Advances in Clinical and Experimental Medicine

MONTHLY ISSN 1899-5276 (PRINT) ISSN 2451-2680 (ONLINE) advances.umw.edu.pl

2026, Vol. 35, No. 1 (January)

Impact Factor (IF) – 1.9
Ministry of Science and Higher Education – 70 pts
Index Copernicus (ICV) – 161.00 pts

Wroclaw Medical University

Advances
in Clinical and Experimental
Medicine

Advances
in Clinical and Experimental Medicine

ISSN 1899-5276 (PRINT) ISSN 2451-2680 (ONLINE) advances.umw.edu.pl

MONTHLY 2026
Vol. 35, No. 1
(January)

Advances in Clinical and Experimental Medicine (*Adv Clin Exp Med*) publishes high-quality original articles, research-in-progress, research letters and systematic reviews and meta-analyses of recognized scientists that deal with all clinical and experimental medicine.

Editorial Office
ul. Marcinkowskiego 2–6
50-368 Wrocław, Poland
Tel.: +48 71 784 12 05
E-mail: acem.journal@umw.edu.pl

Publisher
Wroclaw Medical University
Wybrzeże L. Pasteura 1
50-367 Wrocław, Poland

Online edition is the original version of the journal

Editorial Policy

Advances in Clinical and Experimental Medicine (Adv Clin Exp Med) is an independent multidisciplinary forum for exchange of scientific and clinical information, publishing original research and news encompassing all aspects of medicine, including molecular biology, biochemistry, genetics, biotechnology and other areas. During the review process, the Editorial Board conforms to the "Uniform Requirements for Manuscripts Submitted to Biomedical Journals: Writing and Editing for Biomedical Publication" approved by the International Committee of Medical Journal Editors (www.ICMJE.org). The journal publishes (in English only) original papers and reviews. Short works considered original, novel and significant are given priority. Experimental studies must include a statement that the experimental protocol and informed consent procedure were in compliance with the Helsinki Convention and were approved by an ethics committee.

For all subscription-related queries please contact our Editorial Office: acem.journal@umw.edu.pl
For more information visit the journal's website: advances.umw.edu.pl

Pursuant to the ordinance of the Rector of Wroclaw Medical University No. 37/XVI R/2024, from March 1, 2024, authors are required to pay a fee for each manuscript accepted for publication in the journal Advances in Clinical and Experimental Medicine. The fee amounts to 1600 EUR for all types of papers.

Indexed in: MEDLINE, Science Citation Index Expanded, Journal Citation Reports/Science Edition, Scopus, EMBASE/Excerpta Medica, Ulrich's™ International Periodicals Directory, Index Copernicus

Typographic design: Piotr Gil, Monika Kolęda
DTP: Wydawnictwo UMW
Cover: Monika Kolęda
Printing and binding: Drukarnia I-BiS Bierońscy Sp.k.

Advances
in Clinical and Experimental Medicine

MONTHLY 2026, Vol. 35, No. 1 (January)

ISSN 1899-5276 (PRINT)
ISSN 2451-2680 (ONLINE)
advances.umw.edu.pl

Contents

Reviews

From consensus to action: Implementing cardiovascular prevention guidelines in primary healthcare

Donata Kurpas[1,A–F], Ferdinando Petrazzuoli[2,A–F], Eduard Shantsila[3,A–F], Maria Antonopoulou[4,A–F], Ruxandra Christodorescu[5,A–F], Oleksii Korzh[6,A–F], Thomas Kümler[7,8,A–F], Martha Kyriakou[9,A–F], Lis Neubeck[10,A–F], Panteleimon E. Papakonstantinou[11,A–F], Dimitrios Richter[12,A–F], Anne Grete Semb[13,A–F], Manuel Frias Vargas[14,A–F], Marc Ferrini[15,A–F]

[1] Division of Research Methodology, Department of Nursing, Faculty of Nursing and Midwifery, Wroclaw Medical University, Poland
[2] WONCA Europe & EURIPA, Department of Clinical Sciences, Centre for Primary Health Care Research, Lund University, Malmö, Sweden
[3] Department of Primary Care and Mental Health, University of Liverpool, UK
[4] Spili Primary Care Center, Crete Regional Health System, Greece
[5] Department V Internal Medicine, University of Medicine and Pharmacy V. Babes Timișoara, Research Center Institute of Cardiovascular Diseases, Romania
[6] Department of General Practice–Family Medicine, Kharkiv National Medical University, Ukraine
[7] Institute for Clinical Medicine, University of Copenhagen, Denmark
[8] Complications Research, Steno Diabetes Center Copenhagen, Department of Cardiology, Herlev-Gentofte University Hospital, Denmark
[9] Department of Health Sciences, School of Sciences, European University Cyprus, Nicosia, Cyprus
[10] Centre for Cardiovascular Health, Edinburgh Napier University, UK
[11] Heart and Vascular Centre, Mater Private Hospital, Dublin, Ireland
[12] Athens EUROCLINIC Hospital, Greece
[13] Division for Research and Innovation, REMEDY Center, Diakonhjemmet Hospital, Oslo, Norway
[14] Daroca Primary Care Health Centre, Madrid, Spain
[15] Department of Cardiology and Vascular Pathology, Centre Hospitalier Saint Joseph Saint Luc, Lyon, France

A – research concept and design; B – collection and/or assembly of data; C – data analysis and interpretation;
D – writing the article; E – critical revision of the article; F – final approval of the article

Advances in Clinical and Experimental Medicine, ISSN 1899–5276 (print), ISSN 2451–2680 (online) *Adv Clin Exp Med*. 2026;35(1):5–10

Address for correspondence
Donata Kurpas
E-mail: dkurpas@hotmail.com

Funding sources
None declared

Conflict of interest
None declared

Received on October 3, 2025
Reviewed on October 20, 2025
Accepted on October 29, 2025
Published online on November 20, 2025

Cite as
Kurpas D, Petrazzuoli F, Shantsila E, et al. From consensus to action: Implementing cardiovascular prevention guidelines in primary healthcare. *Adv Clin Exp Med*. 2026;35(1):5–10. doi:10.17219/acem/213742

DOI
10.17219/acem/213742

Abstract

Cardiovascular prevention guidelines are based on robust evidence, yet their implementation in primary healthcare remains inconsistent due to systemic barriers, workload pressures and insufficiently adapted tools. The 2025 European consensus emphasizes the need for multidisciplinary teamwork, digital innovation and equity-focused strategies to strengthen prevention across diverse healthcare systems. Translating these recommendations into actionable, context-specific approaches is essential to close the evidence-practice gap and improve population cardiovascular outcomes.

Key words: primary healthcare, cardiovascular diseases, implementation science, preventive health services, guideline adherence

Highlights

- Cardiovascular prevention guidelines remain under-implemented in primary care due to systemic barriers and workload challenges.
- The 2025 European consensus calls for multidisciplinary teamwork and equity-driven approaches in prevention strategies.
- Digital health tools and context-specific adaptation are essential for improving cardiovascular risk management.
- Closing the evidence–practice gap can enhance population-level cardiovascular outcomes across healthcare systems.

Introduction: From guidelines to everyday practice

The past 2 decades have witnessed a proliferation of cardiovascular prevention guidelines produced by national, European and global professional societies. Their scientific quality is rarely questioned; most are grounded in robust evidence and formulated through rigorous consensus processes. Yet, many of these recommendations cannot be implemented equitably at scale in real-world practice. As the frontline of prevention and long-term management of cardiovascular disease (CVD), primary healthcare has a pivotal role, but systemic and structural barriers frequently constrain implementation efforts. The paradox is striking. Even though we now possess unprecedented knowledge about reducing cardiovascular risk, incorporating this evidence into routine clinical care continues to pose a significant challenge. The COVID-19 pandemic underscored the fragility of preventive services and amplified existing inequities.[1] Although the acute disruptions have eased, persistent health inequalities – driven by structural determinants – remain a key obstacle to improving cardiovascular outcomes.

Several factors underpin this gap. Primary care clinicians face heavy caseloads, limited consultation times and competing priorities. Guidelines, frequently designed with hospital-based populations in mind and without adequate consultation with primary care providers, may not fully account for the complexity of multimorbidity or the social determinants of health that shape outcomes in the community.[2] Moreover, the lack of standardized tools for continuous professional feedback and quality improvement limits effective implementation.[3] The consequence is a pattern of underdiagnosis, therapeutic inertia and wide disparities in preventive care across Europe.

Against this backdrop, the 2025 scientific statement jointly issued by the European Association of Preventive Cardiology, the European Society of Cardiology (ESC) Council for Cardiology Practice, the Association of Cardiovascular Nursing and Allied Professions, WONCA (World Organization of National Colleges, Academies and Academic Associations of General Practitioners/Family Physicians) Europe, and European Rural and Isolated Practitioners Association (EURIPA) represents a critical step forward.[2] By explicitly addressing the realities of primary care, it seeks to harmonize recommendations, highlight implementation gaps and promote system-level engagement. Its central message is clear: Cardiovascular prevention cannot succeed without stronger integration of guidelines into the daily practice of general practitioners, nurses and allied professionals.

Why is implementation so difficult?

Despite decades of progress in cardiovascular medicine, translating preventive recommendations into primary care remains fraught with obstacles. One of the most persistent is the structural fragmentation of healthcare systems across Europe. Such gaps are difficult to overcome, since they reflect structural differences in how health systems are organized. While complete harmonization across countries is unlikely, progress may come from shared principles and adaptable coordination models.

At the same time, primary care professionals carry a workload that continues to expand in volume and complexity. Rising numbers of older patients with multimorbidity, coupled with limited workforce growth, leave general practitioners and nurses with little time to address prevention systematically. Large multicountry programs consistently document these shortfalls, including suboptimal risk factor control and persistent care gaps in patients with multimorbidity.[4,5]

Another major challenge lies in the limited availability of locally adapted tools that fit into the daily routines of family practice. Risk calculators, decision support systems and patient education resources often remain inaccessible, overly complex or poorly integrated into electronic health records. This limits their use during short consultations and reduces their relevance in resource-constrained environments.

Finally, clinicians face a paradox of abundance. The sheer volume of guidelines produced by multiple professional bodies, each with nuanced recommendations, creates confusion rather than clarity.[6] Without concise, operational guidance adapted to primary care realities, preventive cardiology risks remaining aspirational rather than actionable,[7] a conclusion echoed by EUROASPIRE V/VI[4] and AFFIRMO,[5] which highlight the gap between recommendations and everyday delivery of care.

Key messages of the consensus

The 2025 consensus highlights that prevention cannot be delivered by physicians alone. Multidisciplinary and team-based models are the foundation of effective cardiovascular risk management. General practitioners, nurses, dietitians, pharmacists, psychologists, and community health workers each bring complementary expertise that can improve adherence and continuity of care. The most tangible pathway to scaling prevention across European health systems is shifting from a physician-centered to a team-centered approach. Digital innovation is another defining feature of the statement. Integrating telemedicine and decision support into everyday workflows offers the potential to extend the reach of primary care, particularly in underserved or remote regions. Technology should be regarded as an enabler rather than a substitute for clinical judgment. The challenge is to ensure that digital tools are interoperable, user-friendly and accessible across settings with variable resources. Ongoing training in digital literacy for healthcare staff is essential to maximize the benefits of these innovations.

The document draws special attention to vulnerable populations. People with multimorbidity, migrants and residents of rural or deprived communities often experience systematic disadvantages in access to timely prevention.[8] The consensus sets a benchmark for more inclusive cardiovascular health strategies by explicitly acknowledging these groups. It frames prevention as a biomedical issue and a matter of equity and social responsibility. Including clinical illustrations such as chronic venous disease, elevated lipoprotein(a) and inflammatory rheumatic disorders exemplifies the need for broader thinking in primary care. These examples highlight conditions that cut across specialties, often overlooked in standard prevention frameworks, yet highly relevant to everyday practice.[9] Their selection signals a call to widen the lens of cardiovascular prevention and adapt strategies to the complex realities of patients in primary care.[2] The consensus also emphasizes the importance of ongoing professional development to keep abreast of new scientific evidence and improve communication skills, cultural competence and motivational interviewing – core elements of effective preventive counseling across diverse populations.

Implications for general practitioners

For general practitioners, the challenge is translating recommendations into the constraints of a brief consultation and keeping pace with the increasing complexity of evolving guidance, which reinforces the need for continuous professional development. With only 10–15 min available, including the time required to review prior history and document decisions, preventive cardiology must often be reduced to its most pragmatic elements. While longer consultations would be preferable, realistic prioritization and alignment with patient expectations remain essential. This requires focusing on tools and approaches that can be used efficiently, without adding excessive burden to already crowded agendas.

Risk assessment remains the cornerstone of prevention. Instruments such as SCORE2 or mobile-based calculators allow rapid cardiovascular risk estimation and seamlessly integrate into electronic health records. Their most significant value lies in enabling clinicians to stratify patients quickly, identify those requiring intensified intervention and open conversations about behavior change. To be effective, these tools must be simple, reliable and embedded into clinical routines rather than existing as standalone resources.[10]

Equally important is the emphasis on shared decision-making and personalization of therapy, yet these processes are time-intensive and difficult to achieve fully within the constraints of short consultations. Preventive care gains credibility and durability when it reflects patient values and priorities. General practitioners who engage patients in goal setting, acknowledge barriers and tailor interventions are more likely to achieve sustainable behavior changes and treatment adherence.

The role of the general practitioner must also be understood within a broader team context. Nurses, pharmacists and link workers can take responsibility for education, follow-up and care coordination. By redistributing tasks across a multidisciplinary team, preventive strategies become more feasible and less dependent on the physician alone.[11] This team-based approach is essential to bring guidelines to life in the day-to-day practice of primary care.[12] It is important to note that digital literacy and adequate training in decision support tools are prerequisites for successful implementation, ensuring that technologies reduce, rather than increase, the workload of physicians.

The evidence-practice gap

The promise of cardiovascular prevention remains only partially realized, with wide gaps between evidence and routine practice. Persistent regional inequalities across Europe illustrate the challenge. In some countries, structured prevention programs and strong primary care systems have delivered measurable progress, while in others, resource limitations and fragmented services have left high-risk populations without consistent support. Such variation reflects not only differences in funding but also disparities in health literacy, workforce capacity and political commitment to prevention.

Even where guidelines are well disseminated, clinical targets remain poorly achieved. Rates of optimal control for low-density lipoprotein cholesterol, blood pressure and glycemia are consistently inadequate. This failure

is not simply the result of patient non-adherence but also of therapeutic inertia, insufficient follow-up and the absence of systematic monitoring within primary care.[13] The consequence is that millions of Europeans live with preventable cardiovascular risk that remains unaddressed despite clear evidence on how to reduce it.

Compounding the problem is the lack of reliable indicators to assess implementation in real-world practice. Most health systems can report prescription volumes or hospital outcomes, yet very few collect data on whether preventive strategies are delivered during primary care consultations. Without suitable ways to assess implementation, quality improvement efforts risk lacking direction and accountability. However, indicators alone are unlikely to provide the solution unless co-designed with practitioners and embedded in supportive systems. The development and integration of standardized processes and outcome measures within electronic health systems are urgently needed to close this gap.[14]

Closing the evidence–practice gap requires a stronger focus on real-world evidence and practice-based research. Embedding pragmatic trials and observational studies in everyday primary care would provide the insights needed to adapt guidelines, overcome barriers and deliver prevention that is both evidence-based and feasible in daily clinical work.[15] Equally important is patient participation in the co-design of prevention strategies, where patients act not simply as recipients of care but also as partners in developing, testing and refining interventions that fit their life realities.[16]

The rural primary care setting

The specificity of the rural primary care setting deserves a more profound analysis. Rural primary care teams face persistent barriers to following CVD prevention guidelines, including workforce shortages, brief consultations and competing acute demands that crowd out structured prevention.[2] Limited on-site diagnostics and referral bottlenecks (e.g., natriuretic peptide testing and echocardiography access) delay risk stratification and timely treatment initiation. Fragmented information flows and poor interoperability of electronic systems hinder the use of decision support, audits and shared records across dispersed services.[17]

Guidelines are often lengthy and hospital-centric, offering insufficiently tailored, feasible steps for multi-morbid, older patients commonly seen in rural practice. Socioeconomic determinants – lower health literacy, travel costs and limited access to nutritious food – compound adherence challenges and widen prevention gaps. Time constraints and digital literacy gaps reduce uptake of risk tools (e.g., SCORE2/QRISK) and undermine shared decision-making during short visits. Telehealth and remote monitoring could mitigate distance barriers, but added data processing and workflow burden can offset benefits without resourcing. Policy-level enablers (e.g., European Health Data Space; national CVD strategies) require local funding and adaptation to become usable in small practices.

Overall, practical, concise and context-adapted guidance – embedded into interoperable IT with team-based pathways – is essential to close rural implementation gaps.[16,18] Community collaborations, such as those involving local schools, employers and municipalities, can expand prevention efforts beyond clinics and help create healthier rural environments. A short, structured self-care coaching intervention combined with assessment of caregiver contribution is beneficial in rural settings.[19]

A system-level perspective

Sustainable cardiovascular prevention depends not only on clinical knowledge but also on the organization of health systems. What is required are prevention models that are simple, scalable and financially sustainable.[15] Strategies must focus on streamlined pathways that can be delivered consistently across diverse settings, from urban centers to rural practices with limited resources.

European and global health policies provide a framework for such efforts. The European Health Data Space promises to improve data interoperability and facilitate monitoring of preventive care. Initiatives such as the European Commission's Healthier Together strategy and the World Health Organization's (WHO) commitment to Universal Health Coverage underline the importance of equity in prevention. These frameworks highlight the need for patient-centered, transparent and accountable systems.

Yet, international declarations alone are insufficient. Translation into local practice requires strong national strategies, adequate funding and political will. Primary care providers must be supported by reimbursement schemes, workforce planning and digital infrastructure that make prevention practical and sustainable. Policy strategies that enable integrated healthcare and build strong multidisciplinary healthcare networks to enhance interprofessional communication and referral pathways are also crucial to implementing recommendations in primary care settings.[19]

Cardiovascular prevention will remain fragmented and uneven without alignment between global ambitions and national implementation.

Innovations and the future of prevention

The future of cardiovascular prevention in primary care may be shaped by innovations that extend beyond traditional models of care. Remote monitoring and telehealth

are already transforming the management of chronic conditions.[20] Continuous tracking of blood pressure, heart rate or rhythm through wearable devices enables earlier detection of deterioration and more timely interventions.[21] Artificial intelligence applied to these data streams offers the possibility of personalized risk prediction and decision support that adapts to the complexity of multimorbidity often encountered in general practice.

At the same time, personalized medicine must move beyond genomics to encompass psychosocial and cultural determinants of health. Effective prevention depends on biological risk and behaviors shaped by family dynamics, education, employment, and community environments. Recognizing and integrating these determinants into risk assessment and management strategies can make preventive care more relevant and sustainable.[22]

Community resources represent another frontier for innovation. Link workers, peer support groups and culturally adapted education programs help bridge gaps between clinical advice and lived reality.[23] Religiosity and spirituality, too often overlooked in biomedical discourse, may provide resilience, reduce stress and encourage adherence to healthy behaviors. Incorporating such dimensions does not replace evidence-based medicine but enriches it, anchoring prevention in the context of patients' lives.[24]

Taken together, these innovations point to a future in which prevention is more technologically sophisticated and more human-centered. The challenge will be integrating digital advances with social and cultural realities, ensuring equitable access and meaningful outcomes.[25]

Call to action

The implementation of cardiovascular prevention in primary care represents a dual challenge that is both medical and societal. Success requires the rigorous application of evidence-based medicine combined with explicit recognition of the social, cultural and economic determinants that shape health behaviors and access to services. Without an integrated perspective, guidelines risk remaining scientifically robust but operationally ineffective, with limited impact on population-level outcomes.

Strengthening the evidence base specific to primary care is a critical priority. Recommendations relying on hospital-based studies do not adequately capture the multimorbidity, diagnostic uncertainty, and socioeconomic diversity characteristic of community populations. Pragmatic trials, practice-based research networks and real-world evidence are necessary to evaluate preventive interventions' feasibility, effectiveness and scalability within everyday consultations. In parallel, sustained investment in education and professional development is required to equip clinicians with the competencies to deliver high-quality prevention in settings constrained by time and resources. Guidelines must evolve toward simplicity and operational clarity, providing concise and actionable recommendations bridging the research and practice gap.

International collaboration remains central to progress. Professional societies, policymakers and patient organizations should work collectively to promote coherent standards while allowing adaptation to national and local contexts. Equity must be the guiding principle, ensuring that vulnerable populations are prioritized in implementation strategies.[26]

The consensus statement provides a critical platform. The next step is to translate shared aspirations into coordinated action that strengthens primary care and mitigates the global burden of CVD. A transition from aspiration to implementation requires naming specific levers that can be activated without adding complexity to already pressured primary care. At system level, embedding concise and context-adapted preventive steps into existing electronic workflows – rather than creating parallel processes – is essential to make adherence feasible during brief consultations. Implementation can further be enabled through financing schemes that allow redistribution of preventive tasks within multidisciplinary primary care teams, and through co-design of care pathways with patients and communities to ensure cultural fit, equity and uptake across heterogeneous settings.

Use of AI and AI-assisted technologies

Not applicable.

ORCID iDs

Donata Kurpas https://orcid.org/0000-0002-6996-8920
Ferdinando Petrazzuoli https://orcid.org/0000-0003-1058-492X
Eduard Shantsila https://orcid.org/0000-0002-2429-6980
Maria Antonopoulou https://orcid.org/0000-0001-5259-2819
Ruxandra Christodorescu https://orcid.org/0000-0001-8267-5404
Oleksii Korzh https://orcid.org/0000-0001-6838-4360
Thomas Kümler https://orcid.org/0000-0001-9102-3862
Martha Kyriakou https://orcid.org/0000-0003-1786-4668
Lis Neubeck https://orcid.org/0000-0001-5852-1034
Panteleimon E. Papakonstantinou https://orcid.org/0000-0003-4691-7183
Dimitrios Richter https://orcid.org/0000-0003-0245-4690
Anne Grete Semb https://orcid.org/0000-0003-2730-2853
Manuel Frias Vargas https://orcid.org/0000-0003-2692-5063
Marc Ferrini https://orcid.org/0000-0002-2595-2433

References

1. Petrazzuoli F, Gokdemir O, Antonopoulou M, et al. Resilience of primary healthcare facilities: Experiences from 16 European countries during the COVID-19 pandemic. A mixed-methods study conducted by EURIPA. *Adv Clin Exp Med*. 2024;34(4):487–505. doi:10.17219/acem/194212
2. Kurpas D, Petrazzuoli F, Shantsila E, et al. Implementation of prevention guidelines in primary healthcare: A scientific statement of the European Association of Preventive Cardiology of the ESC, the ESC Council for Cardiology Practice, the Association of Cardiovascular Nursing & Allied Professions of the ESC, WONCA Europe, and EURIPA [published online as ahead of print on July 17, 2025]. *Eur J Prev Cardiol*. 2025. doi:10.1093/eurjpc/zwaf384

3. Kotseva K, De Backer G, De Bacquer D, et al. Primary prevention efforts are poorly developed in people at high cardiovascular risk: A report from the European Society of Cardiology EURObservational Research Programme EUROASPIRE V survey in 16 European countries. *Eur J Prev Cardiol*. 2021;28(4):370–379. doi:10.1177/2047487320908698
4. EUROASPIRE Study Group. EUROASPIRE: A European Society of Cardiology survey of secondary prevention of coronary heart disease. Principal results. *Eur Heart J*. 1997;18(10):1569–1582. doi:10.1093/oxfordjournals.eurheartj.a015136
5. AFFIRMO Project. The Project. AFFIRMO Project; 2025. https://www.affirmo.eu/the-project. Accessed November 14, 2025.
6. Wang T, Tan JY, Liu XL, Zhao I. Barriers and enablers to implementing clinical practice guidelines in primary care: An overview of systematic reviews. *BMJ Open*. 2023;13(1):e062158. doi:10.1136/bmjopen-2022-062158
7. Uchmanowicz I, Czapla M, Lomper K, et al. Effective implementation of preventive cardiology guidelines: Pathways to success [published online as ahead of print on July 18, 2025]. *Eur J Prev Cardiol*. 2025. doi:10.1093/eurjpc/zwaf448
8. Fu Y, Price C, Haining S, et al. Cardiovascular-related conditions and risk factors in primary care for deprived communities before and during the COVID-19 pandemic: An observational study in Northern England. *BMJ Open*. 2022;12(11):e066868. doi:10.1136/bmjopen-2022-066868
9. Hanarz M, Siniarski A, Gołębiowska-Wiatrak R, Nessler J, Malinowski KP, Gajos G. Gender-related and PUFA-related differences in lipoprotein-associated phospholipase A2 levels in patients with type 2 diabetes and atherosclerotic cardiovascular disease. *Adv Clin Exp Med*. 2023;33(6):593–600. doi:10.17219/acem/171002
10. Elias S, Chen Y, Liu X, et al. Shared decision-making in cardiovascular risk factor management: A systematic review and meta-analysis. *JAMA Netw Open*. 2024;7(3):e243779. doi:10.1001/jamanetworkopen.2024.3779
11. Tu Q, Lin S, Hyun K, et al. The effects of multidisciplinary collaborative care on cardiovascular risk factors among patients with diabetes in primary care settings: A systematic review and meta-analysis. *Primary Care Diabetes*. 2024;18(4):381–392. doi:10.1016/j.pcd.2024.05.003
12. German CA, Baum SJ, Ferdinand KC, et al. Defining preventive cardiology: A clinical practice statement from the American Society for Preventive Cardiology. *Am J Prev Cardiol*. 2022;12:100432. doi:10.1016/j.ajpc.2022.100432
13. Ray KK, Haq I, Bilitou A, et al. Treatment gaps in the implementation of LDL cholesterol control among high- and very high-risk patients in Europe between 2020 and 2021: The multinational observational SANTORINI study. *Lancet Reg Health Eur.* 2023;29:100624. doi:10.1016/j.lanepe.2023.100624
14. Aktaa S, Gencer B, Arbelo E, et al. European Society of Cardiology Quality Indicators for Cardiovascular Disease Prevention: Developed by the Working Group for Cardiovascular Disease Prevention Quality Indicators in collaboration with the European Association for Preventive Cardiology of the European Society of Cardiology. *Eur J Prev Cardiol*. 2022;29(7):1060–1071. doi:10.1093/eurjpc/zwab160
15. Królikowska A, Prill R, Klugar M. Evidence-based healthcare: Bridging the gap between research and practice. *Adv Clin Exp Med*. 2025;34(2):139–147. doi:10.17219/acem/201184
16. Szczepanowski R, Uchmanowicz I, Pasieczna AH, et al. Application of machine learning in predicting frailty syndrome in patients with heart failure. *Adv Clin Exp Med*. 2024;33(3):309–315. doi:10.17219/acem/184040
17. Kefala AM, Triantafyllou A, Symvoulakis EK, Tzouganatou EM, Kapellas N, Smyrnakis E. Working as a healthcare professional at island primary care: An exploratory qualitative study on the Cyclades Islands, Greece. *Healthcare (Basel)*. 2024;12(9):882. doi:10.3390/healthcare12090882
18. Grice-Jackson T, Rogers I, Ford E, et al. A community health worker led approach to cardiovascular disease prevention in the UK – SPICES-Sussex (scaling-up packages of interventions for cardiovascular disease prevention in selected sites in Europe and Sub-saharan Africa): An implementation research project. *Front Health Serv*. 2024;4:1152410. doi:10.3389/frhs.2024.1152410
19. Iovino P, Uchmanowicz I, Vellone E. Self-care: An effective strategy to manage chronic diseases. *Adv Clin Exp Med*. 2024;33(8):767–771. doi:10.17219/acem/191102
20. Caiani EG, Kemps H, Hoogendoorn P, et al. Standardized assessment of evidence supporting the adoption of mobile health solutions: A clinical consensus statement of the ESC Regulatory Affairs Committee. *Eur Heart J Digital Health*. 2024;5(5):509–523. doi:10.1093/ehjdh/ztae042
21. Guasti L, Dilaveris P, Mamas MA, et al. Digital health in older adults for the prevention and management of cardiovascular diseases and frailty: A clinical consensus statement from the ESC Council for Cardiology Practice/Taskforce on Geriatric Cardiology, the ESC Digital Health Committee and the ESC Working Group on e-Cardiology. *ESC Heart Fail*. 2022;9(5):2808–2822. doi:10.1002/ehf2.14022
22. Kupper N, Van Den Houdt S, Kuijpers PMJC, Widdershoven J. The importance, consequences and treatment of psychosocial risk factors in heart disease: Less conversation, more action! *Neth Heart J*. 2024;32(1):6–13. doi:10.1007/s12471-023-01831-x
23. Petrazzuoli F, Vidall Alabal J, Kenkre J, et al. Best practice approaches to social prescribing in European primary care: A Delphi protocol focused on link workers. *Adv Clin Exp Med*. 2025;34(9):1589–1595. doi:10.17219/acem/208216
24. Hassen HY, Ndejjo R, Van Geertruyden JP, Musinguzi G, Abrams S, Bastiaens H. Type and effectiveness of community-based interventions in improving knowledge related to cardiovascular diseases and risk factors: A systematic review. *Am J Prev Cardiol*. 2022;10:100341. doi:10.1016/j.ajpc.2022.100341
25. Składanek JA, Leśkiewicz M, Gumiężna K, et al. Long COVID and its cardiovascular consequences: What is known? *Adv Clin Exp Med*. 2023;33(3):299–308. doi:10.17219/acem/167482
26. Piccoliori G, Barbieri V, Wiedermann C, Engl A. Special roles of rural primary care and family medicine in improving vaccine hesitancy. *Adv Clin Exp Med*. 2023;32(4):401–406. doi:10.17219/acem/162349

Personalized medicine for patients with chronic diseases in Europe: From concept to clinical practice

Dorota Stefanicka-Wojtas[A–D], Donata Kurpas[B,C,E,F]

Division of Research Methodology, Department of Nursing, Faculty of Nursing and Midwifery, Wroclaw Medical University, Poland

A – research concept and design; B – collection and/or assembly of data; C – data analysis and interpretation;
D – writing the article; E – critical revision of the article; F – final approval of the article

Advances in Clinical and Experimental Medicine, ISSN 1899–5276 (print), ISSN 2451–2680 (online) *Adv Clin Exp Med*. 2026;35(1):11–16

Address for correspondence
Dorota Stefanicka-Wojtas
E-mail: dorota.stefanicka-wojtas@umw.edu.pl

Funding sources
None declared

Conflict of interest
None declared

Received on August 14, 2025
Reviewed on October 24, 2025
Accepted on October 30, 2025

Published online on November 13, 2025

Abstract

The rising prevalence of chronic diseases presents a major challenge to healthcare systems worldwide, particularly within primary care. While advances in diagnostics and therapeutics have improved disease management, traditional care models often neglect the individual contexts and lived experiences of patients. Personalized medicine (PM) offers a paradigm shift from standardized treatment approaches toward patient-specific care, integrating biological, behavioral and psychosocial dimensions to optimize outcomes. This editorial synthesizes findings from the Regions4PerMed (Horizon 2020) project, encompassing focus groups, stakeholder surveys and best practice analyses across 20 European countries. Stakeholders from government, academia, patient organizations and healthcare practice, identified key barriers to PM implementation, including fragmented data systems, insufficient clinician training and limited patient engagement. Cross-border data exchange standards, integration of real-world evidence (RWE) and sustainable funding mechanisms emerged as critical enablers of progress.

The transition from concept to practice requires aligning policy, technology and human factors. Personalized care extends beyond genomics and precision therapies to encompass communication, motivation and shared decision-making. Training healthcare professionals in holistic competencies, enhancing digital literacy and promoting trust in data-driven systems are essential for successful adoption. By reframing personalization as both a scientific and relational endeavor, PM can strengthen chronic disease care through more adaptive, patient-centered models. Coordinated action across policy, education and technology domains is vital to embed personalization into everyday clinical practice and ensure sustainable, equitable healthcare delivery across Europe.

Key words: health policy, patient-centered care, primary health care, chronic disease, personalized medicine

Cite as
Stefanicka-Wojtas D, Kurpas D. Personalized medicine for patients with chronic diseases in Europe: From concept to clinical practice. *Adv Clin Exp Med*. 2026;35(1):11–16. doi:10.17219/acem/213758

DOI
10.17219/acem/213758

Highlights

- Personalized medicine advances chronic disease management through patient-specific strategies, improving treatment precision, response and long-term outcomes.
- Cross-border data sharing, real-world evidence (RWE) integration and sustainable funding models are vital for the successful implementation of personalized medicine in Europe.
- Coordinated health policies, clinician education and active patient engagement are essential to translate personalized medicine into clinical practice and enhance healthcare quality.

Introduction

The growing burden of chronic diseases poses a major challenge to healthcare systems, particularly in primary healthcare. While medical progress has improved diagnostics and treatments, care delivery often overlooks patients' individual contexts. There is a clear shift from a "one size fits all" model toward patient-specific strategies, including targeted therapies, to achieve optimal outcomes.[1,2] Personalized medicine (PM) reflects this shift, focusing on differences between patients with the same disease and matching treatments to subgroups to improve precision and effectiveness, while also predicting individual therapy responses.

However, implementing PM faces systemic and practical barriers. Stakeholder consultations across 20 European countries highlighted the need for cross-border data exchange standards, better integration of real-world evidence (RWE) into decisions and sustainable funding. Successful implementation demands coordination between health policy, healthcare system capacity and patient organizations.[3]

This editorial examines the practical implications of PM, drawing on studies involving stakeholders from government, patient organizations, academia, clinical practice, and law at national and international levels. Personalized care goes beyond technology; it requires a deep understanding of the individual within the healthcare ecosystem. Key areas shaping the PM agenda include: evolving definitions, medical data systems, health policy, economic sustainability, clinical training, patient engagement, and dissemination of reliable information.

We also address barriers such as inadequate training and lack of incentives, as well as potential solutions: holistic care models, increased research investment, and development of interactive tools for self-monitoring and share decision-making. By addressing these challenges, PM can shift from concept to practice, enhancing outcomes for patients with chronic diseases.

The increasing prevalence of chronic diseases – such as cardiovascular conditions, diabetes and chronic respiratory illnesses – has become a defining feature of global health in the 21st century.[4,5] These conditions account for most morbidity, mortality and healthcare expenditures worldwide. Significant advances have been made in pharmacotherapy, diagnostics and clinical guidelines. Yet despite these developments, a critical disconnect persists between the biomedical management of chronic illness and the broader lived experience of patients.[6]

Personalized medicine has emerged as a promising paradigm to bridge this gap. Initially rooted in genomics and biomarker-driven treatment, the field has gradually expanded its scope to include a more comprehensive understanding of the patient. According to Epstein and Street, patient-centered communication goes beyond a clinical technique to represent a moral obligation.[7] In this context, personalization must encompass not only biology, but also behavior, beliefs and biopsychosocial environments.

The findings presented in this editorial are grounded in multiple qualitative and mixed-method studies conducted within the framework of the Regions4PerMed (Horizon 2020) project. One study employed focus group methodology, bringing together stakeholders including representatives of Polish government institutions, patient advocacy organizations and financial bodies to explore barriers and facilitators to implementing PM.[8] Another research phase involved a semi-structured survey of 85 respondents from 20 countries. Participants included policy officers, project managers, scientists, physicians, and legal advisors, offering diverse perspectives on PM implementation challenges and enablers at micro-, meso- and macro-regional levels. The 3rd component drew from the findings of the conference Health Technology in Connected & Integrated Care, held under the Horizon 2020 project "Interregional Coordination for a Fast and Deep Uptake of Personalized Health" (Regions4PerMed).[3] The event brought together experts from academia, industry and regional and governmental health policy institutions across the EU. Best practice brochures developed within the project were also analyzed to summarize the current state of PM implementation across Europe. Analysis of European studies indicates that the implementation of eHealth and mHealth in chronic disease care requires not only technological readiness but also adaptation to patients' skills and motivation. Barriers include low levels of digital literacy among older adults, a lack of user-friendly interfaces and fragmented legislation. Overcoming these obstacles calls for the training of healthcare professionals, the integration of data systems and the development of solutions tailored to patient needs. Consultations with stakeholders from 20 European countries revealed the necessity

of developing cross-border data exchange standards, improving the integration of RWE into decision-making processes, and creating sustainable funding mechanisms. Effective implementation of PM requires coordinated action between health policy, healthcare system capacity and patient organizations. Focus group discussions emphasized that PM should balance technological advancement with socio-economic realities. Participants pointed out that international guidelines, such as those from the American Diabetes Association (ADA), already incorporate personalization by adapting treatments and prevention strategies to comorbidities, economic status and patient preferences. These complementary methods – focus groups, semi-structured surveys and analysis of best practice materials – were applied to capture both the depth and diversity of stakeholder perspectives on PM implementation across Europe.

This editorial synthesizes those findings and situates them within the broader discourse on personalized primary care. We examine how theoretical models of behavior and health regulation intersect with practical considerations in the clinical setting, and we propose directions for transforming personalization from an abstract ideal into a functional component of everyday practice.

Reframing chronic disease care: Why personalization matters

The burden of chronic diseases continues to rise globally, placing increasing demands on primary healthcare systems. While medical advancements have contributed significantly to the improved management of chronic illnesses, the human aspect of care – the unique needs, preferences and life contexts of individual patients – is too often overlooked. This disconnection between biomedical progress and holistic patient-centered care has led to growing interest in integrating PM into everyday clinical practice.

In recent years, the concept of PM has evolved beyond its molecular and genomic origins to include psychosocial, behavioral and environmental factors that shape health trajectories. Nowhere is this shift more needed than in the care of patients with chronic conditions, who often face not only the physiological burden of illness but also the psychological and social challenges of living with a long-term diagnosis. As the first and usually most continuous point of contact for these patients, the primary care setting is uniquely positioned to implement personalized care models beyond clinical protocols.

Personalization in practice: What does it mean?

Personalized care in chronic disease management should not be confused with highly technical precision medicine. While genomic data, biomarkers and advanced diagnostics have a role, personalized care at the primary care level involves recognizing the patient's lived experience and aligning interventions with their values, beliefs and capabilities.

This means asking "What is the matter with the patient?" and "What matters to the patient?". It means exploring motivation, readiness to change, perceived control over health, and social support systems – all of which influence behavior and outcomes. For example, systematic reviews confirm that a higher sense of coherence is positively associated with health-promoting behaviors – including physical activity and healthy eating – and negatively associated with risk behaviors.[9] Moreover, population-based data analyses indicate that better subjective health perception, regardless of objective disease status, is linked to improved health behaviors such as normal weight, proper sleep and regular exercise.[10] Recognizing and responding to these factors requires time, empathy, and often a rethinking of how clinical encounters are structured. Tools such as motivational interviewing, brief behavioral interventions and risk stratification models can support clinicians in integrating personalization into routine visits.[11] As evidenced by findings from both the focus group discussions and stakeholder surveys, real-world examples of personalized care are already emerging across Europe. For instance, national initiatives in primary care in Poland, Germany and Italy have introduced personalized lifestyle coaching combined with remote monitoring tools for patients with diabetes and heart failure. These programs use mobile health applications and telemonitoring systems to track symptoms and treatment adherence, enabling clinicians to dynamically adjust care plans based on real-time patient feedback.[3,4,8] However, the most critical ingredient is clinician awareness – an openness to understanding the person behind the patient.

The data dilemma: Integration, protection and validity

Effective personalized care depends on the thoughtful collection and use of patient data. However, significant obstacles remain. In our studies, stakeholders expressed concerns about data fragmentation, limited system interoperability and a lack of standardization. The ethical dimension is equally important – particularly about data security, privacy and the potential misuse of health information.[12]

Participants also noted that personalized therapies offer great promise but often apply to narrowly defined patient populations, making it difficult to generate robust, generalizable evidence. Cross-border collaboration and harmonization of legal frameworks were seen as essential steps to enable data-driven personalization that is safe, trustworthy and beneficial for patients across diverse healthcare systems.[13]

Recent studies also highlight how artificial intelligence (AI)-driven predictive models can enhance data

interpretation and support early intervention in chronic disease management, further strengthening the potential of personalized care pathways.[14,15]

Systems in transition: Policy, regulation and the role of evidence

The successful implementation of PM depends heavily on coherent health policies and political will.[16] Our findings, based on qualitative focus group discussions and cross-national survey data collected from policymakers and healthcare stakeholders in 20 European countries, revealed that the regulatory landscape across Europe remains fragmented, characterized by lengthy legislative cycles and inconsistent funding structures. These factors delay the translation of innovative practices into routine care.

A recurring recommendation from our respondents was the need to scale up the dissemination of RWE and best practices. This would demonstrate the value of personalized care and support advocacy efforts aimed at integrating personalization into national health strategies. Structural reforms – such as the appointment of case managers or patient navigators – were also cited as promising enablers of change.

Financing the future: Economic models for personalized medicine

The economic sustainability of PM is a central concern. On the one hand, PM offers the potential for long-term cost savings by avoiding ineffective treatments and reducing hospitalizations. Conversely, the high costs of specific targeted therapies – especially for small patient subgroups – pose challenges to reimbursement and equity.[17]

Stakeholders emphasized the importance of rigorous cost-effectiveness analysis and flexible funding models. Public payers and insurers should be equipped to evaluate the value of innovation in terms of clinical efficacy and through the lens of quality of life and long-term outcomes. Furthermore, respondents emphasized that successful pilot programs must be adequately supported beyond their initial funding cycles to ensure a sustainable impact.

The practitioner's role: From specialist knowledge to holistic competence

A transformative approach to clinician education is essential for realizing personalized care. Many medical professionals are still trained primarily in disease-specific silos, with limited exposure to behavioral science, patient communication and interprofessional collaboration. This makes it difficult to engage patients as active participants in their care.

Our findings suggest that medical training should emphasize holistic competencies –including empathy, active listening and cultural sensitivity – as foundational skills for all healthcare professionals. Personalized medicine is not just a clinical model, but a relational one, requiring a mindset shift as much as a skillset expansion.[18]

Empowered patients: Engagement, education and digital trust

Personalization also requires a new kind of patient who is informed, engaged and confident in navigating digital health tools. Respondents highlighted the need to strengthen digital literacy, ensure transparency in data use, and involve patients in the design of tools and services.[19] Findings from qualitative and quantitative studies also pointed to the growing role of distance monitoring in chronic disease management. Participants noted that digital tools, such as mobile health apps and wearable sensors, can enhance patient engagement by providing continuous feedback and enabling more responsive, personalized interventions.[3,4,8]

Patients should also be educated about the potential benefits of data sharing,[20] as public support for the implementation of personalized medicine policies (PMPs) in routine care is crucial – not only due to the high financial costs involved but also because of the potential diversion of resources from other healthcare services.[21]

When patients are empowered with information and feel their voices are heard, they are more likely to adhere to treatment, participate in self-care and experience greater satisfaction. Building trust in the digital ecosystem – through robust data protection, clear communication and co-creation strategies – is integral to the personalization agenda.

Spreading the word: Why dissemination is not optional

A frequently overlooked component of PM implementation is the dissemination of knowledge. Our research indicates that public awareness of personalized care remains limited, particularly outside academic and specialist settings. Strategic communication – via traditional media, digital platforms and community engagement – is essential to foster acceptance and demand.[22]

Stakeholders stressed the importance of sharing success stories and scientific findings with the broader public, including patients and caregivers. Widening access

to understandable, evidence-based information is key to building a supportive environment for personalized innovation.

Conclusions

As the epidemiological landscape shifts toward the predominance of chronic diseases, the importance of personalized care in primary care settings becomes increasingly evident. Our findings, together with those of others, point toward a future in which medical practice is scientifically informed, emotionally intelligent, socially conscious, and behaviorally adaptive.

Personalized care is not a luxury reserved for cutting-edge institutions – it is a necessity that can and should be embedded into everyday practice. The first step toward that future is to recognize the diversity of patients – not only in their diagnoses, but also in their experiences, values and capacities. The second is to build systems and develop skills that translate this recognition into practice.

Moreover, findings from qualitative studies and patient narratives highlight the necessity of integrating emotional, cognitive and relational dimensions into care planning – especially in the context of increasingly complex needs among individuals with chronic conditions.[23,24] Addressing these needs requires empathy and communication, as well as digital technologies that enable real-time health monitoring, information exchange and shared decision-making.[3]

Strategies grounded in a holistic, biopsychosocial approach – supported by technological solutions and embedded within secure and regulation-compliant (e.g., General Data Protection Regulation (GDPR)) information systems – have the potential to significantly improve treatment adherence, satisfaction with care and health outcomes.[8]

If we are to improve outcomes for people living with chronic illness, we must begin not just with protocols, but with people. In the European context, where healthcare systems and policies remain diverse yet increasingly interconnected, these insights highlight the shared need for harmonized, patient-centered strategies in chronic disease management.

Use of AI and AI-assisted technologies

Not applicable.

ORCID iDs

Dorota Stefanicka-Wojtas https://orcid.org/0000-0002-8162-7299
Donata Kurpas https://orcid.org/0000-0002-6996-8920

References

1. Suwinski P, Ong C, Ling MHT, Poh YM, Khan AM, Ong HS. Advancing personalized medicine through the application of whole exome sequencing and big data analytics. *Front Genet*. 2019;10:49. doi:10.3389/fgene.2019.00049
2. Iovino P, Uchmanowicz I, Vellone E. Self-care: An effective strategy to manage chronic diseases. *Adv Clin Exp Med*. 2024;33(8):767–771. doi:10.17219/acem/191102
3. Stefanicka-Wojtas D, Kurpas D. Barriers and facilitators to the implementation of personalised medicine across Europe. *J Pers Med*. 2023;13(2):203. doi:10.3390/jpm13020203
4. Stefanicka-Wojtas D, Kurpas D. eHealth and mHealth in chronic diseases: Identification of barriers, existing solutions, and promoters based on a survey of EU stakeholders involved in Regions4PerMed (H2020). *J Pers Med*. 2022;12(3):467. doi:10.3390/jpm12030467
5. Szlenk-Czyczerska E, Kurpas D. Indicators of integrated care for patients with chronic cardiovascular disease in ambulatory care. *Adv Clin Exp Med*. 2023;32(10):1159–1166. doi:10.17219/acem/161462
6. Duman H, Duman H, Puşuroğlu M, Yılmaz AS. Anxiety disorders and depression are associated with resistant hypertension. *Adv Clin Exp Med*. 2023;33(2):111–118. doi:10.17219/acem/166304
7. National Cancer Institute (NCI), National Institutes of Health (NIH). Patient-Centered Communication in Cancer Care: Promoting Healing and Reducing Suffering. Bethesda, USA: National Cancer Institute (NCI), National Institutes of Health (NIH); 2007. https://cancercontrol.cancer.gov/sites/default/files/2020-06/pcc_monograph.pdf. Accessed August 12, 2025.
8. Stefanicka-Wojtas D, Kurpas D. Personalised medicine: Implementation to the healthcare system in Europe (focus group discussions). *J Pers Med*. 2023;13(3):380. doi:10.3390/jpm13030380
9. da-Silva-Domingues H, del-Pino-Casado R, Palomino-Moral PÁ, López Martínez C, Moreno-Cámara S, Frías-Osuna A. Relationship between sense of coherence and health-related behaviours in adolescents and young adults: A systematic review. *BMC Public Health*. 2022;22(1):477. doi:10.1186/s12889-022-12816-7
10. Kwak S, Lee Y, Baek S, Shin J. Effects of subjective health perception on health behavior and cardiovascular disease risk factors in patients with prediabetes and diabetes. *Int J Environ Res Public Health*. 2022;19(13):7900. doi:10.3390/ijerph19137900
11. Vinker S. Innovations in family medicine and the implication to rural and remote primary care. *Adv Clin Exp Med*. 2023;32(2):147–150. doi:10.17219/acem/158171
12. Shabani M, Borry P. Rules for processing genetic data for research purposes in view of the new EU General Data Protection Regulation. *Eur J Hum Genet*. 2018;26(2):149–156. doi:10.1038/s41431-017-0045-7
13. Schleidgen S, Klingler C, Bertram T, Rogowski WH, Marckmann G. What is personalized medicine: Sharpening a vague term based on a systematic literature review. *BMC Med Ethics*. 2013;14(1):55. doi:10.1186/1472-6939-14-55
14. Dong C, Ji Y, Fu Z, et al. Precision management in chronic disease: An AI empowered perspective on medicine-engineering crossover. *iScience*. 2025;28(3):112044. doi:10.1016/j.isci.2025.112044
15. Li C, Zhao Y, Bai Y, et al. Unveiling the potential of large language models in transforming chronic disease management: Mixed methods systematic review. *J Med Internet Res*. 2025;27:e70535. doi:10.2196/70535
16. Doxzen KW, Signé L, Bowman DW. Advancing Precision Medicine through Agile Governance: Bridging Innovation and Regulation for the Greater Good. Washington D.C., USA: Brookings Institution; 2022. https://www.brookings.edu/research/advancing-precision-medicine-through-agile-governance. Accessed August 12, 2025.
17. Kalouguina V, Wagner J. Challenges and solutions for integrating and financing personalized medicine in healthcare systems: A systematic literature review. *Journal of Risk and Financial Management*. 2020;13(11):283. doi:10.3390/jrfm13110283
18. Haiech J, Kilhoffer MC. Personalized medicine and education: The challenge. *Croat Med J*. 2012;53(4):298–300. doi:10.3325/cmj.2012.53.298
19. Greenhalgh T, Wherton J, Papoutsi C, et al. Beyond adoption: A new framework for theorizing and evaluating nonadoption, abandonment, and challenges to the scale-up, spread, and sustainability of health and care technologies. *J Med Internet Res*. 2017;19(11):e367. doi:10.2196/jmir.8775
20. Aronson SJ, Rehm HL. Building the foundation for genomics in precision medicine. *Nature*. 2015;526(7573):336–342. doi:10.1038/nature15816
21. McMichael AJ, Kane JPM, Rolison JJ, O'Neill FA, Boeri M, Kee F. Implementation of personalised medicine policies in mental healthcare: Results from a stated preference study in the UK. *BJPsych Open*. 2022;8(2):e40. doi:10.1192/bjo.2022.9

22. Hicks-Courant K, Shen J, Stroupe A, et al. Personalized cancer medicine in the media: Sensationalism or realistic reporting? *J Pers Med*. 2021;11(8):741. doi:10.3390/jpm11080741
23. Dissen A, Uchmanowicz I, Czapla M. Obesity: A call to action. *Adv Clin Exp Med*. 2025;34(4):473–477. doi:10.17219/acem/203269
24. Dissen A, Riccardo C. Nutrition-related needs and considerations in the transgender and gender non-conforming (TGNC) population: Current gaps and future directions in research. *Adv Clin Exp Med*. 2025;34(5):663–667. doi:10.17219/acem/204177

Risk assessment of human monkeypox infections: A systematic review and meta-analysis

Yue Wang[A–F], Jianlei Wang[A–F]

Department of Dermatology, Beijing Civil Aviation General Hospital, China

A – research concept and design; B – collection and/or assembly of data; C – data analysis and interpretation;
D – writing the article; E – critical revision of the article; F – final approval of the article

Advances in Clinical and Experimental Medicine, ISSN 1899–5276 (print), ISSN 2451–2680 (online) *Adv Clin Exp Med*. 2026;35(1):17–26

Address for correspondence
Yue Wang
E-mail: wy667283@163.com

Funding sources
None declared

Conflict of interest
None declared

Received on July 1, 2024
Reviewed on December 29, 2024
Accepted on March 19, 2025

Published online on August 1, 2025

Abstract

Background. Human monkeypox is a zoonotic disease with increasing global prevalence. Although several studies have identified its potential risk factors, findings remain inconsistent, highlighting the need for a systematic evaluation.

Objectives. To systematically investigate risk factors associated with human monkeypox infections using meta-analysis.

Materials and methods. A comprehensive search of PubMed, Scopus, Web of Science, Embase, and The Cochrane Library databases was conducted on all records up to February 19, 2024. Eligible studies assessing risk factors for monkeypox were included. Odds ratios (ORs) and 95% confidence intervals (95% CIs) were calculated, and heterogeneity was evaluated using I^2 statistics.

Results. Of the 1,844 articles identified, 9 studies met the inclusion criteria after screening, no publication bias was identified, and the meta-analysis results showed strong robustness. Human immunodeficiency virus (HIV) infection significantly increased monkeypox risk (OR = 2.21, 95% CI: 1.13–4.34, p = 0.02, I^2 = 93%). Concurrent sexually transmitted infections (STIs) were also a significant risk factor (OR = 1.84, 95% CI: 1.46–2.33), as was body mass index (BMI) higher than 30 kg/m^2 (OR = 1.18, 95% CI: 0.19–7.53, p = 0.86), lower economic status (OR = 0.33, 95% CI: 0.01–9.36, p = 0.52), education level (OR = 0.74, 95% CI: 0.30–1.79, p = 0.50), or men who have sex with men (MSM) status (OR = 1.22, 95% CI: 0.84–1.75, p = 0.29).

Conclusions. HIV infection and concurrent STIs significantly increase monkeypox risk, underscoring the need for targeted prevention, including screening and risk reduction strategies in vulnerable populations, particularly MSM.

Key words: meta-analysis, risk assessment, virus, human monkeypox, literature search

Cite as
Wang Y, Wang J. Risk assessment of human monkeypox infections: A systematic review and meta-analysis. *Adv Clin Exp Med*. 2026;35(1):17–26. doi:10.17219/acem/203099

DOI
10.17219/acem/203099

Highlights

- HIV infection significantly elevates risk of human monkeypox: Meta-analysis reveals HIV-positive individuals have more than double the risk of monkeypox infection (odds ratio (OR) = 2.21), highlighting an urgent need for targeted public health interventions.
- Concurrent sexually transmitted infection (STIs) are strongly linked to higher honkeypox susceptibility: Individuals with STIs face significantly increased monkeypox risk (OR = 1.84), reinforcing the importance of integrated STI and monkeypox screening programs.
- Sociodemographic factors show no significant association with monkeypox risk: BMI, income, education level, and men who have sex with men (MSM) status did not show statistically significant associations, suggesting that biological risk factors may outweigh sociodemographic ones.
- Systematic review supports focused prevention for vulnerable populations: Findings emphasize the need for prevention strategies targeting high-risk groups, particularly those with HIV or STIs, to curb rising global monkeypox transmission.

Background

Human monkeypox is a sporadic zoonotic disease caused by the monkeypox virus (MPXV), a double-stranded DNA virus belonging to the orthopoxvirus genus.[1,2] The clinical presentation of monkeypox shares similarities with smallpox but is generally less severe, with key symptoms including fever, severe headaches, swollen lymph nodes, back pain, muscle aches, and fatigue.[3] Within 1–3 days of the onset of fever, a characteristic rash typically develops, predominantly affecting the face and limbs. At this stage, individuals become contagious.

Monkeypox virus transmission occurs through direct contact with bodily fluids, lesions on the skin or mucous membranes, contaminated objects, or respiratory droplets from infected individuals.[4] Two distinct genetic clades of MPXV have been identified: the Central African clade, which is associated with more severe disease, and the West African clade. The first human case of monkeypox was reported in 1970 in a 9-year-old boy from the Democratic Republic of the Congo. Historically, human monkeypox was endemic to regions in West and Central Africa.[1] However, in recent years, the incidence has been increasing.[3] In 2022, a major outbreak occurred, involving more than 30 countries outside of Africa, including the UK, Spain, Portugal, Germany, Italy, the USA, and Canada.[5,6] This outbreak, the largest recorded outside Africa, prompted significant concern and led the World Health Organization (WHO) to declare a Public Health Emergency on July 23, 2022.[7]

As of September 2023, more than 90,000 cases of monkeypox had been confirmed globally, with over 30,000 reported in the USA.[8] Studies indicate that monkeypox primarily spreads rapidly among men who have sex with men (MSM), rendering this group particularly vulnerable to infection.[9] The modified vaccinia virus Ankara (MVA), an attenuated non-replicating orthopoxvirus, is currently the preferred vaccine for reducing the risk of human monkeypox infections.[10] However, the global supply of vaccines falls significantly short of meeting the demand, particularly given the large population of MSM worldwide.[9]

Monkeypox continues to be a significant and ongoing threat to public health. The 2022 outbreak emphasized the urgent need to identify risk factors, particularly to safeguard vulnerable groups, including LGBTQ populations. Despite this urgency, existing studies are characterized by inconsistent findings, significant heterogeneity and the absence of standardized methodologies, which have hindered the development of effective prevention and treatment strategies. Furthermore, most research to date has been limited to descriptive epidemiology, lacking comprehensive analyses of potential risk factors. These limitations underscore the necessity of a systematic review and meta-analysis to consolidate available evidence, identify critical risk factors and provide actionable insights for improving clinical practice and public health responses.

Objectives

Based on current evidence, we hypothesized that human immunodeficiency virus (HIV) infection and other sexually transmitted infections (STIs) are significant risk factors for human monkeypox, particularly in vulnerable groups. To test this hypothesis, we designed this study to systematically analyze existing evidence and address 2 key research questions: 1) What are the main risk factors for human monkeypox infections? 2) Do these risk factors vary across different populations?

Materials and methods

Search strategies

To comprehensively evaluate the scientific evidence related to the risk assessment of human monkeypox infections,

an integrated literature search strategy was developed in strict adherence to the Preferred Reporting Items for Systematic Reviews and Meta-Analyses (PRISMA) guidelines on databases, including PubMed, Scopus, Web of Science, Embase, and The Cochrane Library, covering records from the inception of each database to February 19, 2024. The search strategy was formulated using controlled vocabulary (MeSH terms) and free-text terms. For PubMed, the search strategy was as follows: (#1) (((((Monkeypox[MeSH Terms]) OR (Mpox[MeSH Terms])) OR (Orthopoxvirus infections[MeSH Terms])) OR (Monkeypox virus[MeSH Terms])) OR (Human Monkeypox[MeSH Terms])); (#2) (((Human Infection) OR (Human Illness)) OR (Infectious Disease)) OR (Infection); (#3) ((((Risk Factors[MeSH Terms]) OR (Epidemiology[MeSH Terms])) OR (Disease Surveillance[MeSH Terms])) OR (Public Health[MeSH Terms])) OR (Epidemiological Studies[MeSH Terms]); (#4) (((Risk Assessment) OR (Risk Evaluation)) OR (Risk Analysis)); (#5) (((#1) AND (#2)) AND (#3)) AND (#4). The detailed search strategy is shown in Supplementary Table 1. Logical operators and Boolean connectors were used for other databases, ensuring consistent search terms tailored to their respective syntaxes. Corresponding Chinese search terms were used for Chinese-language databases.

To ensure a comprehensive search, the reference lists of relevant studies and review articles were manually screened to identify additional eligible literature that may have been missed during the electronic database search. Grey literature was excluded to ensure methodological rigor. To handle duplicates, we employed systematic deduplication using bibliographic management software, followed by manual verification to identify studies recorded in multiple databases.

Literature inclusion criteria

Studies were included if they met the following criteria: 1) Original research on the risk assessment of human monkeypox infections, including but not limited to epidemiological studies, case-control studies, cohort studies, randomized controlled trials (RCTs), and observational studies; 2) Research providing quantitative data on risk factors, epidemiological characteristics, clinical manifestations, or treatment outcomes of monkeypox infections; 3) Peer-reviewed and published articles; 4) Studies published in English or Chinese to ensure comprehensive coverage of relevant research; 5) Studies with clear research design and methodology, including explicit research objectives, well-defined sample selection criteria, and robust data collection and analysis methods.

Literature exclusion criteria

Studies were excluded based on the following criteria: 1) Articles not subjected to peer review, including preprints, conference abstracts, expert opinions, and review articles; 2) Research not directly relevant to the study objectives, such as studies focused solely on the basic science of MPXV, animal models or non-human infection cases; 3) Studies with incomplete data or unclear findings; 4) For duplicate studies identified across multiple databases, only 1 version of the most complete study was retained.

Literature screening and data extraction

During the initial phase of literature screening, 2 researchers independently reviewed the titles and abstracts of the retrieved publications. Studies unrelated to the research topic were excluded based on the above inclusion and exclusion criteria. For publications that passed this preliminary screening, a full-text review was conducted to evaluate whether each study met the final inclusion criteria for analysis.

In the data extraction phase, 2 researchers independently extracted relevant information from each study using a standardized template comprising details such as the authors, publication year, study design, participant characteristics, and other essential data. Any disagreements during the data extraction process were resolved through open discussion or consultation with a 3rd researcher to ensure accuracy and consistency.

Quality and bias risk assessment of included literature

We evaluated the quality and risk of bias for the included studies using the Newcastle–Ottawa scale (NOS), a tool commonly used for observational studies. For cross-sectional studies, the assessment included checking how well the sample represented the population, whether the sample size was justified, how non-respondents were addressed and how exposure was measured. The comparability of studies was based on adjustments for important factors like age, sex and socioeconomic status. The outcome section focused on how the results were assessed and whether the statistical tests used were appropriate.

For case-control studies, the assessment looked at how cases and controls were defined and selected, whether they were comparable, and how exposure was measured. It also checked if the same method was used to measure exposure for both cases and controls and if non-responses were correctly handled.

Each study was given a score from 0 to 9. Scores of 6–9 indicated high quality, 4–5 meant moderate quality and 3 or less denoted low quality. Two reviewers carried out the assessments independently, and any disagreements were resolved by discussion or with help from a 3rd reviewer. This process ensured a consistent and fair evaluation.

Statistical analyses

A comprehensive meta-analysis was conducted to quantify the primary outcomes and effect sizes related

to monkeypox infection risk assessment. Data analysis was performed using the R v. 4.3.1 (R Foundation for Statistical Computing, Vienna, Austria). Combined odds ratios (ORs) and 95% confidence intervals (95% CIs) were calculated to estimate the pooled effect sizes. Heterogeneity among studies was evaluated using the I^2 statistic, where an I^2 value greater than 50% indicated substantial heterogeneity. A random-effects model was specified for all analyses, as it was anticipated that the studies would exhibit considerable variability in terms of participants, interventions, study designs, and outcome measures, which, in turn, suggests that the true effect size might differ across studies. Funnel plots and Egger's regression tests were employed to assess potential publication bias. Statistical significance was determined at $p < 0.05$ for all analyses.

Results

Search results

The initial database search identified 1,844 articles. After removing duplicates (n = 267), 1,577 records were screened based on their titles and abstracts. Of these, 1,334 articles were excluded as they were unrelated to the research objectives. Subsequently, 237 articles with accessible full texts were subjected to a thorough review in line with the inclusion and exclusion criteria. At this stage, 190 articles were excluded due to the absence of key data or because the data could not be extracted. Additionally, 36 studies involving animal experiments and 2 studies of poor quality were excluded. Ultimately, 9 studies met the inclusion criteria[4,8,9,11–16] and were included in the meta-analysis (Fig. 1).

Basic characteristics and quality assessment of literature

Most of the included studies were cross-sectional in design, while 1 was classified as a case-control study. Their sample sizes varied significantly, ranging from 72 to 8,088 participants. The median age of participants across the studies was 18 to 45 years, with the majority being male. The quality assessment of the included literature yielded scores ranging from 6 to 8, reflecting a moderate-to-high overall quality, and confirming that the studies met the quality standards required for inclusion in this analysis.

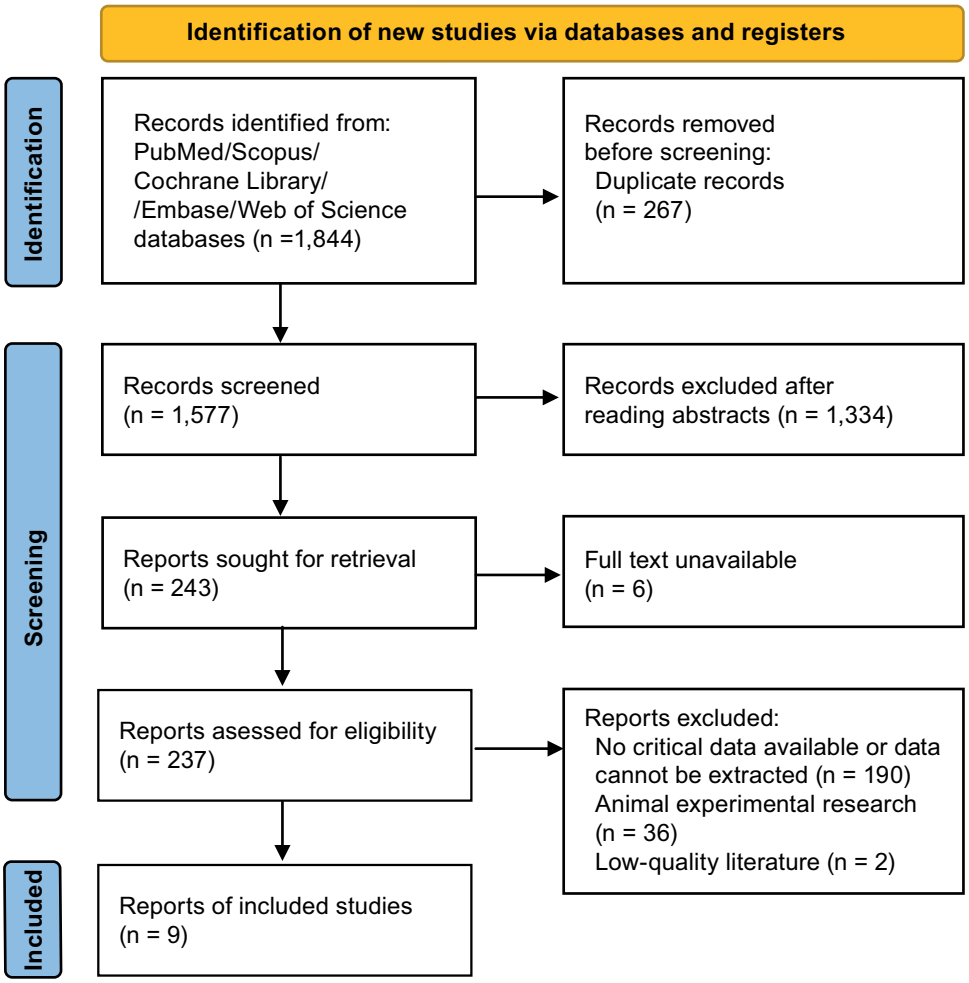

Fig. 1. Flowchart of the literature screening process, showing the number of studies identified, excluded and included

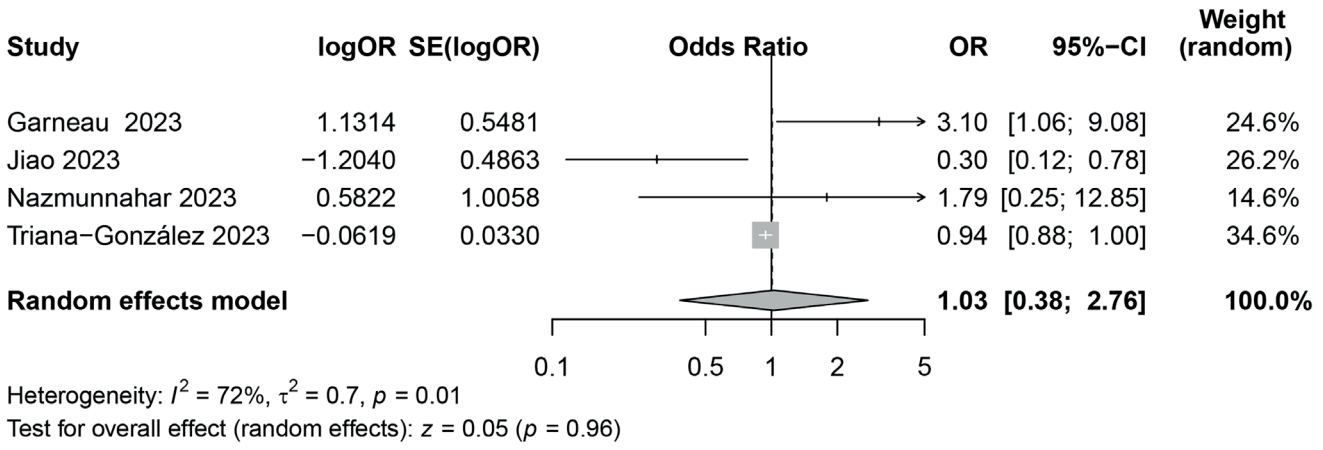

Fig. 2. Meta-analysis of the association between age and monkeypox risk. Pooled odds ratio (OR) and 95% confidence interval (95% CI) were calculated. The size of the boxes represents the study weight, and the diamond indicates the overall effect size

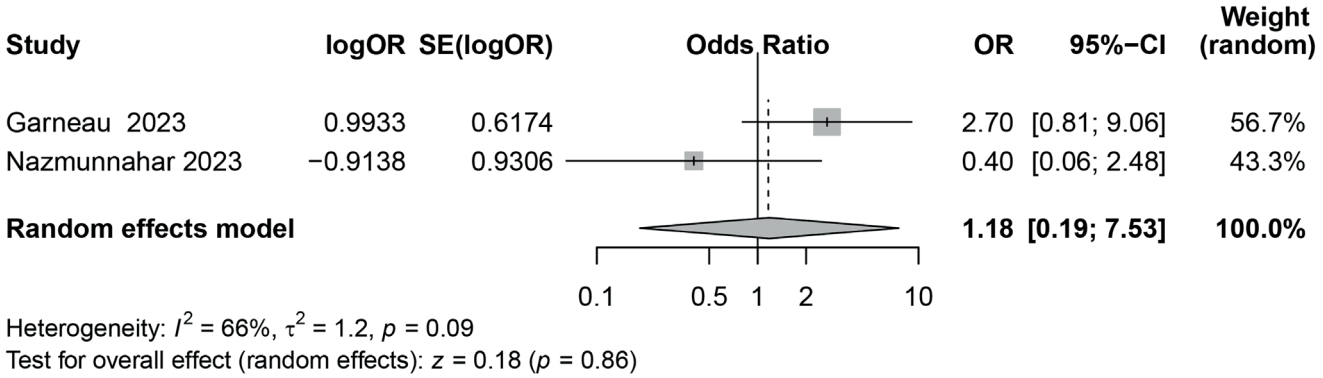

Fig. 3. Meta-analysis of the impact of body mass index (BMI) >30 kg/m^2 on monkeypox risk. Pooled odds ratio (OR) and 95% confidence interval (95% CI) were calculated

Meta-analysis results

Age

This section examines whether demographic factors, such as age, contribute significantly to the risk of monkeypox infection. To assess the impact of age as a predictive factor for the risk of monkeypox infections, this meta-analysis included 4 studies covering various regions, populations and research designs. The analysis revealed high statistical heterogeneity (I^2 = 72%, p = 0.01), which may indicate significant differences among the studies in terms of methodology, population characteristics, geographical locations, and age group categorization. The combined data showed that the overall effect size for age (OR = 1.03, 95% CI: 0.38–2.76, p = 0.96) did not demonstrate statistical significance (Fig. 2). The high heterogeneity observed across the included studies (I^2 = 72%) suggests substantial variability in study design, population characteristics and age group categorizations.

Body mass index >30 kg/m^2

This meta-analysis synthesized the results of 2 studies to explore the potential impact of body mass index (BMI) >30 kg/m^2 on the risk of monkeypox infections. The studies showed significant heterogeneity in the included literature (I^2 = 66%, p = 0.09). The overall effect size (OR = 1.18, 95% CI: 0.19–7.53, p = 0.86) suggested that BMI > 30 kg/m^2 did not constitute a significant risk factor for monkeypox infections (Fig. 3). The analysis revealed substantial heterogeneity (I^2 = 66%), potentially reflecting differences in sample sizes and study populations.

Economic status

Economic status was assessed to determine whether lower income levels increase susceptibility to monkeypox. Results from 2 studies were synthesized when the meta-analysis was adopted to assess the potential impact of economic status on monkeypox infection risk. The heterogeneity test indicated the significant heterogeneity between the included studies (I^2 = 84%, p = 0.01). The combined overall effect size (OR = 0.33, 95% CI: 0.01–9.36, p = 0.52) revealed that compared to higher economic status, lower economic status did not significantly increase the risk of monkeypox infections (Fig. 4). The high heterogeneity observed (I^2 = 84%) underscores the variability in how economic status was defined and measured across studies.

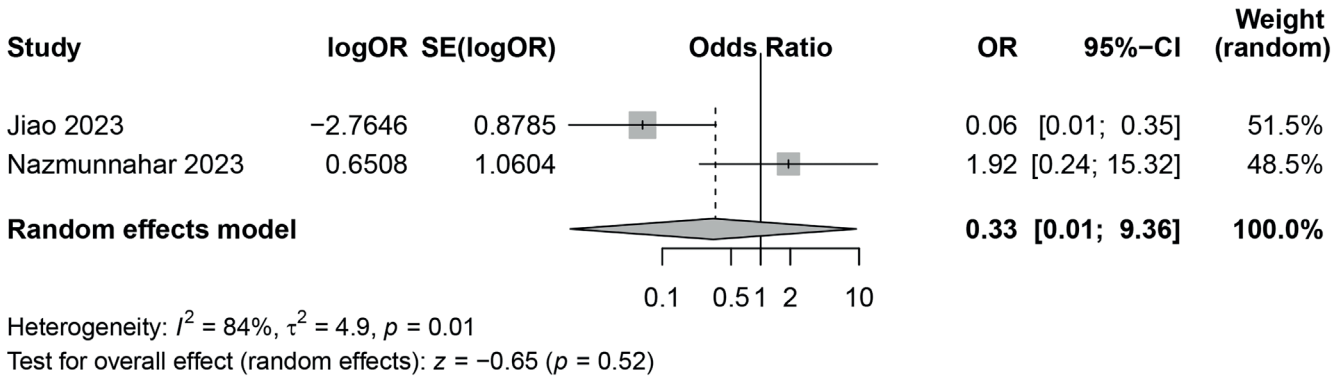

Fig. 4. Meta-analysis of the association between lower economic status and monkeypox risk. Pooled odds ratio (OR) and 95% confidence interval (95% CI) were calculated

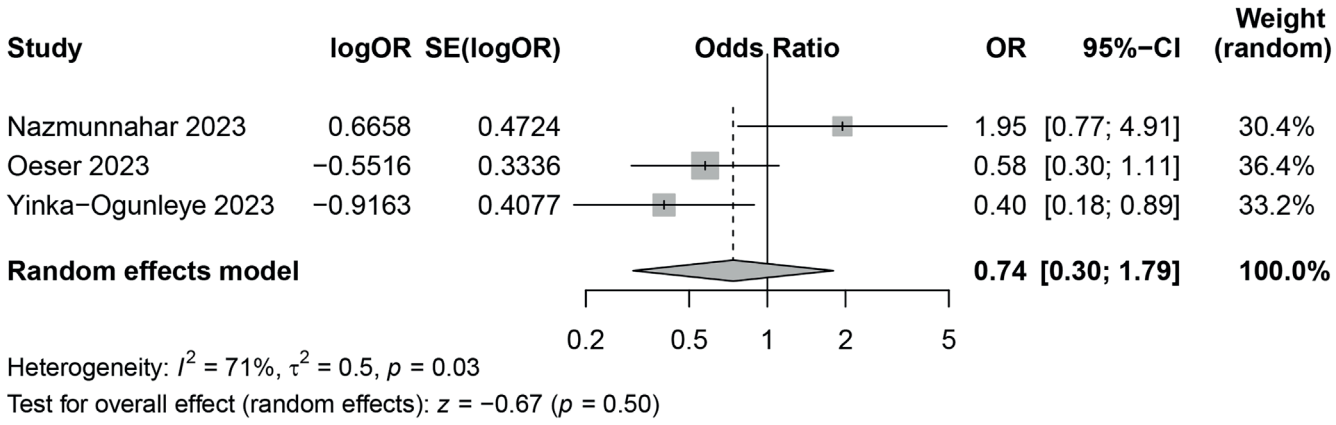

Fig. 5. Meta-analysis of the role of education level in monkeypox risk. Pooled odds ratio (OR) and 95% confidence interval (95% CI) were calculated

Education level

This meta-analysis combined the results of 3 studies to explore the potential impact of education level on the risk of monkeypox infections. The heterogeneity test revealed significant differences among the included studies (I^2 = 71%, p = 0.03). The combined overall effect size (OR = 0.74, 95% CI: 0.30–1.79, p = 0.50) revealed that the education level did not constitute a significant risk factor for monkeypox infections (Fig. 5). Although education level was analyzed to evaluate its role in monkeypox risk, the significant heterogeneity (I^2 = 71%) may arise from variations in educational systems and participant awareness in different regions.

Men who have sex with men

This meta-analysis synthesized the results of 4 studies to explore the potential impact of MSM on the risk of monkeypox infections. The heterogeneity test revealed significant heterogeneity among the included studies (I^2 = 88%, p < 0.01). The combined overall effect size (OR = 1.22, 95% CI: 0.84–1.75, p = 0.29) indicated that the MSM did not significantly increase the risk of monkeypox infections (Fig. 6), likely due to differences in clinical presentations, symptom recognition and healthcare access within this population.

Human immunodeficiency virus infections

The association between HIV infection and monkeypox risk was explored. This meta-analysis synthesized the results of 7 studies to explore the potential impact of HIV infections on the risk of monkeypox infections. The heterogeneity test indicated the high heterogeneity among the included studies (I^2 = 93%, p < 0.01). The combined overall effect size (OR = 2.21, 95% CI: 1.13–4.34, p = 0.02) demonstrated that HIV infections significantly increased the risk of monkeypox infections (Fig. 7). Despite high heterogeneity (I^2 = 93%), the findings consistently demonstrate a significant increase in risk, highlighting the impact of immune suppression.

Other concurrent sexually transmitted infections

This meta-analysis combined the results of 4 studies to discuss the potential impact of other concurrent STIs on the risk of monkeypox infections. The heterogeneity test revealed relatively low heterogeneity among the included studies (I^2 = 32%, p = 0.22). The combined overall effect size (OR = 1.84, 95% CI: 1.46–2.33, p < 0.01) indicated that other concurrent STIs significantly raised the risk of monkeypox infections (Fig. 8). The influence of concurrent STIs on monkeypox risk, with the relatively low heterogeneity (I^2 = 32%), suggests that damaged mucosal barriers may facilitate viral transmission.

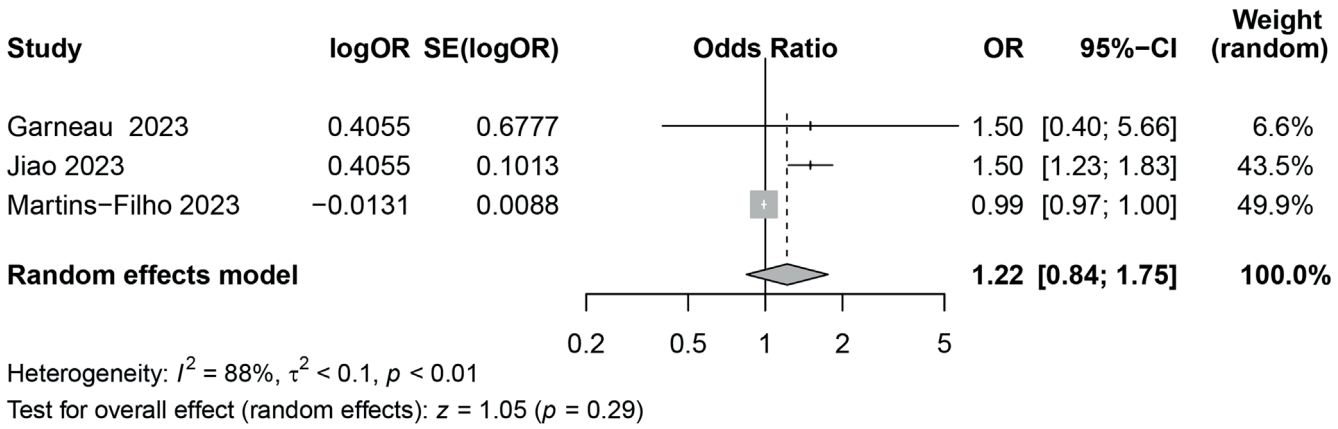

Fig. 6. Meta-analysis of the association between men who have sex with men (MSM) status and monkeypox risk. Pooled odds ratio (OR) and 95% confidence interval (95% CI) were calculated

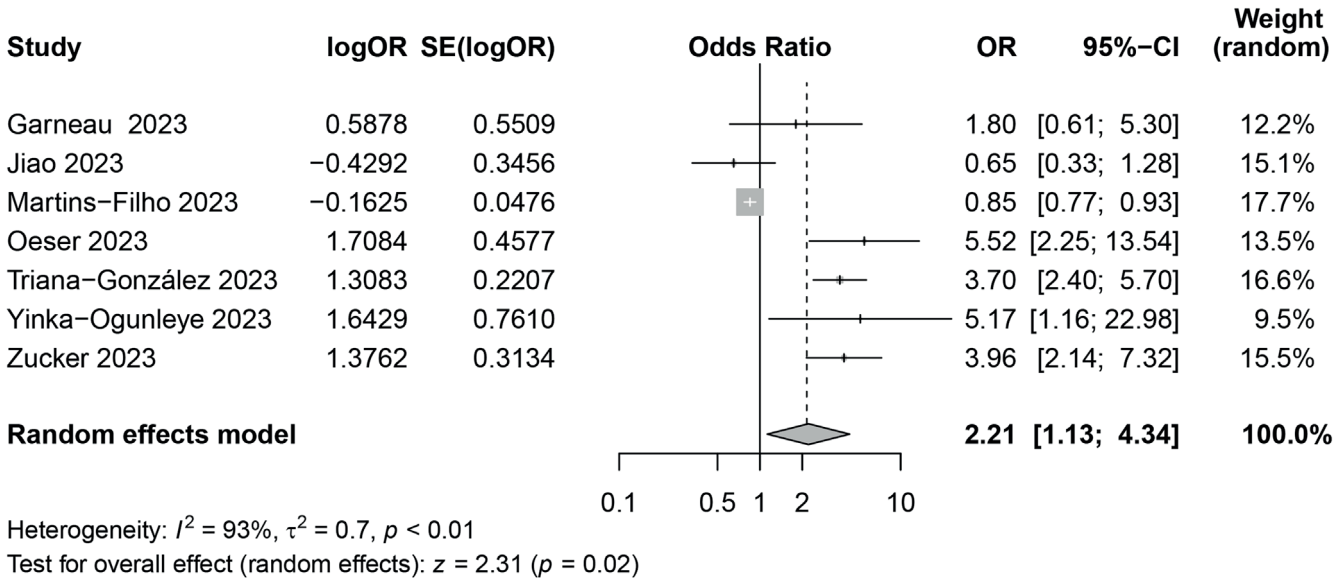

Fig. 7. Meta-analysis of the association between human immunodeficiency virus (HIV) infection and monkeypox risk. Pooled odds ratio (OR) and 95% confidence interval (95% CI) were calculated

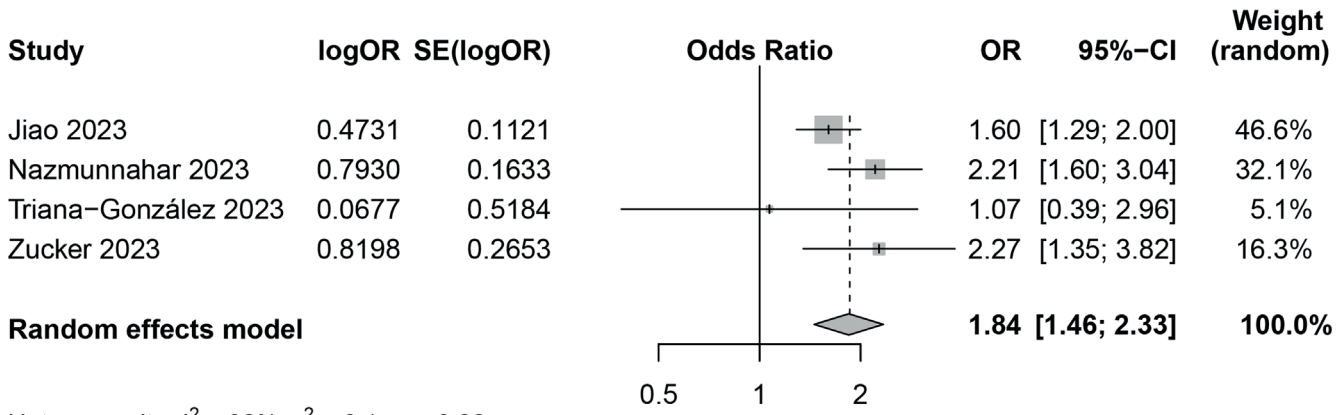

Fig. 8. Meta-analysis of the association between concurrent sexually transmitted infections (STIs) and monkeypox risk. Pooled odds ratio (OR) and 95% confidence interval (95% CI) were calculated

Publication bias

A funnel plot was constructed to assess potential publication bias. The analysis revealed some studies lying outside the funnel, with noticeable asymmetry (Supplementary Fig. 1). To further evaluate publication bias quantitatively, Egger's test was applied. This regression-based method examined the relationship between effect size estimates and their standard errors (SEs). The results indicated minimal publication bias among the included studies.

Sensitivity analysis

Sensitivity analysis was performed to evaluate the robustness of the results. By sequentially excluding each study and reassessing the individual contributions, minimal changes were observed in the combined effect size and its CI, demonstrating consistent findings (Supplementary Fig. 2,3). These results suggest that the study findings are robust and reliable.

Discussion

This study provides a comprehensive and robust risk assessment of human monkeypox infections, distinguishing itself from previous research by integrating diverse datasets in a meta-analysis. Unlike earlier studies, which primarily focused on descriptive epidemiology or isolated populations, this work consolidates findings across multiple regions and populations, providing a global perspective on risk factors. Additionally, the analysis incorporated stringent quality assessments and addressed heterogeneity through advanced statistical modeling. Importantly, the findings challenge previous assumptions about the influence of socioeconomic and demographic factors, while reinforcing the roles of HIV infection and concurrent STIs as significant risk factors. For instance, the data revealed that age, BMI > 30 kg/m^2, lower economic status, education level, and MSM status did not significantly increase the risk of monkeypox infections. However, HIV infections and the presence of other STIs were significantly associated with an elevated risk of monkeypox infections. Overall, this study refines the understanding of monkeypox transmission dynamics and provides important insight into informing targeted public health strategies.

The risk assessment for human monkeypox infections is a complex issue influenced by various demographic and behavioral factors. Garneau et al.[8] reported that age >40 years was not a risk factor for hospitalization in patients with monkeypox infections. Similarly, Jiao et al.[11] conducted a large cross-sectional survey among young MSM in China and found no significant relationship between age and the perception of monkeypox infection risk. In contrast, another study demonstrated a significant association between perceived monkeypox infection risk and sociodemographic attributes, with younger age groups more likely to perceive moderate-to-high risk.[13] This was attributed to their greater engagement with internet-based communication and increased health awareness in the digital era. Consequently, the age range of 18–35 years may not constitute a risk factor for monkeypox infections,[17,18] which aligns with the findings of our study, where age ranging from 18 to 45 years was not identified as significant risk factor for human monkeypox infections.

Some research suggests that BMI is a key factor in assessing the risk of viral infections, as obesity is linked to increased severity of infectious diseases.[19] However, in this study, a BMI > 30 kg/m^2 was not a significant risk factor for monkeypox infections. This may be attributed to the inclusion of individuals with only mild obesity, which may not be sufficient to significantly increase susceptibility to infection. Additionally, Cénat et al.[20] indicated that low-income populations face higher risks of viral infections due to limited access to healthcare services, overcrowded living conditions and poor nutrition. Similarly, individuals with lower education levels may have reduced awareness of preventive measures or engage in behaviors that increase viral exposure.[21,22] While economic status and education level are important determinants of viral infections, the findings of this study revealed that neither factor significantly influenced the risk of monkeypox infections, and we hypothesized that this could be attributed to enhanced efforts in promoting awareness of human monkeypox prevention and other viral infections.

Data from the WHO showed that as of May 9, 2023, the monkeypox outbreak had spread to 111 countries or regions, with 87,314 cases reported globally. A distinctive feature of this outbreak was that most infections occurred in the MSM group. In contrast, the risk of monkeypox infections among the general population remains relatively low, suggesting MSM could represent a potential risk group.[23] However, our meta-analysis findings indicated that MSM status was not a significant risk factor for monkeypox infections. This discrepancy may arise from the variability in the clinical presentation of monkeypox among confirmed MSM cases. Many cases exhibit atypical symptoms, with genital and perianal rashes often appearing as the first symptom, or even progressing to empyesis before systemic symptoms develop. These atypical presentations could lead to misdiagnoses within the MSM group, ultimately contributing to an insignificant risk assessment in this population.[24]

In the risk assessment of human monkeypox infections, HIV infections emerge as significant contributory factors. During the 2022 monkeypox outbreak, approx. 95% of global cases occurred among MSM, with 40% of these cases involving individuals with HIV infections. Surveys have revealed that HIV-positive MSM, primarily aged 18–40 years, are often sexually active, with some reporting more than 3 partners for oral or anal sex and engaging in group or heterosexual sexual activities. While it remains unconfirmed whether monkeypox is transmitted sexually, the detection of the virus in the semen of male patients suggests

the potential for sexual transmission.[25,26] Individuals with lower $CD4^+$ T-cell counts and uncontrolled HIV viral loads exhibit more severe symptoms of monkeypox. In the USA, although HIV-positive individuals account for only 38% of monkeypox cases, they represent up to 94% of monkeypox-related deaths. These observations strongly support the notion that HIV infection is a significant risk factor for human monkeypox infections.[27] In this study, HIV infection was found to significantly increase the risk of monkeypox infection, consistent with findings from previous research. This increased risk can be attributed to 2 primary factors: the more pronounced clinical presentation of monkeypox in individuals with HIV and the immunosuppression associated with HIV infection, which reduces immune defense and increases susceptibility to monkeypox.[28,29]

The presence of concurrent STIs further exacerbates the risk of human monkeypox transmission. Studies have demonstrated that monkeypox can occur in individuals with as little as 1 sexual encounter or those who are sexually active, with the risk amplified among MSM. Additionally, 41% of monkeypox patients reported a recent history of other STIs, such as chlamydia, gonorrhea or syphilis. These findings underscore the necessity of screening individuals diagnosed with monkeypox for HIV and other STIs.[24,30] The results of this study confirmed that concurrent STIs significantly increased the risk of monkeypox infection. This is likely because STIs can damage the skin barrier or mucosal surfaces, facilitating viral entry and spread. Based on these findings, prevention and control measures for human monkeypox should emphasize reducing high-risk behaviors, such as having multiple sexual partners among MSM, and actively screening for HIV and other STIs.

Lastly, vaccination is key to preventing monkeypox, especially in vulnerable groups such as MSM. However, the limited global supply of vaccines shows the need for other preventive measures alongside treatment strategies. Vaccines like the MVA can lower the risk of infection, but they are often unavailable in regions with new outbreaks. Early and regular screening for monkeypox, combined with proper management of HIV, is essential to reduce severe cases. Public health efforts should include educational campaigns to help MSM and the general public understand monkeypox symptoms and how it spreads. Vaccination programs should focus on high-risk groups, including MSM and people with HIV, while addressing vaccine shortages through better planning and international cooperation. Increasing access to antiviral treatments and setting up systems to track outbreaks would also help control the spread of monkeypox.

Limitations

However, this study has some limitations. The included studies primarily focused on specific regions and populations, such as MSM groups in developed countries, limiting the generalizability of our findings to other regions or demographic groups. Regional differences in healthcare systems and cultural factors may influence monkeypox transmission and risk factors. Additionally, small sample sizes in some studies, particularly for BMI, socioeconomic status and education level, reduced statistical power and may have contributed to nonsignificant results. Variability in study quality, as assessed with the NOS, and significant heterogeneity observed in certain analyses highlight the need for larger, high-quality studies involving diverse populations to validate these findings.

Conclusions

This study demonstrated that age, BMI > 30 kg/m^2, lower economic status, education level, and MSM status were not significant risk factors for human monkeypox infection, whereas HIV infection and concurrent STIs were identified as significant risk factors. Therefore, prevention and control measures for human monkeypox should focus on advocating reduced high-risk behaviors, such as limiting multiple sexual partners within the MSM population, and actively screening for HIV and other STIs. These findings provide valuable insights for implementing targeted and effective interventions to prevent and manage monkeypox infections.

Future research should focus on larger multicenter studies to validate these findings across diverse populations and geographic regions. Longitudinal studies are also needed to explore the long-term relationships between HIV, other STIs and monkeypox, particularly in immunocompromised populations. Additionally, efforts to standardize study designs and data collection methods would help reduce heterogeneity and improve comparability across studies. Taken together, the findings from this study could serve as a valuable reference to improve prevention and treatment strategies for human monkeypox infections.

Supplementary data

The supplementary materials are available at https://doi.org/10.5281/zenodo.15188222. The package includes the following files:

Supplementary Table 1. Search strategy.

Supplementary Fig. 1. Funnel plots for assessing publication bias. A. Age; B. BMI; C. Economic status; D. Education level; E. MSM status; F. HIV infection; G. Concurrent STIs.

Supplementary Fig. 2. Sensitivity analysis. A. Age; B. BMI; C. Economic status; D. Education level.

Supplementary Fig. 3. Sensitivity analysis. A. MSM status; B. HIV infection; C. STIs.

Consent for publication

Not applicable.

Use of AI and AI-assisted technologies

Not applicable.

ORCID iDs

Yue Wang https://orcid.org/0000-0001-8293-5915
Jianlei Wang https://orcid.org/0009-0009-3621-4119

References

1. Bunge EM, Hoet B, Chen L, et al. The changing epidemiology of human monkeypox: A potential threat? A systematic review. *PLoS Negl Trop Dis*. 2022;16(2):e0010141. doi:10.1371/journal.pntd.0010141
2. Gessain A, Nakoune E, Yazdanpanah Y. Monkeypox. *N Engl J Med*. 2022;387(19):1783–1793. doi:10.1056/NEJMra2208860
3. Harris E. What to know about monkeypox. *JAMA*. 2022;327(23):2278. doi:10.1001/jama.2022.9499
4. Zheng M, Qin C, Qian X, et al. Knowledge and vaccination acceptance toward the human monkeypox among men who have sex with men in China. *Front Public Health*. 2022;10:997637. doi:10.3389/fpubh.2022.997637
5. Kameli N, Algaissi A, Taha MME, et al. Monkeypox global research: A comprehensive analysis from emergence to present (1961–2023) for innovative prevention and control approaches. *J Infect Public Health*. 2025;18(1):102593. doi:10.1016/j.jiph.2024.102593
6. Thornhill JP, Barkati S, Walmsley S, et al. Monkeypox virus infection in humans across 16 countries: April–June 2022. *N Engl J Med*. 2022;387(8):679–691. doi:10.1056/NEJMoa2207323
7. Puy L, Parry-Jones AR, Sandset EC, Dowlatshahi D, Ziai W, Cordonnier C. Intracerebral haemorrhage. *Nat Rev Dis Primers*. 2023;9(1):14. doi:10.1038/s41572-023-00424-7
8. Garneau WM, Jones JL, Dashler GM, et al. Risk factors for hospitalization and effect of immunosuppression on clinical outcomes among an urban cohort of patients with Mpox. *Open Forum Infect Dis*. 2023;10(12):ofad533. doi:10.1093/ofid/ofad533
9. Zucker R, Lavie G, Wolff-Sagy Y, et al. Risk assessment of human mpox infections: Retrospective cohort study. *Clin Microbiol Infect*. 2023;29(8):1070–1074. doi:10.1016/j.cmi.2023.04.022
10. Poland GA, Kennedy RB, Tosh PK. Prevention of monkeypox with vaccines: A rapid review. *Lancet Infect Dis*. 2022;22(12):e349–e358. doi:10.1016/S1473-3099(22)00574-6
11. Jiao K, Xu Y, Huang S, et al. Mpox risk perception and associated factors among Chinese young men who have sex with men: Results from a large cross-sectional survey. *J Med Virol*. 2023;95(8):e29057. doi:10.1002/jmv.29057
12. Martins-Filho PR, Tanajura DM, Vecina-Neto G. Multi-country monkeypox outbreak: A quantitative evidence synthesis on clinical characteristics, potential transmission routes, and risk factors. *Eur J Intern Med*. 2023;107:102–104. doi:10.1016/j.ejim.2022.09.013
13. Nazmunnahar, Haque MdA, Ahamed B, Tanbir Md, Suhee FI, Islam MdR. Assessment of risk perception and subjective norms related to Mpox (monkeypox) among adult males in Bangladesh: A cross-sectional study. *Health Sci Rep*. 2023;6(6):e1352. doi:10.1002/hsr2.1352
14. Oeser P, Napierala H, Schuster A, Herrmann WJ. Risk factors for monkeypox infection: A cross-sectional study. *Dtsch Arztebl Int*. 2023;120(5):65–66. doi:10.3238/arztebl.m2022.0365
15. Triana-González S, Román-López C, Mauss S, et al. Risk factors for mortality and clinical presentation of monkeypox. *AIDS*. 2023;37(13):1979–1985. doi:10.1097/QAD.0000000000003623
16. Yinka-Ogunleye A, Dalhat M, Akinpelu A, et al. Mpox (monkeypox) risk and mortality associated with HIV infection: A national case–control study in Nigeria. *BMJ Glob Health*. 2023;8(11):e013126. doi:10.1136/bmjgh-2023-013126
17. Hisham R, Ng CJ, Liew SM, Hamzah N, Ho GJ. Why is there variation in the practice of evidence-based medicine in primary care? A qualitative study. *BMJ Open*. 2016;6(3):e010565. doi:10.1136/bmjopen-2015-010565
18. Diviani N, Camerini AL, Reinholz D, Galfetti A, Schulz PJ. Health literacy, health empowerment and health information search in the field of MMR vaccination: A cross-sectional study protocol. *BMJ Open*. 2012;2(6):e002162. doi:10.1136/bmjopen-2012-002162
19. Zhou Y, Chi J, Lv W, Wang Y. Obesity and diabetes as high-risk factors for severe coronavirus disease 2019 (Covid-19). *Diabetes Metab Res Rev*. 2021;37(2):e3377. doi:10.1002/dmrr.3377
20. Cénat JM, Broussard C, Darius WP, et al. Social mobilization, education, and prevention of the Ebola virus disease: A scoping review. *Prev Med*. 2023;166:107328. doi:10.1016/j.ypmed.2022.107328
21. Visser ME, Durao S, Sinclair D, Irlam JH, Siegfried N. Micronutrient supplementation in adults with HIV infection. *Cochrane Database Syst Rev*. 2017;2017(5):CD003650. doi:10.1002/14651858.CD003650.pub4
22. Tiyou A, Belachew T, Alemseged F, Biadgilign S. Food insecurity and associated factors among HIV-infected individuals receiving highly active antiretroviral therapy in Jimma zone (southwest Ethiopia). *Nutr J*. 2012;11(1):51. doi:10.1186/1475-2891-11-51
23. Feng Y, Zhang Y, Liu S, et al. Unexpectedly higher levels of anti-orthopoxvirus neutralizing antibodies are observed among gay men than general adult population. *BMC Med*. 2023;21(1):183. doi:10.1186/s12916-023-02872-0
24. Liu X, Zhu Z, He Y, et al. Monkeypox claims new victims: The outbreak in men who have sex with men. *Infect Dis Poverty*. 2022;11(1):84. doi:10.1186/s40249-022-01007-6
25. Lapa D, Carletti F, Mazzotta V, et al. Monkeypox virus isolation from a semen sample collected in the early phase of infection in a patient with prolonged seminal viral shedding. *Lancet Infect Dis*. 2022;22(9):1267–1269. doi:10.1016/S1473-3099(22)00513-8
26. Edman-Wallér J, Jonsson O, Backlund G, Muradrasoli S, Sondén K. Results of PCR analysis of Mpox clinical samples, Sweden, 2022. *Emerg Infect Dis*. 2023;29(6):1220–1222. doi:10.3201/eid2906.230253
27. Aldred B, Scott JY, Aldredge A, et al. Associations between HIV and severe Mpox in an Atlanta cohort. *J Infect Dis*. 2024;229(Suppl 2):S234–S242. doi:10.1093/infdis/jiad505
28. Angelo KM, Smith T, Camprubí-Ferrer D, et al. Epidemiological and clinical characteristics of patients with monkeypox in the GeoSentinel Network: A cross-sectional study. *Lancet Infect Dis*. 2023;23(2):196–206. doi:10.1016/S1473-3099(22)00651-X
29. Laurenson-Schafer H, Sklenovská N, Hoxha A, et al. Description of the first global outbreak of mpox: An analysis of global surveillance data. *Lancet Glob Health*. 2023;11(7):e1012–e1023. doi:10.1016/S2214-109X(23)00198-5
30. Nolasco S, Vitale F, Geremia A, et al. First case of monkeypox virus, SARS-CoV-2 and HIV co-infection. *J Infect*. 2023;86(1):e21–e23. doi:10.1016/j.jinf.2022.08.014

Noninvasive ventilation for COPD management: A systematic review & meta-analysis

Jinyu Yang[1,A], Lin Chen[1,B], Lihong Zhao[1,C], Chengyi Liu[1,C], Xiujuan Gu[1,B], Wanjun Qi[2,E,F], Lei Wang[2,D]

[1] Department of Respiratory and Critical Care Medicine, The Third Hospital of Mianyang (Sichuan Mental Health Center), China
[2] Department of Nursing, The Third Hospital of Mianyang (Sichuan Mental Health Center), China

A – research concept and design; B – collection and/or assembly of data; C – data analysis and interpretation;
D – writing the article; E – critical revision of the article; F – final approval of the article

Advances in Clinical and Experimental Medicine, ISSN 1899–5276 (print), ISSN 2451–2680 (online) *Adv Clin Exp Med*. 2026;35(1):27–43

Address for correspondence
Lei Wang
E-mail: wl13778102345@outlook.com

Funding sources
This study was supported by the Research Project Subsidy of the Mianyang Health Commission, 2022 (grant No. 202209).

Conflict of interest
None declared

Received on December 14, 2024
Reviewed on March 11, 2025
Accepted on March 26, 2025

Published online on January 5, 2026

Abstract

Background. Noninvasive ventilation (NIV) is an important treatment modality in the management of chronic obstructive pulmonary disease (COPD) by reducing respiratory distress, improving gas exchange and reducing exacerbations without the need for intubation and invasive airways.

Objectives. To synthesize data from randomized controlled trials (RCTs) and perform a meta-analysis to understand the beneficial effects of NIV across different COPD stages.

Materials and methods. A systematic literature review was performed using MEDLINE (PubMed) and Cochrane Register of Controlled Trials (CENTRAL) al databases for RCTs that involved the administration of NIV vs usual treatment (oxygen supplementation, pharmacological agents, nasal cannulation) in patients with stable COPD, acute exacerbations of COPD (AECOPD), and post-exacerbation COPD (PECOPD). Mortality, exacerbation and intubation rates, and arterial blood gases ($PaCO_2$ and PaO_2 levels) were assessed in both groups. RevMan software was used to assess the risk of bias and calculate the pooled odds ratio (OR), mean differences (MDs) and subgroup analyses with a random-effects model.

Results. A total of 51 RCTs were included in the meta-analysis with information from 3,775 patients. Meta-analysis of the data showed that there was a significant decrease in mortality outcomes ($p < 0.001$), intubation frequency ($p < 0.001$) and $PaCO_2$ levels ($p < 0.001$) but no significant improvement in exacerbation frequency ($p = 0.12$) and PaO_2 levels ($p = 0.69$). Subgroup analyses demonstrated no significant difference between COPD stage on mortality outcomes ($p = 0.32$), $PaCO_2$ level ($p = 0.12$) and PaO_2 level ($p = 0.64$). There was a significant decrease in intubation rate in AECOPD patients receiving NIV and a statistically nonsignificant difference in exacerbation frequency in stable COPD patients using NIV.

Conclusions. The findings of this meta-analysis indicate a substantial overall enhancement in the frequency of exacerbations and intubations, mortality outcomes, and arterial gas levels among patients in various stages of COPD. Consequently, it is imperative to identify patients with COPD that are most likely to benefit from the use of NIV.

Key words: chronic obstructive pulmonary disease, exacerbation, noninvasive ventilation, arterial blood gases, BiPAP

Cite as
Yang J, Chen L, Zhao L, et al. Noninvasive ventilation for COPD management: A systematic review and meta-analysis. *Adv Clin Exp Med*. 2026;35(1):27–43. doi:10.17219/acem/203397

DOI
10.17219/acem/203397

Highlights

- Noninvasive ventilation (NIV) in chronic obstructive pulmonary disease (COPD) alleviates dyspnea, optimizes arterial blood gases, and cuts exacerbation rates without requiring intubation.
- Acute-exacerbation benefits of NIV include reduced mortality, fewer complications and shorter hospital stays – while benefits in stable COPD (no flare-ups in 4 weeks) show mixed evidence.
- Pooled randomized controlled trial (RCT) meta-analysis across COPD stages rigorously evaluated NIV's efficacy from mild to severe disease, offering a unified evidence base.
- Meta-analysis outcomes revealed significant improvements in arterial gas exchange, enhanced survival and lower frequencies of exacerbations and intubations among COPD patients.

Introduction

Chronic obstructive pulmonary disease (COPD), encompassing emphysema and chronic bronchitis, is a common, progressive disorder characterized by irreversible airflow limitation resulting from damage to both the airways and the lung parenchyma.[1,2] Globally, COPD remains a leading cause of morbidity and mortality, responsible for an estimated 3.1 million deaths in 2021, with the heaviest burden observed in low- and middle-income countries.[3] Beyond its mortality toll, COPD significantly impairs daily functioning and quality of life, and drives substantial healthcare utilization through recurrent exacerbations that often necessitate hospitalization and intensified pharmacotherapy.[4]

Key risk factors for COPD encompass cigarette smoking; exposure to ambient air pollution; a history of childhood asthma; and α_1-antitrypsin deficiency, a rare genetic disorder.[4] These insults provoke pathological remodeling of the lung parenchyma, including destruction of alveolar walls, that impairs gas exchange, precipitating hypoxemia and hypercapnia, and in severe cases leading to acute hypercapnic respiratory failure (AHRF).[5,6] Resultant hypoxemia and systemic inflammation manifest as respiratory symptoms (dyspnea, fatigue, wheezing, cough, and chest tightness) and drive extrapulmonary complications, notably pulmonary hypertension and right heart failure, as well as adverse effects on endocrine, gastrointestinal, neuromuscular, and musculoskeletal systems.[7,8]

Stable COPD refers to a state where symptoms are manageable and not worsening. Acute exacerbation of COPD (AECOPD) is a sudden worsening of COPD symptoms. Post-exacerbation COPD (PECOPD) describes the recovery phase after an acute exacerbation. The diagnosis of COPD is based on symptom assessment, imaging tests, pulmonary function tests (spirometry), and physical examinations. The Global Initiative for Chronic Obstructive Lung Disease (GOLD) has developed diagnostic criteria, including a post-bronchodilator forced expiratory volume (FEV_1)/forced vital capacity (FVC) ratio <0.7. The GOLD criteria also classify the severity of airflow limitations into various stages and are used with patient-reported outcomes and exacerbation history to guide COPD management decisions.[2] Treatment plans for COPD aim to improve quality of life, alleviate symptoms and prevent disease progression.

Pharmacological management of acute COPD exacerbations typically includes systemic corticosteroids, inhaled short-acting bronchodilators, and antibiotics when there is clinical or microbiological suspicion of bacterial infection.[9,10] Adjunctive ventilatory support, preferentially noninvasive ventilation (NIV) in cases of hypercapnic respiratory failure, can avert the need for invasive mechanical ventilation, which is reserved for NIV failure or contraindications. However, systemic corticosteroids, while accelerating recovery and reducing relapse rates, carry risks of hyperglycemia, fluid retention and steroid-induced myopathy, and repeated high-dose bronchodilator use may precipitate tachycardia, tremor and tolerance. Pulmonary rehabilitation, although pivotal for restoring functional capacity and reducing future exacerbations, often struggles with poor adherence, transport barriers and limited program availability. Invasive mechanical ventilation requires endotracheal intubation or tracheostomy and increases the risk of ventilator-associated pneumonia, barotrauma and prolonged weaning difficulties in COPD patients.

Noninvasive ventilation is an alternative to invasive ventilation techniques in which ventilator support (pressure-supported airflow) is provided through a noninvasive interface such as a nasal, oronasal or full-face mask to ventilator muscles. It is a comfortable alternative to intubation and avoiding immobility, and is used for managing conditions like acute COPD exacerbations and cardiogenic pulmonary edema-related respiratory failure. It reduces complications like ventilator-associated pneumonia and sinusitis by eliminating the need for sedation and endotracheal intubation, thereby minimizing hospital and intensive care unit (ICU) stays. Bi-level positive airway pressure (BiPAP), continuous positive airway pressure (CPAP) and negative pressure ventilation (NPV) are the most common types of NIV. BiPAP delivers 2 pressure levels for improved ventilation and airway stability, while CPAP provides constant pressure, typically used for milder respiratory issues and sleep apnea. The American Thoracic Society and *European Respiratory Journal* guidelines recommend the use

of BiPAP for acute-on-chronic respiratory acidosis secondary to COPD exacerbations. Studies have shown that NIV has reduced mortality outcomes in patients with acute exacerbations and decreased complications and length of hospital stay.[11–13]

Previous meta-analyses have shown mixed results regarding the benefits of NIV in stable COPD patients (generally defined as no exacerbation in last 4 weeks). In general, long-term or domiciliary NIV use resulted in a decrease in mortality and improved quality of life, whereas outcomes such as hospital admissions and gas exchange were variable.[10,14] Effects of NIV in AECOPD patients were associated with lower deaths, intubation rates, and hospital stays in a meta-analysis by Osadnik et al.[9] In a meta-analysis comparing NIV with usual care in PECOPD patients, the exacerbation frequency was decreased when NIV was employed, with no significant differences in mortality rates or arterial gases.[15] Thus, the beneficial effects of NIV in patients in different COPD stages are heterogeneous in terms of outcomes which can limit its applicability.

Objectives

This study aims to systematically synthesize and critically analyze the available literature on NIV across all GOLD stages of COPD, quantifying its effects on mortality, hospital length of stay, exacerbation frequency, arterial blood gas parameters, and health-related quality of life in both acute exacerbations and stable disease, while comparing different NIV modalities, initiation timings and ventilator settings by patient phenotype, and ultimately developing an evidence-based clinical framework to guide optimal NIV selection, timing and management in acute and chronic COPD.

Materials and methods

Study selection or inclusion/exclusion criteria

We included randomized controlled trials (RCTs) that compared any type of NIV device (BiPAP, nocturnal) or administration device (full face, oronasal or nasal mask) with usual therapy such as oxygen supplementation, long-term oxygen therapy (LTOT), pharmacological treatment (antibiotics, bronchodilators, steroids, theophylline, mucolytic agents, etc.), or sham NIV for our analysis. We included adult patients (≥18 years) with various phases of COPD, including stable COPD, PECOPD and AECOPD in our analysis. Patients diagnosed with COPD as per the Global Initiative for Chronic Obstructive Lung Disease (GOLD) system that uses the FEV_1/FVC ratio <0.7 were included. Exclusion criteria included non-randomized studies and prospective and retrospective study designs.

Information sources

We conducted a systematic literature search of MEDLINE (PubMed) and Cochrane Register of Controlled Trials (CENTRAL) in November 2024, encompassing the period of 1990–2024.

Search strategy

We conducted comprehensive searches of PubMed, Embase and the Cochrane Library from inception through May 2025 using both free-text keywords – "non-invasive ventilation," "NIV," "non-invasive positive pressure ventilation," "BiPAP," "VPAP," "chronic obstructive pulmonary disease," "pulmonary disease," and "pulmonary emphysema" – and their corresponding Medical Subject Headings (MeSH) terms. Titles and abstracts of all retrieved records were screened for relevance, and full texts of potentially eligible studies were reviewed in detail. To ensure completeness, we also examined the reference lists of included articles for additional reports (Table 1).

Data extraction process

Data extraction was performed using a standardized, pre-piloted form to capture key study characteristics and outcomes: study identifiers (authors, publication year), design (e.g. randomized trial, cohort study), intervention and comparator details, duration of follow-up, COPD phase (stable vs exacerbation), participant demographics (mean age), exacerbation frequency and severity, and arterial partial pressure of carbon dioxide ($PaCO_2$) levels.

Data items

We analyzed the following outcomes – mortality, exacerbation frequency, endotracheal intubation rates, and arterial blood gas parameters ($PaCO_2$ and PaO_2) – comparing patients receiving NIV with control groups. Article screening and data extraction were performed by a single reviewer using the predefined extraction form to ensure consistency and completeness of the collected data.

Risk of bias assessment

We used the Cochrane Collaboration's risk of bias tool to assess the methodological quality of the included studies.[16] This tool includes the following criteria: randomization, allocation concealment, blinding and completeness of follow-up. The risk of bias for each item was graded as high, low or unclear risk.

Quantitative data synthesis

We performed the meta-analysis and statistical calculations were performed using Review Manager (RevMan, v. 5;

Table 1. Search strategy

Search terms	MeSH terms and keywords
Search term 1 (#1)	("Noninvasive Ventilation"[MeSH Terms] OR "Continuous Positive Airway Pressure"[MeSH Terms] OR ("BiPAP"[All Fields] OR "CPAP"[All Fields] OR ("positive pressure respiration"[MeSH Terms] OR ("positive pressure"[All Fields] AND "respiration"[All Fields]) OR "positive pressure respiration"[All Fields] OR ("positive"[All Fields] AND "pressure"[All Fields] AND "ventilation"[All Fields]) OR "positive pressure ventilation"[All Fields] OR "intermittent positive pressure ventilation"[MeSH Terms] OR ("intermittent"[All Fields] AND "positive pressure"[All Fields] AND "ventilation"[All Fields]) OR "intermittent positive pressure ventilation"[All Fields]) OR ("non-invasive"[All Fields] AND ("positive pressure respiration"[MeSH Terms] OR ("positive pressure"[All Fields] AND "respiration"[All Fields]) OR "positive pressure respiration"[All Fields] OR ("positive"[All Fields] AND "pressure"[All Fields] AND "ventilation"[All Fields]) OR "positive pressure ventilation"[All Fields] OR "intermittent positive pressure ventilation"[MeSH Terms] OR ("intermittent"[All Fields] AND "positive pressure"[All Fields] AND "ventilation"[All Fields]) OR "intermittent positive pressure ventilation"[All Fields])) OR (("noninvasive"[All Fields] OR "noninvasively"[All Fields] OR "noninvasiveness"[All Fields]) AND ("positive pressure respiration"[MeSH Terms] OR ("positive pressure"[All Fields] AND "respiration"[All Fields]) OR "positive pressure respiration"[All Fields] OR ("positive"[All Fields] AND "pressure"[All Fields] AND "ventilation"[All Fields]) OR "positive pressure ventilation"[All Fields] OR "intermittent positive pressure ventilation"[MeSH Terms] OR ("intermittent"[All Fields] AND "positive pressure"[All Fields] AND "ventilation"[All Fields]) OR "intermittent positive pressure ventilation"[All Fields])))
Search term 2 (#2)	("pulmonary disease, chronic obstructive"[MeSH Terms] OR "pulmonary disease, chronic obstructive"[MeSH Terms] OR "pulmonary disease, chronic obstructive"[MeSH Terms] OR (("chronic"[All Fields] OR "chronical"[All Fields] OR "chronically"[All Fields] OR "chronicities"[All Fields] OR "chronicity"[All Fields] OR "chronicization"[All Fields] OR "chronics"[All Fields]) AND ("respiratory tract diseases"[MeSH Terms] OR "respiration disorders"[MeSH Terms])) OR "pulmonary disease, chronic obstructive"[MeSH Terms] OR "pulmonary disease, chronic obstructive"[MeSH Terms] OR "pulmonary emphysema"[MeSH Terms]))
Search term 3 (#3)	#1 and #2

MeSH – Medical Subject Headings.

The Nordic Cochrane Center, Cochrane Collaboration, Copenhagen, Denmark). Binary outcomes such as mortality, exacerbation, and intubation rates were reported as odds ratios (OR) with corresponding 95% confidence intervals (95% CIs). Meta-analyses for binary outcomes were done using a random-effects model (Mantel–Haenszel method). Continuous outcomes such as $PaCO_2$ and PaO_2 levels were reported as mean differences (MDs) with associated 95% CIs using the random-effects model (inverse variance method). Heterogeneity in the included studies was evaluated using I^2 statistic, with small heterogeneity for I^2 values of <25%, moderate heterogeneity for I^2values of 25% to 50% and high heterogeneity for I^2 values >50%.[17] Forest plots were constructed and $p < 0.05$ was statistically significant. Subgroup analyses were also performed according to stage of COPD (stable COPD, PECOPD and AECOPD) and type of control treatment or comparator (pharmacological treatment + oxygen, LTOT, high-flow nasal cannula (HFNC), or only pharmacological treatment). Publication bias was assessed using Egger's test and a funnel plot, where the log OR for each study was plotted against its standard error (SE) for the mortality outcome. The vertical line indicates the pooled OR representing the overall summary effect size.

Results

Identification of studies

A total of 874 records were identified through database searching. After removing 345 duplicates and irrelevant records, 581 titles and abstracts were screened. Of these, 236 RCTs were assessed for eligibility. However, 185 RCTs were excluded due to reasons such as inappropriate comparator, intervention, condition, or population, missing required outcomes, or duplicate data. The selection process is illustrated in Fig. 1. Table 2 shows the results of search strategy and Hits for COPD and NIV literature review.

Study characteristics

A total of 51 RCTs, comprising 3,775 participants, met the inclusion criteria. These included patients with stable COPD (n = 1,187), PECOPD (n = 1,314) and acute exacerbation of AECOPD (n = 1,274). The RCTs compared nocturnal or domiciliary NIV to other COPD treatments, such as LTOT, oxygen supplementation, pharmacologic therapies, HFNC, standard nasal cannula, or sham interventions. Participants were male and female across different COPD stages, with varying baseline $PaCO_2$ levels, presence of hypercapnia, history of recent exacerbations, and differing durations of NIV administration and follow-up. Most studies used BiPAP systems for NIV delivery, administered via nasal, full-face or oronasal masks. Detailed information on interventions and control groups is provided in Table 3.[18–69]

Characteristics of participants

The included studies involved patients with stable COPD (19 studies), PECOPD (14 studies) and AECOPD (18 studies). Across all studies, the mean age of participants was over 60 years. In most studies, baseline $PaCO_2$ levels exceeded 6 kPa, and the majority of patients presented with hypercapnia (Table 4).[18–69]

Bias assessment

The results of the risk of bias evaluation are presented in Fig. 2. Overall, the studies demonstrated a high risk

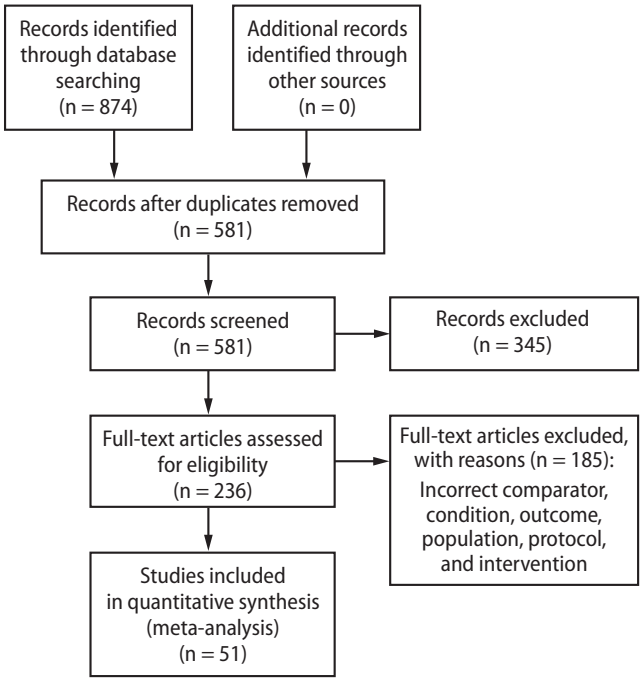

Fig. 1. Flow chart for identification and inclusion of studies in the meta-analysis according to Preferred Reporting Items for Systematic and Meta-Analyses (PRISMA)

Table 2. Search strategy and hits for chronic obstructive pulmonary disease (COPD) and noninvasive ventilation (NIV) literature review

ID	Search	Hits
#1	MeSH descriptor: [Pulmonary Disease, Chronic Obstructive] explode all trees	8385
#2	MeSH descriptor: [Pulmonary Emphysema] explode all trees	409
#3	("chronic obstructive airway disease"):ti,ab,kw (Word variations have been searched)	199
#4	("chronic obstructive lung disease"):ti,ab,kw (Word variations have been searched)	8617
#5	#1 or #2 or #3 or #4	14621
#6	MeSH descriptor: [Noninvasive Ventilation] explode all trees	580
#7	MeSH descriptor: [Continuous Positive Airway Pressure] explode all trees	1929
#8	(BiPAP):ti,ab,kw (Word variations have been searched)	478
#9	(CPAP):ti,ab,kw (Word variations have been searched)	5890
#10	("bilevel positive airway pressure"):ti,ab,kw (Word variations have been searched)	289
#11	("positive pressure ventilation"):ti,ab,kw (Word variations have been searched)	2366
#12	#6 or #7 or #8 or #9 or #10 or #11	9033
#13	#5 and #12	433

MeSH – Medical Subject Headings.

Table 3. Details of intervention and control groups of the studies included in the meta-analysis

Study name	Intervention	Control
Avdeev, 1998[18]	NIV (BiPAP) + usual care	oxygen + bronchodilators + steroids + theophylline
Barbe et al., 1996 [19]	NIV (BiPAP) + usual care	salbutamol + prednisolone + oxygen
Barrett et al., 2022[20]	NIV (ICU ventilator in NIV mode)	extracorporeal carbon dioxide removal ($ECCO_2R$)
Bhatt et al., 2013[21]	domiciliary NPPV (oronasal mask/nasal pillows, BiPAP)	usual therapy
Bott et al., 1993[22]	NPPV + usual care	oxygen, bronchodilators, antibiotics, diuretics, respiratory stimulants, corticosteroids
Braunlich et al., 2019[23]	NIV	nasal high flow (NHF)
Brochard et al., 1995[24]	NIV (ARM 25)	oxygen, subcutaneous heparin, antibiotics, bronchodilators
Budweiser et al., 2007[25]	NIV (BiPAP, Twin Air®, Smart Air®) + pharmacological treatment	usual pharmacological agents
Carrera et al., 2009[26]	NIV (BiPAP and facial mask)	sham NIV
Casanova et al., 2000[27]	nocturnal nasal NPPV (nasal mask)	standard care + LTOT
Celikel et al., 1998[28]	continuous NIV + usual care	oxygen + pharmacological treatment
Cheung et al., 2010[29]	nocturnal NIV (BiPAP)	placebo home NIV
Clini et al., 1998[30]	Nocturnal NIV + LTOT	LTOT
Clini et al., 2002[31]	nocturnal NPPV (BiPAP, nasal mask) + LTOT	LTOT
Collaborative Research Group of Noninvasive Mechanical Ventilation for Chronic Obstructive Pulmonary Disease, 2005[32]	NIV (oronasal mask, BiPAP) + pharmacological treatment	oxygen via nasal cannula + pharmacological treatment
Cortegiani et al., 2020[33]	NIV (full-face or oronasal mask)	high flow nasal therapy (HFNT)
del Castillo et al., 2003[34]	NIV (BiPAP, mask)	oxygen + pharmacological treatment
DeBacker et al., 2011[35]	nocturnal NIV pharmacological treatment	pharmacological treatment
Dickensoy et al., 2002[36]	NIV (BiPAP) + usual care	oxygen + pharmacological treatment
Duiverman et al., 2008[37]	nocturnal NPPV (BiPAP, nasal/oronasal mask)	pulmonary rehabilitation

Table 3. Details of intervention and control groups of the studies included in the meta-analysis – cont

Study name	Intervention	Control
Duiverman et al., 2011[38]	nocturnal NPPV + rehabilitation	rehabilitation
Funk et al. 2011[39]	nocturnal NIV (BiPAP)	no NIV
Garrod et al., 2000[40]	nocturnal NPPV + exercise training program (BiPAP, nasal mask)	exercise training program
Gay et al., 1996[41]	nocturnal NIV (BiPAP, nasal mask)	sham NIV
Hedsund et al., 2023[42]	long-term NIV + standard of care	standard of care
Jing et al., 2019[43]	NIV (VPAP)	HFNC
Khilnani et al., 2010[44]	NIV (BiPAP)	oxygen + pharmacological treatment
Köhnlein et al., 2014[45]	nocturnal NPPV (nasal/face mask) + pharmacological treatment	pharmacological treatment
Kramer et al., 1995[46]	NIV (BiPAP) + pharmacological treatment + oxygen	oxygen + pharmacological treatment
Liu et al., 2005[47]	NIV (BiPAP, face mask) + pharmacological treatment + oxygen	pharmacological treatment + oxygen
Liu et al., 2023[48]	NPPV (BiPAP)	transnasal high-flow humidified oxygen therapy
Majorski et al., 2021[49]	portable NIV device	no NIV device
Martin-Marquez et al., 2014[50]	nocturnal NIV (BiPAP) + training program	training program
Matsuka et al., 2006[51]	NIV (BiPAP) + oxygen + pharmacological treatment	oxygen + pharmacological treatment
McEvoy et al., 2019[52]	nocturnal NIV + usual care + LTOT	usual care + LTOT
Meecham-Jones et al., 1995[53]	nocturnal NIV (BiPAP) + oxygen therapy	oxygen therapy
Murphy et al., 2017[54]	nocturnal NIV + home oxygen therapy	home oxygen therapy
Plant et al., 2001[55]	NIV (BiPAP) + oxygen + pharmacological treatment	oxygen + pharmacological treatment
Rezaei et al., 2020[56]	NIV (VPAP)	high-oxygen nasal cannula
Samaria., 2009[57]	NIV (BiPAP) + oxygen + pharmacological treatment	oxygen + pharmacological treatment
Shebl et al., 2015[58]	nocturnal NPPV (BiPAP) + pharmacological treatment	pharmacological treatment
Sin et al., 2007[59]	NIV (VPAP, nasal/oronasal mask)	sham treatment
Struik et al., 2014[60]	nocturnal NIV + standard treatment	pharmacological treatment + LTOT
Strumpf et al., 1991[61]	nocturnal NIV (BiPAP, nasal mask)	oxygen + pharmacological treatment
Tan et al., 2020[62]	NIV (BiPAP, oronasal mask)	NFNC oxygen therapy
Tan et al., 2024[63]	NIV (BiPAP, oronasal mask)	HFNC oxygen therapy
Thys et al., 2002[64]	NIV (BiPAP) + supplemental oxygen	supplemental oxygen + pharmacological treatment
Tsolaki et al., 2008[65]	NIV (BiPAP, face mask)	LTOT + pharmacological treatment
Vargas et al., 2017[66]	NIV (face mask)	standard oxygen therapy
Xiang et al., 2007[67]	home NPPV + standard treatment	standard treatment
Zhou et al., 2001[68]	NIV (BiPAP, nasal/face mask) + oxygen + pharmacological treatment	pharmacological treatment
Zhou et al., 2017[69]	nocturnal NIV + pharmacological treatment	LTOT + pharmacological treatment

NIV – noninvasive ventilation; BiPAP – bilevel positive airway pressure; NPPV – noninvasive positive pressure ventilation; VPAP – variable positive airway pressure; LTOT – long-term oxygen therapy; HFNC – high flow nasal cannula.

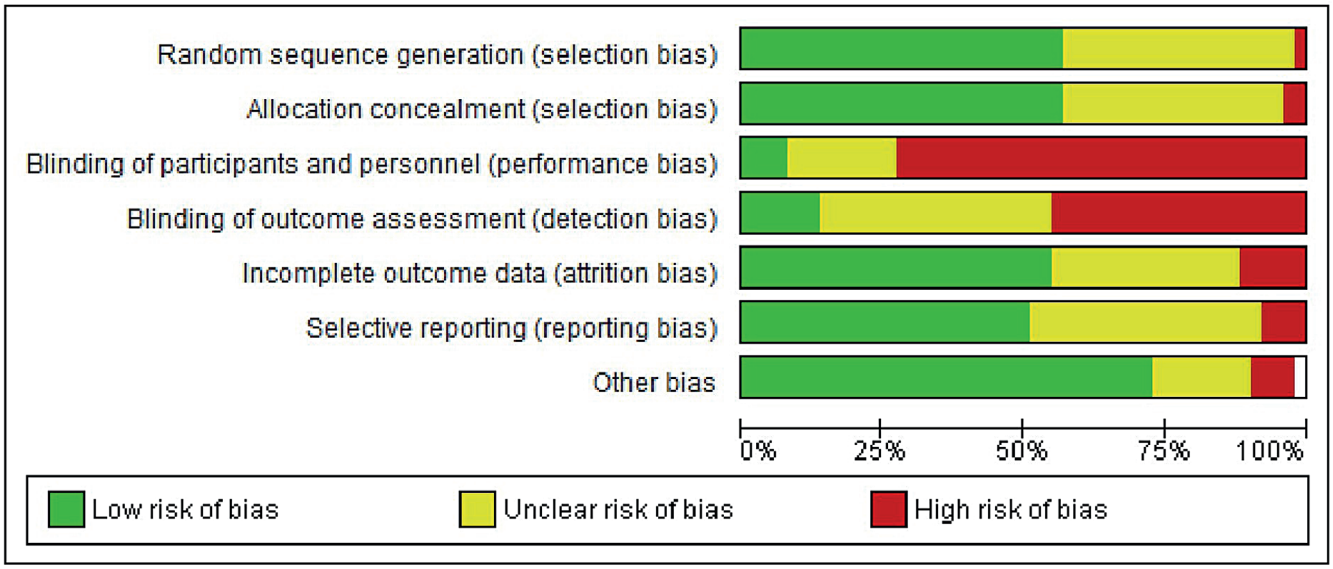

Fig. 2. Risk of bias summary for studies included in the meta-analysis

Table 4. Characteristics of the included randomized controlled trials (RCTs)

Study name	COPD type	Patient characteristics	Length of follow-up
Avdeev, 1998[18]	AECOPD	male and female, acute respiratory failure, mean age 65 years	N/A
Barbe et al., 1996 [19]	AECOPD	Male, 68 ±2 years, acute respiratory failure	N/A
Barrett et al., 2022[20]	AECOPD	male and female, ≥18 years, hypercapnia pH < 7.3	N/A
Bhatt et al., 2013[21]	stable COPD	male and female, mean age: 69.4 years, no exacerbations in last 4 weeks, $PaCO_2$ < 52 mm Hg	6 weeks, 3 and 6 months
Bott et al., 1993[22]	AECOPD	male and female, ≤80 years, acute exacerbation of COPD	At least 30 days
Braunlich et al., 2019[23]	stable COPD	male and female, mean age: 65.3 years, no exacerbations in last 4 weeks, BMI ≤ 30 kg/m^2	12 weeks
Brochard et al., 1995[24]	AECOPD	male and female, acute exacerbation with respiratory acidosis	N/A
Budweiser et al., 2007[25]	PECOPD	male and female, mean age: 65 years, $PaCO_2$ > 50 mm hg after treatment of exacerbation, $PaCO_2$ 59 mm Hg	6 months
Carrera et al., 2009[26]	AECOPD	male and female, 67 ±9 years,	N/A
Casanova et al., 2000[27]	stable COPD	male and female, mean age: 66.6 years, no exacerbations in last 3 months, mean $PaCO_2$: 6.8 kPa	12 months
Celikel et al., 1998[28]	AECOPD	male and female, hypercapnic acute respiratory failure	N/A
Cheung et al., 2010[29]	PECOPD	male and female, mean age: 70.3 years, acute respiratory failure and treatment with pharmacological agents, $PaCO_2$ 7.5 kPa	12 months
Clini et al., 1998[30]	stable COPD	male and female, mean age: 66 years, no exacerbation in last 4 weeks, $PaCO_2$: 6–8 kPa	36 months
Clini et al., 2002[31]	stable COPD	male and female, ≤75 years, no exacerbation in last 4 weeks, $PaCO_2$ > 6.6 kPa	24 months
Collaborative Research Group of Noninvasive Mechanical Ventilation for Chronic Obstructive Pulmonary Disease, 2005[32]	AECOPD	male and female, <85 years, pH>7.25	N/A
Cortegiani et al., 2020[33]	PECOPD	male and female, mean age: 75 years, acute hypercapnic respiratory failure and exacerbation, $PaCO_2$ ≥ 55 mm Hg	N/A
del Castillo et al., 2003[34]	AECOPD	male and female, acidotic hypercapnic respiratory failure, mean age: 67 years	N/A
DeBacker et al., 2011[35]	PECOPD	male and female, mean age: 65.6 years, persistent hypercapnia $PaCO_2$ > 6 kPa, hospitalized due to exacerbation	12 months
Dickensoy et al., 2002[36]	AECOPD	male, mean age: 65 years	N/A
Duiverman et al., 2008[37]	stable COPD	male and female, 40–76 years, no exacerbation in last 4 weeks, $PaCO_2$ > 6 kPa	24 months
Duiverman et al., 2011[38]	stable COPD	male and female, mean age: 62 years, no exacerbation in last 4 weeks, $PaCO_2$ > 6 kPa	24 months
Funk et al. 2011[39]	PECOPD	male and female, mean age: 63 years, requiring invasive or noninvasive mechanical ventilation, $PaCO_2$ 94 mm Hg	N/A
Garrod et al., 2000[40]	stable COPD	male and female, 38–84 years, no exacerbations in last 4 weeks, mean $PaCO_2$ 6.1 kPa	8 weeks
Gay et al., 1996[41]	stable COPD	male and female, mean age: 67.6 years, BMI ≤ 30 kg/m^2, $PaCO_2$ > 6 kPa	3 months
Hedsund et al., 2023[42]	PECOPD	male and female, mean age: 72 years, admission with acute hypercapnic respiratory failure, $PaCO_2$ 9 kPa	12 months
Jing et al., 2019[43]	PECOPD	male and female, mean age: 74 years, intubated for exacerbation, $PaCO_2$ 53 mm Hg	N/A
Khilnani et al., 2010[44]	AECOPD	male and female, AECOPD leading to hypoxemia and respiratory acidosis pH < 7.35, mean age: 60 years	N/A
Köhnlein et al., 2014[45]	stable COPD	male and female, mean age: 63.2 years, no exacerbations in last 4 weeks, $PaCO_2$ 7.8 kPa	12 months
Kramer et al., 1995[46]	AECOPD	male and female, respiratory distress, pH < 7.35	N/A
Liu et al., 2005[47]	AECOPD	acute exacerbation, pH 7.25–7.35, mean age: 70 years	N/A
Liu et al., 2023[48]	PECOPD	male and female, mean age: 69 years, AECOPD and type II respiratory failure $PaCO_2$ 53 mm Hg	N/A
Majorski et al., 2021[49]	stable COPD	male and female, mean age: 67 years, no exacerbation in last 4 weeks, $PaCO_2$ 42kPa	N/A
Martin-Marquez et al., 2014[50]	stable COPD	male and female, mean age: 68.3 years, clinically stable for last 3 months, $PaCO_2$ 6.7 kPa	3 months

Table 4. Characteristics of the included randomized controlled trials – cont

Study name	COPD type	Patient characteristics	Length of follow-up
Matsuka et al., 2006[51]	AECOPD	male and female, pH < 7.35, mean age: 67 years	N/A
McEvoy et al., 2019[52]	stable COPD	male and female, mean age: 68 years, stable hypercapnic respiratory failure in last 6 months, $PaCO_2$ 7.3 kPa	6 months
Meecham-Jones et al., 1995[53]	stable COPD	male and female, mean age: 65.9 years, stable clinical state, $PaCO_2$ 7.4 kPa	6 months
Murphy et al., 2017[54]	PECOPD	male and female, mean age: 66 years, acute decompensated hypercapnic exacerbations of COPD, $PaCO_2$ 7.9 kPa	12 months
Plant et al., 2001[55]	AECOPD	male and female, mean age: 69 years, tachypnoea, pH 7.25–7.35	N/A
Rezaei et al., 2020[56]	PECOPD	male and female, mean age: 60 years, moderate-to-severe COPD exacerbation, $PaCO_2$ 64 mm Hg	N/A
Samaria, 2009[57]	AECOPD	NA	N/A
Shebl et al., 2015[58]	stable COPD	male and female, mean age: 65.5 years, no exacerbation in last 4 weeks, $PaCO_2$ 7.3 kPa	6 months
Sin et al., 2007[59]	stable COPD	male and female, mean age: 65.4 years, $PaCO_2$ 5.8 kPa	3 months
Struik et al., 2014[60]	PECOPD	male and female, mean age: 63.4 years, $PaCO_2$ 7.8 kPa	12 months
Strumpf et al., 1991[61]	stable COPD	male and female, mean age: 65.6 years, no exacerbation in last 1 week, $PaCO_2$ 6.2 kPa	6 months
Tan et al., 2020[62]	PECOPD	male and female, mean age: 69 years, hypercapnic respiratory failure with invasive ventilation, $PaCO_2$ 51 mm Hg	N/A
Tan et al., 2024[63]	PECOPD	male and female, mean age: 71 years, hypercapnic respiratory failure, $PaCO_2$ 62 mm Hg	N/A
Thys et al., 2002[64]	AECOPD	male and female, mean age: 73 years, acute respiratory distress, $PaCO_2$ 57 mm Hg	N/A
Tsolaki et al., 2008[65]	stable COPD	male and female, mean age: 66 years, no exacerbations in last 4 weeks, chronic hypercapnic respiratory failure, $PaCO_2$ 54 mm Hg	12 months
Vargas et al., 2017[66]	PECOPD	male and female, mean age: 64 years, patients intubated for at least 48 h, $PaCO_2$ > 45 mm Hg	3 months
Xiang et al., 2007[67]	PECOPD	male and female, severe COPD and hospitalized, $PaCO_2$ > 55 mm Hg	24 months
Zhou et al., 2001[68]	AECOPD	Male and female, mean age: 64 years, respiratory failure, $PaCO_2$ > 55 mm Hg	N/A
Zhou et al., 2017[69]	stable COPD	male and female, mean age: 67.7 years, clinically stable and chronic hypercapnia, $PaCO_2$ 8 kPa	3 months

AECOPD – acute exacerbation of chronic obstructive pulmonary disease; stable COPD – stable chronic obstructive pulmonary disease; PECOPD – pulmonary embolism with chronic obstructive pulmonary disease; BMI – body mass index; N/A – not applicable.

of detection and performance bias. This was primarily due to the inherent differences between NIV devices and their comparators, including interface types (e.g., nasal or oronasal masks), and the practical inability to blind participants and personnel to the intervention. These limitations may have influenced subjective and patient-reported outcomes. However, the funnel plot showed relative symmetry (Fig. 3), and Egger's test returned a p-value of 0.324, exceeding the conventional significance threshold of 0.05, suggesting a low risk of publication bias.

Meta-analysis results

The overall risk of mortality was significantly lower in the NIV group compared to the control group (OR = 0.67, 95% CI: 0.52–0.85, p < 0.001), with low heterogeneity observed across studies (I^2 = 20%). However, when stratified by COPD stage, the difference in mortality was not statistically significant (p = 0.32). Mortality outcomes were reported across all COPD subgroups, each exhibiting low-to-moderate heterogeneity (I^2 range: 0–35%). The highest heterogeneity was observed in the AECOPD subgroup (I^2 = 35%), possibly

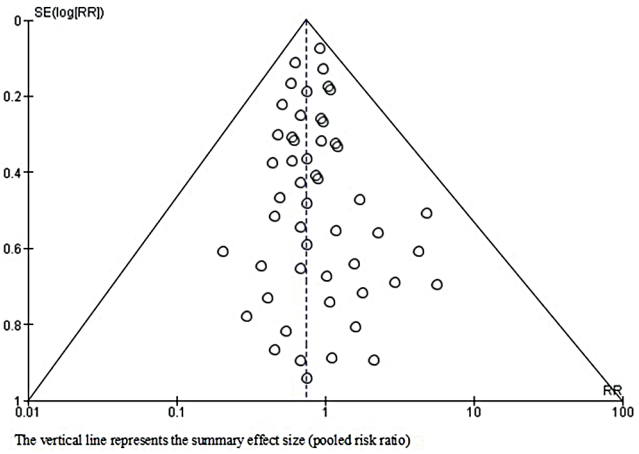

Fig. 3. Funnel plot for overall publication bias for studies included in the meta-analysis

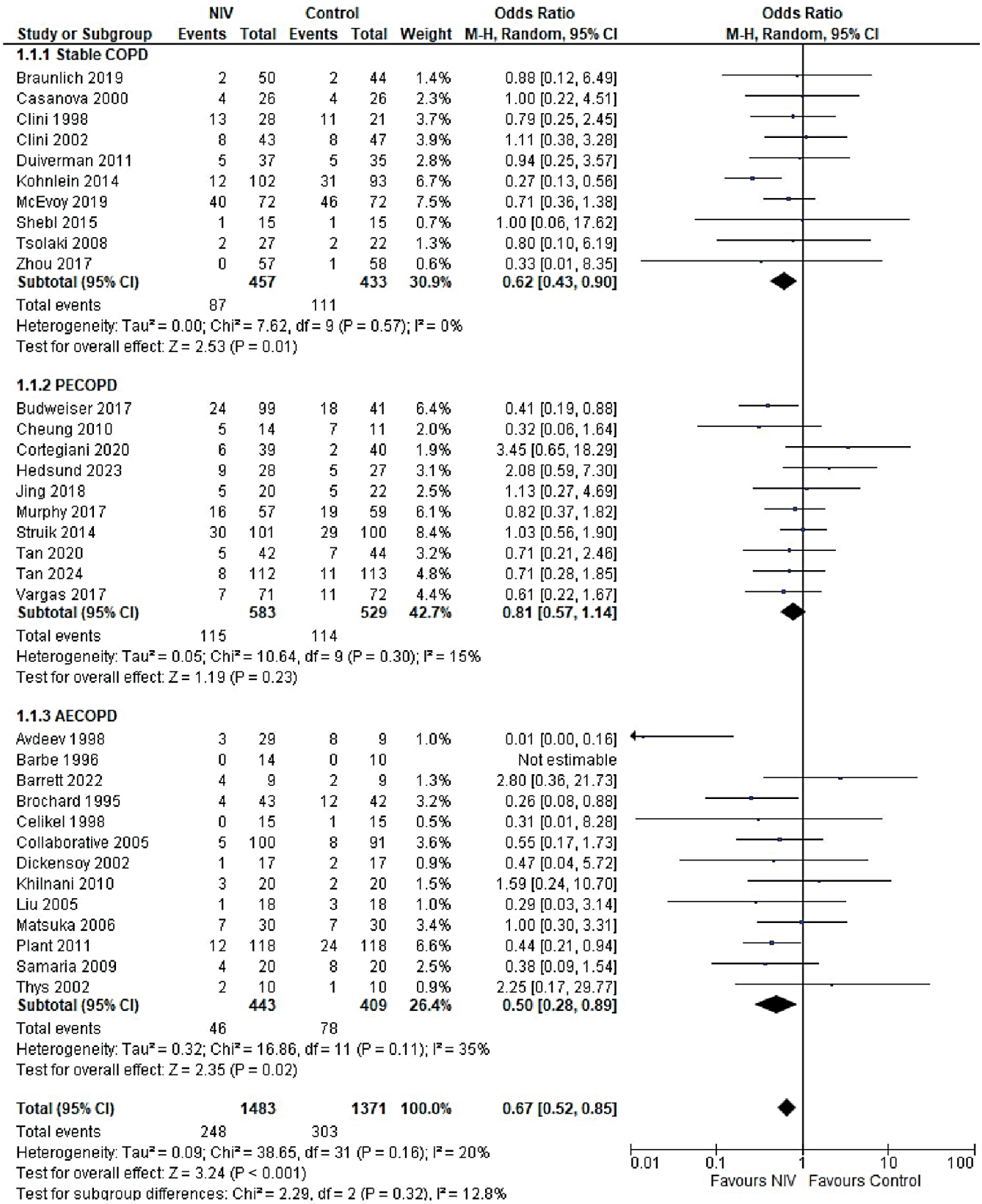

Fig. 4. Forest plot for mortality outcomes: A. Stable chronic obstructive pulmonary disease (COPD) patients; B. Post-exacerbation COPD (PECOPD) patients; C. Acute exacerbation COPD (AECOPD) patients

due to variations in follow-up duration (Fig. 4). The funnel plot for mortality outcomes demonstrated approximate symmetry, suggesting a low risk of publication bias, which was supported by Egger's test results: stable COPD (p = 0.136), PECOPD (p = 0.211) and AECOPD (p = 0.141) (Supplementary Fig. 1).

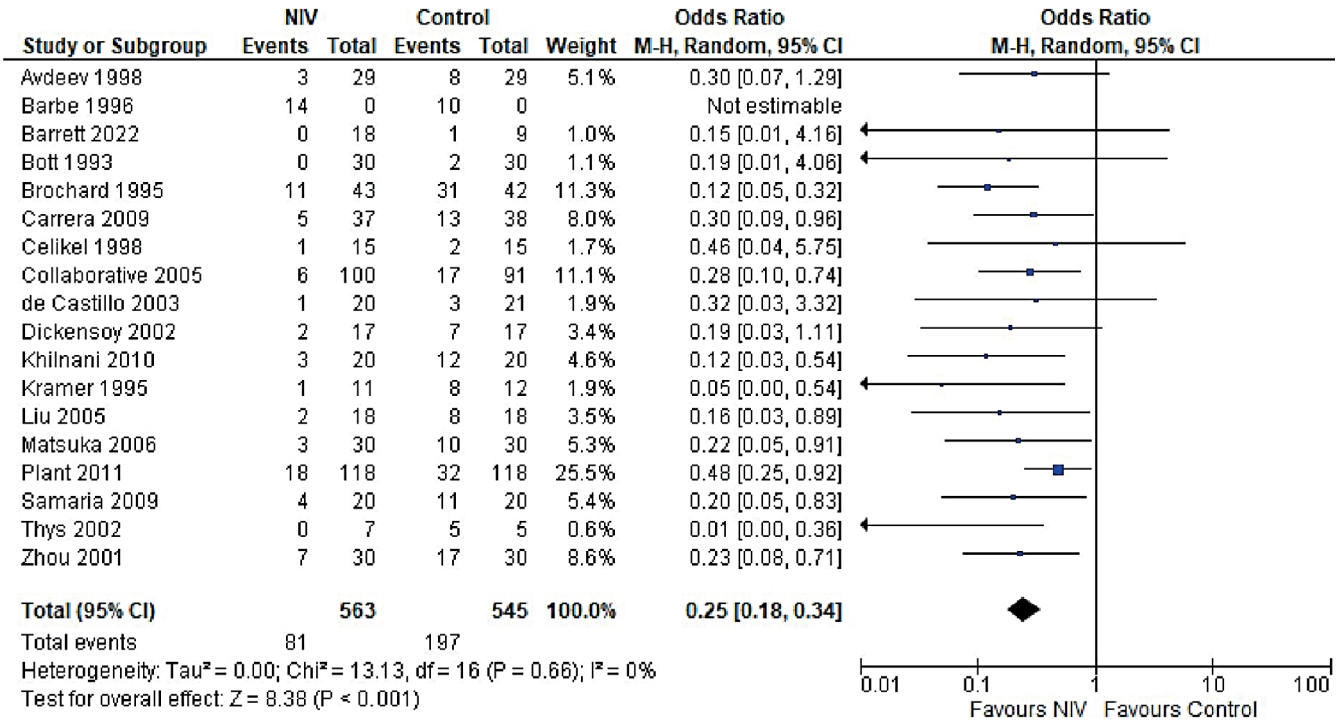

Fig. 5. Forest plot for intubation in AECOPD patients

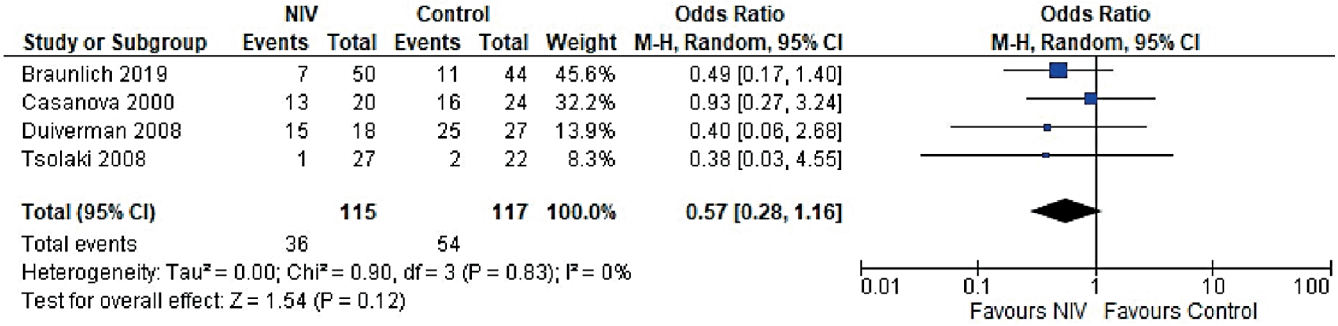

Fig. 6. Forest plot for exacerbation in stable chronic obstructive pulmonary disease (COPD) patients

In patients with AECOPD, NIV significantly reduced the risk of intubation compared to the control group (OR = 0.25, 95% CI: 0.18–0.34, p < 0.001). This analysis, based on 18 trials, showed no heterogeneity (I^2 = 0%), suggesting consistency in patient characteristics and study conditions (Fig. 5). The funnel plot appeared symmetrical, and Egger's test confirmed a low risk of publication bias (p = 0.173) (Supplementary Fig. 2). In patients with stable COPD, the exacerbation rate did not differ significantly between the NIV and control groups (OR = 0.57, 95% CI: 0.28–1.16, p = 0.83), based on data from 4 studies. The low heterogeneity (I^2 = 0%) likely reflects similar patient profiles and consistent definitions of stable COPD (i.e., no exacerbations within the last 4 weeks). One trial[27] (Casanova et al.) showed a nonsignificant result, possibly due to a slightly different definition of stability (no exacerbations in the past 3 months). The type of control intervention did not influence the direction of the results (Fig. 6). The funnel plot suggested a low risk of publication bias (Supplementary Fig. 3). Continuous outcomes, such as $PaCO_2$ and PaO_2 levels, were analyzed across COPD subgroups, reported as changes in arterial blood gases from baseline to follow-up. Noninvasive ventilation was associated with a significantly greater reduction in $PaCO_2$ levels compared to the control group (MD = −0.36, 95% CI: −0.63 to −0.09; p < 0.001), although high heterogeneity was observed (I^2 = 95%). When stratified by COPD subgroup, trials involving Acute exacerbation chronic obstructive pulmonary disease (AECOPD) patients demonstrated a significant reduction in $PaCO_2$ with NIV (MD = −0.79, 95% CI: −1.19 to −0.40; p < 0.001; I^2 = 89%), while trials in stable COPD and PECOPD populations did not show statistically significant benefits. The high heterogeneity likely reflects variations in patient characteristics, control interventions and follow-up durations (ranging from 3 to 12 months) (Fig. 7). The funnel plot appeared symmetrical, suggesting a low risk of publication bias, which was supported by Egger's test for the stable COPD subgroup

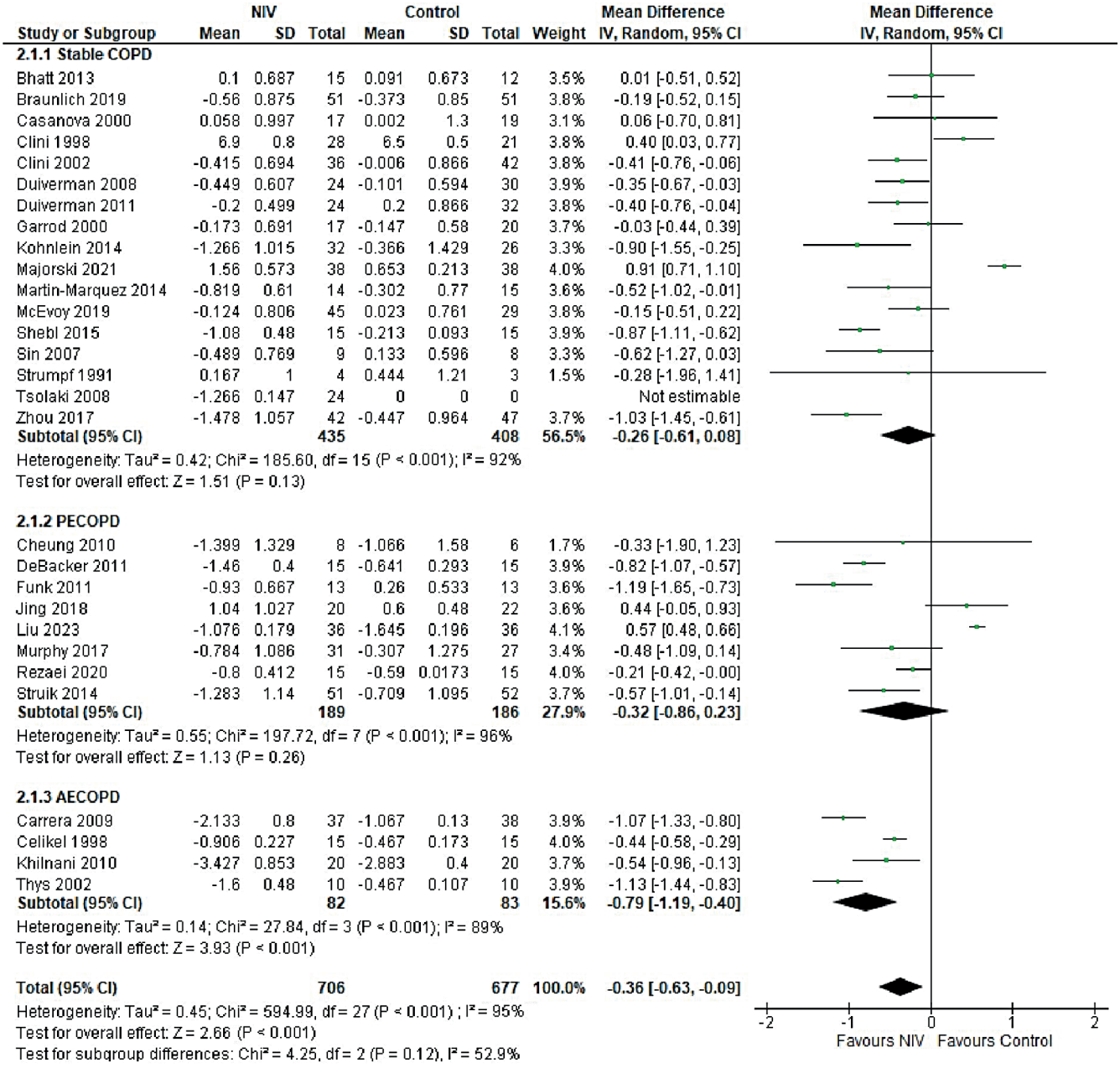

Fig. 7. Forest plot for $PaCO_2$ levels: A. Stable chronic obstructive pulmonary disease (COPD) patients; B. Post-exacerbation COPD (PECOPD) patients; C. Acute exacerbation COPD (AECOPD) patients

(p = 0.119) (Supplementary Fig. 4). No significant difference in PaO_2 levels was observed between the NIV and control groups in trials involving stable COPD and PECOPD patients (MD = 0.14, 95% CI: −0.55 to 0.84; p = 0.69) (Fig. 8). High heterogeneity (I^2 = 100%) was likely attributable to differences in patient characteristics, ventilator settings, comparator treatments, and follow-up durations. The subgroup analysis did not reveal a statistically significant difference (p = 0.64). The funnel plot appeared symmetrical (Supplementary Fig. 5), indicating a low risk of publication bias, which was confirmed by Egger's test for the stable COPD subgroup (p = 0.159). Subgroup analyses based on the type of control treatment revealed a significant reduction in mortality when the comparator was pharmacological therapy combined with oxygen supplementation (OR = 0.38, 95% CI: 0.17–0.83; p = 0.02; I^2 = 42%) or pharmacological therapy alone (OR = 0.34, 95% CI: 0.20–0.57; p < 0.001; I^2 = 0%) (Fig. 9). However, no significant reduction in mortality was observed when NIV was compared with LTOT or HFNC. The funnel plot for control-treatment subgroups (Supplementary Fig. 6) displayed high symmetry, suggesting a low likelihood of publication bias. Similar effects were observed for $PaCO_2$ levels (Fig. 10), with a significant reduction associated with NIV compared to pharmacological treatment combined with oxygen (MD = −0.72, 95% CI: −1.34 to −0.10, p = 0.02, I^2 = 88%) and pharmacological treatment alone (MD = −0.85, 95% CI: −1.02 to −0.68, p < 0.001, I^2 = 0%).

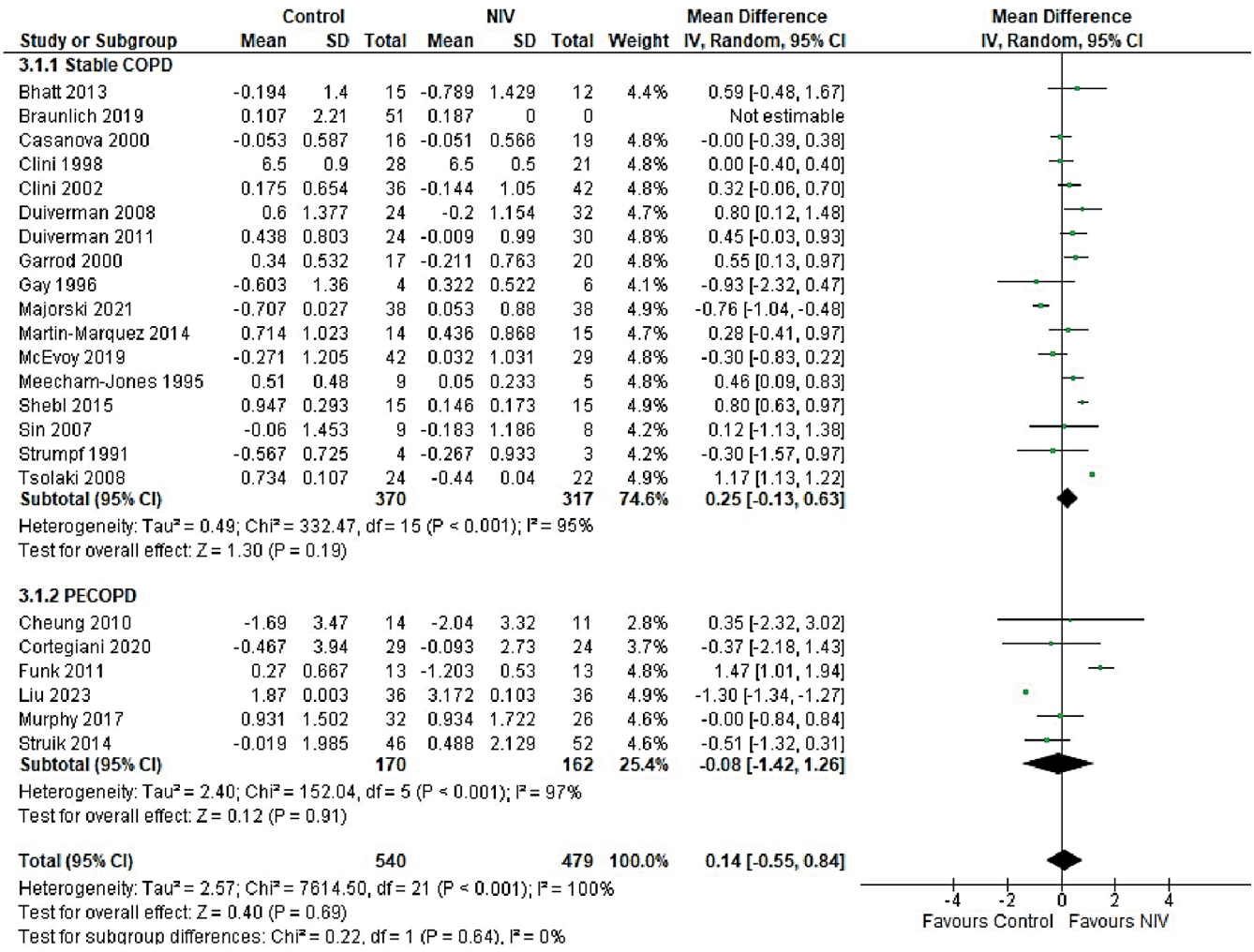

Fig. 8. Forest plot for PaO_2 levels: A. Stable chronic obstructive pulmonary disease (COPD) patients; B. Post-exacerbation COPD (PECOPD) patients

The funnel plot (Supplementary Fig. 7) displayed a high degree of symmetry across various control treatments, indicating a low risk of publication bias.

Discussion

This paper provides an updated synthesis of the evidence for using NIV instead of usual care to manage different stages of COPD. Important outcomes such as mortality, exacerbations, intubation, and arterial gas levels (e.g. $PaCO_2$ and PaO_2 were assessed to determine the long- and short-term effects of NIV on patients at different stages of COPD. The findings of this study emphasize the importance of NIV in reducing mortality and morbidity, as well as the incidence of adverse events such as exacerbations and intubations, in COPD patients. Although several trials and meta-analyses have demonstrated the beneficial effects of NIV on survival, hospital admissions and length of stay, as well as improving quality of life, there are challenges associated with NIV devices that limit their applicability. These include mask leaks, difficulty wearing the device, mask discomfort, and severe hypoxia. Therefore, it is necessary to understand which patient baseline characteristics are most likely to benefit from NIV, the ideal length of treatment and continuous monitoring protocols, and training on the appropriate use of devices and ventilator settings.

The risk of bias assessment using the Cochrane tool revealed high performance and detection biases. Blinding of personnel and participants was not possible, as NIV devices and interfaces differ from usual care. Such treatments as pharmacological interventions and sham treatments may not always be feasible. This introduces an inherent bias when subjective outcomes such as quality of life and symptom assessment are measured. Therefore, this study only included objective measurements such as mortality, intubation and exacerbation rates, and arterial blood gases, which are not subject to bias and provide more reliable results regarding the efficacy of NIV. Our study showed that NIV use across different COPD stages decreases mortality. However, there was no significant difference in mortality outcomes between PECOPD patients receiving NIV or usual care.

The effect of NIV on COPD varies between patients with stable COPD and those with PECOPD. Some meta-analyses have reported nonsignificant differences

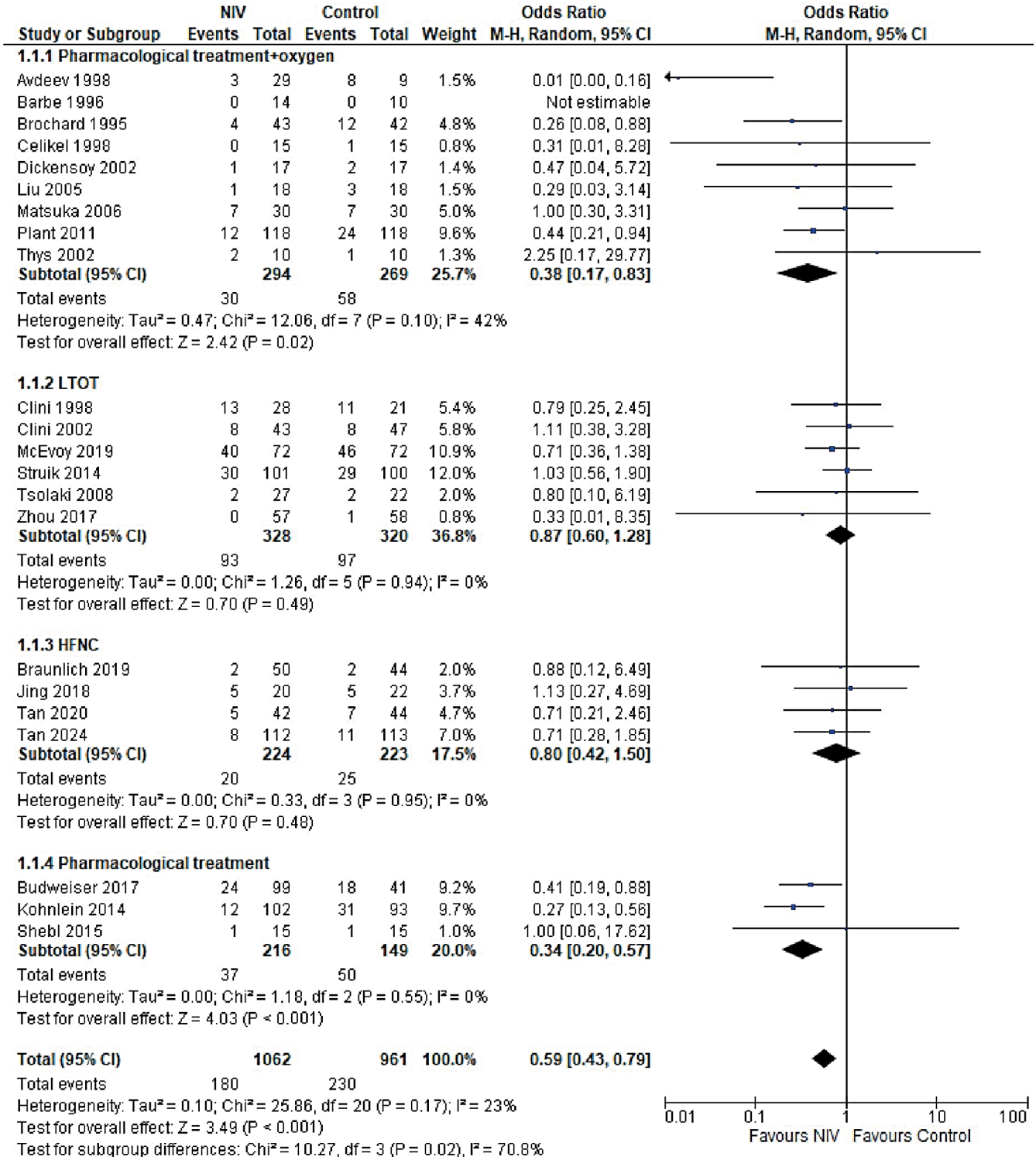

Fig. 9. Forest plot for mortality in intervention group stratified by type of control treatment

in mortality outcomes among patients with stable COPD and PECOPD. However, other studies, including our analysis, have demonstrated a mortality benefit in patients with stable COPD.[14,70] This benefit may be attributed to persistent hypercapnia commonly observed in stable COPD patients, in contrast to PECOPD patients, where hypercapnia may be transient and often accompanied by additional complications. In patients with AECOPD, NIV was found to significantly reduce mortality rates, which could be linked to a reduced need for intubation – thus minimizing the risk of prolonged hospital and ICU stays and associated infections. The exacerbation rate among patients with stable COPD was significantly lower with NIV compared to usual care. Although this analysis included only a limited number of studies (n = 4), it provides preliminary evidence that long-term or chronic use

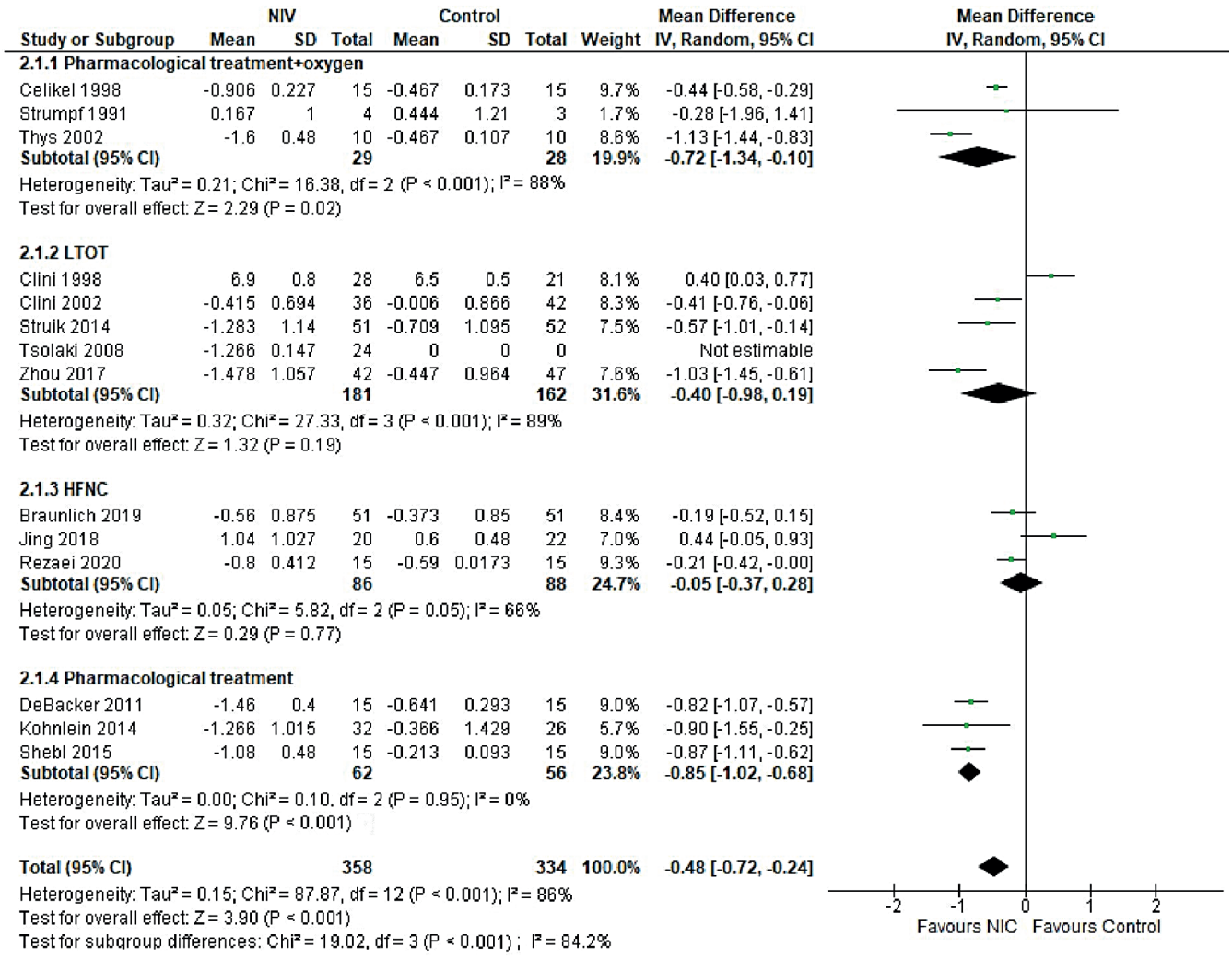

Fig. 10. Forest plot for $PaCO_2$ levels in intervention group stratified by type of control treatment

of NIV may help reduce exacerbation frequency in COPD patients. A greater reduction in $PaCO_2$ levels in stable COPD patients likely contributes to improved alveolar ventilation and respiratory muscle function, particularly in cases of chronic hypercapnia, which may predispose patients to fewer exacerbations. Consistent with previous meta-analyses and the GOLD report, our findings demonstrated a significant improvement in $PaCO_2$ levels in all patients receiving NIV compared to usual care. However, no significant improvement was observed in PaO_2 levels between the 2 groups. The beneficial effect of NIV in lowering $PaCO_2$ is attributed to enhanced alveolar ventilation, increased tidal volume and reduced respiratory muscle fatigue as a result of the positive airway pressure delivered by NIV devices, which facilitates more effective CO_2 elimination.[2,11,71] However, destruction of alveolar units and underlying lung pathology can impair oxygen diffusion into the bloodstream, thereby limiting the impact of NIV on arterial oxygenation and often necessitating supplemental oxygen. Moreover, because several studies included oxygen supplementation or LTOT in the standard treatment arms, the differences in PaO_2 levels between NIV and comparator groups were often attenuated, rendering the effect of NIV on oxygenation statistically nonsignificant. Subgroup analyses revealed that NIV significantly reduced both mortality and $PaCO_2$ levels when compared to pharmacological or standard oxygen therapy. In contrast, differences were nonsignificant when compared to LTOT and HFNC therapy. These findings may be attributed to the superior ventilatory support provided by NIV, which enhances alveolar ventilation and facilitates CO_2 clearance – mechanisms not fully addressed by oxygen or pharmacologic therapy alone. Notably, HFNC delivers heated and humidified oxygen while also generating low-level positive airway pressure, promoting CO_2 washout, which may explain its comparable or potentially superior efficacy to NIV in certain clinical scenarios.

Limitations

Despite our study proving a comprehensive and current review and quantitative evidence on the use of NIV in COPD patients in different stages, it has certain limitations that require consideration when generalizing these

results. The high heterogeneity present in the results of this analysis, particularly for arterial blood gas levels, $PaCO_2$ and PaO_2 is related to heterogenous patient populations and baseline demographics. Differences in baseline $PaCO_2$ levels, comorbidities, and severity of COPD can affect the magnitude of effect of NIV, thereby affecting the efficacy of NIV. Other factors, such as ventilator pressure settings and duration of application, concomitant treatments, comparators such as supplemental oxygen treatment, variable lengths of follow-up between different studies, also result in heterogeneity. However, analyzing studies with homogenous populations regarding patient characteristics results in a limited number of studies included in each subgroup, underpowering the study. Differences in the definitions of outcomes, such as exacerbation, which are often not specified in the trials, also makes combining of results challenging. The numbers of exacerbations and intubations have not been reported for most studies prior to the use of NIV. This lack of information makes it difficult to determine the effectiveness of NIV in decreasing the frequency of attacks. As discussed above, the high risk of detection bias makes it necessary to interpret the results with caution as they may not be generalizable in larger patient populations and the efficacy of NIV can be overestimated without blinding. To provide more robust evidence on the use of NIV, it is important to identify patient subgroups, such as those with hypercapnic respiratory failure, certain comorbidities, and stages of COPD, that are most likely to benefit from NIV use. Additionally, since the efficacy of NIV depends upon its correct use and adherence particularly in case of long-term use, trained personnel are required to administer it, and patients and their caregivers should be educated on the proper use of masks to maximize the benefits offered by NIV.

Since NIV devices demonstrated particular benefit in AECOPD patients by reducing mortality, intubation rates and $PaCO_2$ levels, their integration into clinical practice appears most justified in this subgroup. Moreover, the inconsistent effects of NIV on PaO_2 and $PaCO_2$ levels suggest that NIV may not be the optimal ventilation strategy when oxygenation is the primary therapeutic goal. Instead, its use should be focused on improving alveolar ventilation and respiratory muscle function. Understanding the differential effects of NIV across COPD stages may assist clinicians in selecting appropriate candidates who are most likely to derive significant benefit from this intervention.

Conclusions

In this meta-analysis, we demonstrated that NIV devices reduce mortality, exacerbation frequency and intubation rates in patients across different stages of COPD, including stable COPD, PECOPD and AECOPD. The impact of NIV on gas exchange was variable: NIV significantly reduced $PaCO_2$ levels, but the improvement in PaO_2 was not statistically significant. The efficacy of NIV also varied depending on the COPD stage, with the greatest benefit observed in patients with AECOPD. The high heterogeneity among studies likely reflects differences in patient populations, baseline characteristics, NIV settings, and duration of use. These findings highlight the need to individualize NIV therapy based on patient-specific factors to optimize clinical outcomes.

Supplementary data

The supplementary materials are available at https://doi.org/10.5281/zenodo.17072868. The package includes the following files:

Supplementary Fig. 1. Funnel plot for mortality outcome a) in stable COPD patients b) in PECOPD patients and c) in AECOPD.

Supplementary Fig. 2. Funnel plot for intubation in AECOPD patients.

Supplementary Fig. 3. Funnel plot for exacerbation in stable COPD patients.

Supplementary Fig. 4. Funnel plot for $PaCO_2$ levels a) in stable COPD patients b) in PECOPD patients and c) in AECOPD.

Supplementary Fig. 5. Funnel plot for PaO_2 level a) in stable COPD patients b) in PECOPD patients.

Supplementary Fig. 6. Funnel plot for mortality in intervention group stratified by type of control treatment.

Supplementary Fig. 7. Funnel plot for $PaCO_2$ levels in intervention group stratified by type of control treatment.

Use of AI and AI-assisted technologies

Not applicable.

ORCID iDs

Jinyu Yang https://orcid.org/0009-0000-7137-039X
Lin Chen https://orcid.org/0009-0005-8306-6535
Lihong Zhao https://orcid.org/0009-0003-5373-6986
Chengyi Liu https://orcid.org/0009-0003-9650-9556
Xiujuan Gu https://orcid.org/0009-0003-6311-5198
Wanjuan Qi https://orcid.org/0009-0007-2889-480X
Lei Wang https://orcid.org/0009-0002-3057-3961

References

1. Yoon HK, Park YB, Rhee CK, Lee JH, Oh YM; Committee of the Korean COPD Guideline 2014. Summary of the Chronic Obstructive Pulmonary Disease Clinical Practice Guideline Revised in 2014 by the Korean Academy of Tuberculosis and Respiratory Disease. *Tuberc Respir Dis*. 2017;80(3):230. doi:10.4046/trd.2017.80.3.230
2. Vestbo J, Hurd SS, Agustí AG, et al. Global Strategy for the Diagnosis, Management, and Prevention of Chronic Obstructive Pulmonary Disease: GOLD Executive Summary. *Am J Respir Crit Care Med*. 2013; 187(4):347–365. doi:10.1164/rccm.201204-0596PP
3. World Health Organization (WHtO). Chronic obstructive pulmonary disease (COPD): Fact sheet. Geneva, Switzerland: World Health Organization (WHO); 2024. https://www.who.int/news-room/fact-sheets/detail/chronic-obstructive-pulmonary-disease-(copd). Accessed August 15, 2024.

4. Agustí A, Celli BR, Criner GJ, et al. Global Initiative for Chronic Obstructive Lung Disease 2023 Report: GOLD Executive Summary. *Am J Respir Crit Care Med*. 2023;207(7):819–837. doi:10.1164/rccm.202301-0106PP
5. Müllerova H, Maselli DJ, Locantore N, et al. Hospitalized exacerbations of COPD: Risk factors and outcomes in the ECLIPSE cohort. *Chest*. 2015;147(4):999–1007. doi:10.1378/chest.14-0655
6. Soriano JB, Lamprecht B, Ramírez AS, et al. Mortality prediction in chronic obstructive pulmonary disease comparing the GOLD 2007 and 2011 staging systems: A pooled analysis of individual patient data. *Lancer Respir Med*. 2015;3(6):443–450. doi:10.1016/S2213-2600(15)00157-5
7. Xiang Y, Luo X. Extrapulmonary comorbidities associated with chronic obstructive pulmonary disease: A review. *Int J Chron Obstruct Pulmon Dis*. 2024;19:567–578. doi:10.2147/COPD.S447739
8. Jo YS. Long-term outcome of chronic obstructive pulmonary disease: A review. *Tuberc Respir Dis*. 2022;85(4):289–301. doi:10.4046/trd.2022.0074
9. Osadnik CR, Tee VS, Carson-Chahhoud KV, Picot J, Wedzicha JA, Smith BJ. Non-invasive ventilation for the management of acute hypercapnic respiratory failure due to exacerbation of chronic obstructive pulmonary disease. *Cochrane Database Syst Rev*. 2017;2017(7):CD004104. doi:10.1002/14651858.CD004104.pub4
10. Raveling T, Vonk J, Struik FM, et al. Chronic non-invasive ventilation for chronic obstructive pulmonary disease. *Cochrane Database Syst Rev*. 2021;2021(8):CD002878. doi:10.1002/14651858.CD002878.pub3
11. Ram F, Picot J, Lightowler J, Wedzicha J. Non-invasive positive pressure ventilation for treatment of respiratory failure due to exacerbations of chronic obstructive pulmonary disease. *Cochrane Database Syst Rev*. 2003;2004(1):CD004104.pub2. doi:10.1002/14651858.CD004104.pub2
12. Corrêa TD, Sanches PR, De Morais LC, Scarin FC, Silva E, Barbas CSV. Performance of noninvasive ventilation in acute respiratory failure in critically ill patients: A prospective, observational, cohort study. *BMC Pulm Med*. 2015;15(1):144. doi:10.1186/s12890-015-0139-3
13. Mukherjee R, Nenna R, Turner A. Early ward-based acute noninvasive ventilation: A paper that changed practice. *Breathe*. 2018;14(2):153–155. doi:10.1183/20734735.001618
14. Park SY, Yoo KH, Park YB, et al. The long-term efficacy of domiciliary noninvasive positive-pressure ventilation in chronic obstructive pulmonary disease: A meta-analysis of randomized controlled trials. *Tuberc Respir Dis*. 2022;85(1):47–55. doi:10.4046/trd.2021.0062
15. He X, Luo L, Ma Y, Chen Y. Efficacy of domiciliary noninvasive ventilation on clinical outcomes in posthospital chronic obstructive pulmonary disease patients: A meta-analysis of randomized controlled trials. *Ann Palliat Med*. 2021;10(5):5137–5145. doi:10.21037/apm-20-2017
16. Higgins JPT, Thomas J, Chandler J, et al., eds. *Cochrane Handbook for Systematic Reviews of Interventions*. 2nd ed. Chichester, UK: Wiley; 2019. doi:10.1002/9781119536604
17. Higgins JPT, Thompson SG, Deeks JJ, Altman DG. Measuring inconsistency in meta-analyses. *BMJ*. 2003;327(7414):557–560. doi:10.1136/bmj.327.7414.557
18. Avdeev SN. Non-invasive ventilation in acute respiratory failure [in Russian]. *Pulmonologia (Mosk)*. 2005;6:37–54. doi:10.18093/0869-0189-2005-0-6-37-54
19. Barbe F, Togores B, Rubi M, Pons S, Maimo A, Agusti A. Noninvasive ventilatory support does not facilitate recovery from acute respiratory failure in chronic obstructive pulmonary disease. *Eur Respir J*. 1996;9(6):1240–1245. doi:10.1183/09031936.96.09061240
20. Barrett NA, Hart N, Daly KJR, et al. A randomised controlled trial of non-invasive ventilation compared with extracorporeal carbon dioxide removal for acute hypercapnic exacerbations of chronic obstructive pulmonary disease. *Ann Intensive Care*. 2022;12(1):36. doi:10.1186/s13613-022-01006-8
21. Bhatt S, Peterson M, Wilson J, Durairaj L. Noninvasive positive pressure ventilation in subjects with stable COPD: A randomized trial. *Int J Chron Obstruct Pulmon Dis*. 2013;8:581–589. doi:10.2147/COPD.S53619
22. Bott J, Carroll MP, Conway JH, et al. Randomised controlled trial of nasal ventilation in acute ventilatory failure due to chronic obstructive airways disease. *Lancet*. 1993;341(8860):1555–1557. doi:10.1016/0140-6736(93)90696-E
23. Bräunlich J, Dellweg D, Bastian A, et al. Nasal high-flow versus noninvasive ventilation in patients with chronic hypercapnic COPD. *Int J Chron Obstruct Pulmon Dis*. 2019;14:1411–1421. doi:10.2147/COPD.S206111
24. Brochard L, Mancebo J, Wysocki M, et al. Noninvasive ventilation for acute exacerbations of chronic obstructive pulmonary disease. *N Engl J Med*. 1995;333(13):817–822. doi:10.1056/NEJM199509283331301
25. Budweiser S, Hitzl AP, Jörres RA, et al. Impact of noninvasive home ventilation on long-term survival in chronic hypercapnic COPD: A prospective observational study. *Int J Clin Pract*. 2007;61(9):1516–1522. doi:10.1111/j.1742-1241.2007.01427.x
26. Carrera M, Marín JM, Antón A, et al. A controlled trial of noninvasive ventilation for chronic obstructive pulmonary disease exacerbations. *J Crit Care*. 2009;24(3):473.e7–473.e14. doi:10.1016/j.jcrc.2008.08.007
27. Casanova C, Celli BR, Tost L, et al. Long-term controlled trial of nocturnal nasal positive pressure ventilation in patients with severe COPD. *Chest*. 2000;118(6):1582–1590. doi:10.1378/chest.118.6.1582
28. Çelikel T, Sungur M, Ceyhan B, Karakurt S. Comparison of noninvasive positive pressure ventilation with standard medical therapy in hypercapnic acute respiratory failure. *Chest*. 1998;114(6):1636–1642. doi:10.1378/chest.114.6.1636
29. Cheung APS, Chan VL, Liong JT, et al. A pilot trial of non-invasive home ventilation after acidotic respiratory failure in chronic obstructive pulmonary disease. *Int J Tuberc Lung Dis*. 2010;14(5):642–649. PMID:20392360.
30. Clini E, Sturani C, Porta R, et al. Outcome of COPD patients performing nocturnal non-invasive mechanical ventilation. *Respir Med*. 1998;92(10):1215–1222. doi:10.1016/S0954-6111(98)90424-3
31. Clini E, Sturani C, Rossi A, et al. The Italian multicentre study on noninvasive ventilation in chronic obstructive pulmonary disease patients. *Eur Respir J*. 2002;20(3):529–538. doi:10.1183/09031936.02.02162001
32. Collaborative Research Group of Noninvasive Mechanical Ventilation for Chronic Obstructive Pulmonary Disease. Early use of non-invasive positive pressure ventilation for acute exacerbations of chronic obstructive pulmonary disease: A multicentre randomized controlled trial. *Chin Med J (Engl)*. 2005;118(24):2034–2040. PMID:16438899.
33. Cortegiani A, Longhini F, Madotto F, et al; the HF-AECOPD study investigators. High flow nasal therapy versus noninvasive ventilation as initial ventilatory strategy in COPD exacerbation: A multicenter non-inferiority randomized trial. *Crit Care*. 2020;24(1):692. doi:10.1186/s13054-020-03409-0
34. Del Castillo D, Barrot E, Laserna E, Otero R, Cayuela A, Castillo Gómez J. Noninvasive positive pressure ventilation for acute respiratory failure in chronic obstructive pulmonary disease in a general respiratory ward [in Spanish]. *Med Clin (Barc)*. 2003;120(17):647–651. doi:10.1016/S0025-7753(03)73798-1
35. De Backer L, Vos W, Dieriks B, et al. The effects of long-term noninvasive ventilation in hypercapnic COPD patients: A randomized controlled pilot study. *Int J Chron Obstruct Pulmon Dis*. 2011;6:615–624. doi:10.2147/COPD.S22823
36. Schreiber A, Fusar Poli B, Bos LD, Nenna R. Noninvasive ventilation in hypercapnic respiratory failure: From rocking beds to fancy masks. *Breathe*. 2018;14(3):235–237. doi:10.1183/20734735.018918
37. Duiverman ML, Wempe JB, Bladder G, et al. Nocturnal non-invasive ventilation in addition to rehabilitation in hypercapnic patients with COPD. *Thorax*. 2008;63(12):1052–1057. doi:10.1136/thx.2008.099044
38. Duiverman ML, Wempe JB, Bladder G, et al. Two-year home-based nocturnal noninvasive ventilation added to rehabilitation in chronic obstructive pulmonary disease patients: A randomized controlled trial. *Respir Res*. 2011;12(1):112. doi:10.1186/1465-9921-12-112
39. Funk GC, Breyer MK, Burghuber OC, et al. Long-term non-invasive ventilation in COPD after acute-on-chronic respiratory failure. *Respir Med*. 2011;105(3):427–434. doi:10.1016/j.rmed.2010.09.005
40. Garrod R, Mikelsons C, Paul EA, Wedzicha JA. Randomized controlled trial of domiciliary noninvasive positive pressure ventilation and physical training in severe chronic obstructive pulmonary disease. *Am J Respir Crit Care Med*. 2000;162(4):1335–1341. doi:10.1164/ajrccm.162.4.9912029
41. Gay PC, Hubmayr RD, Stroetz RW. Efficacy of nocturnal nasal ventilation in stable, severe chronic obstructive pulmonary disease during a 3-month controlled trial. *Mayo Clin Proc*. 1996;71(6):533–542. doi:10.4065/71.6.533

42. Hedsund C, Linde Ankjærgaard K, Peick Sonne T, et al. Long-term non-invasive ventilation for COPD patients following an exacerbation with acute hypercapnic respiratory failure: A randomized controlled trial. *Eur Clin Respir J*. 2023;10(1):2257993. doi:10.1080/20018525.2023.2257993
43. Jing G, Li J, Hao D, et al. Comparison of high flow nasal cannula with noninvasive ventilation in chronic obstructive pulmonary disease patients with hypercapnia in preventing postextubation respiratory failure: A pilot randomized controlled trial. *Res Nurs Health*. 2019;42(3):217–225. doi:10.1002/nur.21942
44. Khilnani G, Saikia N, Banga A, Sharma S. Non-invasive ventilation for acute exacerbation of COPD with very high $PaCO_2$: A randomized controlled trial. *Lung India*. 2010;27(3):125. doi:10.4103/0970-2113.68308
45. Köhnlein T, Windisch W, Köhler D, et al. Non-invasive positive pressure ventilation for the treatment of severe stable chronic obstructive pulmonary disease: A prospective, multicentre, randomised, controlled clinical trial. *Lancer Respir Med*. 2014;2(9):698–705. doi:10.1016/S2213-2600(14)70153-5
46. Kramer N, Meyer TJ, Meharg J, Cece RD, Hill NS. Randomized, prospective trial of noninvasive positive pressure ventilation in acute respiratory failure. *Am J Respir Crit Care Med*. 1995;151(6):1799–1806. doi:10.1164/ajrccm.151.6.7767523
47. Liu L, Qui HB, Zheng RQ, Yang Y. Prospective randomized controlled clinical study of early use of noninvasive positive pressure ventilation in the treatment for acute exacerbation of chronic obstructive pulmonary disease [in Chinese]. *Zhongguo Wei Zhong Bing Ji Jiu Yi Xue*. 2005;17(8):477–480. PMID:16105426.
48. Liu A, Zhou Y, Pu Z. Effects of high-flow nasal cannula oxygen therapy for patients with acute exacerbation of chronic obstructive pulmonary disease in combination with type II respiratory failure. *J Int Med Res*. 2023;51(6):03000605231182558. doi:10.1177/03000605231182558
49. Majorski DS, Magnet FS, Thilemann S, Schmoor C, Windisch W, Schwarz SB. Portable NIV for patients with moderate to severe COPD: Two randomized crossover trials. *Respir Res*. 2021;22(1):123. doi:10.1186/s12931-021-01710-2
50. Márquez-Martín E, Ruiz FO, Ramos PC, López-Campos JL, Azcona BV, Cortés EB. Randomized trial of non-invasive ventilation combined with exercise training in patients with chronic hypercapnic failure due to chronic obstructive pulmonary disease. *Respir Med*. 2014;108(12):1741–1751. doi:10.1016/j.rmed.2014.10.005
51. Matuska P, Pilarová O, Merta Z, Skrická J. Non-invasive ventilation support in patients with acute exacerbation of chronic obstructive pulmonary disease (COPD) [in Czech]. *Vnitr Lek*. 2006;52(3):241–248. PMID:16722155.
52. McEvoy RD, Pierce RJ, Hillman D, et al. Nocturnal non-invasive nasal ventilation in stable hypercapnic COPD: A randomised controlled trial. *Thorax*. 2009;64(7):561–566. doi:10.1136/thx.2008.108274
53. Meecham Jones DJ, Paul EA, Jones PW, Wedzicha JA. Nasal pressure support ventilation plus oxygen compared with oxygen therapy alone in hypercapnic COPD. *Am J Respir Crit Care Med*. 1995;152(2):538–544. doi:10.1164/ajrccm.152.2.7633704
54. Murphy PB, Rehal S, Arbane G, et al. Effect of home noninvasive ventilation with oxygen therapy vs oxygen therapy alone on hospital readmission or death after an acute COPD exacerbation: A randomized clinical trial. *JAMA*. 2017;317(21):2177. doi:10.1001/jama.2017.4451
55. Plant PK, Owen JL, Elliott MW. Non-invasive ventilation in acute exacerbations of chronic obstructive pulmonary disease: Long term survival and predictors of in-hospital outcome. *Thorax*. 2001;56(9):708–712. doi:10.1136/thorax.56.9.708
56. Rezaei A, Fakharian A, Ghorbani F, Idani E, Abedini A, Jamaati H. Comparison of high-flow oxygenation with noninvasive ventilation in COPD exacerbation: A crossover clinical trial. *Clin Respir J*. 2021;15(4):420–429. doi:10.1111/crj.13315
57. Samaria JK. Need for mechanical ventilation and in-hospital mortality in patients of acute exacerbation of COPD (AECOPD) on conventional treatment versus noninvasive oositive airway pressure (NIPPV). In: *A41. CHRONIC Obstructive Pulmonary Disease Exacerbations: Epidemiology and Outcomes. American Thoracic Society 2010 International Conference, May 14-19, 2010; New Orleans, USA*. American Thoracic Society; 2010:A1515. doi:10.1164/ajrccm-conference.2010.181.1_MeetingAbstracts.A1515
58. Eman Shebl R, Abderaboh MM. Bi-level positive airway pressure ventilation for patients with stable hypercapnic chronic obstructive pulmonary disease. *Egypt J Chest Dis Tuberc*. 2015;64(2):395–398. doi:10.1016/j.ejcdt.2015.02.004
59. Sin DD, Wong E, Mayers I, et al. Effects of nocturnal noninvasive mechanical ventilation on heart rate variability of patients with advanced COPD. *Chest*. 2007;131(1):156–163. doi:10.1378/chest.06-1423
60. Struik FM, Sprooten RTM, Kerstjens HAM, et al. Nocturnal non-invasive ventilation in COPD patients with prolonged hypercapnia after ventilatory support for acute respiratory failure: A randomised, controlled, parallel-group study. *Thorax*. 2014;69(9):826–834. doi:10.1136/thoraxjnl-2014-205126
61. Strumpf DA, Millman RP, Carlisle CC, et al. Nocturnal positive-pressure ventilation via nasal mask in patients with severe chronic obstructive pulmonary disease. *Am Rev Respir Dis*. 1991;144(6):1234–1239. doi:10.1164/ajrccm/144.6.1234
62. Tan D, Walline JH, Ling B, et al. High-flow nasal cannula oxygen therapy versus non-invasive ventilation for chronic obstructive pulmonary disease patients after extubation: A multicenter, randomized controlled trial. *Crit Care*. 2020;24(1):489. doi:10.1186/s13054-020-03214-9
63. Tan D, Wang B, Cao P, et al. High flow nasal cannula oxygen therapy versus non-invasive ventilation for acute exacerbations of chronic obstructive pulmonary disease with acute-moderate hypercapnic respiratory failure: A randomized controlled non-inferiority trial. *Crit Care*. 2024;28(1):250. doi:10.1186/s13054-024-05040-9
64. Thys F, Roeseler J, Reynaert M, Liistro G, Rodenstein DO. Noninvasive ventilation for acute respiratory failure: A prospective randomised placebo-controlled trial. *Eur Respir J*. 2002;20(3):545–555. doi:10.1183/09031936.02.00287402
65. Tsolaki V, Pastaka C, Karetsi E, et al. One-year non-invasive ventilation in chronic hypercapnic COPD: Effect on quality of life. *Respir Med*. 2008;102(6):904–911. doi:10.1016/j.rmed.2008.01.003
66. Vargas F, Clavel M, Sanchez-Verlan P, et al. Intermittent noninvasive ventilation after extubation in patients with chronic respiratory disorders: A multicenter randomized controlled trial (VHYPER). *Intensive Care Med*. 2017;43(11):1626–1636. doi:10.1007/s00134-017-4785-1
67. Xiang PC, Zhang X, Yang JN, et al. The efficacy and safety of long term home noninvasive positive pressure ventilation in patients with stable severe chronic obstructive pulmonary disease [in Chinese]. *Zhonghua Jie He He Hu Xi Za Zhi*. 2007;30(10):746–750. PMID:18218204.
68. Zhou R, Chen P, Luo H, Xiang XD. Effects of noninvasive positive pressure ventilation on gas exchange and patients' transformation in chronic obstructive pulmonary disease and respiratory failure [in Chinese]. *Hunan Yi Ke Da Xue Xue Bao*. 2001;26(3):261–262. PMID:12536700.
69. Zhou LQ, Li XY, Guan LL, et al. Home noninvasive positive pressure ventilation with built-in software in stable hypercapnic COPD: A short-term prospective, multicenter, randomized, controlled trial. *Int J Chron Obstruct Pulmon Dis*. 2017;12:1279–1286. doi:10.2147/COPD.S127540
70. Dretzke J, Moore D, Dave C, et al. The effect of domiciliary noninvasive ventilation on clinical outcomes in stable and recently hospitalized patients with COPD: A systematic review and meta-analysis. *Int J Chron Obstruct Pulmon Dis*. 2016;11:2269–2286. doi:10.2147/COPD.S104238
71. Ambrosino N, Vagheggini G. Noninvasive positive pressure ventilation in the acute care setting: Where are we? *Eur Respir J*. 2008;31(4):874–886. doi:10.1183/09031936.00143507

Association of 41 circulating inflammatory factors, C-reactive protein, and procalcitonin with sepsis risk and 28-day mortality: A bidirectional Mendelian randomization and mediation analysis

Jinchan Peng[1,A], Liqun Li[2,B], Guangyao Wang[2,B], Jinxiu Wei[2,C], Bingbing Lei[1,C], Jinjing Tan[2,D], Lijian Liu[2,E], Sheng Xie[2,F]

[1] Department of Graduate School, Guangxi University of Chinese Medicine, Nanning, China
[2] Department of Gastroenterology and Critical Care Medicine, The First Affiliated Hospital of Guangxi University of Chinese Medicine, Nanning, China

A – research concept and design; B – collection and/or assembly of data; C – data analysis and interpretation;
D – writing the article; E – critical revision of the article; F – final approval of the article

Advances in Clinical and Experimental Medicine, ISSN 1899–5276 (print), ISSN 2451–2680 (online) *Adv Clin Exp Med*. 2026;35(1):45–55

Address for correspondence
Sheng Xie
E-mail: xsh6566@163.com

Funding sources
This work was supported by the Guangxi Science and Technology Department Project (grant No. Gui Ke AB23026098), the Guangxi Science and Technology Department Project (grant No. GZKJ2307), and the National Natural Science Foundation of China (grant No. 82305151).

Conflict of interest
None declared

Acknowledgements
The authors express their sincere gratitude to the researchers who generously shared the GWAS data used in this study.

Received on July 14, 2024
Reviewed on February 8, 2025
Accepted on March 20, 2025

Published online on January 5, 2026

Cite as
Peng J, Li L, Wang G, et al. Association of 41 circulating inflammatory factors, C-reactive protein, and procalcitonin with sepsis risk and 28-day mortality: A bidirectional Mendelian randomization and mediation analysis. *Adv Clin Exp Med*. 2026;35(1):45–55. doi:10.17219/acem/203155

DOI
10.17219/acem/203155

Abstract

Background. The precise causal relationship between circulating inflammatory factors and sepsis has not yet been fully elucidated.

Objectives. To identify biomarkers that enable earlier and more accurate diagnosis of sepsis.

Materials and methods. The causal relationships between 41 circulating inflammatory factors, C-reactive protein (CRP), and procalcitonin (PCT) with sepsis and 28-day sepsis-related mortality were evaluated using two-sample bidirectional Mendelian randomization (MR) analyses.

Results. This study revealed negative causal associations between genetically predicted circulating inflammatory factors–interleukin-6 (IL-6) (odds ratio [OR] = 0.923; 95% confidence interval [CI], 0.854–0.998; p = 0.044), RANTES (OR = 0.926; 95% CI, 0.862–0.994; p = 0.033), and macrophage inflammatory protein-1β (MIP1β) (OR = 0.957; 95% CI, 0.919–0.996; p = 0.032) – and the risk of sepsis. Furthermore, positive causal relationships were observed between CRP and sepsis (OR = 1.140; 95% CI: 1.055–1.232; p = 0.001), as well as between CRP and 28-day sepsis-related mortality (OR = 1.241; 95% CI: 1.034–1.489; p = 0.020). Platelet-derived growth factor-BB (PDGF-BB) levels were also elevated in sepsis (OR = 1.136; 95% CI: 1.003–1.286; p = 0.044). Mediation analysis indicated that CRP mediated the effects of IL-6 and RANTES on sepsis, accounting for 25.87% (OR = 0.980; 95% CI: 0.961–0.998) and 2.04% (OR = 1.002; 95% CI: 0.991–1.012) of the total effect, respectively. The robustness of these associations was confirmed through leave-one-out sensitivity analysis and funnel plots.

Conclusions. This study enhances our understanding of the mechanisms underlying sepsis and its associated mortality, and underscores the therapeutic potential of targeting inflammatory factors in its management.

Key words: C-reactive protein, procalcitonin, sepsis, Mendelian randomization analysis, circulating inflammatory factors

Highlights

- The study investigated causal relationships between 41 circulating inflammatory factors, including C-reactive protein (CRP) and procalcitonin (PCT) – and the risk of sepsis and 28-day sepsis-related mortality using Mendelian randomization analysis.
- Genetically predicted inflammatory mediators, including interleukin-6 (IL-6), RANTES, and macrophage inflammatory protein-1β (MIP-1β), showed negative causal associations with sepsis risk.
- Positive causal relationships were identified between CRP and both sepsis incidence and 28-day sepsis-associated mortality.
- Platelet-derived growth factor-BB (PDGF-BB) levels were found to be significantly elevated in patients with sepsis.
- CRP acted as a mediating factor linking IL-6 and RANTES to the development of sepsis, suggesting a key pathway in sepsis pathophysiology.

Background

Sepsis is a syndrome characterized by a systemic inflammatory response triggered by infection of the host with pathogenic agents such as bacteria, viruses, fungi, or parasites, and it is often secondary to trauma, burns or shock.[1–3] This condition frequently leads to dysfunction or failure of multiple organs, posing a serious threat to human life. It has been reported that the global burden of sepsis includes 48.9 million cases and 11 million sepsis-related deaths annually,[4] while the overall incidence of sepsis among intensive care unit (ICU) patients in Asian countries is 22.4%.

The 30-day mortality rate of sepsis is approx. 17.4%, while that of severe sepsis can reach 26%, and may rise to 32.6% in low- and middle-income countries.[5–7] Additionally, studies have reported that the incidence of sepsis can be as high as 38.6%, with mortality rates reaching 43.0% and continuing to increase at an alarming pace.[8–10] Sepsis remains a major focus in the field of critical and emergency medicine, underscoring the urgent need to deepen our understanding of its pathophysiology, improve prevention strategies, and strengthen therapeutic approaches.

Identifying the etiology of sepsis is essential for reducing its incidence and improving treatment outcomes. The physiological and pathological processes of sepsis are highly complex, but the systemic inflammatory response remains one of its core pathological mechanisms. An excessive inflammatory reaction can lead to organ dysfunction in sepsis. Numerous preclinical studies have demonstrated significant increases in the protein levels of interleukin 6 (IL-6) and tumor necrosis factor alpha (TNF-α) in the liver tissue of septic rats.[11]

Serum concentrations of TNF-α, IL-6 and IL-10 are markedly elevated in rats with sepsis.[12] In cellular models of sepsis, the secretion of IL-6, TNF-α and IL-1β increases sharply, amplifying the inflammatory response.[13,14] Clinical studies have confirmed these findings, demonstrating that procalcitonin (PCT) serves as a potential indicator of disease severity, whereas IL-6 is associated with the clinical progression of the syndrome.[15] Both PCT and C-reactive protein (CRP) are significantly upregulated in sepsis.[16] Moreover, increased IL-27 levels and decreased RANTES concentrations have been observed in neonates with sepsis.[17]

Observational studies often carry a risk of bias and false associations. The Mendelian randomization (MR) approach addresses this limitation by using genetic variants as instrumental variables (IVs) to infer causality. Mendelian randomization reduces confounding factors and bias, providing stronger evidence for causal relationships.[18,19] The two-sample MR method further minimizes distortion and interference by employing pooled statistical data from multiple studies. Moreover, this approach has been widely applied to improve causal inference through larger sample sizes and greater statistical power.

Objectives

To identify potential causal relationships and mediators between inflammatory factors and sepsis, this study employed a bidirectional MR design combined with mediation analysis. Additionally, the study aimed to provide guidance for the development of diagnostic and therapeutic strategies based on 41 circulating inflammatory factors (Table 1), as well as CRP and procalcitonin PCT, which may assist in the early diagnosis and treatment of sepsis.

Materials and methods

Research design

A genome-wide association study (GWAS) is a research approach used to identify genetic variants associated with specific diseases or traits. This method involves scanning the entire genome of a large number of individuals to detect genetic markers linked to the condition or

Table 1. Circulating inflammatory factors

Number	Inflammatory factors
1	interleukin 1β
2	interleukin 1-receptor antagonist
3	interleukin 2
4	interleukin 2-receptor antagonist
5	interleukin 4
6	interleukin 5
7	interleukin 6
8	interleukin 7
9	interleukin 8
10	interleukin 9
11	interleukin 10
12	interleukin 12p70
13	interleukin 13
14	interleukin 16
15	interleukin 17
16	interleukin 18
17	cutaneous T-cell attracting
18	stromal-cell-derived factor 1 alpha
19	regulated on activation, normal T cell expressed and secreted
20	macrophage inflammatory protein 1β
21	macrophage inflammatory protein 1α
22	monokine induced by interferon gamma
23	monocyte chemoattractant protein-3
24	monocyte chemoattractant protein-1
25	interferon γ-induced protein 10
26	growth-regulated protein α
27	eotaxin
28	beta-nerve growth factor
29	vascular endothelial growth factor
30	stem cell growth factor beta
31	stem cell factor
32	platelet-derived growth factor BB
33	macrophage colony stimulating factor
34	hepatocyte growth factor
35	granulocyte-colony stimulating factor
36	fibroblast growth factor basic
37	macrophage migration inhibitory factor
38	tumor necrosis factor-related apoptosis inducing ligand
39	tumor necrosis factor alpha
40	tumor necrosis factor beta
41	interferon gamma

characteristic of interest. The present study is based on the most recent and comprehensive GWAS datasets from large populations to investigate the causal relationships of CRP, PCT and 41 circulating inflammatory factors with sepsis and 28-day mortality.

To ensure the validity of the research findings, the IV model in MR must satisfy 3 key assumptions: 1) the genetic variants are strongly associated with the exposure variables; 2) the genetic variants are independent of confounding factors that may influence the results (e.g., smoking, diabetes); and 3) the genetic variants affect the outcome variables only through the exposure variables. The overall research process is illustrated in Fig. 1.

Collection of data on circulating inflammatory factors

Genetic instruments for the 41 circulating inflammatory factors were obtained from the most recent and comprehensive GWAS datasets, which combined summary statistics from 3 Finnish cohorts – the Cardiovascular Risk in Young Finns Study, FINRISK 1997, and FINRISK 2002 (n = 8,293);[20,21] 13 European-ancestry cohorts (n = 21,758);[22] and the Lothian Birth Cohort 1936 (n = 1,091).[23] The GWAS data on 41 circulating inflammatory factors involved a total of 31,142 individuals.

The GWAS data for CRP were obtained from the UK Biobank (n = 427,367) and the Cohorts for Heart and Aging Research in Genomic Epidemiology (CHARGE) consortium (n = 148,164), comprising a total of 575,531 participants.[24] The GWAS data for PCT were derived from 3,301 healthy participants from the INTERVAL study.[25]

Further details regarding genomic (GM) statistics are available in the original publications. As indicated in Supplementary Table 1, the IEU OpenGWAS project also provides access to the corresponding GWAS datasets.

Collection of sepsis datasets

The OpenGWAS database includes summary statistics for sepsis and sepsis-related 28-day mortality, obtained from the IEU OpenGWAS project, which is based on data from the UK Biobank.[26] This dataset comprises 11,643 sepsis patients of European ancestry and 474,841 controls, with a total of 12,243,539 SNP loci analyzed. Patients were classified as having confirmed sepsis according to the International Classification of Diseases (ICD-9 and ICD-10) codes.[4] Because data on circulating inflammatory factors and sepsis were obtained from different research projects, there was no sample overlap. As this study did not involve the collection of individual participant data, ethical approval was not required.

Selection of genetic instrumental variables

First, a strong correlation must exist between the exposure factors and the instrumental variables selected for analysis. To ensure adequate screening of instrumental variables, single-nucleotide polymorphisms (SNPs) with p-values below the genome-wide significance threshold (1×10^{-5}) were selected. Subsequently, the genetic distance

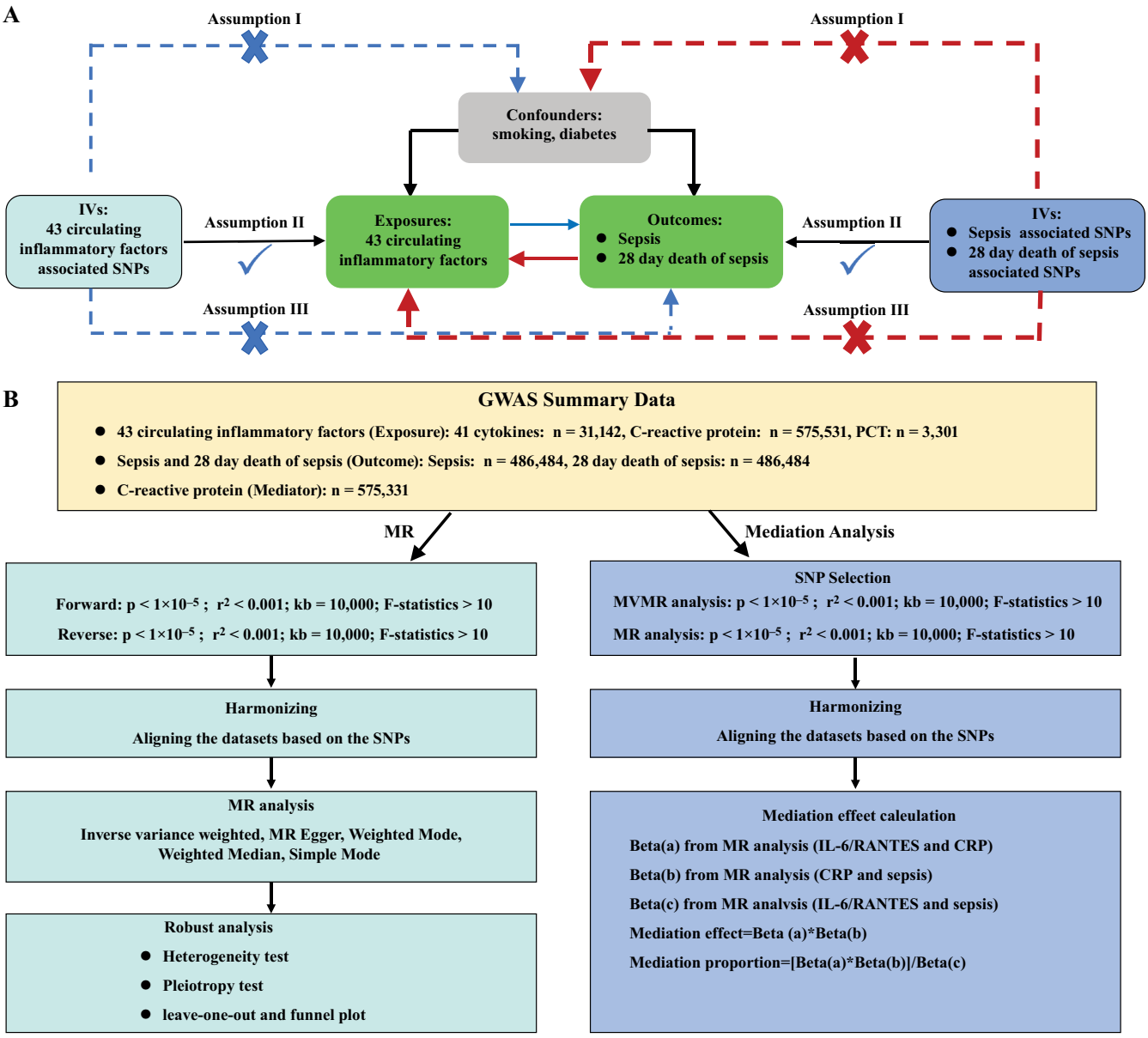

Fig. 1. The bidirectional Mendelian randomization (MR) and mediation analysis study of the associations between 41 circulating inflammatory factors, C-reactive protein (CRP), procalcitonin (PCT) and sepsis

was set to 10,000 kb, and the linkage disequilibrium (LD) parameter (R^2) for the SNPs was set to 0.001. Next, we calculated the F-statistic using the formula:

$$F = [(R^2/(1 - R^2)) \times (N - K - 1)/K]$$

Instrumental variables with F-values <10 were excluded to ensure a strong correlation between the exposure factors and IVs. Additionally, IVs showing associations with outcome variables at a p-value < 1.0×10^{-5} were removed. The Phenoscanner database[27] (http://www.phenoscanner.medschl.cam.ac.uk/) was used to identify and exclude potential confounding factors (e.g., smoking, diabetes) related to the IVs. Finally, the exposure and outcome datasets were harmonized to remove non-concordant SNPs, leaving the remaining SNPs as valid genetic instrumental variables.

Bidirectional MR analysis

A bidirectional MR approach was used to assess the causal relationships between circulating inflammatory factors and sepsis. Mendelian randomization analysis was performed using the inverse-variance weighted (IVW) method as the primary analytical strategy. The IVW approach combines all SNPs in a meta-analysis framework to generate a pooled causal estimate. Four additional complementary methods – MR-Egger, weighted mode, weighted median, and simple mode – were also applied. Sensitivity analyses were conducted using the MR-Egger and weighted median methods. When IVs account for at least half of the total weight in the analysis, the weighted median method provides robust and reliable causal estimates.

Pleiotropy was assessed and corrected using the MR-Egger intercept test. Heterogeneity among SNPs selected for each exposure variable was evaluated by calculating Cochran's Q statistic. The Mendelian Randomization Pleiotropy RESidual Sum and Outlier (MR-PRESSO) method was applied to detect outliers and provide corrected causal estimates. The p-value from the MR-Egger intercept test was used to assess the presence of pleiotropy among SNPs. A nonsignificant difference between Q and Q' ($p > 0.05$) indicated that the IVW model was more appropriate for the analysis. Sensitivity analyses, including the leave-one-out method and funnel plots, were conducted to evaluate the robustness of the results and identify potential outliers.

After Bonferroni correction for multiple comparisons, a p-value < 0.001 (0.05/43) was considered indicative of a strong causal relationship, whereas p-values between 0.001 and 0.05 were regarded as evidence of a general association. Reverse causality analyses were performed using MR, MR-PRESSO, and the TwoSampleMR package in R v. 4.3.1 (R Foundation for Statistical Computing, Vienna, Austria). The results were reported in accordance with the Strengthening the Reporting of Observational Studies in Epidemiology–Mendelian Randomization (STROBE-MR) guidelines (Supplementary Table 2).[28]

Mediation analysis

Mediation analysis is a statistical approach used to examine the mechanisms through which an independent variable (X) influences a dependent variable (Y) via a mediator (M). The objective is to determine whether the effect of X on Y is direct or occurs indirectly through M. This technique is particularly valuable for identifying the underlying pathways that explain relationships between variables. In this study, we applied a simple mediation model in which the independent variables (41 circulating inflammatory factors) influence the mediator (CRP), which in turn affects the dependent variables (sepsis and sepsis-related 28-day mortality).

The effects of the 41 circulating inflammatory factors on sepsis and sepsis-related 28-day mortality can be divided into direct and indirect components. The indirect effect represents the influence of these inflammatory factors on sepsis and 28-day mortality mediated through CRP, whereas the direct effect reflects their influence independent of CRP.[29] The proportion of the total effect explained by mediation was estimated by dividing the indirect effect by the overall effect and calculating the 95% confidence interval (95% CI) using the delta method.

Results

Selection of genetic IVs

We screened IVs for CRP, PCT and 41 circulating inflammatory factors and sepsis, respectively. Ultimately, 1,198 SNPs for inflammatory factor, 627 sepsis-associated SNPs, and 1,036 SNPs related to 28-day mortality of sepsis were included. The F-statistics of the genetic IVs that were strongly correlated with inflammatory factors were all greater than 10, indicating a low likelihood of bias influencing the estimates (Supplementary Tables 3,4).

Two-sample MR

Impacts of 41 circulating inflammatory factors, CRP, and PCT on sepsis

This study identified 2 causal correlations between CRP, PCT and 41 circulating inflammatory factors and the risk of sepsis (Fig. 2, Supplementary Table 3). Interleukin 6 (odds ratio (OR) = 0.923, 95% CI: 0.854–0.998; p = 0.044), RANTES (OR = 0.926, 95% CI: 0.862–0.994; p = 0.033), and macrophage inflammatory protein 1 beta (MIP1β) (OR = 0.957, 95% CI: 0.919–0.996; p = 0.032) were all related to the reduced risk of sepsis. Elevated CRP levels were positively associated with the risk of sepsis (OR = 1.140, 95% CI: 1.055–1.232; p = 0.001). Platelet-derived growth factor-BB (PDGFbb) noticeably increased in sepsis (OR = 1.136, CI: 1.003–1.286; p = 0.044). According to Cochran's Q test results, the selected SNPs did not exhibit significant heterogeneity (p > 0.05; Supplementary Table 5). Similarly, the MR-Egger intercept test indicated no evidence of pleiotropy or outliers (p > 0.05; Supplementary Table 5). Finally, the leave-one-out analysis confirmed the robustness of the results (Supplementary Fig. 1–5).

The influence of 41 circulating inflammatory factors, CRP, and PCT on the 28-day mortality of sepsis

The IVW results indicated that CRP, PCT and the 41 circulating inflammatory factors were causally associated with 28-day sepsis-related mortality (Fig. 3; Supplementary Table 4). Genetically predicted CRP was associated with an increased risk of 28-day sepsis mortality (OR = 1.241; 95% CI: 1.034–1.489; p = 0.020). Cochran's Q test results showed no significant heterogeneity among the selected SNPs (p > 0.05; Supplementary Table 6), and the MR-Egger intercept test revealed no evidence of pleiotropy or outliers (p > 0.05; Supplementary Table 6). Finally, the leave-one-out analysis and funnel plot confirmed the stability of the CRP results (Supplementary Fig. 11,12). The Bonferroni-corrected analysis revealed a strong association between CRP levels and the prevalence of sepsis, although this does not imply direct causation (OR = 1.140; 95% CI: 1.055–1.232; p = 0.001).

The mediating proportion of CRP in the relation between 41 circulating inflammatory factors and sepsis

We analyzed whether CRP acted as a mediator to strengthen the effects of 41 circulating inflammatory factors on sepsis. It was found that IL-6 and RANTES

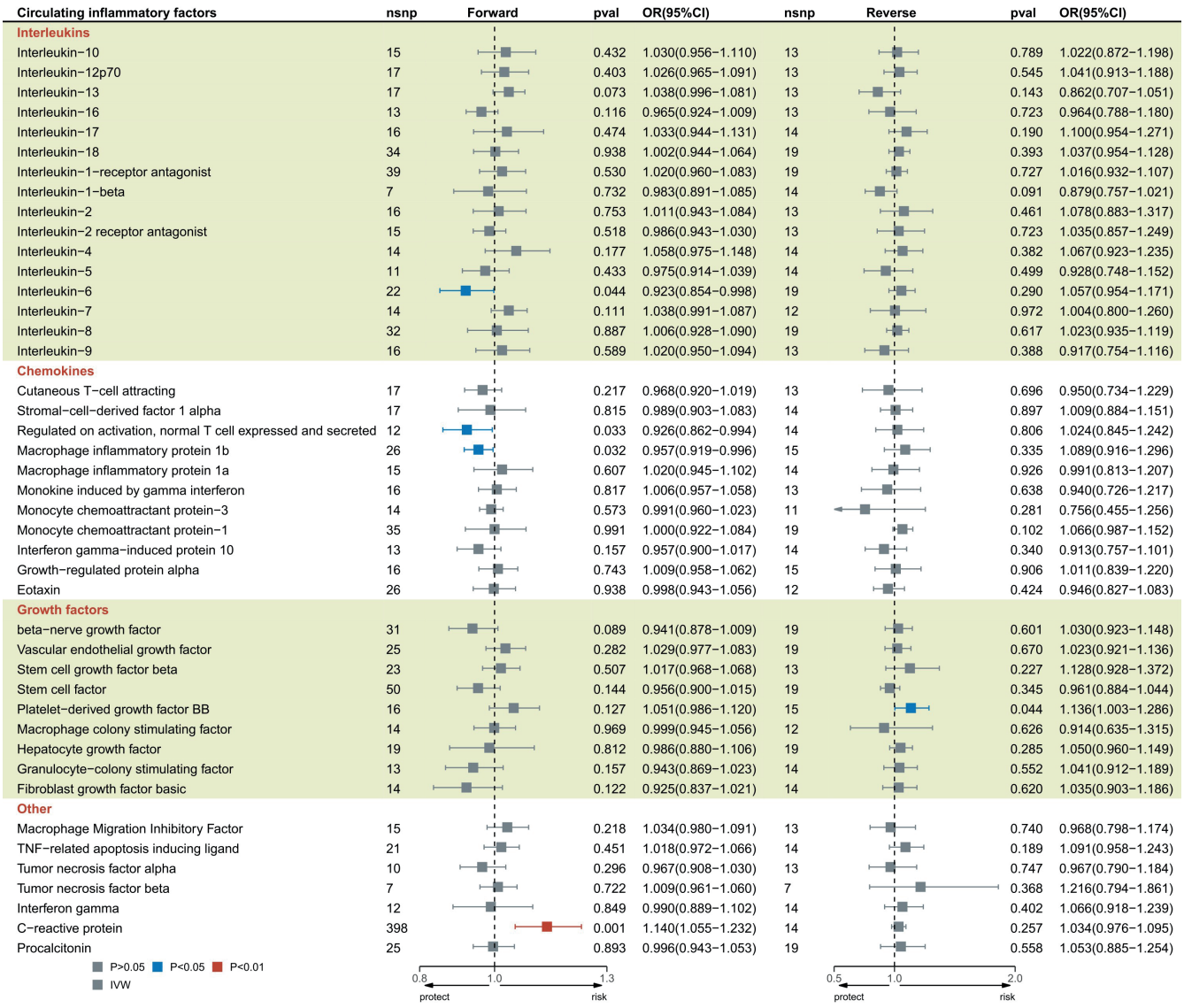

Fig. 2. Forest plot for 41 circulating inflammatory factors, C-reactive protein (CRP) and procalcitonin (PCT) on sepsis

OR – odds ratio; 95% CI – 95% confidence interval; IVW – inverse variance weighted.

were associated with elevated CRP, and in turn, elevated CRP correlated with an enhanced risk of sepsis. As presented in Supplementary Table 7, our research showed that the mediating proportion of CRP in IL-6-based prediction of sepsis was 25.87% (OR = 0.980, 95% CI: 0.961–0.998), and that of CRP in RANTES-based prediction of sepsis was 2.04% (OR = 1.002, 95% CI: 0.991–1.012).

Discussion

This research evaluated the causation between CRP, PCT and 41 circulating inflammatory factors and sepsis/28-day sepsis-associated mortality. Also, mediation analysis was utilized to reveal the mediators of their causal relationships. Important findings were obtained: IL-6, RANTES and MIP1β were protective factors for sepsis, while CRP was a risk factor for the onset and 28-day mortality of sepsis. No significant causal relationships were observed between 39 inflammatory factors – including IL-10, PCT and β-NGF – and sepsis or 28-day sepsis-related mortality. Sepsis was identified as the cause of elevated PDGFbb levels. The mediation analysis indicated that the CRP-mediated predictive contribution of IL-6 and RANTES to the onset of sepsis was 25.87% and 2.04%, respectively.

The abnormal production and regulation of inflammatory factors play a crucial role in the pathogenesis of sepsis. Imbalances in these mediators can trigger dysregulated immune responses, leading to an excessive inflammatory cascade. Interleukin 6 is produced rapidly and transiently during infection or trauma, contributing to host defense by promoting acute-phase responses, hematopoiesis and immune activation, thereby playing a key role in the inflammatory process.[30,31]

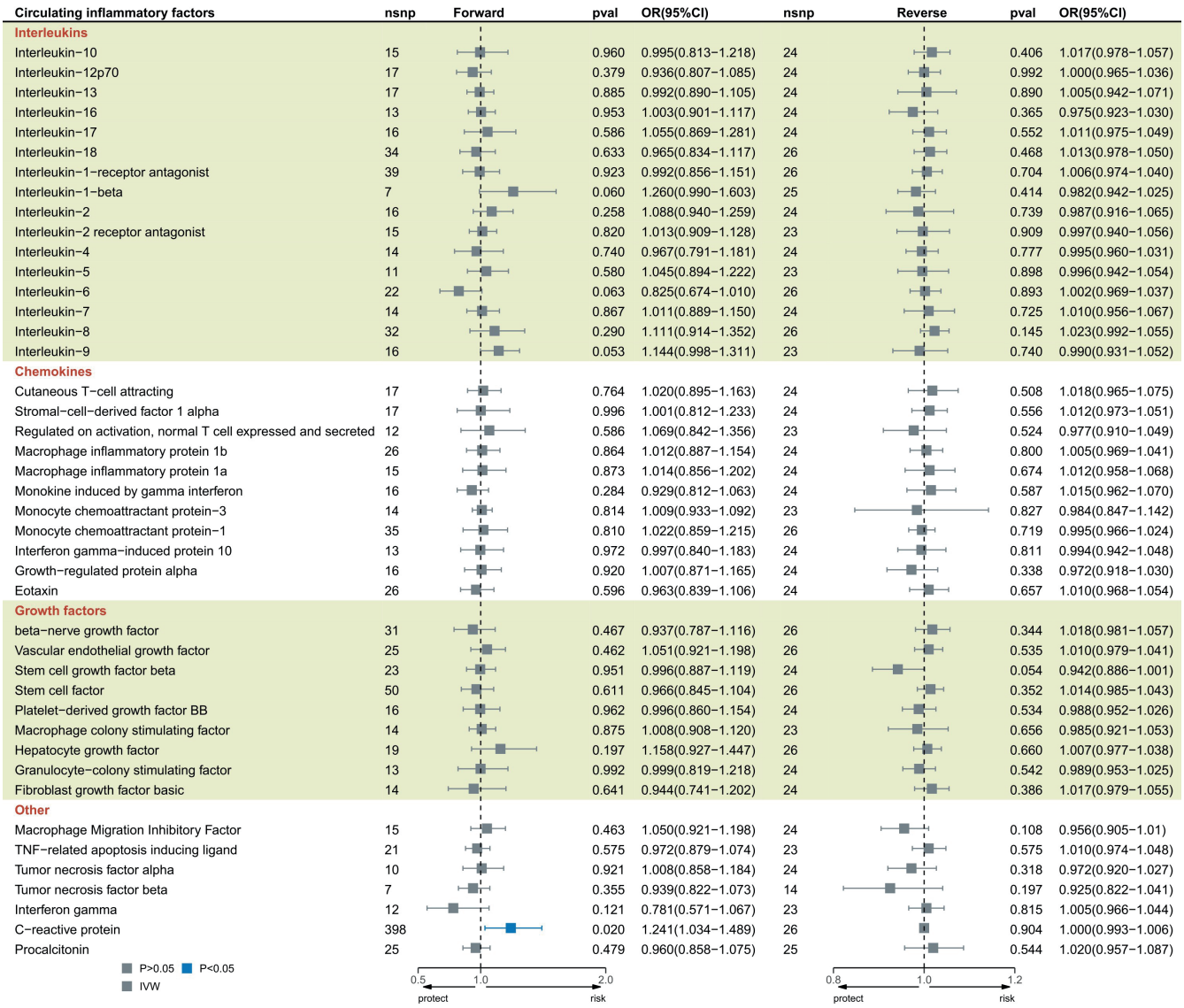

Fig. 3. Forest plot for 41 circulating inflammatory factors, C-reactive protein (CRP) and procalcitonin (PCT) on sepsis (28-day death)

OR – odds ratio; 95% CI – 95% confidence interval; IVW – inverse variance weighted.

Several previous studies have examined the relationship between IL-6 and sepsis. Clinical research has shown that IL-6 levels are elevated in septic patients admitted to the ICU,[32,33] and that IL-6 is strongly correlated with sepsis severity.[34] These findings suggest that IL-6 may serve as a potential biomarker for disease severity in sepsis. Elevated IL-6 levels may also indicate treatment response and prognosis.[35] This conclusion is further supported by animal studies.[36] Moreover, the combined measurement of TNF-α, IL-1β and IL-6 has demonstrated strong predictive value for sepsis-associated myocardial injury and is closely related to patient outcomes.[37]

However, our research findings did not support these conclusions. More studies are necessary in the future to elucidate the causation. While some studies have shown that IL-6 can have protective effects in specific contexts, such as protecting cardiomyocytes from oxidative stress at the early stage of lipopolysaccharide (LPS)-induced sepsis, it is important to note that literature and experimental results show that IL-6 is a complex marker with both pro-inflammatory and anti-inflammatory roles in sepsis. Given the complex and dual roles of IL-6 in sepsis, clinicians should interpret elevated IL-6 levels with caution.

RANTES is a chemokine involved in regulating cell migration, and its levels progressively increase during infection in patients with sepsis.[38,39] Elevated concentrations of RANTES have also been observed in plasma samples from cats with sepsis and septic shock.[40] A small-scale MR analysis previously reported that higher RANTES levels were associated with a reduced risk of sepsis,[2] indirectly supporting our findings that elevated RANTES concentrations may be protective. RANTES plays an important role in promoting inflammation and activating

other inflammatory mediators such as IL-6. It may serve as an early biomarker of inflammation, aiding in the early diagnosis and monitoring of sepsis. However, similar to CRP, these markers should be interpreted with caution.

Clinical evidence shows no noticeable correlation of MIP1β with the high risk of sepsis.[41] However, an opposite conclusion was proposed in another prospective and retrospective case-control study that MIP1β acted as a useful clinical marker in children with sepsis, distinguishing it from other febrile illnesses.[42] Another prospective clinical study also corroborated that MIP1β could be applied to distinguish patients with and without sepsis. Our MR analysis illustrated that MIP1β shared a negative causal association with sepsis and might have a protective impact on sepsis, which warrants verification. Mechanistically, MIP1β is a member of the chemokine family with chemotactic and pro-inflammatory properties. The release of MIP1β can activate TCC88 at the site of infection, enhancing the host's resistance to pathogens.[43] Future research should further investigate its causal role in sepsis, particularly its influence on inflammatory pathways, and large-scale clinical studies are needed to validate its prognostic significance.

C-reactive protein is an acute-phase protein synthesized in response to cytokine secretion.[44] Clinical observational studies have demonstrated that CRP possesses the highest diagnostic accuracy for sepsis[45,46] and serves as one of the most effective prognostic biomarkers for this condition,[47] making it valuable for predicting treatment outcomes in sepsis.[48]

This research supports our results that CRP is a significant risk factor and acts as a mediator for IL-6 and RANTES to predict 25.87% and 2.04% of sepsis, respectively. Although our study demonstrates a strong link between CRP levels and the prevalence of sepsis, it is important to note that CRP is not an ideal indicator of therapy effectiveness and can be influenced by factors other than infection, such as trauma, surgery, immune system dysregulation, and medications. Given the complexity of sepsis and the multifactorial nature of CRP elevation, further studies are necessary to elucidate the exact role of CRP in the pathogenesis and management of sepsis. This will help in developing more accurate diagnostic tools and therapeutic strategies.

It has been revealed that many inflammatory factors, including IL-1RA, IL-1β, IL-7, IL-4, IL-9, IL-10, IL-12, IL-13, IL-16, IL-17, and IL-18, are feasible serum biomarkers for sepsis and exert a significant predictive role in the prognosis of this disease.[2,36,37,41,42,49–52] CAP-1 and TNF-α levels are elevated in patients with sepsis.[36,49] While TNF-α is a key mediator of the inflammatory response in sepsis, genetic polymorphisms may influence individual susceptibility to its development.[53]

Studies have shown that sepsis is associated with granulocyte colony-stimulating factor (G-CSF) and monocyte chemoattractant protein-1 (MCP-1) levels, while severe sepsis-related mortality or sequelae are linked to reduced interferon gamma (IFN-γ) concentrations.[41] TRAIL levels are inversely correlated with sepsis severity,[54] whereas PCT, IP10 and HGF have been identified as potential serum biomarkers with high diagnostic value and strong prognostic utility in sepsis.[42,50,55] Serum vascular endothelial growth factor (VEGF) and stromal cell-derived factor 1 (SDF-1) are remarkably correlated with the survival rate of septic patients.[56,57] Additionally, previous MR analyses have reported a positive causal relationship between beta nerve growth factor (β-NGF) and sepsis.[2,3] However, in our study, 39 of the circulating inflammatory factors examined did not show significant causal associations.

The reverse MR analysis showed an increase in PDGFbb in sepsis. Previous clinical and preclinical research results supported our finding that the PDGFbb levels are significantly elevated in sepsis.[58] The mechanism of this correlation may be related to the inhibitory function of PDGFbb in immune cell activation and cytokine production. Platelet-derived growth factor-BB protects against sepsis by reducing the secretion of pro-inflammatory cytokines and chemokines.[58] This discovery suggests a potential role for PDGFbb in sepsis treatment. While our analysis suggests a potential role for PDGFbb in sepsis treatment, it is important to note that the current understanding of PDGFbb as a therapeutic target in sepsis is still in its early stages. Further studies are necessary to validate the therapeutic potential of PDGFbb and to explore its mechanisms of action in the context of sepsis.

To our knowledge, although previous studies have conducted two-sample MR analyses investigating the causal relationships between 41 circulating inflammatory factors and sepsis, our study offers distinct advantages and provides several novel and suggestive findings. Fang et al. used the MR approach to demonstrate that β-NGF increased the risk of sepsis, whereas RANTES and fibroblast growth factor (FGF) were associated with a reduced risk.[2] However, their study employed a two-sample unidirectional MR design and was limited by a relatively small GWAS sample size.

Lin et al. conducted a two-sample bidirectional MR study, demonstrating that the predicted circulating RANTES, basic-FGF and β-NGF levels were causally correlated with changes in the risk of sepsis.[3] However, these 2 MR analyses did not examine the association between inflammatory factors and sepsis-related mortality, nor did they perform mediation analysis.

Zhi et al. performed a bidirectional MR analysis of circulating inflammatory factors and 28-day sepsis-related mortality, revealing inverse associations between IL-10 and sepsis, as well as between MCP-1 and sepsis-related mortality. In contrast, elevated MIP1β concentrations showed a positive association with both the incidence and mortality of sepsis.[59] However, their study did not include mediation analysis. In contrast, our research

employed a bidirectional MR approach using the most recent and comprehensive GWAS datasets to investigate the risk of sepsis and 28-day mortality. Furthermore, we performed mediation analysis to identify potential mediators underlying the observed causal relationships. Notably, although previous MR analyses identified β-NGF and MCP-1 as significant factors, our results showed no significant causal associations between these 2 markers and the risk of sepsis or 28-day sepsis-related mortality. Meanwhile, CRP was identified as a significant predictor of sepsis onset and 28-day mortality, as well as the principal mediator through which IL-6 and RANTES influenced sepsis risk. In addition, PDGFbb emerged as a potential key therapeutic target for sepsis. Heterogeneity and pleiotropy were evaluated, and the results were rigorously tested using multiple sensitivity analyses, confirming the robustness and validity of our findings. C-reactive protein levels rise later than those of IL-6 and, therefore, are not an ideal indicator of therapeutic effectiveness. Although elevated CRP concentrations can indicate the presence of inflammation, they may also be influenced by non-infectious factors such as trauma, surgery or immune dysregulation. Our findings suggest a potential link between IL-6, RANTES, MIP1β, CRP, PDGFbb, and sepsis severity, but further studies are warranted to elucidate whether these biomarkers play a causative role in the progression of sepsis or if they are merely markers of the underlying disease process.

Limitations

The limitations should also be mentioned. First, because most of the participants recruited in GWAS are from Europe, this population restriction might limit the application of our findings to other populations. Second, although our findings identify the mediators and causal links between CRP, PCT and 41 circulating inflammatory factors and sepsis, the underlying mechanisms require more investigation.

Conclusions

We identified strong causal associations between IL-6, RANTES and MIP1β and the risk of sepsis. C-reactive protein showed a robust causal relationship with an increased risk of sepsis and was also associated with 28-day sepsis-related mortality. In contrast, 39 inflammatory factors, including IL-10, PCT and β-NGF, showed no significant causal relationships with sepsis risk or 28-day mortality. Platelet-derived growth factor-BB levels were elevated in septic patients. Moreover, CRP acted as a mediating factor in the effects of IL-6 and RANTES on sepsis. These findings may provide valuable insights for the early identification of sepsis and the development of potential therapeutic strategies.

Supplementary data

The supplementary materials are available at https://doi.org/10.5281/zenodo.15881855. The package includes the following files:

Supplementary Fig. 1. Leave-one-out sensitivity analysis for the effect of IL-6 on sepsis risk.

Supplementary Fig. 2. Leave-one-out sensitivity analysis for the effect of RANTES on sepsis risk.

Supplementary Fig. 3. Leave-one-out sensitivity analysis for the effect of MIP1β on sepsis risk.

Supplementary Fig. 4. Leave-one-out sensitivity analysis for the effect of CRP on sepsis risk.

Supplementary Fig. 5. Leave-one-out sensitivity analysis for the effect of sepsis on PDGF-BB levels.

Supplementary Fig. 6. Funnel plot assessing asymmetry in the MR estimates for the effect of IL-6 on sepsis risk.

Supplementary Fig. 7. Funnel plot assessing asymmetry in the MR estimates for the effect of RANTES on sepsis risk.

Supplementary Fig. 8. Funnel plot assessing asymmetry in the MR estimates for the effect of MIP1β on sepsis risk.

Supplementary Fig. 9. Funnel plot assessing asymmetry in the MR estimates for the effect of CRP on sepsis risk.

Supplementary Fig. 10. Funnel plot assessing asymmetry in the MR estimates for the effect of sepsis on PDGFbb levels.

Supplementary Fig. 11. Leave-one-out sensitivity analysis for the effect of CRP on sepsis (28-day death) risk.

Supplementary Fig. 12. Funnel plot assessing asymmetry in the MR estimates for the effect of CRP on sepsis (28-day death) risk.

Supplementary Table 1. Sources and details of the GWAS summary statistics used for CRP, PCT and 41 circulating inflammatory factors.

Supplementary Table 2. Analytical methods used for MR and mediation analysis.

Supplementary Table 3. Bidirectional MR estimating causal effects between circulating inflammatory factors and sepsis risk.

Supplementary Table 4. Bidirectional MR results estimating causal effects between circulating inflammatory factors and sepsis (28-day death).

Supplementary Table 5. Heterogeneity and horizontal pleiotropy assessments for MR analyses of circulating inflammatory factors on sepsis risk.

Supplementary Table 6. Heterogeneity and horizontal pleiotropy assessments for MR analyses of circulating inflammatory factors on sepsis (28-day death).

Supplementary Table 7. Two-step MR analysis quantifying mediation effects of IL-6 and RANTES on the relationship between CRP and sepsis risk.

Data Availability Statement

Summaries of sepsis and circulating inflammatory factors were acquired from the IEU OpenGWAS Project (https://gwas.mrcieu.ac.uk/) and OpenGWAS databases.

Consent for publication

Not applicable.

Use of AI and AI-assisted technologies

Not applicable.

ORCID iDs

Jinchan Peng https://orcid.org/0009-0002-3357-0002
Liqun Li https://orcid.org/0000-0002-0202-1951
Guangyao Wang https://orcid.org/0000-0001-7342-7644
Jinxiu Wei https://orcid.org/0000-0002-4446-390X
Bingbing Lei https://orcid.org/0009-0006-4467-6004
Jinjing Tan https://orcid.org/0009-0008-5339-0002
Lijian Liu https://orcid.org/0009-0006-0952-817X
Sheng Xie https://orcid.org/0000-0003-4276-3068

References

1. Singer M, Deutschman CS, Seymour CW, et al. The Third International Consensus Definitions for Sepsis and Septic Shock (Sepsis-3). *JAMA*. 2016;315(8):801. doi:10.1001/jama.2016.0287
2. Fang W, Chai C, Lu J. The causal effects of circulating cytokines on sepsis: A Mendelian randomization study. *PeerJ*. 2024;12:e16860. doi:10.7717/peerj.16860
3. Lin S, Mao X, He W. Causal association of circulating cytokines with sepsis: A Mendelian randomization study. *Front Immunol*. 2023;14: 1281845. doi:10.3389/fimmu.2023.1281845
4. Rudd KE, Johnson SC, Agesa KM, et al. Global, regional, and national sepsis incidence and mortality, 1990–2017: Analysis for the Global Burden of Disease Study. *Lancet*. 2020;395(10219):200–211. doi:10.1016/S0140-6736(19)32989-7
5. García-Rodríguez JF, Mariño-Callejo A. The factors associated with the trend in incidence of bacteraemia and associated mortality over 30 years. *BMC Infect Dis*. 2023;23(1):69. doi:10.1186/s12879-023-08018-0
6. Fleischmann C, Scherag A, Adhikari NKJ, et al. Assessment of global incidence and mortality of hospital-treated sepsis: Current estimates and limitations. *Am J Respir Crit Care Med*. 2016;193(3):259–272. doi:10.1164/rccm.201504-0781OC
7. Li A, Ling L, Qin H, et al. Epidemiology, management, and outcomes of sepsis in ICUs among countries of differing national wealth across Asia. *Am J Respir Crit Care Med*. 2022;206(9):1107–1116. doi:10.1164/rccm.202112-2743OC
8. Kiya GT, Mekonnen Z, Melaku T, et al. Prevalence and mortality rate of sepsis among adults admitted to hospitals in sub-Saharan Africa: A systematic review and meta-analysis. *J Hosp Infect*. 2024;144:1–13. doi:10.1016/j.jhin.2023.11.012
9. Ma Z, Jiang Z, Li H, et al. Prevalence, early predictors, and outcomes of sepsis in neurocritical illnesses: A prospective cohort study. *Am J Infect Control*. 2024;52(7):827–833. doi:10.1016/j.ajic.2024.01.017
10. Yang X, Man MY, Heng H, et al. Molecular epidemiology and clinical impact of *Klebsiella* spp. causing bloodstream infections in Hong Kong. *eBioMedicine*. 2024;101:104998. doi:10.1016/j.ebiom.2024.104998
11. Yang M, Liu Z, Xu Z, et al. Inhibition of Toll-like receptor 4 pathway by TAK242 protects the liver in sepsis [in Chinese]. *Zhonghua Wei Zhong Bing Ji Jiu Yi Xue*. 2022;34(8):814– 818. doi:10.3760/cma.j.cn121430-20220420-00395
12. Liu J, Li J, Tian P, et al. H2S attenuates sepsis-induced cardiac dysfunction via a PI3K/Akt-dependent mechanism. *Exp Ther Med*. 2019;17(5):4064–4072. doi:10.3892/etm.2019.7440
13. Ma F, Liu F, Ding L, et al. Anti-inflammatory effects of curcumin are associated with downregulating microRNA-155 in LPS-treated macrophages and mice. *Pharm Biol*. 2017;55(1):1263–1273. doi:10.1080/13880209.2017.1297838
14. Liu Z, Gao J, Ban Y, et al. Synergistic effect of paeoniflorin combined with luteolin in alleviating lipopolysaccharides-induced acute lung injury. *J Ethnopharmacol*. 2024;327:118022. doi:10.1016/j.jep.2024.118022
15. Ling H, Chen M, Dai J, Zhong H, Chen R, Shi F. Evaluation of qSOFA combined with inflammatory mediators for diagnosing sepsis and predicting mortality among emergency department. *Clin Chim Acta*. 2023;544:117352. doi:10.1016/j.cca.2023.117352
16. Zhang GM, Gu YY. Diagnostic value of procalcitonin, C-reactive protein-to-lymphocyte ratio (CLR), C-reactive protein and neutrophil-to-lymphocyte ratio (NLR) for predicting patients with bacteraemia in the intensive care unit. *J Crit Care*. 2024;81:154538. doi:10.1016/j.jcrc.2024.154538
17. Fahmy EM, Kamel NM, Abdelsadik A, et al. Assessment of interleukin-27 and chemokine RANTES as biomarkers for early onset neonatal sepsis. *Egypt J Immunol*. 2020;27(1):9–18. PMID:33180383.
18. Emdin CA, Khera AV, Kathiresan S. Mendelian randomization. *JAMA*. 2017;318(19):1925. doi:10.1001/jama.2017.17219
19. Walker VM, Zheng J, Gaunt TR, Smith GD. Phenotypic causal inference using genome-wide association study data: Mendelian randomization and beyond. *Annu Rev Biomed Data Sci*. 2022;5(1):1–17. doi:10.1146/annurev-biodatasci-122120-024910
20. Ahola-Olli AV, Würtz P, Havulinna AS, et al. Genome-wide association study identifies 27 loci influencing concentrations of circulating cytokines and growth factors. *Am J Hum Genet*. 2017;100(1):40–50. doi:10.1016/j.ajhg.2016.11.007
21. Kalaoja M, Corbin LJ, Tan VY, et al. The role of inflammatory cytokines as intermediates in the pathway from increased adiposity to disease. *Obesity*. 2021;29(2):428–437. doi:10.1002/oby.23060
22. Folkersen L, Gustafsson S, Wang Q, et al. Genomic and drug target evaluation of 90 cardiovascular proteins in 30,931 individuals. *Nat Metab*. 2020;2(10):1135–1148. doi:10.1038/s42255-020-00287-2
23. Hillary RF, Trejo-Banos D, Kousathanas A, et al. Multi-method genome- and epigenome-wide studies of inflammatory protein levels in healthy older adults. *Genome Med*. 2020;12(1):60. doi:10.1186/s13073-020-00754-1
24. Said S, Pazoki R, Karhunen V, et al. Genetic analysis of over half a million people characterises C-reactive protein loci. *Nat Commun*. 2022;13(1):2198. doi:10.1038/s41467-022-29650-5
25. Sun BB, Maranville JC, Peters JE, et al. Genomic atlas of the human plasma proteome. *Nature*. 2018;558(7708):73–79. doi:10.1038/s41586-018-0175-2
26. Hamilton FW, Thomas M, Arnold D, et al. Therapeutic potential of IL6R blockade for the treatment of sepsis and sepsis-related death: A Mendelian randomisation study. *PLoS Med*. 2023;20(1):e1004174. doi:10.1371/journal.pmed.1004174
27. Wang E, Zhao H, Zhao D, Li L, Du L. Functional prediction of chronic kidney disease susceptibility gene *PRKAG2* by comprehensively bioinformatics analysis. *Front Genet*. 2018;9:573. doi:10.3389/fgene.2018.00573
28. Skrivankova VW, Richmond RC, Woolf BAR, et al. Strengthening the Reporting of Observational Studies in Epidemiology Using Mendelian Randomization: The STROBE-MR Statement. *JAMA*. 2021;326(16):1614. doi:10.1001/jama.2021.18236
29. Carter AR, Sanderson E, Hammerton G, et al. Mendelian randomisation for mediation analysis: Current methods and challenges for implementation. *Eur J Epidemiol*. 2021;36(5):465–478. doi:10.1007/s10654-021-00757-1
30. Tanaka T, Narazaki M, Kishimoto T. IL-6 in inflammation, immunity, and disease. *Cold Spring Harb Perspect Biol*. 2014;6(10):a016295-a016295. doi:10.1101/cshperspect.a016295
31. Unver N, McAllister F. IL-6 family cytokines: Key inflammatory mediators as biomarkers and potential therapeutic targets. *Cytokine Growth Factor Rev*. 2018;41:10–17. doi:10.1016/j.cytogfr.2018.04.004
32. Nader D, Abdelmaseeh M, Al Sharif R, Samir N. Serum level of microRNA 15a and interleukin 6 as biomarkers for sepsis in critically ill patients. *Egypt J Immunol*. 2023;30(3):162–170. PMID:37440665.
33. Jiang S, Shi D, Bai L, Niu T, Kang R, Liu Y. Inhibition of interleukin-6 trans-signaling improves survival and prevents cognitive impairment in a mouse model of sepsis. *Int Immunopharmacol*. 2023;119:110169. doi:10.1016/j.intimp.2023.110169
34. Cao Z, Wu M, Li Y, et al. Predictive effect of combined procalcitonin, interleukin-6 and antithrombin III on the severity and prognosis of patients with sepsis [in Chinese]. *Zhonghua Wei Zhong Bing Ji Jiu Yi Xue*. 2023;35(10):1033–1038. doi:10.3760/cma.j.cn121430-20221114-00981

35. Palalıoğlu B, Erdoğan S, Atay G, Tugrul H, Özer Ö. Diagnostic and prognostic value of pentraxin 3, interleukin-6, CRP, and procalcitonin levels in patients with sepsis and septic shock. *Niger J Clin Pract*. 2024;27(3):317–324. doi:10.4103/njcp.njcp_615_23
36. Cao YZ, Tu YY, Chen X, Wang BL, Zhong YX, Liu MH. Protective effect of ulinastatin against murine models of sepsis: Inhibition of TNF-α and IL-6 and augmentation of IL-10 and IL-13. *Exp Toxicol Pathol*. 2012;64(6):543–547. doi:10.1016/j.etp.2010.11.011
37. Deng P, Tang N, Li L, Zou G, Xu Y, Liu Z. Diagnostic value of combined detection of IL-1β, IL-6, and TNF-α for sepsis-induced cardiomyopathy. *Med Clin (Barc)*. 2022;158(9):413–417. doi:10.1016/j.medcli.2021.04.025
38. Stojewska M, Wąsek-Buko M, Jakub B, et al. Evaluation of serum chemokine RANTES concentration as a biomarker in the diagnosis of early-onset severe infections in neonates. *Postepy Hig Med Dosw*. 2016;70:272–279. doi:10.5604/17322693.1198990
39. Cavalcanti NV, Torres LC, Da Matta MC, et al. Chemokine patterns in children with acute bacterial infections. *Scand J Immunol*. 2016;84(6):338–343. doi:10.1111/sji.12492
40. Troia R, Mascalzoni G, Agnoli C, Lalonde-Paul D, Giunti M, Goggs R. Cytokine and chemokine profiling in cats with sepsis and septic shock. *Front Vet Sci*. 2020;7:305. doi:10.3389/fvets.2020.00305
41. Leal YA, Álvarez-Nemegyei J, Lavadores-May AI, Girón-Carrillo JL, Cedillo-Rivera R, Velazquez JR. Cytokine profile as diagnostic and prognostic factor in neonatal sepsis. *J Matern Fetal Neonatal Med*. 2019;32(17):2830–2836. doi:10.1080/14767058.2018.1449828
42. Frimpong A, Owusu EDA, Amponsah JA, et al. Cytokines as potential biomarkers for differential diagnosis of sepsis and other non-septic disease conditions. *Front Cell Infect Microbiol*. 2022;12:901433. doi:10.3389/fcimb.2022.901433
43. Naghavian R, Faigle W, Oldrati P, et al. Microbial peptides activate tumour-infiltrating lymphocytes in glioblastoma. *Nature*. 2023;617(7962):807–817. doi:10.1038/s41586-023-06081-w
44. Plebani M. Why C-reactive protein is one of the most requested tests in clinical laboratories? *Clin Chem Lab Med*. 2023;61(9):1540–1545. doi:10.1515/cclm-2023-0086
45. Goyal M, Mascarenhas D, Rr P, Haribalakrishna A. Diagnostic accuracy of point-of-care testing of C-reactive protein, interleukin-6, and procalcitonin in neonates with clinically suspected sepsis: A prospective observational study. *Med Princ Pract*. 2024;33(3):291–298. doi:10.1159/000536678
46. Cui N, Zhang YY, Sun T, Lv XW, Dong XM, Chen N. Utilizing procalcitonin, C-reactive protein, and serum amyloid A in combination for diagnosing sepsis due to urinary tract infection. *Int Urol Nephrol*. 2024;56(7):2141–2146. doi:10.1007/s11255-024-03959-0
47. Tocu G, Mihailov R, Serban C, Stefanescu BI, Tutunaru D, Firescu D. The contribution of procalcitonin, C-reactive protein and interleukin-6 in the diagnosis and prognosis of surgical sepsis: An observational and statistical study. *J Multidiscip Healthc*. 2023;16:2351–2359. doi:10.2147/JMDH.S422359
48. Jimoh A, Bolaji O, Adelekan A, et al. Clinical utility of procalcitonin and C-reactive protein in the management of neonatal sepsis in a resource-limited Nigerian hospital. *Niger J Clin Pract*. 2023;26(12):1895–1901. doi:10.4103/njcp.njcp_397_23
49. Li G, Yang Z, Yang C, et al. Single-cell RNA sequencing reveals cell–cell communication and potential biomarker in sepsis and septic shock patients. *Int Immunopharmacol*. 2024;132:111938. doi:10.1016/j.intimp.2024.111938
50. Zhang W, Wang W, Hou W, et al. The diagnostic utility of IL-10, IL-17, and PCT in patients with sepsis infection. *Front Public Health*. 2022;10:923457. doi:10.3389/fpubh.2022.923457
51. Eidt MV, Nunes FB, Pedrazza L, et al. Biochemical and inflammatory aspects in patients with severe sepsis and septic shock: The predictive role of IL-18 in mortality. *Clin Chim Acta*. 2016;453:100–106. doi:10.1016/j.cca.2015.12.009
52. Froeschle GM, Bedke T, Boettcher M, Huber S, Singer D, Ebenebe CU. T cell cytokines in the diagnostic of early-onset sepsis. *Pediatr Res*. 2021;90(1):191–196. doi:10.1038/s41390-020-01248-x
53. Georgescu AM, Banescu C, Azamfirei R, et al. Evaluation of TNF-α genetic polymorphisms as predictors for sepsis susceptibility and progression. *BMC Infect Dis*. 2020;20(1):221. doi:10.1186/s12879-020-4910-6
54. Yoo H, Lee JY, Park J, Yang JH, Suh GY, Jeon K. Association of plasma level of TNF-related apoptosis-inducing ligand with severity and outcome of sepsis. *J Clin Med*. 2020;9(6):1661. doi:10.3390/jcm9061661
55. Peng F, Liang C, Chang W, et al. Prognostic significance of plasma hepatocyte growth factor in sepsis. *J Intensive Care Med*. 2022;37(3):352–358. doi:10.1177/0885066621993423
56. Patry C, Stamm D, Betzen C, et al. CXCR-4 expression by circulating endothelial progenitor cells and SDF-1 serum levels are elevated in septic patients. *J Inflamm (Lond)*. 2018;15(1):10. doi:10.1186/s12950-018-0186-7
57. Siavashi V, Asadian S, Taheri-Asl M, Keshavarz S, Zamani-Ahmadmahmudi M, Nassiri SM. Endothelial progenitor cell mobilization in preterm infants with sepsis is associated with improved survival. *J Cell Biochem*. 2017;118(10):3299–3307. doi:10.1002/jcb.25981
58. Wang M, Wei J, Shang F, Zang K, Ji T. Platelet-derived growth factor B attenuates lethal sepsis through inhibition of inflammatory responses. *Int Immunopharmacol*. 2019;75:105792. doi:10.1016/j.intimp.2019.105792
59. Zhi F, Ma JW, Ji DD, Bao J, Li QQ. Causal associations between circulating cytokines and risk of sepsis and related outcomes: A two-sample Mendelian randomization study. *Front Immunol*. 2024;15:1336586. doi:10.3389/fimmu.2024.1336586

Effects of a cystic artery–first Calot's triangle laparoscopic approach versus conventional laparoscopic cholecystectomy on therapeutic efficacy and complications in acute cholecystitis

Qiang Wu[A–F], Yin Fang[B,C], Lei Wang[B,C,E], Hao Wu[B,C,E], Lai-Zhi Yang[A–F]

Department of Emergency Surgery, The First People's Hospital of Wuhu, China

A – research concept and design; B – collection and/or assembly of data; C – data analysis and interpretation;
D – writing the article; E – critical revision of the article; F – final approval of the article

Advances in Clinical and Experimental Medicine, ISSN 1899–5276 (print), ISSN 2451–2680 (online) *Adv Clin Exp Med*. 2026;35(1):57–64

Address for correspondence
Lai-Zhi Yang
E-mail: 15375689086@163.com

Funding sources
None declared

Conflict of interest
None declared

Received on June 30, 2024
Reviewed on December 13, 2024
Accepted on March 21, 2025

Published online on January 5, 2026

Abstract

Background. Acute cholecystitis (AC) is a common biliary disorder, most often caused by gallstones obstructing the cystic duct and leading to gallbladder inflammation.

Objectives. This study aimed to compare the therapeutic efficacy and complication rates of laparoscopic cholecystectomy (LC) performed using the Calot's triangle approach vs traditional LC techniques in the treatment of AC.

Materials and methods. A retrospective analysis was conducted on 120 patients diagnosed with AC, with 60 patients undergoing LC using the Calot's triangle approach (study group) and 60 patients treated with traditional LC techniques (control group). Surgical parameters, including operation time, intraoperative hemorrhage, postoperative recovery times, and 30-day postoperative complications were recorded. Intraoperative adhesion formation was evaluated through direct visualization and graded based on severity. Postoperative pain was assessed using the visual analogue scale (VAS).

Results. There was no statistically significant difference in the baseline characteristics between the 2 groups, confirming their comparability. The study group (Calot's triangle approach) demonstrated significantly shorter average operation time, postoperative exhaust time, and diet recovery time compared to the control group. Additionally, patients in the study group had significantly lower intraoperative bleeding, lower VAS pain scores at 24 h and 72 h postoperatively, and a lower overall complication rate compared to the control group ($p < 0.05$).

Conclusions. The LC Calot's triangle approach demonstrated shorter operation times and lower rates of certain complications compared with traditional LC techniques. However, the absence of statistically significant differences in some key outcomes highlights the need for further research to fully evaluate its clinical advantages and long-term benefits.

Key words: laparoscopic cholecystectomy, acute cholecystitis, Calot's triangle approach

Cite as
Wu Q, Fang Y, Wang L, Wu H, Yang LZ. Effects of a cystic artery–first Calot's triangle laparoscopic approach versus conventional laparoscopic cholecystectomy on therapeutic efficacy and complications in acute cholecystitis. *Adv Clin Exp Med*. 2026;35(1):57–64. doi:10.17219/acem/203217

DOI
10.17219/acem/203217

Highlights

- Laparoscopic Calot's triangle approach outperforms traditional laparoscopic cholecystectomy (LC) in acute cholecystitis by directly targeting critical anatomy for safer dissection.
- Calot's triangle technique cuts operative and recovery times significantly compared to standard LC methods.
- Lower rates of bile duct injuries and hemobilia are seen with the Calot's triangle LC approach, enhancing patient safety.
- Calot's triangle-guided LC improves surgical outcomes and accelerates recovery for acute cholecystitis patients.

Background

Acute cholecystitis (AC) is a common biliary disorder that typically results from obstruction or inflammation of the gallbladder caused by gallstones.[1] Patients commonly present with severe upper abdominal pain, nausea, vomiting, and fever. Without prompt intervention, AC may lead to serious complications, such as gallbladder perforation, abscess formation, or even pancreatitis.[2] Therefore, timely and effective treatment is essential for preserving the health and preventing disease progression in patients with AC.

Laparoscopic surgery is a minimally invasive surgical technique performed through small incisions located in the abdomen. Compared with traditional open surgery, laparoscopic surgery offers several advantages, including reduced tissue trauma, faster postoperative recovery, and fewer complications.[3] Laparoscopic cholecystectomy (LC) has been widely recognized as the standard treatment for AC. However, the selection of an appropriate surgical approach is critical to the success of the surgical procedure and the recovery of patients. Various surgical techniques are available for LC, including the conventional approach and the Calot-based approach (termed as Calot-guided LC in our present study).[4,5] Conventional LC techniques generally include the 4-port,[6], 3-port[7] and transumbilical single-port approaches.[8]

A comprehensive review of the literature on the efficacy and complications associated with the Calot-guided LC compared to conventional LC techniques, particularly in the context of AC, reveals distinct advantages and disadvantages for each method. Calot-guided LC enhances visualization of the cystic duct and artery, thereby reducing the risk of bile duct injuries.[9] Additionally, this approach decreases the need for conversion to open surgery by enabling more accurate anatomical identification and facilitating early recognition of anatomical variations that are crucial in preventing complications.[10] In contrast, conventional LC techniques benefit from greater familiarity and extensive clinical experience among surgeons, which may contribute to lower complication rates and shorter operative times, as they typically require less meticulous dissection compared with the Calot-guided approach.[10] However, despite improved visualization, Calot's triangle-guided LC still carries a risk of bile duct injuries, particularly in cases with significant inflammation or fibrosis, and may be associated with higher postoperative complication rates, such as bile leakage and infection, due to the complexity of the dissection.[10]

Conventional LC techniques also present a notable risk of bile duct injury and may result in a higher likelihood of conversion to open surgery when anatomical structures are difficult to identify.[10] Notably, early LC (ELC) is generally recognized as the optimal treatment for AC, with Calot-guided LC offering particular advantages in this setting due to its superior anatomical identification and reduced risk of bile duct injuries.[10,11] Moreover, performing ELC within 24 h of presentation is associated with lower complication rates compared to delayed surgery.[11] Overall, the surgeon's experience should guide the selection of surgical approach, the patient's condition, and the presence of inflammation or anatomical anomalies. Nonetheless, ELC remains the preferred treatment for AC, and the Calot-guided method may provide better intraoperative visualization and potentially fewer complications.

The LC Calot's triangle approach is a relatively new approach for LC, which emphasizes the delicate dissection and protection of the LC Calot's triangle structure to reduce complications such as common bile duct injury and thereby enhance surgical safety and success rates.[12] However, most of the current clinical studies have focused on the clinical outcomes of different Calot-based approaches or the comparison of outcomes between previous conventional LC techniques (such as the 3-port approach and 4-port approach). Fewer studies have been conducted on the comparison of conventional LC techniques and the Calot-guided LC.

Objectives

This study aimed to compare the efficacy and complication rate of conventional LC techniques and the Calot's triangle approach in the treatment of AC, with the goal of maximizing surgical success rates and improving postoperative recovery outcomes.

Materials and methods

General information

A single-center retrospective study protocol was conducted, enrolling patients diagnosed with AC who underwent elective cholecystectomy at the First People's Hospital of Wuhu (China) between December 2021 and October 2022. Patients were assigned to 2 groups. The study group was treated using a Calot-guided LC technique, which emphasized precise dissection within the anatomical landmarks of Calot's triangle to minimize the risk of injury to vital structures. The control group underwent conventional LC, which involved broader anatomical exposure without the targeted precision of the Calot-based technique. Group allocation was determined based on factors such as anatomical complexity and disease severity, allowing surgeons to select the most appropriate technique for each patient to optimize operative safety and outcomes. In this study, the Calot-based approach was defined as a laparoscopic technique focused on the precise identification and dissection of the anatomical structures within LC Calot's triangle, namely the cystic duct, cystic artery and common bile duct, to minimize the risk of injuries and complications during LC. In contrast, conventional LC included established methods such as the 3-port and 4-port techniques, which prioritized general exposure of the gallbladder and adjacent tissues without specific attention to detailed anatomical structures.

Based on a literature review, the postoperative visual analogue scale (VAS) score in the control group was 3.32 ±0.59, and it was expected to decrease by 1.22 in the study group; both of them had a similar standard deviation (SD). Additionally, $\alpha = 0.05$ (two-sided) and 90% power were set. According to the formula for calculating sample size $[N = (Z\alpha/2 + Z\beta)^2 \times (p1(1-p1) + p2(1-p2))/\delta^2]$, the sample size was calculated to be 90 cases. To account for a projected 15% loss to follow-up, a total of 120 patients were enrolled, with 60 in each group.

This study received approval from the Ethics Committee of the First People's Hospital of Wuhu (approval No. YYLL20230051), and patient privacy was strictly maintained to ensure data confidentiality and security. Prior informed consent was obtained from all participating patients and their families. The research team collected relevant clinical and laboratory data from all patients while ensuring the anonymization and confidentiality of all included cases. Data collection encompassed a range of parameters, including sex, age, disease duration, family history, comorbidities, gallbladder wall thickness, type of disease (simple, gangrenous, or suppurative), and routine blood parameters.

Inclusion and exclusion criteria

Cases were selected for inclusion based on the following criteria: 1) Patients with physical examination findings and imaging results that fulfilled the diagnostic criteria for AC, including those with acute attacks of chronic cholecystitis[13]; 2) Patients who required surgical intervention and met the clinical indications for LC following a thorough clinical evaluation[14]; 3) Only those with complete clinical data were considered for inclusion to ensure comprehensive analysis and reporting.[14]

Patients were excluded from the study based on the following criteria: 1) Patients who developed serious complications, such as gallbladder perforation, abscess formation or pancreatitis; 2) Patients with a history of open surgery that might have impacted the surgical approach or outcomes; 3) Patients with significant comorbidities, including severe cardiovascular disease, respiratory disease, malignant tumors, or immune system disorders; 4) Patients deemed suitable for LC but were intolerant to anesthesia; 5) Patients with a history of mental disorders or those who demonstrated poor compliance; 6) Patients with incomplete or insufficient clinical information that hindered a definitive diagnosis of AC or those deemed inappropriate for enrollment by other research teams.

Surgical techniques

Study group (LC Calot's triangle approach)

For the Calot-guided LC approach, 1 key criterion was the anatomical consideration, which included the presence of clear visualization of the Calot's triangle. This technique was typically favored in patients with identifiable anatomical landmarks in this region, allowing for safe dissection. Additionally, patients were required to have minimal or no prior surgical history that could lead to significant adhesions around the gallbladder or surrounding structures. The type and severity of AC also influenced the selection process. Patients presenting with uncomplicated AC, where the risk of biliary injury was lower, were often considered ideal candidates.

In the study group, LC was performed using the Calot's triangle approach, which focused on the precise identification and dissection of the anatomical structures within the Calot's triangle, specifically the cystic duct, cystic artery and common bile duct, to minimize the risk of injury to vital structures and reduce the incidence of intraoperative complications. Briefly, patients were placed in the supine position and underwent general anesthesia with endotracheal intubation. After routine disinfection and surgical draping, the surgical field was fully exposed. A 1-cm transverse incision was made at the lower edge of the umbilicus, and a pneumoperitoneum needle was inserted to establish pneumoperitoneum via CO_2 insufflation, with abdominal pressure maintained at 12–14 mm Hg (1 mm Hg = 0.133 kPa). The pneumoperitoneum needle was then removed, and a 10 mm trocar was inserted for the laparoscope.

A second 1-cm transverse incision was created 1 cm below the xiphoid process to insert a 10-mm trocar, through which an electrocautery hook was introduced. Additionally, a 5-mm

incision was made along the midclavicular line, 1 cm below the costal margin, and a 5-mm trocar was inserted to serve as the operation hole for a grasper. If severe adhesions were encountered, a 5-mm incision was established at the right anterior axillary line to function as a 4th port. Under laparoscopic visualization, the size of the gallbladder and its relationship with surrounding tissues were assessed. Adhesions were separated using a suction device, and Calot's triangle, along with the porta hepatis, were carefully dissected.

The serous layer of Calot's triangle was opened, followed by meticulous dissection of the cystic artery first, and then the cystic duct was identified. Once the anatomical relationship among the cystic artery, cystic duct, common bile duct, and common hepatic duct was confirmed, the cystic artery was prioritized for transection. After secondary confirmation of both the cystic artery and cystic duct, the cystic duct was subsequently clipped and transected. The gallbladder was excised and removed through the incision below the xiphoid process. Upon completion of the procedure, CO_2 was released from the abdominal cavity, and all incisions were closed with routine suturing techniques. The emphasis on precise dissection and preservation of anatomical structures within Calot's triangle differentiates this approach from more generalized dissection techniques.

Control group (conventional LC techniques)

The conventional LC techniques were selected based on specific clinical criteria. Anatomical challenges were a key consideration; for example, patients with a history of prior abdominal surgery or significant intra-abdominal scarring were more likely to require traditional approaches that provide broader surgical exposure. Additionally, patients suffering from severe or complicated AC, such as those with perforation or abscess formation, often necessitated the generalized exposure provided by traditional methods.

In the control group, LC was performed using conventional LC techniques, including both the 3-port and 4-port techniques. Unlike the LC Calot's triangle approach, these conventional LC techniques prioritized general exposure of the gallbladder and surrounding tissues without a specific focus on the precise dissection of Calot's triangle structures. The patients were positioned supine, and general anesthesia with endotracheal intubation was administered. Once a satisfactory level of muscle relaxation was achieved, an artificial pneumoperitoneum was established using the subumbilical closed technique, with an abdominal pressure maintained between 1.3 kPa and 2.0 kPa. Laparoscopic cholecystectomy was conducted through either the 3-port or 4-port approach, depending on the surgeon's assessment of the case. For the 3-port approach, a 10-mm trocar was inserted at the lower margin of the umbilicus for the laparoscope, while 2 additional 5-mm ports were placed – 1 below the xiphoid process and the other at the intersection of the right midclavicular line and the costal margin. For the 4-port approach, an additional 5-mm port was inserted 5 mm below the right anterior axillary line to assist in cases of severe adhesions.

During the procedure, the gallbladder was elevated, and general dissection was performed to expose the cystic duct and cystic artery. These structures were subsequently clipped and transected with Hem-o-lok clips. The gallbladder was then detached from the liver bed and retrieved through the umbilical incision. Hemostasis was secured, and routine subhepatic drainage was performed when indicated. Although conventional LC techniques also required identification of the cystic duct and cystic artery, they did not prioritize the same degree of precision in the dissection and preservation of Calot's triangle structures as was applied in the study group.

Observation indicators

Both groups received identical pre- and postoperative care. The following parameters were recorded for comparative analysis: operation time, intraoperative hemorrhage, conversion to open cholecystectomy, time to first postoperative flatus, time to diet resumption, postoperative length of stay, and 30-day postoperative complications.

Pain was evaluated using the VAS, where higher scores indicated more severe pain. The VAS scores were compared preoperatively and at 24 h and 72 h postoperatively.

The incidence of 30-day postoperative complications, including biliary leakage, hemobilia, bile duct injury, intestinal adhesion, and incision infection, was recorded.

Statistical analyses

Data analysis was conducted using IBM SPSS v. 22.0 (IBM Corp., Armonk, USA). The normality of continuous variables was assessed by the Shapiro–Wilk test. Data that conformed to a normal distribution were expressed as mean ±SD, and differences between the 2 groups were analyzed using the independent samples Student's t-test. Data that did not follow a normal distribution were presented as median with interquartile range (IQR; M (25%, 75%)), and differences between the 2 groups were analyzed using the Mann–Whitney U test. Differences among 3 or more related samples were analyzed using Friedman's test for nonparametric repeated measures. Categorical data were reported as counts and percentages (n (%)) and statistically analyzed using Pearson's χ^2 test of independence with Yates's continuity correction. The significance level was set at $p < 0.05$ to establish statistical significance.

Results

Comparison of baseline data

A total of 120 patients with AC were included in this study. All patients were randomly divided into 2 groups and

underwent LC using either the Calot-guided LC technique or conventional LC techniques. Results from the Shapiro–Wilk test assessing the normality of continuous variables are shown in Supplementary Table 1. The baseline characteristics of both groups are presented in Table 1. No statistically significant differences were found between groups in terms of sex, age, disease duration, family history, comorbidities, type of disease, gallbladder wall thickness, white blood cell count, hemoglobin, and platelet count (Pearson's χ^2 test/Mann–Whitney U test/independent samples Student's t-test: $p > 0.05$), indicating comparability for subsequent analyses.

Comparison of surgery status

The surgical status of the 2 groups is shown in Table 2. The results of whether the continuous variables conformed to a normal distribution were shown in Supplementary Table 2. Compared with conventional LC, the Calot-guided technique was associated with significantly shorter operation time, reduced intraoperative blood loss and earlier postoperative recovery, including shorter times to first flatus and diet resumption (Mann–Whitney U test/independent samples Student's t-test: $p < 0.001$). At the 30-day follow-up, the LC Calot's triangle approach had 3 readmissions (5.0%, 3/60), whereas the conventional LC techniques had 6 (10.0%, 6/60). There were no significant differences in readmission rates (Pearson's χ^2 test of independence with Yates's continuity correction: $p = 0.488$), conversion to open cholecystectomy (Pearson's χ^2 test of independence with Yates's continuity correction: $p > 0.999$), and postoperative length of stay (Mann–Whitney U test: $p = 0.351$) between the groups. Overall, the Calot-guided LC demonstrated improved surgical outcomes, including reduced operation times and postoperative recovery metrics, without significant differences in readmission

Table 1. Comparison of baseline data between the 2 groups

Variable		Study group (n = 60)	Control group (n = 60)	df	χ^2/t/Z	p-value
Sex, n (%)	male	35 (58.3)	39 (65.0)	1	0.564	0.453
	female	25 (41.7)	21 (35.0)			
Age [years]		51.00 (34.50, 59.00)	50.00 (41.25,64.90)	–	–0.037	0.971
Disease duration [years]		4.50 (4.00, 5.00)	4.50 (4.00, 5.00)	–	–0.252	0.801
Family history, n (%)	no	47 (78.3)	44 (73.3)	1	0.409	0.522
	yes	13 (21.7)	16 (26.7)			
Comorbidities, n (%)	no	29 (48.3)	33 (55.0)	1	0.534	0.465
	yes	31 (51.7)	27 (45.0)			
Type of disease, n (%)	simple	28 (46.7)	26 (43.3)	2	0.622	0.733
	gangrenous	11 (18.3)	9 (15.0)			
	suppurative	21 (35.0)	25 (41.7)			
Gallbladder wall thickness [mm]		3.46 ±0.45	3.47 ±0.51	118	–0.146	0.884
White blood cell count [10^9/L]		12.79 ±3.57	12.50 ±3.36	118	0.464	0.644
Hemoglobin [g/L]		98.18 ±8.54	96.56 ±7.80	118	1.079	0.283
Platelet count [10^9/L]		154.61 ±15.51	158.66 ±14.26	118	–1.490	0.139

Data were expressed as n (%) or median (25%, 75%) or mean ± standard deviation; df – degrees of freedom.

Table 2. Comparison of surgery status in the 2 groups of patients

Variable		Study group (n = 60)	Control group (n = 60)	df	χ^2/t/Z	p-value
Operation time [min]		56.42 ±16.01	74.15 ±14.23	118	6.413	<0.001
Intraoperative hemorrhage [mL]		36.30 ±5.23	63.47 ±7.78	118	–22.455	<0.001
Postoperative exhaust time [h]		21.49 ±3.29	32.46 ±3.62	118	–17.391	<0.001
Diet recovery time [days]		4.00 (3.00, 5.00)	7.00 (6.00, 8.00)	–	–9.010	<0.001
Readmission, n (%)	yes	57 (95.0)	54 (90.0)	1	0.480	0.488
	no	3 (5.0)	6 (10.0)			
Conversion to open cholecystectomy, n (%)	yes	60 (100)	59 (98.3)	1	–	>0.999
	no	0 (0)	1 (1.7)			
Postoperative length of stay [days]		4.00 (3.00, 5.00)	4.00 (3.00, 5.00)	–	–0.952	0.341

Data were expressed as n (%) or median (25%, 75%) or mean ± standard deviation; df – degrees of freedom.

rates or conversion to open surgery compared to the conventional LC techniques.

Comparison of pain scores before and after surgery

Pre- and postoperative pains were evaluated using the VAS, with higher scores indicating more severe pain. Normality analysis revealed that pre- and postoperative VAS scores in both groups were non-normally distributed (Supplementary Table 3). Therefore, the Friedman test was employed for statistical analysis. Patients in the study group experienced significantly greater pain relief at both 24 h and 72 h postoperatively (degrees of freedom (df) = 2, Z = 187.995, p < 0.001) (Table 3), suggesting improved postoperative pain control in this group.

Comparison of postoperative complications

The incidence of biliary leakage and incision infection was slightly lower in the Calot-based approach (1 case and 2 cases, respectively) than in the conventional LC techniques (2 cases and 3 cases, respectively), although this difference was not statistically significant (Pearson's χ^2 test of independence with Yates's continuity correction: df = 1, p > 0.999). In contrast, subjects receiving Calot-guided LC exhibited a significantly lower incidence of hemobilia (0% vs 11.7%, Pearson's χ^2 test of independence with Yates's continuity correction: df = 1, p = 0.019), bile duct injury (1.7% vs 15%, Pearson's χ^2 test of independence with Yates's continuity correction: df = 1, p = 0.008) and intestinal adhesion (0% vs 10%, Pearson's χ^2 test of independence with Yates's continuity correction: df = 1, p = 0.036). The complication rate was significantly lower in the study group (6.7%) compared to the conventional LC group (26.7%) (Pearson's χ^2 test of independence with Yates's continuity correction: df = 1, p = 0.003) (Table 4). These findings suggested that the LC Calot's triangle approach may reduce the risk of postoperative complications, underscoring its potential advantages in terms of surgical safety and clinical efficacy.

Discussion

This study demonstrated that, compared with conventional LC techniques, the Calot-guided approach significantly improved key surgical outcomes, including shorter operative time, faster postoperative recovery duration, and a reduced incidence of specific complications such as bile duct injuries and hemobilia. Although no statistically significant differences were found in postoperative hospital stay or conversion rates to open surgery, these findings indicated that Calot's triangle approach might offer unique benefits in enhancing surgical safety and recovery for patients with AC. These benefits are especially evident in cases with minimal inflammation and clearly identifiable anatomical structures, highlighting the potential of Calot's triangle approach in supporting individualized treatment choices in clinical practice.

Acute cholecystitis is a common cause of abdominal emergencies, with LC being the standard of care. While conventional LC techniques – including the 4-port, 3-port and single-port methods – have been widely adopted, each comes with its own set of limitations. For example, although the 3-port method reduces the number of incisions, it still requires multiple entries, which can increase postoperative discomfort and visible scarring.[15,16] In contrast, the Calot-guided LC emphasizes precise dissection within Calot's triangle, facilitating safer identification of vital

Table 3. Comparison of pain scores before and after surgery in the 2 groups of patients

Groups	n	Before surgery	24 h after surgery	72 h after surgery	df	Z	p-value
Study group	60	6 (5, 7)	4 (3, 5)	2 (2, 3)	2	187.995	<0.001
Control group	60	6 (5, 7)	5 (4, 6)	3 (3, 4)			

Data were expressed as median (25%, 75%); df – degrees of freedom.

Table 4. Comparison of postoperative complications in the 2 groups of patients

Variable	Study group (n = 60)	Control group (n = 60)	df	χ^2	p-value
Biliary leakage (%)	1 (1.7)	2 (3.3)	1	0.000	>0.999
Incision infection (%)	2 (3.3)	3 (5.0)	1	0.000	>0.999
Hemobilia (%)	0 (0)	7 (11.7)	1	5.461	0.019
Bile duct injury (%)	1 (1.7)	9 (15.0)	1	6.982	0.008
Intestinal adhesion (%)	0 (0)	6 (10.0)	1	4.386	0.036
Total incidence (%)	4 (6.7)	16 (26.7)	1	8.640	0.003

Data were expressed as n (%); df – degrees of freedom.

anatomical structures, including the cystic artery, common bile duct and common hepatic artery.[17] Compared with conventional LC techniques, the Calot-guided LC emphasizes meticulous anatomical precision, potentially reducing intraoperative complications and improving patient outcomes.

Our findings align with previous research. Al-Rekabi et al.[14] demonstrated that isolating and clipping the cystic artery outside Calot's triangle minimized stapler-related injuries and improved bleeding control. Additionally, studies by Fateh et al. confirmed the benefits of Calot's triangle approach in reducing risks such as bile duct injury due to its emphasis on precise anatomical dissection.[18,19] However, unlike previous studies, our findings showed no statistically significant differences in conversion rates to open surgery or postoperative length of stay. These discrepancies may stem from variations in patient characteristics or the surgeon's level of experience. Furthermore, the Calot-guided approach may reduce the risk of gastrointestinal paralysis and bowel distension after surgery, thereby supporting faster restoration of intestinal function.[20] In addition, the overall incidence of complications was significantly lower in the study group compared to the control group in this study. A surgical strategy using the LC Calot's triangle approach emphasizes the fine dissection and protection of the structures surrounding the gallbladder, including the gallbladder artery and the common bile duct. As a result, the risk of postoperative complications such as bleeding and biliary leakage and consequent readmission can be reduced.[21] Cholecystitis and surgical trauma can trigger inflammatory and immune responses. Compared with conventional techniques, the Calot-based strategy may minimize tissue injury and allow for more refined dissection, thus attenuating inflammation, edema and associated complications.[22] Additionally, patients in the study group experienced significantly greater pain relief at both 24 h and 72 h after surgery, suggesting the advantages of the Calot-guided LC in postoperative pain management.

The lack of statistically significant differences in certain outcomes warrants further consideration. First, it is essential to determine whether the study was adequately powered to detect clinically meaningful differences, particularly in rare events such as conversion to open surgery. A post hoc power analysis based on the observed effect sizes could clarify whether the sample size was sufficient. Furthermore, while the benefits of the Calot-guided approach are evident in several aspects, its broader clinical impact should be interpreted in the context of existing literature and variability in practice. Comparison with previous studies evaluating alternative surgical techniques may offer valuable insights into the relative efficacy and safety of the Calot-guided LC approach, thereby supporting evidence-based clinical decision-making. Additionally, the challenges in patient selection and surgical execution inherent to each method might influence outcomes and warrant further exploration in future research.

Limitations

While our study aimed to demonstrate differences between Calot's triangle approach and conventional LC techniques in treating AC, it is essential to evaluate whether the study had sufficient statistical power to detect these differences across all measured outcomes. The initial sample size calculation was based on anticipated differences in postoperative pain scores between the 2 groups. However, for secondary outcomes such as conversion rates to open surgery and incidence of specific complications, the sample size may have been insufficient to identify smaller yet clinically significant effects. Conducting a post hoc power analysis could elucidate the potential limitations related to statistical power. Moreover, future studies with larger sample sizes are warranted to validate the observed trends with greater confidence. In addition, this study is subject to several inherent limitations, including its single-center setting, retrospective design, and lack of stratification based on surgeon experience. To comprehensively assess the relative efficacy and safety of these surgical approaches, future research should employ multicenter, prospective designs with standardized assessments of operator proficiency.

Conclusions

The findings of this study suggest that the LC Calot's triangle approach may provide significant benefits over conventional LC techniques, particularly in reducing operation time, expediting postoperative recovery, and minimizing specific complications like bile duct injuries and hemobilia. However, no statistically significant differences were observed in the conversion to open surgery, length of hospital stay or overall complication rates. These findings suggest that while the Calot-guided LC has distinct advantages, its broader clinical impact may vary based on surgeon experience and patient selection criteria. Further multicenter, prospective studies are needed to fully validate these findings and better assess the role of Calot's triangle approach in managing AC.

Supplementary data

The supplementary materials are available at https://doi.org/10.5281/zenodo.15381600. The package includes the following files:

Supplementary Table 1. The results of the normality test of baseline data.

Supplementary Table 2. The results of the normality test of surgery status.

Supplementary Table 3. The results of the normality test of pain scores.

Consent for publication

Not applicable.

Use of AI and AI-assisted technologies

Not applicable.

ORCID iDs

Qiang Wu https://orcid.org/0000-0003-3856-7945
Yin Fang https://orcid.org/0009-0008-0774-5925
Lei Wang https://orcid.org/0009-0007-9558-5150
Hao Wu https://orcid.org/0009-0003-2078-9686
Lai-zhi Yang https://orcid.org/0009-0002-9558-7694

References

1. Kurihara H, Binda C, Cimino MM, Manta R, Manfredi G, Anderloni A. Acute cholecystitis: Which flow-chart for the most appropriate management? *Digest Liver Dis*. 2023;55(9):1169–1177. doi:10.1016/j.dld.2023.02.005
2. Jacoby H, Rayman S, Oliphant U, et al. Current operative approaches to the diseased gallbladder: Diagnosis and management updates for general surgeons. *Am Surg*. 2024;90(1):122–129. doi:10.1177/00031348231198107
3. ElSherbiney M, Khawaja A, Noureldin K, Issa M, Varma A. Single incision laparoscopy versus conventional multiport laparoscopy for colorectal surgery: A systematic review and meta-analysis. *Ann R Coll Surg Engl*. 2023;105(8):709–720. doi:10.1308/rcsann.2022.0132
4. Timerbulatov MV, Grishina EE, Aitova LR, Aziev MM. Modern principles of safety in laparoscopic cholecystectomy [in Russian]. *Khirurgiia (Mosk)*. 2022;12:104. doi:10.17116/hirurgia2022121104
5. Vidrio Duarte R, Martínez Martínez AR, Ortega León LH, et al. Transillumination of Calot's triangle on laparoscopic cholecystectomy: A feasible approach to achieve a critical view of safety. *Cureus*. 2020;12(7):e9113. doi:10.7759/cureus.9113
6. Kartal K, Uludag M. Can 4-port laparoscopic cholecystectomy remain the gold standard for gallbladder surgery? *Ann Ital Chir*. 2016;87:13–17. PMID:27026289
7. Hassan I, Hassan L, Alsalameh M, Abdelkarim H, Hassan W. Cost-effective scarless cholecystectomy using a modified endoscopic minimally invasive reduced appliance technique (Emirate). *Front Surg*. 2023;10:1200973. doi:10.3389/fsurg.2023.1200973
8. Yang N, Tao QY, Niu JY, et al. Effect of a local anesthetic injection kit on pain relief and postoperative recovery after transumbilical single-incision laparoscopic cholecystectomy. *J Pain Res*. 2023;16:2791–2801. doi:10.2147/JPR.S422454
9. Ortenzi M, Corallino D, Botteri E, et al. Safety of laparoscopic cholecystectomy performed by trainee surgeons with different cholangiographic techniques (SCOTCH): A prospective non-randomized trial on the impact of fluorescent cholangiography during laparoscopic cholecystectomy performed by trainees. *Surg Endosc*. 2024;38(2):1045–1058. doi:10.1007/s00464-023-10613-w
10. Song J, Chen J, Zheng S. Lateral dorsal infundibular approach: An alternative option for the safe completion of difficult laparoscopic cholecystectomy. *BMC Surg*. 2022;22(1):439. doi:10.1186/s12893-022-01894-4
11. Mencarini L, Vestito A, Zagari RM, Montagnani M. The diagnosis and treatment of acute cholecystitis: A comprehensive narrative review for a practical approach. *J Clin Med*. 2024;13(9):2695. doi:10.3390/jcm13092695
12. Shinde J, Pandit S. Innovative approach to a frozen Calot's triangle during laparoscopic cholecystectomy. *Indian J Surg*. 2015;77(6):554–557. doi:10.1007/s12262-015-1354-0
13. Hernandez M, Murphy B, Aho JM, et al. Validation of the AAST EGS acute cholecystitis grade and comparison with the Tokyo guidelines. *Surgery*. 2018;163(4):739–746. doi:10.1016/j.surg.2017.10.041
14. Al-Rekabi AM. Isolation & clipping of cystic artery outside versus inside Calot's triangle minimizes the intraoperative complications in laparoscopic cholecystectomy. *Syst Rev Pharm*. 2020;11(10):123–127. https://www.sysrevpharm.org/articles/isolation--clipping-of-cystic-artery-outside-versus-inside-calots-triangle-minimizes-the-intraoperative-complications-in.pdf
15. Nip L, Tong KS, Borg CM. Three-port versus four-port technique for laparoscopic cholecystectomy: Systematic review and meta-analysis. *BJS Open*. 2022;6(2):zrac013. doi:10.1093/bjsopen/zrac013
16. Lin H, Zhang J, Li X, Li Y, Su S. Comparative outcomes of single-incision laparoscopic, mini-laparoscopic, four-port laparoscopic, three-port laparoscopic, and single-incision robotic cholecystectomy: A systematic review and network meta-analysis. *Updates Surg*. 2023;75(1):41–51. doi:10.1007/s13304-022-01387-2
17. Lin YR, Ding GF, Huo MX. The "Hand as Foot" teaching method in the Calot's triangle. *Asian J Surg*. 2022;45(11):2538–2539. doi:10.1016/j.asjsur.2022.05.142
18. Fateh O, Wasi MSI, Bukhari SA. Anaotmical variability in the position of cystic artery during laparoscopic visualization. *BMC Surg*. 2021;21(1):263. doi:10.1186/s12893-021-01270-8
19. Fu JN, Liu SC, Chen Y, Zhao J, Ma T. Analysis of risk factors for complications after laparoscopic cholecystectomy. *Heliyon*. 2023;9(8):e18883. doi:10.1016/j.heliyon.2023.e18883
20. Gupta R, Kumar A, Hariprasad CP, Kumar M. Anatomical variations of cystic artery, cystic duct, and gall bladder and their associated intraoperative and postoperative complications: An observational study. *Ann Med Surg (Lond)*. 2023;85(8):3880–3886. doi:10.1097/MS9.0000000000001079
21. Fujinaga A, Endo Y, Etoh T, et al. Development of a cross-artificial intelligence system for identifying intraoperative anatomical landmarks and surgical phases during laparoscopic cholecystectomy. *Surg Endosc*. 2023;37(8):6118–6128. doi:10.1007/s00464-023-10097-8
22. Sewefy AM, Elsageer EM, Kayed T, Mohammed MM, Taha Zaazou MM, Hamza HM. Nasobiliary guided laparoscopic cholecystectomy following endoscopic retrograde cholangiopancreatography, randomized controlled trial. *Surgeon*. 2023;21(4):230–234. doi:10.1016/j.surge.2022.06.003

ERa inhibits the progression of hepatocellular carcinoma by regulating the circRNA/miRNA/SMADs network

Changfeng Liu[A–D,F], Zujian Wu[B,C,E,F], Bing Zhang[B,C,E,F], Zhi Chen[A,E,F]

Department of Hepatobiliary and Pancreatic Surgery, Tongde Hospital of Zhejiang Province, Hangzhou, China

A – research concept and design; B – collection and/or assembly of data; C – data analysis and interpretation;
D – writing the article; E – critical revision of the article; F – final approval of the article

Advances in Clinical and Experimental Medicine, ISSN 1899–5276 (print), ISSN 2451–2680 (online) *Adv Clin Exp Med*. 2026;35(1):65–76

Address for correspondence
Zhi Chen
E-mail: ZhiCHenn_n@outlook.com

Funding sources
This work was supported by grants from the Zhejiang Province medical and health science and technology project (grant No. 2022KY699) and Chinese Medicine Research Program of Zhejiang Province (grants No. 2022ZB080 and No. GZY-ZJ-KJ-24060).

Conflict of interest
None declared

Received on September 23, 2024
Reviewed on December 24, 2024
Accepted on March 24, 2025

Published online on January 5, 2026

Abstract

Background. Hepatocellular carcinoma (HCC) shows significant differences in incidence and mortality between genders.

Objectives. This study investigates the mechanisms by which estrogen receptors (ER), specifically *ERa*, influence HCC outcomes.

Materials and methods. Bioinformatics approaches were used to study estrogen and its related pathways in relation to HCC. Estrogen receptor expression levels, along with downstream circular RNAs (circRNAs) and microRNAs (miRNAs), were measured in MHCC97H cells via quantitative reverse transcription polymerase chain reaction (RT-qPCR). Western blot was used to assess estrogen receptor 1 (*ESR1*) and SMAD family member 7 (*SMAD7*) protein expression. Cell proliferation, migration and cell cycle status of MHCC97H cells were measured using Cell Counting Kit-8 (CCK-8), Transwell assays and flow cytometry for cell cycle analysis.

Results. Bioinformatics analysis revealed that *ERa* acts as a transcription factor (TF) for 9 circRNAs with differential expression in HCC. We constructed the *ERa*/circRNA/miRNA/SMADs network based on the downstream targets of circRNAs, which were associated with the SMADs family. Survival studies revealed that *ESR1* is correlated with favorable patient survival in liver cancer. In MHCC97H cells, qRT-PCR findings showed low expression of *ESR1*, hsa_circ_0004913 and *SMAD7*, but significant expression of hsa-miR-96-5p. Overexpression of *ESR1* significantly increased the expression of hsa_circ_0004913 and *SMAD7* while suppressing hsa-miR-96-5p. Western blot analysis confirmed these findings. Furthermore, *ESR1* overexpression reduced MHCC97H cell proliferation and migration while inhibiting growth through G1 phase arrest. *ESR1* acts as a TF that binds to the promoter of hsa_circ_0004913, as demonstrated using chromatin Immunoprecipitation followed by chromatin immunoprecipitation-quantitative real-time PCR (ChIP-qPCR). A dual-luciferase reporter experiment confirmed that hsa_circ_0004913 targets and regulates hsa-miR-96-5p.

Conclusions. *ERa* can function as aTF, modulating the expression of various circRNAs with differential expression in HCC. Through this regulation, it modulates the circRNA/miRNA/SMADs network, thereby inhibiting the progression of HCC.

Key words: hepatocellular carcinoma, ceRNA network, transcription factor, estrogen receptor alpha, circular RNAs

Cite as
Liu C, Wu Z, Zhang B, Chen Z. *ERa* inhibits the progression of hepatocellular carcinoma by regulating the circRNA/miRNA/SMADs network. *Adv Clin Exp Med*. 2026;35(1):65–76. doi:10.17219/acem/203285

DOI
10.17219/acem/203285

Highlights

- *ERα* drives circRNA expression in hepatocellular carcinoma (HCC): Estrogen receptor α controls key differentially expressed circular RNAs, revealing new epigenetic regulators in HCC.
- *ESR1* overexpression inhibits HCC cell growth: Restoring *ESR1* function in MHCC97H liver cancer cells significantly reduces proliferation and migration.
- *ERα* modulates the circRNA/miRNA/SMAD signaling axis: This hormone receptor-driven network suppresses HCC development by coordinating noncoding RNA and SMAD pathways.
- hsa_circ_0004913 directly targets hsa-miR-96-5p: Dual-luciferase reporter assays validate this circRNA–miRNA interaction, highlighting a promising therapeutic target.

Background

Liver cancer was the 6th most common cancer worldwide in 2022 and the 3rd leading cause of cancer-related deaths, with hepatocellular carcinoma (HCC) accounting for 75–85% of cases.[1] The prognosis of HCC is closely associated with the stage of the disease. While advancements in targeted immunotherapy have improved survival rates in recent years, 2023 cancer statistics indicate that the 5-year survival rate for HCC remains low. Specifically, it is approx. 36% for early-stage cases and only 13% for advanced metastatic cases.[2] Furthermore, HCC ranks as the 2nd leading cause of cancer mortality among men. In most regions globally, the incidence and mortality rates of HCC are 2–3 times higher in men than in women.[1] Research has shown that the duration of estrogen exposure and the age at which HCC first appears are positively correlated, with a notable increase in HCC incidence observed among postmenopausal women.[3] Research by O'Brien et al. revealed a significant rise in HCC prevalence in female mice following ovariectomy. Additionally, female mice with knockout *ESR1* genes, which encode the estrogen receptor alpha (*ERα*), exhibited a 9-fold increase in HCC incidence. In contrast, the absence of the *ESR2* gene, encoding the estrogen receptor beta (*ERβ*), did not influence HCC development.[4] These findings suggest that the estrogen signaling pathway, mediated by *ERα*, could be a crucial target for HCC therapy. However, the exact mechanisms remain unclear, highlighting the need for further investigation into the role and regulatory pathways of the estrogen signaling system in HCC.

The circular RNAs (circRNAs) are evolutionarily conserved non-coding RNAs that form circular structures without 3' or 5' ends.[5] The unique closed-loop conformation of circRNAs imparts a higher degree of stability compared to most linear RNAs, and these molecules demonstrate significantly differential expression between malignant tissues and their adjacent non-malignant counterparts.[1] Unbalanced circRNA expression has been found as a possible biomarker for HCC diagnosis and treatment targeting.[6,7] Recent studies have shown that circRNAs can act as "gene sponges" for miRNAs, indirectly influencing the expression of miRNA target genes through competitive binding interactions.[8] MiRNAs are key regulators of gene expression at the post-transcriptional level, exerting their effects by base pairing with target sequences in the 3'UTR of messenger RNAs. They play an integral role in the pathogenesis of liver cancer.[9,10] Nevertheless, although these studies have elucidated the downstream regulatory mechanisms of circRNAs, the upstream regulatory mechanisms and the factors regulating circRNAs expression remain unclear. Wang et al. demonstrated that circCCDC66 was significantly elevated in non-small cell lung cancer, with *STAT3* directly interacting with the circCCDC66 promoter to enhance its transcriptional activity.[11] Our preliminary bioinformatics analysis suggests that *ERα* may serve as a transcription factor (TF) for several circRNAs that are differentially expressed in HCC tissues.

Objectives

Based on the above findings, we hypothesized that *ERα*, acting as a, regulates the production of circRNAs associated with HCC, thereby influencing its progression. The SMAD family plays an important role in the transition from liver fibrosis to HCC and has emerged as a prominent area of emphasis in liver cancer research.[12]

We employed bioinformatics methodologies to construct the *ERα*/circRNA/miRNA/SMADs network. A substantial body of evidence suggests that several coding and non-coding RNAs within this network, including hsa_circ_0004913, hsa-miR-96-5p and SMAD proteins, are involved in the development of HCC.[12–16]

SMAD7 acts as a suppressive element in HCC. A Kaplan–Meier analysis of HCC patients indicated that higher expression levels of *SMAD7* were associated with longer survival durations.[17] Moreover, previous research has shown that hsa-miR-96-5p may inhibit *SMAD7* expression through target regulation.[18,19] Consequently, the present study focuses on the *ERα*/hsa_circ_0004913/hsa-miR-96-5p/SMAD7 axis, aiming to elucidate the mechanisms

by which *ERα*, as a TF for circular RNAs (circRNAs), regulates the *ERα*/circRNA/miRNA/SMADs network to inhibit HCC progression.

Materials and methods

Ethics approval and consent to participate

Our study is based on publicly available data from open-source databases. The Tongde Hospital of Zhejiang Province (Hangzhou, China) does not require ethics committee review for research utilizing publicly available data. As a result, our study does not raise any ethical concerns or conflicts of interest.

Bioinformatics analysis

The Hepatocellular Carcinoma Database (HCCDB; http://lifeome.net/database/hccdb/home.html) was used to investigate the expression of *ESR1* in liver tumors and neighboring normal tissues, as well as in normal liver tissues. The Cancer Genome Atlas (TCGA; https://portal.gdc.cancer.gov) database was utilized to compare the difference in overall survival (OS) between HCC patients in various expression groups. The circRNA expression data for HCC were retrieved from the Gene Expression Omnibus (GEO) database (https://www.ncbi.nlm.nih.gov/geo) using the keywords "circRNA" and "hepatocellular carcinoma". Furthermore, the circRNA names were standardized according to the circBase database (http://www.circbase.org). All GEO data sets were analyzed using R v. 4.2.2 (R Foundation for Statistical Computing, Vienna, Austria) and the limma package. Only circRNAs with a log2 > 2 and $p < 0.05$ were selected. The circRNA promoter sequence was retrieved from the University of California Santa Cruz (UCSC) database (http://genome.ucsc.edu). To anticipate possible TFs, we utilized the JASPAR database (http://jaspar.genereg.net). The target miRNAs of the circRNA were predicted using the online tool circBank (https://www.circbank.cn/#/home). The target miRNAs of the circRNA were predicted using the online tool CircNetVis (https://www.meb.ki.se/shiny/truvu/CircNetVis/), retaining only the intersection of the prediction results from the Miranda and TargetScan databases for further analysis. Only those predicted by at least 2 of the databases to have potential regulatory effects were included in the study.

Cell culture and transfection

The Chinese Academy of Sciences Cell Bank (Shanghai, China) provided the human HCC cells (MHCC97H). The cells were grown at 37°C in a humidified atmosphere with 5% CO_2 and were maintained in Dulbecco's modified Eagle's medium (DMEM) supplemented with 10% fetal bovine serum (FBS). *ESR1*-pcDNA3.1 plasmids and the corresponding control vectors were generated by Genecreate (Wuhan, China). MHCC97H cells were transfected using the Lipofectamine 2000 reagent (Invitrogen, Waltham, USA).

Total RNA preparation and RT-qPCR

Total RNA and miRNA were extracted from MHCC97H cells using the miRcute miRNA Isolation Kit (DP501; Tiangen, Beijing, China) following the manufacturer's instructions. Briefly, 1×10^5–10^7 cells were lysed with Lysis Buffer. RNA was transferred to miRspin columns and eluted after buffer washing. Reverse transcription was performed using the ReverTra Ace qPCR RT Kit (FSQ-101; Toyobo, Osaka, Japan) for mRNA and the miRNA 1st Strand cDNA Synthesis Kit (MR101-02; Vazyme, Nanjing, China) for miRNA. Quantitative reverse transcription polymerase chain reaction (RT-qPCR) was performed using SYBR®Green Real time PCR Master Mix (QPK-201; Toyobo) for mRNA and miRNA Universal SYBR qPCR Master Mix (MQ101-02; Vazyme) for miRNA, and Real-time PCR System (SLAN-48P; Hongshi, Shanghai, China). The relative expression levels of the target genes were determined using the $2^{\wedge-\Delta\Delta Ct}$ method. This method made it possible to compare the expression of the genes in relation to *GAPDH* (for mRNA) or *U6* (for miRNA), the internal control gene. To ensure the reproducibility and reliability of the RT-qPCR results, each sample was amplified 3 times. Table 1 lists the specific primer sequences used in this study.

Cell Counting Kit-8 assay

A total of 1,000 cells were seeded into each well of a 96-well plate and incubated in a 5% CO_2 incubator for 0, 24 and 48 h. Ten microliters of Cell Counting Kit-8 (CCK-8) solution (CCK-8 Cell Proliferation and Cytotoxicity Assay Kit, CA1210; Solarbio, Beijing, China) were added to each well, and the plates were incubated for an additional 30 min. After incubation, the absorbance was measured at approx. 450 nm using a microplate reader (MB-530; Heales, Shenzhen, China). The IC50 (half-maximal inhibitory concentration) values were calculated by fitting concentration-response curves using the 4-parameter method. The color intensity was found to be proportional to the number of viable cells, as living cells reduced the CCK-8 dye to a colored formazan product.

Transwell assay

Cells were trypsinized, resuspended in serum-free DMEM, and counted using a hemocytometer. A total of 1×10^4 MHCC97H cells were seeded in the upper chamber of a 24-well Transwell insert (Corning Company, Corning, USA), while the lower chamber was filled with DMEM containing 10% FBS. The Transwell insert was then incubated in a humidified atmosphere of 5%

Table 1. Primer sequences

Primer	Sequence (5'to3')
ESR1 F	TCCTGATGATTGGTCTCGTCTGG
ESR1 R	GGTTCCTGTCCAAGAGCAAGTTAG
hsa_circ_0004913 F	GCCTGGGTGAATGCCTTGC
hsa_circ_0004913 R	ACTGTTGTGTCTGCTGTGTGC
hsa-miR-96-5p F	ACACTCCAGCTGGGTTTGGCACTAGCACATT
hsa-miR-96-5p R	CTCAACTGGTGTCGTGGAGTCGGCAATTCAGTTGAGAGCAAAAA
SMAD7 F	AACCCCCATCACCTTAG
SMAD7 R	CTCGTCTTCTCCTCCCA
U6 F	GCTTCGGCAGCACATATACTAAAAT
U6 R	CGCTTCACGAATTTGCGTGTCAT
GAPDH F	ACAACAGCCTCAAGATCATCAGC
GAPDH R	GCCATCACGCCACAGTTTCC

CO_2 at 37°C for 24 h to allow cell migration. After incubation, the insert was removed, and the medium was aspirated. Cells were fixed with 4% paraformaldehyde for 15 min and subsequently stained with 0.1% crystal violet for 20 min to visualize migrated cells. The insert was then rinsed 3 times with phosphate-buffered saline (PBS) to remove the unbound stain. A cotton swab was used to gently remove non-migrated cells from the upper surface of the membrane. Finally, migrated cells on the lower surface of the membrane were imaged under a light microscope (DSY5000X, COIC, Chongqing, China).

Flow cytometry assay for the cell cycle

After collecting and fixing the cell suspension, 5 mL of cold 70% ethanol was added, and the mixture was then incubated at 4°C overnight. Following 2 washes with 5 mL of PBS, the cells were stained for 10 min with 50 μg/mL propidium iodide (PI). After passing the suspension through a 300-mesh filter, it was centrifuged for 5 min at 1,000 rpm. To remove any remaining PI, 5 mL of PBS was used to rinse the cells. Subsequently, the cells were reconstituted in 200 μL of PBS and subjected to analysis using a Beckman Coulter flow cytometer (Beckman Coulter, Brea, USA).

Luciferase reporter assay

Both wild-type (WT) and mutant (MT) sequences were generated to investigate the role of hsa_circ_0004913 in cellular biology. Several recombinant reporter constructs were created by inserting these sequences into the pGL3 reporter gene vector. These recombinant reporters were then co-transfected into 293T cells along with hsa-miR-96-5p. Luciferase activity was precisely assessed 48 h after transfection using a dual-luciferase detection kit and the dual-luciferase reporter assay method. An internal control was included using the Renilla luciferase expression vector pRLTK (Takara, Beijing, China).

Chromatin immunoprecipitation-quantitative real-time PCR (ChIP-qPCR)

Following a seeding of MHCC97H cells (3×10^6) on 100 mm dishes and treatment with 1% formaldehyde, 600 μL of radioimmunoprecipitation assay (RIPA) lysis solution was used to lyse the cells. The sonicator was used to separate genomic DNA and shear it into 20–600-bp pieces. The chromatin was precipitated and incubated for an overnight duration at 4°C using either immunoglobulin G (IgG; Beyotime Biotechnology, Shanghai, China) or *ERα*-antibodies (Abcam, Shanghai, China) after centrifugation and removal of supernatants. The immune complexes were then cleaned using several washing buffers, including Tris-EDTA buffer, high salt, low salt, and LiCl. The immune precipitates were cross-linked overnight at 65°C after being eluted with 500 μL of elution buffer. hsa_circ_0004913 promoter primers were used to amplify *ESR1* binding sites. The promoter primers were as follow:

Primer 1:
forward (5'-ACTTCTCCCTCTGATACTCGTTCC-3'),
reverse (5'-ACTCCTCCTCCTTGATGCTGTAG-3');

Primer 2:
forward (5'-GGGAAGTGAGGACCCTAAGAAGC-3'),
reverse (5'-AAAAGCCCTGGAGCCAAGAAG-3');

Primer 3:
forward (5'-CGACTGACCGAGTATGGTATGG-3'),
reverse (5'-AGGAGGCAGGAAGTAGAGCGA-3').

Ultimately, DNA was extracted following the method recommended by the manufacturer, and RT-qPCR was used for analysis.

Western blot analysis

For immunoblotting, cells were lysed using preheated 2% sodium dodecyl sulfate (SDS) and then boiled for 30 min. Protein concentrations were determined using a bicinchoninic acid (BCA) assay (CW0014S; CoWin Biotech, Taizhou, China). Proteins were separated using SDS-polyacrylamide

gel electrophoresis (SDS-PAGE) and transferred to a nitrocellulose membrane (GE Healthcare, Chicago, USA) using the Genscript eBlot transfer technique. Membranes were blocked for 1 h at room temperature with 5% milk in 1× Tris-buffered saline with Tween-20 (TBST; 25 mM Tris, 150 mM NaCl, 2 mM KCl, pH 7.4, supplemented with 0.2% Tween-20) and probed overnight at 4°C with the indicated primary antibodies: *ERα* antibody (ab32063; Abcam) or *SMAD7* antibody (25840-1-AP; Proteintech, Wuhan, China). After washing with TBST 3 times for 30 min, membranes were incubated with peroxidase-conjugated secondary antibodies (SA00001-2; Proteintech) at room temperature for 1 h. The membranes were washed with TBST 3 times and detection was performed using Sensitive Chemiluminescence Test Kit (S6008M; UElany, Suzhou, China)

Statistical analyses

The normality assumption was assessed using the Shapiro–Wilk test, and the homogeneity of variance was evaluated with Levene's test. For data that met the test assumptions, differences between 2 groups were analyzed using the Student's t-test, and comparisons among multiple groups were performed using one-way analysis of variance (ANOVA). For small-sample data with a sample size below 7, the Mann–Whitney test was used for comparisons between 2 groups, and the Kruskal–Wallis test was applied for comparisons among multiple groups. Statistical significance was defined as $p < 0.05$. The corresponding results are provided in the shared data. The time from patient death or a 5-year follow-up is defined as the OS time. Kaplan–Meier method and log-rank test were used for survival analysis, and receiver operating characteristic (ROC) curve analysis was used to evaluate the discriminatory power of biomarkers. To evaluate heterogeneity among datasets, we used Cochran's Q test and the I^2 statistic. A fixed-effect model was applied when heterogeneity was minimal ($I^2 < 50\%$), assuming a consistent effect size across datasets. Conversely, a random-effects model was employed for analyses with substantial heterogeneity ($I^2 \geq 50\%$), accounting for between-study variability. Data analysis was performed using GraphPad Prism v. 7.0 (GraphPad Software, San Diego, USA), R v. 4.2.2 software (limma package v. 3.62.2; pheatmap package v. 1.0.12; survminer package v. 0.5.0) or IBM SPSS Statistics for Windows v. 24 (IBM Corp., Armonk, USA).

Results

ERα/circRNA/miRNA/*SMADs* network construction

CircRNA data from GSE97332 microarrays in the GEO database were analyzed using R v. 4.2.2. The top 30 differentially expressed circRNAs between cancer tissues and paired normal tissues were selected, including 15 with high expression and 15 with low expression. A heatmap was generated to display the hierarchical clustering of circRNA expression values (Fig. 1). The promoter sequence of circRNA was obtained from the UCSC database. The JASPAR database (https://jaspar.elixir.no) was used to predict potential TFs. ERα was the potential TF for 10 of these differentially expressed circRNA (Fig. 2).

The target miRNAs of circRNA were predicted using the online tool circBank. In the miRwalk online tool, predicted *SMADs* that overlap in at least 2 of the following databases–miRPathDB, miRWalk, and TargetScan–were considered, with a score greater than 0.95. Cytoscape was used to construct the *ERα*/circRNA/miRNA/*SMADs* network. We identified 8 circRNAs that were differentially expressed in HCC and ultimately target the *SMAD* family (Fig. 3).

Differential expression of the *ERα*/circRNA/miRNA/*SMADs* network is associated with poor prognosis in HCC

We used the HCCDB database to investigate *ESR1* expression in liver tumors and adjacent liver tissues, as well as in HCC and normal patient samples. Compared to the surrounding non-cancerous tissues, HCC tissues exhibited significantly lower *ESR1* expression (Fig. 4). Furthermore, *ESR1* expression was consistently lower in HCC

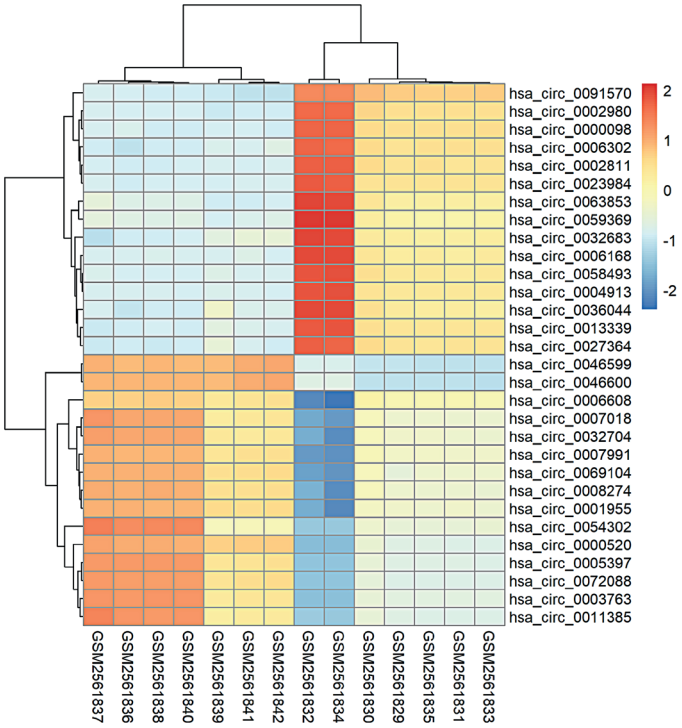

Fig. 1. Heatmap of 30 differentially expressed circular RNAs (circRNAs) in hepatocellular carcinoma (HCC). Differential expression analysis of circRNAs in the GSE97332 datasets was performed using the limma package. The top 30 differentially expressed circRNAs in HCC were selected, comprising 15 with high expression and 15 with low expression, based on a selection criterion of a log2 fold change ($|\log2FC| > 2$) and a $p < 0.05$. A heatmap illustrating these differential expression patterns was generated using the pheatmap package

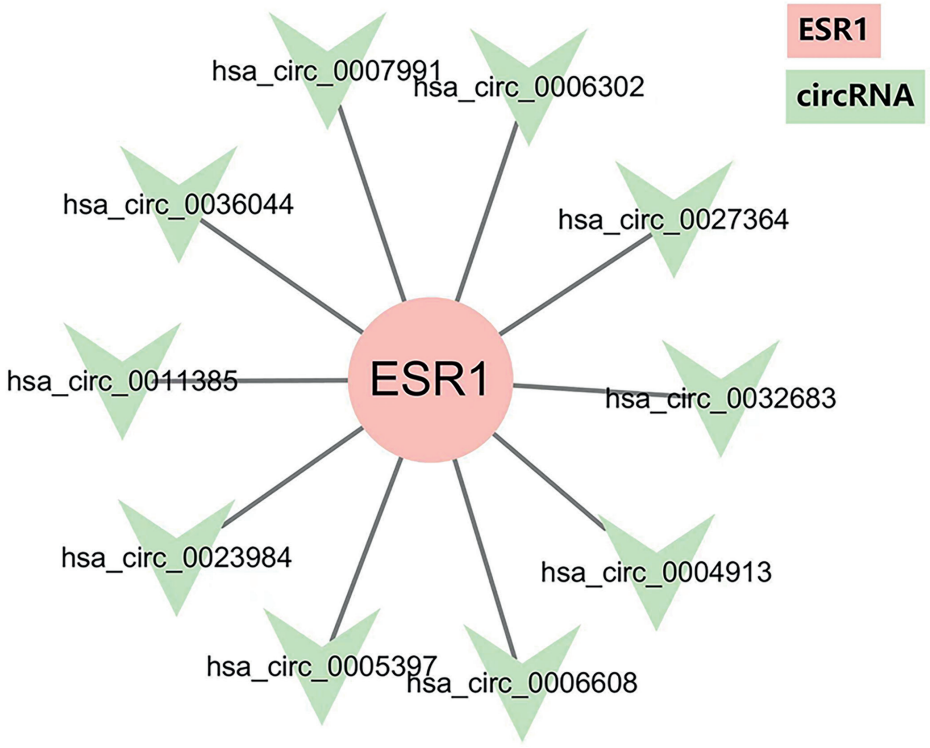

Fig. 2. Estrogen receptor alpha (*ERa*) is predicted as a transcription factor for 10 circular RNAs (circRNAs). Transcription factors of 30 differentially expressed circRNAs in hepatocellular carcinoma (HCC) were predicted using the JASPAR database. Among them, *ERa* was identified as a potential transcription factor for 10 circRNAs

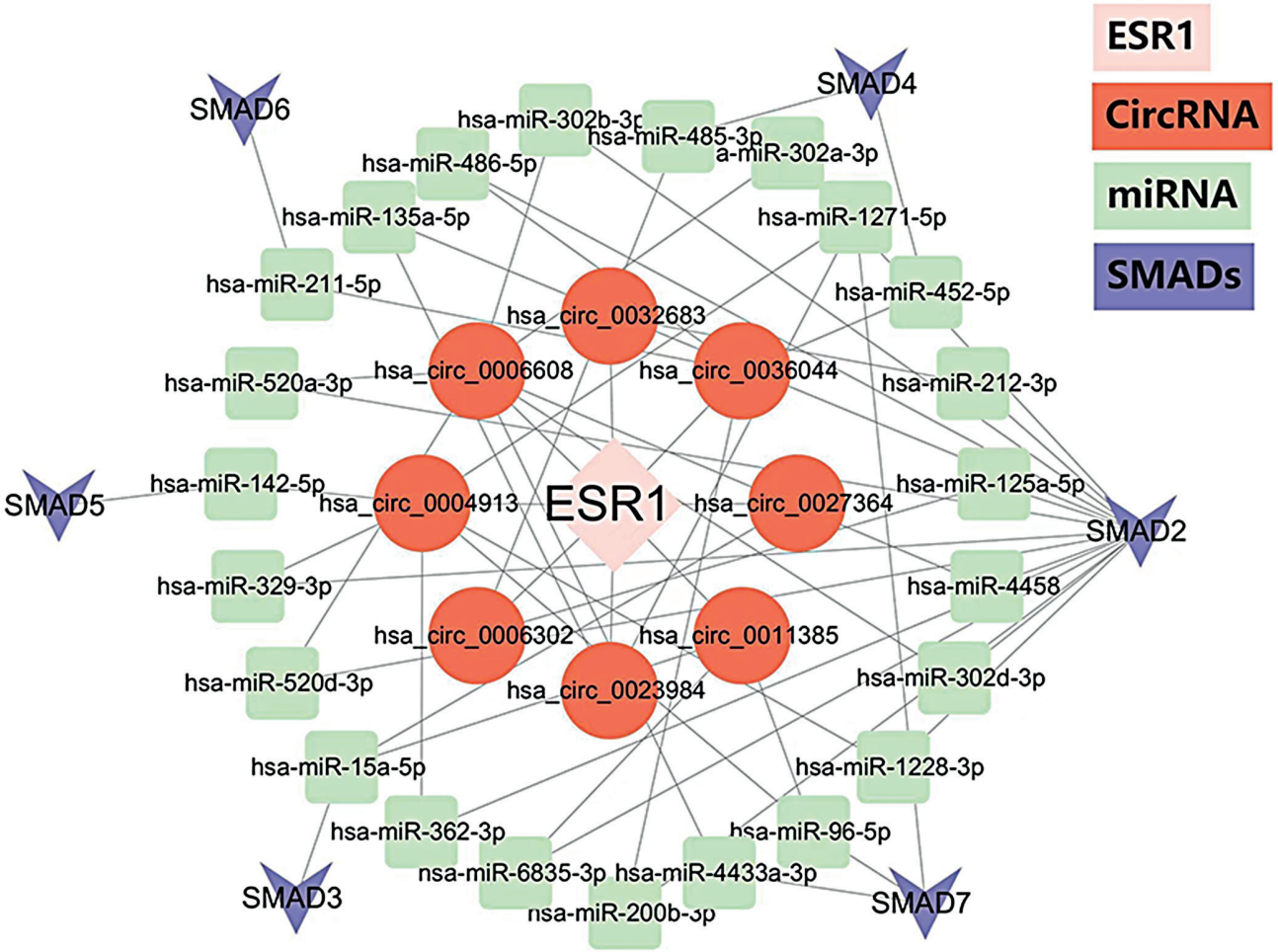

Fig. 3. Potential *ERa*/circRNA/miRNA/SMADs regulatory axis in hepatocellular carcinoma (HCC). Potential target miRNAs of circular RNAs (circRNAs) were predicted using the online tool circBank, while miRNA-targeted SMAD family genes were predicted using the online tool miRwalk. Ultimately, 8 circRNAs, 14 miRNAs and 4 genes from the SMAD family (*SMAD2*, *SMAD3*, *SMAD4*, *SMAD5*, *SMAD6*, and *SMAD7*) were identified, forming a potential *ERa*/circRNA/miRNA/SMADs regulatory axis in HCC

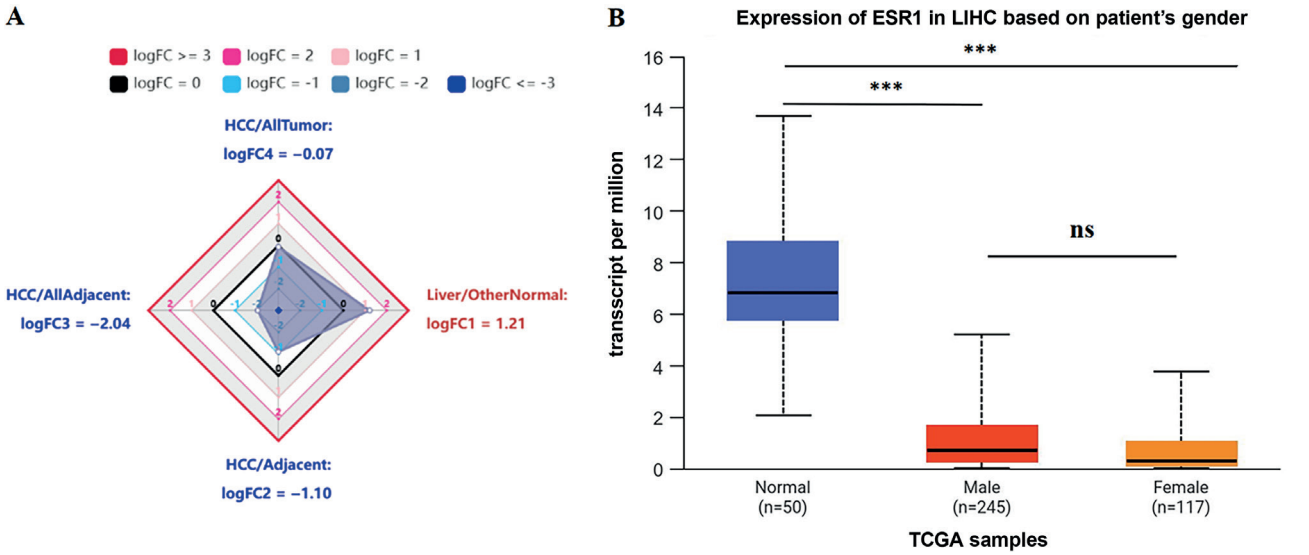

Fig. 4. *ESR1* expression in hepatocellular carcinoma (HCC) and adjacent tissues. A. Analysis of *ESR1* expression levels in HCC/All tumour, HCC/All Adjacent, HCC/Adjacent, and Liver/Other Normal tissues using the Hepatocellular Carcinoma Database (HCCDB) database. *ESR1* expression is significantly reduced in HCC tissues compared to adjacent non-cancerous tissues and healthy controls, regardless of gender, based on HCCDB analysis. Statistical significance is defined by |log2FC| > 1; B. Analysis of *ESR1* expression levels in liver tissues from 362 HCC patients (245 males and 117 females) and 50 normal individuals using The Cancer Genome Atlas (TCGA) data from the UALCAN website (https://ualcan.path.uab.edu). The results show that *ESR1* expression is significantly decreased in both male and female HCC patients compared to normal individuals ($p < 0.001$). However, there is no statistically significant difference in *ESR1* expression between male and female tumor patients ($p = 0.61$). Differences were analyzed using Welch's t-test and are presented as box plots showing the median and range

* $p < 0.05$; **$p < 0.01$; ***$p < 0.001$.

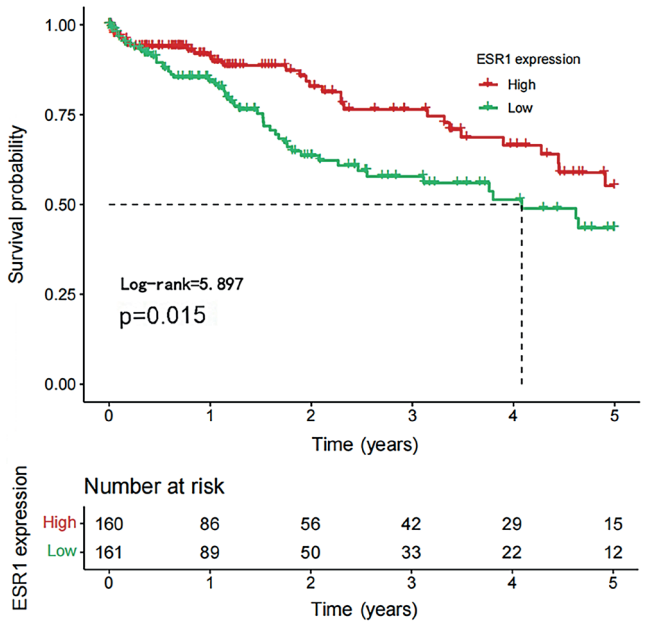

Fig. 5. Kaplan–Meier analysis shows that higher *ESR1* expression correlates with longer survival. Kaplan–Meier analysis and log-rank test were used to determine the relationship between *ESR1* expression and clinical prognosis in The Cancer Genome Atlas (TCGA) database. Overall survival (OS) time was defined as the time to patient death or the time of the last follow-up (up to 5 years). A total of 321 patients with non-zero OS were selected for the analysis, indicating a positive correlation between *ESR1* expression and OS in these patients ($p < 0.05$)

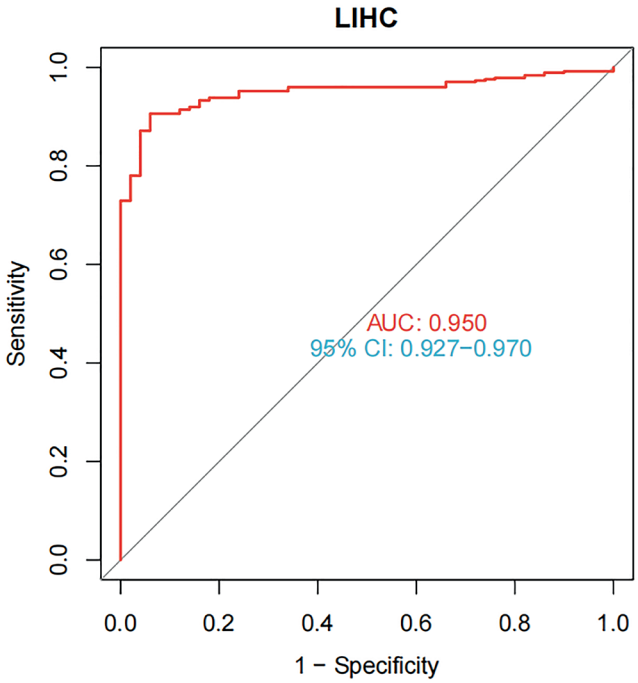

Fig. 6. Receiver operating characteristic (ROC) curve analysis showed that *ESR1* expression effectively distinguished tumor tissue from paired adjacent tissue, with an area under the curve (AUC) of 0.950 (95% confidence interval (95% CI): 0.927–0.970)

patients than in healthy individuals, regardless of gender (Fig. 4; $p < 0.001$). Based on our research, patients with high *ESR1* expression levels had significantly longer OS times compared to those with low expression levels (Fig. 5; $p = 0.015$). Additionally, ROC curve analysis demonstrated that *ESR1* expression effectively distinguished tumor tissue from paired adjacent tissue, with an area under the curve (AUC) of 0.950 (95% confidence interval (95% CI): 0.927–0.970; Fig. 6). The RT-qPCR results revealed that the liver

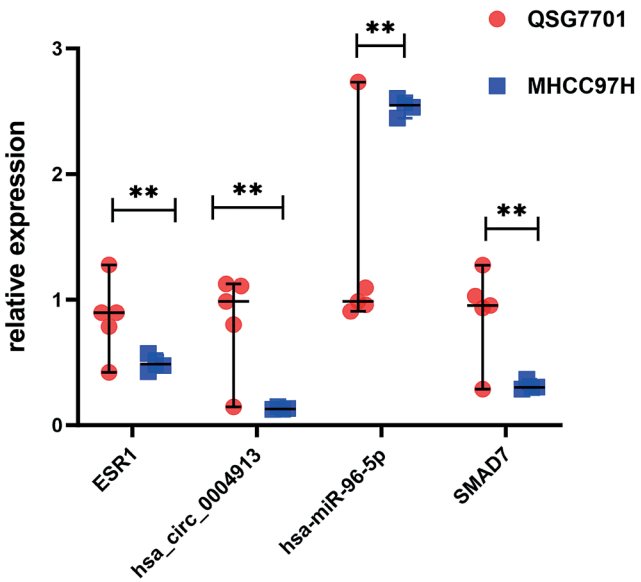

Fig. 7. Reverse transcription quantitative polymerase chain reaction (RT-qPCR) results between MHCC97H and QSG7701. RT-qPCR was performed to measure the expression levels of *ESR1*, hsa_circ_0004913, hsa-miR-96-5p, and *SMAD7* in the hepatocellular carcinoma (HCC) cell line MHCC97H and the normal liver cell line QSG7701. The results showed that, compared to normal QSG7701 liver cells, the MHCC97H liver cancer cells had higher levels of hsa-miR-96-5p, and lower levels of *ESR1*, hsa_circ_0004913 and *SMAD7*. Differences were analyzed using Mann–Whitney test and are expressed as median and range

* $p < 0.05$; ** $p < 0.01$; *** $p < 0.001$.

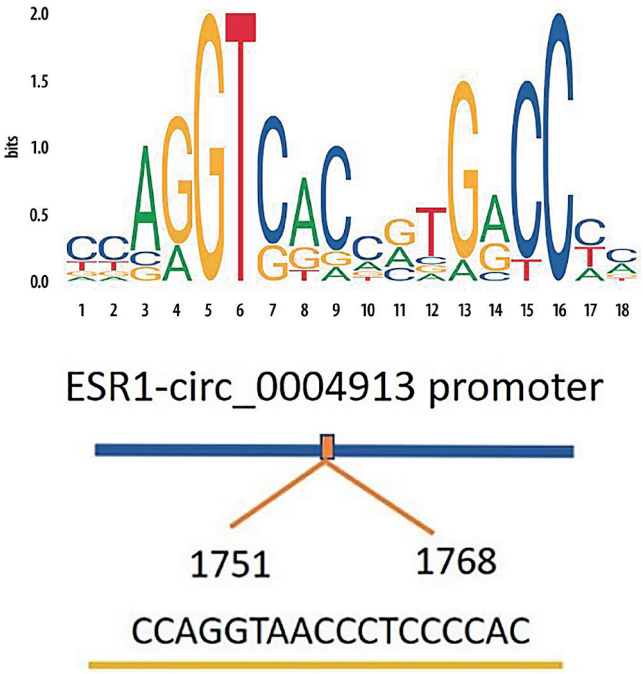

Fig. 8. Prediction of binding sites between *ESR1* and hsa_circ_0004913. Bioinformatics analyses predicted *ESR1* as a transcription factor for hsa_circ_0004913, with binding motifs identified using the JASPAR database

cancer cell line MHCC97H expressed higher levels of hsa-miR-96-5p and lower levels of *ESR1*, hsa_circ_0004913 and *SMAD7* compared to the normal control cell line QSG7701 (Fig. 7, $p = 0.008$). These findings suggest that a poor prognosis in HCC patients is associated with high expression of hsa-miR-96-5p and low expression of *ESR1* and *SMAD7*.

ERα promotes hsa_circ_0004913 expression in MHCC97H cells

To explore the upstream regulatory mechanisms of hsa_circ_0004913, we identified *ESR1* as a predicted TF using the JASPAR database. The JASPAR database was employed to predict the motif of *ESR1* (Fig. 8). Additionally, potential binding sites between *ERα* and the hsa_circ_0004913 promoter were predicted using the JASPAR database (Fig. 8). We used RT-qPCR to confirm that *ESR1* was overexpressed after plasmid transfection, and we found that there was a significant increase in hsa_circ_0004913 expression following *ESR1* overexpression (Supplementary Fig. 1). Additionally, ChIP-qPCR analysis revealed a strong binding affinity between the hsa_circ_0004913 promoter and *ESR1* at the sites targeted by the 3 primers (Fig. 9). Western blot analysis confirmed the successful extraction of protein samples with *GAPDH* as the internal control (Fig. 9). Collectively, these findings suggest that *ESR1* activates the transcription of hsa_circ_0004913, thereby enhancing its expression in MHCC97h cells.

ESR1 overexpression regulates the hsa_circ_0004913/hsa-miR-96-5p/*SMAD7* axis in MHCC97H

According to RT-qPCR data, *ESR1* overexpression significantly increased the expression of *SMAD7* while substantially decreasing the expression of hsa-miR-96-5p compared to the control group (Supplementary Fig. 2). Western blot analysis provided additional confirmation of these results (Supplementary Fig. 3). Hsa_circ_0004913 WT and MT sequences were created and transfected into 293T cells based on the anticipated binding sites (Supplementary Fig. 4). The results demonstrated that in the circ_0004913-WT group, the fluorescence of hsa-miR-96-5p mimics was significantly increased compared to negative control (NC) mimics ($p = 0.008$). Nevertheless, no significant difference in fluorescence was observed between NC mimics and hsa-miR-96-5p mimics in the circ_0004913-MT group (Supplementary Fig. 5). In summary, *ESR1* regulates the expression of the circRNA/miRNA/*SMADs* axis and hsa_circ_0004913 interacts with hsa-miR-96-5p in MHCC97H cells.

ESR1 overexpression suppresses the biological activity of MHCC97H cells

To investigate the biological effects of *ESR1* on MHCC97H cells, we transfected the cells with an *ESR1* plasmid and an empty vector, as well as with siRNAs targeting *ESR1* and a NC. Next, we evaluated MHCC97H

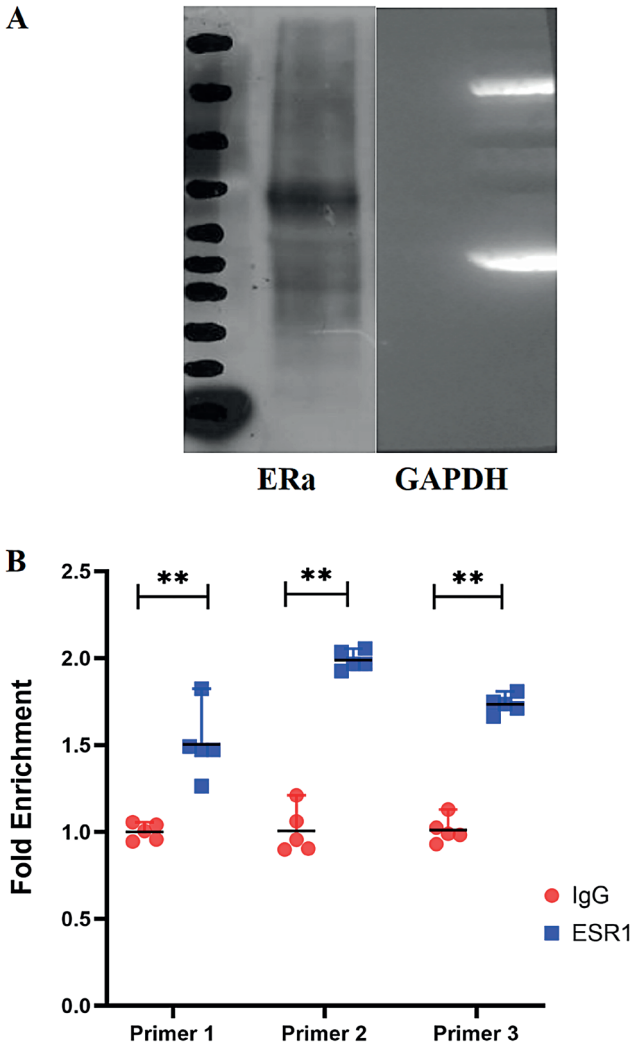

Fig. 9. Chromatin immunoprecipitation-quantitative real-time polymerase chain reaction (ChIP-qPCR) results. A. Western blot analysis showing *GAPDH* expression as an internal control for the estrogen receptor alpha (*ERα*) samples; B. The ChIP-qPCR experiment demonstrated that all 3 primers targeting the *ESR1* and hsa_circ_0004913 binding sites exhibited strong affinity, confirming the binding ability of *ESR1* to the hsa_circ_0004913 promoter. Differences were analyzed using Mann–Whitney test and are expressed as median and range

*p < 0.05; **p < 0.01; ***p < 0.001.

cells proliferation with the CCK-8 test, cell migration with the Transwell assay, and cell cycle distribution with flow cytometry. The results indicated that overexpression of *ESR1* significantly reduced cell proliferation, while silencing *ESR1* significantly enhanced cell proliferation ($p < 0.01$; Supplementary Fig. 6). The migratory capacity was much lower in the *ESR1* overexpression group than in the *ESR1* silencing group ($p < 0.01$; Supplementary Fig. 7). Furthermore, compared to the *ESR1* silencing group, the *ESR1* overexpression group showed an increase in the proportion of cells in the G1 phase, accompanied by a decrease in cells in the S and G2 phases. This suggests that *ESR1* inhibits tumor growth in MHCC97H cells by inducing G1 phase arrest (Supplementary Fig. 8; $p < 0.01$).

Discussion

The incidence and mortality of HCC vary significantly by gender.[1] In comparison to men, women had lower incidence and mortality rates from HCC. We found that, compared to normal liver tissues, HCC tissues exhibit a marked downregulation of *ESR1* expression, as confirmed with analysis of the TCGA database. Moreover, the concentration of *ESR1* in adjacent non-tumor tissues was significantly higher compared to that in HCC tissues. The results of the survival study showed a favorable association between the patient's survival times and *ESR1* levels. Kaplan–Meier analysis further demonstrated that higher *ESR1* expression was associated with longer survival in HCC patients. These findings suggest that the estrogen signaling pathway may play a protective role in HCC development and progression, offering a promising target for therapeutic intervention.

While substantial research has investigated the downstream regulatory mechanisms of circRNAs, their upstream regulatory pathways remain largely unexplored. Several studies have suggested that TFs can bind to circRNA promoter sequences, thereby regulating their expression.[20,21] Emerging evidence indicates that TFs, including *ERα*, can bind to circRNA promoter sequences, thereby modulating their transcriptional activity.

In this study, we analyzed differentially expressed circRNAs between adjacent non-tumor tissues and HCC using the GEO database and investigated potential TFs via the JASPAR database. We found that *ESR1* may function as a TF for multiple differentially expressed circular RNAs (circRNAs). Of these circRNAs, hsa_circ_0004913 was identified as a key regulator of the *ERα*/circRNA/miRNA/*SMADs* network.

Based on the "gene sponge" theory, we analyzed the potential miRNAs and mRNAs targeted by these circRNAs, constructing a circRNA-miRNA-mRNA network. This network comprises several pathways that converge on the *SMAD* family, primarily utilizing the *TGF-β/SMAD* signaling pathway to influence HCC development.[12,22] This network is closely associated with the *TGF-β/SMAD* signaling pathway, a critical driver in HCC pathogenesis. Several circRNAs and miRNAs within this network have been implicated in HCC initiation and progression through diverse mechanisms. For instance, hsa_circ_0058493 accelerates HCC progression by binding to *YTH* domain-containing protein 1.[23] Hsa_circ_0001955 acts as a miR-646 sponge, promoting angiogenesis in HCC.[24] MiR-200b-3p suppresses HCC cell growth by targeting *ERG* and *VEGF*-mediated angiogenesis.[25] MiR-329-3p enhances tumor cell responsiveness to T cell-induced cytotoxicity.[26] These findings suggest that this network is closely associated with the development of HCC and may be involved in various processes such as tumor angiogenesis, cellular activity, and immune sensitivity. Collectively, this network holds promise as a novel therapeutic target for HCC.

In this study, we hypothesize that *ESR1*, acting as a TF, differentially modulates the expression of specific circRNAs in HCC. This modulation influences the *SMADs* family expression and inhibits hepatocyte proliferation. The RT-qPCR analysis revealed that *ESR1* overexpression upregulates the expression of hsa_circ_0004913 and *SMAD7*, while downregulating hsa-miR-96-5p. Furthermore, ChIP-qPCR results confirmed that *ERα* interacts with the hsa_circ_0004913 promoter, enhancing its expression as a transcriptional regulator. Dual-luciferase reporter assays verified that hsa_circ_0004913 directly targets and regulates hsa-miR-96-5p. In vitro studies demonstrated that *ESR1* overexpression hinders HCC progression by inhibiting the proliferation and migration of MHCC97H cells, thereby inducing cell cycle arrest.

Many studies have also corroborated our findings. For instance, Li et al. conducted a study involving 150 HCC patients who underwent surgical treatment, with tissue specimens analyzed and clinical follow-up performed. The results indicated that the expression of hsa_circ_0004913 was significantly downregulated in liver cancer tissues compared to paired adjacent normal tissues. They reported significantly downregulated hsa_circ_0004913 in HCC tissues compared to adjacent normal tissues, correlating with shorter patient survival.[14]

Wu et al. demonstrated that hsa_circ_0004913 overexpression inhibits HCC progression by targeting miR-184, suppressing the *JAK2/STAT3/AKT* signaling pathway.[13] Additionally, hsa-miR-96-5p has been discovered to be significantly expressed in HCC, and its suppression can increase HCC apoptosis while reducing migration and invasion.[15,16]

Our study confirmed that hsa_circ_0004913 can target and regulate the expression of hsa-miR-96-5p. Similarly, Tang et al. demonstrated that in liver cancer cells, hsa-miR-96-5p is regulated by circ_0000972 through a gene-sponge mechanism, inhibiting HCC.[27] As mentioned earlier, several experiments have confirmed the targeting regulatory effect of hsa-miR-96-5p on *SMAD7*, which is consistent with our bioinformatics predictions.[18,19,28] Therefore, we did not perform further experimental validation. Besides *SMAD7*, *SMAD2*, *SMAD3*, and *SMAD4* are also potential targets within our predicted network, all of which belong to the *SMAD* family. Recent studies have demonstrated that the *SMAD* family mediates TF activation and the transmission of membrane-to-nucleus signals through the *TGF-β/SMAD* signaling pathway.[12] This pathway regulates multiple functions, including the tumor microenvironment, immune responses, tumor cell activity, and sensitivity to targeted therapies.[29–32] Additionally, it can crosstalk with other pathways, such as the *MAPK*, *PI3K/AKT* and *WNT/β*-catenin pathways, thereby amplifying its impact on tumor progression.[12] Thus, it plays a critical role in the initiation and progression of HCC.

In summary, the above indicates that the *ERα*/circRNA/miRNA/*SMADs* network may serve as a potential therapeutic target for HCC.

Limitations

Our study has several limitations. Our primary focus was on the gender differences in the incidence and mortality of HCC. Our analyses identified ERα as a TF regulating multiple differentially expressed circRNAs in HCC. It also modulates the circRNA/miRNA/SMAD network to suppress HCC progression. However, our study does not explore the potential pathways involved, nor does it examine the diagnostic value of *ERα* and hsa_circ_0004913 in HCC. Additionally, the small sample size may limit the statistical significance of our findings. Future large-scale studies are necessary.

Conclusions

The *ERα* signaling pathway represents a potential therapeutic target for HCC. We propose that *ERα*, functioning as a TF, , regulates the production of circRNAs that are differentially expressed in HCC. This modulates the circRNA/miRNA/SMAD network and slows the progression of the cancer. We hope this research will contribute to securing additional funding for further studies aimed at improving the survival rates of HCC patients.

Supplementary data

The supplementary materials are available at https://doi.org/10.5281/zenodo.15004445. The package includes the following files:

Supplementary Fig. 1. qRT-PCR detection of the relationship between *ESR1* and hsa_circ_0004913 expression. qRT-PCR analysis validated the overexpression of *ESR1* in the MHCC97H cell line transfected with the *ESR1* plasmid (OE-*ESR1*), showing a significant increase compared to the pcDNA3.1 empty vector group (pcDNA3.1). Additionally, the overexpression of *ESR1* resulted in an upregulation of hsa_circ_0004913 expression. Differences were analyzed using Mann–Whitney test and are expressed as median and range (*$p < 0.05$, **$p < 0.01$, ***$p < 0.001$).

Supplementary Fig. 2. qRT-PCR detection of the relationship between *ESR1* hsa-miR-96-5p and SMAD7 expression. qRT-PCR data showed that overexpression of *ESR1* significantly increased the expression of *SMAD7*, while significantly decreased the expression of hsa-miR-96-5p. Differences were analyzed using Mann–Whitney test and are expressed as median and range (*$p < 0.05$, **$p < 0.01$, ***$p < 0.001$).

Supplementary Fig. 3. Western blot analysis confirmed that *ESR1* overexpression increases the expression level of *SMAD7*.

Supplementary Fig. 4. The target between hsa_circ_0004913 and hsa-miR- 96-5p were predicted through TargetScan.

Supplementary Fig. 5. Luciferase reporter assay revealed that in the circ-0004913-WT group, fluorescence

significantly increased in the hsa-miR-96-5p mimic group (miR-96-5p) compared to the NC mimics empty vector group (NC mimic) ($p < 0.05$), confirming the interaction and targeted regulation between hsa_circ_0004913 and hsa-miR-96-5p. Differences were analyzed using Mann–Whitney test and are expressed as median and range (*$p < 0.05$, **$p < 0.01$,***$p < 0.001$).

Supplementary Fig. 6. CCK-8 assay showed that overexpression of *ESR1* (OE-*ESR1*) reduced MHCC97H cell proliferation, while silencing of *ESR1* (si-*ESR1*) enhanced proliferation. Differences were analyzed using Mann–Whitney test and are expressed as median and range (*$p < 0.05$, **$p < 0.01$,***$p < 0.001$).

Supplementary Fig. 7. Transwell assay demonstrating that *ESR1* overexpression decreased cell migration, while silencing *ESR1* had the opposite effect. Differences were analyzed using Mann–Whitney test and are expressed as median and range (*$p < 0.05$, **$p < 0.01$,***$p < 0.001$).

Supplementary Fig. 8. Results of cell cycle. Compared to the *ESR1* silencing group, the *ESR1* overexpression group showed an increased proportion of cells in the G1 phase and a decreased proportion in the S and G2 phases. This suggests that *ESR1* inhibits tumor growth in MHCC97H cells by inducing G1 phase arrest. Differences were analyzed using Mann–Whitney test and are expressed as median and range (*$p < 0.05$, **$p < 0.01$,***$p < 0.001$).

Data Availability Statement

The datasets used and/or analyzed during the current study were obtained from publicly available sources, including from the HCCDB, TCGA, GEO, circBase, UCSC, and JASPAR.

Consent for publication

Not applicable.

Use of AI and AI-assisted technologies

Not applicable.

ORCID iDs

Changfeng Liu https://orcid.org/0000-0002-5129-127X
Zujian Wu https://orcid.org/0009-0005-7064-1895
Bing Zhang https://orcid.org/0009-0005-7018-054X
Zhi Chen https://orcid.org/0009-0002-1829-7861

References

1. Bray F, Laversanne M, Sung H, et al. Global cancer statistics 2022: GLOBOCAN estimates of incidence and mortality worldwide for 36 cancers in 185 countries. *CA Cancer J Clin*. 2024;74(3):229–263. doi:10.3322/caac.21834
2. Siegel RL, Miller KD, Wagle NS, Jemal A. Cancer statistics, 2023. *CA Cancer J Clin*. 2023;73(1):17–48. doi:10.3322/caac.21763
3. Hassan MM, Botrus G, Abdel-Wahab R, et al. Estrogen replacement reduces risk and increases survival times of women with hepatocellular carcinoma. *Clin Gastroenterol Hepatol*. 2017;15(11):1791–1799. doi:10.1016/j.cgh.2017.05.036
4. O'Brien MH, Pitot HC, Chung SH, Lambert PF, Drinkwater NR, Bilger A. Estrogen receptor-α suppresses liver carcinogenesis and establishes sex-specific gene expression. *Cancers (Basel)*. 2021;13(10):2355. doi:10.3390/cancers13102355
5. Mumtaz PT, Taban Q, Dar MA, et al. Deep insights in circular RNAs: From biogenesis to therapeutics. *Biol Proced Online*. 2020;22(1):10. doi:10.1186/s12575-020-00122-8
6. Hu Z, Chen G, Zhao Y, et al. Exosome-derived circCCAR1 promotes $CD8^+$ T-cell dysfunction and anti-PD1 resistance in hepatocellular carcinoma. *Mol Cancer*. 2023;22(1):55. doi:10.1186/s12943-023-01759-1
7. Zhou Y, Mao X, Peng R, Bai D. CircRNAs in hepatocellular carcinoma: Characteristic, functions and clinical significance. *Int J Med Sci*. 2022;19(14):2033–2043. doi:10.7150/ijms.74713
8. Zhao X, Zhong Y, Wang X, Shen J, An W. Advances in circular RNA and its applications. *Int J Med Sci*. 2022;19(6):975–985. doi:10.7150/ijms.71840
9. Hajizadeh M, Hajizadeh F, Ghaffarei S, et al. MicroRNAs and their vital role in apoptosis in hepatocellular carcinoma: MiRNA-based diagnostic and treatment methods. *Gene*. 2023;888:147803. doi:10.1016/j.gene.2023.147803
10. El-Mahdy HA, Sallam AAM, Ismail A, Elkhawaga SY, Elrebehy MA, Doghish AS. miRNAs inspirations in hepatocellular carcinoma: Detrimental and favorable aspects of key performers. *Pathol Res Pract*. 2022;233:153886. doi:10.1016/j.prp.2022.153886
11. Wang Y, Zhao W, Zhang S. STAT3-induced upregulation of circCCDC66 facilitates the progression of non-small cell lung cancer by targeting miR-33a-5p/KPNA4 axis. *Biomed Pharmacother*. 2020;126:110019. doi:10.1016/j.biopha.2020.110019
12. Xin X, Cheng X, Zeng F, Xu Q, Hou L. The role of TGF-β/SMAD signaling in hepatocellular carcinoma: From mechanism to therapy and prognosis. *Int J Biol Sci*. 2024;20(4):1436–1451. doi:10.7150/ijbs.89568
13. Wu M, Sun T, Xing L. Circ_0004913 inhibits cell growth, metastasis, and glycolysis by absorbing miR-184 to regulate *HAMP* in hepatocellular carcinoma. *Cancer Biother Radiopharm*. 2023;38(10):708–719. doi:10.1089/cbr.2020.3779
14. Li X, Yang J, Yang X, Cao T. Dysregulated circ_0004913, circ_0008160, circ_0000517, and their potential as biomarkers for disease monitoring and prognosis in hepatocellular carcinoma. *Clin Lab Anal*. 2021;35(6):e23785. doi:10.1002/jcla.23785
15. Yuan F, Tang Y, Cao M, et al. Identification of the hsa_circ_0039466/miR-96-5p/FOXO1 regulatory network in hepatocellular carcinoma by whole-transcriptome analysis. *Ann Transl Med*. 2022;10(14):769–769. doi:10.21037/atm-22-3147
16. Li ZR, Xu G, Zhu LY, Chen H, Zhu JM, Wu J. GPM6A expression is suppressed in hepatocellular carcinoma through miRNA-96 production. *Lab Invest*. 2022;102(11):1280–1291. doi:10.1038/s41374-022-00818-3
17. Feng T, Dzieran J, Gu X, et al. *SMAD7* regulates compensatory hepatocyte proliferation in damaged mouse liver and positively relates to better clinical outcome in human hepatocellular carcinoma. *Clin Sci (Lond)*. 2015;128(11):761–774. doi:10.1042/CS20140606
18. Gu H, Duan Y, Li S, et al. miR-96-5p regulates myocardial infarction-induced cardiac fibrosis via *SMAD7*/Smad3 pathway. *Acta Biochim Biophys Sin*. 2022;54(12):1874–1888. doi:10.3724/abbs.2022175
19. Kang J, Li Y, Zou Y, Zhao Z, Jiao L, Zhang H. miR-96-5p induces orbital fibroblasts differentiation by targeting *SMAD7* and promotes the development of thyroid-associated ophthalmopathy. *Evid Based Complement Alternat Med*. 2022;2022:8550307. doi:10.1155/2022/8550307
20. Zhou H, Huang J, Wang F. Increased transcription of hsa_circ_0000644 upon RUNX family transcription factor 3 downregulation participates in the malignant development of bladder cancer. *Cell Signal*. 2023;104:110590. doi:10.1016/j.cellsig.2023.110590
21. Ren L, Jiang M, Xue D, et al. Nitroxoline suppresses metastasis in bladder cancer via EGR1/circNDRG1/miR-520h/*SMAD7*/EMT signaling pathway. *Int J Biol Sci*. 2022;18(13):5207–5220. doi:10.7150/ijbs.69373
22. Zaidi S, Gough NR, Mishra L. Mechanisms and clinical significance of TGF-β in hepatocellular cancer progression. *Adv Cancer Res*. 2022;156:227–248. doi:10.1016/bs.acr.2022.02.002
23. Wu A, Hu Y, Xu Y, et al. Methyltransferase-like 3-mediated m6A methylation of Hsa_circ_0058493 accelerates hepatocellular carcinoma progression by binding to YTH domain-containing protein 1. *Front Cell Dev Biol*. 2021;9:762588. doi:10.3389/fcell.2021.762588

24. Li X, Lv J, Hou L, Guo X. Circ_0001955 acts as a miR-646 sponge to promote the proliferation, metastasis and angiogenesis of hepatocellular carcinoma. *Dig Dis Sci*. 2022;67(6):2257–2268. doi:10.1007/s10620-021-07053-8
25. Wang Y, Moh-Moh-Aung A, Wang T, et al. Exosomal delivery of miR-200b-3p suppresses the growth of hepatocellular carcinoma cells by targeting ERG- and VEGF-mediated angiogenesis. *Gene*. 2024; 931:148874. doi:10.1016/j.gene.2024.148874
26. Wang Y, Cao K. KDM1A promotes immunosuppression in hepatocellular carcinoma by regulating PD-L1 through demethylating MEF2D. *J Immunol Res*. 2021;2021:9965099. doi:10.1155/2021/9965099
27. Tang J, Tang R, Xue F, Gu P, Han J, Huang W. Circ_0000972 inhibits hepatocellular carcinoma cell stemness by targeting miR-96-5p/PFN1 [published online as ahead of print on December 2, 2024]. *Biochem Genet*. 2024. doi:10.1007/s10528-024-10975-3
28. Zhan J, Qi Y, Fu Y, et al. LncRNA ZFAS1 alleviated NLRP3 inflammasome-mediated pyroptosis through regulating miR-96-5p/*SMAD7* signaling in allergic rhinitis. *Int Arch Allergy Immunol*. 2024;185(7): 704–717. doi:10.1159/000535646
29. Gu J, Zhou J, Chen Q, et al. Tumor metabolite lactate promotes tumorigenesis by modulating MOESIN lactylation and enhancing TGF-β signaling in regulatory T cells. *Cell Rep*. 2022;39(12):110986. doi:10.1016/j.celrep.2022.110986
30. Bao W, Wang J, Fan K, Gao Y, Chen J. PIAS3 promotes ferroptosis by regulating TXNIP via TGF-β signaling pathway in hepatocellular carcinoma. *Pharmacol Res*. 2023;196:106915. doi:10.1016/j.phrs.2023.106915
31. Xin X, Li Z, Yan X, et al. Hepatocyte-specific Smad4 deficiency inhibits hepatocarcinogenesis by promoting CXCL10/CXCR3-dependent $CD8^+$-T cell-mediated anti-tumor immunity. *Theranostics*. 2024;14(15): 5853–5868. doi:10.7150/thno.97276
32. Ding J, Yang YY, Li PT, et al. TGF-β1/SMAD3-driven GLI2 isoform expression contributes to aggressive phenotypes of hepatocellular carcinoma. *Cancer Lett*. 2024;588:216768. doi:10.1016/j.canlet.2024.216768

The diagnostic performance of shear-wave elastography combined with ultrasound and magnetic resonance imaging in breast lesions: A single center retrospective study

*Wen-Yan Zhou[1,A–F], *Lian-Lian Zhang[1,A–F], Xiao Zhou[1,A–F], Xian-Bin Pan[1,A–C,E,F], Long-Xiu Qi[2,A,C,E,F]

[1] Department of Ultrasound , Yancheng No. 1 People's Hospital (The First People's Hospital of Yancheng), Affiliated Hospital of Medical School, Nanjing University, China
[2] Department of Radiology, Yancheng No. 1 People's Hospital (The First People's Hospital of Yancheng), Affiliated Hospital of Medical School, Nanjing University, China

A – research concept and design; B – collection and/or assembly of data; C – data analysis and interpretation;
D – writing the article; E – critical revision of the article; F – final approval of the article

Advances in Clinical and Experimental Medicine, ISSN 1899–5276 (print), ISSN 2451–2680 (online) *Adv Clin Exp Med*. 2026;35(1):77–87

Address for correspondence
Long-Xiu Qi
E-mail: Lx080306520@163.com

Funding sources
None declared

Conflict of interest
None declared

*Wen-Yan Zhou and Lian-Lian Zhang contributed equally to this work.

Received on July 2, 2024
Reviewed on January 17, 2025
Accepted on March 31, 2025

Published online on August 1, 2025

Cite as
Zhou WY, Zhang LL, Zhou X, Pan XB, Qi LX. The diagnostic performance of shear-wave elastography combined with ultrasound and magnetic resonance imaging in breast lesions: A single center retrospective study. *Adv Clin Exp Med*. 2026;35(1):77–87. doi:10.17219/acem/203584

DOI
10.17219/acem/203584

Abstract

Background. Breast cancer remains a major healthcare challenge, highlighting the need for early and accurate diagnosis. Shear-wave elastography (SWE), an ultrasound-based imaging technique that quantifies tissue elasticity, has emerged as a promising tool. Recent studies suggest that SWE may provide additional diagnostic value when used alongside conventional imaging methods.

Objectives. This study aimed to assess the diagnostic performance of SWE when combined with conventional ultrasound and magnetic resonance imaging (MRI) in the evaluation of breast lesions.

Material and methods. This retrospective study included patients with breast lesions who underwent SWE, conventional ultrasound and MRI. The diagnostic performance of each modality was evaluated individually and in combination. Histopathological results served as the gold standard for diagnosis. Key performance metrics – sensitivity, specificity, positive predictive value (PPV), negative predictive value (NPV), and overall accuracy – were calculated for each imaging approach.

Results. A total of 99 patients were included in the study, comprising 64 with benign lesions and 35 with malignant lesions. Malignant lesions were generally larger and exhibited distinct imaging characteristics across ultrasound, SWE and MRI. When assessed individually, SWE, ultrasound and MRI showed comparable diagnostic accuracy (64.6%, 62.6% and 62.6%, respectively). However, combining all 3 modalities significantly improved diagnostic performance, yielding sensitivity, specificity, PPV, NPV, and overall accuracy of 94.3%, 89.1%, 82.5%, 96.6%, and 90.9%, respectively ($p < 0.001$). The area under the curve (AUC) for the combined approach was significantly higher than for any single modality (0.917 vs 0.642, 0.627 and 0.633; $p < 0.001$).

Conclusions. While SWE alone offers diagnostic performance comparable to that of ultrasound and MRI individually, its greatest value lies in combination with these imaging modalities. Integrating ultrasound, SWE and MRI significantly enhances diagnostic accuracy, sensitivity and specificity, offering a promising multimodal approach for more reliable differentiation between benign and malignant breast lesions.

Key words: breast cancer, magnetic resonance imaging, ultrasonography, shear-wave elastography, breast diseases

Highlights

- Advanced breast imaging with shear-wave elastography (SWE): Combining SWE with conventional ultrasound and MRI provides a state-of-the-art, triple-modality breast imaging strategy for superior diagnostic confidence.
- Shear-wave elastography leads in diagnostic precision: SWE offers higher specificity (65.6%) and a significantly improved positive predictive value (PPV = 50%) compared to traditional ultrasound and MRI alone.
- Unmatched accuracy in breast lesion diagnosis: Integrating ultrasound, SWE and MRI achieves an impressive 90.9% overall diagnostic accuracy, setting a new standard in breast cancer screening.
- Enhanced sensitivity and specificity with multimodal imaging: This combined workflow boosts sensitivity to 94.3% and specificity to 89.1%, reducing both false positives and false negatives.
- Early detection and better outcomes: Incorporating SWE into routine breast imaging can accelerate early breast cancer detection, leading to improved patient outcomes and more efficient care pathways.

Background

Cancer is a disease characterized by the uncontrolled proliferation of abnormal cells within the body. It disrupts the usual regulatory processes that govern cellular growth and proliferation. Among different types of cancers, breast cancer is a prominent cause of cancer-related deaths in women.[1] According to GLOBOCAN 2018, there were over 2 million new breast cancer cases, making it the most frequently diagnosed cancer among women in 154 of the 185 countries assessed.[2] Its epidemiological spread has not only highlighted disparities in incidence between developed and developing nations, but also brought to the fore the critical role of early diagnosis.[3] Early-stage detection, primarily through mammographic screenings, can improve 5-year survival rates to over 90% in developed countries.[2,4] However, in low-income countries, where diagnosis often occurs at more advanced stages, 5-year survival rates can fall below 40%.[2–4] Therefore, early and accurate diagnosis is crucial for improving patient outcomes.

To distinguish between benign and malignant breast disease, traditional imaging modalities such as mammography, ultrasonography and magnetic resonance imaging (MRI) are typically employed.[5] The choice of modality depends on the patient's age and clinical scenario. For example, in patients under 30 years of age presenting with a palpable breast mass, the National Comprehensive Cancer Network (NCCN)[6] and the American College of Radiology (ACR) recommend breast ultrasonography as the initial imaging modality.[7] When evaluating with ultrasound, the breast imaging-report and data system (BI-RADS) using ACR is commonly used as an assessment tool to assist imaging report interpretation,[8] which reportedly has a high sensitivity of 74% and specificity of 84%.[9] However, while these traditional methods are effective in initial screening, they have limitations in specificity, often leading to unnecessary biopsies and overtreatment. This limitation calls for the development of more advanced imaging techniques to reduce false positives and improve the diagnostic accuracy of breast cancer detection.

In this context, advanced imaging modalities have emerged as valuable adjuncts to traditional methods. For instance, transmission electron microscopy (TEM) provides high-resolution visualization of cellular ultrastructure, enabling a deeper understanding of cellular components such as the cytoskeleton, membrane systems and organelles. This technique has shown potential in the study of breast cancer, offering insights into the morphology and structural changes at the cellular level.[10] Although TEM is more commonly used in research and pathology studies, its ability to identify subcellular features may have diagnostic implications in the future.

Another advanced technique is ultrasound elastography, which builds upon traditional grayscale ultrasound by assessing tissue stiffness. Two primary elastography methods have been explored: static elastography and shear-wave elastography (SWE). Static elastography provides qualitative information about the stiffness, allowing for better differentiation between benign and malignant lesions.[11,12] However, its application is limited due to the similar diagnostic performance as conventional ultrasound and inconsistency among multiple observers.[13,14] In contrast, SWE offers a more advanced and quantitative approach, providing objective measurements of lesion stiffness in kilopascals (kPa).[15] Studies have shown that SWE can yield accurate information with regard to benign or malignant differentiation of solid breast masses.[15,16] A recent meta-analysis by Langdon et al. indicated that SWE may be useful in downgrading BI-RADS 4A lesions or upgrading BI-RADS 3 lesions.[17] Despite its apparent advantages, SWE has not yet been recommended by current guidelines. This is largely due to several factors, including the lack of standardized diagnostic thresholds for SWE parameters, operator dependency and limited multicenter validation studies. Additionally, the high cost of elastography-capable ultrasound devices poses a significant challenge, especially for resource-limited healthcare settings.[5,18] These barriers hinder the widespread adoption of SWE, even though its diagnostic potential has been demonstrated.

Objectives

There is currently limited research on the combined use of SWE with conventional imaging modalities such as ultrasound and MRI. Our study addresses this gap by exploring the diagnostic potential of this multimodal approach. By leveraging the complementary strengths of these imaging techniques and addressing key barriers, we hope to facilitate the integration of SWE into standardized clinical guidelines, thereby advancing the precision and efficiency of breast cancer diagnosis.

This retrospective study aims to assess the diagnostic efficacy of combining SWE with ultrasound BI-RADS classification and MRI in distinguishing between benign and malignant breast lesions.

Materials and methods

Study design

This was a single-center retrospective study.

Participants

Patients included in this study were individuals with benign or malignant breast lesions who were diagnosed and treated by surgery. All cases were confirmed and classified the lesions into either benign group or malignant group through pathological evidence. The inclusion criteria were: 1) patients who underwent breast SWE, ultrasound and MRI before surgery in Yancheng No. 1 People's Hospital (The First People's Hospital of Yancheng), Affiliated Hospital of Medical School, Nanjing University (Nanjing, China); 2) resection of the lesion site in the breast and pathological examination were performed in this hospital; and 3) complete clinical data. The exclusion criteria were: 1) a history of prior breast surgeries or chemoradiation therapy; 2) coexisting malignancies; 3) metastatic diseases; 4) indeterminate pathology findings; 5) breast implant(s); 6) current pregnancy or breastfeeding status; 7) breast lesions exceeding 3 cm; 8) contraindications for MRI; and 9) critical illness.

Variables

Patient demographic and clinical data included: age, body mass index (BMI), family history of cancer, menstrual status, lesion type, lesion size, nodal involvement, lesion location, and histological grade. The single modality evaluation using either SWE, ultrasound or MRI was documented. A combination diagnosis, combining all 3 modalities, was performed using the existing information to comprehensively reassess included lesions. The above examination used the 2013 BI-RADS guidelines issued by the ACR to evaluate the lesions.[8] Pathologic diagnoses were used as the gold standard. If the imaging diagnosis matched with pathology, it was then considered a true positive. Otherwise, it was defined as a false positive.

Data measurement

Ultrasonic examination

A senior sonographer performed the exam by using a standard ultrasound scanner (AixPlorer; SuperSonic Imagine, Aix-en-Provence, France). The patient was placed in a supine position with both arms raised to adequately expose the breast area. Starting from the upper outer quadrant, the scanning continued gradually in a clockwise manner from the breast edges towards the nipple. Bilateral breasts were both scanned. Sonographic characteristics recorded included tissue composition, lesion-related parameters (shape, orientation, margin, echo pattern, posterior features), calcifications, associated features (architectural distortion, duct changes, skin changes, edema, vascularity, elasticity assessment), and other features (cysts, lymph nodes, vascular abnormalities, fat necrosis).

Shear-wave elastography

After the standard ultrasound evaluation, the probe was then placed on the skin to locate the lesion again. The level with the largest cross-sectional area was identified and selected, followed by switching to the SWE elasticity imaging mode. The sonographer then instructed the patient to hold their breath for 3 s and capture the image. The quantitative analysis sampling box (Q-box) was placed to cover the entire lesion as much as possible, with no red compression marks on the box outlines. The Q-box was then adjusted to cover the area with high elasticity surrounding the lesion. The areas extending beyond the Q-box were divided into multiple sections and measured individually. The elastic parameters included the maximum elastic modulus (E-max), average elastic modulus (E-mean), elastic standard deviation (E-sd), and lesion-to-fat elastic ratio (E-ratio). The lesion was measured 3 times, and the average was calculated.

Magnetic resonance imaging

Pre-menopausal patients underwent breast MRI using a 3.0T MRI machine (MAGNETOM Skyra; Siemens AG, Erlangen, Germany) during the 7^{th} to 14^{th} day of their menstrual cycle. No time restrictions applied to post-menopausal patients. The patient was placed in a prone position, and the breasts were appropriately positioned using a dedicated 4-channel coil. Non-enhanced studies included continuous axial slices (thickness: 3 mm, distance factor = 0), and T1-weighted images were captured using turbo spin-echo sequences, while T2-weighted fat-saturated images were obtained via short tau inversion

recovery sequences. Dynamic contrast-enhanced studies used three-dimensional (3D) T1-weighted gradient-echo sequences with the following parameters: repetition time (TR)/echo time (TE): 4.66/1.68 ms; matrix: 448 × 362; field of view. Gadoteric acid was intravenously injected at a dose of 0.2 mL/kg, followed by a 15 mL saline flush. The post-contrast imaging was repeated 5 times. Image processing included subtraction (obtained by subtracting pre-contrast images from the 5 sets of post-contrast images on a pixel-by-pixel basis), multi-planar reconstruction, maximum intensity projection, and time-intensity curves (TIC). The size, shape, border, intensity, and enhancement on the MRI imaging were documented.

Statistical analyses

Statistical analyses were performed using IBM SPSS v. 21.0 (IBM Corp., Armonk, USA). Continuous variables were expressed as means and standard deviation (SD) if the data were normally distributed. Normality was assessed using the Shapiro–Wilk test for sample sizes between 10 and 50 (n = 35 for the malignant group), and by examining skewness values and Q–Q plots for larger samples (n = 64 for the benign group). Skewness values close to 0 and data points aligning closely along the diagonal in Q–Q plots were considered indicative of normal distribution. For variables that did not meet the normality assumption, data were presented as median (Q1, Q3). Categorical variables were expressed as numbers or proportions (%).

For normally distributed continuous variables, we conducted an independent samples Student's t-test to compare differences between the 2 groups, with Welch's correction applied if variances were unequal (assessed with Levene's test). For non-normally distributed continuous variables, Mann–Whitney U test was used as a nonparametric alternative to compare the 2 groups. For categorical variables, Pearson's χ^2 test was used to assess independence and compare proportions between the groups.

Diagnostic performance metrics, including sensitivity, specificity, positive predictive value (PPV), negative predictive value (NPV), and accuracy, were calculated and reported as descriptive statistics without statistical comparisons. The receiver operating characteristic (ROC) curve was plotted, and the area under the curve (AUC) was calculated to assess diagnostic performance. DeLong's test, implemented using the roc.test(roc1, roc2, method="delong") function in R (R Foundation for Statistical Computing, Vienna, Austria), was conducted to compare AUC values across diagnostic modalities.

For analyses involving multiple comparisons, Bonferroni correction was applied to control for type I error, with adjusted significance thresholds calculated based on the number of comparisons. The significance threshold was adjusted for the number of comparisons made to reduce the risk of false positives. However, for exploratory analyses (e.g., baseline clinical characteristics, evaluation of SWE, ultrasound, and MRI features), no correction for multiple comparisons was applied. Given the exploratory nature of these analyses, the statistical significance was defined as $p < 0.05$.

Results

Clinical characteristics of included patients

A total of 99 patients were enrolled in this study; 64 had benign lesions, while 35 had malignant diseases, including 5 invasive ductal carcinomas, 7 cases of ductal carcinoma in situ, 5 mucinous carcinomas, 5 invasive lobular carcinomas, 6 solid papillary carcinomas, 3 borderline phyllodes tumors, and 4 advanced lymphomas. As shown in Table 1, there were significant differences in the age of patients with (49.33 ±8.71 vs 53.49 ±6.47; $t(97) = -2.47$, $p = 0.015$), BMI (24.39 (22.45, 26.27) vs 25.78 (23.67, 27.69); $z = 2.10$, $p = 0.036$) and the lesions size (1.70 cm vs 2.07 cm; $t(97) = -4.19$, $p < 0.001$) between the benign group and malignant group. Also, malignant group patients tend to have more family members with a oncologic diagnosis (42.9% vs 20.3%; $\chi^2 = 5.67$, degrees of freedom (df) = 1, $p = 0.017$), higher proportion of menopause status (51.4% vs 29.7%; $\chi^2 = 4.57$, $df = 1$, $p = 0.033$) and histology grading III (42.9% vs 17.2%; $\chi^2 = 10.72$, $df = 2$, $p = 0.005$). There was no statistically significant difference in lesion laterality between the benign and malignant groups ($\chi^2 = 3.41$, $df = 1$, $p = 0.065$) (Table 1).

Shear-wave elastography evaluation of breast lesions

Table 2 summarizes the 4 SWE parameters measured. The malignant group demonstrated higher E-max (151.96 kPa vs 69.65 kPa; $t(97) = -9.66$, $p < 0.001$), E-mean (92.30 ±13.05 vs 30.04 ±9.28; $t(53) = -24.97$, $p < 0.001$), E-sd (13.09 ±2.45 vs 8.98 ±2.47; $t(97) = -7.93$, $p < 0.001$), and E-ratio (14.77 ±3.50 vs 3.39 ±0.80; $t(35) = -18.99$, $p < 0.001$) compared to the benign group (Table 2). Representative SWE images from the malignant and benign groups are presented in Fig. 1.

Ultrasound evaluation of breast lesions

The incidence of discovering a mass in the malignant cohort was higher than that in the benign group (37.1% vs 14.1%; $\chi^2 = 6.97$, $df = 1$, $p = 0.008$). It is also more likely to detect heterogeneous echogenicity in malignant lesions (45.7% vs 15.6%; $\chi^2 = 10.58$, $df = 1$, $p = 0.001$). Benign lesions tended to have well-defined borders ($\chi^2 = 19.92$, $df = 1$, $p < 0.001$) and regular shapes ($\chi^2 = 11.25$, $df = 1$, $p = 0.001$). Calcifications were more frequently detected in patients with malignant diseases ($\chi^2 = 6.24$, $df = 1$, $p = 0.013$). There was a higher

Table 1. Clinical characteristics of included patients

Variable		Benign group (n = 64)	Malignant group (n = 35)	t/Z/^{2}	df	p-value
Age [years]		49.33 ±8.71	53.49 ±6.47	–2.47	97	0.015
BMI [kg/m^2]		24.39 (22.45, 26.27)	25.78 (23.67, 27.69)	2.10	97	0.036
Family oncology history, n (%)	no	51 (79.7)	20 (57.1)	5.67	1	0.017
	yes	13 (20.3)	15 (42.9)			
Menopause status, n (%)	no	45 (70.3)	17 (48.6)	4.57	1	0.033
	yes	19 (29.7)	18 (51.4)			
Lesion size [cm]		1.70 ±0.39	2.07 ±0.45	–4.19	97	<0.001
Lesion side, n (%)	left	26 (40.6)	21 (60.0)	3.41	1	0.065
	right	38 (59.4)	14 (40.0)			
Histology grading, n (%)	I	34 (53.1)	8 (22.9)	10.72	2	0.005
	I	19 (29.7)	12 (34.3)			
	III	11 (17.2)	15 (42.9)			

Data were presented as mean ± standard deviation (±SD), median (Q1, Q3) or n (%). Independent samples t-test was used for normally distributed continuous variables, Mann–Whitney U test was used for non-normally distributed continuous variables, and χ^2 test was used for categorical variables; df – degrees of freedom; BMI – body mass index.

Table 2. Shear-wave elastography (SWE) evaluation of breast lesions

Variable	Benign group (n = 64)	Malignant group (n = 35)	t	df	p-value
E-max	69.65 ±36.64	151.96 ±46.94	–9.66	97	<0.001
E-mean	30.04 ±9.28	92.30 ±13.05	–24.97	53 (Welch)	<0.001
E-sd	8.98 ±2.47	13.09 ±2.45	–7.93	97	<0.001
E-ratio	3.39 ±0.80	14.77 ±3.50	–18.99	36 (Welch)	<0.001

Data were presented as mean ± standard deviation (±SD). Welch's t-test was applied for E-mean and E-ratio due to unequal variances between groups, while the independent samples t-test was used for E-max and E-sd. df – degrees of freedom.

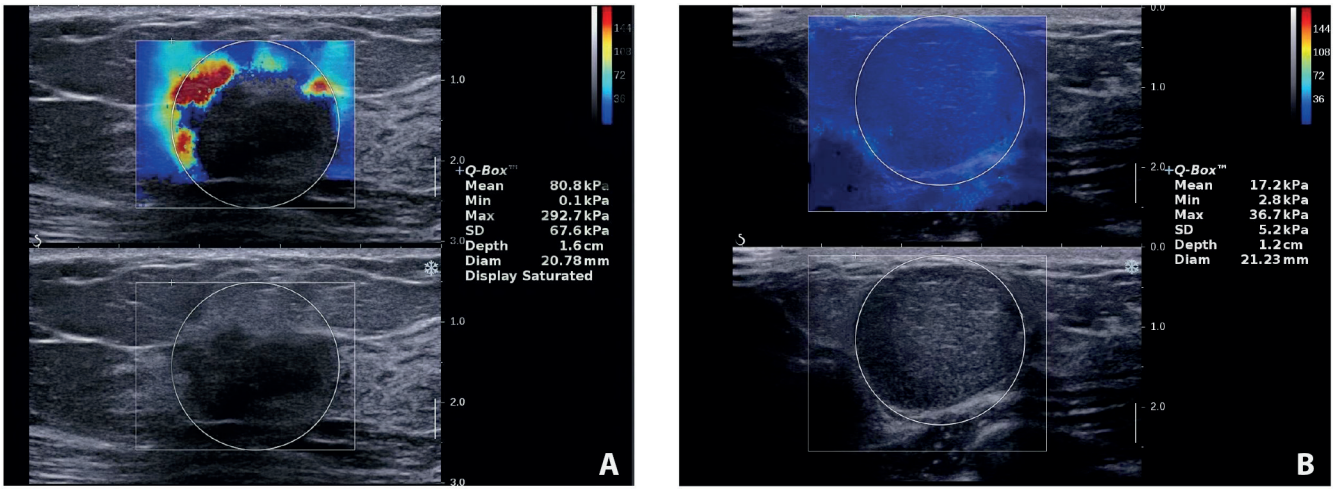

Fig. 1. Shear-wave elastography (SWE) images of breast lesions showing stiffness differences between malignant and benign lesions. A. Malignant breast lesion with high stiffness and heterogeneity, indicated by an E-mean of 80.8 kPa and E-max of 292.7 kPa in the Q-Box (measurement area). The color scale on the right shows stiffness values, with red indicating higher stiffness; B. Benign breast lesion with lower, more uniform stiffness, with an E-mean of 17.2 kPa and E-max of 36.7 kPa. The lesion appears primarily in blue on the color scale, reflecting lower stiffness

proportion of malignant lesions showing posterior attenuation (42.9% vs 21.9%; $\chi^2 = 4.81$, df = 1, p = 0.028). Benign lesions were less likely to be associated with abnormal axillary node findings (76.6% vs 34.3%; $\chi^2 = 17.01$, df = 1, p < 0.001) (Table 3). The typical ultrasound images from the malignant and benign groups are shown in Fig. 2.

Table 3. Ultrasound evaluation of breast lesions

Variable		Benign group (n = 64)	Malignant group (n = 35)	2	df	p-value
Mass presentation, n (%)	no	55 (85.9)	22 (62.9)	6.97	1	0.008
	yes	9 (14.1)	13 (37.1)			
Echo, n (%)	hypoechoic	54 (84.4)	19 (54.3)	10.58	1	0.001
	heterogenous echogenicity	10 (15.6)	16 (45.7)			
Borders, n (%)	well-defined	56 (87.5)	16 (45.7)	19.92	1	0.001
	poor-defined	8 (12.5)	19 (54.3)			
Shape, n (%)	regular	58 (90.6)	22 (62.9)	11.25	1	0.001
	irregular	6 (9.4)	13 (37.1)			
Calcifications, n (%)	no	53 (82.8)	21 (60.0)	6.24	1	0.013
	yes	11 (17.2)	14 (40.0)			
Posterior attenuation, n (%)	no	50 (78.1)	20 (57.1)	4.81	1	0.028
	yes	14 (21.9)	15 (42.9)			
Axillary abnormal nodes, n (%)	no	49 (76.6)	12 (34.3)	17.10	1	<0.001
	yes	15 (23.4)	23 (65.7)			

Data were presented as n (%); χ^2 test was used to compare categorical variables between groups; df – degrees of freedom.

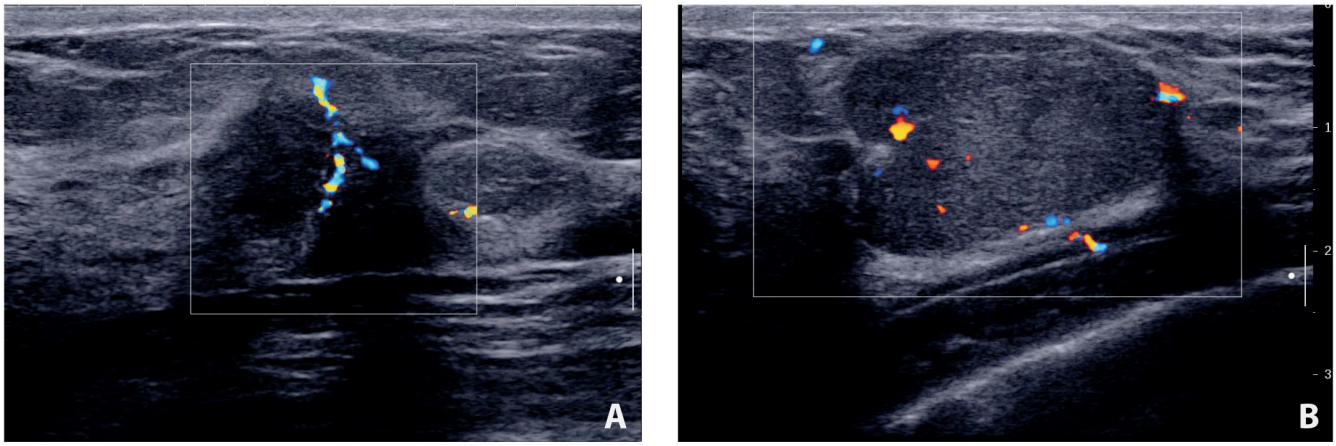

Fig. 2. Ultrasound images of malignant and benign breast lesions with color Doppler imaging. A. Malignant breast lesion showing heterogeneous echogenicity, irregular shape and posterior attenuation. Color Doppler imaging demonstrates irregular vascularization, which is indicative of neovascularization within the tumor; B. Benign breast lesion displaying well-defined borders, regular shape and homogeneous echogenicity. Color Doppler imaging shows minimal and regular vascularization, typical of benign lesions

Magnetic resonance imaging evaluation of breast lesions

The shape and border differences of lesions evaluated with MRI were similar to the ultrasound features. More irregular shapes were found in malignant group compared to patients with the benign group (48.6% vs 23.4%; $\chi^2 = 6.53$, df = 1, p = 0.011) and more lesions with poor-defined borders were identified (51.4% vs 26.6%; $\chi^2 = 6.12$, df = 1, p = 0.013). The benign group demonstrated more homogeneous enhancement, whereas the malignant group showed greater heterogeneity ($\chi^2 = 14.74$, df = 1, p < 0.001). The average apparent diffusion coefficient (ADC) was 1.18 (0.95, 1.34) in the malignant group, which was higher than 0.80 (0.65, 0.91) in the benign group (z = 6.14, p < 0.001). Type III time-intensity curves (TICs) were more frequently observed in the malignant group compared to the benign group (51.4% vs 25%). Conversely, type I and type II TICs were more commonly seen in the benign group (42.2% vs 17.1% and 32.8% vs 31.4%, respectively). The differences were statistically significant ($\chi^2 = 8.87$, df = 2, p = 0.012) (Table 4). The typical MRI images and TIC from the malignant and benign groups are shown in Fig. 3.

Diagnostic value evaluation

Pathologic diagnosis was used as the gold standard. When evaluating the lesions using individual modality, SWE detected 22 true positive cases and 42 true negative cases. Similarly, ultrasound was also able to detect 22 true positive cases and 40 true negative cases. As for MRI, it had more false negative cases and fewer true negative cases

Table 4. Magnetic resonance imaging (MRI) evaluation of breast lesions

Variable		Benign group (n = 64)	Malignant group (n = 35)	t/Z/^{2}	df	p-value
Shape, n (%)	round/oval	49 (76.6)	18 (51.4)	6.53	1	0.011
	irregular	15 (23.4)	17 (48.6)			
Borders, n (%)	well-defined	47 (73.4)	17 (48.6)	6.12	1	0.013
	poor-defined	17 (26.6)	18 (51.4)			
Enhancement, n (%)	homogenous	53 (82.8)	16 (45.7)	14.74	1	<0.001
	heterogeneous/circular	11 (17.2)	19 (54.3)			
ADC		0.80 (0.65, 0.91)	1.18 (0.95, 1.34)	6.14	78	<0.001
TIC, n (%)	type I	27 (42.2)	6 (17.1)	8.87	2	0.012
	type II	21 (32.8)	11 (31.4)			
	type III	16 (25.0)	18 (51.4)			

Data were presented as median (Q1, Q3) or n (%); Mann–Whitney U test was used for non-normally distributed continuous variables and χ^2 test was used for categorical variables. ADC – apparent diffusion coefficient; TIC – time-intensity curves; df – degrees of freedom.

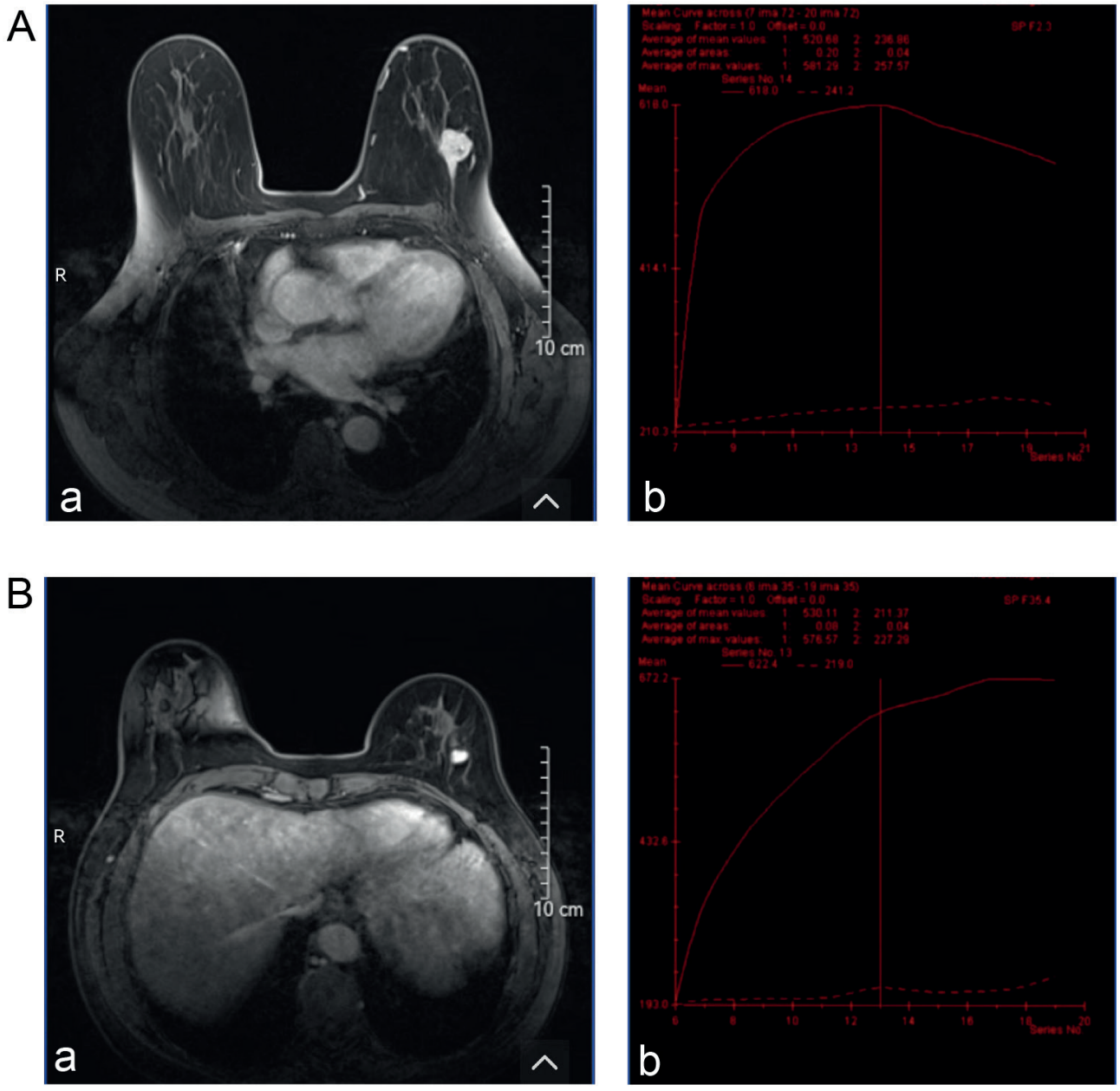

Fig. 3. Magnetic resonance imaging (MRI) images and time-intensity curves (TIC) for malignant and benign breast lesions. A. Malignant breast lesion: MRI image showing irregular shape and heterogeneous enhancement, characteristics commonly associated with malignancy (a) and corresponding TIC shows a rapid initial enhancement followed by a washout phase (type III), which is indicative of aggressive tumor behavior (b); B. Benign breast lesion: MRI image displaying well-defined borders and homogeneous enhancement, typical of benign features (a) and corresponding TIC shows gradual and persistent enhancement (type I), which is characteristic of benign lesions (b)

Table 5. Diagnostic results of shear-wave elastography (SWE), ultrasound, magnetic resonance imaging (MRI), and their combination

Diagnostic modality	True positive, n	False positive, n	True negative, n	False negative, n
SWE	22	22	42	13
Ultrasound	22	24	40	13
MRI	23	25	39	12
Combination	33	7	57	2

Table 6. Diagnostic value evaluation of shear-wave elastography (SWE), ultrasound, magnetic resonance imaging (MRI), and their combination

Diagnostic modality	Sensitivity (%)	Specificity (%)	PPV (%)	NPV (%)	Accuracy (%)
SWE	62.9	65.6	50.0	76.4	64.6
Ultrasound	62.9	62.5	47.8	75.5	62.6
MRI	65.7	60.9	47.9	76.5	62.6
Combination	94.3	89.1	82.5	96.6	90.9

PPV – positive predictive value; NPV – negative predictive value.

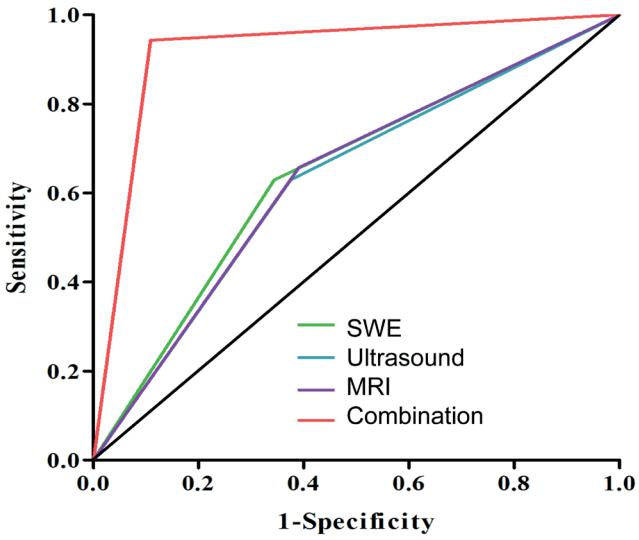

Fig. 4. Receiver operating characteristic (ROC) curves for diagnostic performance of shear-wave elastography (SWE), ultrasound, magnetic resonance imaging (MRI), and their combination. Area under the curve (AUC) of SWE: 0.642 (0.528–0.757), AUC of ultrasound: 0.627 (0.511–0.742), AUC of MRI: 0.633 (0.518–0.748), AUC of the combination: 0.917 (0.853–0.980). The AUC represents the overall diagnostic accuracy, with higher values indicating better performance

(Table 5). When all 3 modalities were combined, the diagnostic approach most closely matched the pathological results, identifying 33 true positive cases and 57 true negative cases. It also yielded the lowest false positive and false negative cases (Table 5).

Magnetic resonance imaging demonstrated the highest sensitivity for detecting malignancies (65.7%), while SWE had the highest specificity (65.6%) and the highest positive predictive value (PPV; 50.0%). Magnetic resonance imaging also showed a strong negative predictive value (NPV; 76.5%). The diagnostic accuracy of SWE, ultrasound and MRI was comparable, with SWE having the highest accuracy (64.6%). When combining all 3 modalities, the diagnostic performance improved substantially, with sensitivity increasing to 94.3% and specificity reaching 89.1%. The combination also yielded the highest PPV (82.5%) and NPV (96.6%), resulting in an overall accuracy of 90.9% (Table 6).

Figure 4 demonstrates the ROC of each modality as well as the combination of 3 techniques. The AUC values were as follows: SWE (0.642), ultrasound (0.627), MRI (0.633), and the combination of all 3 modalities (0.917). Pairwise comparisons using DeLong's test showed that the AUC for the combined modalities was significantly higher than those for individual modality ($p_{adjusted} < 0.001$). However, no significant differences were observed between SWE, ultrasound and MRI ($p_{adjusted} > 0.05$ for all comparisons) (Table 7).

Discussion

Early diagnosis of breast cancer is critical for determining appropriate management strategies and improving patient outcomes; however, current screening and diagnostic modalities still require further refinement. Although SWE can enhance diagnostic efficacy when used alongside ultrasound,[17,19] it has not yet been incorporated into the BI-RADS system. Interestingly, the combined use of all 3 commonly employed modalities for diagnostic assistance has only rarely been explored. Our study identified that using SWE alone did not yield significant diagnostic benefit, but combining it with ultrasound and MRI showed the sensitivity of 94.3% and the specificity 89.1%, which was significantly higher than single modality evaluation. Our results suggest the potential and value of combining 3 different imaging modalities to enhance diagnostic accuracy, warranting further investigation.

Our results from the ultrasound evaluations underscore the salient differences between benign and malignant breast lesions. Previous literature highlights similar distinctions. The higher frequency of mass presentation

Table 7. Comparison of area under the curve (AUC) values for shear-wave elastography (SWE), ultrasound, magnetic resonance imaging (MRI), and their combination

Comparison	AUC 1	AUC 2	p-value	Adjusted p-value
Combination vs SWE	0.917	0.642	<0.001	<0.001
Combination vs ultrasound	0.917	0.627	<0.001	<0.001
Combination vs MRI	0.917	0.633	<0.001	<0.001
SWE vs MRI	0.642	0.633	0.45	1.000
SWE vs ultrasound	0.642	0.627	0.65	1.000
MRI vs ultrasound	0.633	0.627	0.75	1.000

Data were presented as n. DeLong's test was used to compare the diagnostic performance metrics across the 4 modalities. Adjusted p-values higher than 1 were presented as p = 1, as p-values cannot exceed this value.

in malignant lesions compared to benign ones (37.1% vs 14.1%) aligns with findings by Berg et al.,[20] who emphasized that malignant masses are more prominently visualized on ultrasound. This observation of a higher proportion of cases with heterogeneity, calcifications and posterior attenuation in malignant lesions also matches the previous findings.[21–23] Lastly, the markedly higher association of malignant lesions with abnormal axillary lymph node findings compared to benign lesions (65.7% vs 23.4%) reinforces the diagnostic importance of nodal assessment in breast imaging, as highlighted by Lee et al.[24] In our study, we found the sensitivity, specificity, PPV, NPV, and AUC of ultrasonography to be 62.9%, 62.5%, 47.8%, 75.5%, and 0.627 respectively. The average diagnostic efficacy was lower than reported in studies,[11,25,26] which could be due to geographic location and small samples in this study.

Magnetic resonance imaging evaluations of breast lesions presented in our study align with some of our ultrasound results, emphasizing the differences between benign and malignant lesions. Malignant lesions consistently exhibited irregular shapes (48.6% vs 23.4%, p = 0.011), poorly defined borders (51.4% vs 26.6%, p = 0.013) and heterogeneous enhancement patterns, consistent with findings in the literature.[27–29] Notably, the higher average ADC values in malignant lesions (1.18 vs 0.80, p < 0.001) reaffirm their diagnostic significance.[30] The distribution of TIC types further differentiated the lesions, with type III being predominant in malignancies, aligning with prior studies.[31,32] Meanwhile, MRI, recognized for its superior soft tissue contrast, demonstrated a sensitivity of 65.7%, specificity of 60.9% and an AUC of 0.633 in our study – values that are lower than those reported in previous literature.[33,34] This discrepancy may be attributed to our relatively small sample size and the inclusion of a substantial number of benign cases, suggesting that despite the lower performance in this study, MRI retains significant diagnostic value in detecting malignant breast lesions.

The SWE evaluation in our cohorts demonstrated that the elastic parameters (E-max, E-mean, E-sd, and E-ratio) in the malignant lesions were all significantly higher than those in benign diseases. Our results are consistent with the findings by Schaefer et al. that significantly higher elasticity in malignant lesions was observed.[11] Though the exact mechanism of the "stiffness" of malignant lesions is unknown, several possibilities have been proposed. Wang's team evaluated the extracellular matrix (ECM) components in benign and malignant breast lesions and found a higher concentration of collagen and elastic fibers in the ECM of cancerous tissues. These findings suggest that alterations in ECM composition may contribute to the increased stiffness observed on ultrasound elastography.[35] Xue et al. conducted a more in-depth molecular investigation and found that hypoxia-inducible factor 1-alpha (HIF-1α), in conjunction with Kindlin-2, plays a role in promoting collagen formation in breast cancer tissues.[36,37] Other possible mechanism might involve more intense immune response around cancer cells or rapid growth of cancer cells, which all remains to be proven by more research.

Although the diagnostic potential of SWE is well recognized, its integration into clinical guidelines has been delayed due to several limitations. Key barriers to implementation include operator dependency, variability in cut-off thresholds, limited equipment availability, and the high cost of elastography devices. These factors continue to hinder the adoption of SWE into standardized diagnostic protocols.[5,18] Addressing these barriers, such as through the standardization of diagnostic thresholds and increased availability of training programs for healthcare professionals, may help facilitate its adoption in clinical practice. Nevertheless, our study demonstrated that using SWE alone yielded a sensitivity of 62.9%, specificity of 62.5%, PPV of 50%, NPV of 76.4%, and an AUC of 0.642. These findings align with those reported by Evans et al.,[38] who observed that while SWE and greyscale BI-RADS had comparable diagnostic performance individually, their combination significantly improved sensitivity – reaching 100% for malignancy detection. Shi et al. also evaluated the combined use of SWE and greyscale ultrasound in 251 patients and reported similarly improved diagnostic performance, with a sensitivity of 96.7% and an accuracy of 93.8%.[19] Shear-wave elastography has rarely been combined with MRI, as both are typically employed as independent imaging

modalities for lesion assessment. The study by Plecha et al. demonstrated that using SWE-based second-look ultrasound following MRI can improve the detection rate of breast cancers.[39] In our study, we integrated all 3 imaging modalities – ultrasound, SWE and MRI – for the initial assessment and found that this comprehensive approach significantly enhanced diagnostic performance, achieving a sensitivity of 94.3%, specificity of 89.1%, PPV of 82.5%, NPV of 96.6%, and an AUC of 0.917. There were limited studies available for direct comparison; however, our results demonstrated a relatively favorable diagnostic performance when SWE was added to ultrasound alone.[17,19,40] Although the diagnostic accuracy of SWE in our study appeared lower than that reported in previous studies,[17] this discrepancy may be attributed to our relatively small sample size and potential inconsistencies in the application of the SWE technique. Additionally, our combination results highlighted the emerging need to investigate and evaluate the multimodal approach for early breast cancer diagnosis.

Besides the diagnostic value of SWE, its capability to be integrated in breast cancer prognosis prediction has also been investigated. Higher E-ratio has been reported to be associated with negative hormonal receptor expression and positive p53 and Ki-67.[41] Chang et al. studied 337 patients with invasive breast cancer and found that elevated elastic parameters were significantly associated with more aggressive tumor subtypes.[42] Another research group reported similar findings and additionally observed that high tissue elasticity was associated with nodal metastases.[43] Furthermore, a growing body of evidence supports the use of SWE in predicting responses to neoadjuvant chemotherapy.[25,44,45] While these aspects were beyond the scope of our study, the encouraging results underscore the prognostic potential of SWE and its possible role in informing future treatment strategies for patients with breast cancer.

Limitations

Our study has several limitations. First, this is a single-center retrospective study, and our sample size is relatively small. Second, the inter-observer reliability of SWE is not consistent;[46] thus, the interpretation and techniques performed may not be completely standard. Third, since mammography is not frequently used as an initial assessment modality in China, we did not include it in our study, which might limit the generality of our findings to countries that place more emphasis on screening mammography. Moreover, although the Bonferroni correction was applied to some hypotheses to control for type I error, it was not consistently applied across all comparisons, thereby increasing the risk of false positives – particularly in exploratory analyses. This limitation should be considered when interpreting the results. Future research should implement more rigorous adjustments for multiple comparisons to reduce the risk of type I error.

Conclusions

Shear-wave elastography exhibits similar diagnostic performance as ultrasound and MRI when used as single modality. However, when combining all 3 together, it can yield significantly higher sensitivity, specificity, PPV, NPV, and accuracy. Future studies should focus on how to integrate SWE into BI-RADS system for more accurate detection for malignancies.

Data availability

The datasets generated and/or analyzed during the current study are available from the corresponding author on reasonable request.

Consent for publication

Not applicable.

Use of AI and AI-assisted technologies

Not applicable.

ORCID iDs

Wen-Yan Zhou https://orcid.org/0009-0006-0489-5421
Lian-Lian Zhang https://orcid.org/0000-0003-0966-4228
Xiao Zhou https://orcid.org/0009-0007-5312-1067
Xian-Bin Pan https://orcid.org/0009-0009-4960-2276
Long-Xiu Qi https://orcid.org/0009-0004-4914-8097

References

1. Vaiphei KK, Prabakaran A, Snigdha S, et al. Impact of PEGylated liposomes on cytotoxicity of tamoxifen and piperine on MCF-7 human breast carcinoma cells. *J Drug Deliv Sci Technol*. 2024;102(Pt A):106331. doi:10.1016/j.jddst.2024.106331
2. Bray F, Ferlay J, Soerjomataram I, Siegel RL, Torre LA, Jemal A. Global cancer statistics 2018: GLOBOCAN estimates of incidence and mortality worldwide for 36 cancers in 185 countries. *CA Cancer J Clin*. 2018;68(6):394–424. doi:10.3322/caac.21492
3. DeSantis CE, Ma J, Goding Sauer A, Newman LA, Jemal A. Breast cancer statistics, 2017, racial disparity in mortality by state. *CA Cancer J Clin*. 2017;67(6):439–448. doi:10.3322/caac.21412
4. Torre LA, Islami F, Siegel RL, Ward EM, Jemal A. Global cancer in women: Burden and trends. *Cancer Epidemiol Biomarkers Prev*. 2017;26(4):444–457. doi:10.1158/1055-9965.EPI-16-0858
5. Wildeboer RR, Van Sloun RJG, Mannaerts CK, et al. Synthetic elastography using B-mode ultrasound through a deep fully convolutional neural network. *IEEE Trans Ultrason Ferroelect Freq Contr*. 2020;67(12):2640–2648. doi:10.1109/TUFFC.2020.2983099
6. National Comprehensive Cancer Network (NCCN). Breast Cancer Version 4 (NCCN Guidelines). Plymouth Meeting, USA: National Comprehensive Cancer Network (NCCN); 2023. https://www.nccn.org/guidelines/guidelines-detail?category=1&id=1419. Accessed September 18, 2023.
7. Moy L, Heller SL, Bailey L, et al. ACR Appropriateness Criteria® Palpable Breast Masses. *J Am Coll Radiol*. 2017;14(5 Suppl):S203–S224. doi:10.1016/j.jacr.2017.02.033
8. American College of Radiology (ACR). BI-RADS® ACR Breast Imaging Reporting and Data System. Reston, USA: American College of Radiology (ACR); 2024. https://www.acr.org/Clinical-Resources/Reporting-and-Data-Systems/Bi-Rads. Accessed March 1, 2025.
9. Berg WA, Zhang Z, Lehrer D, et al; ACRIN 6666 Investigators. Detection of breast cancer with addition of annual screening ultrasound or a single screening MRI to mammography in women with elevated breast cancer risk. *JAMA*. 2012;307(13):1394–1404. doi:10.1001/jama.2012.388

10. Torge D, Bernardi S, Ciciarelli G, Macchiarelli G, Bianchi S. Dedicated protocol for ultrastructural analysis of farmed rainbow trout (*Oncorhynchus mykiss*) tissues with red mark syndrome. The skin: Part one. *Methods Protoc*. 2024;7(3):37. doi:10.3390/mps7030037
11. Schaefer FKW, Heer I, Schaefer PJ, et al. Breast ultrasound elastography: Results of 193 breast lesions in a prospective study with histopathologic correlation. *Eur J Radiol*. 2011;77(3):450–456. doi:10.1016/j.ejrad.2009.08.026
12. Fleury E de FC, Fleury JCV, Piato S, Roveda D. New elastographic classification of breast lesions during and after compression. *Diagn Interv Radiol*. 2009;15(2):96–103. PMID:19517379.
13. Regner DM, Hesley GK, Hangiandreou NJ, et al. Breast lesions: Evaluation with US strain imaging. Clinical experience of multiple observers. *Radiology*. 2006;238(2):425–437. doi:10.1148/radiol.2381041336
14. Burnside ES, Hall TJ, Sommer AM, et al. Differentiating benign from malignant solid breast masses with US strain imaging. *Radiology*. 2007;245(2):401–410. doi:10.1148/radiol.2452061805
15. Athanasiou A, Tardivon A, Tanter M, et al. Breast lesions: Quantitative elastography with supersonic shear imaging. Preliminary results. *Radiology*. 2010;256(1):297–303. doi:10.1148/radiol.10090385
16. Evans A, Whelehan P, Thomson K, et al. Quantitative shear wave ultrasound elastography: Initial experience in solid breast masses. *Breast Cancer Res*. 2010;12(6):R104. doi:10.1186/bcr2787
17. Pillai A, Voruganti T, Barr R, Langdon J. Diagnostic accuracy of shear-wave elastography for breast lesion characterization in women: A systematic review and meta-analysis. *J Am Coll Radiol*. 2022;19(5):625–634.e0. doi:10.1016/j.jacr.2022.02.022
18. Cè M, D'Amico NC, Danesini GM, et al. Ultrasound elastography: Basic principles and examples of clinical applications with artificial intelligence. A review. *BioMedInformatics*. 2023;3(1):17–43. doi:10.3390/biomedinformatics3010002
19. Shi XQ, Li JL, Wan WB, Huang Y. A set of shear wave elastography quantitative parameters combined with ultrasound BI-RADS to assess benign and malignant breast lesions. *Ultrasound Med Biol*. 2015;41(4):960–966. doi:10.1016/j.ultrasmedbio.2014.11.014
20. Berg WA, Bandos AI, Mendelson EB, Lehrer D, Jong RA, Pisano ED. Ultrasound as the primary screening test for breast cancer: Analysis from ACRIN 6666. *J Natl Cancer Inst*. 2016;108(4):djv367. doi:10.1093/jnci/djv367
21. Tarchi SM, Pernia Marin M, Hossain MdM, Salvatore M. Breast stiffness, a risk factor for cancer and the role of radiology for diagnosis. *J Transl Med*. 2023;21(1):582. doi:10.1186/s12967-023-04457-0
22. Zhang S, Shao H, Li W, et al. Intra- and peritumoral radiomics for predicting malignant BiRADS category 4 breast lesions on contrast-enhanced spectral mammography: A multicenter study. *Eur Radiol*. 2023;33(8):5411–5422. doi:10.1007/s00330-023-09513-3
23. Irshad A, Leddy R, Pisano E, et al. Assessing the role of ultrasound in predicting the biological behavior of breast cancer. *Am J Roentgenol*. 2013;200(2):284–290. doi:10.2214/AJR.12.8781
24. Lee B, Lim AK, Krell J, et al. The efficacy of axillary ultrasound in the detection of nodal metastasis in breast cancer. *Am J Roentgenol*. 2013;200(3):W314–W320. doi:10.2214/AJR.12.9032
25. Qi J, Wang C, Ma Y, et al. The potential role of combined shear wave elastography and superb microvascular imaging for early prediction the pathological response to neoadjuvant chemotherapy in breast cancer. *Front Oncol*. 2023;13:1176141. doi:10.3389/fonc.2023.1176141
26. Monticciolo DL, Newell MS, Moy L, Niell B, Monsees B, Sickles EA. Breast cancer screening in women at higher-than-average risk: Recommendations from the ACR. *J Am Coll Radiol*. 2018;15(3):408–414. doi:10.1016/j.jacr.2017.11.034
27. Li X, Fan Z, Jiang H, et al. Synthetic MRI in breast cancer: Differentiating benign from malignant lesions and predicting immunohistochemical expression status. *Sci Rep*. 2023;13(1):17978. doi:10.1038/s41598-023-45079-2
28. Ghuman N, Ambinder EB, Oluyemi ET, Sutton E, Myers KS. Clinical and imaging features of MRI screen-detected breast cancer. *Clin Breast Cancer*. 2024;24(1):45–52. doi:10.1016/j.clbc.2023.09.012
29. Billy CA, Darmiati S, Prihartono J. Diagnostic accuracy of diffusion weighted imaging compared to magnetic resonance spectroscopy in differentiation of benign and malignant breast lesions: A systematic review and meta-analysis. *Eur J Radiol*. 2023;168:111124. doi:10.1016/j.ejrad.2023.111124
30. Ozkul O, Sever I, Ozkul B. Assessment of apparent diffusion coefficient parameters and coefficient of variance in discrimination of receptor status and molecular subtypes of breast cancer. *Curr Med Imaging*. 2023;20:e060923220760. doi:10.2174/1573405620666230906092253
31. Li Y, Yang Z, Lv W, et al. Role of combined clinical-radiomics model based on contrast-enhanced MRI in predicting the malignancy of breast non-mass enhancements without an additional diffusion-weighted imaging sequence. *Quant Imaging Med Surg*. 2023;13(9):5974–5985. doi:10.21037/qims-22-1199
32. Li Y, Chen J, Yang Z, et al. Contrasts between diffusion-weighted imaging and dynamic contrast-enhanced MR in diagnosing malignancies of breast nonmass enhancement lesions based on morphologic assessment. *J Magn Reson Imaging*. 2023;58(3):963–974. doi:10.1002/jmri.28600
33. Aristokli N, Polycarpou I, Themistocleous SC, Sophocleous D, Mamais I. Comparison of the diagnostic performance of magnetic resonance imaging (MRI), ultrasound and mammography for detection of breast cancer based on tumor type, breast density and patient's history: A review. *Radiography*. 2022;28(3):848–856. doi:10.1016/j.radi.2022.01.006
34. Gao Y, Reig B, Heacock L, Bennett DL, Heller SL, Moy L. Magnetic resonance imaging in screening of breast cancer. *Radiol Clin North Am*. 2021;59(1):85–98. doi:10.1016/j.rcl.2020.09.004
35. Liu G, Zhang MK, He Y, Li XR, Wang ZL. Shear wave elasticity of breast lesions: Would it be correlated with the extracellular matrix components? *Gland Surg*. 2019;8(4):399–406. doi:10.21037/gs.2019.04.09
36. Xue X, Xue S, Wan W, Li J, Shi H. HIF-1α interacts with Kindlin-2 and influences breast cancer elasticity: A study based on shear wave elastography imaging. *Cancer Med*. 2020;9(14):4971–4979. doi:10.1002/cam4.3130
37. Xue X, Li J, Wan W, Shi X, Zheng Y. Kindlin-2 could influence breast nodule elasticity and improve lymph node metastasis in invasive breast cancer. *Sci Rep*. 2017;7(1):6753. doi:10.1038/s41598-017-07075-1
38. Evans A, Whelehan P, Thomson K, et al. Differentiating benign from malignant solid breast masses: Value of shear wave elastography according to lesion stiffness combined with greyscale ultrasound according to BI-RADS classification. *Br J Cancer*. 2012;107(2):224–229. doi:10.1038/bjc.2012.253
39. Plecha DM, Pham RM, Klein N, Coffey A, Sattar A, Marshall H. Addition of shear-wave elastography during second-look MR imaging–directed breast US: Effect on lesion detection and biopsy targeting. *Radiology*. 2014;272(3):657–664. doi:10.1148/radiol.14132491
40. Farghadani M, Barikbin R, Rezaei MH, Hekmatnia A, Aalinezhad M, Zare H. Differentiating solid breast masses: Comparison of the diagnostic efficacy of shear wave elastography and magnetic resonance imaging. *Diagnosis (Berl)*. 2021;8(3):382–387. doi:10.1515/dx-2020-0056
41. Choi WJ, Kim HH, Cha JH, et al. Predicting prognostic factors of breast cancer using shear wave elastography. *Ultrasound Med Biol*. 2014;40(2):269–274. doi:10.1016/j.ultrasmedbio.2013.09.028
42. Chang JM, Park IA, Lee SH, et al. Stiffness of tumours measured by shear-wave elastography correlated with subtypes of breast cancer. *Eur Radiol*. 2013;23(9):2450–2458. doi:10.1007/s00330-013-2866-2
43. Kim HJ, Kim HH, Choi WJ, Chae EY, Shin HJ, Cha JH. Correlation of shear-wave elastography parameters with the molecular subtype and axillary lymph node status in breast cancer. *Clin Imaging*. 2023;101:190–199. doi:10.1016/j.clinimag.2023.06.006
44. Yuan S, Shao H, Na Z, Kong M, Cheng W. Value of shear wave elasticity in predicting the efficacy of neoadjuvant chemotherapy in different molecular types. *Clin Imaging*. 2022;89:97–103. doi:10.1016/j.clinimag.2022.06.008
45. Duan Y, Song X, Guan L, et al. Comparative study of pathological response evaluation systems after neoadjuvant chemotherapy for breast cancer: Developing predictive models of multimodal ultrasound features including shear wave elastography combined with puncture pathology. *Quant Imaging Med Surg*. 2023;13(5):3013–3028. doi:10.21037/qims-22-910
46. Togawa R, Pfob A, Büsch C, et al. Intra- and interobserver reliability of shear wave elastography in breast cancer diagnosis. *J Ultrasound Med*. 2024;43(1):109–114. doi:10.1002/jum.16344

Expression and correlation of SMAD2/3 and Th1/Th2/Th17 cytokines in embryonic tissues of idiopathic recurrent miscarriage

Huiqin Xue[1,A,E,F], Min Guo[2,C,E], Jingbo Gao[1,B–D], Rong Guo[1,B], Guizhi Cao[1,B], Xinyan Li[1,B], Xiayu Sun[1,B], Hongyong Lu[1,B], Jianrui Wu[1,B]

[1] Department of Cytogenetic Laboratory, Shanxi Women and Children Hospital, Shanxi Children's Hospital, Affiliated Hospital of Shanxi Medical University, Taiyuan, China

[2] Department of Pediatric Medicine, Shanxi Medical University, Taiyuan, China

A – research concept and design; B – collection and/or assembly of data; C – data analysis and interpretation; D – writing the article; E – critical revision of the article; F – final approval of the article

Advances in Clinical and Experimental Medicine, ISSN 1899–5276 (print), ISSN 2451–2680 (online) *Adv Clin Exp Med*. 2026;35(1):89–96

Address for correspondence
Huiqin Xue
E-mail: pyxhq315@163.com

Funding sources
This work was supported by the Shanxi Scholarship Council of China (grant No. 2023-180), the Shanxi Provincial Key Laboratory of Medical Genetics under the 2020 "Fourteenth Batch" Science and Technology Innovation Program (grant No. 2020SYS24), and the Shanxi Provincial Health and Wellness Committee (grant No. 2023016).

Conflict of interest
None declared

Received on December 4, 2024
Reviewed on February 10, 2025
Accepted on April 11, 2025

Published online on January 7, 2026

Cite as
Xue H, Guo M, Gao J, et al. Expression and correlation of SMAD2/3 and Th1/Th2/Th17 cytokines in embryonic tissues of idiopathic recurrent miscarriage. *Adv Clin Exp Med*. 2026;35(1):89–96. doi:10.17219/acem/203971

DOI
10.17219/acem/203971

Abstract

Background. Recurrent miscarriage (RM), the loss of 2 or more consecutive pregnancies before 28 weeks' gestation, has become increasingly common in recent years, imposing significant physical and psychological burdens on affected women. Despite comprehensive evaluation, approx. 40–50% of RM cases remain unexplained and are therefore classified as idiopathic.

Objectives. This study aimed to investigate the expression of *SMAD2* and *SMAD3* and characterize Th1, Th2 and Th17 cytokine profiles in placental villous tissues from women with idiopathic RM.

Materials and methods. Forty-nine women with idiopathic RM in early pregnancy and 41 gestational age-matched women with normal pregnancies (NP) were recruited at Shanxi Maternal and Child Health Hospital (Taiyuan, China) . Following informed consent, placental villous tissues were obtained via ultrasound-guided vacuum aspiration, rinsed in saline and stored at –80°C. Total RNA was extracted from each sample, and *SMAD2* and *SMAD3* mRNA levels were quantified using real-time quantitative PCR (qPCR) using the $2^{-\Delta\Delta Cq}$ method. Parallelly, tissue homogenates were assayed with enzyme-linked immunosorbent assay (ELISA) for Th1 cytokines (interleukin (IL)-2, intereron gamma (IFN-γ), tumor necrosis factor alpha (TNF-α)), Th2 cytokine (IL-10), and Th17 cytokines (IL-6, IL-17). Spearman's rank correlation was used to evaluate associations between *SMAD2/3* expression and cytokine concentrations. All statistical analyses were performed in IBM SPSS v. 27.0, with two-tailed $p < 0.05$ denoting significance.

Results. The qPCR analysis demonstrated that *SMAD2* mRNA levels in villous tissues were significantly higher in the RM group than in NP controls ($p < 0.05$). Consistent with this, ELISA revealed a marked increase in IL-6 concentration ($p < 0.05$) alongside significant reductions in IL-2, IL-10, TNF-α, and IFN-γ levels in RM samples vs NP (all $p < 0.05$). Spearman correlation analysis showed that *SMAD2* expression was inversely correlated with IFN-γ ($\rho < 0$, $p < 0.05$), while *SMAD3* expression was negatively associated with both IL-2 and IFN-γ levels ($\rho < 0$, $p < 0.05$).

Conclusions. SMAD2/3 can affect the expression of Th1 and Th17 cytokines, which may in turn affect normal embryonic development.

Key words: cytokines, embryo, SMAD2, SMAD3, idiopathic recurrent miscarriage

Highlights

- SMAD2/3 may serve as a novel therapeutic target for recurrent miscarriage (RM).
- This study represents the first human investigation elucidating the association between SMAD2/3 and miscarriage pathogenesis.
- During early pregnancy, SMAD2/3 potentially regulates normal embryonic development by modulating the expression of cytokines.
- Elevated SMAD2 mRNA expression in early gestation may contribute to the pathogenesis of RM.

Background

Recurrent miscarriage (RM) is defined as the consecutive loss of 2 or more pregnancies in the same woman before 28 weeks of gestation. Patients with RM face an approx. 40% risk of embryo loss in subsequent pregnancies,[1] a burden that profoundly impacts reproductive health. The etiology of RM is multifactorial, encompassing infectious agents, uterine anatomical abnormalities, immune dysregulation, endocrine disorders, and chromosomal anomalies. Nevertheless, despite comprehensive evaluation, a substantial proportion of RM cases remain unexplained, highlighting a critical and active area of clinical research.

Cases in which no cause can be identified are classified as idiopathic RM. Immune regulation at the maternal–fetal interface is critical for pregnancy maintenance. At the maternal interface, the decidua not only supports embryo implantation and development but also mediates maternal immune tolerance.[2,3] At the fetal interface, trophoblast cells adhere to and invade the maternal endometrium to secure nutritional exchange and collaborate with decidual immune cells to establish a specialized immune microenvironment[4]. Recurrent miscarriage has been associated with disruptions in this maternal–fetal immune balance[5], most notably an altered Th1/Th2 cytokine ratio at the interface. Th17 cells are integral to maintaining immune equilibrium at the maternal–fetal interface and supporting healthy pregnancies. Disruption of this balance can trigger maternal immune rejection of the embryo, resulting in miscarriage.[6] In early gestation, a Th1-dominant response-mediated by cytokines such as interferon gamma (IFN-γ) and tumor necrosis factor alpha (TNF-α) drives the inflammatory milieu necessary for successful implantation. As pregnancy advances, Th2 cytokines (e.g., interleukin (IL)-4 and IL-10) increasingly promote maternal–fetal tolerance, shielding the fetus from immune attack. Whether the Th1/Th2 balance further shifts toward Th2 during the second and third trimesters to facilitate labor remains controversial,[7] underscoring the need for additional research into cytokine dynamics throughout gestation. Meanwhile, SMAD2 and SMAD3-key transcriptional mediators of tumor growth factor beta (TGF-β) signaling, govern critical processes in cell differentiation, immune regulation and embryonic development.[8,9]

SMAD2 and SMAD3 are also key regulators of Th1, Th2 and Th17 cell proliferation and differentiation.[10,11] Downregulation of the TGF-β–mTOR–hypoxia-inducible factor 1 alpha (HIF-1α) pathway has been shown to increase cytotoxicity, reduce apoptosis, and alter cytokine secretion by decidual natural killer (dNK) cells, thereby contributing to the pathogenesis of RM.[12] Inhibition of SMAD2/3 similarly impairs dNK cell function and promotes pregnancy-related disorders via modulation of this pathway. In animal models, icaritin (ICT) has been demonstrated to decrease fetal loss by restoring Th17-mediated immune balance through activation of the TGF-β–SMAD2/3 axis.[13] However, most studies to date have focused on model organisms, and data on SMAD2/3 expression in human RM patients remain scarce. Moreover, investigations of immune mechanisms in RM have largely centered on the maternal–fetal interface, with relatively little exploration of the fetal interface. Our previous work revealed significant alterations in TGF-β/BMP pathway gene expression in villous tissues from RM compared to normal pregnancy groups.[14]

Objectives

This study aims to further elucidate the role of SMAD2/3 in RM by conducting an in-depth investigation of embryonic villous tissue from RM patients, and explore the role of SMAD2/3 in immune response through analyzing its relationship with cytokines. In addition, immunological studies of fetal villous tissue will provide new evidence for understanding the mechanism of RM.

Materials and methods

Research subjects

Between July 2023 and October 2024, we enrolled 49 women with RM who presented to the Shanxi Maternal and Child Health Hospital (Shanxi Children's Hospital; Taiyuan, China). All had experienced at least 2 consecutive

Table 1. *SMAD2/3* real-time polymerase chain reaction (qPCR) primer sequences

Gene	Primer	Sequence	Amplicon length (bp)
SMAD2 (NM_005901.6)	forward primer reverse primer	GCTGGCCTGATCTTCACAGT CCAGAGGCGGAAGTTCTGTT	183
SMAD3 (NM_005902.4)	forward primer reverse primer	CCAGAGGCGGAAGTTCTGTT CTGCCCCGTCTTCTTGAGTT	137

embryonic losses before 12 weeks' gestation, confirmed with transvaginal ultrasound. Detailed histories, including thromboembolic disorders and prior pregnancy losses, were obtained, and classical RM risk factors (parental chromosomal abnormalities, uterine anatomical defects, infectious diseases, luteal phase insufficiency, diabetes mellitus, thyroid dysfunction, and hyperprolactinemia) were systematically excluded. As a control group, we recruited 41 women with uncomplicated, clinically normal pregnancies (NP) who were undergoing elective termination.

All participants were screened for established risk factors for pregnancy loss. After obtaining informed consent, both RM patients and NP controls underwent ultrasound-guided curettage abortion, and villous tissue specimens were collected. Samples were accepted only if they met both of the following criteria: 1) absence of uterine bleeding or cramping, with ultrasound confirmation of an empty gestational sac or an embryo without cardiac activity; and 2) retrieval of a fresh specimen, free of blood clots, via vacuum aspiration. Collected tissues were rinsed in sterile saline and snap-frozen at –80°C. This study protocol was reviewed and approved by the Ethics Committee of Shanxi Children's Hospital (approval No. IRB-KYSB-2023-030). All experimental participants signed the written informed consent form.

Experimental methods

The expression of *SMAD2/3* mRNA transcript levels in RM and NP samples detected with qPCR

Total RNA were extracted from 10–20 mg villous tissue of RM and NP samples according to the instructions of RNAprep Pure Tissue Kit (Tiangen Biotech, Bejing, China). The concentration and purity of RNA were quantified with NanoDrop microspectrophotometer (Thermo Fisher Scientific, Waltham, USA). RNA samples were examined using a Bio-Rad (Hercules, USA) electrophoresis apparatus and RNA integrity was assessed by observing 28S and 18S RNAs strips. Then 3 μg total RNA was reverse transcribed into cDNA using Universal RT-PCR Kit (M-MLV) (Solarbio, Beijing, China). Reverse transcription reactions were carried out in a total volume of 20 μL containing 2 μg total RNA, 2 μL Oligo(dT)^{16}, Supplement RNase-free ddH_2O to 14.5 μL. After initial denaturation at 70°C for 5 min, the mixture was immediately cooled on ice for 2 min and briefly centrifuged. Subsequently, 4 μL 5 × M-MLV Buffer, 1 μL dNTPs, 0.5 μl RNasin, and 1 μL M-MLV were added. The reaction proceeded at 42°C in a PCR instrument for 60 min, followed by enzyme inactivation at at 95°C for 5 min. The resulting cDNA was diluted to 50 μL with RNase-free ddH_2O. Real-time qualitative polymerase chain reaction (qPCR) was performed using the SYBR Green qPCR Master Mix (Bioss, Beijing, China) kit, with Human ACTB Endogenous Reference Genes Primers (Sangon Biotech, Shanghai, China) used as internal reference. Thermal cycling conditions comprised: initial denaturation at 95°C for 30 s; 40 cycles of 95°C for 3 s and 60°C for 30 s; followed by melt curve analysis (65–95°C, 0.5°C increments). All reactions were performed on a CFX Real-Time PCR Detection System (Bio-Rad) thermocycler. Primers for *SMAD2* and *SMAD3* were designed using the Primer-BLAST tool of the National Center for Biotechnology Information (NCBI) database (Bethesda, USA). Data concerning primers used are shown in Table 1. The relative expression of samples were calculated using Bio-Rad CFX Manager v. 3.0.

Detection of Th1/Th2/Th17 cytokine expression levels in the villous of patients in the RM and NP samples using ELISA

Total protein was extracted from ~50 mg of villous tissue using the Total Protein Extraction Kit (Solarbio, Beijing, China) per the manufacturer's instructions. Protein concentrations were determined using bicinchoninic acid (BCA) assay (Tiangen Biotech), and equal amounts of protein, normalized to these measurements, were applied to 96-well plates pre-coated with the appropriate capture antibodies. Cytokine levels (IL-2, IFN-γ, IL-6, TNF-α, IL-17, and IL-10) were quantified using enzyme-linked immunosorbent assay (ELISA) kits (Bioss Antibodies, Beijing, China; cat. No. bsk11002, bsk11013, bsk11007, bsk11014, bsk11028, and bsk11010, respectively). Absorbance at 450 nm was read on a Diatek microplate reader (Diatek, Wuxi, China), and sample concentrations were calculated against standard curves using WPS Office (Kingsoft, Beijing, China).

Statistical analyses

Statistical analyses were performed in IBM SPSS v. 27.0 (IBM Corp., Armonk, USA). Data distribution was assessed using the Shapiro–Wilk test. For variables that followed a normal distribution, group comparisons were

made with independent-samples t-tests and are reported as mean ± standard deviation (SD). Non-normally distributed data were compared using the Mann–Whitney U test and are presented as median with interquartile range (IQR, 25–75th percentiles). Associations between *SMAD2/3* expression and cytokine levels were evaluated using Spearman's rank correlation. Multiple comparisons were corrected using the Bonferroni method: Each p-value was multiplied by the number of cytokines tested (k = 6) and truncated to a maximum of 1.0, with significance defined as an adjusted $p < 0.05$. *SMAD2* and *SMAD3* relative expression levels were quantified using the $2^{-\Delta\Delta Cq}$ method, and differences were considered statistically significant at $p < 0.05$.

Results

Clinical information

There were no significant differences in either maternal age or gestational age between the RM (recurrent miscarriage) and NP (normal pregnancy) groups (Table 2).

qPCR results

The qPCR analysis revealed that *SMAD2* expression was significantly upregulated in the RM group compared to NP controls, whereas *SMAD3* expression was markedly reduced in the RM group (Table 3).

Th1, Th2 and Th17 cytokine expression levels

In placental villous tissues, IL-2, TNF-α, IFN-γ, and IL-10 concentrations were significantly reduced in the RM group compared to NP controls ($p < 0.05$), whereas IL-6 levels were significantly elevated ($p < 0.05$). Although IL-17 appeared lower in RM samples, this difference did not reach statistical significance ($p > 0.05$) (Table 4).

Cytokines ratios in placental villous tissue

The ratios of IL-2/IL-10, IFN-γ/IL-10 and IL-17/IL-10 were significantly higher in the RM group compared to the NP group ($p < 0.05$), while the TNF-α/IL-10 ratio was also elevated but did not reach statistical significance ($p > 0.05$) (Table 5).

Table 2. Clinical data

Clinical feature	RM (n = 49)	NP (n = 41)	Statistics	p-value
Age [years]	31.51 ±3.98	31.58 ±5.52	t = –0.073	0.942
Gestational cycle [days]	49.00 (45.00–53.00)	50 (43.50–50.00)	Z = –0.586	0.558

RM – recurrent miscarriage; NP – normal pregnancy.

Table 3. Comparison of the relative expression of SMAD2/3 between RM patients and NP women

Gene	RM (n = 49)	NP (n = 41)	Z	p-value
SMAD2	4.03 (2.8–7.78)	2.83 (1.89–3.85)	–3.447	<0.001
SMAD3	19.16 (5.39–63.57)	27.28 (6.04–71.06)	–0.502	0.615

RM – recurrent miscarriage; NP – normal pregnancy.

Table 4. Cytokine levels in the villous tissue of the RM group and the NP group

Variable	IL-2 (pg/mL)	TNF-α (pg/mL)	IFN-γ (pg/mL)	IL-6 (pg/mL)	IL-10 (pg/mL)	IL-17 (pg/mL)
RM (n = 49)	19.07 (16.42–27.99)	3.27 (1.35–5.24)	33.58 (14.45–46.36)	123.34 (94.89–178.29)	15.49 (8.87–26.55)	92.74 (53.32–131.22)
NP (n = 41)	42.44 (33.76–49.36)	6.64 (2.58–15.26)	58.63 (44.4–73.84)	56.22 (39.82–67.86)	70.37 (21.04–100.04)	94.49 (68.58–142.97)
Z	–6.688	–2.682	–4.509	–6.024	–5.222	–0.604
p-value	<0.001	0.007	<0.001	<0.001	<0.001	0.546

$p < 0.05$ was considered statistically significant; IL – interleukin; IFN – interferon; TNF – tumor necrosis factor; RM – recurrent miscarriage; NP – normal pregnancy.

Table 5. Th1/Th2 ratio in placental villous tissue

Group	RM (n = 49)	NP (n = 41)	Z	p-value
IL-2/IL-10	1.55 (0.82–3.17)	0.63 (0.42–2.11)	–2.402	0.016
TNF-α/IL-10	0.15 (0.07–0.44)	0.09 (0.03–0.21)	–1.738	0.082
IFN-γ/IL-10	1.60 (0.57–4.34)	1.04 (0.61–2.25)	–1.981	0.048
IL17/IL10	4.59 (2.66–11.22)	1.48 (0.90–3.35)	–4.898	<0.001

$p < 0.05$ was considered statistically significant; IL – interleukin; IFN – interferon; TNF – tumor necrosis factor; RM – recurrent miscarriage; NP – normal pregnancy.

Table 6. Results of correlation analysis between *SMAD2/3* and Th1/Th2/Th17 type cytokine levels in RM group

Gene	Variable	IL-2	IL-6	IL-10	IL-17	TNF-α	IFN-γ
SMAD2	correlation coefficient	–0.314	0.156	0.043	–0.183	–0.084	–0.459
	significance	0.168	1	1	1	1	0.005
SMAD3	correlation coefficient	–0.448	0.214	0.215	–0.366	–0.211	–0.497
	significance	0.006	0.834	0.822	0.060	0.870	0.002

IL – interleukin; IFN – interferon; TNF – tumor necrosis factor.

Correlation analysis of *SMAD2/3* and Th1/Th2/Th17 cytokine levels in RM group

Spearman's correlation analysis demonstrated that *SMAD2* expression was significantly negatively correlated with IFN-γ levels, while *SMAD3* expression was significantly negatively correlated with both IL-2 and IFN-γ levels (Table 6).

Discussion

Recurrent miscarriage is among the most common complications affecting women of reproductive age.[1] Women with a history of RM face an elevated risk of miscarriage in subsequent pregnancies and are more likely to experience other obstetric complications, such as fetal growth restriction and stillbirth. The pathogenesis of RM is closely linked to dysregulation of the maternal–fetal immune interface, highlighting the critical role of immune factors in maintaining a successful pregnancy.

SMAD2/3 are intracellular kinase substrates of TGF-β receptors, facilitating intracellular signal transduction of TGF-β. They regulate the expression of downstream target genes by interacting with other transcription factors, thereby affecting the initiation and development of various biological processes such as cell growth, proliferation, apoptosis, migration, adhesion, and differentiation.[15] Although SMAD2/3 have been reported to play critical roles in early embryonic development, the relationship between SMAD2/3 in embryonic villous tissue and miscarriage remains unexplored. SMAD2/3 influence the trajectory of the embryo by directly transcribing target genes via Nodal/Activin-mediated TGF-β signaling cascades.[16,17] In addition, SMAD2 plays an important role in establishing embryonic axial patterns and specifying deterministic endoderm. Mouse embryos with SMAD2 deficiency are unable to undergo normal embryo transformation and establish the anterior posterior axis, resulting in embryonic mortality.[18,19] SMAD2 is also vital for embryo elongation and mesoderm induction. A deficiency in SMAD2 prevents mouse embryos from undergoing these crucial processes before the embryonic stage.[20] Meanwhile, the synergistic activity of SMAD2/3 regulate mesoderm formation and patterning as well as embryonic morphogenesis in mice. While SMAD3 provides essential signals during early implantation, dual absence of SMAD2/3 completely blocks mesoderm formation and embryonic development.[21] In human embryonic stem cells (hESCs), SMAD2 and SMAD3 coordinate the maintenance of pluripotency and the onset of differentiation by modulating distinct transcriptional networks and engaging with chromatin-modifying complexes.[9] In our study, *SMAD2* was significantly higher in RM than NP. The major role of SMAD2 in early embryonic development is to control epigenetic modifications through the activin/SMAD2 signaling pathway and to cooperate with the Wnt/β-catenin signaling to regulate mesoderm gene expression.[22,23] Therefore, we speculate that high expression of *SMAD2* may affect mesoderm development, but further validation is needed.

The roles of Th1, Th2 and Th17 cells in embryonic development involve the production and regulation of various essential immune system cytokines. Th1 cells mainly produce cytokines such as il-2, IFN-γ and TNF-α, promoting cell-mediated immune responses.[24] Interleukin 10 is mainly secreted by Th2 cells, but can also be produced by regulatory T cells (Treg), Th1 cells and Th17 cells. Th2 cytokines contribute to promoting immune tolerance at the mother-fetal interface and ensuring the maintenance of normal pregnancy.[25] While IL-6 is commonly recognized as a proinflammatory cytokine, it also exhibits anti-inflammatory properties.[26] This dual functionality allows IL-6 to play a nuanced and intricate role in maintaining inflammatory homeostasis. The number of Th17 cells at the mother–fetal interface significantly increases during early pregnancy, potentially playing a crucial role in the proliferation and invasion of trophoblastic cells, as well as subsequent placental formation. In addition, Th17 cells regulate the biological activity of trophoblast cells by secreting cytokines, especially IL-17 and play an important role in placental development in early pregnancy.[27] In this period, TNF-α supports the pregnancy process by regulating hormone synthesis, placental structure and embryonic development. The increased expression level of TNF-α contributes to the maturation of the placenta and the normal development of the embryo.[28] IFN-γ can induce trophoblast apoptosis and MHC II antigen expression, thereby protecting placental function.[29] Furthermore, IFN-γ helps to inhibit immune rejection and protect the embryo by regulating the polarization of Treg cells and

Th17 cells.[30] Interleukin 2 can stimulate the proliferation and function of regulatory Tregs, regulate the activity of immune cells, promote maternal immune tolerance to the fetus, and contribute to placental stability and normal fetal development.[31,32]

Our study demonstrated that women in the RM group exhibited significantly lower levels of IL-2, TNF-α, IFN-γ, and IL-10 compared to the NP cohort, a finding that parallels the majority of previous reports. The level of IL-6 was significantly increased. Beyond its role in inflammation, IL-6 contributes to embryo implantation, placental development and pregnancy maintenance.[27] Previous research has suggested inadequate expression or secretion of IL-6 at the fetal–maternal interface in patients with RM.[33] However, increased IL-6 expression in the decidua has been reported in recent studies.[34,35] Elevated levels of IL-6in decidual tissue indicate increased inflammation at the fetus–maternal interface, which may potentially endanger embryo implantation and pregnancy. Therefore, both low and high levels of IL-6 can disrupt the inflammatory network at the fetus-maternal interface, thereby affecting pregnancy outcomes. Although studies on the expression of IL-6 in villous tissues are limited, our preceding study found that the expression of IL-6 was significantly higher in the villous tissues of RM patients compared to NP group. This finding was verified in the present study.[14] Given that IL-6 can attenuate maternal immune rejection of the fetus, we hypothesized that persistently elevated IL-6 levels in RM reflect ongoing alloimmune reactions at the fetal interface; as these responses intensify, IL-6 expression rises further, ultimately contributing to pregnancy loss.[36] Analysis of the four indicators IL-2/IL-10, TNF-α/IL-10, IFN-γ/IL-10 and IL-7/IL-10 revealed higher levels in the RM group, mainly because the expression of IL-10 in the RM group was much lower than that in the NP group. Interleukin 10 maintains a homeostasis between mother and embryo by suppressing inflammation and regulating the immune system.[37] For example,IL-10 protects embryo from inflammation-mediated damage by inhibiting TNF-α production in macrophages.[24] Moreover, IL-10 inhibits invasion of placental interstitial cells by inhibiting the expression of matrix metalloproteinase 9 (MMP-9), which is crucial for embryo implantation and growth in the uterus.[38] In early-pregnancy decidual tissues from women with RM, concentrations of IL-17, IL-6 and TNF-α were significantly elevated,[33,39,40] whereas IL-10 expression was markedly reduced.[41] Notably, IFN-γ levels did not differ between RM and control groups.[42] These observations contrast with the cytokine profiles seen in villous tissues, highlighting distinct maternal vs fetal immune signatures during the first trimester.

SMAD2 and SMAD3 are essential downstream effectors of the TGF-β/SMAD signaling pathway, and multiple studies have established TGF-β as a pivotal regulator of T helper cell differentiation.[43,44] Takimoto et al. found that Smad2/3-dependent TGFβ inhibited Th1 and Th2 differentiation.[45] In Nile tilapia (*Oreochromis niloticus*), TGF-β1 has been shown to activate the canonical TGF-β/SMAD signaling pathway.[46] This leads to subsequent phosphorylation and nuclear translocation of SMAD2/3. Furthermore, SMAD3 interacts with various transcription partners to inhibit the transcription of cytokines IL-2 and IFN-γ.[47] Wang also found that SMAD3 inhibits Th17 cell differentiation by interfering with the transcriptional activity of RORγt.[48] In our research, *SMAD2* was significantly negatively correlated with IFN-γ. *SMAD3* was significantly negatively correlated with IL-2 and IFN-γ. These findings suggest that SMAD2/3 may inhibit the production of Th1 and Th2 cytokines.

Limitations

This single-center study was conducted exclusively in Shanxi Province, and may therefore have limited generalizability. We confined our analysis to early pregnancy to capture the critical window of embryo implantation and immune-microenvironment establishment; however, extending investigations into the second and third trimesters would yield valuable insights into immune dynamics throughout gestation. Additionally, we did not examine pathological correlations – an important avenue for future research given the complexity of immune–tissue interactions. Finally, our modest sample size precluded the development of robust statistical models, underscoring the need for larger, multicenter cohorts.

Conclusions

SMAD2/3 can affect the expression of Th1 and Th17 cytokines to alter the immune environment of embryonic villous tissue, which may in turn affect normal embryonic development. SMAD2 and SMAD3 represent promising novel biomarkers and therapeutic targets for the diagnosis and management of idiopathic recurrent miscarriage.

Data availability statement

The datasets supporting the findings of the current study are openly available in the Zenodo repository at https://doi.org/10.5281/zenodo.15234132.

Consent for publication

Not applicable.

Use of AI and AI-assisted technologies

Not applicable.

ORCID iDs

Huiqin Xue https://orcid.org/0000-0002-9005-367X
Min Guo https://orcid.org/0000-0002-9005-367X
Jingbo Gao https://orcid.org/0009-0002-8246-5815
Rong Guo https://orcid.org/0009-0005-1203-3939
Guizhi Cao https://orcid.org/0009-0009-7297-0624
Xinyan Li https://orcid.org/0009-0009-1019-3567
Xiayu Sun https://orcid.org/0009-0004-5047-886X
Hongyong Lu https://orcid.org/0000-0002-1012-2584
Jianrui Wu https://orcid.org/0009-0001-5312-7940

References

1. Obstetrics Subgroup, Chinese Society of Obstetrics and Gynecology, Chinese Medical Association; Chinese Expert Consensus Group on Diagnosis and Management of Recurrent Spontaneous Abortion. Chinese expert consensus on diagnosis and management of recurrent spontaneous abortion (2022) [in Chinese]. *Zhonghua Fu Chan Ke Za Zhi*. 2022;57(9):653–667. doi:10.3760/cma.j.cn112141-20220421-00259
2. Whettlock EM, Woon EV, Cuff AO, Browne B, Johnson MR, Male V. Dynamic changes in uterine NK cell subset frequency and function over the menstrual cycle and pregnancy. *Front Immunol*. 2022;13:880438. doi:10.3389/fimmu.2022.880438
3. Ticconi C, Di Simone N, Campagnolo L, Fazleabas A. Clinical consequences of defective decidualization. *Tissue Cell*. 2021;72:101586. doi:10.1016/j.tice.2021.101586
4. Di Simone N, Caliandro D, Castellani R, Ferrazzani S, Caruso A. Interleukin-3 and human trophoblast: In vitro explanations for the effect of interleukin in patients with antiphospholipid antibody syndrome. *Fertil Steril*. 2000;73(6):1194–1200. doi:10.1016/s0015-0282(00)00533-1
5. Zhao X, Jiang Y, Luo S, Zhao Y, Zhao H. Intercellular communication involving macrophages at the maternal-fetal interface may be a pivotal mechanism of URSA: A novel discovery from transcriptomic data. *Front Endocrinol (Lausanne)*. 2023;14:973930. doi:10.3389/fendo.2023.973930
6. Guo L, Guo A, Yang F, et al. Alterations of cytokine profiles in patients with recurrent implantation failure. *Front Endocrinol (Lausanne)*. 2022;13:949123. doi:10.3389/fendo.2022.949123
7. Shi L, Wei L, Lu M, Ding H, Bo L. Analysis of gene expression difference and biological process in chorionic villi of unexplained recurrent spontaneous abortion. *BMC Pregnancy Childbirth*. 2024;24(1):880. doi:10.1186/s12884-024-07099-2
8. Sakaki-Yumoto M, Liu J, Ramalho-Santos M, Yoshida N, Derynck R. Smad2 is essential for maintenance of the human and mouse primed pluripotent stem cell state. *J Biol Chem*. 2013;288(25):18546–18560. doi:10.1074/jbc.M112.446591
9. Yang J, Jiang W. The role of SMAD2/3 in human embryonic stem cells. *Front Cell Dev Biol*. 2020;8:653. doi:10.3389/fcell.2020.00653
10. Dahmani A, Delisle JS. TGF-β in T cell biology: Implications for cancer immunotherapy. *Cancers (Basel)*. 2018;10(6):194. doi:10.3390/cancers10060194
11. Zhang S. The role of transforming growth factor β in T helper 17 differentiation. *Immunology*. 2018;155(1):24–35. doi:10.1111/imm.12938
12. Zhu J, Song G, Zhou X, et al. CD39/CD73 dysregulation of adenosine metabolism increases decidual natural killer cell cytotoxicity: Implications in unexplained recurrent spontaneous abortion. *Front Immunol*. 2022;13:813218. doi:10.3389/fimmu.2022.813218
13. Huang SQ, Xia L, Xia YQ, Huang HL, Dong L. Icaritin attenuates recurrent spontaneous abortion in mice by modulating Treg/Th17 imbalance via TGF-β/SMAD signaling pathway. *Biochim Biophys Acta Mol Cell Res*. 2024;1871(1):119574. doi:10.1016/j.bbamcr.2023.119574
14. Xue H, Ma L, Xue J, et al. Low expression of LEFTY1 in placental villi is associated with early unexplained miscarriage. *J Reprod Med*. 2017;62(5–6):305–310. PMID:30027725.
15. Bertero A, Brown S, Madrigal P, et al. The SMAD2/3 interactome reveals that TGFβ controls m6A mRNA methylation in pluripotency. *Nature*. 2018;555(7695):256–259. doi:10.1038/nature25784
16. Guzman-Ayala M, Lee KL, Mavrakis KJ, Goggolidou P, Norris DP, Episkopou V. Graded Smad2/3 activation is converted directly into levels of target gene expression in embryonic stem cells. *PLoS One*. 2009;4(1):e4268. doi:10.1371/journal.pone.0004268
17. Redshaw N, Camps C, Sharma V, et al. TGF-β/Smad2/3 signaling directly regulates several miRNAs in mouse ES cells and early embryos. *PLoS One*. 2013;8(1):e55186. doi:10.1371/journal.pone.0055186
18. Heyer J, Escalante-Alcalde D, Lia M, et al. Postgastrulation Smad2-deficient embryos show defects in embryo turning and anterior morphogenesis. *Proc Natl Acad Sci U S A*. 1999;96(22):12595–12600. doi:10.1073/pnas.96.22.12595
19. Wei S, Wang Q. Molecular regulation of Nodal signaling during mesendoderm formation. *Acta Biochim Biophys Sin (Shanghai)*. 2018;50(1):74–81. doi:10.1093/abbs/gmx128
20. Kim YS, Fan R, Kremer L, et al. Deciphering epiblast lumenogenesis reveals proamniotic cavity control of embryo growth and patterning. *Sci Adv*. 2021;7(11):eabe1640. doi:10.1126/sciadv.abe1640
21. Senft AD, Bikoff EK, Robertson EJ, Costello I. Genetic dissection of Nodal and Bmp signalling requirements during primordial germ cell development in mouse. *Nat Commun*. 2019;10(1):1089. doi:10.1038/s41467-019-09052-w
22. Xu X, Wang L, Liu B, Xie W, Chen YG. Activin/Smad2 and Wnt/β-catenin up-regulate HAS2 and ALDH3A2 to facilitate mesendoderm differentiation of human embryonic stem cells. *J Biol Chem*. 2018;293(48):18444–18453. doi:10.1074/jbc.RA118.003688
23. Wang L, Xu X, Cao Y, et al. Activin/Smad2-induced histone H3 Lys-27 trimethylation (H3K27me3) reduction is crucial to initiate mesendoderm differentiation of human embryonic stem cells. *J Biol Chem*. 2017;292(4):1339–1350. doi:10.1074/jbc.M116.766949
24. Cheng SB, Sharma S. Interleukin-10: A pleiotropic regulator in pregnancy. *Am J Reprod Immunol*. 2015;73(6):487–500. doi:10.1111/aji.12329
25. Spence T, Allsopp PJ, Yeates AJ, Mulhern MS, Strain JJ, McSorley EM. Maternal serum cytokine concentrations in healthy pregnancy and preeclampsia. *J Pregnancy*. 2021;2021:6649608. doi:10.1155/2021/6649608
26. Vilotić A, Nacka-Aleksić M, Pirković A, Bojić-Trbojević Ž, Dekanski D, Jovanović Krivokuća M. IL-6 and IL-8: An overview of their roles in healthy and pathological pregnancies. *Int J Mol Sci*. 2022;23(23):14574. doi:10.3390/ijms232314574
27. Wang W, Sung N, Gilman-Sachs A, Kwak-Kim J. T helper (Th) cell profiles in pregnancy and recurrent pregnancy losses: Th1/Th2/Th9/Th17/Th22/Tfh cells. *Front Immunol*. 2020;11:2025. doi:10.3389/fimmu.2020.02025
28. Romanowska-Próchnicka K, Felis-Giemza A, Olesińska M, Wojdasiewicz P, Paradowska-Gorycka A, Szukiewicz D. The role of TNF-α and anti-TNF-α agents during preconception, pregnancy, and breastfeeding. *Int J Mol Sci*. 2021;22(6):2922. doi:10.3390/ijms22062922
29. Devvanshi H, Kachhwaha R, Manhswita A, Bhatnagar S, Kshetrapal P. Immunological changes in pregnancy and prospects of therapeutic pla-xosomes in adverse pregnancy outcomes. *Front Pharmacol*. 2022;13:895254. doi:10.3389/fphar.2022.895254
30. Liu X, Chen L, Peng W, et al. Th17/Treg balance: The bloom and wane in the pathophysiology of sepsis. *Front Immunol*. 2024;15:1356869. doi:10.3389/fimmu.2024.1356869
31. Turka LA, Walsh PT. IL-2 signaling and $CD4^+$ $CD25^+$ $Foxp3^+$ regulatory T cells. *Front Biosci*. 2008;13:1440–1446. doi:10.2741/2773
32. Chen Z, Zhang Y, Kwak-Kim J, Wang W. Memory regulatory T cells in pregnancy. *Front Immunol*. 2023;14:1209706. doi:10.3389/fimmu.2023.1209706
33. Pitman H, Innes BA, Robson SC, Bulmer JN, Lash GE. Altered expression of interleukin-6, interleukin-8 and their receptors in decidua of women with sporadic miscarriage. *Hum Reprod*. 2013;28(8):2075–2086. doi:10.1093/humrep/det233
34. Zhao L, Han L, Hei G, et al. Diminished miR-374c-5p negatively regulates IL (interleukin)-6 in unexplained recurrent spontaneous abortion. *J Mol Med (Berl)*. 2022;100(7):1043–1056. doi:10.1007/s00109-022-02178-3
35. Chen P, Zhou L, Chen J, et al. The immune atlas of human deciduas with unexplained recurrent pregnancy loss. *Front Immunol*. 2021;12:689019. doi:10.3389/fimmu.2021.689019
36. Wakabayashi A, Sawada K, Nakayama M, et al. Targeting interleukin-6 receptor inhibits preterm delivery induced by inflammation. *Mol Hum Reprod*. 2013;19(11):718–726. doi:10.1093/molehr/gat057
37. Mobini M, Mortazavi M, Nadi S, Zare-Bidaki M, Pourtalebi S, Arababadi MK. Significant roles played by interleukin-10 in outcome of pregnancy. *Iran J Basic Med Sci*. 2016;19(2):119–124. PMID:27081455. PMCID:PMC4818358.

38. Roth I, Fisher SJ. IL-10 is an autocrine inhibitor of human placental cytotrophoblast MMP-9 production and invasion. *Dev Biol*. 1999; 205(1):194–204. doi:10.1006/dbio.1998.9122
39. Li S, Wang L, Xing Z, Huang Y, Miao Z. Expression level of TNF-α in decidual tissue and peripheral blood of patients with recurrent spontaneous abortion. *Cent Eur J Immunol*. 2017;42(2):156–160. doi:10.5114/ceji.2017.69357
40. Li N, Wu HM, Hang F, Zhang YS, Li MJ. Women with recurrent spontaneous abortion have decreased 25(OH) vitamin D and VDR at the fetal-maternal interface. *Braz J Med Biol Res*. 2017;50(11):e6527. doi:10.1590/1414-431X20176527
41. Cai J, Li M, Huang Q, Fu X, Wu H. Differences in cytokine expression and STAT3 activation between healthy controls and patients of unexplained recurrent spontaneous abortion (URSA) during early pregnancy. *PLoS One*. 2016;11(9):e0163252. doi:10.1371/journal.pone.0163252
42. Herkiloglu D, Gokce S, Cevik O. Relationship of interferon regulator factor 5 and interferon-γ with missed abortion. *Exp Ther Med*. 2022;23(5):356. doi:10.3892/etm.2022.11283
43. Huss DJ, Winger RC, Peng H, Yang Y, Racke MK, Lovett-Racke AE. TGF-beta enhances effector Th1 cell activation but promotes self-regulation via IL-10. *J Immunol*. 2010;184(10):5628–5636. doi:10.4049/jimmunol.1000288
44. Li MO, Wan YY, Flavell RA. T cell-produced transforming growth factor-beta1 controls T cell tolerance and regulates Th1- and Th17-cell differentiation. *Immunity*. 2007;26(5):579–591. doi:10.1016/j.immuni.2007.03.014
45. Takimoto T, Wakabayashi Y, Sekiya T, et al. Smad2 and Smad3 are redundantly essential for the TGF-beta-mediated regulation of regulatory T plasticity and Th1 development. *J Immunol*. 2010;185(2):842–855. doi:10.4049/jimmunol.0904100
46. Zhan XL, Ma TY, Wu JY, et al. Cloning and primary immunological study of TGF-β1 and its receptors TβR I/TβR II in tilapia (Oreochromis niloticus). *Dev Comp Immunol*. 2015;51(1):134–140. doi:10.1016/j.dci.2015.03.008
47. Zhang Q, Geng M, Li K, et al. TGF-β1 suppresses the T-cell response in teleost fish by initiating Smad3- and Foxp3-mediated transcriptional networks. *J Biol Chem*. 2023;299(2):102843. doi:10.1016/j.jbc.2022.102843
48. Wang J, Zhao X, Wan YY. Intricacies of TGF-β signaling in Treg and Th17 cell biology. *Cell Mol Immunol*. 2023;20(9):1002–1022. doi:10.1038/s41423-023-01036-7

Bioinformatics-driven discovery of shared biomarkers linking depression and cognitive impairment

Weizhi Chen[B–D], Bin Li[A,D–F]

Department of Neurology, Washington Scientific Institute, Fairfax, USA

A – research concept and design; B – collection and/or assembly of data; C – data analysis and interpretation;
D – writing the article; E – critical revision of the article; F – final approval of the article

Advances in Clinical and Experimental Medicine, ISSN 1899–5276 (print), ISSN 2451–2680 (online) *Adv Clin Exp Med*. 2026;35(1):97–106

Address for correspondence
Bin Li
E-mail: wihscontact@gmail.com

Funding sources
None declared

Conflict of interest
None declared

Received on June 15, 2025
Reviewed on August 13, 2025
Accepted on August 25, 2025

Published online on January 7, 2026

Abstract

Background. Major depressive disorder (MDD) is frequently comorbid with mild cognitive impairment (MCI), yet its molecular basis remains unclear.

Objectives. This study aimed to identify shared differentially expressed genes (DEGs) and biological pathways that may underlie the comorbidity between MDD and MCI. Using integrative bioinformatics approaches applied to transcriptomic datasets, we sought to uncover molecular biomarkers that could inform early diagnosis and provide novel targets for mechanism-based therapeutic strategies.

Materials and methods. Transcriptomic datasets from MDD (GSE58430) and MCI (GSE140831) patients were analyzed to identify DEGs. Functional enrichment analyses were performed using the Gene Ontology (GO) and Kyoto Encyclopedia of Genes and Genomes (KEGG) databases. Protein–protein interaction (PPI) networks were constructed to identify core genes.

Results. A total of 301 DEGs were shared between MDD and MCI. Gene Ontology and KEGG enrichment analyses revealed key biological processes involved in neuroinflammation, oxidative stress, synaptic dysfunction, and apoptotic signaling. The PPI network analysis identified nine hub genes with high connectivity: *HSP90AB1*, *CDC42*, *NFKB1*, *CD8A*, *CALM3*, *PARP1*, *CD44*, *H2BC21*, and *MYH9*.

Conclusions. These findings reveal shared molecular biomarkers and pathways linking MDD and MCI, providing insights into their comorbidity. The identified core genes, particularly *PARP1* and *CDC42*, may serve as novel targets for early diagnosis and mechanism-based therapeutic strategies in psychiatry and neurodegenerative disorders.

Key words: biomarkers, bioinformatics, gene expression, major depressive disorder, mild cognitive impairment

Cite as
Chen W, Li B. Bioinformatics-driven discovery of shared biomarkers linking depression and cognitive impairment. *Adv Clin Exp Med*. 2026;35(1):97–106. doi:10.17219/acem/209879

DOI
10.17219/acem/209879

Highlights

- 301 shared differentially expressed genes (DEGs) identified in MDD and MCI, including 9 hub genes (*HSP90AB1*, *CDC42*, *NFKB1*, *CD8A*, *CALM3*, *PARP1*, *CD44*, *H2BC21*, *MYH9*) with high network connectivity and strong functional roles in comorbidity.
- Shared DEGs linked to key molecular pathways – NF-κB signaling, small GTPase signaling, TNF-mediated signaling, and apoptosis – suggest common pathogenic mechanisms driving MDD–MCI overlap.
- Novel biomarkers and therapeutic targets discovered, offering potential for earlier diagnosis and personalized, mechanism-based treatment strategies in patients with coexisting major depressive disorder and mild cognitive impairment.

Background

Major depressive disorder (MDD) is a prevalent mental health condition. According to a 2020 World Health Organization (WHO) report, approx. 280 million people worldwide suffer from MDD.[1] It is not only a leading cause of emotional distress but is also frequently associated with cognitive impairments, including comorbidity with mild cognitive impairment (MCI). Furthermore, individuals diagnosed with MCI are at an increased risk of developing depression. For instance, a meta-analysis of 57 studies involving 20,892 participants revealed that the overall pooled prevalence of depression in patients with MCI was 32%.[2] This highlights the substantial overlap between these 2 disorders.[3]

Clinically, there is a strong correlation between MDD and MCI. Studies have shown that the prevalence of cognitive impairment is higher in MDD patients hospitalized during the acute phase.[4] Specifically, a study conducted in 2024 found that the prevalence of cognitive impairment among MDD patients hospitalized during the acute phase was as high as 63.49%.[5] Longitudinal studies have also consistently established a connection between MDD and MCI, showing that individuals with a history of depression are more likely to develop cognitive impairments, including MCI and even dementia, as they age.[6,7] In some cases, cognitive symptoms resembling MCI may manifest as part of depressive episodes.[8,9] Several studies indicate that neuroinflammation, oxidative stress and synaptic dysfunction may serve as shared pathological mechanisms between the 2 disorders.[10] For example, chronic inflammation has been implicated in both depression and neurodegeneration, with cytokine dysregulation playing a key role in disease progression.[11] Additionally, impairments in neurotransmitter signaling and neuronal plasticity have been observed in both MDD and MCI,[12] further suggesting a common underlying biological basis. Despite evidence supporting this connection, the biological and neurological mechanisms underlying the link between MDD and MCI remain poorly understood. Further investigations into their interactions on a genetic and molecular basis are urgently needed.

Objectives

The objective of this study was to identify differentially expressed genes (DEGs) and biological pathways underlying the comorbidity between MDD and MCI. To achieve this, we applied integrative bioinformatic methods,[13] selecting the shared DEGs from transcriptomic datasets and subjecting them to enrichment analysis and protein–protein interaction (PPI) network construction to investigate the mechanisms and biomarkers involved in their interactions and mutual influence. This approach was intended to uncover molecular biomarkers that may provide insights into molecular overlaps, support early diagnosis, and serve as novel targets for mechanism-based therapeutic strategies and clinical interventions in patients with concurrent mood and cognitive symptoms.

Materials and methods

Microarray data sources

Microarray gene expression data were obtained from the Gene Expression Omnibus (GEO) database (https://www.ncbi.nlm.nih.gov/geo/). Two transcriptomic datasets, GSE58430 and GSE140831, were selected. GSE58430 contains gene expression data from 12 patient samples (6 MDD and 6 healthy controls), while GSE140831 includes 664 samples (134 MCI and 530 healthy controls).

DEG analysis

Differential gene expression analysis was performed using GEO2R, an interactive web tool provided by the NCBI GEO that applies the limma (Linear Models for Microarray Data) package.[14] For GSE58430, genes were considered differentially expressed if $p < 0.05$ and $|\log2FC| > 0.5$. For GSE140831, the same threshold was applied ($p < 0.05$ and $|\log2FC| > 0.5$). Probe annotations were verified using the respective platform annotation files. Differentially expressed genes identified in each dataset were then compared to determine the shared genes between MDD and MCI.

GO and KEGG pathway enrichment

Once the DEGs were identified, functional enrichment analysis was performed using Gene Ontology (GO) and Kyoto Encyclopedia of Genes and Genomes (KEGG) pathways. Gene Ontology analysis classifies genes into functional categories based on their molecular functions, biological processes and cellular components, while KEGG analysis maps genes to specific signaling pathways and biological processes. Both analyses used the Database for Annotation, Visualization and Integrated Discovery (DAVID; https://david.ncifcrf.gov/), which performs functional annotation clustering (FAC) to identify overrepresented or enriched biological processes, pathways, functional categories, and diseases/phenotypic annotations associated with the DEGs. Adjusted p-values < 0.05 were considered statistically significant.

Protein–protein interaction analysis and core genes identification

Protein–protein interaction analysis was used to investigate interactions between proteins in the cell. Core genes were identified according to their importance in cellular functions. The PPI network was constructed using the STRING database (Search Tool for the Retrieval of Interacting Genes/Proteins; https://string-db.org/) and analyzed with Cytoscape (https://cytoscape.org/). Differentially expressed genes with a high degree of connectivity to other genes were selected as core or hub genes.

Results

Identification of DEGs

A total of 3,122 genes were identified as depression-related DEGs in the GSE58430 dataset, of which 1,537 were downregulated and 1,585 were upregulated, as shown in the volcano plot (Fig. 1A). In the GSE140831 dataset, 1,739 MCI-related DEGs were identified, all of which were upregulated (Fig. 1B). The 301 genes shared between MDD- and MCI-related DEGs are shown in the Venn diagram (Fig. 2).

GO and KEGG pathway enrichment analysis results

A total of 301 DEGs were submitted to GO analysis on the DAVID online platform, using $p < 0.05$ as the significance threshold. The results were visualized accordingly.

The GO terms were categorized into 3 domains: biological processes (BP), molecular functions (MF) and cellular components (CC). In the BP domain, significantly enriched GO terms among DEGs shared between MDD and MCI included positive regulation of canonical NF-κB signaling, actin filament organization, small GTPase-mediated signal transduction, tumor necrosis factor (TNF)-mediated signaling pathway, and regulation of cell shape. In the CC domain, significantly enriched GO terms included cytosol, cytoplasm and extracellular exosome. In the MF domain, protein binding, identical protein binding, and structural

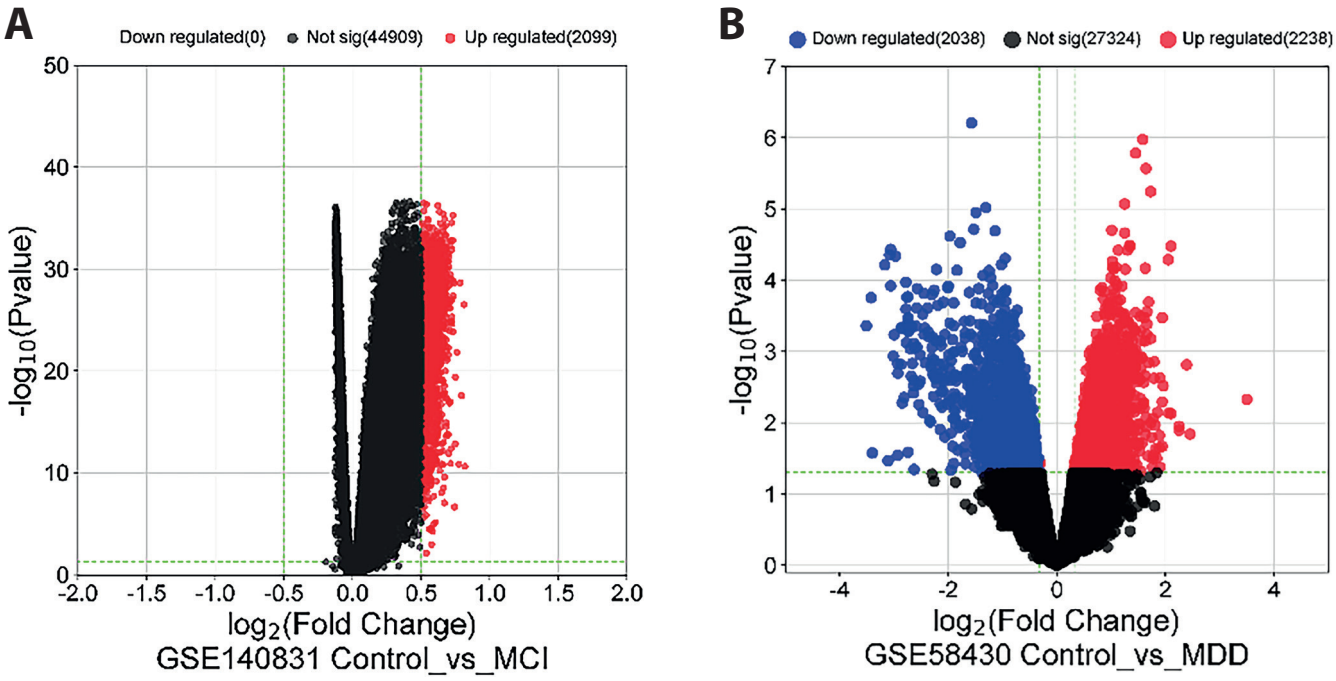

Fig. 1. Volcano plots of differentially expressed genes (DEGs) for 2 datasets (GSE58430 and GSE140831). Red and blue dots indicate upregulation and downregulation, respectively. A. GSE58430; B. GSE140831

constituent of the cytoskeleton were enriched. Figure 3 shows a comprehensive set of significantly enriched GO terms in bubble plots. The KEGG enrichment analysis identified several pathways that may play important roles in infection and apoptosis. Figure 4 shows these pathways, including *Salmonella* infection, pathogenic *Escherichia coli* infection, human immunodeficiency virus 1 (HIV-1) infection, shigellosis, human cytomegalovirus infection, and apoptosis.

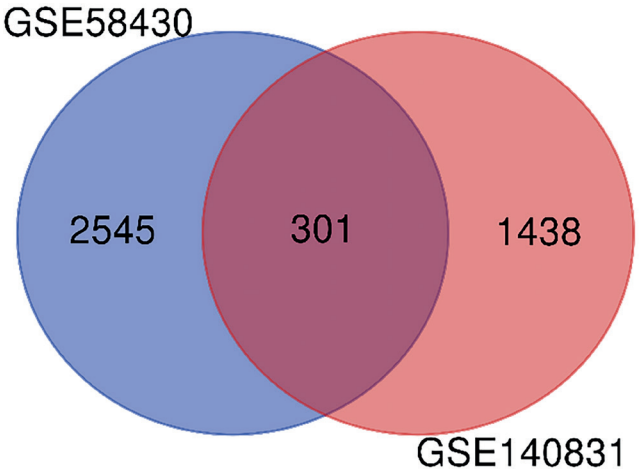

Fig. 2. Venn intersection diagram showing the identification of 301 common differentially expressed genes (DEGs) from 2 datasets (GSE58430 and GSE140831)

PPI analysis and core genes

To further explore the interactions among DEGs shared between MDD and MCI, we performed a PPI network analysis, constructed with the STRING database (Fig. 5A) and visualized in Cytoscape (Fig. 5B). The network revealed 127 nodes with a degree greater than 10. Among the nine core genes identified as having the highest degree in the PPI network – *HSP90AB1*, *CDC42*, *NFKB1*, *CD8A*, *CALM3*, *PARP1*, *CD44*, *H2BC21*, and *MYH9* – several are notable for their well-established roles in neuropsychiatric and neurodegenerative conditions. Their centrality in the network and functional relevance suggest they may serve as candidate targets for early intervention or therapeutic development in the comorbidity of MDD and MCI.

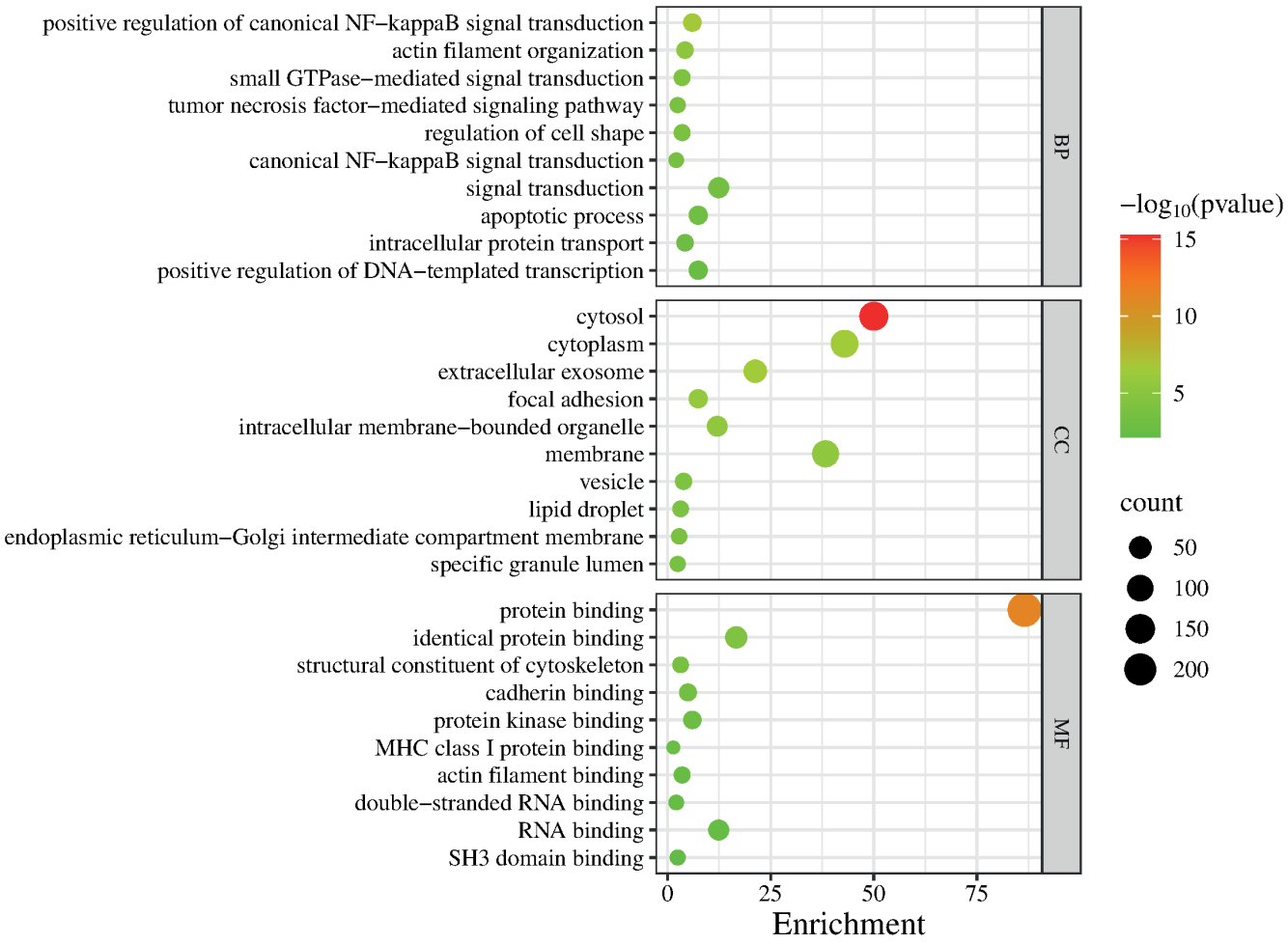

Fig. 3. Gene Ontology (GO) enrichment analysis of differentially expressed genes (DEGs). Horizontal axis represents the frequency of processes. Top – bubble plot of biological processes (BP); middle – bubble plot of cellular components (CC); bottom – bubble plot of molecular functions (MF)

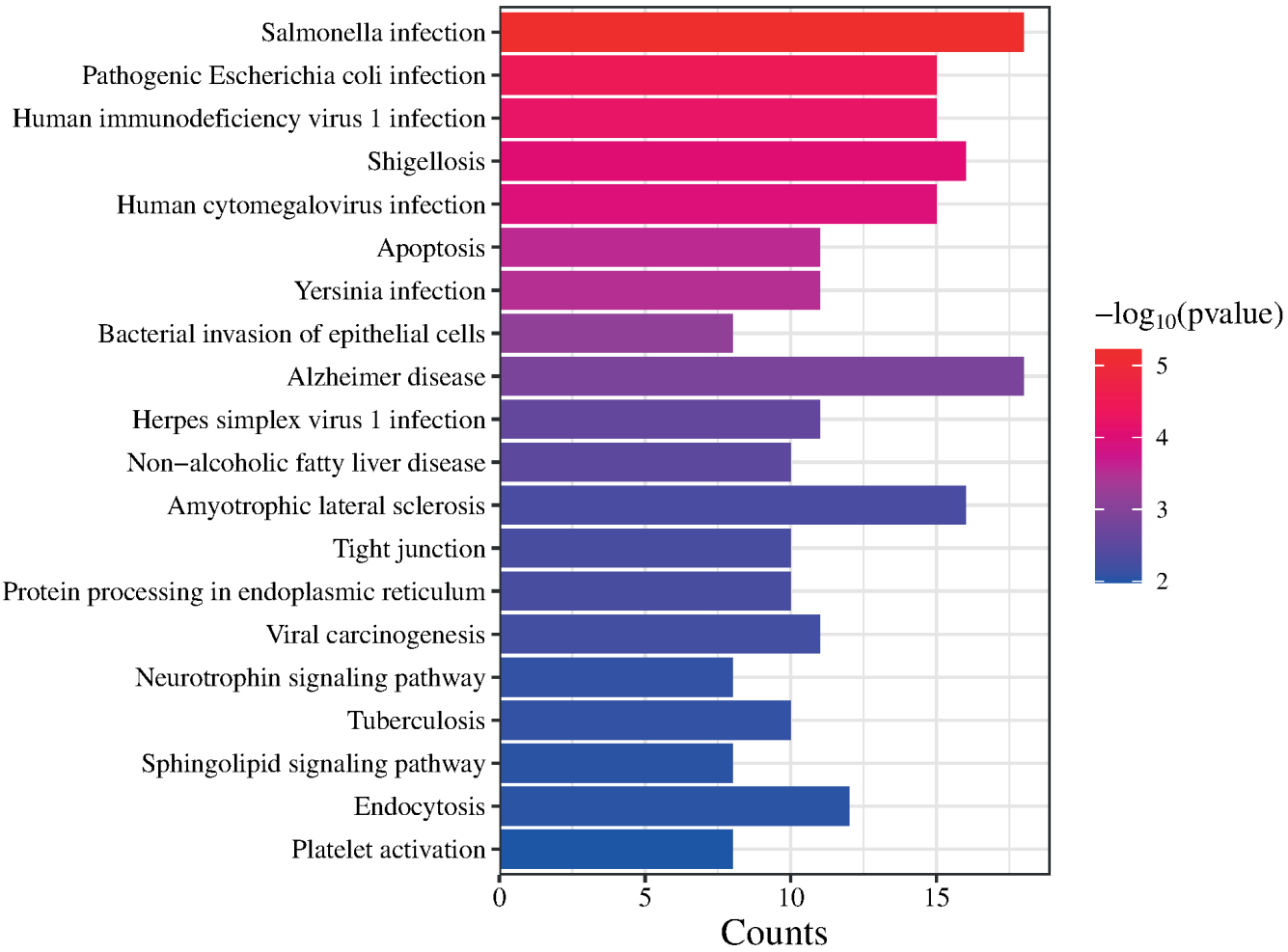

Fig. 4. Kyoto Encyclopedia of Genes and Genomes (KEGG) enrichment analysis of differentially expressed genes (DEGs) between major depressive disorder (MDD) and mild cognitive impairment (MCI). Horizontal axis represents the number of genes associated with each enriched KEGG pathway

Discussion

In this study, we identified 301 DEGs shared between MDD and MCI, many of which are implicated in key biological processes, including neuroinflammation, oxidative stress, synaptic dysfunction, and apoptotic signaling. Among these, *HSP90AB1*, *CDC42*, *NFKB1*, *CD8A*, *CALM3*, *PARP1*, *CD44*, *H2BC21*, and *MYH9* were central within the PPI network. The functions of these genes and their associated pathways support the hypothesis that MDD and MCI share molecular mechanisms contributing to their comorbidity.

Identified biomarkers in regulating MDD and MCI

In our study, 9 hub genes mediating MDD and MCI were identified. Among them, the functions of *HSP90AB1*, *CD8A*, *CD44*, *NFKB1*, and *CDC42* in linking MDD and MCI are supported by existing evidence from literature retrieval. *HSP90AB1* may serve as a potential biomarker in the pathophysiology of depression and could influence the comorbidity of MDD and MCI. As a molecular chaperone, *HSP90AB1* has also been identified as a major hub in the posterior cingulate cortex, an area significantly related to MDD.[15] It has also been implicated in regulating posterior cingulate cortex microRNA dysregulation, which differentiates cognitive resilience, MCI, and Alzheimer's disease.[16] In our study, *NFKB1* was identified as a central marker in the NF-κB (nuclear factor kappa-light-chain-enhancer of activated B cells) signaling pathway. The involvement of the NF-κB signaling pathway is critical, as it acts as a key regulator of neuroinflammatory responses. This pathway is known to be hyperactive in both MDD and neurodegenerative diseases such as MCI.[17] Chronic neuroinflammation markers, including CD44 and CD8A, may be involved in responses to axon terminal degeneration and neuronal reorganization. In MDD, CD44 expression is dysregulated and is associated with immune cell infiltration. CD8A, a marker of $CD8^+$ T cells, is more abundant in MDD samples. Together, changes in CD44 and CD8A may reflect altered immune responses in MDD.[18] Neuroinflammation triggered by CD44 and CD8A contributes to MCI by promoting amyloid beta (Aβ) plaque deposition and tau pathology, which are key features of MCI progression.[19]

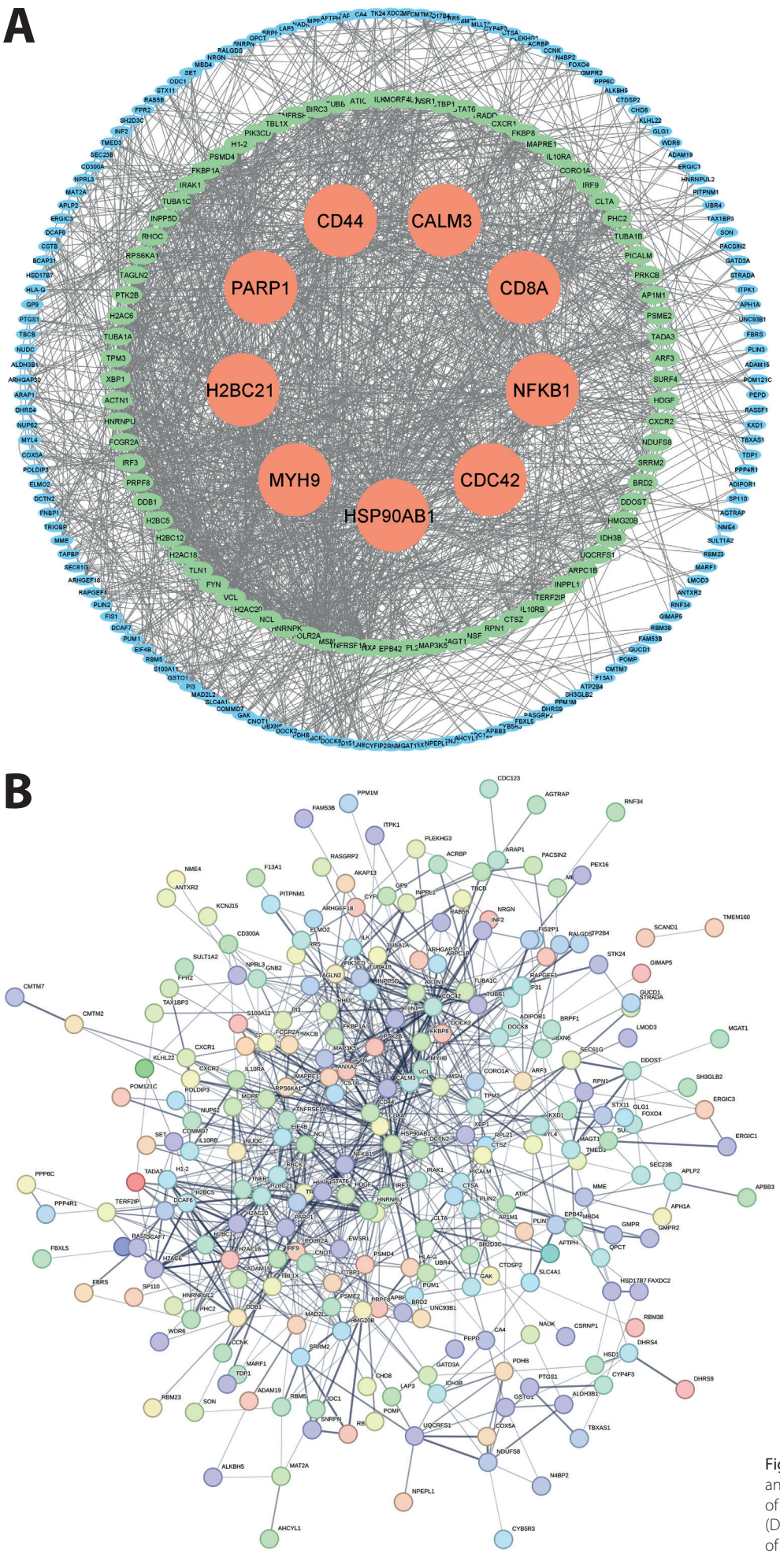

Fig. 5. Protein–protein interaction (PPI) analysis and core genes. A. PPI analysis of the 301 differentially expressed genes (DEGs); B. Cytoscape network visualization of the 301 DEGs (top 9 DEGs are in red)

This indicates a potential link between MDD and MCI mediated by neuroinflammation. These targets may be considered candidate genes for the comorbidity of MDD and MCI. *CDC42* is a key regulator of neuronal cytoskeletal dynamics and synaptic plasticity, which are critical for cognitive function and emotional regulation. The centrality and functional relevance of CDC42 in the network suggest that it may serve as a candidate target for early intervention or therapeutic development in MDD–MCI comorbidity.[20]

Identified pathways and mechanisms in regulating comorbidity of MDD and MCI

Among the enriched signaling pathways, positive regulation of canonical NF-κB signaling, small GTPase-mediated signal transduction, TNF-mediated signaling, apoptosis, and regulation of cell shape have been supported by existing evidence as relevant to the comorbidity of MDD and MCI. These pathways may therefore be highlighted as particularly important in modulating this comorbidity. The identified signaling pathways indicated that NF-κB signaling acts as a crucial inflammatory mediator in the comorbidity of MDD and MCI. Chronic stress and cellular damage activate NF-κB, driving pro-inflammatory cytokine production. This neuroinflammation can impair neurogenesis and synaptic plasticity in limbic and cognitive brain regions, thereby promoting neuronal dysfunction and contributing to both depressive symptoms (mood circuits) and cognitive decline (hippocampus, cortex).[21] Overactivation of the TNF-mediated signaling pathway, a key pro-inflammatory pathway, drives the release of cytokines such as TNF-α, interleukin (IL)-1β, and IL-6, leading to sustained neuroinflammation.[22,23] Chronic inflammation exacerbates mood disturbances in MDD and contributes to synaptic degeneration and cognitive decline, hallmarks of MCI.[24] The identification of the TNF-mediated signaling pathway in our study reinforces the hypothesis that inflammatory dysregulation is a shared driver of pathology in both disorders. Small GTPase-mediated signal transduction is also implicated in both MDD and MCI. These signaling pathways regulate essential cellular processes, and their dysregulation may contribute to neuroinflammation and synaptic dysfunction, common to both disorders. For instance, RhoA can activate NADPH oxidase (NOX) to generate superoxide ions, contributing to oxidative stress and neuronal cell death in conditions such as Alzheimer's disease.[25] Oxidative stress and inflammation can also affect cognitive function and mood regulation, potentially influencing the comorbidity of MDD and MCI.[25,26] The enriched apoptosis pathway may also contribute to the comorbidity of MDD and MCI through the neuroinflammatory processes discussed above. Neuroinflammation may disrupt normal synaptic activity and neuronal structure via the regulation of cell shape pathway identified in our KEGG analysis, which is implicated in both MDD and MCI.[27]

Possible mechanisms of neuroinflammation, synaptic signaling and apoptotic mechanisms in linking the progression of MDD and MCI

Our findings on biomarkers and pathways jointly indicate that neuroinflammation, synaptic signaling and apoptotic mechanisms play fundamental roles in linking the progression of MDD and MCI. Beyond these mechanisms, neuroinflammation in this comorbidity can activate CD44 and CD8A molecules and trigger pathways such as NF-κB signaling, TNF-mediated signaling and apoptosis. Furthermore, neuroinflammation may compromise the blood–brain barrier (BBB), allowing peripheral immune cells and inflammatory factors to infiltrate the central nervous system. Disruption of the BBB has been implicated in both depression-related cognitive dysfunction and early-stage MCI.[28] *PARP1* and *NCL*, which play roles in DNA repair and inflammatory responses, may contribute to BBB dysfunction.[29,30] Dysregulation of these genes could lead to increased neuroinflammation and neuronal damage, further linking MDD and MCI at a molecular level. Our findings indicate that synaptic signaling, mediated by CDC42, a marker identified in our study, is closely associated with synaptic plasticity and neuronal network formation. Research shows that synaptic plasticity and neurotransmission are significantly altered in MDD patients, contributing to mood and cognitive dysfunction. These alterations may also be involved in the pathophysiological changes underlying MCI. The interplay between synaptic signaling and other molecular pathways may provide insights into the comorbidity of MDD and MCI. Apoptotic mechanisms have also been proposed as contributing to this link. In MDD, inflammation-induced apoptosis in the hippocampus can lead to neuronal loss and cognitive dysfunction. Similarly, apoptotic processes may exacerbate neuronal damage in MCI, potentially involving the release of pro-apoptotic factors such as p53, which is elevated in MCI. These mechanisms may drive further cognitive decline and emotional dysregulation underlying the comorbidity of MDD and MCI.[10,31]

Taken together, these processes are interrelated. Neuroinflammation mediated by CD44, CD8A, and NF-κB activation can induce oxidative stress and apoptosis, leading to synaptic dysfunction and neuronal loss. Additionally, cytoskeletal regulators such as CDC42 integrate inflammatory signals and modulate synaptic remodeling and plasticity. *PARP1* acts as a molecular bridge between DNA damage responses and inflammatory cascades. This interplay creates a self-reinforcing cycle in which neuroinflammation, synaptic impairment and apoptosis converge on a common set of molecular effectors. These shared pathogenic pathways likely underlie the consistent differential expression of the hub genes identified in both MDD and MCI.

Possible mechanisms of oxidative stress and mitochondrial dysfunction in linking the progression of MDD and MCI

Oxidative stress represents another major contributor to both depression and cognitive impairment. It leads to mitochondrial dysfunction, neuronal apoptosis and impaired neurotransmission.[32] Among the DEGs identified, *PARP1* is a key gene mediating oxidative DNA damage repair in MDD and MCI. However, excessive activation of *PARP1* can deplete cellular energy, promoting neuronal death through a process known as parthanatos.[33] This mechanism is relevant to both MDD and MCI, where mitochondrial dysfunction related to oxidative stress has been widely reported.[34]

The interaction between oxidative stress and inflammation further exacerbates disease progression. Given its dual role in inflammation and DNA damage repair, *PARP1* serves as a mechanistic bridge between chronic inflammation and neuronal dysfunction in MDD and MCI. *PARP1* inhibitors, such as olaparib, are currently in clinical trials for neurodegenerative diseases, suggesting their potential for therapeutic repurposing in MDD-MCI comorbidity.[35] The NF-κB pathway, previously described, is also activated by oxidative stress and induces chronic inflammatory signaling.[36] This vicious cycle of inflammation and oxidative stress is a well-documented feature of both MDD and neurodegenerative disorders.[37,38]

Notably, this mechanistic cascade also involves transcriptional upregulation of *NFKB1*, as oxidative stress and *PARP1* activation can induce NF-κB autoregulatory feedback loops. Increased expression of *NFKB1* and persistent NF-κB activation perpetuate chronic inflammation and neuronal injury. This reciprocal relationship between *PARP1* and *NFKB1* likely underlies their consistent identification as shared hub genes in our analysis, highlighting a convergent pathway linking oxidative damage, inflammatory signaling and neurodegeneration in both MDD and MCI.

Functions of neural connectivity signaling in linking MDD and MCI

Currently, cognitive dysfunction in both MDD and MCI is considered to be linked to disrupted synaptic plasticity, which can subsequently impair neuronal connectivity. Several key genes identified in our study, including *CDC42* and *CALM3*, are known regulators of neuronal cytoskeletal dynamics and calcium signaling.

CDC42 plays a critical role in dendritic spine formation and axonal remodeling, both of which are essential for maintaining functional neural circuits. Impaired *CDC42* function leads to defective neuronal connectivity and synaptic signaling. This may result in disrupted or misconnected neural circuits, reducing communication efficiency across brain regions. Experimental models show that *CDC42* knockout causes deficits in long-term potentiation (LTP) and remote memory recall,[39] functions impaired in both MDD and MCI. Modulating CDC42 activity presents a promising approach for restoring cognitive resilience.[40,41]

CALM3 is a key modulator of calcium-dependent neurotransmitter release and neural connectivity. Dysfunction in *CALM3*-related pathways could impair LTP and long-term depression (LTD), which are essential for learning and memory.[42] *CALM3* also interacts with multiple kinases and phosphatases that regulate neuronal excitability and neural connectivity, suggesting its dysfunction could underlie both affective and cognitive symptoms. Clinically, altered calmodulin levels have been detected in postmortem brain tissues and peripheral samples of patients with neuropsychiatric disorders, indicating a potential role for *CALM3* as a biomarker of dysfunction in synaptic plasticity and neural connectivity.[43] Additionally, modulators of calcium signaling pathways are being explored as therapeutic agents in both depression and dementia,[44,45] highlighting the translational relevance of *CALM3* in comorbid MDD-MCI treatment strategies. Thus, the convergence of *CDC42* and *CALM3* dysregulation likely reflects their shared roles as critical mediators of synaptic remodeling in response to cellular stress. Neuroinflammation and oxidative stress, previously described, can disrupt calcium homeostasis and cytoskeletal dynamics, leading to compensatory or maladaptive changes in the expression of these genes. This mechanistic interplay provides a plausible explanation for the emergence of *CDC42* and *CALM3* as shared hub genes in our analysis, as their dysregulation integrates inflammatory signaling, impaired neurotransmission and deficits in cognitive processing characteristic of both MDD and MCI.

Pathway enrichment highlights overlapping biological mechanisms

In addition to gene-level insights, our pathway enrichment analysis identified several pathways that further support the shared pathophysiology of MDD and MCI. The shigellosis pathway enriched in our KEGG results, associated with immune activation and inflammatory responses, may contribute to neuroinflammation and BBB integrity disruption.[46] The platelet activation pathway, enriched in our KEGG analysis, and platelet aggregation, enriched in our GO-BP analysis, are linked to vascular dysfunction, which has been implicated in both MDD and neurodegenerative diseases.[28] The neurotrophin signaling pathway, enriched in our KEGG analysis and regulating neuronal survival and synaptic plasticity, is often dysregulated in both mood and cognitive disorders.[47] These pathways highlight the intricate interplay between immune dysregulation, vascular integrity and neuroplasticity, all critical to the development of both conditions. While certain KEGG pathways, such as shigellosis and *Salmonella* infection, were enriched, this likely reflects

involvement of shared immune-related genes rather than direct pathogen-specific processes. This observation underscores the central role of immune activation in MDD and MCI.

Moreover, many of the hub genes identified in our PPI analysis, such as *NFKB1*, *CD44* and *CDC42*, are directly involved in mediating these pathways, underscoring their central role as integrative nodes linking immune activation, vascular dysfunction and impaired neuroplasticity. The convergence of these processes likely drives the shared transcriptional signatures observed in both MDD and MCI datasets. This reinforces the notion that comorbid mood and cognitive symptoms arise from interconnected pathophysiological mechanisms rather than isolated processes.

Limitations

While this study reveals key genes and pathways linking MDD and MCI, further validation in patient-derived tissue and longitudinal cohorts is needed to confirm causality and directionality. Single-cell RNA sequencing and spatial transcriptomics could deepen our understanding of cell-type-specific expression changes, particularly in vulnerable brain regions. Moreover, integrating proteomics and metabolomics may further uncover post-transcriptional and metabolic alterations that gene expression data alone cannot resolve. Finally, although bioinformatics analyses provide valuable hypotheses, we did not experimentally validate gene expression, such as using quantitative polymerase chain reaction (qPCR) or western blot verification of the identified hub genes. This is an important limitation, as experimental confirmation is needed to corroborate the in silico differential expression patterns. Functional studies in animal models and human-derived organoids will be essential to elucidate the mechanistic roles of the identified DEGs and to test targeted therapeutic interventions. We plan to address this in future work through qPCR and protein-level validation in patient-derived samples or relevant preclinical models.

Conclusions

In this study, we identified 301 DEGs shared between MDD and MCI, revealing significant overlap in the molecular mechanisms underlying both conditions. Integrative bioinformatics analyses revealed that these DEGs are enriched in pathways related to neuroinflammation, oxidative stress, synaptic plasticity, and epigenetic regulation – hallmarks of both mood and cognitive disorders. Notably, several hub genes, including *HSP90AB1*, *CD8A*, *CD44*, *NFKB1*, *CALM3*, and *CDC42*, demonstrated strong functional relevance and translational potential.

These findings suggest that the identified genes may serve as novel biomarkers for the early detection of MDD-MCI comorbidity and as mechanism-based therapeutic targets. Although further experimental validation is needed, our study provides a foundation for developing diagnostic tools and personalized treatment strategies for individuals at risk for concurrent mood and cognitive decline.

Data Availability Statement

The datasets supporting the findings of the current study were already openly available when the research project commenced and can be accessed in the NCBI Gene Expression Omnibus (GEO) database (https://www.ncbi.nlm.nih.gov/geo/):

GSE58430: https://www.ncbi.nlm.nih.gov/geo/query/acc.cgi?acc=GSE58430

GSE140831: https://www.ncbi.nlm.nih.gov/geo/query/acc.cgi?acc=GSE140831

Consent for publication

Not applicable.

Use of AI and AI-assisted technologies

Not applicable.

ORCID iDs

Weizhi Chen https://orcid.org/0009-0009-9065-5556
Bin Li https://orcid.org/0000-0002-1051-801X

References

1. Institute of Health Metrics and Evaluation (IHME). Global Health Data Exchange (GHDx). Seattle, USA: Institute of Health Metrics and Evaluation (IHME); 2021. https://vizhub.healthdata.org/gbd-results. Accessed March 4, 2023.
2. Ismail Z, Elbayoumi H, Fischer CE, et al. Prevalence of depression in patients with mild cognitive impairment: A systematic review and meta-analysis. *JAMA Psychiatry*. 2017;74(1):58. doi:10.1001/jamapsychiatry.2016.3162
3. Steffens DC, Otey E, Alexopoulos GS, et al. Perspectives on depression, mild cognitive impairment, and cognitive decline. *Arch Gen Psychiatry*. 2006;63(2):130. doi:10.1001/archpsyc.63.2.130
4. Dotson VM, Beydoun MA, Zonderman AB. Recurrent depressive symptoms and the incidence of dementia and mild cognitive impairment. *Neurology*. 2010;75(1):27–34. doi:10.1212/WNL.0b013e3181e62124
5. Zhao H, Chen J. The prevalence and clinical correlation factors of cognitive impairment in patients with major depressive disorder hospitalized during the acute phase. *Front Psychiatry*. 2024;15:1497658. doi:10.3389/fpsyt.2024.1497658
6. Bartels C, Wagner M, Wolfsgruber S, Ehrenreich H, Schneider A, for the Alzheimer's Disease Neuroimaging Initiative. Impact of SSRI therapy on risk of conversion from mild cognitive impairment to Alzheimer's dementia in individuals with previous depression. *Am J Psychiatry*. 2018;175(3):232–241. doi:10.1176/appi.ajp.2017.17040404
7. Jacob L, Bohlken J, Kostev K. Risk factors for mild cognitive impairment in German primary care practices. *J Alzheimers Dis*. 2017;56(1):379–384. doi:10.3233/JAD-160875
8. Morimoto SS, Kanellopoulos T, Alexopoulos GS. Cognitive impairment in depressed older adults: Implications for prognosis and treatment. *Psychiatr Ann*. 2014;44(3):138–142. doi:10.3928/00485713-20140306-05
9. Guo Y, Pai M, Xue B, Lu W. Bidirectional association between depressive symptoms and mild cognitive impairment over 20 years: Evidence from the Health and Retirement Study in the United States. *J Affect Disord*. 2023;338:449–458. doi:10.1016/j.jad.2023.06.046

10. Zhao K, Zhang Y, Yang S, et al. Neuroinflammation and stress-induced pathophysiology in major depressive disorder: Mechanisms and therapeutic implications. *Front Cell Neurosci*. 2025;19:1538026. doi:10.3389/fncel.2025.1538026
11. Zhang W, Xiao D, Mao Q, Xia H. Role of neuroinflammation in neurodegeneration development. *Sig Transduct Target Ther*. 2023;8(1):267. doi:10.1038/s41392-023-01486-5
12. Aquilani R, Cotta Ramusino M, Maestri R, et al. Several dementia subtypes and mild cognitive impairment share brain reduction of neurotransmitter precursor amino acids, impaired energy metabolism, and lipid hyperoxidation. *Front Aging Neurosci*. 2023;15:1237469. doi:10.3389/fnagi.2023.1237469
13. Zhou TT, Sun JJ, Tang LD, Yuan Y, Wang JY, Zhang L. Potential diagnostic markers and therapeutic targets for rheumatoid arthritis with comorbid depression based on bioinformatics analysis. *Front Immunol*. 2023;14:1007624. doi:10.3389/fimmu.2023.1007624
14. Ritchie ME, Phipson B, Wu D, et al. limma powers differential expression analyses for RNA-sequencing and microarray studies. *Nucl Acids Res*. 2015;43(7):e47. doi:10.1093/nar/gkv007
15. Fan X, Sun L, Qin Y, Liu Y, Wu S, Du L. The role of HSP90 molecular chaperones in depression: Potential mechanisms. *Mol Neurobiol*. 2025;62(1):708–717. doi:10.1007/s12035-024-04284-4
16. Zhang H, Chi M, Feng S, et al. Heat shock protein 90α may serve as a biomarker for mild cognitive impairment in type 2 diabetes mellitus patients without diabetic nephropathy. *Front Immunol*. 2025;16:1516975. doi:10.3389/fimmu.2025.1516975
17. Mattson MP, Camandola S. NF-κB in neuronal plasticity and neurodegenerative disorders. *J Clin Invest*. 2001;107(3):247–254. doi:10.1172/JCI11916
18. Ventorp F, Barzilay R, Erhardt S, et al. The CD44 ligand hyaluronic acid is elevated in the cerebrospinal fluid of suicide attempters and is associated with increased blood–brain barrier permeability. *J Affect Disord*. 2016;193:349–354. doi:10.1016/j.jad.2015.12.069
19. Skaper S, Facci L, Giusti P. Neuroinflammation, microglia and mast cells in the pathophysiology of neurocognitive disorders: A review. *CNS Neurol Disord Drug Targets*. 2015;13(10):1654–1666. doi:10.2174/1871527313666141130224206
20. Zhang H, Ben Zablah Y, Zhang H, Jia Z. Rho signaling in synaptic plasticity, memory, and brain disorders. *Front Cell Dev Biol*. 2021;9:729076. doi:10.3389/fcell.2021.729076
21. Caviedes A, Lafourcade C, Soto C, Wyneken U. BDNF/NF-κB signaling in the neurobiology of depression. *Curr Pharm Des*. 2017;23(21):3154–3163. doi:10.2174/1381612823666170111141915
22. Jang DI, Lee AH, Shin HY, et al. The role of tumor necrosis factor alpha (TNF-α) in autoimmune disease and current TNF-α inhibitors in therapeutics. *Int J Mol Sci*. 2021;22(5):2719. doi:10.3390/ijms22052719
23. Bulua AC, Simon A, Maddipati R, et al. Mitochondrial reactive oxygen species promote production of proinflammatory cytokines and are elevated in TNFR1-associated periodic syndrome (TRAPS). *J Exp Med*. 2011;208(3):519–533. doi:10.1084/jem.20102049
24. Ahmad MA, Kareem O, Khushtar M, et al. Neuroinflammation: A potential risk for dementia. *Int J Mol Sci*. 2022;23(2):616. doi:10.3390/ijms23020616
25. Li L, Wang Q, Sun X, et al. Activation of RhoA pathway participated in the changes of emotion, cognitive function and hippocampal synaptic plasticity in juvenile chronic stress rats. *Int J Biol Macromol*. 2023;233:123652. doi:10.1016/j.ijbiomac.2023.123652
26. Arrazola Sastre A, Luque Montoro M, Gálvez-Martín P, et al. Small GTPases of the Ras and Rho families switch on/off signaling pathways in neurodegenerative diseases. *Int J Mol Sci*. 2020;21(17):6312. doi:10.3390/ijms21176312
27. Fries GR, Saldana VA, Finnstein J, Rein T. Molecular pathways of major depressive disorder converge on the synapse. *Mol Psychiatry*. 2023;28(1):284–297. doi:10.1038/s41380-022-01806-1
28. Chen T, Dai Y, Hu C, et al. Cellular and molecular mechanisms of the blood–brain barrier dysfunction in neurodegenerative diseases. *Fluids Barriers CNS*. 2024;21(1):60. doi:10.1186/s12987-024-00557-1
29. Zhu H, Tang YD, Zhan G, Su C, Zheng C. The critical role of PARPs in regulating innate immune responses. *Front Immunol*. 2021;12:712556. doi:10.3389/fimmu.2021.712556
30. Schwab M, De Trizio I, Ghobrial M, et al. Nucleolin promotes angiogenesis and endothelial metabolism along the oncofetal axis in the human brain vasculature. *JCI Insight*. 2023;8(8):e143071. doi:10.1172/jci.insight.143071
31. Berk M, Köhler-Forsberg O, Turner M, et al. Comorbidity between major depressive disorder and physical diseases: A comprehensive review of epidemiology, mechanisms and management. *World Psychiatry*. 2023;22(3):366–387. doi:10.1002/wps.21110
32. Jomova K, Raptova R, Alomar SY, et al. Reactive oxygen species, toxicity, oxidative stress, and antioxidants: Chronic diseases and aging. *Arch Toxicol*. 2023;97(10):2499–2574. doi:10.1007/s00204-023-03562-9
33. Xu X, Sun B, Zhao C. Poly (ADP-Ribose) polymerase 1 and parthanatos in neurological diseases: From pathogenesis to therapeutic opportunities. *Neurobiol Dis*. 2023;187:106314. doi:10.1016/j.nbd.2023.106314
34. Wen JJ, Yin YW, Garg NJ. PARP1 depletion improves mitochondrial and heart function in Chagas disease: Effects on POLG dependent mtDNA maintenance. *PLoS Pathog*. 2018;14(5):e1007065. doi:10.1371/journal.ppat.1007065
35. Mekhaeil M, Conroy MJ, Dev KK. Elucidating the therapeutic utility of olaparib in sulfatide-induced human astrocyte toxicity and neuroinflammation. *J Neuroimmune Pharmacol*. 2023;18(4):592–609. doi:10.1007/s11481-023-10092-9
36. Gao W, Guo L, Yang Y, et al. Dissecting the crosstalk between Nrf2 and NF-κB response pathways in drug-induced toxicity. *Front Cell Dev Biol*. 2022;9:809952. doi:10.3389/fcell.2021.809952
37. Turunc Bayrakdar E, Uyanikgil Y, Kanit L, Koylu E, Yalcin A. Nicotinamide treatment reduces the levels of oxidative stress, apoptosis, and PARP-1 activity in Aβ(1–42)-induced rat model of Alzheimer's disease. *Free Radic Res*. 2014;48(2):146–158. doi:10.3109/10715762.2013.857018
38. Bobińska K, Gałecka E, Szemraj J, Gałecki P, Talarowska M. Is there a link between TNF gene expression and cognitive deficits in depression? *Acta Biochim Pol*. 1970;64(1):65–73. doi:10.18388/abp.2016_1276
39. Kim IH, Wang H, Soderling SH, Yasuda R. Loss of Cdc42 leads to defects in synaptic plasticity and remote memory recall. *eLife*. 2014;3:e02839. doi:10.7554/eLife.02839
40. Ma H, Chang Q, Jia J, Zhang Y, Wang G, Li Y. Linkage of blood cell division cycle 42 with T helper cells, and their correlation with anxiety, depression, and cognitive impairment in stroke patients. *Braz J Med Biol Res*. 2023;56:e12855. doi:10.1590/1414-431x2023e12855
41. Park G, Jin Z, Lu H, Du J. Clearing amyloid-beta by astrocytes: The role of Rho GTPases signaling pathways as potential therapeutic rargets. *Brain Sci*. 2024;14(12):1239. doi:10.3390/brainsci14121239
42. Meng F, You Y, Liu Z, Liu J, Ding H, Xu R. Neuronal calcium signaling pathways are associated with the development of epilepsy. *Mol Med Rep*. 2015;11(1):196–202. doi:10.3892/mmr.2014.2756
43. Esteras N, Alquézar C, De La Encarnación A, Villarejo A, Bermejo-Pareja F, Martín-Requero Á. Calmodulin levels in blood cells as a potential biomarker of Alzheimer's disease. *Alz Res Ther*. 2013;5(6):55. doi:10.1186/alzrt219
44. Wójcik-Piotrowicz K, Kaszuba-Zwoińska J, Rokita E, Thor P. Cell viability modulation through changes of Ca^2+-dependent signalling pathways. *Prog Biophys Mol Biol*. 2016;121(1):45–53. doi:10.1016/j.pbiomolbio.2016.01.004
45. Wang M, Zhang H, Liang J, Huang J, Wu T, Chen N. Calcium signaling hypothesis: A non-negligible pathogenesis in Alzheimer's disease [published online as ahead of print on January 8, 2025]. *J Adv Res*. 2025. doi:10.1016/j.jare.2025.01.007
46. Ashida H, Mimuro H, Sasakawa C. Shigella manipulates host immune responses by delivering effector proteins with specific roles. *Front Immunol*. 2015;6:219. doi:10.3389/fimmu.2015.00219
47. Li Y, Li F, Qin D, et al. The role of brain derived neurotrophic factor in central nervous system. *Front Aging Neurosci*. 2022;14:986443. doi:10.3389/fnagi.2022.986443

Bioinformatics analysis identified *TCP1* and *NOTCH1* as potential target molecules to overcome 5-fluorouracil resistance in cholangiocarcinoma

Sonexai Kidoikhammouan[1,A–E], Nopkamol Kanchanangkul[2,B,C], Worachart Lert-Itthiporn[2,A,E,F], Raksawan Deenonpoe[3,A,E,F], Charupong Saengboonmee[2,4,A,E,F], Sumalee Obchoei[5,B,F], Sopit Wongkham[2,4,A,D–F], Wunchana Seubwai[6,4,A–F]

[1] Biomedical Sciences Program, Graduate School, Khon Kaen University, Thailand
[2] Department of Biochemistry, Faculty of Medicine, Khon Kaen University, Thailand
[3] Department of Pathology, Faculty of Medicine, Khon Kaen University, Thailand
[4] Center for Translational Medicine, Faculty of Medicine, Khon Kaen University, Thailand
[5] Division of Health and Applied Science, Faculty of Science, Prince of Songkla University, Songkhla, Thailand
[6] Department of Forensic Medicine, Faculty of Medicine, Khon Kaen University, Thailand

A – research concept and design; B – collection and/or assembly of data; C – data analysis and interpretation; D – writing the article; E – critical revision of the article; F – final approval of the article

Advances in Clinical and Experimental Medicine, ISSN 1899–5276 (print), ISSN 2451–2680 (online) *Adv Clin Exp Med*. 2026;35(1):107–119

Address for correspondence
Wunchana Seubwai
E-mail: wunchanas@yahoo.com

Funding sources
This work was supported by the Graduate School, Khon Kaen University, through funding to support lecturers in admitting high-potential students to study and conduct research in their area of expertise. Funding was provided to W. Seubwai and S. Kidoikhammouan [631JH219], with additional support from the Faculty of Medicine, Khon Kaen University, Thailand (grant No. IN68031).

Conflict of interest
None declared

Received on September 26, 2024
Reviewed on December 19, 2024
Accepted on March 27, 2025

Published online on September 4, 2025

Cite as
Kidoikhammouan S, Kanchanangkul N, Lert-Itthiporn W, et al. Bioinformatics analysis identified *TCP1* and *NOTCH1* as potential target molecules to overcome 5-fluorouracil resistance in cholangiocarcinoma. *Adv Clin Exp Med*. 2026;35(1):107–119. doi:10.17219/acem/203446

DOI
10.17219/acem/203446

Abstract

Background. Late diagnosis and chemotherapy resistance, particularly to 5-fluorouracil (5-FU), contribute to the low survival rate in cholangiocarcinoma (CCA) patients. Identifying relevant genes and pathways, as well as novel targeted molecules, is crucial to overcoming 5-FU resistance and improving treatment outcomes for CCA patients.

Objectives. This study aimed to determine the potential molecules associated with 5-FU resistance in CCA cells.

Materials and methods. Transcriptomic datasets from 4 stable 5-FU-resistant cell lines and their corresponding parental lines were retrieved from the Gene Expression Omnibus. A series of bioinformatics analyses were conducted to identify key genes upregulated in 5-FU-resistant cells compared to their parental counterparts. The expression levels of candidate genes identified through bioinformatics analysis were validated in CCA tissues and cell lines.

Results. Differential gene expression, protein–protein interaction, and Hub genes analysis revealed 8 genes that were significantly upregulated in 5-FU resistance cells compared to their parental cells. Six of the 8 genes, including *TCP1*, *RPS6*, *RPS29*, *HSPA5*, *RPS15A*, and *NOTCH1*, were upregulated in patient CCA tissues. Using real-time PCR, only the expression levels of *NOTCH1* and *TCP1* were significantly higher in the 5-FU insensitive CCA cell lines, KKU-213A and KKU-213B, than that of the 5-FU sensitive CCA cell line, KKU-055. A similar result was observed in stable 5-FU-resistant cell lines (KKU-213A-FR and KKU-213B-FR) compared to their parental cells.

Conclusions. The bioinformatic analysis and PCR results revealed that *NOTCH1* and *TCP1* might be associated with 5-FU resistance and serve as potential molecular targets to enhance 5-FU sensitivity in CCA cells.

Key words: 5-fluorouracil, resistance, cholangiocarcinoma, *NOTCH1*, *TCP1*

Highlights

- This study identifies *TCP1* and *NOTCH1* as key genes associated with 5-FU resistance in cholangiocarcinoma (CCA).
- Bioinformatics and real-time PCR analyses confirm the upregulation of *TCP1* and *NOTCH1* in 5-FU-resistant CCA cell lines and patient tissues.
- Targeting *TCP1* and *NOTCH1* may enhance the efficacy of 5-FU treatment, improving therapeutic outcomes for CCA patients.

Background

Cholangiocarcinoma (CCA) is a malignancy arising from the biliary epithelium.[1] Surgical resection remains the cornerstone of therapy for early-stage disease, offering the best chance for long-term survival. In contrast, patients with metastatic or unresectable CCA are typically managed with systemic chemotherapy, most often 5-fluorouracil (5-FU).[2] Unfortunately, response rates to 5-FU in CCA are modest, and the emergence of 5-FU resistance is the principal cause of therapeutic failure, driving disease progression and mortality. Although the molecular mechanisms underpinning 5-FU resistance have been well characterized in other cancers[3,4] those specific to CCA remain poorly understood. A deeper elucidation of these pathways is therefore essential to develop more effective, resistance-overcoming treatment strategies for CCA. Recently, bioinformatics analyses leveraging public transcriptomic repositories, such as the Gene Expression Omnibus (GEO)[5] and The Cancer Genome Atlas (TCGA)[6], have become increasingly prevalent across biomedical research. These approaches have enabled the identification of novel therapeutic targets in gastric cancer,[7] non–small cell lung cancer and esophageal carcinoma,[8] as well as cholangiocarcinoma.[9] Moreover, numerous studies have demonstrated that mining these datasets can reveal molecular drivers of anticancer drug resistance. Accordingly, applying bioinformatics methods to publicly available transcriptomic data represents a promising strategy for uncovering candidate mediators of 5-FU resistance in CCA.

In this study, we combined bioinformatics and experimental approaches to uncover molecules linked to 5-FU resistance in CCA. First, we mined multiple GEO transcriptomic datasets to identify genes consistently associated with 5-FU resistance. Next, we constructed a protein–protein interaction network (PPI) of these candidate genes to highlight central "hub" factors. We then validated the expression of key resistance-associated genes in both CCA patient tissues and established cell lines using quantitative PCR. Finally, we employed PanDrugs to predict existing compounds that target these hub genes, laying the groundwork for potential therapeutic interventions.

Objectives

This study aimed to investigate potential target molecules associated with 5-FU resistance in CCA using bioinformatics, and PCR techniques.

Materials and methods

Cholangiocarcinoma cells

Three human CCA cell lines, KKU-055, KKU-213A, and KKU-213B, were obtained from the Japanese Collection of Research Bioresources Cell Bank.[10] Cells were maintained in Dulbecco's Modified Eagle's Medium (DMEM; Gibco/BRL, Grand Island, NY, USA) supplemented with 10% fetal bovine serum and 100 U/mL penicillin–streptomycin at 37°C in a humidified atmosphere of 5% CO_2. Two 5-FU-resistant sublines (KKU-213A-FR and KKU-213B-FR), kindly provided by Assoc. Prof. S. Obchoei,[11] were cultured in complete DMEM containing the IC_{10} concentration of 5-FU.

Proliferation assay

To assess 5-FU sensitivity, 2,000 cells per well were seeded in 96-well plates and incubated under standard culture conditions. Cell viability was then quantified using the MTT assay: After treatment, MTT solution (0.5 mg/mL) was added to each well and plates were incubated for 4 h at 37°C. The resulting formazan crystals were solubilized by adding 100 µL of DMSO and mixing thoroughly. Absorbance was measured at 540 nm on a microplate reader (Tecan Austria GmbH, Salzburg, Austria) to determine relative cell viability.

Determination of differentially expressed genes

To identify molecules commonly associated with 5-FU resistance, we retrieved transcriptomic profiles of stable 5-FU-resistant cancer cell lines from the GEO database (accession numbers GSE196900, GSE23776, and GSE81005). We then examined the GSE7631 dataset – which comprises 92 non-tumor controls and 91 Thai CCA patient tissue

samples, to evaluate the expression of candidate genes in clinical specimens.

Differentially expressed genes (DEGs) were identified from microarray datasets using GEO2R (https://www.ncbi.nlm.nih.gov/geo/geo2r) and from RNA-seq data via the Galaxy platform (https://usegalaxy.org).[12] Genes meeting the criteria of an adjusted p-value < 0.05 and $|\log_2$ fold change$| > 0.5$ were considered significant. Data visualization, including volcano plots and Venn diagrams, was performed in RStudio (https://rstudio.com) and with the jvenn online tool (https://jvenn.toulouse.inrae.fr/app/index.html), respectively.

Gene Ontology and pathway enrichment analysis

Gene Ontology (GO) and pathway enrichment analyses of the identified DEGs were performed using the DAVID Functional Annotation tool.[13] Differentially expressed genes were classified into GO categories, biological processes, cellular components, and molecular functions, as well as mapped to Reactome pathways.[14] Enrichment results were visualized as a bubble plot in RStudio to illustrate the significance and gene counts for each term.

Protein–protein interaction and hub gene identifications

Protein–protein interaction (PPI) networks for the common DEGs were generated using STRING v. 11.5 (https://string-db.org/). Hub genes within these networks were identified and ranked in Cytoscape (https://cytoscape.org) via the cytoHubba plugin,[15] with the top 30 genes selected based on connectivity degree. A heatmap illustrating the expression patterns of these hub genes across all datasets was then plotted using GraphPad Prism 9.2 (GraphPad Software, San Diego, USA).

Real-time polymerase chain reaction

Total RNA was isolated from CCA cell lines using TRIzol® Reagent (Invitrogen, Carlsbad, USA) according to the manufacturer's protocol. RNA purity and concentration were assessed with a NanoDrop™ 2000 Spectrophotometer (Thermo Fisher Scientific, Waltham, USA). For reverse transcription, total RNA was converted to cDNA using the High-Capacity cDNA Reverse Transcription Kit (Applied Biosystems, Foster City, USA; cat. No. 4368814) following the supplier's instructions.

Real-time quantitative PCR was conducted to assess the mRNA expression of candidate 5-FU resistance genes in CCA cell lines using a LightCycler® 480 system (Roche Diagnostics, Basel, Switzerland). Each 20 µL reaction contained 1× LightCycler® 480 SYBR Green I Master Mix (Roche Diagnostics), 0.5 µM of each primer, and 40 ng of cDNA template. Thermal cycling and fluorescence acquisition were performed according to the manufacturer's recommended protocol.

PCR amplifications were performed on a LightCycler 480 system with the following cycling conditions: An initial denaturation at 95°C for 5 min; 40 cycles of 95°C for 20 s, gene-specific annealing at 65°C (*TCP1*), 58°C (*RPS6*, *RPS15A*, *NOTCH1*), 60°C (*RPS29*), or 63°C (*HSPA5*) for 10 s; and extension at 72°C for 20 s. For each reaction, cycle threshold (Ct) and melting temperature (Tm) values were recorded, and mean ±SD were calculated. Relative gene expression was quantified using the $2^{-\Delta Ct}$ method. Primer sequences and expected amplicon sizes are detailed in Table 1.

Determination of targeted drug for 5-FU sensitizing using PanDrugs analysis

PanDrugs (www.pandrugs.org)[16] was used to identify druggable targets for sensitizing 5-FU-resistant CCA cell lines. Hub genes from the PPI analysis were submitted to PanDrugs, and candidate compounds were selected based on 2 criteria: 1) availability of a clinically approved, specific inhibitor targeting the gene product, and 2) evidence of the drug's efficacy in enhancing chemosensitivity.

Statistical analyses

Real-time PCR data are reported as the mean ±SD from 3 independent biological experiments, each performed in triplicate. Statistical analyses were conducted using IBM SPSS v. 24.0 (IBM Corp., Armonk, USA) and GraphPad Prism 9.2 (GraphPad Software Inc.). For microarray and RNA-seq datasets, p-values were calculated using the Limma and DESeq2 packages in R, respectively,

Table 1. The list of primers for candidate 5-FU associated genes

Genes	Forward primers	Reverse primers	Product sizes (bp)
TCP1	CGACTTCTGCCCATTCTCTC	CTCTTGGAGCATCTGGCTGT	70
RPS6	TGCTCTGAAGAAGCAGCGTA	GGAAAGTCTGCGTCTCTTCG	130
RPS29	TGGCTCTAGAAGTGGCTGGT	GTGAAGGCAAGGTTGGTCAT	110
HSPA5	TAGCGTATGGTGCTGCTGTC	TGACACCTCCCACAGTTTCA	117
RPS15A	CCTGTCCCCTAGTCTCTGCT	GAAGCTGATCCATGCCCCTT	93
NOTCH1	GGAGGCATCCTACCCTTTTC	TGTGTTGCTGGAGCATCTTC	118

5-FU – 5-fluorouracil; bp – base pair.

and adjusted for multiple testing by the Benjamini–Hochberg method. Normality of data distributions was assessed by the Kolmogorov–Smirnov test, and homogeneity of variances was confirmed by Levene's test (Supplementary Table 1). Differences between 5-FU-resistant and parental cell lines were considered statistically significant at $p < 0.05$.

Data meeting normality and homogeneity of variance criteria were compared by Student's t-test, whereas non-normally distributed data or those with unequal variances were analyzed using the Mann–Whitney (M–W) U test. For nonparametric comparisons, box-and-whisker plots display the median and interquartile range (IQR); for parametric analyses, results are presented as mean with 95% confidence intervals (95% CIs). Three-group comparisons – examining the correlation between mRNA levels of 6 upregulated hub genes and 5-FU response rates in CCA cell lines – were performed by the Kruskal–Wallis (K–W) test followed by Dunn's multiple comparisons. The Wilcoxon matched-pairs signed-rank test was used to compare 5-FU sensitivity between resistant and parental cells. A two-sided p-value < 0.05 was considered statistically significant.

Results

Identification of 417 DEGs common to 4 stable 5-FU-resistant cancer cell lines

We searched the GEO database for transcriptome datasets of stable 5-FU-resistant cancer cell lines. Our search revealed 3 transcriptomics datasets from four 5-FU-resistant colorectal cancer cell lines and their corresponding parental cells, including GSE196900, GSE23776, and GSE81005. The DEGs analysis revealed a total of 6,965, 11,899, 2,537 and 7,255 DEGs were identified from GSE196900H (HCT116 5-FU-resistant/HCT116 parental), GSE196900SW (SW480 5-FU-resistant/SW480 parental cell lines), GSE23776 (MIP 5-FU-resistant/MIP parental cell lines), and GSE81005 (HCT8 5-FU-resistant/HCT8 parental cell lines), respectively.

Volcano plots (Fig. 1) depict the distribution of significantly up- and downregulated genes in each 5-FU-resistant colorectal cancer model. By intersecting the DEG lists from all 4 datasets with a Venn diagram, we identified 417 genes that were consistently dysregulated across these resistant cell lines (Fig. 2). The complete breakdown of upregulated vs downregulated DEGs for each dataset is presented in Table 2.

Gene Ontology and pathway enrichment analysis showed several biological processes related to 5-FU resistance

Gene Ontology analysis of the 417 DEGs common to all 4 5-FU-resistant cell lines revealed significant enrichment in biological processes such as negative regulation of transcription from the RNA polymerase II promoter (Fig. 3A). At the cellular-component level, these genes localized predominantly to the cytosol and nucleoplasm (Fig. 3B). Molecular-function analysis showed a strong bias toward protein and RNA binding activities (Fig. 3C). Reactome pathway enrichment further indicated that these DEGs participate broadly in the cellular response to stress and external stimuli, glycosylation processes, and protein translation (Fig. 3D).

Identification of the top 10 hub genes associated with 5-FU resistance using PPIs and hub gene analysis

The PPIs of 417 common DEGs associated with 5-FU resistance were constructed using STRING. From the PPIs network, the hub genes were identified and ranked as the top 30 hub genes according to their connectivity (binding scores) with other genes (Table 3). The top 10 hub genes included *HSPA8*, *UBC*, *HSPA5*, *UBB*, *RPS6*, *CYCS*, *VCP*, *EIF2S1*, *CCND1*, *RPS5*. Node colors reflect the connectivity degree, with a pseudocolor scale ranging from red to yellow, representing gene rankings from 1 to 30 (Fig. 4).

Heatmap analysis (Fig. 5) of the top 30 hub genes identified 8 candidates that were upregulated in at least 3 of the 4 5-FU-resistant cell lines: *TCP1*, *RPS6*, *RPS29*, *HSPA5*, *RPS15A*, *NOTCH1*, *CALR*, and *ACO2*. These genes were therefore designated as the commonly upregulated hubs for further investigation.

To validate the relevance of the 8 upregulated hub genes in cholangiocarcinoma, we examined their expression in Thai CCA patient tissues using GEO dataset GSE7631.[17] Six genes – *TCP1* (M–W U = –7.335, $p < 0.001$), *RPS6* (U = –8.521, $p < 0.001$), *RPS29* (U = –7.527, $p < 0.001$), *RPS15A* (U = –9.657, $p < 0.001$), *NOTCH1* (U = –3.254, $p = 0.001$), and *HSPA5* ($t(181) = 3.505$, $p = 0.001$) – were significantly overexpressed in tumor vs adjacent normal tissues (Fig. 6). Detailed summary statistics (median ±IQR for nonparametric tests; mean ±95% CI for parametric tests) are provided in Supplementary Table 2.

Expression of 6 upregulated hub genes associated with 5-FU resistance varied with the 5-FU sensitivity in CCA cell lines

We next evaluated whether mRNA expression of the 6 upregulated hub genes correlated with 5-FU sensitivity in 3 CCA cell lines. KKU-055, KKU-213A, and KKU-213B were treated with increasing concentrations of 5-FU for 72 h, and cell viability was assessed by MTT assay. Dose–response curves demonstrated differential inhibition of proliferation: KKU-055 exhibited a low IC_{50} and was classified as 5-FU-sensitive, whereas KKU-213A and KKU-213B displayed significantly higher IC_{50} values and were deemed 5-FU-insensitive (Fig. 7A).

Real-time PCR analysis of the 6 upregulated hub genes in CCA cell lines revealed that, of these candidates, *TCP1*

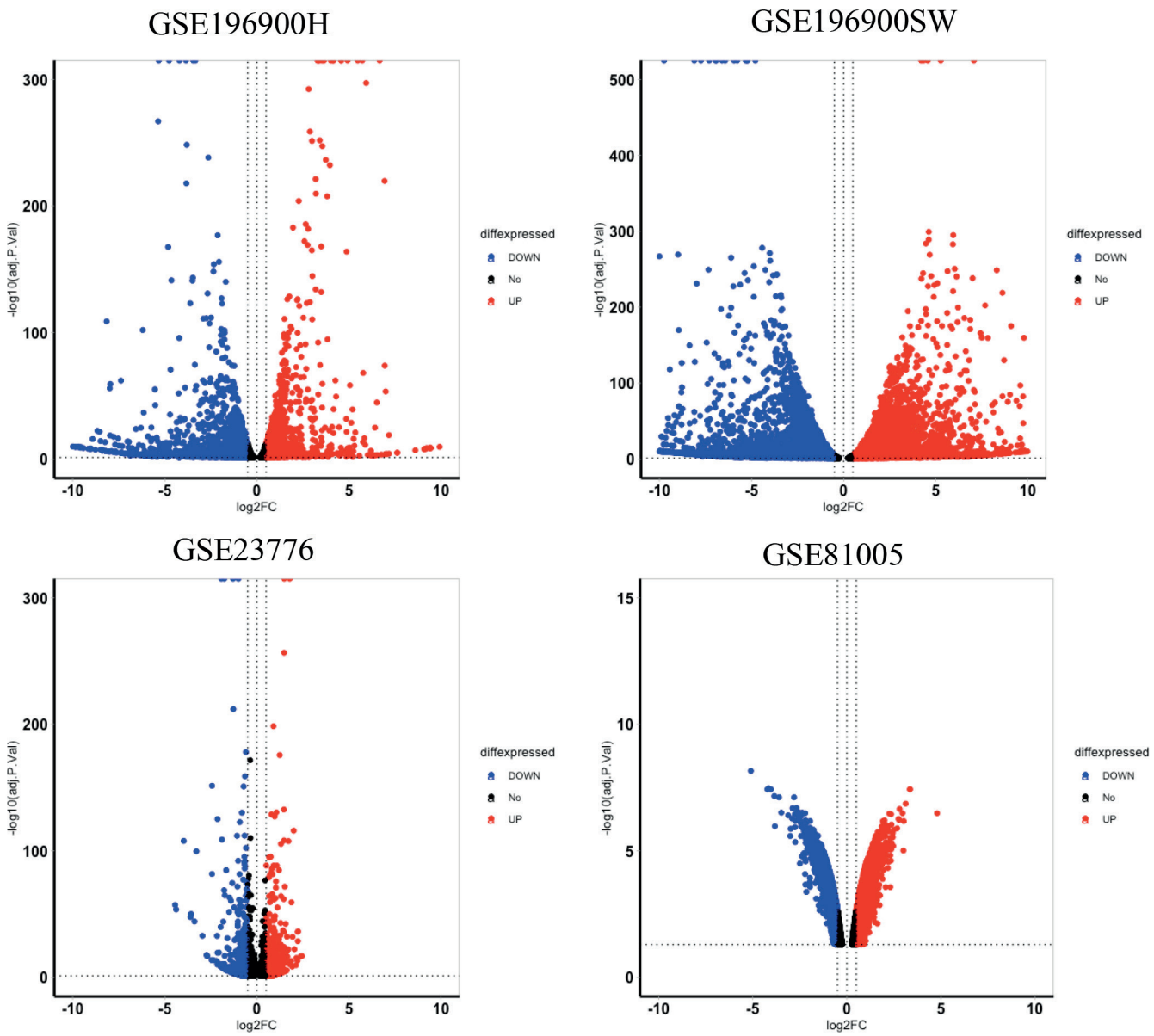

Fig. 1. Volcano plots of DEGs from 4 stable 5-FU-resistant cancer cell lines. The datasets include GSE196900H, GSE196900SW, GSE23776, and GSE81005. The X-axis represents the log2 fold change, and the Y-axis represents the negative logarithm (base 10) of the adjusted p-value. Red dots represent significantly upregulated genes, blue dots represent significantly downregulated genes, and black dots represent genes with no significant genes. GSE – GEO accession number. A p-value < 0.05 was considered statistical significance

Table 2. Transcriptomics datasets from stable 5-FU-resistant cancer cell lines

GSE	Cell lines	Resistance ratio	Total DEGs	Up-DEGs	Down-DEGs	Experiment type
GSE196900	HCT116	49 folds	6,965	657	6,308	RNA sequencing
	SW480	35 folds	11,899	3,578	8,321	
GSE23776	MIP5	10 folds	2,537	197	2,340	RNA sequencing
GSE81005	HCT8	26 folds	7,255	688	6,567	Microarray

GSE – GEO accession number; 5-FU – 5-fluorouracil; DEGs – differentially expressed genes.

(Kruskal–Wallis H = 19.65, p < 0.001), *RPS6* (H = 19.65, p < 0.001), and *NOTCH1* (H = 17.92, p < 0.001) were significantly more abundant in the 5-FU-insensitive lines (KKU-213A and KKU-213B) than in the 5-FU-sensitive line (KKU-055) (Fig. 7B). Median expression values with interquartile ranges for all 6 genes are provided in Supplementary Table 4.

To further validate the link between mRNA expression of the 6 hub genes and 5-FU resistance, we compared parental CCA cell lines (KKU-213A, KKU-213B) with their

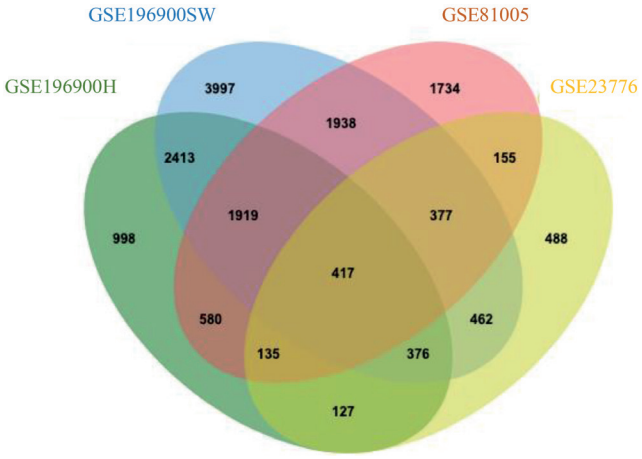

Fig. 2. Common DEGs in 5-FU-resistant cancer cell lines across 3 Gene Expression Omnibus (GEO) datasets. The Venn diagram displays the overlap of DEGs among the 3 datasets. Numbers within the sections indicate the count of DEGs specific to 1 dataset or shared among multiple datasets. GSE196900H, GSE196900SW, GSE81005, and GSE23776 are represented in green, blue, pink and yellow, respectively. The overlap number of all circles demontrates the common DEGs between the datasets

5-FU-resistant counterparts (KKU-213A-FR, KKU-213B-FR). As anticipated, the resistant sublines exhibited significantly reduced sensitivity to 5-FU vs their parental lines, as shown by Wilcoxon matched-pairs signed-rank tests (KKU-213A vs KKU-213A-FR: $Z = -2.366$, $p = 0.018$; KKU-213B vs KKU-213B-FR: $Z = -2.201$, $p = 0.028$) (Fig. 8).

Consistent with our earlier findings, *TCP1* and *NOTCH1* mRNA levels were markedly higher in the 5-FU-resistant sublines than in their parental counterparts. Specifically, *TCP1* expression was significantly elevated in KKU-213A-FR vs KKU-213A (M–W U: $Z = -3.576$, $p < 0.001$) and in KKU-213B-FR vs KKU-213B ($Z = -3.582$, $p < 0.001$). Similarly, *NOTCH1* levels were substantially increased in KKU-213A-FR compared to KKU-213A ($Z = -3.580$, $p < 0.001$) and in KKU-213B-FR compared to KKU-213B ($Z = -3.576$, $p < 0.001$) (Fig. 9). Median values with interquartile ranges (IQR) are detailed in Supplementary Table 5.

Potential therapeutics for *TCP1* and *NOTCH1* were identified using PanDrugs analysis; however, only *NOTCH1* has clinically approved, direct inhibitors available (Table 4).

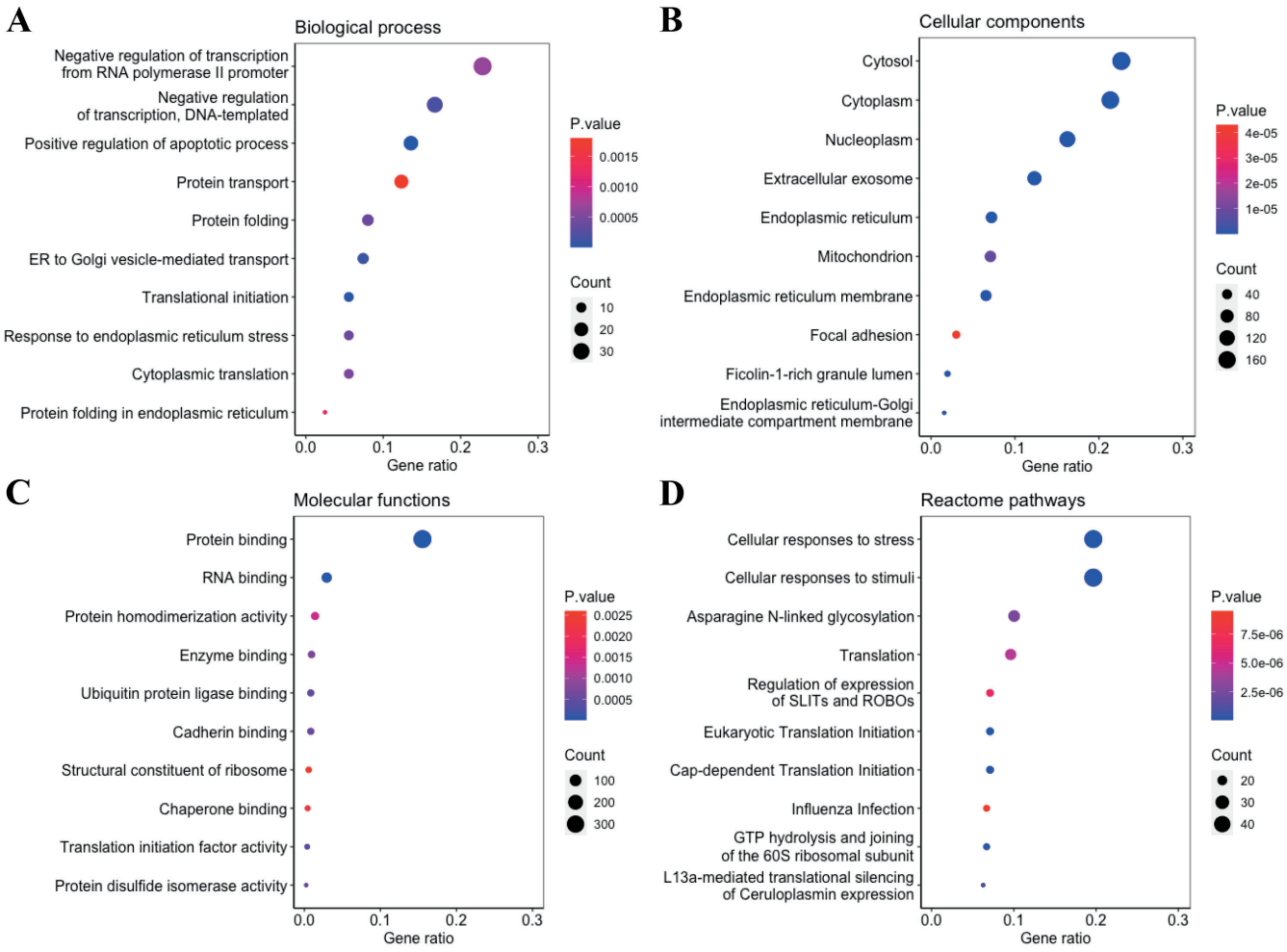

Fig. 3. Gene Ontology and pathway enrichment analysis in the common DEGs associated with 5-FU resistance. The top 10 enriched in (A) biological processes, (B) cellular components, (C) molecular function, and (D) the Reactome pathway, respectively. The size of the dots represents the count of genes, and the color indicates the p-value for the enrichment analysis

Table 3. The top 30 hub genes of common DEGs associated with 5-FU resistance

Rank	Name	Binding scores	Rank	Name	Binding scores
1	*HSPA8*	55.0	16	*RPL10*	32.0
2	*UBC*	52.0	17	*TCP1*	32.0
3	*HSPA5*	52.0	18	*SQSTM1*	30.0
4	*UBB*	47.0	19	*RPL38*	29.0
5	*RPS6*	47.0	20	*RPL28*	29.0
6	*CYCS*	42.0	21	*EIF2S3*	27.0
7	*VCP*	40.0	22	*RPS29*	27.0
8	*EIF2S1*	39.0	23	*CDK4*	27.0
9	*CCND1*	39.0	24	*ACO2*	25.0
10	*RPS5*	38.0	25	*PSMC2*	24.0
11	*EEF1A1*	37.0	26	*MAP1LC3B*	24.0
12	*RPL14*	35.0	27	*CALR*	24.0
13	*RPL15*	33.0	28	*EIF5B*	24.0
14	*RPS15A*	33.0	29	*NOTCH1*	21.0
15	*PARP1*	32.0	30	*ICAM1*	21.0

5-FU – 5-fluorouracil; DEGs – differentially expressed genes.

Table 4. Targeted inhibitors of hub gene interactions by PanDrugs analysis

Gene(s)	Drug name	Status description	Best interaction	DScore	GScore
NOTCH1	KK8645V7LE	clinical trials	direct-target	0.514	0.7973
NOTCH1	NIROGACESTAT	clinical trials	direct-target	0.513	0.7973
NOTCH1	BRONTICTUZUMAB	clinical trials	direct-target	0.512	0.7973
NOTCH1	CRENIGACESTAT	clinical trials	direct-target	0.512	0.7973
NOTCH1	OMP-52M51	clinical trials	direct-target	0.511	0.7973

DScore – the suitability of the treatment for a particular patient; GScore – the biological relevance of a gene in the tumoral process and its druggability.

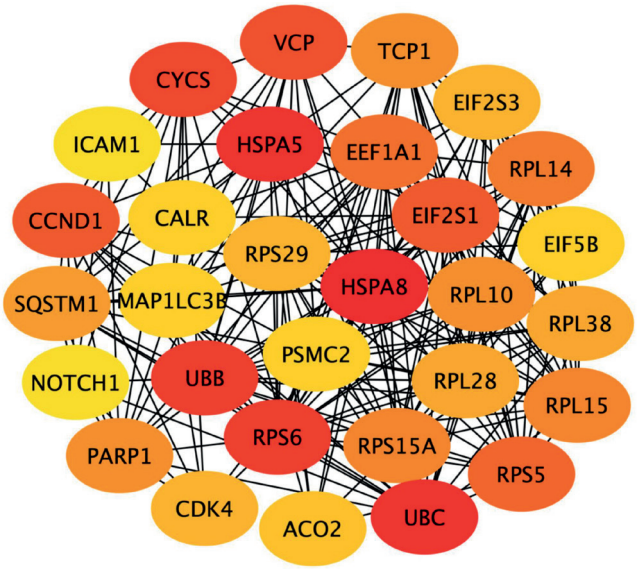

Fig. 4. Hub gene analysis of common DEGs associated with 5-FU resistance. The subnetwork shows the top 30 hub genes from the protein–protein interaction (PPI) network, generated using Cytoscape software. Node color reflects the degree of connectivity, with a pseudocolor scale from red to yellow representing the hub gene ranks from 1 to 30. Dark red color represents the highest degree while an orange color stands for the intermediate degree and yellow color is the lowest degree

Discussion

Chemoresistance to 5-FU poses a major obstacle in cholangiocarcinoma therapy.[18,19] Targeting the molecular drivers of this resistance offers a promising strategy to restore drug sensitivity. In the present study, we integrated bioinformatics analyses with PCR validation to identify *TCP1* and *NOTCH1* as novel mediators of 5-FU resistance in CCA. Both genes were consistently upregulated in stable 5-FU-resistant sublines compared to their parental counterparts, confirming their potential as therapeutic targets.

Chaperonin containing T-complex polypeptide 1 subunit 1 (*TCP1*) is a key molecular chaperone that facilitates the proper folding of nascent and stress-denatured proteins. In our study, *TCP1* was markedly upregulated in 5-FU-resistant CCA cell lines, implicating it as a driver of chemoresistance. This finding is in line with reports from other malignancies, where *TCP1* stabilizes oncogenic client proteins and augments pro-survival signaling. For example, in ovarian cancer, *TCP1* promotes tumor cell proliferation, invasion, and migration through activation of the PI3K/AKT/mTOR pathway.[20]

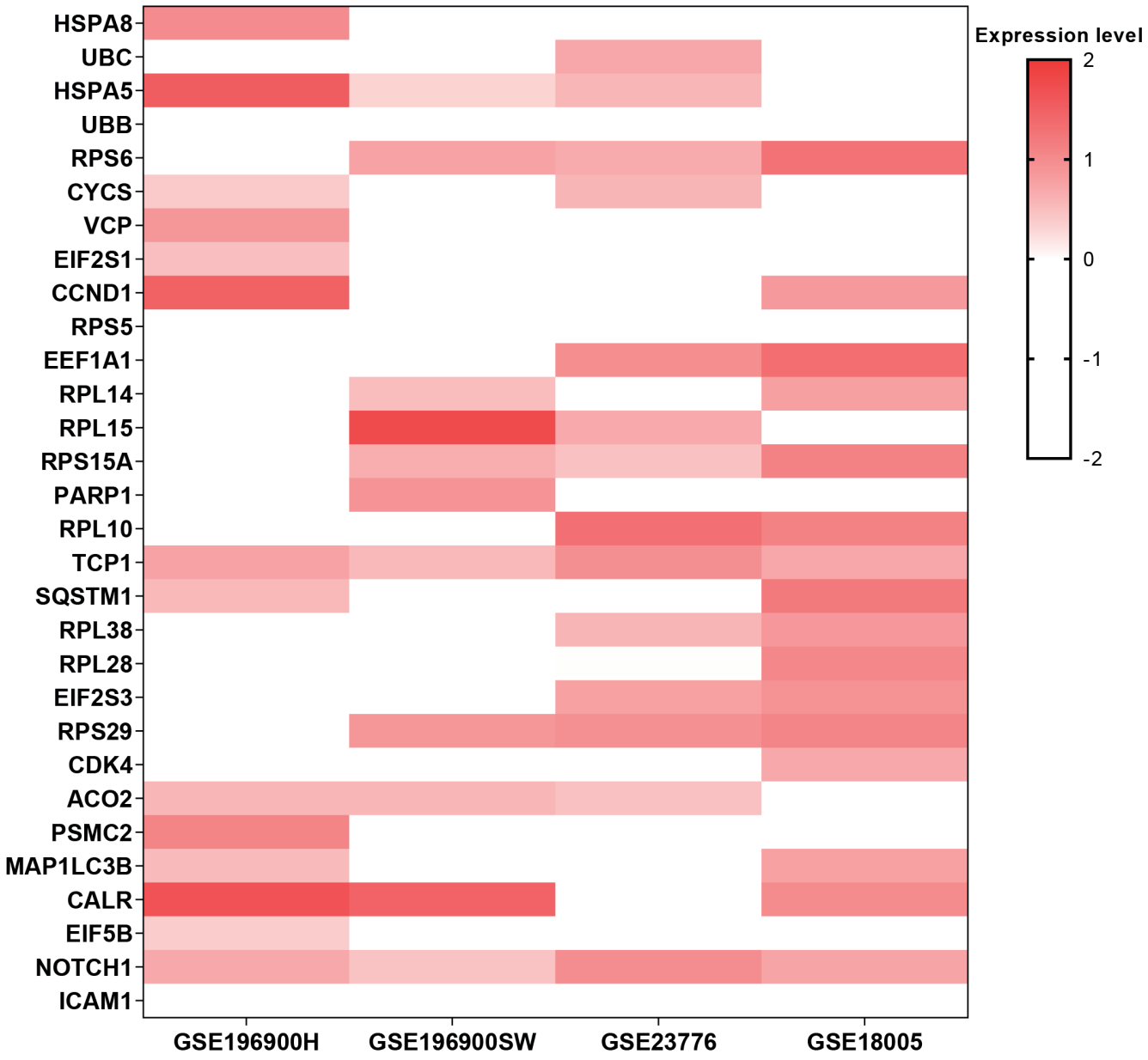

Fig. 5. Heatmap analysis of the commonly upregulated hub genes from the top 30 identified hub genes associated with 5-FU resistance. The heatmap displays the expression levels of hub genes across 4 transcriptomics datasets (GSE196900H, GSE196900SW, GSE23776, and GSE81005). The selection criteria for hub genes were those that showed upregulation in at least 3 out of the 4 5-FU-resistant cell lines. The color intensity represents the gene expression levels. Red indicates upregulation, whereas white represents downregulation

The expression of *TCP1* has been linked to upregulation of oncogenes such as *MYC*, *CCND1*, and *CDK2*, promoting breast cancer progression.[21] Although its role in 5-FU resistance remains unproven, *TCP1* overexpression correlates with poor responses to chemotherapy across multiple malignancies. Elevated *TCP1* levels confer resistance to doxorubicin and paclitaxel in breast and lung _cancer cell lines, while *TCP1* knockdown reduces X-linked inhibitor-of-apoptosis protein (*XIAP*) and β-catenin expression and inhibits metastatic behavior both in vitro and in vivo.[22]

TCP1 has been shown to enhance adriamycin resistance in acute myeloid leukemia by promoting autophagy via AKT/mTOR pathway activation. In the context of 5-FU resistance, key mediators include XIAP, β-catenin, and the AKT/mTOR signaling axis. XIAP, a potent inhibitor of apoptosis, blocks caspase activation, and its overexpression correlates with increased resistance to both radiotherapy and chemotherapy.[23] Activation of the Wnt/β-catenin pathway has been implicated in 5-FU resistance in oral squamous cell carcinoma and colorectal cancer[24,25] while hyperactivation of AKT/mTOR signaling is a hallmark of 5-FU-resistant colorectal tumors. By targeting *TCP1*, which sits upstream of these critical pro-survival networks, it may be possible to disrupt autophagy-mediated drug resistance mechanisms and improve therapeutic outcomes in CCA and other malignancies.

Notch signaling is an evolutionarily conserved pathway that governs development, cell-fate determination,

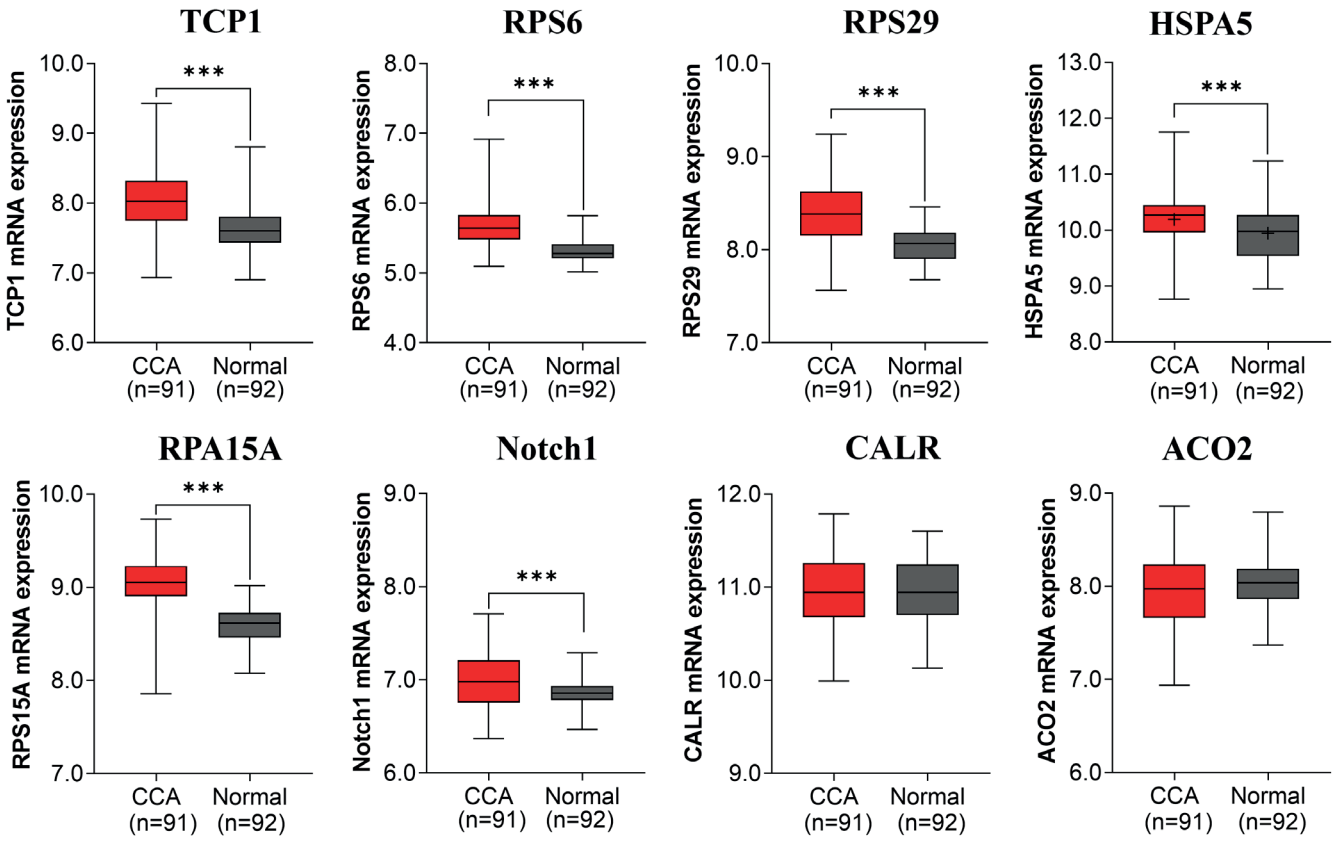

Fig. 6. The relative expression of common upregulated hub genes associated with 5-FU resistance in CCA tissues from Thai patients. Box plots show the mRNA expression levels of *TCP1*, *RPS6*, *RPS29*, *HSPA5*, *RPS15A*, *NOTCH1*, *CALR*, and *ACO2* in CCA tissues (n = 91) compared to normal tissues (n = 92). For genes analyzed using Mann–Whitney U tests, the box plots display median with interquartile range (IQR; Q1 to Q3), while for *HSPA5* (analyzed using a t-test), the box plot presents mean with 95% confidence intervals (CI). Outliers were plotted as individual points; *p < 0.05 was considered statistically significant (**p < 0.01, *** p < 0.001). *TCP1* – chaperonin containing t-complex polypeptide 1 subunit 1; *RPS6* – ribosomal protein S6; *RPS29* – ribosomal protein S29; *HSPA5* – heat shock protein family A (Hsp70) member 5; *RPS15A* – ribosomal protein S15A; *NOTCH1* – notch receptor 1; *CALR* – calreticulin; *ACO2* – aconitase 2

and tissue homeostasis through ligand–receptor interactions between the 4 Notch receptors (*NOTCH1–4*) and their cognate ligands (Jagged1, Jagged2, and Delta-like ligands).[26,27] Aberrant Notch activation contributes to tumorigenesis and cancer progression by upregulating oncogenic transcription factors (e.g., *MYC*, NF-κB), dysregulating cell-cycle regulators (such as p21, p27, cyclin D1, and *CCND3*), and enhancing expression of antiapoptotic proteins (including *BCL-2* and survivin).[27]

In intrahepatic cholangiocarcinoma (ICC), *NOTCH1* is markedly overexpressed compared with normal biliary epithelium, and its suppression induces apoptosis in ICC cell lines, indicating that *NOTCH1* promotes tumor cell survival by inhibiting apoptotic pathways[28]. Likewise, *JAGGED1* expression is elevated in ICC tissues relative to adjacent non-neoplastic mucosa.[29] More broadly, aberrant Notch signaling, especially via *NOTCH1*, drives chemoresistance across multiple malignancies. For example, in esophageal squamous cell carcinoma, *NOTCH1*-high KYSE70 cells display significantly greater resistance to 5-FU than *NOTCH1*-negative KYSE450 cells, and *NOTCH1* knockdown restores 5-FU sensitivity in KYSE70 cells.[30]

Knockdown of *NOTCH1* in CCA cell lines (RBE and HCCC-9810) significantly enhanced 5-FU sensitivity by downregulating the drug-efflux transporters *ABCB1* and *MRP1*, which are key mediators of chemoresistance. Given NOTCH1's role in promoting resistance to multiple chemotherapeutics, including 5-FU, its inhibition may represent a viable strategy to resensitize CCA cells and improve treatment outcomes. Several *NOTCH1* inhibitors are currently undergoing clinical evaluation, such as the γ-secretase inhibitor nirogacestat,[31] the anti-NOTCH1 monoclonal antibody brontictuzumab,[32] and the oral inhibitor crenigacestat.[33]

In our study, *NOTCH1* was markedly upregulated in 5-FU-resistant CCA cell lines compared with their parental counterparts, implicating *NOTCH1* activation in the maintenance of chemoresistance. Importantly, co-treatment with 5-FU and pharmacologic *NOTCH1* inhibitors, such as the γ-secretase inhibitor nirogacestat,[31] the anti-*NOTCH1* antibody brontictuzumab,[32] or the small-molecule crenigacestat,[33] has been shown to restore drug sensitivity in CCA models. These findings support the therapeutic potential of combining *NOTCH1* blockade with 5-FU to overcome resistance and improve clinical outcomes.

The identification of *TCP1* and *NOTCH1* as key mediators of 5-FU resistance in CCA cells opens up new avenues for therapeutic intervention. Targeting *TCP1* with

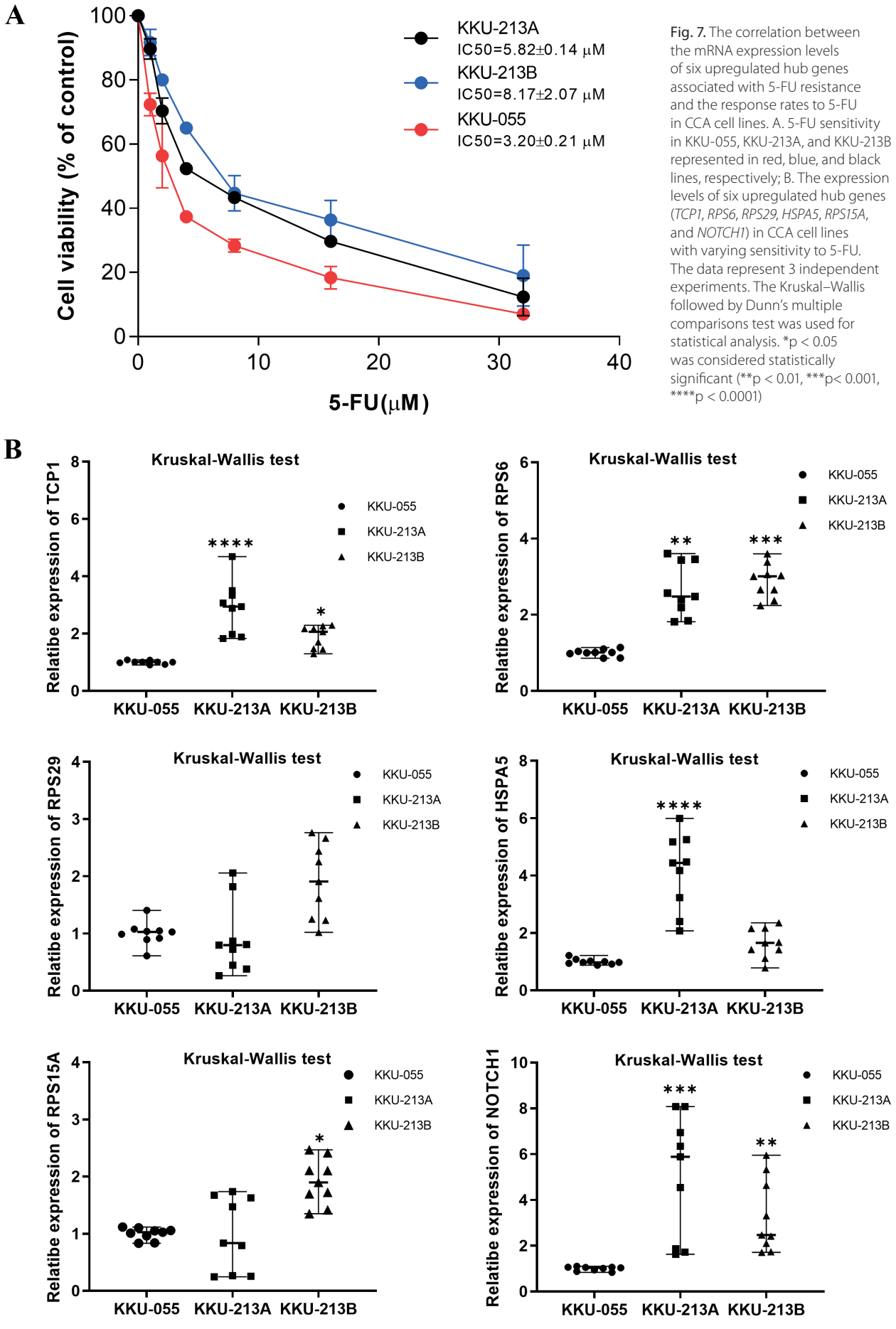

Fig. 7. The correlation between the mRNA expression levels of six upregulated hub genes associated with 5-FU resistance and the response rates to 5-FU in CCA cell lines. A. 5-FU sensitivity in KKU-055, KKU-213A, and KKU-213B represented in red, blue, and black lines, respectively; B. The expression levels of six upregulated hub genes (*TCP1*, *RPS6*, *RPS29*, *HSPA5*, *RPS15A*, and *NOTCH1*) in CCA cell lines with varying sensitivity to 5-FU. The data represent 3 independent experiments. The Kruskal–Wallis followed by Dunn's multiple comparisons test was used for statistical analysis. *p < 0.05 was considered statistically significant (**p < 0.01, ***p< 0.001, ****p < 0.0001)

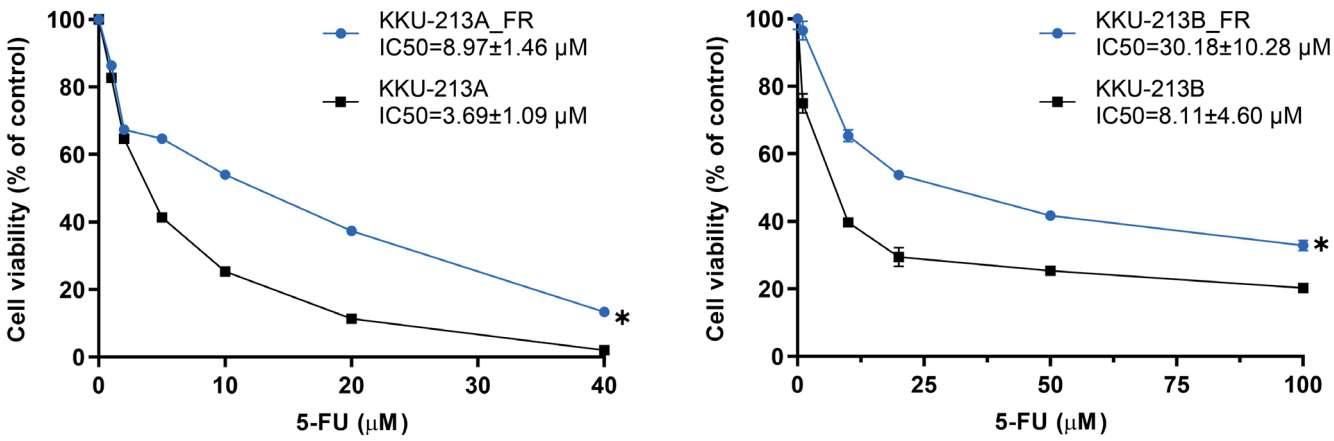

Fig. 8. 5-FU sensitivity in parental and 5-FU-resistant CCA cell lines. (Left) KKU-213A and KKU-213A_FR, and (Right) KKU-213B and KKU-213B_FR. Cell viability was measured using MTT assay after treatment with various concentrations of 5-FU for 72 h. The IC50 values represent the concentration of 5-FU required to inhibit 50% of cell growth. The data represent 3 independent experiments. Two groups were compared using the Wilcoxon matched-pairs signed rank test; *p < 0.05 is considered as the statistical significance

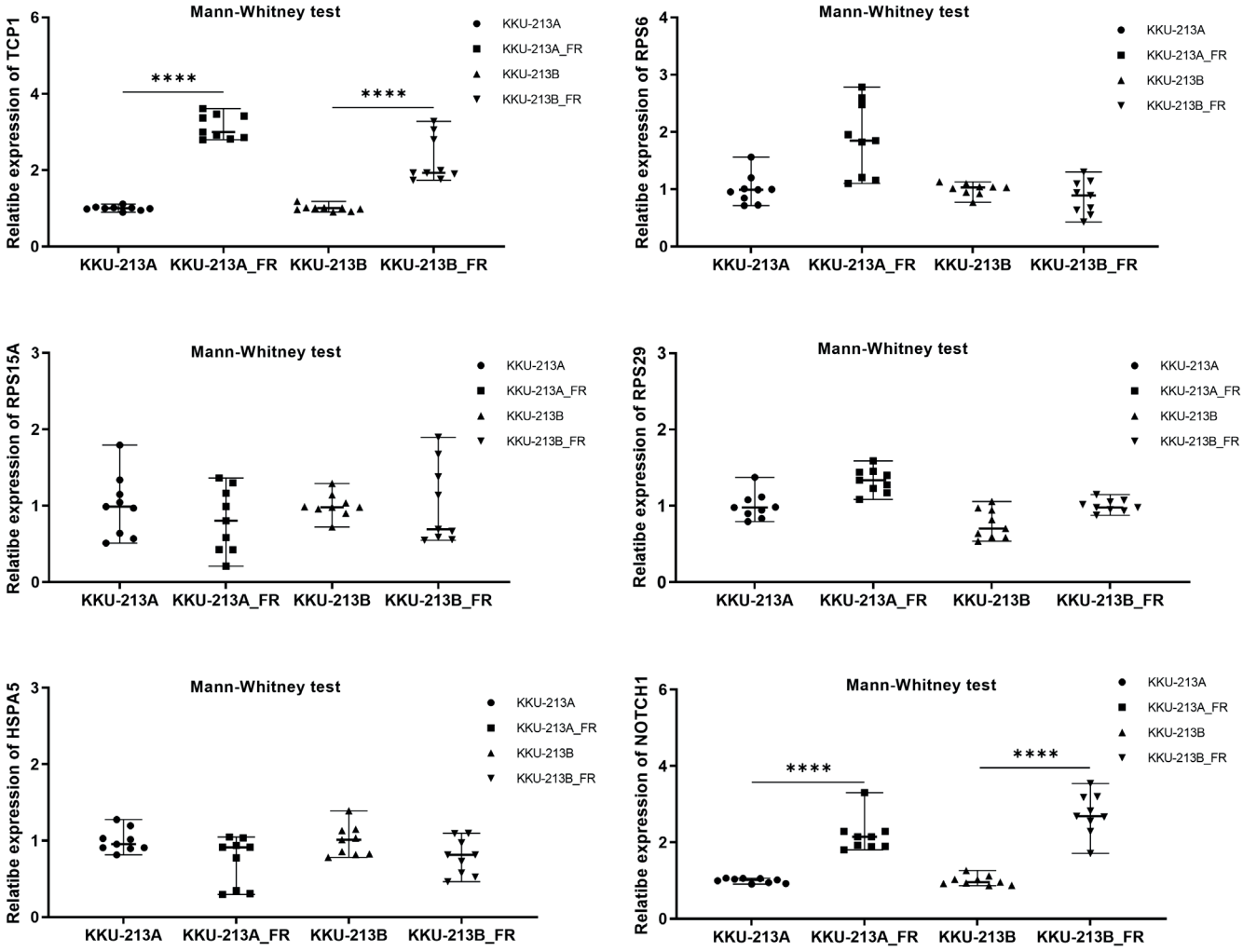

Fig. 9. The correlation between the mRNA expression levels of 6 upregulated hub genes associated with 5-FU resistance in parental CCA cell lines (KKU-213A and KKU-213B) compared to their corresponding stable 5-FU-resistant cell lines (KKU-213A-FR and KKU-213B-FR). The results show significantly higher mRNA levels of TCP1 and NOTCH1 in the stable 5-FU-resistant CCA cell lines compared to the parental cell lines. Mann–Whitney U test was used to evaluate the expression differences between 5-FU-resistant and parental; *p < 0.05 is considered as the statistical significance (**p < 0.01, ***p< 0.001, ****p < 0.0001)

small-molecule inhibitors or RNA-based therapies could disrupt its role in stabilizing oncogenic proteins and sensitizing cancer cells to 5-FU. Similarly, the use of *NOTCH1* inhibitors, such as brontictuzumab or crenigacestat, which are currently in clinical trials for other cancers, may enhance the efficacy of 5-FU in CCA. Combination therapies that include 5-FU and inhibitors of *TCP1* or *NOTCH1* could be explored in preclinical models to evaluate their potential to overcome chemoresistance and improve treatment outcomes.

Limitations

Further research is required to validate these findings in the tissues of CCA patients with resistance to 5-FU treatment vs 5-FU sensitive patients.

Conclusions

This study is the 1st report to identify *TCP1* and *NOTCH1* as key molecules associated with 5-FU resistance in CCA. Our findings suggest that the overexpression of these genes contributes to chemoresistance through mechanisms such as protein folding, cellular stress response, and drug efflux regulation. Importantly, targeting TCP1 and *NOTCH1* holds promise as a strategy to overcome 5-FU resistance and improve therapeutic outcomes in CCA patients. Future studies should validate these findings in clinical samples and explore the efficacy of combining *NOTCH1* inhibitors with 5-FU in preclinical models. These efforts could pave the way for novel therapeutic interventions that enhance the effectiveness of chemotherapy and address the pressing challenge of chemoresistance in CCA.

Data availability statement

The transcriptomic datasets from stable 5-FU-resistant cancer cell lines and Thai CCA patient tissues were retrieved from the GEO database and are openly available in Figshare [https://dx.doi.org/10.6084/m9.figshare.27139791].

ORCID iDs

Sonexai Kidoikhammouan https://orcid.org/0009-0005-1299-4000
Nopkamol Kanchanangkul https://orcid.org/0009-0005-0578-8962
Worachart Lert-Itthiporn https://orcid.org/0000-0002-7223-0169
Raksawan Deenonpoe https://orcid.org/0000-0002-8387-6061
Sopit Wongkham https://orcid.org/0000-0001-9578-3041
Wunchana Seubwai https://orcid.org/0000-0002-9265-5113

References

1. Anchalee N, Thinkhamrop K, Suwannatrai A, Titapun A, Loilome W, Kelly M. Spatio-temporal analysis of cholangiocarcinoma in a high prevalence area of northeastern Thailand: A 10-year large scale screening program. *Asian Pac J Cancer Prev*. 2024;25(2):537–546. doi:10.31557/APJCP.2024.25.2.537
2. Butthongkomvong K, Sirachainan E, Jhankumpha S, Kumdang S, Sukhontharot OU. Treatment outcome of palliative chemotherapy in inoperable cholangiocarcinoma in Thailand. *Asian Pac J Cancer Prev*. 2013;14(6):3565–3568. doi:10.7314/apjcp.2013.14.6.3565
3. Blondy S, David V, Verdier M, Mathonnet M, Perraud A, Christou N. 5-fluorouracil resistance mechanisms in colorectal cancer: From classical pathways to promising processes. *Cancer Sci*. 2020;111(9):3142–3154. doi:10.1111/cas.14532
4. Azwar S, Seow HF, Abdullah M, Faisal Jabar M, Mohtarrudin N. Recent updates on mechanisms of resistance to 5-fluorouracil and reversal strategies in colon cancer treatment. *Biology (Basel)*. 2021;10(9):854. doi:10.3390/biology10090854
5. Clough E, Barrett T. The Gene Expression Omnibus Database. *Methods Mol Biol*. 2016;1418:93–110. doi:10.1007/978-1-4939-3578-9_5
6. The Cancer Genome Atlas Research Network, Weinstein JN, Collisson EA, et al. The Cancer Genome Atlas Pan-Cancer analysis project. *Nat Genet*. 2013;45(10):1113–1120. doi:10.1038/ng.2764
7. Wu Q, Zhang B, Wang Z, et al. Integrated bioinformatics analysis reveals novel key biomarkers and potential candidate small molecule drugs in gastric cancer. *Pathol Res Pract*. 2019;215(5):1038–1048. doi:10.1016/j.prp.2019.02.012
8. Wen P, Dayyani F, Tao R, Zhong X. Screening and verification of potential gene targets in esophageal carcinoma by bioinformatics analysis and immunohistochemistry. *Ann Transl Med*. 2022;10(2):70. doi:10.21037/atm-21-6589
9. Sungwan P, Lert-Itthiporn W, Silsirivanit A, et al. Bioinformatics analysis identified CDC20 as a potential drug target for cholangiocarcinoma. *PeerJ*. 2021;9:e11067. doi:10.7717/peerj.11067
10. Sripa B, Seubwai W, Vaeteewoottacharn K, et al. Functional and genetic characterization of three cell lines derived from a single tumor of an *Opisthorchis viverrini*-associated cholangiocarcinoma patient. *Human Cell*. 2020;33(3):695–708. doi:10.1007/s13577-020-00334-w
11. Klinhom-on N, Seubwai W, Sawanyawisuth K, Obchoei S, Mahalapbutr P, Wongkham S. FOXM1 inhibitor, siomycin A, synergizes and restores 5-FU cytotoxicity in human cholangiocarcinoma cell lines via targeting thymidylate synthase. *Life Sci*. 2021;286:120072. doi:10.1016/j.lfs.2021.120072
12. Afgan E, Baker D, Batut B, et al. The Galaxy platform for accessible, reproducible and collaborative biomedical analyses: 2018 update. *Nucl Acids Res*. 2018;46(W1):W537–W544. doi:10.1093/nar/gky379
13. Huang DW, Sherman BT, Lempicki RA. Systematic and integrative analysis of large gene lists using DAVID bioinformatics resources. *Nat Protoc*. 2009;4(1):44–57. doi:10.1038/nprot.2008.211
14. The Gene Ontology Consortium. Expansion of the Gene Ontology knowledgebase and resources. *Nucleic Acids Res*. 2017;45(D1):D331–D338. doi:10.1093/nar/gkw1108
15. Chin CH, Chen SH, Wu HH, Ho CW, Ko MT, Lin CY. cytoHubba: Identifying hub objects and sub-networks from complex interactome. *BMC Syst Biol*. 2014;8(Suppl 1):S11. doi:10.1186/1752-0509-8-S4-S11
16. Piñeiro-Yáñez E, Reboiro-Jato M, Gómez-López G, et al. PanDrugs: A novel method to prioritize anticancer drug treatments according to individual genomic data. *Genome Med*. 2018;10(1):41. doi:10.1186/s13073-018-0546-1
17. Chaisaingmongkol J, Budhu A, Dang H, et al. Common molecular subtypes among Asian hepatocellular carcinoma and cholangiocarcinoma. *Cancer Cell*. 2017;32(1):57–70.e3. doi:10.1016/j.ccell.2017.05.009
18. Marin JJG, Prete MG, Lamarca A, et al. Current and novel therapeutic opportunities for systemic therapy in biliary cancer. *Br J Cancer*. 2020;123(7):1047–1059. doi:10.1038/s41416-020-0987-3
19. O'Rourke CJ, Munoz-Garrido P, Andersen JB. Molecular targets in cholangiocarcinoma. *Hepatology*. 2021;73(Suppl 1):62–74. doi:10.1002/hep.31278
20. Weng H, Feng X, Lan Y, Zheng Z. TCP1 regulates PI3K/AKT/mTOR signaling pathway to promote proliferation of ovarian cancer cells. *J Ovarian Res*. 2021;14(1):82. doi:10.1186/s13048-021-00832-x
21. Ghozlan H, Showalter A, Lee E, Zhu X, Khaled AR. Chaperonin-containing TCP1 complex (CCT) promotes breast cancer growth through correlations with key cell cycle regulators. *Front Oncol*. 2021;11:663877. doi:10.3389/fonc.2021.663877
22. Chang YX, Lin YF, Chen CL, Huang MS, Hsiao M, Liang PH. Chaperonin-containing TCP-1 promotes cancer chemoresistance and metastasis through the AKT-GSK3β-β-catenin and XIAP-survivin pathways. *Cancers (Basel)*. 2020;12(12):3865. doi:10.3390/cancers12123865
23. Flanagan L, Kehoe J, Fay J, et al. High levels of X-linked inhibitor-of-apoptosis protein (XIAP) are indicative of radio chemotherapy resistance in rectal cancer. *Radiat Oncol*. 2015;10(1):131. doi:10.1186/s13014-015-0437-1

24. Zhang X, Sun K, Gan R, et al. WNT3 promotes chemoresistance to 5-fluorouracil in oral squamous cell carcinoma via activating the canonical β-catenin pathway. *BMC Cancer*. 2024;24(1):564. doi:10.1186/s12885-024-12318-2
25. He L, Zhu H, Zhou S, et al. Wnt pathway is involved in 5-FU drug resistance of colorectal cancer cells. *Exp Mol Med*. 2018;50(8):1–12. doi:10.1038/s12276-018-0128-8
26. Shen W, Huang J, Wang Y. Biological significance of NOTCH signaling strength. *Front Cell Dev Biol*. 2021;9:652273. doi:10.3389/fcell.2021.652273
27. Rauff B, Malik A, Bhatti YA, Chudhary SA, Qadri I, Rafiq S. Notch signalling pathway in development of cholangiocarcinoma. *World J Gastrointest Oncol*. 2020;12(9):957–974. doi:10.4251/wjgo.v12.i9.957
28. Guo J, Fu W, Xiang M, et al. Notch1 drives the formation and proliferation of intrahepatic cholangiocarcinoma. *Curr Med Sci*. 2019;39(6):929–937. doi:10.1007/s11596-019-2125-0
29. Che L, Fan B, Pilo MG, et al. Jagged 1 is a major Notch ligand along cholangiocarcinoma development in mice and humans. *Oncogenesis*. 2016;5(12):e274. doi:10.1038/oncsis.2016.73
30. Liu J, Fan H, Ma Y, et al. Notch1 is a 5-fluorouracil resistant and poor survival marker in human esophagus squamous cell carcinomas. *PLoS One*. 2013;8(2):e56141. doi:10.1371/journal.pone.0056141
31. Gounder M, Ratan R, Alcindor T, et al. Nirogacestat, a γ-secretase inhibitor for desmoid tumors. *N Engl J Med*. 2023;388(10):898–912. doi:10.1056/NEJMoa2210140
32. Ferrarotto R, Eckhardt G, Patnaik A, et al. A phase I dose-escalation and dose-expansion study of brontictuzumab in subjects with selected solid tumors. *Ann Oncol*. 2018;29(7):1561–1568. doi:10.1093/annonc/mdy171
33. Doi T, Tajimi M, Mori J, et al. A phase 1 study of crenigacestat (LY3039478), the Notch inhibitor, in Japanese patients with advanced solid tumors. *Invest New Drugs*. 2021;39(2):469–476. doi:10.1007/s10637-020-01001-5

Precision management of atorvastatin: Cross-sectional analysis of genetic polymorphisms

Razan Ibrahim[1,B–D,F], Mohanad Odeh[2,A,C–F], Eyad Mallah[1,A,C–F], Luay Abu-Qatouseh[1,C–F], Ahmad Abu Awaad[3,B,D–F], Kenza Mansoor[1,C–F], Mohammad I.A. Ahmad[4,5,C–F], Amjad Shdifat[6,B,D–F], Muwafaq Al Hyari[7,B,D–F], Khaled W. Omari[8,C–F], Tawfiq Arafat[9,A,C–F]

[1] Faculty of Pharmacy and Medical Sciences, University of Petra, Amman, Jordan
[2] Department of Clinical Pharmacy and Pharmacy Practice, Faculty of Pharmaceutical Sciences, Hashemite University, Zarqa, Jordan
[3] Faculty of Pharmacy, Jerash University, Jordan
[4] Department of Medical Laboratories Sciences, Faculty of Allied Medical Sciences, Al-Ahliyya Amman University, Jordan
[5] Pharmaceutical and Biomedical Research Centre (PBRC), Al-Ahliyya Amman University, Amman, Jordan
[6] Department of Medicine and Family Medicine, Faculty of Medicine, Hashemite University, Zarqa, Jordan
[7] Center of Diabetes and Endocrinology, Prince Hamza Hospital, Diabetic Center, Amman, Jordan
[8] College of Engineering and Technology, American University of the Middle East, Kuwait
[9] Jordan Center for Pharmaceutical Research, Amman, Jordan

A – research concept and design; B – collection and/or assembly of data; C – data analysis and interpretation;
D – writing the article; E – critical revision of the article; F – final approval of the article

Advances in Clinical and Experimental Medicine, ISSN 1899–5276 (print), ISSN 2451–2680 (online) *Adv Clin Exp Med*. 2026;35(1):121–129

Address for correspondence
Eyad Mallah
E-mail: emallah@uop.edu.jo

Funding sources
None declared

Conflict of interest
None declared

Acknowledgements
We sincerely acknowledge the invaluable support and contributions from the University of Petra, Hashemite University, the Jordan Center for Pharmaceutical Research, and Prince Hamza Hospital, which played a pivotal role in the successful completion of this study.

Received on December 2, 2024
Reviewed on January 26, 2025
Accepted on March 29, 2025

Published online on January 5, 2026

Cite as
Ibrahim R, Odeh M, Mallah E, et al. Precision management of atorvastatin: Cross-sectional analysis of genetic polymorphisms. *Adv Clin Exp Med*. 2026;35(1):121–129. doi:10.17219/acem/203504

DOI
10.17219/acem/203504

Abstract

Background. Hyperlipidemia is a major risk factor for cardiovascular diseases and is associated with complications such as atherosclerosis and tendon injury. Though atorvastatin reduces cholesterol, genetic variants (*CYP2D6-4*, *SULT1A1*, *CYP2C192*) affect its response. These genetic variations influence atorvastatin metabolism, thereby affecting its therapeutic effectiveness.

Objectives. To advance personalized therapeutic drug monitoring and improve lipid profile management, this study aims to develop a robust and LC-MS/MS method for quantifying atorvastatin levels in human plasma. Additionally, to investigate the influence of genetic polymorphisms – particularly *CYP2D6-4*–on plasma concentrations of atorvastatin in patients with hyperlipidemia.

Materials and methods. Ethical approval for the study was obtained from the appropriate institutional review boards, and written informed consent was obtained from all participants. Atorvastatin was measured using LC-MS/MS. PCR-based methods were used for genotyping. Statistical analyses were performed to evaluate relationships between plasma atorvastatin levels and genetic variants.

Results. The LC-MS/MS method demonstrated excellent linearity, accuracy, precision, and stability, for the quantification of atorvastatin in human plasma. Higher atorvastatin concentrations were tied to *CYP2D6-4*. Furthermore, the study validated the analytical method for consistent and reliable measurement of atorvastatin levels in clinical samples.

Conclusions. This study successfully developed and validated a straightforward and reliable LC-MS/MS method for quantifying atorvastatin levels in human plasma. Significant *CYP2D64* – atorvastatin links highlight the value of pharmacogenetic dosing. Integrating pharmacogenetics – especially in the Jordanian population – may enhance the safety, efficacy, and individualization of atorvastatin therapy.

Key words: genotype, polymorphism, atorvastatin, hyperlipidemia, statins

Highlights

- Validated LC-MS/MS assay ensures precise atorvastatin quantification in human plasma, powering accurate therapeutic drug monitoring for hyperlipidemia.
- CYP2D6*4 polymorphism is the chief genetic driver of atorvastatin exposure, underscoring the value of genotype-guided, personalized dosing.
- Dose-dependent pharmacokinetics reveal distinct absorption and metabolism profiles at low vs high atorvastatin doses.
- Elevated plasma atorvastatin strongly correlates with LDL-cholesterol and total-cholesterol reductions, confirming a clear exposure-response link.
- Findings advocate routine pharmacogenetic testing to optimize atorvastatin therapy, maximize efficacy, and cut adverse-event risk in hyperlipidemic patients.

Background

Hyperlipidemia is a condition where blood lipid concentrations exceed normal limits, leading to severe complications like vascular stenosis, atherosclerosis, and heart diseases.[1] It is a significant risk factor for cardiovascular diseases and deaths worldwide, with cardiovascular diseases responsible for 20.5 million deaths in 2021, approx. 80% occurring in low- and middle-income countries.[2]

Hyperlipidemia, a condition causing high mortality and morbidity rates, is triggered by elevated lipid levels in the vascular endothelium. This leads to inflammation, lipid aggregation, foam cell formation, cell death, mitochondrial dysfunction, and fibrotic plaques.[3] Plaque lipids cause cardiovascular diseases, tendon failure, and tendon failure, particularly in the patellar tendon. Over time, hyperlipidemia increases macrophages in tendon tissues, replacing collagen fiber damage with lipids, resulting in less efficient tendons.[4]

Atorvastatin is a statin used for lipid control. It lowers blood cholesterol and triglyceride levels and reduces the risk of cardiac diseases in patients with normal cholesterol levels.[5]

Atorvastatin is an orally administered medication with a low bioavailability of 14% due to its high first-pass metabolism. It binds extensively to plasma proteins and is metabolized to its active metabolites via CYP450 3A4. Its plasma elimination half-life is around 14 h.[6]

Several necessary enzymes are involved in the metabolism of atorvastatin, including *CYP2D6-4*, *SULT1A1*, and *CYP2C19-2*. Many medications, including statins, are metabolized oxidatively by *CYP2D6-4*. Individual differences in medication toxicity and efficacy can result from variations in *CYP2D6* gene variants, which can profoundly impact drug metabolism rates. In the case of atorvastatin, the *CYP2D6-4* polymorphism is associated with higher plasma concentrations, suggesting that individuals with this genetic variant may require lower doses of the drug for the same therapeutic effect. Drugs and endogenous compounds are subject to sulfonation and elimination, which can affect their bioavailability and activity. *SULT1A1* mediates this process. Variations in *SULT1A1* polymorphisms may result in distinct drug responses. Another enzyme involved in drug metabolism is *CYP2C19-2*. Variations in this enzyme's polymorphism can change enzyme activity, impacting drug concentration and treatment results.

Due to the distinct genetic makeup of this population, which may display different frequencies of *CYP2D6-4*, *SULT1A1*, and *CYP2C19-2* polymorphisms, this study focuses on Jordanian patients. Comprehending these genetic variances is essential to creating customized medicine strategies for the Jordanian population. This study's findings could pave the way for a more personalized approach to hyperlipidemia treatment, where medication dosages and types are tailored to an individual's genetic profile. Moreover, cardiovascular illnesses constitute a significant cause of morbidity and death in Jordan, so it is critical to optimize hyperlipidemia treatment approaches in this population.

Objectives

The study aims to develop a simple LC-MS/MS method for determining atorvastatin concentration in human plasma and investigating genetic polymorphisms that affect the response to atorvastatin. The objectives include correlating plasma atorvastatin levels with liver enzymes, examining the relationship between atorvastatin concentration and clinical lipid profile parameters, and assessing the impact of daily dose intake on plasma concentration. Additionally, the study explores drug–drug interactions influencing atorvastatin levels, as well as the influence of demographic factors and patient genotypes on atorvastatin concentration. Finally, the study aims to identify the highest and lowest atorvastatin concentration values and their associations.

Materials and methods

The study employed a robust analytical cross-sectional pragmatic multidisciplinary approach to achieve its

objectives, integrating laboratory preparation for genetic analysis, precise quantification of atorvastatin concentrations, comprehensive clinical data collection from patients, and rigorous statistical analysis to synthesize the findings.

Settings and ethical approval and individual consent

Between March 2022 and August 2024, samples were collected, analyzed, and systematically managed in Jordan. The present study was conducted in accordance with the Declaration of Helsinki and complied with the principles of Good Clinical Practice (GCP) and Good Laboratory Practice (GLP). Ethical approvals for this study were obtained from the Institutional Review Board (IRB) of Prince Hamza Hospital, the Jordanian Ministry of Health, and Hashemite University in Zarqa, Jordan (approval reference numbers 8/3/2021/2022 and MH-14/3/2022, respectively). At Prince Hamza Hospital, separate informed consent forms were provided to each participant. All procedures and interventions were carried out in accordance with the guidelines of the Jordanian Ministry of Health. Data were anonymized and securely stored in compliance with applicable data protection regulations, and patient confidentiality was strictly maintained.

Participants recruitment

The study included patients aged 20–80 years diagnosed with hyperlipidemia and regularly using atorvastatin (ATC code: C10AA05), with complete electronic medical records detailing anthropometric measurements, atorvastatin dosage, and lipid profiles. Exclusion criteria comprised patients using other statin agents, those with incomplete medical records, individuals with secondary hyperlipidemia (e.g., uncontrolled hypothyroidism or nephrotic syndrome), severe comorbidities (e.g., advanced liver disease or malignancies), and non-consenting patients. Only individuals who met the inclusion criteria and provided written informed consent were enrolled in the study.

Variables and measures for LC-MS/MS analysis

Method validation

The European Medicines Agency (EMA) 2012 bioanalytical method validation guidelines[7] stipulated stringent validation procedures for this study's LC-MS/MS analysis method. To avoid bias and guarantee the analytical method's dependability and resilience, validation included thorough evaluations of linearity, accuracy, precision, and stability.

Individuals' plasma sample preparation for analysis

The plasma samples from the individuals were treated the same way as the validation samples before LC-MS/MS analysis. Strict adherence to established protocols was observed during these preparations to minimize analytical variability and preserve sample integrity. The analytical results were more dependable and consistent because standardized sample handling techniques ensured uniformity across all sample preparations.

Variables and measures for genotyping

DNA extraction method

Genomic DNA was extracted from biological samples using the Blood DNA Preparation Column Kit (Jena Bioscience, Jena, Germany). A few minor modifications were made to the manufacturer's suggested protocols to maximize the efficiency of DNA extraction, guaranteeing strong and dependable isolation of high-quality DNA appropriate for further genotyping analyses.

Amplification using polymerase chain reaction

Polymerase chain reaction was used to ramp up the desired genes using the Labnet® PCR System TC6000-G-230V (PCR) (Labnet, international, Edison, USA).o guarantee targeted and effective amplification of the intended genetic loci, PCR reactions were carefully prepared, and amplification conditions were optimized. To verify the accuracy and precision of the amplification procedure, PCR amplification was applied to every DNA sample in conjunction with suitable controls. A mixture with a total volume of 20 µL was created for every DNA sample except the negative samples.

Polymerase chain reaction-restriction fragment length polymorphism

The previously amplified DNA fragments were digested using polymerase chain reaction-restriction fragment length polymorphism (PCR-RFLP). The PCR reaction products were further incubated in the appropriate reaction buffer supplied by the manufacturer using a 25 µL reaction mixture that contained 0.5 µL units of CutSmart HaeII for the *SULTA1* gene and 0.5 µL units of BstN1 for all the CYPs genes. To facilitate enzyme digestion, the mixture for *SULT1A1* was incubated at 37°C for 20 min. After that, the heat was inactivated for 20 min at 80°C. The CYPs were incubated at 60°C for 15 min.

Statistical analyses

The sample size calculation was primarily based on the prevalence of *CYP2C19* genotype in the Jordanian population, which has been documented at 0.3. Based on this prevalence rate, 2 sample size scenarios were calculated: 1) A minimum of 50 patients would be required to detect a 0.25 difference in atorvastatin concentrations;

2) To detect a smaller difference of 0.2, a sample size of 74 patients would be necessary. Both calculations were anchored to the established *CYP2C19* prevalence of 0.3.

Accuracy and completeness were guaranteed by the electronic collection of patient data and associated variables using Microsoft Excel. IBM SPSS for Windows v. 25 was used to code and import the data for statistical analysis (SPSS Inc., Chicago, USA). To reduce errors, bias, and guarantee data integrity, strict quality control procedures were implemented at every stage of the data collection.

The statistical analysis encompassed multiple complementary approaches to ensure robust data interpretation. Descriptive statistics were applied, with categorical variables reported as frequencies and percentages, and continuous variables presented as medians with ranges due to non-normal distribution. Two non-parametric tests were used in this study: The Kruskal–Wallis test and the Mann–Whitney U test, selected based on the results of the Shapiro–Wilk test, which indicated a violation of the normality assumption for atorvastatin concentrations. The Kruskal–Wallis test was used to compare atorvastatin concentrations across 3 independent dose groups (10 mg/day, 20 mg/day and 40 mg/day), followed by post hoc pairwise comparisons using Dunn's procedure with Bonferroni correction to identify specific group differences. To compare atorvastatin concentrations between patients with and without a specific genotype, the Mann–Whitney U test was applied, stratified by daily dose to control for dosing effects. The interaction effects between genotype and dose were not examined, as this was not an objective of the study. Given that Allel/genotype is a naturally occurring, non-manipulated variable, our analysis focused on evaluating atorvastatin concentrations separately by genotype and dose level, rather than exploring potential interactions between these independent variables. A $p < 0.05$ was considered statistically significant for all tests.

Results

Demographic data

Data were collected from a total of 90 patients. The participants' characteristics are summarized in Table 1. The cohort included 41 women (45.6%) and 49 men (54.4%), with an age range of 42 to 81 years. The majority of participants were classified as overweight or having obesity class I (66.6%). Most individuals were non-smokers, and coffee consumption was more frequently reported than tea consumption.

Patient polypharmacy profile

On average, patients were taking 6 medications, with some reporting the use of up to 14. Details on polypharmacy and supplement intake are presented in the accompanying dataset. The most commonly used medications were metformin (64.4%) and aspirin (57.8%), while vitamin D (cholecalciferol, 50,000 IU) was the most frequently reported supplement, used by 37.8% of participants.

Table 1. Descriptive demography

Variable	Description	n (%)
Gender	female	41 (45.6)
	male	49 (54.4)
Age	40–59 years old	26 (28.9)
	60–65 years old	33 (36.7)
	>65 years old	31 (34.4)
BMI	normal weight (18–24.9)	8 (8.9)
	overweight (25–29.9)	30 (33.3)
	obesity class I (30–34.9)	30 (33.3)
	obesity class II (35–39.9)	10 (11.1)
	obesity class III (≥40)	12 (13.3)
Smoking	no	52 (57.8)
	yes	28 (31.1)
	ex	10 (11.1)
Coffee intake (1–3 cups per day)	no	37 (41.1)
	yes	53 (58.9)
Tea intake (1–3 cups per day)	no	56 (62.2)
	yes	34 (37.8)

n – number of participants (their percentage of 90 participants); BMI – body mass index.

Genotyping

Figures 1–3 illustrate the results obtained using Gel-Imaging analysis with a 3% (w/v) agarose gel stained with ethidium bromide, alongside a 100 bp DNA ladder for fragment size reference. As summarized in Table 2, more than half of the recruited patients were homozygous mutants for *SULT1A1* (55.6%). In contrast, the majority of patients were homozygous wild-type for *CYP2C19-2* (76.6%) and *CYP2D6-4* (73.3%).

Dose-dependent variations in atorvastatin concentration

Patients were divided into 3 dosage groups: 10 mg (12.2%), 20 mg (67.8%), and 40 mg (20%). The Kruskal–Wallis test revealed significant differences in atorvastatin concentrations across these groups ($p = 0.003$): 10 mg (n = 11, median = 0.1 ng/mL, range: 0.028–1.35), 20 mg (n = 61, median = 3.6 ng/mL, range: 0.54–6.0), and 40 mg (n = 18, median = 2.7 ng/mL, range: 0.38–5.29). Pairwise comparisons using Dunn's procedure with Bonferroni correction showed a significant difference between the 10 mg and 20 mg groups ($p = 0.002$), and a borderline significant difference between the 10 mg and 40 mg groups ($p = 0.051$). No significant difference was found between the 20 mg and 40 mg groups (Table 3).

In addition to the observed dose-dependent differences, women receiving 10 mg daily had significantly higher plasma

Table 2. Description of the genotype for the patients

Allele	Genotype	Gene expression	n (%)
SULT1A1	wild-type (homozygous)	no	70 (77.8)
		yes	20 (22.2)
	mutant-type (homozygous)	no	40 (44.4)
		yes	50 (55.6)
	heterozygous	no	70 (77.8)
		yes	20 (22.2)
CYP2C19-2	wild-type (homozygous)	no	21 (23.3)
		yes	69 (76.6)
	mutant-type (homozygous)	no	90 (100%)
		yes	0 (0)
	heterozygous	no	69 (76.6)
		yes	21 (23.3)
CYP2D6-4	mutant-type (homozygous)	no	82 (91.1)
		yes	8 (8.9)
	wild-type (homozygous)	no	24 (26.7)
		yes	66 (73.3)
	heterozygous	no	74 (82.2)
		yes	16 (17.8)

n – number of participants (their percentage of 90 participants).

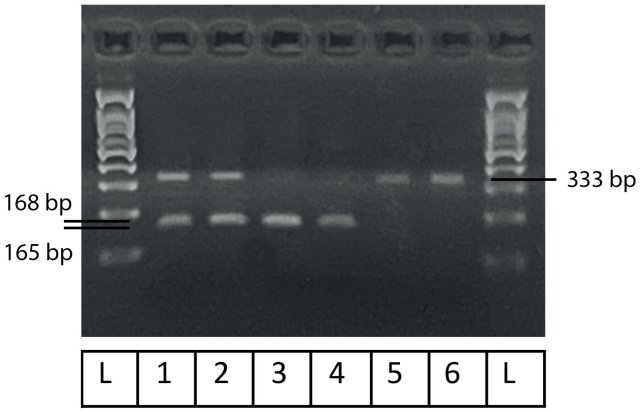

Fig. 1. *SULT1A1* restriction gel-imaging results. Band 1,2: heterozygous, band 3,4: mutant type (homozygous), Band 5,6: wild type (homozygous), and L: 100 bp ladder

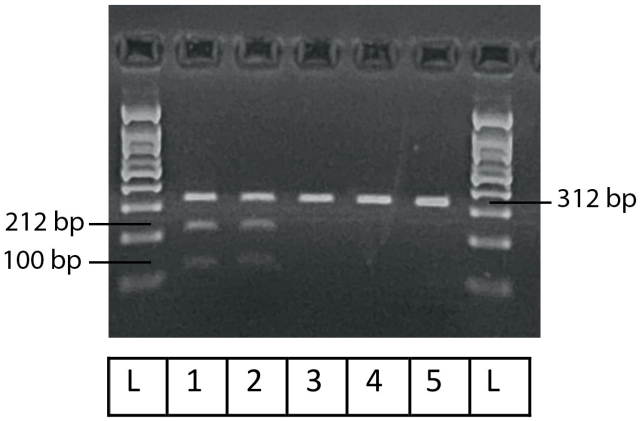

Fig. 2. *CYP2C19-2* restriction gel-imaging results. Band 1,2: Heterozygous, band 3,4,5: wild type (homozygous), and L: 100 bp ladder

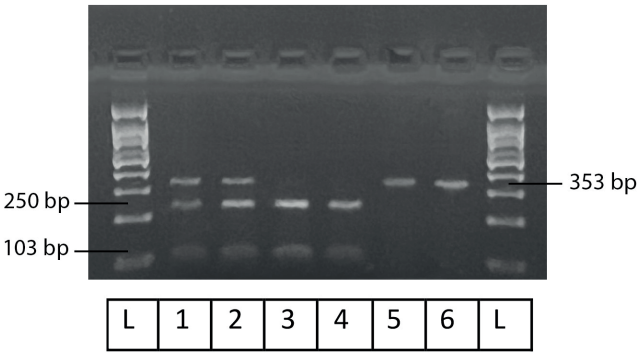

Fig. 3. *CYP2D6-4* restriction gel-imaging results. Band 1,2: heterozygous, band 3,4: wild type (homozygous), band 5,6: mutant type (homozygous), and L: 100 bp ladder

atorvastatin concentrations than men. This gender-based variation may be attributed to differences in pharmacokinetics (PK), enzyme activity, or hormonal factors. No significant associations were observed between atorvastatin plasma concentrations and age, body mass index (BMI), smoking status, or caffeine consumption (coffee or tea).

Atorvastatin drug-drug interactions and polypharmacy

No significant correlations were found between the number of medications or supplements taken and plasma atorvastatin concentrations, nor between any specific medication and atorvastatin levels (see shared data).

Clinical parameters related to lipid profile

The analysis of atorvastatin's impact on lipid profiles revealed compelling associations. A statistically significant, robust negative correlation was found between atorvastatin concentration and low-density lipoprotein (LDL) levels, with a similar correlation for total cholesterol ($rs = -0.45$, $p < 0.001$, and $rs = -0.41$, $p < 0.001$, respectively). A weaker but still statistically significant correlation was observed with triglyceride levels ($rs = -0.28$, $p = 0.016$).

Regarding liver enzymes, most levels, including alanine transaminase (ALT) and aspartate transaminase (AST), were within the normal range, and there was no discernible correlation between their levels and atorvastatin concentration in plasma. Conversely, creatinine serum displayed a moderate positive correlation with creatinine levels ($rs = 0.28$, $p = 0.01$), indicating a potential influence on renal function. Lastly, in the assessment of the uric acid serum, no correlation was detected between atorvastatin plasma concentration and uric acid serum levels, suggesting a distinct metabolic interaction. These findings underscore the multifaceted effects of atorvastatin on various physiological parameters, necessitating comprehensive monitoring in clinical contexts.

Table 3. Atorvastatin concentration based on daily dose intake

Concentration/daily dose	Atorvastatin daily dose			Independent-samples Kruskal–Wallis test	
	10 mg	20 mg	40 mg		
Number of patients (%)	11 (12.2%)	61 (67.8%)	18 (20%)	$\chi^2 = 11.3$, p = 0.003[c]	
Median (range) of concentration	0.10 (0.028–1.35)	3.6 (0.54–6.0)	2.7 (0.38–5.29)		
Shapiro–Wilk[a] test (df)[b]	0.570 (df = 10) p < 0.001	0.75 (df = 60) p < 0.001	0.82 (df = 117) p < 0.001		
Sample 1–Sample 2	test statistic	SE	standard test statistic	Sig.	Adj. Sig.[d]
10–40	–23.874	9.998	–2.388	0.017	0.051
10–20	–28.835	8.558	–3.369	0.001	0.002
40–20	4.961	7.007	0.708	0.479	1.000

[a]assumption of normality was assessed using the Shapiro–Wilk test, which indicated a non-normal distribution of the data (p < 0.05); [b]degrees of freedom (df) correspond to the sample size minus one in each subgroup; [c]comparison to a χ^2-distribution (df, which is k – 1 (where k = number of groups)); p < 0.05 is considered statistically significant; [d]pairwise comparisons using Dunn's procedure with Bonferroni correction; SE – standard error.

Atorvastatin concentrations are due to other variables, including daily dose-dependent

In addition to daily dose intake showing a statistically significant association with atorvastatin plasma concentration, women who received a daily dose of 10 mg showed a significantly higher level of atorvastatin plasma concentration than men. Several factors could contribute to this gender difference, including pharmacokinetic differences, enzyme activity, and hormone differences.

Age, BMI, smoking, coffee, and tea variables exhibited no significant association with the plasma concentration.

Among patients receiving 40 mg daily, those with the *CYP2D6-4* wild-type homozygous genotype showed significantly higher atorvastatin levels

This group exhibited significantly higher plasma levels compared to others at the same dose (Table 4). These findings suggest that the *CYP2D6-4* genotype influences atorvastatin metabolism, with wild-type homozygous individuals potentially requiring lower doses to achieve therapeutic effects. This highlights the role of pharmacogenetics in guiding individualized statin therapy to enhance efficacy and minimize adverse outcomes.

Table 4. Genotype affecting atorvastatin concentration

Allele	Genotype	Atorvastatin daily dose	Patients without genotype (prevalence of genotype/ median (range) atorvastatin concentration in plasma)	Patients with genotype (prevalence of genotype/median (range) atorvastatin concentration in plasma)	Total	Mann–Whitney U test value	p-value
SULT1A1	wild-type (homozygous)	10 mg	4 (100%)	0 (0%)	4 (100%)	N/A	N/A
			0.05 (4.9%)	–	0.05 (4.9)		
		20 mg	44 (72.1%)	17 (27.9%)	61 (100%)	421	0.25
			2.5 (33.6)	4.4 (17.7)	3.3 (33.6)		
		40 mg	16 (88.9%)	2 (11.1%)	18 (100%)	14	0.84
			2.7 (14.2)	1.8 (2.7)	2.7 (14.2)		
	mutant-type (homozygous)	10 mg	1 (9.1%)	10 (90.9%)	11 (100%)	4	0.9
			0.1 (0)	0.05 (4.9)	0.05 (4.9)		
		20 mg	28 (45.9%)	33 (54.1%)	61 (100%)	408	0.58
			4.2 (33.6)	2.7 (18.9)	3.3 (33.6)		
		40 mg	11 (61.1%)	7 (38.9%)	18 (100%)	37	0.93
			2.8 (14.2)	2.6 (6.1)	2.7 (14.2)		
	heterozygous	10 mg	11 (100%)	0 (0%)	11 (100%)	N/A	N/A
			0.05 (4.9)	–	0.05 (4.9)		
		20 mg	50 (82%)	11 (18%)	61 (100%)	238	0.53
			3.8 (18.9)	2.3 (33.6)	3.2 (33.6)		
		40 mg	9 (50%)	9 (50%)	18 (100%)	44	0.79
			2.6 (6.1)	2.6 (14.2)	2.7 (14.2)		

Table 4. Genotype affecting atorvastatin concentration– cont.

Allele	Genotype	Atorvastatin daily dose	Patients without genotype (prevalence of genotype/ median (range) atorvastatin concentration in plasma)	Patients with genotype (prevalence of genotype/median (range) atorvastatin concentration in plasma)	Total	Mann–Whitney U test value	p-value
CYP2C19-2	wild-type (homozygous)	10 mg	3 (27.3%)	8 (72.7%)	11 (100%)	11	0.9
			0.05 (1.3)	0.1 (4.9)	0.05 (4.9)		
		20 mg	14 (23%)	47 (77%)	61 (100%)	246	0.29
			3.6 (33.6)	2.9 (17.7)	3.3 (33.6)		
		40 mg	4 (22.2%)	14 (77.8%)	18 (100%)	10	0.06
			5.1 (11.1)	1.1 (7.1)	2.7 (14.2)		
	mutant-type (homozygous)	10 mg	11 (100%)	0 (0%)	11 (100%)	N/A	N/A
			0.05 (4.9)	–	0.05 (4.9)		
		20 mg	61 (100%)	0 (0%)	61 (100%)	N/A	N/A
			3.3 (33.6)	–	3.3 (33.6)		
		40 mg	18 (10%)	0 (0%)	18 (100%)	N/A	N/A
			2.7 (14.2)	–	2.7 (14.2)		
	heterozygous	10 mg	8 (72.7%)	3 (27.3%)	11 (100%)	13	1
			0.1 (4.9)	0.05 (1.3)	0.05 (4.5)		
		20 mg	47 (77%)	14 (23%)	61 (100%)	365	0.29
			2.9 (17.6)	3.6 (33.6)	3.3 (33.6)		
		40 mg	14 (77.8%)	4 (22.2%)	18 (100%)	46	0.06
			1.1 (7.1)	5.1 (11.1)	2.7 (14.2)		
CYP2D6-4	mutant-type (homozygous)	10 mg	10 (90.9%)	1 (9.1%)	11 (100%)	10	0.18
			0.05 (1.6)	4.9 (0)	0.05 (4.9)		
		20 mg	56 (91.8%)	5 (8.2%)	61 (100%)	364	0.43
			3.8 (33.6)	2.8 (3.8)	3.3 (33.6)		
		40 mg	16 (88.9%)	2 (11.1%)	18 (100%)	3	0.07
			2.9 (14.2)	0.2 (0.3)	2.7 (14.2)		
	wild-type (homozygous)	10 mg	4 (36.4%)	7 (63.6%)	11 (100%)	14.5	1
			0.09 (4.9)	0.05 (1.6)	0.05 (4.9)		
		20 mg	15 (24.6%)	46 (75.4%)	61 (100%)	107	0.65
			2.8 (10.3)	3.9 (33.6)	3.3 (33.6)		
		40 mg	5 (27.8%)	13 (72.2%)	18 (100%)	62	0.002
			0.4 (0.4)	4.2 (14.1)	2.7 (14.2)		
	heterozygous	10 mg	8 (72.7%)	3 (27.3%)	11 (100%)	6.5	0.28
			0.1 (4.9)	0.04 (0.1)	0.05 (4.9)		
		20 mg	51 (83.6%)	10 (16.4%)	61 (100%)	254	0.93
			3.3 (33.6)	3.3 (33.6)	3.3 (33.6)		
		40 mg	15 (83.3%)	3 (16.7%)	18 (100%)	6	0.06
			3.1 (14.2)	0.4 (0.4)	2.7 (14.2)		

N/A – not applicable; values in bold are statistically significant.

Highest and lowest values

Notably, the top 5 patients with the highest atorvastatin plasma concentrations – all receiving either 40 mg or 20 mg daily – shared the *CYP2D6-4* wild-type homozygous genotype. This further supports the association between this genotype and elevated atorvastatin levels.

Discussion

This study investigated the connection between atorvastatin plasma levels in hyperlipidemic patients and drug-metabolizing enzymes, particularly *SULT1A1*, *CYP2D6-4*, and *CYP2C19-2*. Our investigation showed a statistically significant correlation between the plasma

levels of atorvastatin and the homozygous individuals in the *CYP2D6-4* wild type.

According to a 2012 randomized trial, rosuvastatin raises plasma PCSK9 levels by 35% and 28% in men and women after a year of use compared to a placebo. Nonetheless, PCSK9 levels were not predictive of the LDL-C response to statin treatment, as an inverse relationship was observed – participants with lower LDL-C levels tended to have higher PCSK9 concentrations.[8]

A 2012 study examined the relationship between SNP rs1121617 and metformin glycemic response in 5 cohorts. The effectiveness of metformin and genotype were found to be related in patients with decompression sickness (DCS). According to meta-analyses of prior cohorts and studies, the metformin drug efficacy in type 2 diabetic patients in the UK and the Netherlands is strongly correlated with the rs11212617 genotype.[9]

A 2012 study discovered that the CYP2C9 genotype significantly reduces triglycerides and LDL-C in hypercholesterolemic patients taking fluvastatin. However, the rarity of certain CYP genotypes makes it challenging to demonstrate a positive genotype-fluvastatin effect correlation, which is why the study's conclusions are inconclusive.[10]

Interindividual variations in LDL-C response to statins are attributed to genetics. A 2016 study assessed 59 LDL-C SNPs, finding lead SNPs for APOE, SORT1, and NPC1L1 linked to lowered responses and a genetic predisposition for higher LDL-C levels. This suggests that genetic predisposition for elevated LDL-C levels may lower statin therapy's effectiveness.[11]

A 2020 study found that patients with CYP2D6*3 and ABCA1 mutations are less likely to meet therapeutic lipid goals. Findings also suggest that genotyping of *ABCA1*, *CYP2D6*, and *CETP*, pending further validation, could support the selection and dosing of statins in the context of personalized treatment strategies.[12]

In a 2020 study involving 269 Chinese patients with hypercholesterolemia and diabetes mellitus, the ABCG2 421C SNP was found to be the most significant SNP. The study also examined the effect of transport-related SNPs on rosuvastatin PK.[13]

A study published in 2021 investigated the impact of genetic polymorphisms on the therapeutic response to rosuvastatin, atorvastatin, and simvastatin in hyperlipidemic patients. The study enrolled 180 individuals aged 40–75 years. Over a 4-month treatment period, all 3 statins were found to effectively reduce LDL-C and total cholesterol levels. However, patients with the 51CC genotype exhibited a reduced response to statin therapy. In contrast, the MRD1 polymorphism did not show a significant effect on statin efficacy.[14]

Since 2021, Chinese researchers have investigated the relationship between statin efficacy and ApoE gene polymorphisms. In a clinical study, 220 hyperlipidemic patients receiving statin therapy were enrolled to assess how variations in the *ApoE* gene may influence treatment outcomes. Peripheral venous blood samples were obtained from all participants, and genotyping was performed to identify *ApoE* variants (*ApoE2*, *ApoE3*, and *ApoE4*) to assess their potential influence on statin treatment efficacy. The findings of the study demonstrated that *ApoE4* differs from non-*ApoE4* gene carriers. Comparing *ApoE4* to non-*ApoE4* gene carriers, *ApoE4* demonstrated lower rates of TG and LDL reduction as well as lower rates of high-density lipoprotein (HDL) rise. The results of the study indicate that the *ApoE4* polymorphism is not only linked to hyperlipidemia but also significantly influences the therapeutic response to statin treatment.[15]

A significant correlation was found between the *CYP2D6-4* polymorphism and interindividual variability in plasma atorvastatin levels among hyperlipidemic patients, suggesting a potential role in influencing drug metabolism and therapeutic response. This finding emphasizes the value of tailored medicine in treating hyperlipidemia, making it clinically substantial. Genotyping-based personalized dosing can improve patient compliance, minimize side effects, and maximize therapeutic results. Patients with the homozygous *CYP2D6-4* wild-type genotype, in particular, may benefit from therapy at lower dosages, lowering the possibility of adverse effects linked to higher atorvastatin concentrations. By incorporating genotyping into standard clinical practice, physicians can better manage lipid levels and reduce the risk of cardiovascular disease by customizing statin therapy to each patient's genetic profile.

Limitations

Although the findings of this study are significant, certain limitations should be acknowledged. Although 90 patients is a sufficient sample size for preliminary analysis, it might not be enough to extrapolate the findings to the larger Jordanian population or other ethnic groups. Furthermore, only a few genetic polymorphisms (*CYP2D6-4*, *SULT1A1*, and *CYP2C19-2*) were examined in this study; however, other genetic factors may also affect the metabolism and response to atorvastatin. Furthermore, the study's detailed investigation of lifestyle factors that may affect drug metabolism, nor its accounting for possible interactions with other medications, is beyond the scope of this study. Finally, the study's cross-sectional design makes it difficult to determine causality.

Recommendations

Expanding the sample size and incorporating diverse populations into future research is imperative to ensure cross-validation of the findings across genetic backgrounds. Plasmid plasma concentrations and genetic polymorphisms may be related in a causal manner, according to a long-term research design. Comprehensive pharmacogenomics profiling, encompassing a wider variety of genetic variants, may also offer a more comprehensive understanding of the variables influencing statin metabolism and efficacy. Further refining individualized treatment strategies would involve examining the effects of other medications, lifestyle factors, and comorbidities

on atorvastatin levels. Lastly, tests integrating genotyping into standard medical practice illustrate the usefulness and viability of tailored statin treatment, which may result in revised protocols for treating hyperlipidemia.

Conclusions

This study successfully developed a validated LC-MS/MS method for quantifying atorvastatin in plasma and demonstrated its application in therapeutic drug monitoring for hyperlipidemic patients. A key finding was the significant influence of the *CYP2D6-4* wild-type homozygous genotype on atorvastatin plasma concentrations, indicating the potential for dose adjustment based on genetic profile. These results underscore the value of integrating pharmacogenetic testing into routine clinical practice to guide individualized statin therapy, particularly in genetically diverse populations like Jordanians.

Data availability

The datasets supporting the findings of the current study are available from the corresponding author on reasonable request. The data are not publicly available due to legal/ethical reasons. The study adheres to the ethical guidelines of Jordan Ministry of Health, as well as the Helsinki Declaration and Good Clinical Practice (GCP) standards, which emphasize the protection of patient data and confidentiality. Disclosure of sensitive medical data to the public would conflict with these standards and local health regulations.

Other raw data are available here: https://doi.org/10.5281/zenodo.15111777.

Consent for publication

Not applicable.

Use of AI and AI-assisted technologies

Not applicable.

ORCID iDs

Razan Ibrahim https://orcid.org/0009-0005-6059-620X
Mohanad Odeh https://orcid.org/0000-0002-6060-8283
Eyad Mallah https://orcid.org/0000-0003-4794-954X
Luay Abu-Qatouseh https://orcid.org/0000-0003-1551-2343
Ahmad Abu Awaad https://orcid.org/0000-0002-3139-9590
Kenza Mansoor https://orcid.org/0000-0002-8171-2055
Mohammad I. A. Ahmad https://orcid.org/0000-0002-3821-7606
Amjad Shdifat https://orcid.org/0000-0001-7082-4601
Muwafaq Al Hyari https://orcid.org/0009-0004-3394-9615
Khaled W. Omari https://orcid.org/0000-0002-3089-2893
Tawfiq Arafat https://orcid.org/0000-0002-4814-4447

References

1. Shattat GF. A review article on hyperlipidemia: Types, treatments and new drug targets. *Biomed Pharmacol J*. 2014;7(2):399–409. doi:10.13005/bpj/504
2. Di Cesare M, Perel P, Taylor S, et al. The heart of the world. *Glob Heart*. 2024;19(1):11. doi:10.5334/gh.1288
3. Lu H, Rateri DL, Feldman DL, et al. Renin inhibition reduces hypercholesterolemia-induced atherosclerosis in mice. *J Clin Invest*. 2008;118(3):984–993. doi:10.1172/JCI32970
4. Karr S. Epidemiology and management of hyperlipidemia. *Am J Manag Care*. 2017;23(9 Suppl):S139–S148. PMID:28978219
5. Maningat P, Gordon BR, Breslow JL. How do we improve patient compliance and adherence to long-term statin therapy? *Curr Atheroscler Rep*. 2013;15(1):291. doi:10.1007/s11883-012-0291-7
6. Karvaly GB, Karádi I, Vincze I, et al. A pharmacokinetics-based approach to the monitoring of patient adherence to atorvastatin therapy. *Pharmacol Res Perspect*. 2021;9(5):e00856. doi:10.1002/prp2.856
7. European Medicines Agency (EMA). EMA Guideline on bioanalytical method validation. Amsterdam, the Netherlands: European Medicines Agency (EMA); 2011. https://www.ema.europa.eu/en/documents/scientific-guideline/guideline-bioanalytical-method-validation_en.pdf. Accessed November 18, 2024
8. Awan Z, Seidah NG, MacFadyen JG, et al. Rosuvastatin, proprotein convertase subtilisin/kexin type 9 concentrations, and LDL cholesterol response: the JUPITER trial. *Clin Chem*. 2012;58(1):183–189. doi:10.1373/clinchem.2011.172932
9. Van Leeuwen N, Nijpels G, Becker ML, et al. A gene variant near ATM is significantly associated with metformin treatment response in type 2 diabetes: A replication and meta-analysis of five cohorts. *Diabetologia*. 2012;55(7):1971–1977. doi:10.1007/s00125-012-2537-x
10. Buzková H, Pechandová K, Danzig V, et al. Lipid-lowering effect of fluvastatin in relation to cytochrome P450 2C9 variant alleles frequently distributed in the Czech population. *Med Sci Monit*. 2012;18(8):CR512–517. doi:10.12659/msm.883272
11. Smit RA, Postmus I, Trompet S, et al. Rooted in risk: Genetic predisposition for low-density lipoprotein cholesterol level associates with diminished low-density lipoprotein cholesterol response to statin treatment. *Pharmacogenomics*. 2016;17(15):1621–1628. doi:10.2217/pgs-2016-0091
12. Ruiz-Iruela C, Candás-Estébanez B, Pintó-Sala X, et al. Genetic contribution to lipid target achievement with statin therapy: A prospective study. *Pharmacogenomics J*. 2020;20(3):494–504. doi:10.1038/s41397-019-0136-7
13. Zhang D, Ding Y, Wang X, et al. Effects of *ABCG2* and *SLCO1B1* gene variants on inflammation markers in patients with hypercholesterolemia and diabetes mellitus treated with rosuvastatin. *Eur J Clin Pharmacol*. 2020;76(7):939–946. doi:10.1007/s00228-020-02882-4
14. Sivkov A, Chernus N, Gorenkov R, Sivkov S, Sivkova S, Savina T. Relationship between genetic polymorphism of drug transporters and the efficacy of rosuvastatin, atorvastatin and simvastatin in patients with hyperlipidemia. *Lipids Health Dis*. 2021;20(1):157. doi:10.1186/s12944-021-01586-7
15. Cai C, Wen Z, Li L. The relationship between ApoE gene polymorphism and the efficacy of statins controlling hyperlipidemia. *Am J Transl Res*. 2021;13(6):6772–6777. PMID:34306425. PMCID:PMC8290710

The efficacy of carfilzomib and dexamethason (Kd-70) as once-weekly two-drug regimen: The analysis of real-world data from Poland

Magdalena Olszewska-Szopa[1,A–E], Anna Czyż[1,B–F], Maria Węgrzyn[2,B], Tomasz Wróbel[1,A,B,E,F]

[1] Department and Clinic of Hematology, Cellular Therapies and Internal Medicine, University Hospital in Wrocław, Wroclaw Medical University, Poland
[2] Department of Finance, Wroclaw University of Economics and Business, Poland

A – research concept and design; B – collection and/or assembly of data; C – data analysis and interpretation;
D – writing the article; E – critical revision of the article; F – final approval of the article

Advances in Clinical and Experimental Medicine, ISSN 1899–5276 (print), ISSN 2451–2680 (online) *Adv Clin Exp Med*. 2026;35(1):131–136

Address for correspondence
Magdalena Olszewska-Szopa
E-mail: molszopa@gmail.com

Funding sources
None declared

Conflict of interest
None declared

Received on August 8, 2024
Reviewed on December 30, 2024
Accepted on May 15, 2025

Published online on October 29, 2025

Abstract

Background. The two-drug regimen Kd-70 (carfilzomib at a dose of 70 mg/m^2 with dexamethasone) is a recommended treatment option for patients with relapsed or refractory multiple myeloma, according to both American and European guidelines. However, aside from the A.R.R.O.W. trial, real-world data on its effectiveness remain limited.

Objectives. We aimed to assess the effectiveness of the two-drug regimen Kd-70 in real-world practice.

Materials and methods. We analyzed data from the Polish Ministry of Health registry, which included 412 patients treated with the Kd-70 regimen in Poland.

Results. The overall response rate (ORR) was 67.15%, comparable to the A.R.R.O.W. trial. However, the complete response (CR) rate (5.3%) and very good partial response (VGPR) rate (9.59%) were lower than those reported in the A.R.R.O.W. study. Notably, Kd-70 showed significantly lower efficacy in patients who required treatment for primary resistance or disease progression within the 1st year after diagnosis. In contrast, the number of prior treatment lines did not impact the regimen's effectiveness.

Conclusions. In real-world clinical practice, the Kd-70 regimen demonstrated an ORR comparable to that observed in the A.R.R.O.W. trial. However, the CR and VGPR rates were lower. These findings underscore the need for further investigation into factors influencing treatment outcomes in this patient population.

Key words: myeloma, carfilzomib, Kd-70, real-word therapy data, relapsed/refractory myeloma

Cite as
Olszewska-Szopa M, Czyż A, Węgrzyn M, Wróbel T. The efficacy of carfilzomib and dexamethason (Kd-70) as once-weekly two-drug regimen: The analysis of real-world data from Poland. *Adv Clin Exp Med*. 2026;35(1):131–136. doi:10.17219/acem/205167

DOI
10.17219/acem/205167

Highlights

- Real-world Kd-70 regimen matches A.R.R.O.W. trial overall response rate (ORR): Achieved a 67.2% ORR, mirroring pivotal clinical data.
- Lower deep-response rates vs A.R.R.O.W Complete responses (CR; 5.3%) and very good partial responses (VGPR; 9.6%) fell below trial benchmarks.
- Primary resistance limits early efficacy: Patients progressing within 12 months of diagnosis showed significantly reduced Kd-70 effectiveness.
- Prior therapy lines don't impact Kd-70 success: Efficacy remained consistent regardless of the number of previous treatment regimens.

Background

The A.R.R.O.W. trial demonstrated that once-weekly dosing of carfilzomib (70 mg/m^2) in combination with dexamethasone (Kd-70) is more effective than the traditional twice-weekly dosing of carfilzomib (27 mg/m^2) in patients with relapsed and refractory plasma cell myeloma (RRMM).[1] Specifically, progression-free survival (PFS) was significantly improved with the Kd-70 regimen (11.2 months vs 7.6 months, p = 0.003), while maintaining a similar safety profile. This registration study provides the evidence supporting the implementation of the Kd-70 regimen into clinical practice. According to the National Comprehensive Cancer Network (NCCN) guidelines, as well as the European Hematology Association – European Society for Medical Oncology (EHA–ESMO) recommendations, the Kd-70 schedule is a treatment option for selected previously treated myeloma patients.[2,3] Although 6 years have passed since the publication of the A.R.R.O.W. study results, to the best of our knowledge, only 1 publication has been released to date regarding the effectiveness of this two-drug regimen with carfilzomib at a 70 mg/m^2 dosage in clinical practice.

Objectives

We aimed to assess the effectiveness of the two-drug regimen Kd-70 in real-world clinical practice, focusing on its performance in everyday clinical settings. We evaluated the response to Kd-70 and PDS in patients with RRMM, considering factors such as monoclonal protein type, age, the number of prior treatment lines, and the time since diagnosis.

Materials and methods

According to the Polish guidelines published between 2018 and 2023, the standard first-line therapy in Poland for transplant-eligible patients included bortezomib, thalidomide and dexamethasone (VTD). For patients ineligible for transplantation, the recommended regimen was melphalan, prednisone, and thalidomide (MPT).

Kd-70 was available during that period of time for 2nd-, 3rd- and 4th-line treatment under a ministry-regulated drug – access program. Lenalidomide with dexamethasone (LD) and daratumumab with bortezomib and dexamethasone (DVD) were also available through the same program.[4,5] In accordance with the guidelines of the Polish Ministry of Health, baseline patient demographics, clinical data and treatment outcomes for all patients treated within the drug programs had to be reported to the Ministry's registers. We assumed that all patients met the eligibility criteria for the drug program that were in effect during the study period. These criteria included 1–3 prior therapy lines, no heart failure of New York Heart Association (NYHA) class III or IV, and no other cardiac contraindications to the use of carfilzomib, as well as sufficient bone marrow function, indicated by appropriate hematological parameters. We conducted an analysis of data from 412 consecutive patients reported in the Ministry of Health's electronic records in Poland, covering the period from May 1, 2021, to April 5, 2023. The treatment protocol involved administering intravenous carfilzomib at 20 mg/m^2 for the 1st dose in the first cycle, followed by 70 mg/m^2 in subsequent weeks (on days 1, 8 and 15), in combination with oral dexamethasone (40 mg) once weekly, in 28-day cycles. Treatment was to be continued until evidence of disease progression. The primary endpoint of our study was the overall response rate (ORR). We analyzed various clinical data available in the Ministry's records, including monoclonal protein type, age, gender, therapy line, and time since diagnosis, to identify response predictors. The current International Myeloma Working Group (IMWG) criteria were used to assess responses.

Statistical analyses

Data from all eligible patients were collected using a standardized, anonymized case report form. The collected variables included patient age, gender, M protein type, number of previous treatment lines, time from diagnosis to Kd-70 treatment, response to Kd-70 treatment, time to disease progression, and time to death. The distribution of continuous variables was assessed. Since age did not follow

a normal distribution, as confirmed with the Shapiro–Wilk test ($W = 0.9765$, $p < 0.001$), it was reported as the median and interquartile range (IQR). Categorical variables were summarized as frequencies and percentages based on available data. Comparisons between groups based on response to Kd-70 treatment were performed using the χ^2 test for categorical variables. Progression-free survival was defined as the time from the initiation of Kd-70 treatment to disease progression, death from any cause or the end of the observation period. Overall survival (OS) was defined as the time from the initiation of Kd-70 treatment to death from any cause or the end of the observation period. The probabilities of PFS and OS were estimated using the Kaplan–Meier method. All statistical analyses were performed using Statistica v. 13.3 (TIBCO Software Inc., Palo Alto, USA).

This study was conducted in accordance with the principles outlined in the Declaration of Helsinki. The study was approved by the Bioethics Committee of Wroclaw Medical University, Poland (approval No. KB 208/2023).

Results

Patients' characteristics

The median age of the patients was 67 years (IQR: 61–72). There were 190 women (46.1%) and 222 men (53.9%). The majority of patients (74.8%) had an Eastern Cooperative Oncology Group (ECOG) performance status of 1. Monoclonal protein characteristics were typical, with dominance of immunoglobulin G (IgG) (57.6%) in the heavy chain and kappa (67.5%) in the light chain. Selected laboratory and demographic characteristics are provided in Table 1. All patients were required to have adequate heart function, with an ejection fraction ≥40%, as patients with an ejection fraction <40% were excluded. Fifty-one percent of patients had received 1 prior line of treatment.

Table 1. Selected demographic and laboratory characteristics of patients treated with the Kd-70 regimen in Poland

Feature		n (%) or median (Q1–Q3)
Age [years]		67 (61–72)
Sex	female	190 (46.1)
	male	222 (53.9)
ECOG scale	ECOG1	308 (74.8)
	ECOG2	104 (25.3)
M protein type	IgG	237 (57.6)
	IgA	86 (20.9)
	IgM	1 (0.2)
	light chain disease	118 (28.6)
	non-secretory	16 (3.9)
Number of previous therapy lines	1	210 (51.0)
	2	123 (29.8)
	3	79 (19.2)

Q1 – lower quartile; Q3 – upper quartile; ECOG – Eastern Cooperative Oncology Group; M protein – monoclonal protein.

Response rate

Response to treatment was assessed in 344 patients, with 34 early deaths (ED) observed. Early deaths had occurred before assessment was conducted and were considered treatment failure, i.e., lack of response. In an additional 68 patients, the effectiveness of therapy was not assessed at the time of data collection. The ORR was 67.15%. Just under 15% of patients achieved a complete response (CR) or very good partial response (VGPR), approx. 52% met the criteria for a partial response (PR), and nearly 33% did not achieve a sufficient treatment effect (stable disease (SD), progressive disease (PD) or ED). Nearly 10% (34/344) of patients died before response assessment could be conducted. The best response achieved after a median of 2 cycles (range: 1–4) is shown in Fig. 1. There was no difference in response rate based on patients' age or the number of prior therapy lines (Table 2). The stratification into age groups, including the 40–49 age range, also did not reveal statistically significant differences in response to the Kd-70 regimen. However, our observations revealed a significant difference in ORR between patients who received Kd-70 within 1 year of diagnosis and those who received treatment later. Specifically, the ORR was 50% in the former group, compared to 72.7% in the latter group ($p = 0.00003$) (Table 3). Therapy was discontinued in 197 patients (47.8%) after a median of 4 cycles (range: 1–19 cycles) of Kd-70 due to various reasons (n = number of patients): no response (n = 120), death (n = 45) and toxicities (n = 22). In 6 patients, Kd-70 was not continued after autologous stem cell transplantation. In 4 patients, the reason for therapy termination was not provided. Among the 87 patients diagnosed ≤1 year before the introduction of Kd-70, therapy was discontinued in 58 (66.6%) cases, while in those diagnosed >1 year prior, therapy was discontinued in 42.7% (139/325) of cases.

Survival

The median follow-up time was 8 months (range: 1–23 months). The median progression-free survival (PFS) was 7.2 months (95% confidence interval (95% CI): 6.1–8.4), with a 1-year PFS rate of 35.1% (95% CI: 31.1–39.3) and a 1-year OS rate of 85.6% (95% CI: 62.0–95.6). A total of 45 deaths (10.9%) were reported during the follow-up period. The majority of these deaths, 34 in total, occurred before response assessment was conducted (ED). In most cases, no cause of death was reported, except for 5 patients in whom disease progression was noted. The death rate in patients treated with Kd-70 within 1 year of diagnosis was 20.7% (18/87), compared to 8.3% (27/325) in those diagnosed more than 1 year before Kd-70 implementation.

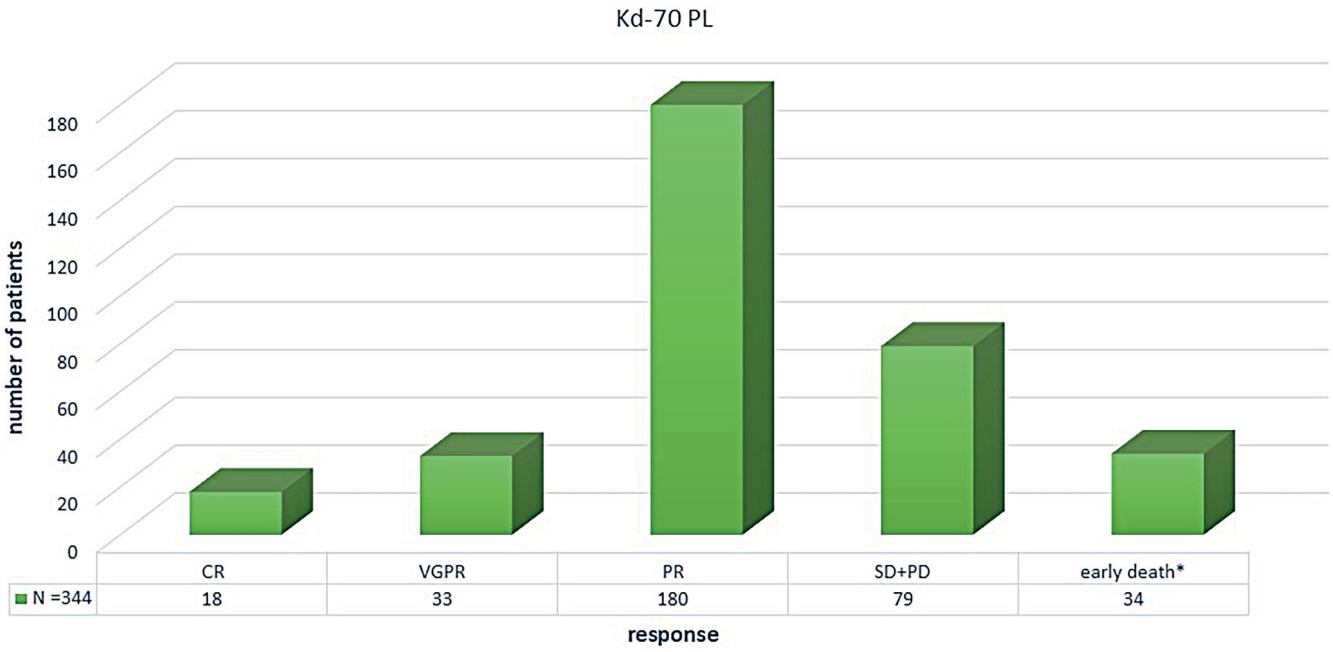

Fig. 1. Best response achieved during Kd-70 therapy

CR – complete response; VGPR – very good partial response; PR – partial response; SD + PD – stable disease and progressive disease.

Table 2. Relationships between response to treatment and patients' age and previous therapy lines in the χ^2 independence test

Parameter	n	CR n (%)	VGPR n (%)	PR n (%)	SD + PD n (%)	ED* n (%)	χ^2	p-value	ORR n (%)	χ^2	p-value
Age											
Age: <60 years	74	5 (6.8)	5 (6.8)	35 (47.3)	22 (29.7)	7 (9.5)	10.89	0.21	45 (60.8)	2.07	0.36
Age: 60–69 years	147	7 (4.8)	15 (10.2)	77 (52.4)	31 (21.1)	17 (11.6)			99 (67.4)		
Age: >69 years	123	6 (4.9)	13 (10.6)	68 (55.3)	26 (21.1)	10 (8.1)			87 (70.7)		
Number of prior therapy lines											
Kd-70 as 2nd line	180	7 (3.9)	21 (11.7)	97 (53.9)	39 (21.7)	16 (8.9)	7.62	0.47	125 (69.4)	0.18	0.91
Kd-70 as 3rd line	97	9 (9.3)	8 (8.3)	46 (47.4)	24 (24.7)	10 (10.3)			63 (64.9)		
Kd-70 as 4th line	67	2 (3)	4 (6)	37 (55.2)	16 (23.9)	8 (11.9)			43 (64.2)		

CR – complete response; VGPR – very good partial response; PR – partial response; ORR – overall response rate (CR + VGPR + PR); SD – stable disease; PD – progressive disease; *in early deaths (ED) response was not assessed; n – number of patients.

Table 3. Relationships between Kd-70 timeline and its effectiveness in the χ^2 independence test

The best response	Kd-70 ≤1 year from diagnosis (n, %) total n = 76	Kd-70 >1 year from diagnosis (n, %) total n = 268	χ^2	p-value
CR	0	18 (6.7)	21.42	0.0003
VGPR	7 (9.2)	26 (9.7)		
PR	29 (38.2)	151 (45.3)		
SD + PD	26 (34.2)	53 (19.8)		
ED before response assessment	14 (18.4)	20 (7.5)		
ORR (CR + VGPR + PR)	38 (50)	195 (72.7)	14.03	0.0002

CR – complete response; VGPR – very good partial response; PR – partial response; ORR – overall response rate (CR + VGPR + PR); SD – stable disease; PD – progressive disease; *in early deaths (ED) response was not assessed.

Discussion

The two-drug Kd-70 regimen (carfilzomib 70 mg/m^2 and dexamethasone) was approved for use in Poland in May 2021 under the ministry-regulated access to the drug program. We analyzed the information available in the ministry's records for all patients treated in the country (n = 412) from May 1, 2021, to April 5, 2023. Upon reviewing

the collected data, we compared the obtained results with the findings of the registry study. Noteworthy distinctions emerged between the Polish Kd-70 population and the A.R.R.O.W. study. Our study group comprised patients treated with Kd-70 after 1–3 prior lines of therapy, whereas in the A.R.R.O.W. study, patients had received 2 or 3 prior lines of treatment, according to the inclusion criteria. Additionally, in our dataset, patients' ECOG scores ranged from 0 to 2, while in the A.R.R.O.W. study, the inclusion criterion was ECOG scores of 0–1.[6]

Recently, an analysis of 114 cases of RRMM treated with Kd-70 in Japan, the "Weekly-CAR" study, was published. However, comparing our observations with the cohort described in this analysis is challenging due to differences in patient characteristics. In the mentioned study, more than 48% of the patients had previously received at least 4 lines of treatment.[7]

The ORR reported in our study, 67.15%, closely mirrored the outcomes documented in the A.R.R.O.W. study, where the ORR ranged between 61% and 65%, and in the Japanese publication, which reported an ORR of 66.3%. However, our Kd-70 population exhibited a lower percentage of CR and VGPR compared to the A.R.R.O.W. and "Weekly-CAR" studies. The therapeutic benefits of Kd-70 were evident regardless of age and the number of prior therapy lines, consistent with observations from the A.R.R.O.W. study.[6]

We were unable to find any publications on the clinical use of Kd-70 beyond the "Weekly-CAR" project. Therefore, we briefly compare our results with studies that exclusively or primarily involve earlier versions of the Kd regimen, including the twice-weekly administration of carfilzomib.

In a prospective observational study (n = 273; carfilzomib at a dose of 20/56 mg/m^2 weekly), the ORR was 63% in patients who had previously received an average of 2 or 3 lines of treatment. The mortality rate ranged from 7% in groups without lenalidomide resistance to 9% in those with lenalidomide resistance.[8]

Comparable ORR values were reported in a study by Terpos et al.,[9] with an ORR of 62.1% (n = 93; carfilzomib at a dose of 20/56 mg/m^2 weekly), and by Onda et al., with an ORR of 62% (n = 41 for Kd-56 and n = 9 for Kd-70).[10]

In another observational study (n = 103; carfilzomib at a dose of 20/56 mg/m^2 weekly), the ORR was 54.7%. Notably, nearly 36% of patients in this cohort were treated with this regimen as the 5th or later line of therapy.[11]

An assessment of the safety profile based on the available data was not possible. We found that Kd-70 therapy was discontinued after an average of 4 cycles in the Polish patient population. The primary reason for discontinuation was lack of efficacy, followed by the occurrence of adverse effects. This is consistent with observations from the "Weekly-CAR" project.[7]

Our analysis revealed a significant distinction among patients treated with Kd-70 within the 1st year of diagnosis. This subgroup demonstrated significantly poorer outcomes compared to those who received Kd-70 at a later stage. These outcomes included a lower response rate, higher mortality and more frequent discontinuation of Kd-70 therapy. This disparity suggests a potential association between treatment refractoriness to Kd-70 in patients treated within 1 year of diagnosis and the presence of primary resistance, characterized by a more aggressive clinical course.

Limitations

This study has several limitations, primarily stemming from its retrospective design and the limited clinical data available in the ministry's drug program registries. Notably, the absence of information on patients' genetic profiles and the specific types of adverse events limits the ability to conduct a more comprehensive and detailed analysis. Nevertheless, it is important to note that these data provide valuable insights derived from real-world practice involving the two-drug Kd-70 regimen in a substantial population of patients with relapsed and refractory multiple myeloma.

Conclusions

In real-world practice, the Kd-70 regimen yielded a comparable ORR to the results observed in the A.R.R.O.W. trial, but with a lower rate of CR and VGPR. Notably, treatment outcomes with the Kd-70 regimen during the 1st year following diagnosis were markedly inferior compared to those in patients with a more extended treatment history. This discrepancy may be attributed to primary resistance and a more aggressive disease profile within this particular subgroup.

Data availability

The datasets generated and/or analyzed during the current study are available from the corresponding author on reasonable request.

Consent for publication

Not applicable.

Use of AI and AI-assisted technologies

Not applicable.

ORCID iDs

Magdalena Olszewska-Szopa https://orcid.org/0000-0002-5828-0872
Anna Czyż https://orcid.org/0000-0001-6641-0182
Maria Węgrzyn https://orcid.org/0000-0002-5063-9238
Tomasz Wróbel https://orcid.org/0000-0002-6612-3535

References

1. Moreau P, Mateos MV, Berenson JR, et al. Once weekly versus twice weekly carfilzomib dosing in patients with relapsed and refractory multiple myeloma (A.R.R.O.W.): Interim analysis results of a randomised, phase 3 study. *Lancet Oncol*. 2018;19(7):953–964. doi:10.1016/S1470-2045(18)30354-1

2. National Comprehensive Cancer Network (NCCN). Multiple myeloma. Version 4. Plymouth Meeting, USA: National Comprehensive Cancer Network (NCCN); 2023. https://www.nccn.org/professionals/physician_gls/pdf/myeloma.pdf. Accessed August 1, 2024.
3. Dimopoulos MA, Moreau P, Terpos E, et al. Multiple myeloma: EHA-ESMO Clinical Practice Guidelines for diagnosis, treatment and follow-up. *Ann Oncol*. 2021;32(3):309–322. doi:10.1016/j.annonc.2020.11.014
4. Giannopoulos K, Jamroziak K, Usnarska-Zubkiewicz L, et al. Zalecenia Polskiej Grupy Szpiczakowej dotyczące rozpoznawania i leczenia szpiczaka plazmocytowego oraz innych dyskrazji plazmocytowych na rok 2018/2019. *Acta Haematol Pol*. 2018;49(4):157–206. doi:10.2478/ahp-2018-0024
5. Giannopoulos K, Jamroziak K, Usnarska-Zubkiewicz L. Zalecenia Polskiej Grupy Szpiczakowej dotyczące rozpoznawania i leczenia szpiczaka plazmocytowego oraz innych dyskrazji plazmocytowych na rok 2022/2023. Warsaw, Poland: Polska Grupa Szpiczakowa; 2022. https://szpiczak.org/wp-content/uploads/aktualnosci/2022/Zalecenia-Polskiej-Grupy-Szpiczakowej-2022_2023.pdf. Accessed August 1, 2024.
6. Dimopoulos MA, Niesvizky R, Weisel K, et al. Once- versus twice-weekly carfilzomib in relapsed and refractory multiple myeloma by select patient characteristics: Phase 3 A.R.R.O.W. study subgroup analysis. *Blood Cancer J*. 2020;10(3):35. doi:10.1038/s41408-020-0300-y
7. Abe Y, Kubonishi S, Ri M, et al. An observational study of once-weekly carfilzomib in patients with multiple myeloma in Japan (Weekly-CAR study). *Future Oncol*. 2024;20(17):1191–1205. doi:10.2217/fon-2023-0834
8. Leleu X, Beksac M, Chou T, et al. Efficacy and safety of weekly carfilzomib (70 mg/m^2), dexamethasone, and daratumumab (KdD70) is comparable to twice-weekly KdD56 while being a more convenient dosing option: A cross-study comparison of the CANDOR and EQUULEUS studies. *Leuk Lymphoma*. 2021;62(2):358–367. doi:10.1080/10428194.2020.1832672
9. Terpos E, Gamberi B, Caers J, et al. Real-world use of carfilzomib among multiple myeloma patients with at least one prior therapy. *J Clin Oncol*. 2019;37(15 Suppl):e19515. doi:10.1200/JCO.2019.37.15_suppl.e19515
10. Onda Y, Kanda J, Kaneko H, et al. Real-world effectiveness and safety analysis of carfilzomib-lenalidomide-dexamethasone and carfilzomib-dexamethasone in relapsed/refractory multiple myeloma: A multicenter retrospective analysis. *Ther Adv Hematol*. 2022;13:20406207221104584. doi:10.1177/20406207221104584
11. Quach H, Yoon SS, Kim K, et al. Carfilzomib use among patients with relapsed/refractory multiple myeloma in the Asia Pacific region: Characteristics and outcomes by regimen from a prospective, real-world study. *Blood*. 2022;140(Suppl 1):4264–4266. doi:10.1182/blood-2022-159324

The correlation between nailfold capillaroscopic findings and adaptive optics imaging of retinal microvasculature in patients with systemic sclerosis

Katarzyna Paczwa[1,A–D], Magdalena Szeretucha[1,B–D], Katarzyna Romanowska-Próchnicka[2,B,C], Sylwia Ornowska[3,B], Marzena Olesińska[3,E], Radosław Różycki[1,E], Joanna Gołębiewska[1,E,F]

[1] Department of Ophthalmology, Military Institute of Aviation Medicine, Warsaw, Poland
[2] Department of Biopysics, Physiology and Pathophysiology, Medical University of Warsaw, Poland
[3] Department and Polyclinic of Systemic Connective Tissue Diseases, National Institute of Geriatrics, Rheumatology and Rehabilitation, Warsaw, Poland

A – research concept and design; B – collection and/or assembly of data; C – data analysis and interpretation; D – writing the article; E – critical revision of the article; F – final approval of the article

Advances in Clinical and Experimental Medicine, ISSN 1899–5276 (print), ISSN 2451–2680 (online) *Adv Clin Exp Med*. 2026;35(1):137–149

Address for correspondence
Katarzyna Paczwa
E-mail: kpaczwa@wiml.waw.pl

Funding sources
None declared

Conflict of interest
None declared

Received on November 11, 2024
Reviewed on January 17, 2025
Accepted on April 15, 2025

Published online on September 17, 2025

Abstract

Background. Vascular injury is a central and early feature of systemic sclerosis (SSc) pathogenesis. Although nailfold capillaroscopy (NC) effectively visualizes characteristic peripheral arteriolar and capillary changes, the retinal microcirculation provides a noninvasive, high-resolution view into subtler vascular dysfunction. Consequently, retinal vascular imaging may offer an ideal modality for monitoring microvascular injury and detecting early manifestations of SSc.

Objectives. To compare retinal microvascular parameters between SSc patients and healthy controls using adaptive optics (AO) imaging, and to evaluate the correlation between adaptive optics-derived retinal measurements and NC findings in SSc.

Materials and methods. The study included 31 patients with SSc and 41 healthy controls. The AO images of the retinal arteries were obtained in both groups and the measurements were compared. Nailfold capillaroscopy was also performed in the SSc cohort, and its findings were directly compared with the AO imaging results.

Results. Retinal arterial wall thickness was significantly lower in SSc patients than in healthy controls ($p = 0.016$), and the wall-to-lumen ratio was similarly reduced in the SSc group ($p = 0.048$). Within the SSc cohort, hypertensive patients exhibited a significantly greater wall cross-sectional area compared to those without hypertension ($p = 0.026$).

Conclusions. Adaptive optics retinal imaging demonstrated a significant reduction in mean arterial wall thickness in SSc patients compared with healthy controls. However, no correlation was identified between the AO findings and the NC parameters or the disease stage. Our analysis revealed that alterations in retinal vascular parameters were confined to SSc patients with comorbid hypertension or those receiving sildenafil therapy. To fully establish the clinical utility of adaptive optics imaging in SSc, and to elucidate its relationship with NC findings, larger, multicenter studies with more diverse patient cohorts are warranted.

Key words: systemic sclerosis, scleroderma, adaptive optics, nailfold capillaroscopy, retinal microvasculature

Cite as
Paczwa K, Szeretucha M, Romanowska-Próchnicka K, et al. The correlation between nailfold capillaroscopic findings and adaptive optics imaging of retinal microvasculature in patients with systemic sclerosis. *Adv Clin Exp Med*. 2026;35(1):137–149. doi:10.17219/acem/204078

DOI
10.17219/acem/204078

Highlights

- Adaptive optics unveils retinal microvascular changes in systemic sclerosis (SSc): First study to apply high-resolution AO imaging in scleroderma patients.
- Concordance between nailfold capillaroscopy and adaptive optics metrics: Combined modalities enhance accuracy in detecting SSc microangiopathy.
- Thinner retinal vessel walls in SSc vs controls: Quantitative AO analysis shows significant retinal wall thinning.
- Adaptive optics as a novel diagnostic tool for SSc microvascular injury: Promises noninvasive, early detection and monitoring of microvascular changes in scleroderma.

Background

Systemic sclerosis (SSc) is a connective tissue disorder caused by autoimmunity. It is characterized by obliterative vasculopathy, widespread fibrosis and a dysregulated immune response.[1,2] Vascular involvement represents an initial and pivotal factor in the pathogenesis of the disease, as well as in the development of multiple organ dysfunction. The vasculopathy in SSc includes thrombosis, vasospasm and vessel lumen obliteration leading to microangiopathy.[2] Microcirculatory changes observed in the capillaries are the hallmark of the disease.

Nailfold capillaroscopy (NC), as a noninvasive imaging technique, is routinely used to assess peripheral capillary abnormalities in scleroderma patients and is included in the diagnostic criteria for SSc.[3,4] Therefore, this tool plays a pivotal role in both diagnosing and monitoring the progression of the disease.

A range of ocular manifestations have been observed in patients with scleroderma, including those affecting the posterior segment of the eye.[5–10] Recent research has concentrated on retinal and choroidal alterations observed in these individuals. Advanced imaging methods, such as optical coherence tomography angiography (OCTA), have facilitated the detection of structural changes in the retinal microvasculature linked to systemic diseases.

Adaptive optics (AO) imaging represents a noninvasive tool for the visualization of retinal structures, including photoreceptors, blood vessels and nerve fibers, in vivo at the microscopic level. The camera employs infrared illumination with a wavelength of 850 nm.[11] The AO technology is employed for the evaluation of retinal vessels in healthy eyes and arterial hypertension, as well as in ocular pathologies such as diabetic retinopathy, glaucoma, retinal vessel occlusion and retinal vasculitis.[12–22]

Objectives

The study aimed to assess and compare the retinal microvasculature parameters in scleroderma patients and healthy controls using AO imaging. Furthermore, we aimed to evaluate the relationship between NC findings, disease characteristics and AO results within the SSc group.

Materials and methods

The study was conducted at the Military Institute of Aviation Medicine (Warsaw, Poland) between March 2022 and May 2023. The study received approval from the Ethics Committee Reviewing Biometric Research at the Military Institute of Aviation Medicine (approval No. 1/2022) and followed the tenets of the Declaration of Helsinki.

The purpose and procedures of the study were thoroughly explained to the participants, and written consent was subsequently obtained from individuals. The study sample comprised patients with SSc from the Department and Polyclinic of Systemic Connective Tissue Diseases at the National Institute of Geriatrics, Rheumatology and Rehabilitation in Warsaw. Healthy participants were enrolled during routine appointments at the Department of Ophthalmology in the Military Institute of Aviation Medicine.

Participants

A total of 31 patients (61 eyes) diagnosed with SSc and 41 healthy controls (81 eyes) were included in this and our previous study.[23] No significant differences were observed between the scleroderma patients and the control group regarding age, gender distribution or axial length (Table 1,2). Within the study cohort, 71.4% of patients were diagnosed with diffuse cutaneous SSc, while 28.6% were diagnosed with limited cutaneous SSc. Nailfold capillaroscopy revealed an early scleroderma pattern in 5 patients, an active pattern in 12 and a late pattern in 9. Within the SSc cohort, 2 patients had pulmonary arterial hypertension (PAH), 8 developed digital ulcers and 8 were hypertensive. A total of 13 participants were treated with sildenafil, while 12 were treated with amlodipine. Interstitial lung disease was identified in 11 patients, of whom 64% were classified as having nonspecific interstitial pneumonia (NSIP) and 36% as having usual interstitial pneumonia (UIP). Elevated pro-B-type natriuretic peptide (proBNP) levels were observed in 16.1% of the studied cases (Table 3).

Table 1. Baseline characteristics of the study cohort

Analyzed trait*		Statistic
Number of participants, n (%)		72 (100.00)
Number of eyes, n (%)		142 (100.00)
Gender	female	49 (60.06)
	male	23 (31.94)
Age [years], Me (Q_1–Q_3)		46 (36–55)
Shapiro–Wilk W test for normality		W = 0.933 p < 0.001

*Statistic parameters used: n – absolute number; % – percentage; Me – median; Q – quartiles.

Table 2. Baseline characteristics of the study cohort by occurrence of scleroderma

Analyzed trait		Scleroderma		p-value
		present	absent	
Number of participants, n (%)		31 (43.06)	41 (56.94)	–
Number of eyes, n (%)		61 (42.96)	81 (57.04)	–
Gender, n (%)	female	22 (70.97)	27 (65.85)	χ^2 = 0.209 df = 1 p = 0.647
	male	9 (29.03)	14 (34.15)	
Age [years], Me (Q_1–Q_3) Shapiro–Wilk test		48 (40–54) W = 0.935 p = 0.003	41 (35–55) W = 0.0867 p < 0.001	Levene's test F (1, 140) = 1.137 p = 0.288 Mann–Whitney test U = 2070.000 $Z_{corr.}$ = 1.651 p = 0.099
AL [mm], Me (Q_1–Q_3) Shapiro–Wilk test		23.53 (22.88–24.20) W = 0.968 p = 0.114	23.78 (23.13–24.35) W = 0.970 p = 0.129	Levene's test F (1, 121) = 0.475 p = 0.492 ANOVA F (1, 121) = 0.138 p = 0.711

*Statistic parameters used: n – absolute number; % – percentage; Me – median; Q – quartiles; ANOVA – analysis of variance; df – degrees of freedom; AL – axial length.

Methods

A comprehensive ophthalmic examination was performed on all participants. This included assessments of best-corrected visual acuity (BCVA), intraocular pressure, refraction, anterior segment examination, fundoscopy with pupillary dilatation, and axial length (AL) measurement. Exclusion criteria were refractive errors beyond –3.0 or +3.0 diopters and any pathological ocular condition, including glaucoma or retinal and choroidal diseases. Moreover, eyes with low-quality AO images were also excluded. The BCVA was measured monocularly using LogMAR charts (Lighthouse International, New York, USA) at 5 m, while AL was assessed using the IOL Master 500 (Carl Zeiss Meditec AG, Jena, Germany).

All participants with scleroderma underwent a clinical evaluation and NC. The clinical data collected from each SSc patient comprised the following: The type of SSc (either limited or diffuse cutaneous scleroderma), the presence of interstitial lung disease (classified as either NSIP or UIP), hypertension, elevated proBNP, and the treatment method (administrations of sildenafil or amlodipine). The NC was conducted using the CapillaryScope 200 Pro (Dino-Lite, Taipei, Taiwan),

Table 3. Baseline characteristics of the scleroderma group (n = 31)

Trait		n M (SD)	% Me (Q_1–Q_3)
Gender	female	22	71.0
	male	9	29.0
Scleroderma	localized	8	28.6
	systemic	20	71.4
	capillaroscopy	27	96.4
Scleroderma pattern	none	2	7.1
	early	5	17.9
	active	12	42.9
	late	9	32.1
anti-PM/SCL		1	3.6
PC TH fibrillarin		3	10.7
anti-Scl-70-antibodies		17	54.8
Centromere		8	25.8
Number of vessels	normal	2	7.1
	reduced	20	71.5
	very reduced	6	21.4
Avascular are		16	57.1
Giant capillaries		14	50.0
Hemorrhages		11	39.3
Branched vessels		10	35.7
MES Shapiro–Wilk test		2.2 (1.1) W = 0.848	2.5 (1.1–3.1) p < 0.001
Interstitial lung disease		12	42.9
PAH		2	7.1
NSIP		7	22.6
UIP		4	14.3
MMF		13	41.9
MTX		7	25.0
mRSS Shapiro–Wilk test		8.1 (7.9) W = 0.771	2.0 (2.0–12.0) p < 0.001
Finger ulcers		8	28.6
RVSP > 35 mm Hg		3	1.1
Elevated proBNP		5	18.5
Arterial hypertension		8	25.8
Administration of sildenafil		13	41.9
Administration of amlodipine		12	38.7

Missing data were pair-wise deleted. For discrete variables: n – number; % – percentage. For numerical traits: M – mean; SD – standard deviation; Me – median; Q – quartiles; anti-PM/SCL – anti-polymyositis/scleroderma antibodies; PAH – pulmonary arterial hypertension; NSIP – non-specific interstitial pneumonia; UIP – usual interstitial pneumonia, MMF – mycophenolat mofetil; MTX – methotrexate, mRSS – modified Rodnan Skin Score; RVSP – right ventricle systolic pressure; MES – the microangiopathy evolution score.

following the manufacturer's guidelines. To ensure consistency, all images were captured by the same expert, maintaining uniformity in lighting, focus and positioning.

The study aimed to categorize scleroderma microangiopathy using the Cutolo classification and to assess multiple capillaroscopic parameters – vessel density, hemorrhages, capillary morphology, giant capillaries, and avascular areas. The classification was based on identifying specific capillary abnormalities linked to different disease stages. In each NC image, vessel density was classified as normal (≥7 capillaries), reduced (4–6 capillaries) or severely reduced (≤3 capillaries). This classification offered valuable insights into the microvascular changes linked to the progression of scleroderma. For each participant, we recorded capillaroscopic features – including hemorrhages, tortuous (branched) vessels, giant capillaries, and avascular zones – offering crucial insight into the microvascular abnormalities characteristic of SSc.[24] The Dino-Lite capillaroscope underwent routine quality control checks, during which calibration images were acquired to confirm accurate color reproduction and resolution.

Images of retinal arterioles using an AO retinal camera (rtx1™; Imagine Eyes, Orsay, France) were captured in both patient groups. Before imaging, participants received 1 drop of 1% tropicamide for pupil dilation. Retinal artery images were analyzed with AOdetectArtery software (rtx1™; Imagine Eyes), focusing on the superior quadrant arterioles with a lumen diameter of at least 40 µm and no bifurcations. Two measurements were taken, and the highest-quality scan was selected for analysis.

The main vascular parameters obtained with AO were total vessel diameter (TD), lumen diameter (LD) and wall thickness (WT). The software also calculates 2 additional vascular metrics: The wall-to-lumen ratio (WLR), defined as wall thickness (WT) divided by lumen diameter (LD), and the wall cross-sectional area (WCSA), computed as $\pi \times [(TD/2)^2 - (LD/2)^2]$, which represents the area occupied by the vessel wall (Fig. 1,2).

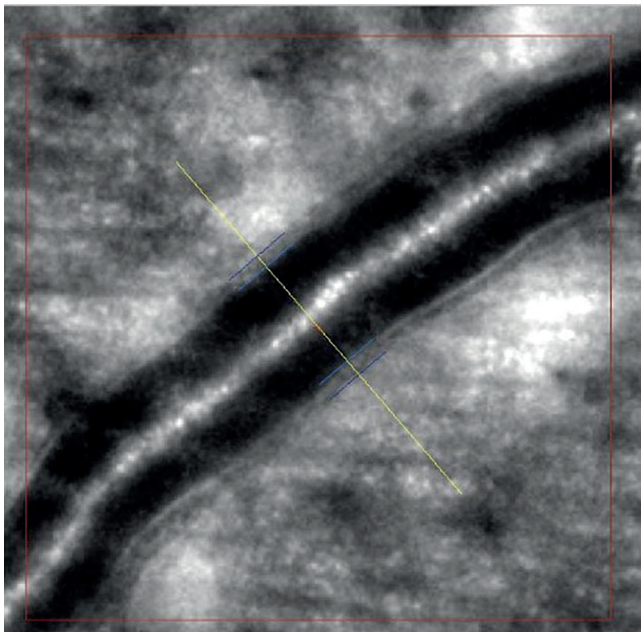

Fig. 1. Adaptive optics (AO) image of the retinal artery in a patient with scleroderma

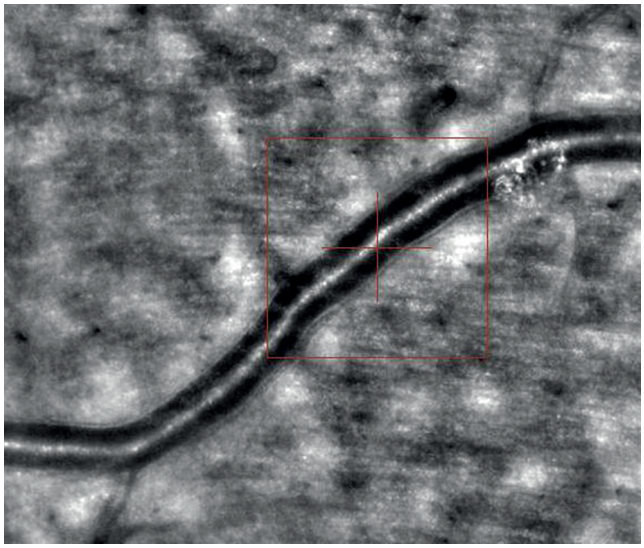

Fig. 2. Adaptive optics (AO) image of the retinal artery in a patient with scleroderma

Statistical analyses

Qualitative variables were shown as integers with percentages. Quantitative parameters were presented according to their weighted arithmetic mean, median, standard deviation (SD), and min–max values. Relationships among the examined qualitative variables were illustrated using contingency tables. Relationships among categorical variables were assessed using Pearson's χ^2 test when all expected cell counts were ≥5, and Fisher's two-tailed exact test when any expected count fell below 5. The Shapiro–Wilk W test was used to assess the normality of distribution and Levene's test was fitted to check the homogeneity of variances. Differences between independent groups for normally distributed numerical variables with homogeneous variances were assessed by one-way analysis of variance (ANOVA) without replication. Variables failing to meet normality or homogeneity of variance assumptions were analyzed with nonparametric tests – namely, the Mann–Whitney U test for dichotomous independent variables and the Kruskal–Wallis H test for variables with more than 2 categories. A level of $p < 0.050$ was deemed statistically significant. All the statistical procedures were performed using STATISTICA v. 13.3 (TIBCO Software Inc., Palo Alto, USA).

Results

The study included 31 SSc patients (61 eyes) and 41 healthy controls (81 eyes). No significant differences between the 2 groups regarding retinal arteries TD, LD, second wall thickness, and WCSA were found (Table 4).

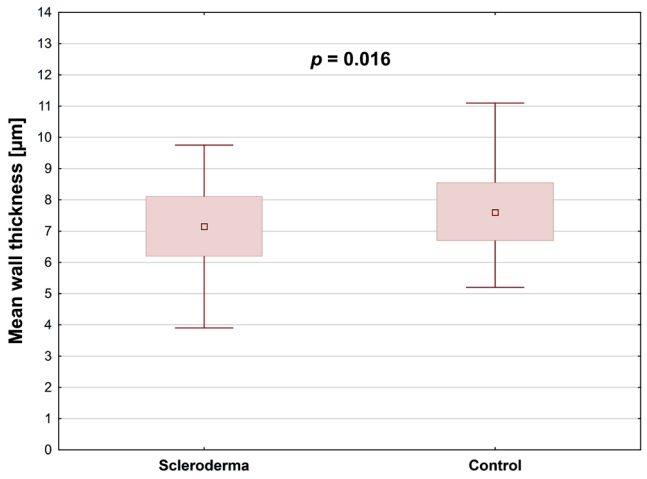

Fig. 3. Graphical presentation of the measures of location (median, quartiles) and dispersion (min–max values) of the mean wall thickness [µm] in the study participants' eyes by occurrence of scleroderma

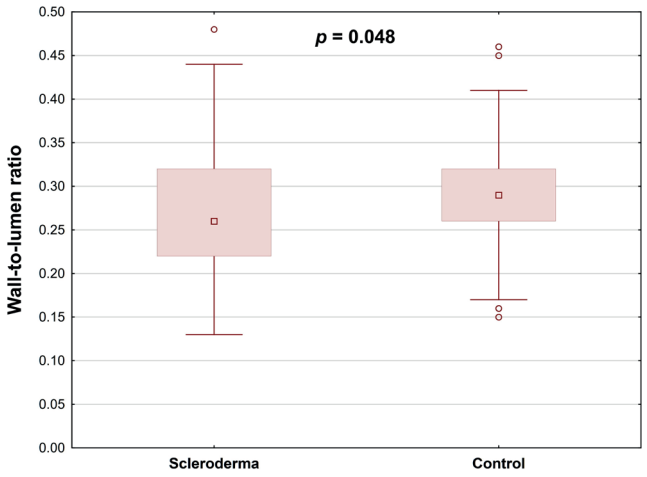

Fig. 4. Graphical presentation of the measures of location (median, quartiles) and dispersion (min–max values) of the wall-to-lumen ratio in the study participants' eyes by occurrence of scleroderma

Mean retinal arterial wall thickness was significantly lower in SSc patients than in healthy controls (p = 0.016), and the wall-to-lumen ratio was also notably decreased in the SSc group (p = 0.048) (Table 4; Fig. 3,4).

Retinal vessel parameters obtained through AO, including TD, LD, wall thicknesses, WLR, and WCSA, were analyzed in relation to NC findings and clinical features of SSc. No statistically significant correlation was observed between retinal vessel parameters and capillaroscopic patterns, nor between these parameters and the type of SSc (Table 5–7). The WCSA was significantly higher in hypertensive SSc patients compared to those without hypertension (p = 0.026; Table 7).

Discussion

Vascular damage is a hallmark of SSc and plays a pivotal role in its pathogenesis. It has been established that microvascular changes primarily affect peripheral arterioles and capillaries. Generalized vasculopathy has been demonstrated to contribute significantly to perfusion disorders in both the retina and the choroid. Therefore, the retinal microvasculature offers an ideal window for monitoring disease progression and detecting early pathological changes. Previous studies have shown that retinal findings, such as hard exudates, vascular tortuosity and arterial narrowing, as well as microhemorrhages, have been discovered in patients with SSc during fundus examination.[25–27] The presence of small retinal capillary abnormalities can be detected through a range of diagnostic techniques, including OCTA and fluorescein angiography (FA). The morphological changes in the retinal caliber, shape, or lumen diameter are valuable for assessing the state of microcirculatory perfusion. Therefore, we hypothesized that adaptive optics retinal imaging, as a novel noninvasive method, could aid in the detection of abnormalities in the structure of retinal vessels.

In this study, AO was used for retinal artery assessment in both groups. To the best of our knowledge, our study is the first to use AO imaging in SSc. A comparison of the 2 groups revealed no statistically significant differences in terms of LD, TD and WLR. According to previous studies, WLR and WCSA are optimal parameters for evaluating vascular remodeling in cases of diabetic retinopathy and arterial hypertension.[11,28–32] Żmijewska et al. analyzed arterial measurements using AO in 36 patients with nonproliferative diabetic retinopathy (DR). Their results demonstrated thicker arterial walls, increased WLR and WCSA in DR group than in controls.[29] Matuszewski et al.[33] and Cristescu et al.[34] also demonstrated comparable outcomes. However, our results showed that the WLR was significantly decreased among SSc patients compared to the healthy group (p = 0.048).

Lombardo et al.[35] reported that, in eyes with nonproliferative DR, the parafoveal capillary lumen diameter was significantly reduced compared to healthy controls. Similarly, Zaleska-Żmijewska et al.[18] demonstrated that prediabetic patients exhibit distinct alterations in both capillary lumen diameter and wall-to-lumen ratio relative to control subjects.

An elevated WLR reflects both thickening of the vessel wall and concomitant narrowing of the lumen. Piantoni et al.[36] used AO in patients with active rheumatoid arthritis treated with abatacept to evaluate cardiovascular risk factors. Their results indicated a significant reduction in the WLR of the arterioles after abatacept treatment. However, our results showed that the mean arterial wall was thinner in the scleroderma group than in the controls (p = 0.016). It is possible that the observed results may be attributed to the vasodilator treatment employed in the management of SSc.[37]

Pache et al.[37] demonstrated that in 10 healthy volunteers, a single dose of sildenafil induced significant dilation of both retinal arterioles and venules 30 minutes

Table 4. Descriptive statistics for the adaptive optics by occurrence of scleroderma (n = 142 eyes)

Adaptive optics	Study group	Statistical parameter				Statistical tests
		M	SD	Me	Q_1–Q_3	
Total diameter [µm]	scleroderma	67.25	11.37	67.15	58.00–75.50	normality test W = 0.979, p = 0.411 W = 0.966, p = 0.033 Levene's test F (1, 135) = 1.083 p = 0.300 Mann–Whitney test U = 2130.000 $Z_{corr.}$ = –0.699 p = 0.484
	control	69.03	12.88	69.30	58.00–78.40	
Wall 1 thickness [µm]	scleroderma	6.53	1.44	6.60	5.60–7.40	normality test W = 0.985, p = 0.677 W = 0.325, p < 0.001 Levene's test F (1, 135) = 1.337 p = 0.250 Mann–Whitney test U = 1323.000 $Z_{corr.}$ = –4.216 **p < 0.001**
	control	8.20	4.78	7.50	6.60–8.90	
Wall 2 thickness [µm]	scleroderma	7.46	1.72	7.45	6.10–8.50	normality test W = 0.976, p = 0.317 W = 0.950, p = 0.004 Levene's test F (1, 135) = 0.686 p = 0.409 Mann–Whitney test U = 2284.500 $Z_{corr.}$ = –0.026 p = 0.979
	control	7.52	1.61	7.20	6.40–8.10	
Mean wall thickness [µm]	scleroderma	6.99	1.34	7.15	6.20–8.10	normality test W = 0.983, p = 0.589 W = 0.512, p < 0.001 Levene's test F (1, 135) = 0.285 p = 0.594 Mann–Whitney test U = 1740.000 $Z_{corr.}$ = –2.398 **p = 0.016**
	control	7.86	2.52	7.60	6.70–8.55	
Lumen diameter [µm]	scleroderma	53.25	10.49	52.65	44.80–61.10	normality test W = 0.983, p = 0.585 W = 0.962, p = 0.018 Levene's test F (1, 135) = 2.123 p = 0.147 Mann–Whitney test U = 2279.000 $Z_{corr.}$ = 0.050 p = 0.960
	control	53.64	14.03	53.30	44.20–62.40	
Wall-to-lumen ratio	scleroderma	0.2710	0.0681	0.2600	0.2200–0.3200	normality test W = 0.970, p = 0.159 W = 0.946, p = 0.002 Levene's test F (1, 135) = 0.024 p = 0.878 Mann–Whitney test U = 1837.000 $Z_{corr.}$ = –1.976 **p = 0.048**
	control	0.2940	0.0724	0.2600	0.2200–0.3300	
Wall cross-sectional area [µm^2]	scleroderma	1338.3	410.0	1386	983–1594	normality test W = 0.952, p = 0.024 W = 0.960, p = 0.015 Levene's test F (1, 135) = 0.006 p = 0.941 Mann–Whitney test U = 1843.000 $Z_{corr.}$ = 0.051 p = 0.051
	control	1479.3	431.3	1498	1129–1724	

M – mean; SD – standard deviation; Me – median; Q – quartiles. Values in bold are statistically significant.

Table 5. Descriptive statistics for the lumen diameter [µm] in the study participants with scleroderma by selected capillaroscopic assessments (n = 61 eyes)

Investigated trait		Statistical parameter		Statistics
		M (SD)	Me (Q_1–Q_3)	
Scleroderma	localized	55.81 (13.23)	58.20 (41.83–61.18)	normality test W = 0.980, p = 0.721 W = 0.929, p = 0.261 Levene's test F (1, 50) = 4.027, p = 0.051 ANOVA F (1, 50) = 2.244 p = 0.140
	systemic	51.15 (8.65)	50.00 (44.73–57.20)	
Scleroderma pattern	early	48.80 (9.92)	52.40 (41.33–55.83)	normality test W = 0.964, p = 0.841 W = 0.970, p = 0.692 W = 0.959, p = 0.612 Levene's test. F (3, 48) = 1.884, p = 0.145 ANOVA F (3, 48) = 1.718 p = 0.176
	active	55.94 (11.75)	57.20 (45.85–64.53)	
	late	49.78 (7.85)	49.00 (43.63–55.97)	
Number of vessels	normal	52.23 (11.12)	58.20 (42.53–58.95)	normality test W = 0.784, p = 0.077 W = 0.982, p = 0.811 W = 0.932, p = 0.403 Levene's test F (2, 49) = 0.365, p = 0.696 ANOVA F (2, 49) = 1.718 p = 0.498
	reduced	51.51 (9.43)	50.00 (44.57–59.77)	
	very reduced	55.59 (12.71)	54.50 (44.07–62.04)	
Avascular areas	yes	52.83 (11.23)	51.35 (44.52–61.70)	normality test W = 0.968, p = 0.667 W = 0.980, p = 0.820 Levene's test F (1, 50) = 0.797, p = 0.376 ANOVA F (1, 50) = 0.072 p = 0.789
	no	52.04 (9.03)	52.50 (43.95–58.83)	
Giant capillaries	yes	52.66 (12.52)	49.95 (42.23–61.24)	normality test W = 0.970, p = 0.613 W = 0.968, p = 0.576 Levene's test F (1, 50) = 6.718, p = 0.012 ANOVA F (3, 48) = 0.014 p = 0.907
	no	52.33 (7.64)	52.90 (44.78–58.28)	
Hemorrhages	yes	49.38 (12.18)	46.65 (40.92–55.28)	normality test W = 0.978, p = 0.726 W = 0.906, p = 0.054 Levene's test F (1, 50) = 1.244, p = 0.270 ANOVA F (1, 50) = 3.127 p = 0.083
	no	54.45 (8.51)	54.55 (48.30–61.49)	
Branched vessels	yes	50.38 (9.78)	49.10 (44.56–57.58)	normality test W = 0.959, p = 0.232 W = 0.975, p = 0.878 Levene's test F (1, 50) = 0.116, p = 0.735 ANOVA F (1, 50) = 1.175 p = 0.283
	no	53.62 (10.49)	53.35 (43.68–59.27)	

Table 5. Descriptive statistics for the lumen diameter [μm] in the study participants with scleroderma by selected capillaroscopic assessments (n = 61 eyes) – cont.

Investigated trait		Statistical parameter		Statistics
		M (SD)	Me (Q_1–Q_3)	
Finger ulcers	yes	54.05 (12.26)	52.70 (46.08–60.95)	normality test W = 0.951, p = 0.114 W = 0.954, p = 0.586 Levene's test F (1, 49) = 0.168, p = 0.683 ANOVA F (1, 50) = 0.399 p = 0.530
	no	52.04 (9.54)	52.50 (43.21–59.10)	
Arterial hypertension	yes	56.30 (13.02)	55.15 (49.00–65.50)	normality test W = 0.975, p = 0.566 W = 0.961, p = 0.731 Levene's test F (1, 49) = 1.248, p = 0.269 ANOVA F (1, 49) = 2.871 p = 0.097
	no	52.29 (9.52)	52.50 (44.70–59.10)	
Sildenafil	yes	48.92 (8.21)	49.00 (44.10–53.60)	normality test W = 0.972, p = 0.676 W = 0.985, p = 0.957 Levene's test F (1, 49) = 2.625, p = 0.112 ANOVA F (1, 49) = 6.062 **p = 0.017**
	no	56.54 (10.94)	58.20 (48.50–64.20)	
Amlodipine	yes	54.44 (10.87)	54.80 (47.80–59.10)	normality test W = 0.967, p = 0.491 W = 0.955, p = 0.392 Levene's test F (1, 49) = 0.024, p = 0.877 ANOVA F (1, 49) = 1.554 p = 0.218
	no	52.53 (10.34)	49.95 (44.70–61.45)	

M – mean; SD – standard deviation; Me – median; Q – quartiles; ANOVA – analysis of variance. Values in bold are statistically significant.

Table 6. Descriptive statistics for the wall-to-lumen ration in the study participants with scleroderma by selected capillaroscopic assessments (n = 61 eyes)

Investigated trait		Statistical parameter		Statistics
		M (SD)	Me (Q_1–Q_3)	
Scleroderma	localized	0.2593 (0.0794)	0.2500 (0.2300–0.2850)	normality test W = 0.983, p = 0.835 W = 0.876, p = 0.041 Levene's test F (1, 50) = 0.009, p = 0.925 Mann–Whitney test U = 212.000 $Z_{corr.}$ = 1.315 p = 0.188
	systemic	0.2816 (0.0641)	0.2800 (0.2267–0.3233)	
Scleroderma pattern	early	0.2989 (0.0924)	0.3000 (0.2500–0.3500)	normality test W = 0.964, p = 0.837 W = 0.917, p = 0.057 W = 0.886, p = 0.040 Levene's test F (3, 48) = 0.574, p = 0.635 Kruskal–Wallis test H (3, n = 52) = 3.453 p = 0.327
	active	0.2626 (0.0726)	0.2500 (0.2117–0.2900)	
	late	0.2753 (0.0516)	0.2700 (0.2267–0.3300)	
Number of vessels	normal	0.2367 (0.0971)	0.2600 (0.1517–0.3100)	normality test W = 0.957, p = 0.600 W = 0.968, p = 0.368 W = 0.963, p = 0.820 Levene's test F (2, 49) = 1.151, p = 0.229 ANOVA F (2, 49) = 2.972 p = 0.061
	reduced	0.2895 (0.0696)	0.2800 (0.2500–0.3300)	
	very reduced	0.2408 (0.0448)	0.2350 (0.2142–0.2658)	

Table 6. Descriptive statistics for the wall-to-lumen ration in the study participants with scleroderma by selected capillaroscopic assessments (n = 61 eyes) – cont.

Investigated trait		Statistical parameter		Statistics
		M (SD)	Me (Q_1–Q_3)	
Avascular areas	yes	0.2753 (0.0707)	0.2700 (0.2292–0.3300)	normality test W = 0.911, p = 0.049 W = 0.975, p = 0.678 Levene's test F (1, 50) = 0.445, p = 0.508 ANOVA F (1, 50) = 0.0003 p = 0.986
	no	0.2750 (0.0678)	0.2600 (0.2475–0.3200)	
Giant capillaries	yes	0.2838 (0.0784)	0.2600 (0.2292–0.3208)	normality test W = 0.953, p = 0.269 W = 0.933, p = 0.090 Levene's test F (1, 50) = 0.447, p = 0.235 ANOVA F (1, 50) = 0.819 p = 0.370
	no	0.2665 (0.0580)	0.2750 (0.2292–0.3200)	
Hemorrhages	yes	0.2945 (0.0833)	0.2750 (0.2383–0.3300)	normality test W = 0.966, p = 0.393 W = 0.943, p = 0.271 Levene's test F (1, 50) = 3.232, p = 0.078 ANOVA F (1, 50) = 2.639 p = 0.111
	no	0.2631 (0.0561)	0.2650 (0.2242–0.3158)	
Branched vessels	yes	0.2861 (0.0750)	0.2750 (0.2200–0.3317)	normality test W = 0.944, p = 0.080 W = 0.939, p = 0.277 Levene's test F (1, 50) = 0.818, p = 0.370 ANOVA F (1, 50) = 0.688 p = 0.411
	no	0.2694 (0.0658)	0.2600 (0.2300–0.3200)	
Finger ulcers	yes	0.2728 (0.0684)	0.2600 (0.2242–0.3200)	normality test W = 0.968, p = 0.373 W = 0.939, p = 0.374 Levene's test F (1, 49) = 0.279, p = 0.599 ANOVA F (1, 49) = 0.001 p = 0.914
	no	0.2720 (0.0652)	0.2700 (0.2300–0.3067)	
Arterial hypertension	yes	0.2760 (0.0626)	0.2600 (0.2300–0.3300)	normality test W = 0.960, p = 0.200 W = 0.978, p = 0.958 Levene's test F (1, 49) = 0.081, p = 0.777 ANOVA F (1, 49) = 0.0002 p = 0.989
	no	0.2700 (0.0704)	0.2650 (0.2200–0.3150)	
Sildenafil	yes	0.2910 (0.0648)	0.2800 (0.2400–0.3300)	normality test W = 0.944, p = 0.162 W = 0.949, p = 0.239 Levene's test F (1, 49) = 0.011, p = 0.918 ANOVA F (1, 49) = 2.449 p = 0.124
	no	0.2560 (0.0677)	0.2600 (0.2200–0.2900)	
Amlodipine	yes	0.2560 (0.0643)	0.2550 (0.2200–0.3000)	normality test W = 0.938, p = 0.089 W = 0.980, p = 0.914 Levene's test F (1, 49) = 0.143, p = 0.707 ANOVA F (1, 49) = 3.051 p = 0.087
	no	0.2800 (0.0697)	0.2700 (0.2250–0.3200)	

M – mean; SD – standard deviation; Me – median; Q – quartiles; ANOVA – analysis of variance.

Table 7. Descriptive statistics for the wall cross-sectional area [μm²] in the study participants with scleroderma by selected capillaroscopic assessments (n = 61 eyes)

Investigated trait		Statistical parameter		Statistics
		M (SD)	Me (Q_1–Q_3)	
Scleroderma	localized	1399.9 (540.5)	1438 (874–1619)	normality test W = 0.907, p = 0.122 W = 0.959, p = 0.187 Levene's test F (1, 50) = 3.233, p = 0.078 ANOVA F (1, 50) = 0.802 p = 0.375
	systemic	1291.3 (323.1)	1379 (1032–1534)	
Scleroderma pattern	early	1235.8 (382.5)	1389 (840–1601)	normality test W = 0.787, p = 0.015 W = 0.951, p = 0.315 W = 0.946, p = 0.391 Levene's test F (3, 48) = 1.493, p = 0.228 Kruskal–Wallis test H (3, n = 52) = 3.104 p = 0.376
	active	1420.4 (458.6)	1428 (1079–1703)	
	late	1210.5 (314.5)	1244 (897–1434)	
Number of vessels	normal	1078.3 (413.4)	912 (796–1444)	normality test W = 0.879, p = 0.322 W = 0.964, p = 0.265 W = 0.828, p = 0.020 Levene's test. F (2, 49) = 0.124, p = 0.883 Kruskal–Wallis test H (2, n = 52) = 1.857 p = 0.395
	reduced	1350.1 (362.8)	1389 (1067–1608)	
	very reduced	1298.8 (493.5)	1325 (922–1446)	
Avascular areas	yes	1322.3 (392.2)	1381 (1048–1496)	normality test W = 0.919, p = 0.025 W = 0.915, p = 0.060 Levene's test F (1, 50) = 0.535, p = 0.468 Mann–Whitney test U = 310.000 $Z_{corr.}$ = –0.361 p = 0.718
	no	1323.0 (409.1)	1433 (866–1605)	
Giant capillaries	yes	1278.2 (461.3)	1405 (892–1620)	normality test W = 0.931, p = 0.083 W = 0.952, p = 0.262 Levene's test F (1, 50) = 1.790, p = 0.187 ANOVA F (1, 50) = 0.657 p = 0.421
	no	1323.0 (319.5)	1356 (981–1532)	
Hemorrhages	yes	1249.4 (440.7)	1195 (864–1467)	normality test W = 0.857, p = 0.007 W = 0.968, p = 0.437 Levene's test F (1, 50) = 0.443, p = 0.509 Mann–Whitney test U = 248.000 $Z_{corr.}$ = 1.345 p = 0.179
	no	1358.3 (364.1)	1397 (1059–1600)	
Branched vessels	yes	1260.5 (324.7)	1353 (899–1530)	normality test W = 0.945, p = 0.353 W = 0.935, p = 0.045 Levene's test. F (1, 50) = 0.925, p = 0.341 Mann–Whitney test U = 267.000 $Z_{corr.}$ = –0.741 p = 0.459
	no	1355.5 (429.1)	1397 (981–1605)	

Table 7. Descriptive statistics for the wall cross-sectional area [μm²] in the study participants with scleroderma by selected capillaroscopic assessments (n = 61 eyes) – cont.

Investigated trait		Statistical parameter		Statistics
		M (SD)	Me (Q_1–Q_3)	
Finger ulcers	yes	1291.3 (376.8)	1353 (896–1576)	normality test W = 0.884, p = 0.054 W = 0.934, p = 0.033 Levene's test. F (1, 49) = 0.154, p = 0.696 Mann–Whitney test U = 263.000 $Z_{corr.}$ = –0.134 p = 0.893
	no	1377.9 (450.1)	1389 (1079–1489)	
Arterial hypertension	yes	1517.5 (476.9)	1466 (1259–1717)	normality test W = 0.929, p = 0.295 W = 0.940, p = 0.047 Levene's test F (1, 49) = 0.296, p = 0.589 ANOVA F (1, 49) = 5.252 **p = 0.026**
	no	1281.2 (374.6)	1324 (905–1547)	
Sildenafil	yes	1224.4 (300.2)	1244 (987–1428)	normality test W = 0.963, p = 0.478 W = 0.931, p = 0.080 Levene's test F (1, 49) = 2.494, p = 0.121 ANOVA F (1, 49) = 2.821 p = 0.099
	no	1424.6 (462.6)	1466 (983–1717)	
Amlodipine	yes	1316.4 (422.9)	1356 (912–1541)	normality test W = 0.895, p = 0.023 W = 0.958, p = 0.291 Levene's test F (1, 49) = 0.015, p = 0.903 Mann–Whitney test U = 308.000 $Z_{corr.}$ = –0.200 p = 0.842
	no	1351.6 (407.4)	1392 (985–1612)	

M – mean; SD – standard deviation; Me – median; Q – quartiles; ANOVA – analysis of variance. Values in bold are statistically significant.

after administration (p < 0.001). Moreover, Polak at al.[38] reported increased retinal blood flow in healthy controls after sildenafil administration. Sildenafil can enhance the vasodilatory effect of nitric oxide (NO), the primary regulator of vascular smooth muscle tone. In addition, we compared the measurements of the retinal arteries obtained in AO with the results of the NC. However, we did not find a statistically significant correlation with the type of scleroderma, finger ulcers and scleroderma patterns, number of vessels, avascular areas, hemorrhages, or branched vessels visualized in NC. In our previous study, we found that scleroderma microangiopathy patterns correlated significantly with both superficial and deep foveal avascular zone (FAZ) areas, as well as with deep retinal vessel density measured by OCTA.[23] Several studies have explored the relationship between peripheral capillary density measured with nailfold capillaroscopy and both choriocapillaris vessel density[39] and overall retinal perfusion.[40] However, these findings have been inconsistent. It is therefore possible that high-resolution imaging of the retinal microvasculature may yield stronger correlations with NC abnormalities.

These findings corroborate earlier reports that hypertension is associated with increased wall cross-sectional area, reflecting arteriolar remodeling.[11] Furthermore, in our study, we evaluated the impact of vasodilator medications employed for the management of complications associated with scleroderma vasculopathy. Contrary to expectations, the findings of this study indicated a decreased LD in patients treated with sildenafil (p = 0.017). It is worth noting that most patients in our NC cohort exhibited a late scleroderma pattern – reflecting severe vasculopathy and advanced disease – so the observed arterial lumen narrowing likely reflects the chronicity and severity of SSc.

Limitations

It is important to acknowledge the limitations of the research, including the relatively small number of participants and the cross-sectional nature of the study.

Conclusions

Our study analysis of the AO retinal imaging data set revealed a reduced mean arterial wall thickness in patients with SSc compared to healthy controls. However, no correlation was identified between the AO findings and the NC parameters or the disease stage. The retinal vessel parameters revealed significant differences only in hypertensive or sildenafil-treated patients. Further studies on a larger cohort of patients are necessary to draw reliable conclusions about the usefulness of AO in the diagnosis of SSc and its possible correlation with capillaroscopic findings.

Data Availability Statement

All data generated or analyzed during this study are included in this article.

Consent for publication

Not applicable.

Use of AI and AI-assisted technologies

Not applicable.

ORCID iDs

Katarzyna Paczwa https://orcid.org/0000-0003-3825-3727
Magdalena Szeretucha https://orcid.org/0000-0002-8944-856X
Katarzyna Romanowska-Próchnicka https://orcid.org/0000-0003-1326-2600
Radosław Różycki https://orcid.org/0000-0001-7040-026X
Joanna Gołębiewska https://orcid.org/0000-0002-3013-4363
Sylwia Ornowska https://orcid.org/0000-0002-2895-4178
Marzena Olesińska https://orcid.org/0000-0003-3028-1061

References

1. Nikpour M, Stevens WM, Herrick AL, Proudman SM. Epidemiology of systemic sclerosis. *Best Pract Res Clin Rheumatol*. 2010;24(6):857–869. doi:10.1016/j.berh.2010.10.007
2. Postlethwaite R, Pattanaik D, Brown M. Vascular involvement in systemic sclerosis (scleroderma). *J Inflamm Res*. 2011;4:105. doi:10.2147/JIR.S18145
3. Pawlik K, Bohdziewicz A, Maciejewska M, et al. Evaluation of cutaneous microcirculation in systemic sclerosis: An update. *Dermatol Rev*. 2023;110(4):499–517. doi:10.5114/dr.2023.131385
4. Lambova SN, Müller-Ladner U. Nailfold capillaroscopy in systemic sclerosis: State of the art. The evolving knowledge about capillaroscopic abnormalities in systemic sclerosis. *J Scleroderma Relat Dis*. 2019;4(3):200–211. doi:10.1177/2397198319833486
5. de AF Gomes B, Santhiago MR, Magalhães P, Kara-Junior N, De Azevedo MNL, Moraes HV. Ocular findings in patients with systemic sclerosis. *Clinics (Sao Paulo)*. 2011;66(3):379–385. doi:10.1590/S1807-59322011000300003
6. de AF Gomes B, Santhiago MR, De Azevedo MNL, Moraes HV. Evaluation of dry eye signs and symptoms in patients with systemic sclerosis. *Graefes Arch Clin Exp Ophthalmol*. 2012;250(7):1051–1056. doi:10.1007/s00417-012-1938-3
7. Sahin Atik S, Koc F, Akin Sari S, Sefi Yurdakul N, Ozmen M, Akar S. Anterior segment parameters and eyelids in systemic sclerosis. *Int Ophthalmol*. 2016;36(4):577–583. doi:10.1007/s10792-015-0165-4
8. Kozikowska M, Luboń W, Kucharz E, Mrukwa-Kominek E. Ocular manifestations in patients with systemic sclerosis. *Reumatologia*. 2020;58(6):401–406. doi:10.5114/reum.2020.102004
9. Tailor R, Gupta A, Herrick A, Kwartz J. Ocular manifestations of scleroderma. *Surv Ophthalmol*. 2009;54(2):292–304. doi:10.1016/j.survophthal.2008.12.007
10. Szucs G, Szekanecz Z, Aszalos Z, et al. A wide spectrum of ocular manifestations signify patients with systemic sclerosis. *Ocul Immunol Inflamm*. 2021;29(1):81–89. doi:10.1080/09273948.2019.1657467
11. Szewczuk A, Zaleska-Żmijewska A, Dziedziak J, Szaflik JP. Clinical application of adaptive optics imaging in diagnosis, management, and monitoring of ophthalmological diseases: A narrative review. *Med Sci Monit*. 2023;29:e941926. doi:10.12659/MSM.941926
12. Yao X, Ke M, Ho Y, et al. Comparison of retinal vessel diameter measurements from swept-source OCT angiography and adaptive optics ophthalmoscope. *Br J Ophthalmol*. 2021;105(3):426–431. doi:10.1136/bjophthalmol-2020-316111
13. Bakker E, Dikland FA, Van Bakel R, et al. Adaptive optics ophthalmoscopy: A systematic review of vascular biomarkers. *Surv Ophthalmol*. 2022;67(2):369–387. doi:10.1016/j.survophthal.2021.05.012
14. Rosenbaum D, Mattina A, Koch E, et al. Effects of age, blood pressure and antihypertensive treatments on retinal arterioles remodeling assessed by adaptive optics. *J Hypertens*. 2016;34(6):1115–1122. doi:10.1097/HJH.0000000000000894
15. Dziedziak J, Zaleska-Żmijewska A, Szaflik JP, Cudnoch-Jędrzejewska A. Impact of arterial hypertension on the eye: A review of the pathogenesis, diagnostic methods, and treatment of hypertensive retinopathy. *Med Sci Monit*. 2022;28:e935135. doi:10.12659/MSM.935135
16. Baltă F, Cristescu IE, Mirescu AE, Baltă G, Zemba M, Tofolean IT. Investigation of retinal microcirculation in diabetic patients using adaptive optics ophthalmoscopy and optical coherence angiography. *J Diabetes Res*. 2022;2022:1516668. doi:10.1155/2022/1516668
17. Gallo A, Dietenbeck T, Giron A, Paques M, Kachenoura N, Girerd X. Noninvasive evaluation of retinal vascular remodeling and hypertrophy in humans: Intricate effect of ageing, blood pressure and glycaemia. *Clin Res Cardiol*. 2021;110(7):959–970. doi:10.1007/s00392-020-01680-3
18. Zaleska-Żmijewska A, Piątkiewicz P, Śmigielska B, et al. Retinal photoreceptors and microvascular changes in prediabetes measured with adaptive optics (rtx1^{TM}): A case-control study. *J Diabetes Res*. 2017;2017:4174292. doi:10.1155/2017/4174292
19. Szewczuk A, Wawrzyniak ZM, Szaflik JP, Zaleska-Żmijewska A. Is primary open-angle glaucoma a vascular disease? Assessment of the relationship between retinal arteriolar morphology and glaucoma severity using adaptive optics. *J Clin Med*. 2024;13(2):478. doi:10.3390/jcm13020478
20. Hugo J, Chavane F, Beylerian M, Callet M, Denis D, Matonti F. Morphologic analysis of peripapillary retinal arteriole using adaptive optics in primary open-angle glaucoma. *J Glaucoma*. 2020;29(4):271–275. doi:10.1097/IJG.0000000000001452
21. Errera MH, Laguarrigue M, Rossant F, et al. High-resolution imaging of retinal vasculitis by flood illumination adaptive optics ophthalmoscopy: A follow-up study. *Ocul Immunol Inflamm*. 2020;28(8):1171–1180. doi:10.1080/09273948.2019.1646773
22. Venkatesh R, Mutalik D, Reddy NG, Akkali MC, Yadav NK, Chhablani J. Retinal vessel wall imaging using fluorescein angiography and adaptive optics imaging in acute branch retinal artery occlusion. *Eur J Ophthalmol*. 2023;33(4):NP85–NP90. doi:10.1177/11206721221113202
23. Paczwa K, Rerych M, Romanowska-Próchnicka K, Olesińska M, Różycki R, Gołębiewska J. Retinal microvasculature in systemic sclerosis patients and the correlation between nailfold capillaroscopic findings and optical coherence angiography results. *J Clin Med*. 2024;13(7):2025. doi:10.3390/jcm13072025
24. Cutolo M, Pizzorni C, Secchi ME, Sulli A. Capillaroscopy. *Best Pract Res Clin Rheumatol*. 2008;22(6):1093–1108. doi:10.1016/j.berh.2008.09.001
25. Waszczykowska A, Goś R, Waszczykowska E, Dziankowska-Bartkowiak B, Jurowski P. Prevalence of ocular manifestations in systemic sclerosis patients. *Arch Med Sci*. 2013;6:1107–1113. doi:10.5114/aoms.2013.39217
26. Ushiyama O, Ushiyama K, Yamada T, et al. Retinal findings in systemic sclerosis: A comparison with nailfold capillaroscopic patterns. *Ann Rheum Dis*. 2003;62(3):204–207. doi:10.1136/ard.62.3.204
27. Shenavandeh S, Afarid M, Hasanaghaei T, Ali Nazarinia M. Prevalence of retinal changes in patients with systemic sclerosis: The association between retinal vascular changes and nailfold capillaroscopic findings. *Reumatologia*. 2021;59(1):27–34. doi:10.5114/reum.2021.103436

28. Mehta R, Akkali M, Jayadev C, Anuj A, Yadav N. Morphometric analysis of retinal arterioles in control and hypertensive population using adaptive optics imaging. *Indian J Ophthalmol*. 2019;67(10):1673. doi:10.4103/ijo.IJO_253_19
29. Zaleska-Żmijewska A, Wawrzyniak ZM, Dąbrowska A, Szaflik JP. Adaptive optics (rtx1) high-resolution imaging of photoreceptors and retinal arteries in patients with diabetic retinopathy. *J Diabetes Res*. 2019; 2019:9548324. doi:10.1155/2019/9548324
30. Meixner E, Michelson G. Measurement of retinal wall-to-lumen ratio by adaptive optics retinal camera: A clinical research. *Graefes Arch Clin Exp Ophthalmol*. 2015;253(11):1985–1995. doi:10.1007/s00417-015-3115-y
31. Rizzoni D, Agabiti Rosei C, De Ciuceis C, Semeraro F, Rizzoni M, Docchio F. New methods to study the microcirculation. *Am J Hypertens*. 2018;31(3):265–273. doi:10.1093/ajh/hpx211
32. Gallo A, Mattina A, Rosenbaum D, Koch E, Paques M, Girerd X. Retinal arteriolar remodeling evaluated with adaptive optics camera: Relationship with blood pressure levels. *Ann Cardiol Angeiol (Paris)*. 2016; 65(3):203–207. doi:10.1016/j.ancard.2016.04.021
33. Matuszewski W, Gontarz-Nowak K, Harazny JM, Bandurska-Stankiewicz E. Evaluation of morphological changes in retinal vessels in type 1 diabetes mellitus patients with the use of adaptive optics. *Biomedicines*. 2022;10(8):1926. doi:10.3390/biomedicines10081926
34. Cristescu IE, Zagrean L, Balta F, Branisteanu DC. Retinal microcirculation investigation in type I and II diabetic patients without retinopathy using an adaptive optics retinal camera. *Acta Endocrinol (Buchar)*. 2019;15(4):417–422. doi:10.4183/aeb.2019.417
35. Lombardo M, Parravano M, Serrao S, Ducoli P, Stirpe M, Lombardo G. Analysis of retinal capillaries in patients with type 1 diabetes and nonproliferative diabetic retinopathy using adaptive optics imaging. *Retina*. 2013;33(8):1630–1639. doi:10.1097/IAE.0b013e3182899326
36. Piantoni S, Regola F, Angeli F, et al. Retinal microvascular alterations in patients with active rheumatoid arthritis without cardiovascular risk factors: The potential effects of T cell co-stimulation blockade. *Front Med (Lausanne)*. 2024;11:1247024. doi:10.3389/fmed.2024.1247024
37. Pache M, Meyer P, Prünte C, Orgül S, Nuttli I, Flammer J. Sildenafil induces retinal vasodilatation in healthy subjects. *Br J Ophthalmol*. 2002;86(2):156–158. doi:10.1136/bjo.86.2.156
38. Polak K, Wimpissinger B, Berisha F, Georgopoulos M, Schmetterer L. Effects of sildenafil on retinal blood flow and flicker-induced retinal vasodilatation in healthy subjects. *Invest Ophthalmol Vis Sci*. 2003; 44(11):4872. doi:10.1167/iovs.03-0177
39. Mihailovic N, Lahme L, Braasch S, et al. Altered ocular microvasculature in patients with systemic sclerosis and very early disease of systemic sclerosis using optical coherence tomography angiography. *Sci Rep*. 2022;12(1):10990. doi:10.1038/s41598-022-14377-6
40. Cutolo CA, Cere A, Toma P, et al. Peripheral and ocular microvascular alterations in systemic sclerosis: Observations from capillaroscopic assessments, perfusion peripheral analysis, and optical coherence tomography angiography. *Rheumatol Int*. 2023;44(1):107–118. doi:10.1007/s00296-023-05495-z

Pharyngeal airway changes after functional orthodontic treatment: A retrospective case-control study on a pediatric population

Zbigniew Paluch[1,A–F], Robert Warnecki[2,A–F], Marta Rogalska[3,C–F], Michał Szlęzak[4,E,F], Katarzyna Miśkiewicz-Orczyk[3,E,F], Wojciech Domka[5,E,F], Maciej Misiołek[3,E,F]

[1] Private Orthodontic Practice, Racibórz, Poland
[2] Private Orthodonctic Practice, Opole, Poland
[3] Department of Otorhinolaryngology and Oncological Laryngology, Faculty of Medical Sciences in Zabrze, Medical University of Silesia in Katowice, Zabrze, Poland
[4] Fizjosport Medical Center, Gliwice, Poland
[5] Department of Otolaryngology, Medical College of the University of Rzeszów, Poland

A – research concept and design; B – collection and/or assembly of data; C – data analysis and interpretation; D – writing the article; E – critical revision of the article; F – final approval of the article

Advances in Clinical and Experimental Medicine, ISSN 1899–5276 (print), ISSN 2451–2680 (online) *Adv Clin Exp Med*. 2026;35(1):151–166

Address for correspondence
Marta Rogalska
E-mail: rogalska_marta@wp.pl

Funding sources
None declared

Conflict of interest
None declared

Received on October 3, 2024
Reviewed on January 11, 2025
Accepted on April 25, 2025

Published online on January 7, 2026

Cite as
Paluch Z, Warnecki R, Rogalska M, et al. Pharyngeal airway changes after functional orthodontic treatment: A retrospective case-control study on a pediatric population. *Adv Clin Exp Med*. 2026;35(1):151–166. doi:10.17219/acem/204393

DOI
10.17219/acem/204393

Abstract

Background. Initiating orthodontic treatment before the pubertal peak results in more pronounced long-term craniofacial changes in the maxilla and adjacent structures. Dental malocclusion correction through maxillary expansion has been shown to significantly increase the patency and decrease the airflow resistance in several airway compartments, ranging from the nares to the epiglottis plane.

Objectives. We aimed to assess the impact of treatment with a removable functional orthodontic appliance on the dimensions of selected sections of the upper respiratory tract in pediatric patients, with the goal of identifying the nasopharyngeal and oropharyngeal regions most susceptible to lateral maxillary and mandibular expansion.

Materials and methods. We retrospectively reviewed the medical records and lateral cephalometric radiographs (LCRs) of all consecutive pediatric patients with deciduous or mixed dentition treated with a functional appliance between 2014 and 2019 at a private orthodontic practice in Racibórz, Poland. To assess the impact of the study group and gender on the dependent variables, a Multivariate Analysis of Covariance (MANCOVA) was performed. The variable T1 (age at treatment initiation) was included as a covariate in the model to control for its potential effect on the outcomes.

Results. The treatment group comprised 55 patients, while 24 subjects served as the control group. In contrast to the nasopharyngeal variables, the average annual increase in the oropharyngeal linear measurements was significantly greater in the treatment group. For the gender factor, after applying the Benjamini–Hochberg correction, no statistically significant differences were observed in any of the assessed variables. In contrast, after correction, the covariate T1 was statistically significant for the following variables: CVM1 and CVM2 (skeletal age before treatment initiation and after treatment completion, respectively), and T2 (chronological age after treatment completion).

Conclusions. Although treatment with a removable functional appliance does not significantly impact the nasopharyngeal airspace, it significantly increases oropharyngeal dimensions, which may help reduce the future risk associated with abnormal breathing patterns in treated patients.

Key words: nasopharynx, cephalometric analysis, functional orthodontic treatment, oropharynx, malocclusion

Highlights

- Dental malocclusion correction through maxillary expansion has been shown to significantly increase the patency and decrease the airflow resistance of several airway compartments.
- Results of this study suggest that functional orthodontic treatment does not considerably impact the nasopharyngeal airspace measurements.
- Expansive treatment using a removable functional appliance significantly increases oropharyngeal dimensions, which might reduce the future risk associated with abnormal breathing patterns in treated patients.

Background

Upper airway obstruction, arising from allergic rhinitis, adenoid and tonsil hypertrophy, congenital nasal deformities, or polyps, has been outlined as a possible contributing factor to the development of dental malocclusion in adolescents.[1,2] Oral respiration pattern due to the nasal obstruction induces incorrect tongue positioning with the loss of its upward pressure on the palate, which hinders the proper development of the upper jaw, resulting in a narrower dental arch and subsequent teeth crowding.[3–5]

Long-term complications of not addressing maxillary and mandibular deficiencies at an early age include articulation disturbances, periodontal disorders, temporomandibular joint dysfunction, obstructive sleep apnea, and psychological sequelae associated with poor facial esthetics.[6] Therefore, many transverse abnormalities require conservative maxillary orthopedic correction during the growth period.[7] Interceptive orthodontic treatment, initiated during the deciduous or early mixed dentition phase,[8] may reduce the complexity of future procedures or even prevent the need for more complicated and costly interventions.[9]

Although several orthodontic treatment modalities have been introduced for maxillary and mandibular deficiencies,[10,11] early extraction of deciduous teeth in an attempt to reduce or avoid future malocclusion has been shown to neither decrease the need for further orthodontic treatment nor reduce its complexity or duration.[12] This has influenced the current trend toward more conservative, non-extraction management.[13]

Notably, the initiation of maxillary expansion before the pubertal peak results in significant long-term craniofacial changes at the skeletal level, both in the maxilla and adjacent structures, which are more pronounced than when intervention occurs during or slightly after the peak in skeletal growth.[14] Furthermore, maxillary expansion has been shown to significantly increase the dimensions of various airway compartments, from the nares to the epiglottis plane, contributing to decreased respiratory airway resistance.[13,15–18]

Objectives

The purpose of our study was to assess the impact of treatment with a removable functional orthodontic appliance on the dimensions of selected sections of the upper respiratory tract in pediatric patients, with the goal of identifying the nasopharyngeal and oropharyngeal regions most susceptible to lateral maxillary and mandibular expansion.

Materials and methods

This study was conducted in accordance with the principles of the Declaration of Helsinki. Due to its retrospective nature, institutional approval from the Ethics Committee was waived. Informed consent was obtained from all enrolled participants and their parents. The paper was prepared following the Strengthening the Reporting of Observational Studies in Epidemiology (STROBE) guidelines.[19]

Subjects

The data were collected retrospectively from the medical and dental history records and lateral cephalometric radiographs (LCRs) of all consecutive pediatric patients diagnosed and/or treated with a functional orthodontic appliance between 2014 and 2019 at a private orthodontic practice in Racibórz, Poland. The inclusion criteria were as follows: 1) deciduous or mixed dentition, 2) presence of at least two teeth distally and mesially from the canines, and 3) adequate radiographic documentation (2 good quality LCRs performed in the period of deciduous and/or mixed dentition). The exclusion criteria comprised: 1) previous head and neck surgeries, 2) presence of congenital craniofacial defects or facial cleft, 3) history of chronic airway/pulmonary diseases (e.g., asthma, chronic obstructive pulmonary disease), and 4) history of previous orthodontic treatment. The management plan included the treatment without extraction of permanent teeth in individuals with deciduous teeth without tremas (between incisors and upper canines, as well as canines and lower molars) and in patients with different forms of malocclusion in 3 planes with deciduous or mixed dentition. The treatment goal

constituted lateral expansion and optimization of shape development of the dental arches, as well as normal and/or optimal alignment of the mandible to the maxilla during this developmental period. The patients were offered two-stage orthodontic treatment: 1) with the functional ERCO appliance created according to the disign of the first author (Z.P.) and 2) with thin-arch fixed orthodontic appliances, correcting the position of the teeth. Patients who completed the first stage of treatment with the ERCO appliance and, according to the patients and their parents, strictly adhered to the orthodontic recommendations (appliance worn 24 h a day except for meals and oral hygiene procedures) were enrolled in the treatment group. The control group included all consecutive patients who had not started treatment with the ERCO appliance after diagnosis and attended regular orthodontic checkups during the study period.

Functional orthodontic appliance

The orthodontic ERCO appliance (Fig. 1) was created according to the design and treatment indications of the first author (Z.P.). The functional appliance was formed using a construction bite with a minimum vertical distance between the upper and lower dental arches (i.e., with the lack of contact of antagonistic teeth). In the sagittal dimension, occlusion was established by bringing upper and lower dental arches close to each other by a maximum of 1 premolar width. In the lateral position, the lower dental arch was placed so as to bring it closer to the mid-sagittal plane. The vertical zone separating the dental arches was filled with acrylic, which could be removed by the clinician. The appliance had 2 active elements, i.e., upper and lower screws, activated once a week. During treatment, the appliance was loosely fitted in the mouth.

Cephalometric analysis

All LCRs were taken using the same device (Vatech, Digital X-ray Imaging System; Voxel Dental Solutions, Houston, USA; PCH-2500, 85 kVp, 10 mA) under the same exposure conditions. Prior to imaging, patients were instructed to hold their heads in a natural position and look at their eyes in the mirror 250 cm away. Teeth were in central occlusion, while the lips and tongue were in the resting position. All subjects were instructed not to swallow saliva or move their heads during image acquisition. All LCRs were saved to a computer disk. The images were corrected for magnification, and a ruler with a scale was visible on the LCRs. The test measurement was performed using the ruler to ensure compatibility with the actual values. The measurements were scaled isotropically. Cephalometric measurements were obtained using DesignCAD software with the Orthodon-MPaluch program (Mateusz Paluch, Racibórz, Poland). The following cephalograms were analyzed: 1) the first diagnostic LCR taken before treatment in both the treatment and control groups, and 2) the second LCR taken after the last expander screw activation in the treatment group, and after the change in the treatment method prior to the insertion of the fixed appliance in the control group.

Figure 2 shows the main cephalometric landmarks used in the study. The definitions of the applied cephalometric landmarks and the variables they formed are presented in Table 1 and Table 2. Some of the landmarks and the variables were defined by the first author (Z.P.) and marked as "zp". In our experience, they can be used as a stable and reproducible alternative for already established points, which may not be clearly visible in many radiographs and might be affected by orthodontic teeth movements and bone

Fig. 1. ERCO appliance

Table 1. Cephalometric landmarks applied in the study

Cephalometric variable	Definition
PNS	the posterior nasal spine, the most posterior point on the hard palate
ANS	the apex of the anterior nasal spine
Me	the most inferior point on the mandibular symphysis in the median plane
Go	the most inferior point on the angle of the mandible representing the intersection of (1) the line tangent to the posterior outline of the ramus of the mandible and (2) the inferior border of the body of the mandible
S	the midpoint of the sella turcica
So	the midpoint of the Ba-S line
Ba	the most anterior point on the foramen magnum
Po	the most superior point of the outline of the external auditory meatus
Ar	the junction between the inferior surface of the cranial base and the posterior border of the ascending rami of the mandible
Go1	the most posterior inferior point on the tangent to the body of the mandible
Go2	the most posterior point on the tangent to the ramus of the mandible, near the angle of the mandible
tu (zp)	the most posterior superior point of the maxillary tuberosity, the deepest point on the anterior outline of the pterygopalatine fossa
Pt1 (zp)	the superior anterior point of the outline of the pterygopalatine fossa
Pt	the superior posterior point of the outline of the pterygopalatine fossa
Or	the most inferior point on the margin of the orbit
ad3	the point formed on the line from the PNS point towards the S point at the intersection with the posterior pharyngeal wall
ad2	the point formed on the line from the PNS point towards the So point at the intersection with the posterior pharyngeal wall
ad1	the point formed on the line from the PNS point towards the Ba point at the intersection with the posterior pharyngeal wall
UPW	the point formed on the line passing through the ANS and the PNS point at the intersection with the posterior pharyngeal wall
U	the most inferior posterior point at the tip of the soft palate
U1	the point on the mesial outline of the soft palate in its largest sagittal dimension
U2	the point on the distal outline of the soft palate in its largest sagittal dimension
TP (zp)	the point on the posterior pharyngeal wall at the intersection with the line passing through the U point, parallel to the line passing through the Po and Or points
MP (zp)	the point on the posterior border of the tongue at the intersection with the line passing through the Go point, parallel to the line passing through the Po and Or points
MM1 (zp)	the point on the posterior pharyngeal wall at the intersection with the line passing through the Et point, parallel to the line passing through the Po and Or points
Et	the superior tip of the epiglottis
Eb	the base of the epiglottis

Table 2. Cephalometric variables applied in the study

Cephalometric variable	Definition
Nasopharynx (zp)	the surface area of the nasopharynx on the lateral cephalometric radiograph – points delineate auxiliary lines, which are based on radiological anatomy: the inferior border forms a line between the PNS and UPW points; the posterior superior border: on the posterior pharyngeal wall from the UPW point upwards through the following points: ad2, ad3, Z4, Pt, Pt1; the anterior border: from the Pt1 point downwards along the anterior border of the pterygopalatine fossa to the tu point, and then connect to the PNS point
PNS-S	the distance from the PNS point to the S point
PNS-ad1	the dimension of the nasopharyngeal airspace, corresponding to the distance from the PNS point to the ad1 point
PNS-ad2	the dimension of the nasopharyngeal airspace, corresponding to the distance from the PNS point to the ad2 point
PNS-ad3	the dimension of the nasopharyngeal airspace, corresponding to the distance from the PNS point to the ad3 point
PNS-Ba	the distance from the PNS point to the Ba point
PNS-UPW	the dimension of the pharyngeal airspace, corresponding to the distance from the PNS point to the UPW point
McN-McN1	the distance between the posterior border of the upper half of the soft palate and the nearest point on the posterior pharyngeal wall
Oropharynx (zp)	the surface area of the oropharynx on the lateral cephalometric radiograph – points delineate auxiliary lines, which are based on radiological anatomy: the superior border forms a line between the PNS and UPW points; the anterior border: from the PNS point downwards on the posterior outline of the soft palate to the U point, from the U point connected perpendicularly with the posterior outline of the body of the tongue, then limited by the downward line along the posterior border of the body of the tongue to the MP point and connected to the Et point; the inferior border: the connection of the Et point with the MM1 point; the posterior border: from the MM1 point upwards through the LP and TP points, along the posterior border of the oropharyngeal airspace to the UPW point
MPW	middle pharyngeal wall, defined as the connection of the U and TP points, corresponding to the retropalatal airspace
MAS	middle airway space, defined as the connection of the MP and LP points, corresponding to the airspace between the posterior border of the body of the tongue and the posterior pharyngeal wall
U1-U2	the largest sagittal dimension of the soft palate measured on the line perpendicular to the line passing through the PNS and U points, corresponding to the soft palate thickness
PNS-U	the length of the soft palate on the line between the PNS and U points
VAL	the length of the pharynx on the line between the Eb and PNS points
Pal1	the anterior length of the entire pharynx, corresponding to the connection of the following cephalometric landmarks on the anterior pharyngeal wall: Eb, MP, U, and PNS
Pal2	the posterior length of the entire pharynx, corresponding to the connection of the following cephalometric landmarks on the posterior pharyngeal wall: MM1, LP, TP, UPW, ad1, ad2, ad3, and Z4

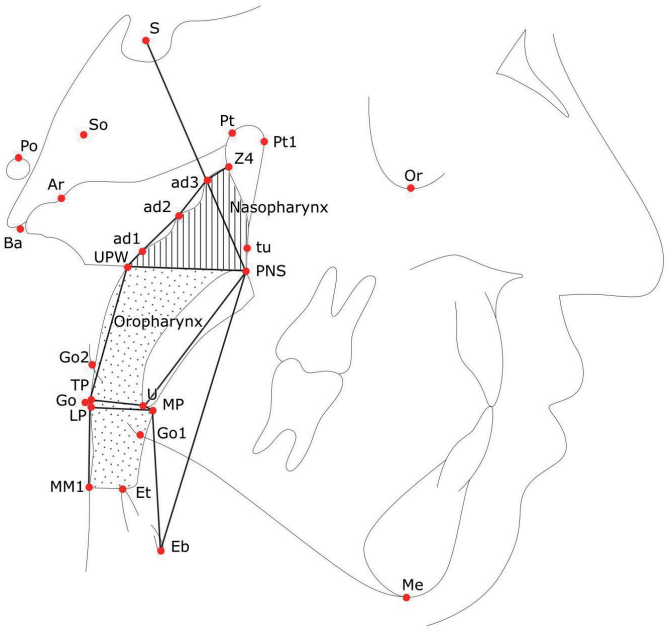

Fig. 2. Selected cephalometric landmarks, linear measurements, and airway areas used in the study – detailed definitions are presented in Tables 1,2

remodeling in relation to growth[20,21]. Landmarks were determined on all LCRs in the treatment and control groups. Subsequently, after 1 month, all landmarks were re-determined to eliminate intra-examiner variability. Craniofacial skeletal maturation was established according to the cervical vertebrae maturation (CVM) method.[22,23]

Statistical analyses

To assess the impact of the study group (study vs. control) and gender (female vs. male) on the dependent variables, a Multivariate Analysis of Covariance (MANCOVA) was conducted. The variable T1 (treatment initiation time) was included as a covariate in the model to control for its potential effect on the outcomes.

Before conducting the MANCOVA, the assumptions were verified. The normality of the dependent variables was assessed using the Shapiro–Wilk test. The homogeneity of covariance matrices was evaluated using Box's M test, while the homogeneity of variances within groups was tested with Levene's test.

If a significant MANCOVA effect was found, post-hoc ANCOVA tests were conducted for each dependent variable separately. The ANCOVA model included Group and Gender as factors and T1 as a covariate. Additionally, to control for the false discovery rate (FDR), the Benjamini–Hochberg procedure was applied. The p-values were sorted in ascending order and adjusted using the formula:, where "n" was the total number of tests, and "rank" was the position of the p-value in the ordered set. The adjusted p-values were then compared to an alpha threshold of 0.05 to determine significance after correction.

Results

The analysis included data from 79 patients (51 men and 28 women): 55 individuals (mean age 8.23 ±1.71 years) constituted the treatment group, while 24 patients (mean age 7.97 ±1.86 years) formed the control group. Detailed group sizes are presented in Table 3. Since this retrospective study included complete data for all participants, statistical analysis was conducted based on 2 LCRs obtained for each individual.

Table 3. Detailed sample sizes

Feature		Group		Total
		study	control	
Gender	male	37	14	51
	female	18	10	28
Total		55	24	79

Before conducting the MANCOVA analysis, the assumptions of this method were verified. The normality of the distribution of dependent variables was assessed using the Shapiro–Wilk test. The results indicated no significant deviations from normality for most variables. Given the general robustness of MANCOVA to violations of normality, the analysis was conducted without data transformation. The homogeneity of covariance matrices was assessed using Box's M test, which yielded $M = 85.47$, $F = 1.570$, $p = 0.002$. The homogeneity of variances within groups was evaluated using Levene's test, which indicated that the variances of 3 dependent variables differed significantly ($p < 0.05$). Consequently, Pillai's trace was used as the primary MANCOVA test statistic instead of Wilks' lambda.

The analysis revealed a significant effect of the experimental group (Group: treated vs control) on the dependent variables (Pillai's trace = 0.625, F(df1, df2) = 3.329, $p < 0.001$, $\eta^2 = 0.625$). The results of the between-subjects effects tests (Table 4) indicated that, before the Benjamini–Hochberg correction, significant differences between groups were observed for 6 variables: middle pharyngeal wall (MPW), corresponding to the retropalatal airspace, the posterior length of the entire pharynx (Pal2), the length of the pharynx (VAL), oropharynx (zp), the dimension of the pharyngeal airspace (PNS-UPW), and the anterior length of the entire pharynx (Pal1).

After applying the false discovery rate (FDR) correction, statistical significance was retained for only 3 variables: MPW ($p\_adj = 0.009$, $\eta^2 = 0.117$), Pal2 ($p\_adj = 0.007$, $\eta^2 = 0.138$), and VAL ($p\_adj < 0.001$, $\eta^2 = 0.154$). For the gender factor, significant differences were observed before correction for the variables CVM and middle airway space (MAS), but after correction, no variables remained significant. The group × gender interaction was not significant for any dependent variable. The covariate T1 (age at treatment

Table 4. Results of the tests of between-subject effects in ANCOVA

Dependent variable	Source	SS, type III	df	Mean square	F	p	p_adj	η_p^2
CVM1	corrected model	15.089	4	3.772	8.723	<0.001	–	0.320
	constant	0.416	1	0.416	0.962	0.330	–	0.013
	T1	12.712	1	12.712	29.396	<0.001	<0.001	0.284
	group	0.536	1	0.536	1.240	0.269	0.635	0.016
	gender	0.824	1	0.824	1.906	0.172	0.527	0.025
	group * gender	0.059	1	0.059	0.136	0.714	0.912	0.002
	error	32.000	74	0.432	–	–	–	–
	total	471.000	79	–	–	–	–	–
	corrected total	47.089	78	–	–	–	–	–
CVM2	corrected model	15.727	4	3.932	6.882	<0.001	–	0.271
	constant	2.798	1	2.798	4.897	0.030	–	0.062
	T1	15.571	1	15.571	27.258	<0.001	<0.001	0.269
	group	0.001	1	0.001	0.002	0.963	0.974	0.000
	gender	0.002	1	0.002	0.003	0.956	0.977	0.000
	group * gender	0.022	1	0.022	0.039	0.843	0.969	0.001
	error	42.273	74	0.571	–	–	–	–
	total	769.000	79	–	–	–	–	–
	corrected total	58.000	78	–	–	–	–	–
CVM	corrected model	1.263	4	0.316	2.238	0.073	–	0.108
	constant	0.131	1	0.131	0.930	0.338	–	0.012
	T1	0.279	1	0.279	1.976	0.164	0.520	0.026
	group	0.098	1	0.098	0.692	0.408	0.751	0.009
	gender	0.688	1	0.688	4.880	0.030	0.251	0.062
	group * gender	0.004	1	0.004	0.029	0.865	0.959	0.000
	error	10.438	74	0.141	–	–	–	–
	total	26.240	79	–	–	–	–	–
	corrected total	11.701	78	–	–	–	–	–
MAS	corrected model	11.233	4	2.808	1.442	0.229	–	0.072
	constant	0.496	1	0.496	0.255	0.615	–	0.003
	T1	0.027	1	0.027	0.014	0.907	0.959	0.000
	group	0.639	1	0.639	0.328	0.569	0.844	0.004
	gender	10.138	1	10.138	5.205	0.025	0.230	0.066
	group * gender	0.122	1	0.122	0.062	0.803	0.959	0.001
	error	144.130	74	1.948	–	–	–	–
	total	165.847	79	–	–	–	–	–
	corrected total	155.363	78	–	–	–	–	–
McN-McN1	corrected model	1.271	4	0.318	0.427	0.789	–	0.023
	constant	1.451	1	1.451	1.947	0.167	–	0.026
	T1	0.323	1	0.323	0.434	0.512	0.812	0.006
	group	0.560	1	0.560	0.752	0.389	0.761	0.010
	gender	0.164	1	0.164	0.220	0.640	0.879	0.003
	group * gender	0.004	1	0.004	0.005	0.944	0.976	0.000
	error	55.126	74	0.745	–	–	–	–
	total	136.690	79	–	–	–	–	–
	corrected total	56.397	78	–	–	–	–	–

Table 4. Results of the tests of between-subjects effects of the ANCOVA analysis – cont

Dependent variable	Source	SS, type III	df	Mean square	F	p	p_adj	η_p^2
MPW	corrected model	11.762	4	2.941	3.443	0.012	–	0.157
	constant	0.605	1	0.605	0.708	0.403	–	0.009
	T1	0.073	1	0.073	0.086	0.770	0.957	0.001
	group	8.408	1	8.408	9.843	0.002	0.031	0.117
	gender	2.362	1	2.362	2.765	0.101	0.404	0.036
	group * gender	0.478	1	0.478	0.560	0.457	0.809	0.008
	error	63.207	74	0.854	–	–	–	–
	total	77.371	79	–	–	–	–	–
	corrected total	74.969	78	–	–	–	–	–
Nasopharynx (zp)	corrected model	4236.518	4	1059.130	2.507	0.049	–	0.119
	constant	31.370	1	31.370	0.074	0.786	–	0.001
	T1	1753.157	1	1753.157	4.149	0.045	0.318	0.053
	group	1169.287	1	1169.287	2.767	0.100	0.418	0.036
	gender	968.316	1	968.316	2.292	0.134	0.514	0.030
	group * gender	724.528	1	724.528	1.715	0.194	0.541	0.023
	error	31268.311	74	422.545	–	–	–	–
	total	71560.307	79	–	–	–	–	–
	corrected total	35504.829	78	–	–	–	–	–
Oropharynx (zp)	corrected model	13467.719	4	3366.930	1.926	0.115	–	0.094
	constant	393.134	1	393.134	0.225	0.637	–	0.003
	T1	1240.647	1	1240.647	0.710	0.402	0.771	0.010
	group	9524.541	1	9524.541	5.449	0.022	0.253	0.069
	gender	1228.107	1	1228.107	0.703	0.405	0.760	0.009
	group * gender	1394.475	1	1394.475	0.798	0.375	0.750	0.011
	error	129339.959	74	1747.837	–	–	–	–
	total	224181.376	79	–	–	–	–	–
	corrected total	142807.678	78	–	–	–	–	–
Pal1	corrected model	28.483	4	7.121	1.555	0.195	–	0.078
	constant	7.105	1	7.105	1.551	0.217	–	0.021
	T1	1.984	1	1.984	0.433	0.512	0.798	0.006
	group	19.865	1	19.865	4.338	0.041	0.314	0.055
	gender	5.052	1	5.052	1.103	0.297	0.666	0.015
	group * gender	0.875	1	0.875	0.191	0.663	0.884	0.003
	error	338.870	74	4.579	–	–	–	–
	total	788.467	79	–	–	–	–	–
	corrected total	367.353	78	–	–	–	–	–
PNS-ad1	corrected model	1.761	4	0.440	0.239	0.916	–	0.013
	constant	0.108	1	0.108	0.059	0.809	–	0.001
	T1	0.609	1	0.609	0.330	0.567	0.855	0.004
	group	0.306	1	0.306	0.166	0.685	0.888	0.002
	gender	0.044	1	0.044	0.024	0.877	0.961	0.000
	group * gender	0.923	1	0.923	0.500	0.482	0.806	0.007
	error	136.438	74	1.844	–	–	–	–
	total	167.083	79	–	–	–	–	–
	corrected total	138.199	78	–	–	–	–	–

Table 4. Results of the tests of between-subject effects in ANCOVA – cont

Dependent variable	Source	SS, type III	df	Mean square	F	p	p_adj	η_p^2
PNS-ad2	corrected model	2.334	4	0.583	0.889	0.475	–	0.046
	constant	0.139	1	0.139	0.212	0.647	–	0.003
	T1	1.388	1	1.388	2.115	0.150	0.493	0.028
	group	0.302	1	0.302	0.460	0.500	0.821	0.006
	gender	0.702	1	0.702	1.069	0.305	0.668	0.014
	group * gender	0.020	1	0.020	0.030	0.863	0.968	0.000
	error	48.585	74	0.657	–	–	–	–
	total	105.006	79	–	–	–	–	–
	corrected total	50.919	78	–	–	–	–	–
PNS-ad3	corrected model	5.912	4	1.478	1.127	0.350	–	0.057
	constant	3.908	1	3.908	2.981	0.088	–	0.039
	T1	1.561	1	1.561	1.191	0.279	0.642	0.016
	group	2.987	1	2.987	2.278	0.135	0.497	0.030
	gender	0.320	1	0.320	0.244	0.623	0.868	0.003
	group * gender	0.041	1	0.041	0.031	0.860	0.977	0.000
	error	97.023	74	1.311	–	–	–	–
	total	109.958	79	–	–	–	–	–
	corrected total	102.935	78	–	–	–	–	–
PNS-Ba	corrected model	5.291	4	1.323	1.202	0.317	–	0.061
	constant	4.439	1	4.439	4.034	0.048	–	0.052
	T1	2.422	1	2.422	2.201	0.142	0.484	0.029
	group	0.304	1	0.304	0.276	0.601	0.864	0.004
	gender	0.718	1	0.718	0.653	0.422	0.761	0.009
	group * gender	2.456	1	2.456	2.232	0.139	0.492	0.029
	error	81.438	74	1.101	–	–	–	–
	total	93.669	79	–	–	–	–	–
	corrected total	86.729	78	–	–	–	–	–
PNS-S	corrected model	11.661	4	2.915	2.176	0.080	–	0.105
	constant	17.711	1	17.711	13.218	0.001	–	0.152
	T1	7.200	1	7.200	5.374	0.023	0.235	0.068
	group	0.077	1	0.077	0.058	0.811	0.944	0.001
	gender	1.239	1	1.239	0.924	0.339	0.709	0.012
	group * gender	3.901	1	3.901	2.912	0.092	0.423	0.038
	error	99.149	74	1.340	–	–	–	–
	total	166.423	79	–	–	–	–	–
	corrected total	110.810	78	–	–	–	–	–
PNS-UPW	corrected model	22.944	4	5.736	2.932	0.026	–	0.137
	constant	1.029	1	1.029	0.526	0.471	–	0.007
	T1	0.369	1	0.369	0.189	0.665	0.874	0.003
	group	11.599	1	11.599	5.929	0.017	0.223	0.074
	gender	6.621	1	6.621	3.384	0.070	0.429	0.044
	group * gender	2.829	1	2.829	1.446	0.233	0.579	0.019
	error	144.769	74	1.956	–	–	–	–
	total	232.627	79	–	–	–	–	–
	corrected total	167.713	78	–	–	–	–	–

Table 4. Results of the tests of between-subject effects in ANCOVA – cont

Dependent variable	Source	SS, type III	df	Mean square	F	p	p_adj	η_p^2
PNS-Z44	corrected model	6.761	4	1.690	1.536	0.201	–	0.077
	constant	2.956	1	2.956	2.686	0.105	–	0.035
	T1	0.238	1	0.238	0.216	0.643	0.870	0.003
	group	4.276	1	4.276	3.885	0.052	0.342	0.050
	gender	1.017	1	1.017	0.924	0.339	0.693	0.012
	group * gender	3.564	1	3.564	3.238	0.076	0.437	0.042
	error	81.437	74	1.101	–	–	–	–
	total	134.805	79	–	–	–	–	–
	corrected total	88.198	78	–	–	–	–	–
Pal2	corrected model	120.196	4	30.049	3.990	0.006	–	0.177
	constant	12.844	1	12.844	1.705	0.196	–	0.023
	T1	0.575	1	0.575	0.076	0.783	0.960	0.001
	group	89.577	1	89.577	11.893	0.001	0.018	0.138
	gender	14.045	1	14.045	1.865	0.176	0.522	0.025
	group * gender	7.128	1	7.128	0.946	0.334	0.715	0.013
	error	557.352	74	7.532	–	–	–	–
	total	1271.383	79	–	–	–	–	–
	corrected total	677.548	78	–	–	–	–	–
U-PNS	corrected model	9.126	4	2.281	1.806	0.137	–	0.089
	constant	0.074	1	0.074	0.059	0.810	–	0.001
	T1	0.317	1	0.317	0.251	0.618	0.875	0.003
	group	3.642	1	3.642	2.883	0.094	0.412	0.037
	gender	2.187	1	2.187	1.731	0.192	0.552	0.023
	group * gender	0.422	1	0.422	0.334	0.565	0.866	0.004
	error	93.494	74	1.263	–	–	–	–
	total	108.900	79	–	–	–	–	–
	corrected total	102.620	78	–	–	–	–	–
U1-U2	corrected model	0.437	4	0.109	0.210	0.932	–	0.011
	constant	0.179	1	0.179	0.344	0.559	–	0.005
	T1	0.064	1	0.064	0.124	0.726	0.915	0.002
	group	0.012	1	0.012	0.024	0.878	0.950	0.000
	gender	0.034	1	0.034	0.066	0.798	0.966	0.001
	group * gender	0.236	1	0.236	0.455	0.502	0.810	0.006
	error	38.478	74	0.520	–	–	–	–
	total	39.445	79	–	–	–	–	–
	corrected total	38.915	78	–	–	–	–	–
VAL	corrected model	47.002	4	11.750	3.597	0.010	–	0.163
	constant	8.536	1	8.536	2.613	0.110	–	0.034
	T1	0.205	1	0.205	0.063	0.803	0.947	0.001
	group	43.905	1	43.905	13.439	<0.001	<0.001	0.154
	gender	0.063	1	0.063	0.019	0.890	0.952	0.000
	group * gender	0.002	1	0.002	0.001	0.980	0.980	0.000
	error	241.765	74	3.267	–	–	–	–
	total	651.574	79	–	–	–	–	–
	corrected total	288.767	78	–	–	–	–	–

Table 4. Results of the tests of between-subject effects in ANCOVA – cont

Dependent variable	Source	SS, type III	df	Mean square	F	p	p_adj	η_p^2
T2	corrected model	210.843	4	52.711	97.877	<0.001	–	0.841
	constant	16.463	1	16.463	30.570	<0.001	–	0.292
	T1	208.366	1	208.366	386.906	<0.001	<0.001	0.839
	group	0.835	1	0.835	1.551	0.217	0.570	0.021
	gender	1.596	1	1.596	2.964	0.089	0.455	0.039
	group * gender	0.279	1	0.279	0.518	0.474	0.823	0.007
	error	39.852	74	0.539	–	–	–	–
	total	7908.914	79	–	–	–	–	–
	corrected total	250.696	78	–	–	–	–	–
Study duration	corrected model	3.515	4	0.879	1.631	0.175	–	0.081
	constant	16.468	1	16.468	30.569	<0.001	–	0.292
	T1	0.893	1	0.893	1.657	0.202	0.547	0.022
	group	0.834	1	0.834	1.549	0.217	0.555	0.021
	gender	1.597	1	1.597	2.964	0.089	0.431	0.039
	group * gender	0.279	1	0.279	0.517	0.474	0.808	0.007
	error	39.865	74	0.539	–	–	–	–
	total	268.555	79	–	–	–	–	–
	corrected total	43.379	78	–	–	–	–	–
Z4-Z44	corrected model	2.725	4	0.681	0.983	0.422	–	0.050
	constant	2.340E–5	1	2.340E–5	0.000	0.995	–	0.000
	T1	0.008	1	0.008	0.012	0.914	0.956	0.000
	group	0.219	1	0.219	0.316	0.576	0.841	0.004
	gender	2.155	1	2.155	3.110	0.082	0.444	0.040
	group * gender	0.881	1	0.881	1.271	0.263	0.637	0.017
	error	51.277	74	0.693	–	–	–	–
	total	54.142	79	–	–	–	–	–
	corrected total	54.002	78	–	–	–	–	–

SS – sum of squares; df – degree of freedom; F – between-groups variance divided by within-groups variance; p_adj – Benjamini–Hochberg adjusted p-value; η_p^2 – partial eta squared; CVM1 – skeletal age before treatment initiation according to the cervical vertebrae maturation method; CVM2 – skeletal age after completion of treatment with the functional appliance according to the cervical vertebrae maturation method; CVM – skeletal age according to the cervical vertebrae maturation method; MAS – middle airway space, defined as the connection of the MP and LP points, corresponding to the airspace between the posterior border of the body of the tongue and the posterior pharyngeal wall; McN-McN1 – the distance between the posterior border of the upper half of the soft palate and the nearest point on the posterior pharyngeal wall; MPW – the distance between the most inferior posterior point at the tip of the soft palate and the posterior pharyngeal wall, corresponding to the retropalatal airspace; nasopharynx (zp) – the surface area of the nasopharynx on the lateral cephalometric radiograph; oropharynx (zp) – the surface area of the oropharynx on the lateral cephalometric radiograph; Pal1 – the anterior length of the entire pharynx, corresponding to the connection of the following cephalometric landmarks on the anterior pharyngeal wall: Eb, MP, U, and PNS; PNS-ad1 – the dimension of the nasopharyngeal airspace, corresponding to the distance from the PNS point to the ad1 point; PNS-ad2 – the dimension of the nasopharyngeal airspace, corresponding to the distance from the PNS point to the ad2 point; PNS-ad3 – the dimension of the nasopharyngeal airspace, corresponding to the distance from the PNS point to the ad3 point; PNS-Ba – the distance from the PNS point to the Ba point; PNS-S – the distance from the PNS point to the S point; PNS-UPW – the dimension of the pharyngeal airspace, corresponding to the distance from the posterior nasal spine to the point formed on the line passing through the anterior and posterior nasal spine at the intersection with the posterior pharyngeal wall; PNS-Z4 – the distance from the PNS point to the Z44 point; Pal2 – the posterior length of the entire pharynx, corresponding to the connection of the following cephalometric landmarks on the posterior pharyngeal wall: MM1, LP, TP, UPW, ad1, ad2, ad3, and Z4; U-PNS – the length of the soft palate on the line between the PNS and U points; U1–U2 – the largest sagittal dimension of the soft palate measured on the line perpendicular to the line passing through the PNS and U points, corresponding to the soft palate thickness; VAL –the length of the pharynx on the line between the base of the epiglottis and posterior nasal spine; T1 – patient chronological age before treatment initiation; T2 – patient chronological age after treatment completion; study duration, length of study T2–T1; Z4–Z44 – the distance from the point at the intersection of the posterior wall of the nasal pharynx with the posterior outline of the pterygopalatine fossa to the point created on a straight line from the PNS point towards the Z4 point, at the intersection with the skull base.

Table 5. Adjusted p-values (Benjamini–Hochberg) for post-hoc ANCOVA comparisons

Source	T1	Group	Gender	Group * Gender
CVM1	<0.001	0.635	0.527	0.912
CVM2	<0.001	0.974	0.977	0.969
CVM	0.520	0.751	0.251	0.959
MAS	0.959	0.844	0.230	0.959
McN-McN1	0.812	0.761	0.879	0.976
MPW	0.957	0.031	0.404	0.809
Nasopharynx (zp)	0.318	0.418	0.514	0.541
Oropharynx (zp)	0.771	0.253	0.760	0.750
Pal1	0.798	0.314	0.666	0.884
PNS-ad1	0.855	0.888	0.961	0.806
PNS-ad2	0.493	0.821	0.668	0.968
PNS-ad3	0.642	0.497	0.868	0.977
PNS-Ba	0.484	0.864	0.761	0.492
PNS-S	0.235	0.944	0.709	0.423
PNS-UPW	0.874	0.223	0.429	0.579
PNS-Z44	0.870	0.342	0.693	0.437
Pal2	0.960	0.018	0.522	0.715
U-PNS	0.875	0.412	0.552	0.866
U1-U2	0.915	0.950	0.966	0.810
VAL	0.947	<0.001	0.952	0.980
T2	<0.001	0.570	0.455	0.823
Study duration	0.547	0.555	0.431	0.808
Z4-Z44	0.956	0.841	0.444	0.637

CVM1 – skeletal age before treatment initiation according to the cervical vertebrae maturation method; CVM2 – skeletal age after completion of treatment with the functional appliance according to the cervical vertebrae maturation method; CVM – skeletal age according to the cervical vertebrae maturation method; MAS – middle airway space, defined as the connection of the MP and LP points, corresponding to the airspace between the posterior border of the body of the tongue and the posterior pharyngeal wall; McN-McN1 – the distance between the posterior border of the upper half of the soft palate and the nearest point on the posterior pharyngeal wall; MPW – the distance between the most inferior posterior point at the tip of the soft palate and the posterior pharyngeal wall, corresponding to the retropalatal airspace; nasopharynx (zp) – the surface area of the nasopharynx on the lateral cephalometric radiograph; oropharynx (zp) – the surface area of the oropharynx on the lateral cephalometric radiograph; Pal1 – the anterior length of the entire pharynx, corresponding to the connection of the following cephalometric landmarks on the anterior pharyngeal wall: Eb, MP, U, and PNS; PNS-ad1 – the dimension of the nasopharyngeal airspace, corresponding to the distance from the PNS point to the ad1 point; PNS-ad2 – the dimension of the nasopharyngeal airspace, corresponding to the distance from the PNS point to the ad2 point; PNS-ad3 – the dimension of the nasopharyngeal airspace, corresponding to the distance from the PNS point to the ad3 point; PNS-Ba – the distance from the PNS point to the Ba point; PNS-S – the distance from the PNS point to the S point; PNS-UPW – the dimension of the pharyngeal airspace, corresponding to the distance from the posterior nasal spine to the point formed on the line passing through the anterior and posterior nasal spine at the intersection with the posterior pharyngeal wall; PNS-Z44 – the distance from the PNS point to the Z44 point; Pal2 – the posterior length of the entire pharynx, corresponding to the connection of the following cephalometric landmarks on the posterior pharyngeal wall: MM1, LP, TP, UPW, ad1, ad2, ad3, and Z4; U-PNS – the length of the soft palate on the line between the PNS and U points; U1–U2 – the largest sagittal dimension of the soft palate measured on the line perpendicular to the line passing through the PNS and U points, corresponding to the soft palate thickness; VAL – the length of the pharynx on the line between the base of the epiglottis and posterior nasal spine; T1 – patient chronological age before treatment initiation; T2 – patient chronological age after treatment completion; Z4-Z44 – the distance from the point at the intersection of the posterior wall of the nasal pharynx with the posterior outline of the pterygopalatine fossa to the point created on a straight line from the PNS point towards the Z4 point, at the intersection with the skull base.

initiation) was statistically significant for the following variables: skeletal age before treatment initiation (CVM1), skeletal age after treatment completion (CVM2), nasopharynx (zp), the distance between the posterior nasal spine and the midpoint of the sella turcica (PNS-S), and chronological age after treatment completion (T2). However, after applying the Benjamini–Hochberg correction, significance remained only for 3 variables: CVM1, CVM2, and T2. The results of the post-hoc ANCOVA with Benjamini–Hochberg correction are presented in Table 5. Box-and-whiskers plots illustrating the results are presented in Fig. 3,4.

Discussion

Oropharyngeal measurements

In the present study, the analysis of changes in upper airway variables on LCRs (taken in the sagittal plane) was conducted in patients where the primary therapeutic forces, due to the presence of 2 screws in the orthodontic appliance, were directed laterally, perpendicular to the sagittal plane. Notably, the MPW values increased significantly more in the treatment group, despite the main expansion forces acting in a plane different from the measurement direction. Our study results align with those presented in the report by Özbek et al., where, however, the forces used in the appliance acted in the anteroposterior direction, thus aligning with the plane of the LCRs.[24] In turn, Ulusoy et al. reported that although a statistically significant increase in the oropharyngeal area was observed in the treatment group during the retention period (after the active treatment phase with an appliance involving anteroposterior and vertical activation), the overall changes in the horizontal oropharyngeal measurements and the surface area of the oropharynx on LCRs did not differ significantly between the analyzed groups. These findings are in line with our observations.[25]

Among patients with sleep-disordered breathing, a retrognathic position of the mandible in relation to the cranial base is often observed, which predisposes to the narrowing of the pharyngeal airway passage.[26–28] The posteriorly positioned tongue and soft palate, which reduce the pharyngeal

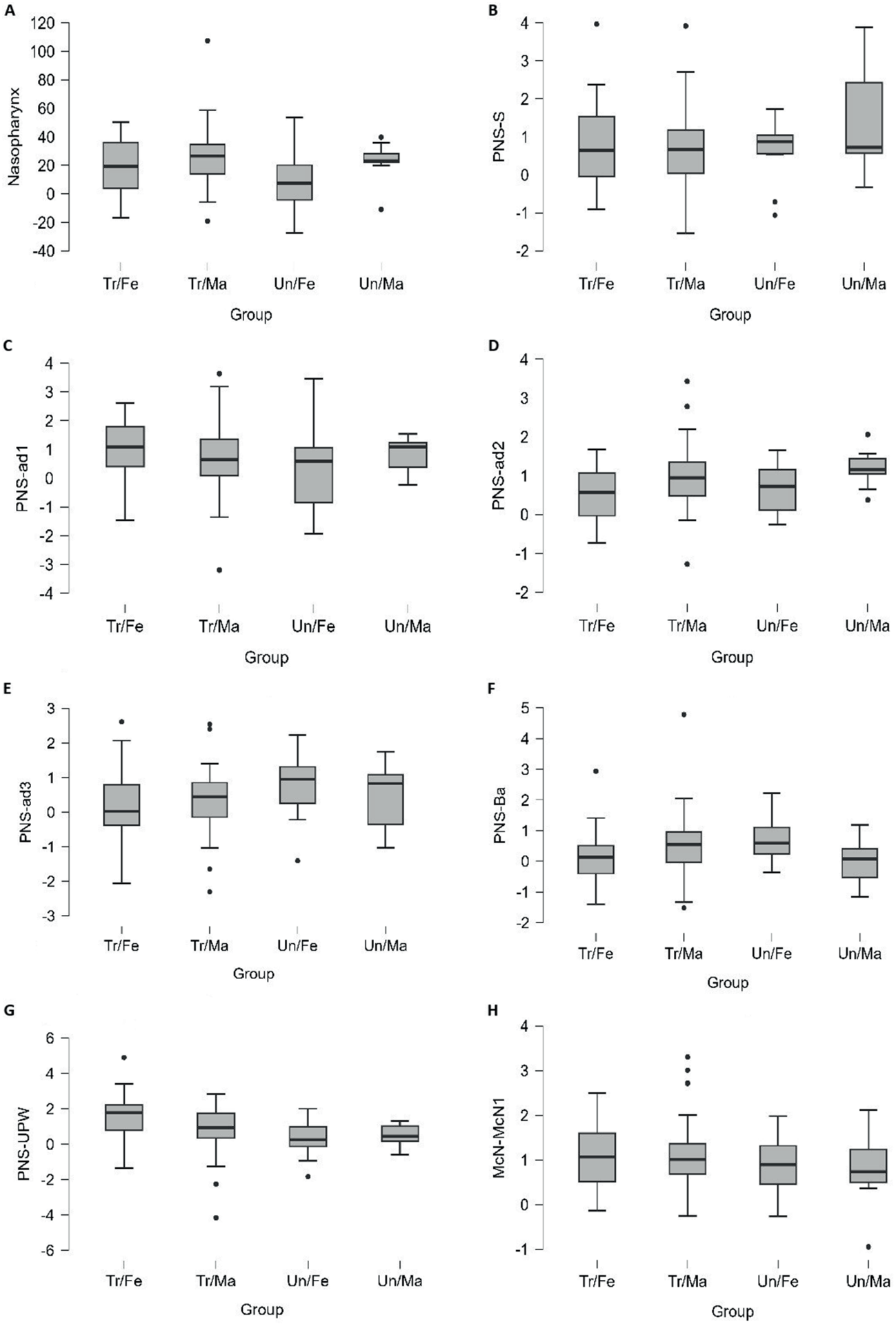

Fig. 3. Box-and-Whisker plots for the following variables: (A) Nasopharynx; (B) PNS-S; (C) PNS-ad1; (D) PNS-ad2; (E) PNS-ad3; (F) PNS-Ba; (G) PNS-UPW; (H) McN-McN1. Detailed definitions are presented in Table 1,2. Tr – study group; Un – control group; Fe – female; Ma – male.

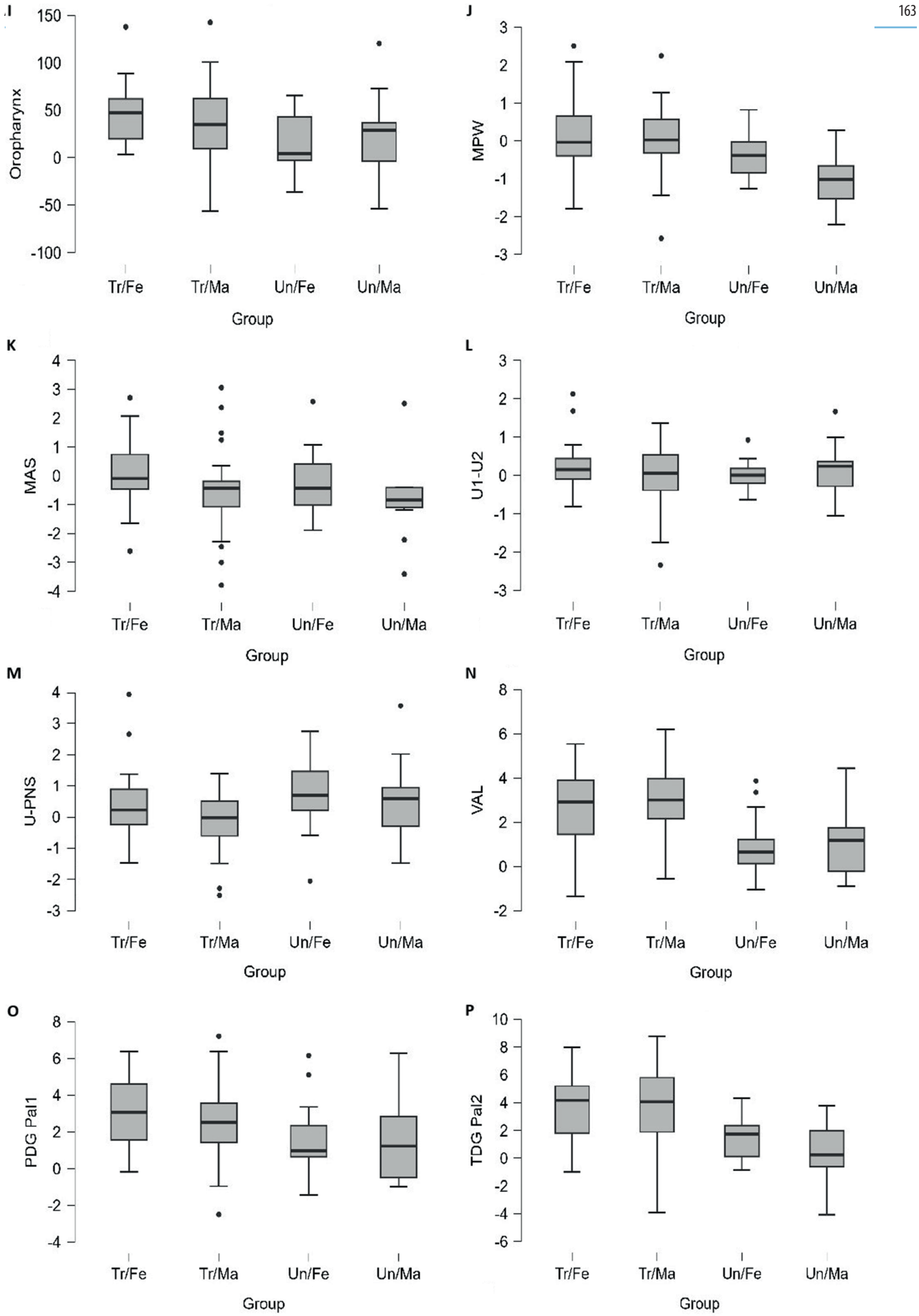

Fig. 4. Box-and-Whisker plots for the following variables: (I) Oropharynx; (J) MPW; (K) MAS; (L) U1-U2; (M) U-PNS; (N) VAL; (O) PDG-Pal1; (P) PDG-Pal2. Detailed definitions are presented in Table 1,2. Tr – study group; Un – control group; Fe – female; Ma – male.

dimensions early in life, may contribute to subsequent impaired respiratory function, snoring, upper airway resistance syndrome, and obstructive sleep apnea.[26,27,29] Concurrent soft tissue changes, attributable to age, obesity, and genetic background, further reduce the oropharyngeal airway.[27] The observed MPW increase following treatment (reflecting the enlargement of the oropharynx depth)[26,27] might be attributed to the mandibular advancement caused by the functional appliances, influencing the position of the hyoid bone and, consequently, leading to the forward relocation of the tongue.[26,27] Since changes in pharyngeal dimensions following functional appliance therapy have been reported to be maintained in the long term, such management may help prevent adaptive changes in the upper airway, thereby potentially influencing the risk of obstructive sleep apnea development later in life.[26,30,31]

Before the functional treatment in patients with mandibular retrognathism, the backward position of the tongue tends to press the soft palate, which leads to a decrease in its thickness, with a concurrent increase in its length and inclination.[26,27] Despite the lack of statistically significant differences in soft palate thickness between the treatment and control groups, we observed a lower average annual increase in soft palate length after expansion treatment. In contrast, Ghodke et al. found a tendency toward improvements in soft palate length, thickness, and inclination after mandibular retrusion correction, with the change in inclination reaching statistical significance.[26] Similarly, Jena et al. observed significant improvements in the adaptation of the soft palate (i.e., an increase in its thickness with a concurrent decrease in its length and inclination) following the treatment of Class II malocclusion using functional appliances. After treatment with a twin-block appliance, the soft palate measurements were found to align with the values seen in healthy controls.[27] Therefore, the positive impact of functional treatment on airway dimensions cannot be attributed solely to the induced skeletal changes but also to the increased genioglossal muscle tone and soft tissue adaptations resulting from the forward positioning of the mandible during treatment.[27,30]

Nasopharyngeal measurements

Contrary to the oropharyngeal variables, we observed that the linear measurements and the surface area of the nasopharynx did not differ significantly between the treatment group and the controls. Similarly, several authors have reported no significant differences in nasopharyngeal measurements when compared with the control group in both the short and long term, despite the favorable alterations in the nasopharyngeal area induced by functional treatment.[25] Therefore, it has been postulated that the growth of the nasopharynx occurs independently of functional appliance treatment, and that nasopharyngeal dimensions may not be influenced by mandibular-sagittal changes but rather by sphenoid wing expansion and the forward sliding of the palate.[27,32] Furthermore, the lack of significant differences was found to be partially attributed to the age of patients at the initiation of functional treatment (beginning of pubertal growth), and thus, no expected alterations in airway size related to the growth process were observed, as the airway capacity was already adequate.[25] Additionally, it has been hypothesized that a more pronounced advancement in airway dimensions could have been observed in patients with retrognathic facial structures or breathing-related sleep disorders, due to their more significant intrinsic stimulus to increase airway capacity.[25] Moreover, the values of the nasopharyngeal measurements on LCRs may be associated with the physiological development pattern of the adenoid tissue, which continues to grow until puberty, followed by a gradual decline.[25,33]

Limitations

The study's limitations include its retrospective design and the use of conventional LCRs in the evaluation of airway spaces, which precluded a detailed multiplanar analysis of the dentomaxillofacial complex. Nevertheless, LCRs are still routinely used in orthodontic practice and, in most conservative treatment cases, serve as a sufficient tool for monitoring growth and conducting accurate treatment progress assessments.[24–27] Since a positive correlation between linear naso- and oropharyngeal cephalometric measurements and the corresponding pharyngeal volume in cone beam computed tomography (CBCT) exams has been described, it becomes even more critical to strictly adhere to the directive of limiting radiation exposure in pediatric patients to the greatest extent possible and to fully justify the acquisition of CBCT scans in routine orthodontic practice.[34–38]

Furthermore, in our study, the division of the treatment and control groups according to skeletal classifications (regarding the anteroposterior relationship between the maxilla and mandible) was not implemented. Mislik et al. found only a few weak correlations between the "p" distance (the shortest distance between the soft palate and the posterior pharyngeal wall) and the "t" distance (the shortest distance between the tongue and the posterior pharyngeal wall) to various cephalometric landmarks with no significant correlations to the angle of the mandible or skeletal class.[39] Additionally, Alves et al. reported no significant correlations between the ANB (the cephalometric parameter of choice for assessing the anteroposterior relationship between the maxilla and mandible) angle (formed between the most concave point of the anterior maxilla, nasion, and the most concave point on mandibular symphysis) and pharyngeal linear and surface measurements.[40] Nevertheless, since discrepancies in pharyngeal airway dimensions depending on the mandibular position have been observed, the implementation of skeletal classifications might have been valuable in interpreting the results.[41]

Moreover, the study's retrospective nature precluded the analysis of confounding factors (such as initial malocclusion severity and patient compliance) on the functional treatment outcomes. Additionally, the presented results should be interpreted with caution due to the lack of long-term follow-up data, which would help define the ultimate sequelae following treatment with the ERCO appliance. Future studies evaluating larger patient cohorts, including those treated during the early permanent dentition phase, and with a more extended follow-up period (e.g., during the retention phase after the active treatment phase) are highly warranted.

Conclusions

Expansive treatment using a removable functional appliance in children during the deciduous or mixed dentition phase does not significantly impact nasopharyngeal airspace dimensions. In contrast, lateral expansion of the maxilla and mandible with the functional appliance significantly increases the oropharyngeal airspace dimensions in the sagittal plane, which may reduce the future risk associated with abnormal breathing patterns in these patients.

Data availability

The datasets supporting the findings of the current study are openly available at https://doi.org/10.5281/zenodo.15126951. The package includes the following files:

Consent for publication

Not applicable

ORCID iDs

Marta Rogalska https://orcid.org/0000-0001-5848-9564
Michał Szlęzak https://orcid.org/0000-0002-9362-8424
Katarzyna Miśkiewicz-Orczyk https://orcid.org/0000-0001-8088-3437
Wojciech Domka https://orcid.org/0000-0003-4429-7638
Maciej Misiołek https://orcid.org/0000-0002-8476-9153

References

1. Abe M, Mitani A, Yao A, Zong L, Hoshi K, Yanagimoto S. Awareness of malocclusion is closely associated with allergic rhinitis, asthma, and arrhythmia in late adolescents. *Healthcare*. 2020;8(3):209. doi:10.3390/healthcare8030209
2. D'Onofrio L. Oral dysfunction as a cause of malocclusion. *Orthod Craniofacial Res*. 2019;22(Suppl 1):43–48. doi:10.1111/ocr.12277
3. Farronato M, Lanteri V, Fama A, Maspero C. Correlation between malocclusion and allergic rhinitis in pediatric patients: A systematic review. *Children*. 2020;7(12):260. doi:10.3390/children7120260
4. Deshkar M, Thosar NR, Kabra SP, Yeluri R, Rathi NV. The influence of the tongue on the development of dental malocclusion. *Cureus*. 2024;16(5):e61281. doi:10.7759/cureus.61281
5. Kuskonmaz CS, Bruno G, Bartolucci ML, Basilicata M, Gracco A, De Stefani A. Correlation between malocclusions, tonsillar grading and Mallampati Modified Scale: A retrospective observational study. *Children*. 2023;10(6):1061. doi:10.3390/children10061061
6. Ruhl CM, Bellian KT, Van Meter BH, Hoard MA, Pham CD, Edlich RF. Diagnosis, complications, and treatment of dentoskeletal malocclusion. *Am J Emerg Med*. 1994;12(1):98–104. doi:10.1016/0735-6757(94)90213-5
7. Ricketts RM, Grummons D. Frontal cephalometrics: Practical applications, part 1. *World J Orthod*. 2003;4:297–316. https://mr.cdn.ignitecdn.com/client_assets/healthconnectionsdentistry_com/media/themes/files/Frontal-Cephalometrics-1.pdf.
8. Leighton BC. The value of prophecy in orthodontics. *Trans Br Soc Study Orthod*. 1970;57:1–14. PMID:5293289.
9. Schneider-Moser UEM, Moser L. Very early orthodontic treatment: when, why and how? *Dental Press J Orthod*. 2022;27(2):e22spe2. doi:10.1590/2177-6709.27.2.e22spe2
10. Jerrold L, Accornero M, Chay C. The extraction of teeth. Part 2: Considerations regarding which teeth to extract. *Semin Orthod*. 2019;25(4):318–322. doi:10.1053/j.sodo.2019.10.002
11. Tang H, Liu P, Liu X, et al. Skeletal width changes after mini-implant–assisted rapid maxillary expansion (MARME) in young adults. *Angle Orthod*. 2021;91(3):301–306. doi:10.2319/052920-491.1
12. Aljabab MA, Algharbi M, Huggare J, Bazargani F. Impact of early extraction of the deciduous canine on relief of severe crowding. *Angle Orthod*. 2021;91(6):743–748. doi:10.2319/020621-109.1
13. Görgülü S, Gokce SM, Olmez H, Sagdic D, Ors F. Nasal cavity volume changes after rapid maxillary expansion in adolescents evaluated with 3-dimensional simulation and modeling programs. *Am J Orthod Dentofacial Orthop*. 2011;140(5):633–640. doi:10.1016/j.ajodo.2010.12.020
14. Baccetti T, Franchi L, Cameron CG, McNamara JA. Treatment timing for rapid maxillary expansion. *Angle Orthod*. 2001;71(5):343–350. PMID:11605867.
15. Buck LM, Dalci O, Darendeliler MA, Papageorgiou SN, Papadopoulou AK. Volumetric upper airway changes after rapid maxillary expansion: A systematic review and meta-analysis. *Eur J Orthod*. 2016;39(5):463–473. doi:10.1093/ejo/cjw048
16. Kim SY, Park YC, Lee KJ, et al. Assessment of changes in the nasal airway after nonsurgical miniscrew-assisted rapid maxillary expansion in young adults. *Angle Orthod*. 2018;88(4):435–441. doi:10.2319/092917-656.1
17. Fastuca R, Perinetti G, Zecca PA, Nucera R, Caprioglio A. Airway compartments volume and oxygen saturation changes after rapid maxillary expansion: A longitudinal correlation study. *Angle Orthod*. 2015;85(6):955–961. doi:10.2319/072014-504.1
18. Bicakci AA, Agar U, Sökücü O, Babacan H, Doruk C. Nasal airway changes due to rapid maxillary expansion timing. *Angle Orthod*. 2005;75(1):1–6. PMID:15747808.
19. Von Elm E, Altman DG, Egger M, Pocock SJ, Gøtzsche PC, Vandenbroucke JP. The Strengthening the Reporting of Observational Studies in Epidemiology (STROBE) statement: Guidelines for reporting observational studies. *Lancet*. 2007;370(9596):1453–1457. doi:10.1016/S0140-6736(07)61602-X
20. Bishnoi A, Kamat NV. New method to assess sagittal jaw position: TWM and TWG angles. A cephalometric study. *J Indian Orthod Soc*. 2023;57(4):286–291. doi:10.1177/03015742231188207
21. Kotuła J, Kuc AE, Lis J, Kawala B, Sarul M. New sagittal and vertical cephalometric analysis methods: A systematic review. *Diagnostics*. 2022;12(7):1723. doi:10.3390/diagnostics12071723
22. Baccetti T, Franchi L, McNamara JA. The cervical vertebral maturation (CVM) method for the assessment of optimal treatment timing in dentofacial orthopedics. *Semin Orthod*. 2005;11(3):119–129. doi:10.1053/j.sodo.2005.04.005
23. McNamara JA, Franchi L. The cervical vertebral maturation method: A user's guide. *Angle Orthod*. 2018;88(2):133–143. doi:10.2319/111517-787.1
24. Ozbek MM, Memikoglu TU, Gögen H, Lowe AA, Baspinar E. Oropharyngeal airway dimensions and functional-orthopedic treatment in skeletal class II cases. *Angle Orthod*. 1998;68(4):327–336. PMID:9709833.
25. Ulusoy C, Canigur Bavbek N, Tuncer BB, Tuncer C, Turkoz C, Gencturk Z. Evaluation of airway dimensions and changes in hyoid bone position following class II functional therapy with activator. *Acta Odontol Scand*. 2014;72(8):917–925. doi:10.3109/00016357.2014.923109
26. Ghodke S, Utreja AK, Singh SP, Jena AK. Effects of twin-block appliance on the anatomy of pharyngeal airway passage (PAP) in class II malocclusion subjects. *Prog Orthod*. 2014;15(1):68. doi:10.1186/s40510-014-0068-3
27. Jena AK, Singh SP, Utreja AK. Effectiveness of twin-block and Mandibular Protraction Appliance-IV in the improvement of pharyngeal airway passage dimensions in class II malocclusion subjects with a retrognathic mandible. *Angle Orthod*. 2013;83(4):728–734. doi:10.2319/083112-702.1

28. Arens R, Marcus CL. Pathophysiology of upper airway obstruction: A developmental perspective. *Sleep*. 2004;27(5):997–1019. doi:10.1093/sleep/27.5.997
29. Ozbek M, Miyamoto K, Lowe AA, Fleetham JA. Natural head posture, upper airway morphology and obstructive sleep apnoea severity in adults. *Eur J Orthod*. 1998;20(2):133–143. doi:10.1093/ejo/20.2.133
30. Hänggi MP, Teuscher UM, Roos M, Peltomaki TA. Long-term changes in pharyngeal airway dimensions following activator-headgear and fixed appliance treatment. *Eur J Orthod*. 2008;30(6):598–605. doi:10.1093/ejo/cjn055
31. Rosenberger HC. XXXVII. Growth and development of the naso-respiratory area in childhood. *Ann Otol Rhinol Laryngol*. 1934;43(2):495–512. doi:10.1177/000348943404300213
32. Yassaei S, Tabatabaei Z, Ghafurifard R. Stability of pharyngeal airway dimensions: Tongue and hyoid changes after treatment with a functional appliance. *Int J Orthod Milwaukee*. 2012;23(1):9–15. PMID:22533023.
33. Preston CB, Tobias PV, Salem OH. Skeletal age and growth of the nasopharynx in the sagittal plane: A cephalometric study. *Semin Orthod*. 2004;10(1):16–38. doi:10.1053/j.sodo.2003.10.002
34. Gul Amuk N, Kurt G, Baysal A, Turker G. Changes in pharyngeal airway dimensions following incremental and maximum bite advancement during Herbst-rapid palatal expander appliance therapy in late adolescent and young adult patients: A randomized non-controlled prospective clinical study. *Eur J Orthod*. 2019;41(3):322–330. doi:10.1093/ejo/cjz011
35. Abdelkarim AA. Appropriate use of ionizing radiation in orthodontic practice and research. *Am J Orthod Dentofacial Orthop*. 2015;147(2):166–168. doi:10.1016/j.ajodo.2014.11.010
36. Zamora N, Llamas JM, Cibrián R, Gandia JL, Paredes V. Cephalometric measurements from 3D reconstructed images compared with conventional 2D images. *Angle Orthod*. 2011;81(5):856–864. doi:10.2319/121210-717.1
37. Vizzotto MB, Liedke GS, Delamare EL, Silveira HD, Dutra V, Silveira HE. A comparative study of lateral cephalograms and cone-beam computed tomographic images in upper airway assessment. *Eur J Orthod*. 2012;34(3):390–393. doi:10.1093/ejo/cjr012
38. Martins LS, Liedke GS, Heraldo LDDS, et al. Airway volume analysis: Is there a correlation between two and three-dimensions? *Eur J Orthod*. 2018;40(3):262–267. doi:10.1093/ejo/cjx067
39. Mislik B, Hanggi MP, Signorelli L, Peltomaki TA, Patcas R. Pharyngeal airway dimensions: A cephalometric, growth-study-based analysis of physiological variations in children aged 6–17. *Eur J Orthod*. 2014;36(3):331–339. doi:10.1093/ejo/cjt068
40. Alves M, Franzotti ES, Baratieri C, Nunes LKF, Nojima LI, Ruellas ACO. Evaluation of pharyngeal airway space amongst different skeletal patterns. *Int J Oral Maxillofac Surg*. 2012;41(7):814–819. doi:10.1016/j.ijom.2012.01.015
41. Paul P, Thakur A, Mathur A, Chitra P. Airway dimensions and mandibular position in adults with different growth patterns: A cone-beam computed tomography study. *J Stomatol*. 2022;75(2):87–92. doi:10.5114/jos.2022.117340

Cornelia de Lange syndrome: What should a dermatologist know?

Omar Shahada[1,A–D,F], Ahmed Kurdi[1,A–C,E,F], Lujain Alrohaily[2,A,C,E,F], Ohoud Alahmadi[3,A,B,D,E], Abdulrahman Tashkandi[4,D–F], Taif Aloufi[4,D–F], Wateen Alloqmani[5,D–F]

[1] Department of Dermatology, King Salman bin Abdulaziz Medical City, Medina, Saudi Arabia
[2] General practitioner, King Salman bin Abdulaziz Medical City, Medina, Saudi Arabia
[3] General practitioner, Ministry of Health, Medina, Saudi Arabia
[4] Department of Pediatrics, King Salman bin Abdulaziz Medical City, Medina, Saudi Arabia
[5] College of Medicine, Alrayan Colleges, Medina, Saudi Arabia

A – research concept and design; B – collection and/or assembly of data; C – data analysis and interpretation; D – writing the article; E – critical revision of the article; F – final approval of the article

Advances in Clinical and Experimental Medicine, ISSN 1899–5276 (print), ISSN 2451–2680 (online) *Adv Clin Exp Med*. 2026;35(1):167–174

Address for correspondence
Lujain Alrohaily
E-mail: lujain.sami44@gmail.com

Funding sources
None declared

Conflict of interest
None declared

Received on November 8, 2024
Reviewed on January 20, 2025
Accepted on February 14, 2025

Published online on January 7, 2026

Abstract

Cornelia de Lange syndrome (CdLS) is a complex genetic disorder affecting multiple body systems. It is characterized by distinctive facial features, skeletal anomalies, neurological and developmental impairments, physiological cutaneous manifestations such as hirsutism and synophrys, and numerous other signs and symptoms. Among affected individuals, the clinical presentation of CdLS varies widely, ranging from relatively mild to severe forms. Additionally, CdLS increases the frequency of certain dermatoses, including cutaneous bacterial infections and idiopathic thrombocytopenic purpura. Six genes have been identified in association with CdLS: *NIPBL* (Nipped-B-like protein), *RAD21* (double-strand break repair protein rad21 homolog), *SMC1A* and *SMC3* (structural maintenance of chromosomes 1A and 3), *BRD4* (bromodomain-containing protein 4), and *HDAC8* (histone deacetylase 8). Cornelia de Lange syndrome is estimated to occur in 1 out of every 10,000–30,000 live births, making it a rare condition and posing diagnostic challenges due to its low incidence. The present review aims to raise awareness of CdLS among dermatologists by providing a brief overview of the syndrome and summarizing the current literature on its dermatological manifestations.

Key words: dermatology, genetics, pediatrics

Cite as
Shahada O, Kurdi A, Alrohaily L, et al. Cornelia de Lange syndrome: What should a dermatologist know? *Adv Clin Exp Med*. 2026;35(1):167–174. doi:10.17219/acem/201419

DOI
10.17219/acem/201419

Highlights

- Cornelia de Lange Syndrome (CdLS) is caused by genetic variations in the cohesin complex.
- Given the variety of symptoms, recognizing the characteristic dermatological features of CdLS is essential for early diagnosis.
- Cutaneous manifestations in CdLS include hirsutism, synophrys and cutis verticis gyrate, which can affect patients' psychosocial wellbeing.
- As self-injury is also common in individuals with CdLS, support groups and psychological counseling should be included in comprehensive care.

Introduction

Cornelia de Lange syndrome (CdLS) is an uncommon and complicated genetic illness characterized by unusual facial traits, developmental delays, limb abnormalities, and several systemic abnormalities.[1,2] Cornelia de Lange Syndrome, initially recognized by Brachmann in 1916 and later named by Cornelia de Lange in 1933, affects approx. 1 in every 10,000–30,000 live births.[3,4] The disorder has been related to genetic differences in the cohesin complex, particularly mutations in 6 genes: *NIPBL*, *RAD21*, *SMC1A*, *SMC3*, *BRD4*, and *HDAC8*.[5–7] These genes play critical roles in chromatin organization, gene expression, and DNA repair. This underscores the causes of the effects of CdLS on various physiological systems.[7,8] Despite their potential relevance for diagnosis and therapeutic management, the dermatological aspects of CdLS have received limited attention in recent research, creating a vacuum in our understanding of the wide range of clinical symptoms of this condition.

Previous research has primarily focused on the developmental, neurological and systemic features of the disease, with dermatological symptoms being highlighted as secondary findings. In the early 1960s and 1970s, investigators described the physical characteristics associated with CdLS, including hirsutism – specifically referring to excessive male-pattern hair growth in women – and hypertrichosis, which describes excessive hair growth in any area, regardless of pattern or gender.

In CdLS, both conditions may be present, with hypertrichosis being more common.[9,10] This study established a framework for understanding the dermatological features of CdLS, although this was constrained by the diagnostic tools available at the time. Additional studies have helped us understand the genetic foundation and clinical presentation of CdLS. A groundbreaking research by Krantz et al. and Tonkin et al. identified *NIPBL* as the first gene related to CdLS.[11,12]

Unfortunately, there is a conspicuous lack of thorough and up-to-date research on dermatological signs of CdLS. While some studies have examined skin symptoms, including cutis marmorata telangiectatic congenita and abnormal dermatoglyphics, studies on the dermatological characteristics of patients with CdLS are limited.[13,14] Kline et al. conducted a detailed clinical examination of CdLS; however, their primary focus was not on its dermatological aspects.[15] The absence of expertise in this field is especially concerning, because skin symptoms can be pivotal for detecting uncommon genetic disorders and impact treatment and general wellbeing of the patients.

New research highlighted the varied appearances of CdLS, underlining the significance of recognizing milder versions of the disorder.[16] Boyle et al. provided valuable insights into the incidence of self-injurious behaviors in CdLS, which might influence the skin.[2] However, previous studies have not adequately examined the numerous skin symptoms observed in people with CdLS.

Objectives

The objectives of this work are to provide an overview of CdLS and to recognize its cutaneous manifestations.

Methods

Our literature search was conducted using PubMed, Cochrane Library, Scopus, Web of Science, and Google Scholar databases, spanning from 1963 to May 2022. All photographs presented in this manuscript are from the authors' own clinical collections and were obtained with appropriate patient consent. The primary search term used in the literature review was "CdLS."A literature review identified all studies that addressed the clinical features of CdLS. All studies discussing the dermatological aspects of this syndrome were selected. Publications discussing the genetic background of this syndrome were also included.

Review

Overview of CdLS

Cornelia de Lange syndrome is a developmental multisystem disorder with variable physical, cognitive, and behavioral characteristics.[17] This prevalence is probably

underestimated, because milder or atypical cases may not have been diagnosed. This syndrome affects both genders equally.[18]

Clinical case illustration

A 6-year-old female patients presented with characteristic facial features, including synophrys and long eyelashes, accompanied by generalized hypertrichosis. The patient showed a low anterior hairline with thick, dark hair and distinctive facial features, including arched eyebrows that met in the midline (synophrys). Generalized hypertrichosis was noted, particularly prominent on the back and extremities. Initial dermatological examination led to suspicion of CdLS, which was subsequently confirmed through genetic testing. This case illustrates how recognition of characteristic dermatological features can facilitate early diagnosis of CdLS.

Genetic background

The etiology of CdLS has been elucidated through molecular investigations of genetic variants affecting the cohesin complex. To date, 6 genes have been implicated: nipped-B-like protein (NIPBL), double-strand break repair protein rad21 homolog (RAD21), structural maintenance of chromosomes 1A (SMC1A) and 3 (SMC3), bromodomain-containing protein 4 (BRD4), and histone deacetylase 8 (HDAC8).. Mutations in the *NIPBL* gene were associated with 50–60% of cases.[17]

The cohesin complex and its associated regulatory proteins help to contact sequence elements and regulate gene expression. In addition to gene expression regulation, the cohesin complex plays a role in sister chromatid cohesion and DNA damage signaling and repair.[17]

Cornelia de Lange syndrome has an autosomal dominant familial or X-linked pattern of inheritance. Nonetheless, most cases result from de novo heterozygous mutations in patients with no family history of CdLS.[17]

Classification

Cornelia de Lange syndrome can be categorized into 3 types based on clinical variability. Type I, the classic form, is characterized by distinctive facial features and significant skeletal abnormalities. Type II, the mild form, presents with typical facial features accompanied by milder skeletal anomalies. Type III refers to cases where CdLS-like phenotypic manifestations are observed either in the presence of chromosomal aneuploidies or following teratogenic exposure. The classic features of CdLS include distinctive craniofacial characteristics, limb anomalies, growth retardation, and intellectual disability.. Additional features include cutaneous manifestations, gastrointestinal disorders, genitourinary malformations, and cardiovascular defects.[17]

Cutaneous manifestations of De Lange syndrome

Hirsutism and hypertrichosis

Hirsutism and hypertrichosis are prominent and typical features of CdLS, observed in most patients (80%).[18] Although hirsutism does not necessarily require treatment, it may affect patients' psychological wellbeing. Therefore, rather than the amount of hair growth, the subjective perception of the patient should be the deciding factor when determining whether the patient needs treatment.[19]

Hypertrichosis in CdLS is typically generalized, with particularly prominent involvement of the nape of the neck, the lateral aspects of the elbows, and the lower sacral area (Fig. 1).[20] Scalp hair is often characterized by low frontal hair implantation and a low posterior hairline, observed in approx. 92% of patients. Additionally, individuals with CdLS tend to have thick scalp hair that frequently extends into the temporal regions.[2] Eyelashes are long and curly in 99% of patients (Fig. 1).[20] The eyebrows are neat, well-penciled, arched, and thick. Moreover, patients almost always have synophry, which is the fusion of the eyebrows above the bridge of the nose (Fig. 2).[21]

Dark hair color

Cornelia de Lange syndrome tends to be associated with dark hair and eyebrows due to a disturbance in hair pigmentation (Fig. 2). However, there has been no evidence of pigmentation disorders in the skin or eyes.[21,22]

Cutis verticis gyrate

Cutis verticis gyrate is an overgrowth of the scalp skin, resulting in deep furrows and convoluted folds of the skin. Cutis verticis can be diagnosed clinically. Surgery is the definitive treatment for cutis verticis. However, appropriate scalp hygiene is important to avoid the accumulation of secretions (Fig. 3).[23] Cutis verticis gyrate has been reported in several patients with CdLS.[24]

Sweat gland abnormalities

Sweat gland density was reduced in 34% of the individuals with CdLS. Decreasing sweat gland density with age is normal; however, individuals with CdLS exhibit a reduction in size that exceeds typical age-related expectations.[25]

Cutis marmorata telangiectatic congenita

Cutis marmorata telangiectatic congenita (CMTC) is a rare congenital rash resulting from vascular malformations. It presents with fixed reticulate erythema, unlike physiological cutis marmorata, which resolves with

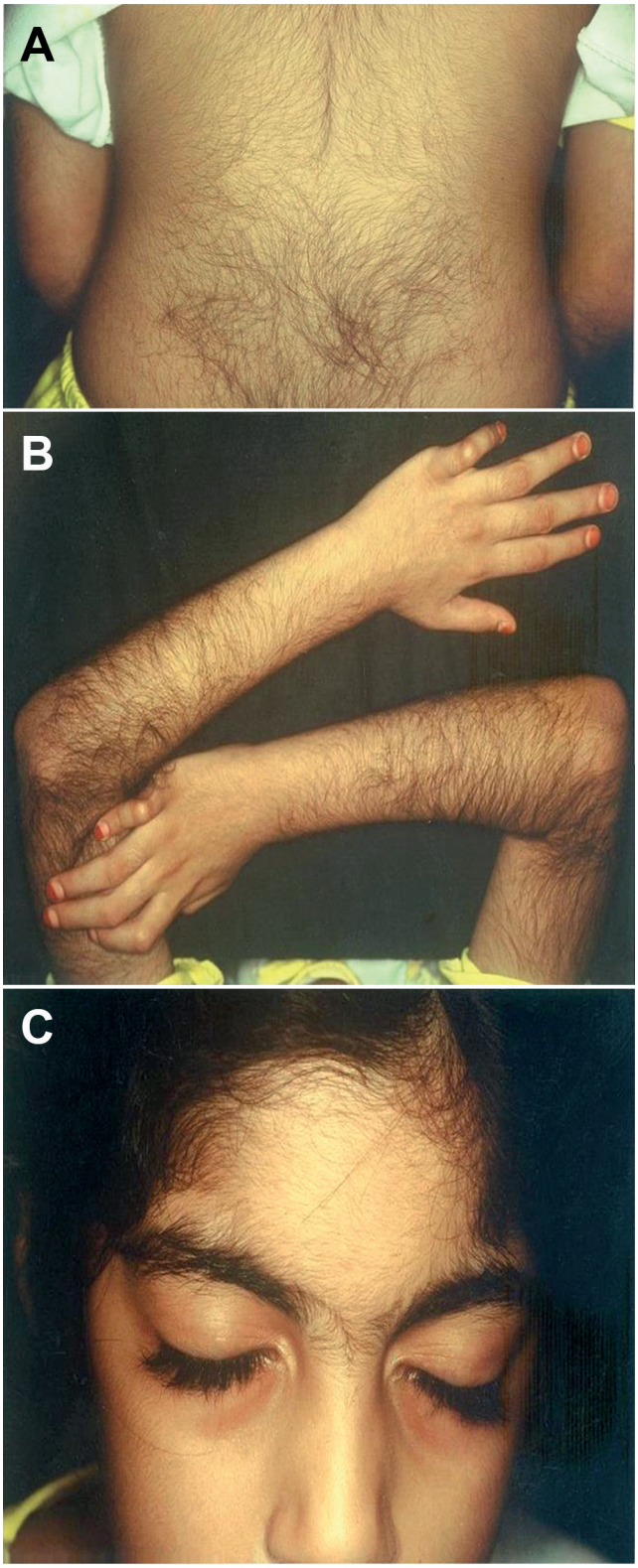

Fig. 1. Hypertrichosis in the back (A) and arm (B) and long curly eyelashes (C)

skin warming. Cutis marmorata telangiectatic congenita is clinically diagnosed, but histopathological examination of the skin is insufficient for diagnosis. It is most associated with reticulate erythema, which is observed in persistent CdLS (Fig. 4).[10] CMTC shows a strong correlation with CdLS, as more than half of the patients with CdLS have CMTC.[26]

Fig. 2. Distinctive facial features of CdLS, including dark hair color, low anterior hairline, hirsutism, and thick, arched, and confluent eyebrows

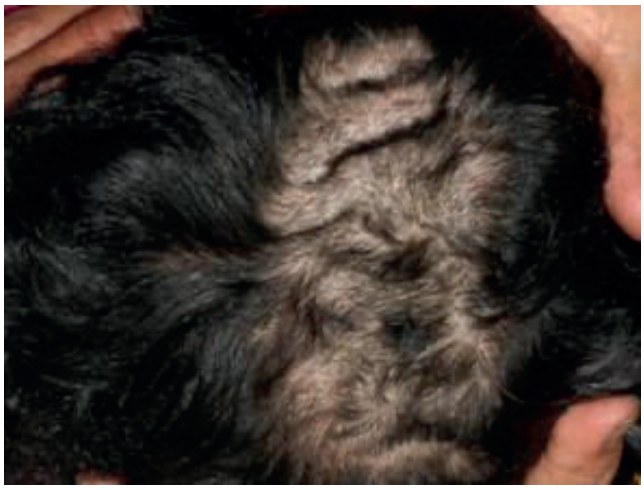

Fig. 3. Cutis verticis gyrate

Nail abnormalities

Approximately 35% of patients with patients with CdLS had aplastic or hypoplastic nails (Fig. 5).[27,28]

Abnormal dermatoglyphics

Patients with CdLS usually have abnormal epidermal ridge patterns, including a hypoplastic ridge pattern, which is characterized by ridges that are reduced in height. This is often accompanied by an excess of white lines on prints (Fig. 6).[13] Under these conditions, the ridges are short, curved and disorganized, instead of running neatly in parallel lines. Dotted ridges are also a type of ridge dissociation associated with CdLS.[29]

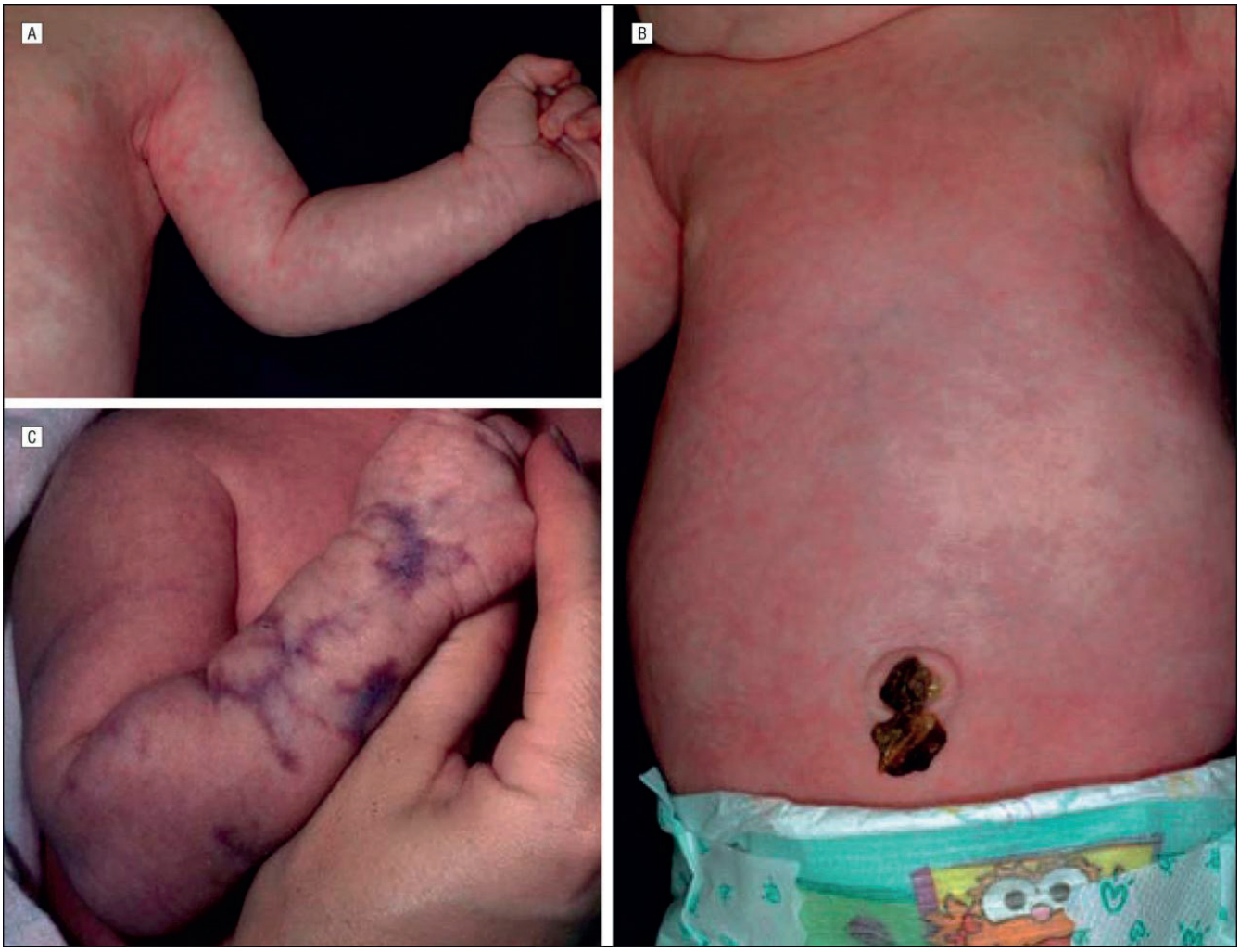

Fig. 4. Cutis marmorata telangiectatic congenita

Fig. 5. Hypoplastic nails of the foot

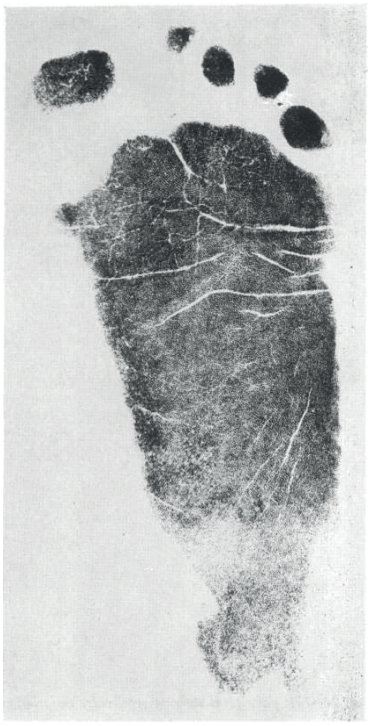

Fig. 6. The dotted ridges pattern in the sole seen in patients with CdLS

Crease anomalies

Many syndromes are associated with abnormal palmar creases, and CdLS is among them, with approx. 60% of patients exhibiting a single transverse palmar crease (Fig. 7).[28]

Cutaneous syndactyly

Cutaneous syndactyly is a malformation that arises during limb development, characterized by the fusion of adjacent digits involving only the skin. Cutaneous syndactyly of the toes is illustrated in Fig. 8.[28,30]

Fig. 7. Single transverse palmar crease

Fig. 8. Cutaneous syndactyly of the toes

Cutaneous bacterial infection

Due to CdLS-associated antibody deficiency and impaired T-cell function, a high frequency of recurrent infections has been reported, with bacterial skin infections occurring in approx. 4% of cases.[31]

Hypoplastic nipples and umbilicus

Hypoplastic nipples and the absence of nipples or the umbilicus have been observed in approx. 50% of patients, most commonly among individuals with classic CdLS (Fig. 9).[18,32]

Fig. 9. Absence of the nipples

Thrombocytopenia and its complications

Although thrombocytopenia in CdLS typically resolves over time, in some cases it may persist, leading to the development of idiopathic thrombocytopenic purpura.[18,33]

Self-injury and aggressive behaviors

Self-injury is common in individuals with CdLS, with roughly of them exhibiting clinically significant self-injury.[18] This includes some behaviors that may concern dermatologists, including onychotillomania, trichotillomania and dermatillomania, which refer to the impulse or urge to pick or pull out nails, hair and skin, respectively.[34] Parent management training (PMT) and cognitive behavioral therapy (CBT) are 2 effective interventions for these behavioral problems and are well supported in randomized controlled trials (RCTs). Parent management training aims to improve family interactions through aggressive behaviors. The basic principle of PMT is that there is a direct relationship between aggressive behavior and the consequences that follow that behavior. Cognitive behavioral therapy aims to enhance social problem-solving skills, using techniques such as identifying patterns of anger expression, recognizing the consequences of self-injurious behavior, and reshaping aggressive reactions into more socially appropriate responses.[35]

Differential diagnosis

Several conditions may present with features resembling CdLS, including Fryns syndrome, Coffin–Siris syndrome, and Rubinstein–Taybi syndrome.[1] Each of these conditions shares some dermatological features with CdLS but can be distinguished through careful clinical examination and genetic testing.[1,36]

Impact on quality of life

The dermatological manifestations of CdLS can significantly impact patients' psychosocial wellbeing. Visible features such as hirsutism and facial differences may affect self-image and social interactions. Support groups and psychological counseling should be considered as part of comprehensive care.[37,38]

Limitations

This review has several limitations. First, the available literature on the dermatological manifestations of Cornelia de Lange syndrome (CdLS) is scarce, and most published studies focus primarily on systemic or developmental aspects. As a result, much of the dermatological evidence is derived from case reports or small case series, which may reduce the generalizability of the findings. Second, variability in diagnostic approaches and reporting styles across studies makes it difficult to establish precise prevalence rates of skin manifestations. Third, because this work was conducted as a narrative review rather than a systematic review, some relevant studies may not have been captured despite a broad database search. Finally, the rarity of CdLS itself and the frequent under-recognition of milder phenotypes may have led to underreporting of dermatological features in the literature.

Conclusions

This review achieves its stated aim of providing a comprehensive overview of CdLS and its cutaneous manifestations. Key findings include the high prevalence of hair abnormalities, the significance of cutaneous markers for diagnosis, and the importance of dermatological care in management. Future research should focus on genotype-phenotype correlations in skin manifestations, long-term outcomes of dermatological interventions, and impact of cutaneous features on quality of life.

Use of AI and AI-assisted technologies

Not applicable.

ORCID iDs

Omar Shahada https://orcid.org/0009-0003-5378-9228
Ahmed Kurdi https://orcid.org/0009-0003-4812-4133
Lujain Alrohaily https://orcid.org/0009-0009-8585-3814
Ohoud Alahmadi https://orcid.org/0009-0007-7187-0037
Abdulrahman Tashkandi https://orcid.org/0009-0009-9105-6344
Taif Aloufi https://orcid.org/0009-0000-8017-0533
Wateen Alloqmani https://orcid.org/0009-0004-5874-7120

References

1. Kline AD, Moss JF, Selicorni A, et al. Diagnosis and management of Cornelia de Lange syndrome: First international consensus statement. *Nat Rev Genet*. 2018;19(10):649–666. doi:10.1038/s41576-018-0031-0
2. Boyle MI, Jespersgaard C, Nazaryan L, et al. Deletion of 11q12.3–11q13.1 in a patient with intellectual disability and childhood facial features resembling Cornelia de Lange syndrome. *Gene*. 2015;572(1):130–134. doi:10.1016/j.gene.2015.07.016
3. de Lange C. Sur un type nouveau de degenerescence (typus Amstelodamensis). *Arch Med Enfants*. 1933;36:713–719
4. Barisic I, Tokic V, Loane M, et al. Descriptive epidemiology of Cornelia de Lange syndrome in Europe. *Am J Med Genet A*. 2008;146A(1):51–59. doi:10.1002/ajmg.a.32016
5. Liu J, Krantz I. Cornelia de Lange syndrome, cohesin, and beyond. *Clin Genet*. 2009;76(4):303–314. doi:10.1111/j.1399-0004.2009.01271.x
6. Parenti I, Teresa-Rodrigo ME, Pozojevic J, et al. Mutations in chromatin regulators functionally link Cornelia de Lange syndrome and clinically overlapping phenotypes. *Hum Genet*. 2017;136(3):307–320. doi:10.1007/s00439-017-1758-y
7. Kaur M, Blair J, Devkota B, et al. Genomic analyses in Cornelia de Lange syndrome and related diagnoses: Novel candidate genes, genotype–phenotype correlations and common mechanisms. *Am J Med Genet A*. 2023;191(8):2113–2131. doi:10.1002/ajmg.a.63247
8. Watrin E, Kaiser FJ, Wendt KS. Gene regulation and chromatin organization: Relevance of cohesin mutations to human disease. *Curr Opin Genet Dev*. 2016;37:59–66. doi:10.1016/j.gde.2015.12.004
9. Falek A, Schmidt R, Jervis GA. Brachmann/De Lange syndrome. *Lancet*. 1965;285(7387):706–707. doi:10.1016/S0140-6736(65)91863-5
10. Ptacek LJ, Opitz JM, Smith DW, Gerritsen T, Waisman HA. The Cornelia de Lange syndrome. *J Pediatr*. 1963;63(5):1000–1020. doi:10.1016/S0022-3476(63)80234-6
11. Krantz ID, McCallum J, DeScipio C, et al. Cornelia de Lange syndrome is caused by mutations in NIPBL, the human homolog of *Drosophila melanogaster* Nipped-B. *Nat Genet*. 2004;36(6):631–635. doi:10.1038/ng1364
12. Tonkin ET, Wang TJ, Lisgo S, Bamshad MJ, Strachan T. NIPBL, encoding a homolog of fungal Scc2-type sister chromatid cohesion proteins and fly Nipped-B, is mutated in Cornelia de Lange syndrome. *Nat Genet*. 2004;36(6):636–641. doi:10.1038/ng1363
13. Basile E, Villa L, Selicorni A, Molteni M. The behavioural phenotype of Cornelia de Lange syndrome: A study of 56 individuals. *J Intellect Disabil Res*. 2007;51(9):671–681. doi:10.1111/j.1365-2788.2007.00977.x
14. Barr A, Grabow J, Matthews C, Grosse F, Motl M, Opitz J. Neurologic and psychometric findings in the Brachmann–De Lange syndrome. *Neuropediatrics*. 1971;3(1):46–66. doi:10.1055/s-0028-1091799
15. Kline AD, Krantz ID, Sommer A, et al. Cornelia de Lange syndrome: Clinical review, diagnostic and scoring systems, and anticipatory guidance. *Am J Med Genet A*. 2007;143A(12):1287–1296. doi:10.1002/ajmg.a.31757
16. Moss J, Penhallow J, Ansari M, et al. Genotype–phenotype correlations in Cornelia de Lange syndrome: Behavioral characteristics and changes with age. *Am J Med Genet A*. 2017;173(6):1566–1574. doi:10.1002/ajmg.a.38228
17. Selicorni A, Mariani M, Lettieri A, Massa V. Cornelia de Lange syndrome: From a disease to a broader spectrum. *Genes (Basel)*. 2021;12(7):1075. doi:10.3390/genes12071075
18. Solovyeva NA, Kurmaeva EA, Kulakova GA, et al. Cornelia de Lange syndrome. *Ross Vestn Perinatol Pediatr*. 2022;67(5):211–215. doi:10.21508/1027-4065-2022-67-5-211-215
19. Escobar-Morreale HF, Carmina E, Dewailly D, et al. Epidemiology, diagnosis and management of hirsutism: A consensus statement by the Androgen Excess and Polycystic Ovary Syndrome Society. *Hum Reprod Update*. 2012;18(2):146–170. doi:10.1093/humupd/dmr042

20. Malik LM, Khan GA, Azfar NA, Jahangir M. Cornelia de Lange syndrome: A cause of hypertrichosis in children. Case report and review of literature. *J Pak Assoc Dermatol*. 2011;21:211–214. https://jpad.com.pk/index.php/jpad/article/view/475
21. Panaitescu AM, Duta S, Gica N, et al. A broader perspective on the prenatal diagnosis of Cornelia de Lange syndrome: Review of the literature and case presentation. *Diagnostics (Basel)*. 2021;11(1):142. doi:10.3390/diagnostics11010142
22. McArthur RG, Edwards JH. De Lange syndrome: Report of 20 cases. *Can Med Assoc J*. 1967;96(17):1185–1198. PMID:6022788. PMCID: PMC1922865
23. Larsen F. Cutis verticis gyrata. Auckland, New Zealand: DermNet (New Zealand Dermatological Society); 2007, revised 2021. https://dermnetnz.org/topics/cutis-verticis-gyrata. Accessed August 15, 2024
24. Kline AD, Grados M, Sponseller P, et al. Natural history of aging in Cornelia de Lange syndrome. *Am J Med Genet C Semin Med Genet*. 2007;145C(3):248–260. doi:10.1002/ajmg.c.30137
25. Pablo MJ, Pamplona P, Haddad M, et al. High rate of autonomic neuropathy in Cornelia de Lange syndrome. *Orphanet J Rare Dis*. 2021;16(1):458. doi:10.1186/s13023-021-02082-y
26. Wright DR, Frieden IJ, Orlow SJ, et al. The misnomer "macrocephaly–cutis marmorata telangiectatica congenita syndrome": Report of 12 new cases and support for revising the name to macrocephaly–capillary malformations. *Arch Dermatol*. 2009;145(3):287–293. doi:10.1001/archdermatol.2008.545
27. Parenti I, Mallozzi MB, Hüning I, et al. *ANKRD11* variants: KBG syndrome and beyond. *Clin Genet*. 2021;100(2):187–200. doi:10.1111/cge.13977
28. Biesecker LG, Aase JM, Clericuzio C, Gurrieri F, Temple IK, Toriello H. Elements of morphology: Standard terminology for the hands and feet. *Am J Med Genet A*. 2009;149A(1):93–127. doi:10.1002/ajmg.a.32596
29. David TJ. Congenital malformations of human dermatoglyphs. *Arch Dis Child*. 1973;48(3):191–198. doi:10.1136/adc.48.3.191
30. Stevenson RE, Scott CI. Discordance for Cornelia de Lange syndrome in twins. *J Med Genet*. 1976;13(5):402–404. doi:10.1136/jmg.13.5.402
31. Jyonouchi S, Orange J, Sullivan KE, Krantz I, Deardorff M. Immunologic features of Cornelia de Lange syndrome. *Pediatrics*. 2013;132(2):e484–e489. doi:10.1542/peds.2012-3815
32. Tadini G, Santagada F, Brena M, Pezzani L, Nannini P. Ectodermal dysplasias: The p63 tail. *G Ital Dermatol Venereol*. 2013;148(1):53–58. PMID:23407076
33. Lambert MP, Jackson LG, Clark D, Kaur M, Krantz ID, Deardorff MA. The incidence of thrombocytopenia in children with Cornelia de Lange syndrome. *Am J Med Genet A*. 2011;155(1):33–37. doi:10.1002/ajmg.a.33631
34. Mulder PA, Huisman SA, Hennekam RC, Oliver C, Van Balkom IDC, Piening S. Behaviour in Cornelia de Lange syndrome: A systematic review. *Devel Med Child Neurol*. 2017;59(4):361–366. doi:10.1111/dmcn.13361
35. Sukhodolsky DG, Smith SD, McCauley SA, Ibrahim K, Piasecka JB. Behavioral interventions for anger, irritability, and aggression in children and adolescents. *J Child Adolesc Psychopharmacol*. 2016;26(1):58–64. doi:10.1089/cap.2015.0120
36. Vergano SS, Deardorff MA. Clinical features, diagnostic criteria, and management of Coffin–Siris syndrome. *Am J Med Genet C Semin Med Genet*. 2014;166(3):252–256. doi:10.1002/ajmg.c.31411
37. Christensen RE, Jafferany M. Psychiatric and psychologic aspects of chronic skin diseases. *Clin Dermatol*. 2023;41(1):75–81. doi:10.1016/j.clindermatol.2023.03.006
38. Costeris C, Petridou M, Ioannou Y. Psychological impact of skin disorders on patients' self-esteem and perceived social support. *J Dermatol Skin Sci*. 2021;3(1):14–22. https://www.dermatoljournal.com/articles/psychological-impact-of-skin-disorders-on-patients-self-esteem-and-perceived-social-support.html

Diagnosis and management of traumatic injuries in pediatric patients secondary to dental local anesthesia: A systematic review

Aneta Olszewska[1,A–D,F], Julia Kensy[2,B–D], Agata Czajka-Jakubowska[1,E], Daniele Pergolini[3,D,E], Maurizio Bossù[3,E], Umberto Romeo[3,E], Jacek Matys[4,A–C,E–F]

[1] Department of Orthodontics and Temporomandibular Disorders, Poznan University of Medical Sciences, Poland
[2] Faculty of Dentistry, Wroclaw Medical University, Poland
[3] Department of Oral and Maxillofacial Sciences, Sapienza University of Rome, Italy
[4] Department of Dental Surgery, Wroclaw Medical University, Poland

A – research concept and design; B – collection and/or assembly of data; C – data analysis and interpretation; D – writing the article; E – critical revision of the article; F – final approval of the article

Advances in Clinical and Experimental Medicine, ISSN 1899–5276 (print), ISSN 2451–2680 (online) *Adv Clin Exp Med*. 2026;35(1):175–190

Address for correspondence
Jacek Matys
E-mail: jacek.matys@umw.edu.pl

Funding sources
None declared

Conflict of interest
None declared

Received on February 16, 2025
Reviewed on April 1, 2025
Accepted on April 25, 2025

Published online on August 26, 2025

Abstract

This study examines soft tissue injuries secondary to the prevalence of local anesthesia, differential diagnosis and therapeutic approaches.

In October 2024, a comprehensive search was performed in PubMed, Web of Science and Scopus along with gray literature sources, adhering to the PRISMA (Preferred Reporting Items for Systematic reviews and Meta-Analyses) guidelines, using the following keywords: "bite", "traumatic injuries", "soft tissue injuries", "self-inflicted injuries", "topical anesthesia", "local anesthesia", "pediatric", or "children". The search was limited to English-language publications. Additional manual screening of reference lists was performed. The risk of bias was assessed using the checklist developed by the Joanna Briggs Institute (JBI).

Out of 574 identified studies, 21 were included in the qualitative analysis (9 randomized controlled trials (RCTs), 6 case reports and 6 cohort studies), mainly focusing on children aged 6–12. Anesthesia methods included traditional techniques (12 studies) and computer-controlled injection (5 studies). The role of articaine (9) and lidocaine (10) was analyzed. Suggested interventions to mitigate injury risks and improve recovery included the use of phentolamine mesylate (2 studies) and non-pharmacological strategies: intraoral appliances (2 studies) and photobiomodulation (2 studies). The included studies varied in design, sample size and duration, limiting direct comparisons. Effect sizes and confidence intervals were inconsistently reported, and the risk of bias assessment using the Cohen's kappa test highlighted methodological heterogeneity and potential reporting bias.

Soft tissue injuries from local anesthesia in children can cause significant pain and cooperation issues. Effective strategies include early intervention with pharmacological and non-pharmacological approaches. Increased awareness and patient-specific management are essential for reducing risks and improving outcomes.

Key words: children, local anesthesia, soft tissue injuries, anesthesia

Cite as
Olszewska A, Kensy J, Czajka-Jakubowska A, et al. Diagnosis and management of traumatic injuries in pediatric patients secondary to dental local anesthesia: A systematic review. *Adv Clin Exp Med*. 2026;35(1):175–190. doi:10.17219/acem/204391

DOI
10.17219/acem/204391

Highlights

- Self-inflicted soft-tissue injuries after pediatric dental anesthesia are common, most often involving the lips, cheeks and tongue.
- These wounds can progress to infection, allergic reaction or neuropathy, so each must be considered in the clinical differential diagnosis.
- Rapid anesthetic reversal with intra-oral splints, phentolamine mesylate (OraVerse®) or photobiomodulation therapy shortens numbness time and lowers injury risk.
- Standardized anesthesia protocols and long-term, multicenter studies are essential to refine prevention, diagnosis and treatment of soft-tissue injuries in children.

Introduction

Lesions secondary to local anesthesia in children are rare but may occur as the child's response to the procedure. These lesions are typically related to the local anesthetic agent used by the technique. However, they are mainly the result of inappropriate behavior of the child due to prolonged numbness after administration of local anesthesia.[1,2] After the procedure, when stress levels have subsided and the child is still under anesthesia, they may be unfamiliar with the sensation of numbness. As a result, they might bite or chew on their lips, cheeks or tongue, potentially causing painful injuries.[1] Timely diagnosis and appropriate management help minimize complications and promote healing of soft tissue injuries caused by local anesthesia.

Regular follow-up is crucial to monitor recovery and prevent complications.[2] If the lesion does not resolve or worsens, it is recommended to seek the help of a pediatric dentist, oral surgeon or appropriate specialist. All cases with severe or non-healing ulcers should be indicated when considering malignancies or systemic causes such as autoimmune diseases, as well as complicated infections requiring surgical drainage or hospitalization.[3] If the lesions recur or appear in different areas, neuropathy should be considered, as this may indicate persistent sensory disturbances or underlying nerve damage.[4] These injuries are usually preventable with careful planning of the time needed for anesthesia for the procedure, a precise technique of anesthetic administration, considering the use of local anesthetic reversal agents such as phentolamine mesylate, and careful post-procedure education of healthcare professionals to monitor the child.[5,6]

To effectively address this often misdiagnosed condition, a thorough understanding of proper diagnostic techniques is essential.[7,8] The differential diagnosis of soft tissue injury should consider trauma during anesthesia delivery, which may present as redness, swelling or ulceration caused by mechanical or physical damage during injection.[7,9] Rare allergic reactions to local anesthesia may manifest as itching, swelling or rash, while infection may present with localized pain, warmth, erythema, or systemic symptoms.[9] Chemical or thermal burns resulting from exposure to caustics or excessive heat should also be assessed. Injection site complications, such as localized hematoma, edema or necrosis caused by improper injection technique, can lead to swelling or discoloration. In addition, neuropathy resulting from temporary or permanent nerve injury can cause symptoms such as paresthesia (tingling or numbness) or dysesthesia (abnormal, often painful sensations). Accurate identification of these potential causes is essential for effective management and the prevention of complications.[9,10]

Although often self-limiting, traumatic soft tissue injuries following local anesthesia in children can lead to complications such as ulceration, secondary infection or neuropathic pain, highlighting the importance of early recognition and management. Despite their clinical significance, research on these injuries remains fragmented, with most studies limited to case reports or small-scale observations rather than comprehensive evidence-based assessments. There is a lack of high-quality evidence on effective prevention and management strategies, and inconsistencies in age-specific clinical approaches further complicate decision-making. Given these gaps, a systematic review is needed to consolidate existing knowledge, evaluate diagnostic and preventive strategies – such as anesthetic reversal agents and post-procedural education – and assess treatment effectiveness, ultimately guiding standardized, evidence-based clinical practices.

Objectives

There is no current published literature review on soft tissue injuries resulting from local anesthesia in children. While most complications occur immediately, late-onset issues can affect essential functions like eating, speaking and chewing, particularly in young children and those with behavioral challenges. These complications may cause pain and impact future dental cooperation. This review aims to synthesize existing research, provide insights into prevalence, diagnosis and management strategies, and raise clinical awareness to improve patient outcomes.

Materials and methods

Focused question

This systematic review was conducted using the PICO framework to address the following clinical question: In children undergoing local anesthesia (Population), how does the diagnosis of traumatic injuries related to anesthesia (Intervention) and the strategies for their management (Comparison) influence the reduction of postoperative trauma (Outcome) compared to no specific intervention or standard care?[11]

Protocol

The process of selecting articles in the systematic review was carefully outlined following the Preferred Reporting Items for Systematic reviews and Meta-Analyses (PRISMA) flowchart (Fig. 1).[12] The systematic review was registered on the Open Science Framework at the following link: https://osf.io/4xwdz (accessed December 9, 2024).

Eligibility criteria

Studies were considered acceptable for inclusion in the review if they met the following criteria[12]:

– children up to 18 years old;
– use of local anesthesia;
– observation of soft tissue trauma in a few postoperative days;
– clinical cases;
– studies in English;
– prospective case series;
– non-randomized controlled clinical trials (NRS);
– randomized controlled clinical trials (RCTs).

The exclusion criteria on which the reviewers agreed were as follows[12]:

– adult patients;
– studies have focused on pain or numbness of tissues without paying attention to self-inflicted trauma;
– articles not in English;
– opinions;

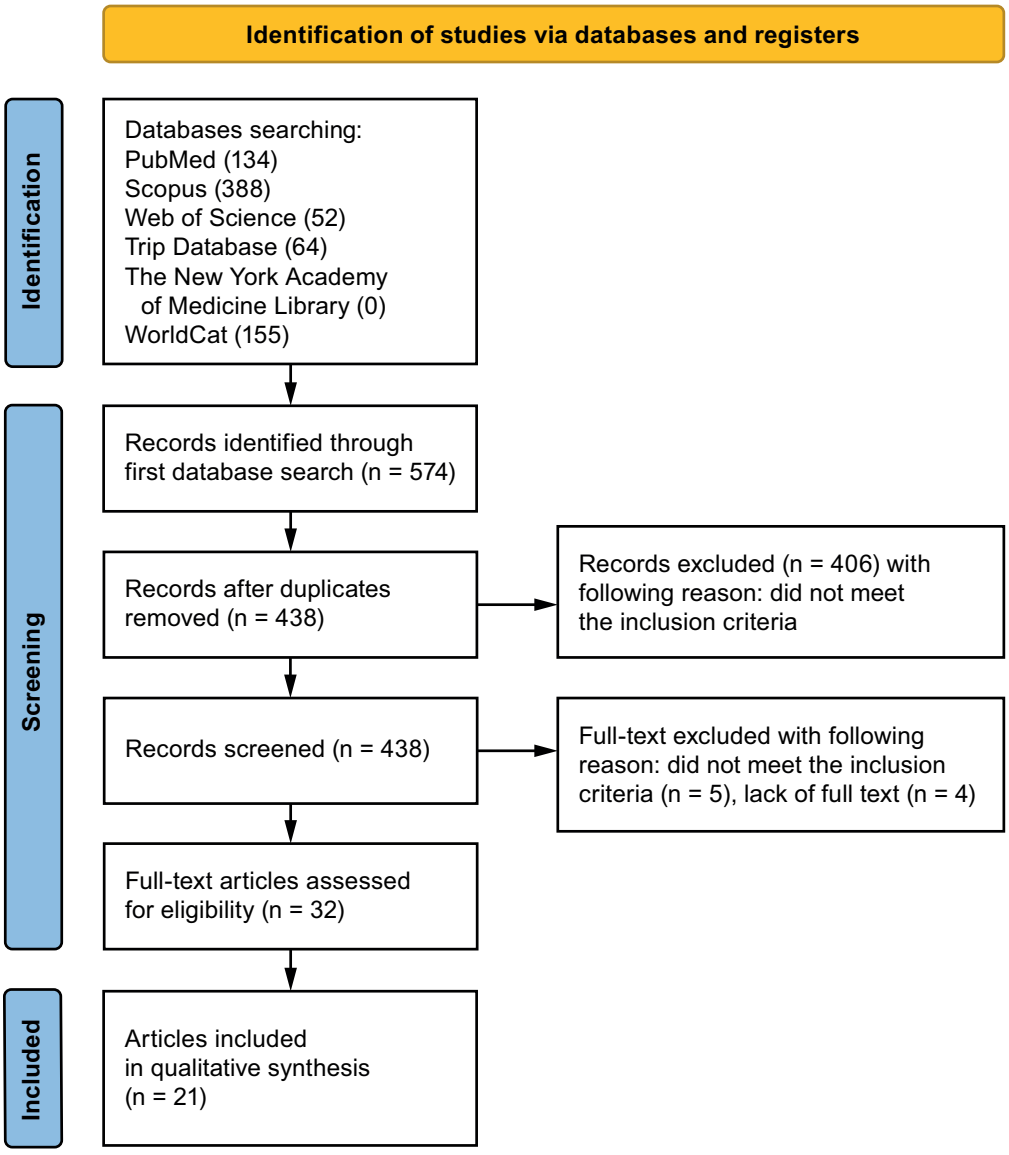

Fig. 1. Preferred Reporting Items for Systematic Reviews and Meta- Analyses (PRISMA) 2020 flow diagram illustrating the study selection process

– editorial articles;
– review articles;
– it is not possible to access the full text;
– duplicate publications.

No restrictions have been applied with regard to the year of publication.

Sources of information, search strategy and selection of studies

In October 2024, a comprehensive search was performed in the PubMed, Scopus and Web of Science (WoS) databases to identify articles that meet the predefined inclusion criteria. Additionally, searches were conducted in gray literature sources, including WorldCat, The New York Academy of Medicine Library and the Trip Database. The search criteria were meticulously crafted, utilizing a strategic blend of the specified keywords. For PubMed, we used ((biting[Title/Abstract]) OR (bite[Title/Abstract]) OR (traumatic injuries) OR (soft-tissue injury[Title/Abstract]) OR (soft tissue injury[Title/Abstract]) OR (self-inflicting injuries[Title/Abstract])) AND ((topical anesthesia[Title/Abstract]) OR (local anesthesia[Title/Abstract])) AND ((pediatric[Title/Abstract]) OR (children[Title/Abstract])). For WoS, we used ALL= ((biting OR bite OR Traumatic injuries OR Soft-tissue injury OR soft tissue injury OR self-inflicting injuries) AND (topical anesthesia OR local anesthesia) AND (pediatric OR children)). For Scopus, we used ((biting OR bite OR Traumatic injuries OR Soft-tissue injury OR soft tissue injury OR self-inflicting injuries) AND (topical anesthesia OR local anesthesia) AND (pediatric OR children)). For WorldCat and The New York Academy of Medicine Library, we used biting OR biting OR traumatic injuries OR soft tissue injuries OR soft tissue injuries OR self-inflicted injuries) AND (topical anesthesia OR local anesthesia) AND (pediatric or children. For Trip Database, we searched (self-inflicted injuries) AND (topical anesthesia OR local anesthesia) AND (children). Following the database search, a thorough and systematic literature review was conducted to identify any papers that were initially considered potentially irrelevant to this study. Only articles with available full-text versions were considered for inclusion.

Data collection process and data elements

Two reviewers (A.O. and J.K.) independently reviewed and extracted articles that met the inclusion criteria. Relevant data collected included the names of the authors, the year of publication, the study design, the title of the article, the type of laser used, and the results related to its effectiveness in the healing process and pain management. The extracted data was systematically recorded in a standardized Excel spreadsheet (Microsoft Excel 2013; Microsoft Corp., Redmond, USA) for subsequent analysis.

Risk of bias and quality assessment

During the initial selection phase of the study, each reviewer independently evaluated the titles and abstracts to minimize potential bias. The Cohen's kappa test was used to assess the level of agreement among reviewers. Any discrepancies regarding the inclusion or exclusion of articles were resolved by the 3rd reviewer.[13]

Quality assessment

Two independent reviewers (A.O. and J.K.) systematically evaluated the methodological quality of each study to determine its suitability for inclusion. If there was a disagreement among the reviewers about whether to include a study, a 3rd reviewer was consulted to make the final decision. The quality assessment was conducted using a set of critical assessment tools designed by the Joanna Briggs Institute (JBI; https://jbi.global/critical-appraisal-tools). Cohen's kappa test was conducted to evaluate inter-rater reliability using MedCalc v. 23.1.7 (MedCalc Software Ltd., Ostend, Belgium). The analysis yielded a kappa value of 0.9 ($p < 0.001$), indicating almost perfect agreement and high consistency among the reviewers' assessments.

Results

Selection of studies

An initial search of databases, including PubMed, WoS and Scopus, yielded a total of 574 studies potentially relevant for review. After the duplicate entries were removed, 438 articles remained for screening. During the preliminary evaluation of the titles and abstracts, 406 studies were excluded as they did not meet the inclusion criteria. Subsequently, 32 articles were subjected to a detailed analysis of the full text, which led to the exclusion of 5 articles for non-compliance with the inclusion criteria and 4 for unavailability of the full text. In the end, 21 articles were deemed eligible and included in the qualitative summary of this review.[1,4–6,14–30]

General characteristics of the studies included

This systematic review includes a wide range of studies examining the diagnosis and management of traumatic injuries resulting from local anesthesia in pediatric dentistry. The studies consist of RCTs,[5,6,16–18,21,24,25,27] clinical cases[1,4,14,15,23,30] and cohort studies,[19,22,26,28] which reflects a comprehensive investigation into this topic. Sample sizes varied considerably between the included studies, with case reports focusing on individual patients or small groups[1,4,14,15,23,30] and large-scale studies that include up

to several hundred participants.[5,19,20,22,24–26,29] A general feature of the included studies was demonstrated in Table 1.

Study participants ranged from children to adolescents, with most studies focusing on children aged 6–12 years, as this group is most commonly placed under local anesthesia during routine dental procedures.[4,5,16,18,21,30] A key theme in all studies is the high prevalence of self-inflicted soft tissue injuries after administration of local anesthesia. These lesions, which often affect the lips, cheeks or tongue, result from the temporary loss of sensation, leading to accidental bites and trauma.[1,4,6,14,15,17,18,23,24,26,27,30] Studies have also explored specific types of injuries, such as traumatic ulcers caused by unintentional tissue damage.[1,4,14,15,23,30]

Anesthesia methods varied between studies and included traditional inferior alveolar nerve blocks,[4,6,15–17,19–21,23,25,26,30] topical anesthetics[14,19] and innovative techniques such as computer-controlled intraosseous injections[29] or intraligamental anesthesia.[17] Comparison of these methods provided insight into the different risks and outcomes associated

Table 1. General characteristics of the studies

Study	Aim of the study	Material and methods	Results	Conclusions
Kot et al.[1]	Presentation of 3 cases of self-inflicted injuries in children after local anesthesia and outline preventive and therapeutic approaches.	Patient 1: – 4.5 years – Tooth 84 – Infiltration anesthesia with Citocartin 200 (4% articaine with epinephrine 1:200,000) (1/2 cartridge) – Treatment: Tantum Verde aerosol and Solcoseryl paste Patient 2: – 9 years – Tooth 36 – Anesthesia of inferior alveolar nerve block with Citocartin 200 (1/2 Cartridge) – Treatment: Sulcoseyl paste Patient 3: – 7 years – Tooth 54 – Infiltration anesthesia with Citocartin 200 (1/2 cartridge) – Treatment: Sulcoseyl paste	Patient 1: – After 3 days: Extensive and painless ulceration of the lower lip on the right side; fibrin-coated lesion, no symptoms of inflammation – One week: Ulceration healed Patient 2: – After 2 days: Healing of ulcerations on the mucosa of the cheek at the level of the treated tooth and at the corner of the lips – Five days after the ulceration subsided and 10 days after healing Patient 3: – After 2 h: Extensive damage to the mucous membrane of the upper lip – After 1 week: Injury healed	Injuries to the lips or cheeks after anesthesia with mandibular block are common. Parents should supervise the child to avoid biting. These lesions heal quickly with symptomatic treatment only, unless reinfection occurs.
Chi et al.[4]	Report the case of a child who presents with a self-inflicted injury as a result of inferior alveolar nerve block (IANB).	– 10 years – Inferior alveolar nerve block – 2% lidocaine Treatment of dental caries	– After the procedure: Lip bite with mild bleeding – Next day: Swollen, white right lower lip, ulcerated lesion (7 × 4 mm); similar lesion on the right buccal mucosa adjacent to the tooth 46 – The patient was transferred to the hospital After the medical examination, the patient was discharged after 7 h.	This case highlights the need to improve medical-dental communication. Pediatric hospital workers are critical to preventing misdiagnosis and unnecessary treatment of self-inflicted lip ulcers after dental anesthesia.
Tavares et al.[5]	Evaluation of the efficacy of a phentolamine mesylate (PM) in accelerating the recovery of normal sensation in children after receiving lidocaine with epinephrine for dental procedures.	– 152 children – 4–11 years – Lidocaine 2% with Epinephrine 1:100,000 – After the procedure, if anesthesia was administered for 60 min or less, soft tissues persisted, anesthetized, one group received a PM injection (96 children) and another group received a sham injection (56 children)	– In the PM group, the recovery of normal soft tissue sensation was shorter than in the control group. There was no difference in pain reduction or episodes of adverse reactions.	Phentolamine mesylate can be a great substance to reduce the duration of anesthesia, which can reduce the number of self-inflicted soft tissue injuries in children.
Nourbakhsh et al.[6]	To evaluate the effect of phentolamine mesylate on the duration of anesthesia and soft tissue injury.	– 54 patients aged 4–11 years – IANB with lidocaine 2% with epinephrine 1:80,000 – Group 1: Phentolamine mesylate injection after lidocaine anesthesia – Group 2: The same children at the next visit received only local anesthesia and placebo	A few hours after the procedure: – 8 patients self-injured after placebo and only 1 patient after application of phentolamine mesylate – No trauma to the tongue or cheeks was observed.	Phentolamine mesylate is a safe and effective option for reducing soft tissue anesthesia after dental procedures and self-inflicted soft tissue trauma.

Table 1. General characteristics of the studies – cont

Study	Aim of the study	Material and methods	Results	Conclusions
Tiwari[14]	Present a case of self-inflicted injury following topical anesthesia.	– 4 years – Restorations in 74 and 75 – Topical anesthesia: benzocaine 20% from the buccal and lingual side – Infiltrative anesthesia: 2% lidocaine	After 2 days: – White patchy ulcer 1 × 2 cm on the left side of the lower lip extending from the midline to the corner of the mouth – The ulcer was painful and raised – All other diseases have been excluded – Treatment: paracetamol oral suspension 5 mL, ice pack applications and saline leavening After 10 days, the injury has healed	Topical anesthesia can cause numbness in the lips as it disperses to the lip area through saliva. Effective risk assessment and preventive monitoring can help prevent accidental bites in anesthetized pediatric patients.
Calazans et al.[15]	Outline the use of low-level laser therapy (LLLT) for the treatment of traumatic ulcers on the lower lip following anesthesia with inferior alveolar nerve block (IANB).	Patient: – 3 years – Tooth 74 – Inferior alveolar nerve block with 2% lidocaine with 1:100,000 epinephrine – LLLT (low-level laser therapy) treatment – 808 nm, 100 mW, 105 J/cm^2, 5 s	– After 1 day: An ulcer with a whitish coating located on the left side of the lower lip; the patient who complains of difficulty eating and pain – After 1 week: Improvement of condition and pain, no problem eating – After 30 days: lesion treated	Self-harm is common in pediatric dentistry after nerve blocks; Low-level laser therapy offers rapid pain relief, healing and anti-inflammatory benefits for traumatic ulcers.
Ghajari et al.[16]	The inverse effect of PBMT (photobiomodulation therapy) on alveolar block anesthesia in children.	– 36 children aged 6–9 years – Inferior alveolar nerve block with 2% lidocaine with epinephrine 1:100,000 – Deciduous molar pulpotomy – Diode laser (808 nm, 250 mW, 11.5 J/cm^2, 23 s) on one side of the jaw and dummy laser on the other side	Among the 36 patients subjected to the experiment, 1 patient suffered self-inflicted soft tissue trauma, while in the sham laser group, 2 children suffered trauma.	The diode laser can reduce the duration of local anesthesia, but it does not prevent self-inflicted soft tissue trauma.
Helmy et al [17]	Evaluation of pain and efficacy of intraligamentous anesthesia (CC-ILA) during mandibular primary molar injection and extraction in children.	– 50 children aged 5–7 years with first deciduous molar to be extracted – Randomly assessed at inferior alveolar nerve block or intraligamental anesthesia – Heart rate, pain and lip biting were assessed after 24 h	Children after CC-ILA did not present any post-anesthesia trauma unlike the IANB group.	CC-ILA turns out to be a better choice in baby anesthesia as it causes fewer side effects such as biting the lips or other mucosal trauma.
Olszewska et al.[18]	To evaluate the efficacy of photobiomodulation in reversing local anesthesia in children.	– 50 children aged 8–10 years – Two maxillary permanent molars for carious treatment – Infiltration anesthesia 4% articaine (Citocartin 200) with epinephrine 1:200,000 – After the procedure, the area of a tooth was treated with laser (635 nm or 808 nm, 250 mW, 500 mW/cm^2, 15 J or 200 mW, 400 mW/cm^2, 12 J); the control tooth was treated with the laser applicator turned off	Four cases of cheek bite were reported in the control groups after the procedure. The next day, 1 case of self-inflicted injury was reported in the laser group and 5 cases in the sham group.	The use of PBM can be a good method to reverse the results of local anesthesia, especially in terms of self-inflicted lesions.
Bagattoni et al.[19]	To evaluate the frequency with which self-inflicted injuries (SSI) occur after dental anesthesia in children, both with and without intellectual disabilities.	– Group A: 159 children without intellectual disability – Group B: 82 children with intellectual disabilities – Topical anesthesia: 15% lidocaine – IANB: mepivacaine 2% with 1:100,000 epinephrine – Anesthesia by infiltration: articaine 4% with 1:100,000 epinephrine – Phone call after 2 days to identify soft tissue injuries	Self-inflicted injuries were more frequent in group B. However, in both groups injuries appeared more after the IANB.	Close supervision is critical to prevent self-inflicted injuries in children after dental anesthesia, especially for those with intellectual disabilities.

Table 1. General characteristics of the studies – cont

Study	Aim of the study	Material and methods	Results	Conclusions
Alghamidi et al.[20]	To evaluate the opinions of professionals on cheek, lip and tongue bites post-anesthesia and the effectiveness of 3 intraoral appliances in preventing them.	– 301 operators were provided with a questionnaire on the occurrence of soft tissue bites after local anesthesia – Intraoral appliances in 3 sizes depending on age: 3–6, 6–9 and 9–12 years (apparatus No. 1 – anterior extension with numerous perforations, No. 2 – with buccal flap extension, No. 3 – with serrated edges); each device is held in the mouth 3 h after anesthesia – Children from 3 to 15 years old – Inferior alveolar nerve block (IANB) using 2% lidocaine with epinephrine (1:50,000 or 1:100,000)	– 31.9% of professionals were familiar with post-anesthesia lesions, which are more common in children aged 3–6 years – The intraoral device No. 1 proved to be the most favorable, showing the best comfort during use	Clear guidance and parental supervision are key to preventing self-harm in children after anesthesia, with the design of the device 1 being shown to be most effective.
Alinejhad et al.[21]	Comparison of lidocaine blockade and buccal articaine infiltration for primary mandibular second molar anesthetization in children.	– 40 children aged 6–8 and 8–10 years – Group I: 2% lidocaine with epinephrine 1:100,000 – Group II: 4% articaine with epinephrine 1:100,000	Children noticed less pain in the articaine infiltration group than in the lidocaine group.	Articaine is an effective anesthetic that can be used in children aged 6–8 years to achieve proper numbness during dental procedures.
Baillargeau et al.[22]	To assess pain, analgesic use, and the incidence of bites or bleeding to the lips or cheeks after primary tooth extractions in children.	– 125 children aged 3–13 years indicated for tooth extractions – Infiltration anesthesia 4% articaine with epinephrine 1:200,000 – Parents advised supervising and giving soft and mixed foods to prevent self-inflicted injuries	Only 6 children suffered post-extraction bite injuries. The wound was painful for 5 of the injured children.	Dentists can predict postoperative discomfort and tailor care to the patient's needs.
Bendgude et al.[23]	Report 2 cases of self-inflicted chin injury after IANB and nasal wing injury after buccal infiltration anesthesia.	Case 1: – 4 years – Caries treatment of 85 – IANB Case 2: – 5 years – Caries treatment of 63 – Anesthesia for buccal infiltration	Case 1: – The next day: An ulcerative lesion on the right side of the lower lip; scratch injury on the right side of the chin – Treatment: Analgesics and antiseptic gel for the mouth – After 2 weeks: Injuries healed Case 2: – Next day: Scratch injuries on the wing of the nose – Treatment with topical antiseptic – After 10 days: The injury had healed	Parents or supervisors should be aware during the first few hours after anesthesia to prevent self-inflicted injury.
Coulthard et al.[24]	To improve the pain experience in children after oral surgery under general anesthesia.	– 142 patients aged 4–12 years – Extractions of 1–10 teeth – The procedure was conducted under general anesthesia – To study postoperative pain reduction, children were provided with 2 mL of 2% lidocaine with 1:200,000 epinephrine or placebo 2 mL of 0.9% sodium chloride as buccal infiltration	In total, 4 patients reported biting their lips or cheeks 24 h after surgery. Three were from the anesthetic group and 1 from the placebo group.	Local anesthesia is safe to use, but it has no benefit for pain control and can lead to self-inflicted lesions on the lips/cheeks.
College et al.[25]	To compare unilateral and bilateral mandibular IANB in terms of postoperative soft tissue trauma in children.	– 320 children 2–18 years old – Control group: unilateral IANB – Investigation group (107 patients): Bilateral IANB – 2% lidocaine with 1:100,000 epinephrine (97% of patients) or 2% mepivacaine with 1:20,000 levonordefrin (3% of patients)	– The highest rate of trauma was observed in children under the age of 4 – 16% of unilateral IANBs reported trauma and 11% of bilateral IANBs	The postoperative lesion decreases with increasing age; there was a greater tendency to soft tissue trauma in the case of bilateral IANB.

Table 1. General characteristics of the studies – cont

Study	Aim of the study	Material and methods	Results	Conclusions
Adewumi et al.[26]	Report adverse reactions after use of 4% articaine with 1:100,000 epinephrine in children receiving routine dental treatment.	– 264 children aged 2–14 years – 4% articaine with 1:100,000 adrenaline – Four short phone calls after 3, 5, 24, and 48 h to ascertain paresthesias, pain and soft tissue injuries	After 3 h: – 14% had soft tissue lesions After 5 h: – 2% had soft tissue lesions The highest incidence of self-inflicted injury was reported in the 3–7 age group; the lip was the most affected site	Soft tissue injuries tend to occur in younger children, which should be supervised by parents until the effect of anesthesia is completely reduced.
Townsend et al.[27]	To evaluate whether the combination of local anesthesia with an intravenous nonsteroidal anti-inflammatory drugs (NSAID) improves children's recovery after general anesthesia.	– 27 children aged 3–5.5 years – Group 1: 15 children receiving 1 mg/kg ketorolac tromethamine together with 2% lidocaine with epinephrine 1: 100,000, – Group 2: 12 children receiving only children receiving 1 mg/kg ketorolac tromethamine	Only 23 children were reached for a postoperative follow-up call. Four out of 11 children in the group in which local anesthesia was used reported soft tissue bites and 2 out of 15 reported oral tissue damage. Meanwhile, in the control group, only 1 parent reported bites to the baby's soft tissues and no one deported oral tissue damage.	Children who received local anesthesia were exposed to a higher incidence of self-inflicted soft tissue injuries.
Ram et al.[28]	To evaluate whether an unsweetened popsicle improves children's comfort and prevents self-harm after dental treatment with local anesthesia.	– 31 children aged 4–11 years – Children who need 2 similar treatments on either side of the jaw – Lidocaine 2% with Epinephrine 1:100,000 – After the 1st procedure, the children received an unsweetened toy or popsicle and received the other price after the 2nd procedure, which took place over a week	There was no significant difference in soft tissue biting in the toy group and ice group immediately after the procedure. However, 10 min after the procedure, only 3 children still bite themselves in the ice group compared to 11 children in the toy group.	Unsweetened ice popsicles effectively improve children's comfort and reduce self-inflicted soft tissue injuries after dental treatment with local anesthesia compared to receiving a toy.
Sixou et al.[29]	To evaluate the efficacy of intraosseous anesthetic as the primary method in children.	– 181 children – Usual dental care – Intraosseous anesthesia with The Quick Sleeper 2 articaine 4% with 1:200,000 epinephrine	Numbness of the lips was noted in 14 cases, which were only cases where anesthesia was performed in the jaw. Self-inflicted mucosal injury was not noted in each case.	Computerized intraosseous anesthesia can be a valid alternative or supplement to infiltration techniques in children.
Flaitz and Felefli[30]	Present a case of self-inflicted trauma to the lips and cheeks.	– 8 years – Positioning of the stainless steel crown on the mandibular second molar – IANB	2 h after the procedure: – Two ulcerations dispersed on the lower lip and buccal mucosa – Edematous, tender, covered with white exudate, with irregular margins – Mild submandibular lymphadenopathy	Self-inflicted soft tissue trauma after IANB is a common case in children. It does not require any specific treatment but requires a correct diagnosis and differentiation with other pathologies.

with the different techniques. For example, Helmy et al.[17] highlighted the potential benefits of computer-controlled intraligamental injections in minimizing complications, while other studies have examined the relative effectiveness of bilateral compared to unilateral nerve blocks.[25] In addition, the role of specific anesthetics, such as articaine and lidocaine, in terms of safety and duration of numbness was analyzed.[26]

Several studies have introduced innovative interventions to mitigate injury risks and improve recovery. These include the use of phentolamine mesylate[5,6] as well as non-pharmacological strategies, intraoral appliances designed to protect soft tissue from damage[10] or unsweetened popsicles to reduce the tendency to bite and provide a soothing effect post-procedure.[28] Photobiomodulation (PBMT) therapy has been prominently characterized as an effective approach to accelerate the reversal of local anesthesia, reducing the duration of numbness and potentially decreasing the risk of self-inflicted injury.[16,18] A detailed feature of the included studies was demonstrated in Table 2.

Main findings of the study

The studies included in this systematic review provide valuable insights into the diagnosis and management of traumatic injuries caused by local anesthesia in pediatric patients. A predominant finding reported in multiple studies has been the high incidence of lesions particularly on the lower lip, cheeks and tongue bites, which are directly attributed to residual numbness after administration of anesthesia.[1,4,6,14,15,17,18,23,24,26,27,30] These injuries often appear as ulcers or tears in the tissues, leading to discomfort,

Table 2. Detailed characteristics of the studies included

Authors	Age of children	Type of anesthesia and anesthesia used	Procedure conducted	Location and type of lesion	Differential diagnosis	Treatment and time needed to heal
Kot et al.[1]	Patient 1: – 4.5 years Patient 2: – 9 years Patient 3: – 7 years	Infiltration anesthesia (4% articaine with epinephrine 1:200,000) (1/2 cartridge) in all 3 cases	Patient 1: – 84 – removal of caries and pulp from the chamber Patient 2: – 36 – removal of caries Patient 3: – 54 – tooth extraction	Patient 1: – Extensive, painless ulceration on the right side of the lower lip with no symptoms of inflammation Patient 2: – Ulcerations on the mucosa of the cheek at the level of the treated tooth and at the corner of the lips Patient 3: – Extensive and swollen damage to the mucous membrane of the upper lip	N/A	Treatment: Patient 1: – Tantum Green Aerosol and Solcoseryl paste – Healing time: 1 week Patient 2: – Sulcoserile paste – Healing time: 10 days Patient 3: – Sulcoserile paste – Healing time: 1 week
Chi et al.[4]	10 years	Inferior alveolar nerve block with 2% lidocaine	Treatment of dental caries	Biting the lips with mild bleeding after the procedure. The next day: The lower lip on the right side was swollen, ulcerated with a white coating. The size of the lesion: 7 × 4 mm. A similar lesion was found on the right vestibular mucosa adjacent to the tooth 46.	Infectious ulcer	N/A
Tavares et al.[5]	4–11 years	Lidocaine 2% with adrenaline 1:100,000	Routine dental treatments	N/A	N/A	N/A
Nourbakhsh et al.[6]	4–11 years	Inferior alveolar block: Lidocaine 2% with epinephrine 1:80,000	Routine dental treatments	Lip, no trauma to the cheeks or tongue has been described.	N/A	N/A
Tiwari[14]	4 years	Topical anesthesia: Benzocaine 20% from the buccal and lingual side Infiltrative anesthesia: 2% lidocaine	Restorations in 74 and 75	Patch, white ulcer seen on the left side of the lower lip. The size of the lesion was 1 × 2 cm and extended from the midline to the corner of the lips. The texture has been described as tender. The injury was slightly relieved.	Herpes simplex virus infection, traumatic fibroid, allergic contact stomatitis aphthous stomatitis	Treatment: paracetamol oral suspension 5 mL, applications of ice packs and salt reliefs. The injury healed after 10 days.
Ghajari et al.[16]	6–9 years	Anesthesia of the inferior alveolar nerve block (2% lidocaine with 1:100,000 epinephrine); 1 cartridge	Deciduous molar pulpotomy	In the experimental group: – A child suffered self-inflicted injuries In the fictitious group: – Two children suffered self-inflicted injuries	N/A	808 nm, 250 mW, 11.5 J/cm^2, 23-s diode laser applied after the dental procedure to reduce the effect of numbness and reduce the potential risk of post-treatment soft tissue trauma.
Helmy et al.[17]	5–7 years	Before injection: topical anesthetic gel with 20% benzocaine Inferior alveolar nerve block or intraligamentous anesthesia (4% articaine with epinephrine 1:100,000)	Extraction of the first deciduous molars	Inferior alveolar block anesthesia group: – 32% of participants suffered trauma to the lips from biting	N/A	No treatment has been applied.

Table 2. Detailed characteristics of the studies included – cont

Authors	Age of children	Type of anesthesia and anesthesia used	Procedure conducted	Location and type of lesion	Differential diagnosis	Treatment and time needed to heal
Olszewska et al.[18]	8–10 years	Infiltration anesthesia 4% articaine with epinephrine 1:200,000	Treatment of caries of permanent molars.	After the procedure: – 4 cases of self-harm of the cheek mucosa in both groups (laser treatment and sham group) One day after the procedure: – 1 case of self-inflicted injury in the laser assembly – 5 cases of injuries in the sham group	N/A	Diode laser application (635 nm or 808 nm, 250 mW, 500 mW/cm^2, 15 J or 200 mW, 400 mW/cm^2, 12 J) 45 min after injection; the control tooth was treated with the laser applicator turned off. The laser was applied using the contact technique.
Bagattoni et al.[19]	3–13 years	Before injection: 15% topical anesthetic spray. Lidocaine-inferior alveolar nerve block: Mepivacaine 2% with 1:100000 epinephrine. Anesthesia by infiltration: Articaine 4% with epinephrine 1:100,000.	N/A	19% of children with disabilities have experienced soft tissue trauma compared to 9% of children without disabilities. In both groups, children under 6 were more likely to suffer the injury. The highest frequency of injuries in both groups was recorded after the IANB. The highest frequency of injuries in both groups occurred after conservative treatments.	N/A	No treatment has been applied. One child in the group without a disability and 2 in the group with disabilities were prescribed ibuprofen to control pain.
Alghamidi et al.[20]	3–15 years	Inferior alveolar nerve block: 2% lidocaine with epinephrine (1:50,000 or 1:100,000)	N/A	N/A	N/A	Intraoral appliances produced in 3 standard sizes depending on age: 3–6, 6–9 and 9–12 years (apparatus No. 1 – anterior extension with numerous perforations, No. 2 – with buccal flap extension, No. 3 – with serrated edges); each device is kept in the mouth 3 h after anesthesia.
Alinejhad et al.[21]	6–10 years	Inferior alveolar block: 2% or 4% lidocaine with epinephrine 1:100,000	Pulpotomy of primary and secondary molars	N/A	N/A	N/A
Baillargeau et al.[22]	3–13 years	Infiltration anesthesia 4% articaine with epinephrine 1:200,000	Dental extractions	Six children reported self-harm, which was painful for 5 of them.	N/A	No treatment
Bendgude et al.[23]	Patient 1: – 4 years Patient 2: – 5 years	Patient 1: – Lower alveolar block Patient 2: – Buccal infiltration	Caries treatment	Case 1: – An ulcerative lesion on the right side of the lower lip and a scratch lesion on the right side of the chin the next day Case 2: – Injuries to the wing of the nose the next day	N/A	Case 1: – Treatment: analgesics and antiseptic gel for the mouth – The injuries healed after 14 days Case 2: – Treatment with topical antiseptic – The injury healed after 10 days

Table 2. Detailed characteristics of the studies included – cont

Authors	Age of children	Type of anesthesia and anesthesia used	Procedure conducted	Location and type of lesion	Differential diagnosis	Treatment and time needed to heal
Coulthard et al.[24]	4–12 years	General anesthesia: 2 mL 2% lidocaine with 1:200,000 epinephrine or placebo 2 mL 0.9% sodium chloride as buccal infiltration to reduce postoperative pain	Extractions of 1–10 teeth	Three children in the lidocaine group reported biting their lips or cheeks 24 h after the procedure, while only 1 child reported this problem from the placebo group.	N/A	N/A
College et al.[25]	2–18 years	2% lidocaine with 1:100,000 epinephrine or 2% mepivacaine with 1:20,000 levonordephrin; inferior and buccal long alveolar local nerve block anesthesia	N/A	There has been a higher incidence of trauma in the case of unilateral inferior alveolar nerve block, especially in the case of children under the age of 4.	N/A	N/A
Adewumi et al.[26]	2–14 years	4% of articaine with 1:100,000 of adrenaline; infiltrations or block of the inferior alveolar nerve as appropriate	Routine dental treatments	The lip was the most affected area of the injury.	N/A	N/A
Townsendet al.[27]	3–5.5 years	General anesthesia: group 1: 1 mg/kg ketorolac tromethamine together with 2% lidocaine with epinephrine 1: 100,000 infiltration; group 2: 1 mg/kg ketorolac tromethamine	Anterior extractions or placement of stainless steel crowns.	Biting lips or cheeks	N/A	No treatment applied
Ram et al.[28]	4–11 years	Lidocaine 2% with adrenaline 1:100,000; type of anesthesia adapted to the procedure	Two similar treatments on both sides of the jaw (fillings, pulpotomies, crowns or extractions).	There was no significant difference in soft tissue bite in either the toy or ice groups. However, 10 min after the procedure, only 3 children in the ice group continued to bite each other compared to 11 children in the toy group.	N/A	N/A
Sixou et al.[29]	4–16 years	Intraosseous anesthesia: 4% articaine with 1:200,000 epinephrine	Usual dental care	No self-inflicted soft tissue injury was detected.	N/A	N/A
Flaitz and Felefli[30]	8 years	Lower alveolar block	Positioning of the stainless steel crown on the mandibular second molar.	Two widespread ulcerations on the right side of the mucous membrane of the lip and cheek. The lesion was covered with fibrinous exudate. The ulcer was painful until palpation. Mild submandibular lymphadenopathy has been observed.	Allergic contact stomatitis, smokeless tobacco lesions-white spongy nevus	Oral lubricants (OralBalance gel), psychological counseling

CC-ILA – computer-controlled intraligamentary anesthesia; IANB – inferior alveolar nerve block; LLLT – low-Level laser therapy; – milliwatt per square centimeter; N/A – not applicable; NSAID – non-steroidal anti-inflammatory drug; PBMT – photobiomodulation therapy; PM – phentolamine mesylate.

delayed healing and psychological distress in affected children.[1,4,6,14,15,23]

Several studies have evaluated the effectiveness of innovative preventive strategies. Intraoral appliances significantly reduce the incidence of bite injuries by serving as mechanical barriers during the period of anesthesia-induced numbness.[22] Similarly, non-pharmacological approaches, such as the use of icicles, have demonstrated potential to mitigate tissue trauma by promoting sensory awareness and calming post-operative behavior.[28] The effectiveness of low-level laser therapy in speeding up anesthesia reversal and decreasing the duration of numbness has also been emphasized, with studies showing quicker recovery times and fewer complications.[16,18] A similar preventive strategy that introduced pharmacological intervention was applied in studies conducted by Tavares et al.[5] and Nourbakhsh et al.,[6] where phentolamine mesylate was administered to patients following the injection of local anesthesia. These methods have proven effective in shortening numbness duration after local anesthesia, thereby preventing self-inflicted soft tissue trauma.

Comparative results of different anesthesia techniques were another significant goal. Studies have found that computer-controlled intraligamental injections resulted in fewer postoperative injuries than traditional nerve block techniques, particularly in younger patients undergoing dental extractions.[17] It happens due to the lack of anesthetization of local soft tissues – anesthesia is applied directly to the periodontal ligament of a treated tooth. Pain management and patient comfort have been evaluated in several studies, with results indicating that improved anesthetic techniques, such as intraosseous injections, can improve the patient experience by providing more localized and controlled anesthesia.[29] The type of anesthetic agent used also influenced the outcomes; e.g., adverse effects such as prolonged numbness or an increased risk of soft tissue trauma have been linked to specific agents, such as articaine, particularly when administered at concentrations as high as 4%.[26]

The studies we reviewed show that different methods for preventing self-inflicted soft tissue injuries after local anesthesia vary in both safety and effectiveness. For example, phentolamine mesylate can cut down on how long a child stays numb, which lowers the chance of accidental bites,[5,6] though it might cause mild side effects like a brief drop in blood pressure or dizziness.[31,32] Photobiomodulation therapy can also speed up recovery from numbness and help tissues heal, but it is not always easy to access or afford.[15,16,18] Non-drug strategies, such as using a custom mouth appliance or offering popsicles, can be effective in preventing biting; however, success largely depends on the child's willingness to cooperate.[20,28] Meanwhile, alternative anesthesia techniques – like intraligamentary or intraosseous anesthesia – can significantly cut down on injuries, but they require special tools and training.[17,29]

In the future, comparing these different methods in head-to-head studies will be helpful to determine which ones are most effective in various situations. We also need longer-term research to find out how well each approach holds up over time. Ultimately, creating clear guidelines for dentists – based on both practical experience and solid evidence – can help protect children from these injuries while ensuring they receive safe, comfortable dental care.[5,6,15,16,18,20,28,29]

Quality assessment

Six case reports were assessed using a checklist, with 2 scoring the highest score by 8 points,[14,23] while the other 4 received 7 points[1,4] and 6 points.[15,30] Among the 9 RCTs, 5 had a low risk of bias, gaining 13 points,[5] 12 points[17,27] or 11 points[6,24] out of 13, while the other showed a moderate risk of sprain with a score of 9 points[16,25] or 10 points[18,21] on the 13 point-scale. In addition, 4 cohort studies were analyzed, with a score of 9 points,[19], 7 points[22] or 6 points[26,28] out of 11 possible. Score details for these studies are summarized in Tables 3–5.

Discussion

This systematic review provided a comprehensive overview of the diagnosis and management of soft tissue injuries caused by local anesthesia in pediatric dental practice. The main findings highlight the high prevalence of traumatic lesions among pediatric patients, with the most common accidental bites to the lips, cheeks and tongue. These injuries are strongly associated with the temporary loss of sensation caused by local anesthesia, which impairs the child's ability to perceive and control oral movements.[1,4,15,17,18,22–24,26,27,30] Many cases have emphasized the risk of soft tissue damage following inferior alveolar block anesthesia.[4,6,15–17,19–21,23,25,26,30] Although generally self-limiting, these injuries can cause considerable discomfort and delay healing, as evidenced in previous work.[1,14,15,26,30]

Consistent with the results of Helmy et al.,[17] anesthetic techniques significantly influence the incidence of post-operative trauma. In particular, computer-assisted intraligamentous anesthesia has been shown to reduce complications compared to traditional nerve block techniques. Computer-controlled anesthetic delivery is associated with reduced injection pain, better control of the anesthetized area and a decreased risk of traumatic bites by providing localized numbness without affecting surrounding soft tissues. This precise administration with preselected speed of anesthetic delivery not only enhances patient comfort but also minimizes post-procedural discomfort and swelling, leading to a smoother recovery.[17,18] In addition, innovative approaches such as PBMT and phentolamine mesylate

Table 3. Assessment of the risk of bias of the included studies – cohort studies

Cohort studies	Bagattoni et al.[19]	Baillargeau et al.[22]	Adewumi et al.[26]	Ram et al.[28]
Were the 2 groups similar and recruited from the same population?	yes	yes	yes	yes
Were exposures measured similarly to assign people to both exposed and unexposed groups?	yes	insecure	no	insecure
Has exposure been measured validly and reliably?	yes	yes	yes	yes
Have confounding factors been identified?	yes	yes	no	no
Have strategies been indicated to deal with confounding factors?	yes	no	no	no
Were the groups/participants outcome free at the start of the study (or at the time of exposure)?	yes	yes	yes	yes
Were the results measured validly and reliably?	yes	yes	yes	yes
Has the follow-up time been reported and sufficient to be long enough for the results to occur?	yes	yes	yes	yes
Was the follow-up complete and, if not, were the reasons for the loss described and explored to follow?	no	no	no	insecure
Were strategies used to address incomplete follow-up?	no	no	no	no
Was an appropriate statistical analysis used?	yes	yes	yes	yes

Table 4. Assessment of the risk of bias of the included studies – randomized controlled trials

Randomized controlled trials	Tavares et al.[5]	Nourbakhsh et al.[6]	Ghajari et al.[16]	Helmy et al.[17]	Olszewska et al.[18]	Alinejhad et al.[21]	Coulthard et al.[24]	College et al.[25]	Townsend et al.[27]
Was true randomization used for the assignment of participants to treatment groups?	yes	yes	yes	yes	yes	yes	yes	yes	yes
Was the assignment to treatment groups hidden?	yes	insecure	insecure	yes	insecure	insecure	yes	insecure	insecure
Were the treatment groups similar at baseline?	yes	yes	yes	yes	yes	yes	yes	yes	yes
Were participants blinded to treatment assignment?	yes	yes	no	yes	yes	no	no	no	yes
Were those providing treatment blinded to the treatment assignment?	yes	yes	no	no	no	insecure	no	no	yes
Were outcome evaluators blinded to treatment assignment?	yes	insecure	insecure	yes	no	yes	yes	insecure	yes
Were the treatment groups treated identically different from the intervention of interest?	yes	yes	yes	yes	yes	yes	yes	yes	yes
Was the follow-up complete and, if not, were the differences between the groups in terms of follow-up adequately described and analyzed?	yes	yes	yes	yes	yes	yes	yes	yes	yes
Were the participants analyzed in the groups to which they were randomized?	yes	yes	yes	yes	yes	yes	yes	yes	yes
Were the outcomes measured in the same way for the treatment groups?	yes	yes	yes	yes	yes	yes	yes	yes	yes
Were the results reliably measured?	yes	yes	yes	yes	yes	yes	yes	yes	yes
Was an appropriate statistical analysis used?	yes	yes	yes	yes	yes	yes	yes	yes	yes
Was the study design appropriate and were any deviations from the standard randomized controlled trial (RCT) design (individual randomization, parallel groups) taken into account in the conduct and analysis of the study?	yes	yes	yes	yes	yes	yes	yes	yes	yes

Table 5. Assessment of the risk of bias of the included studies – clinical cases

Clinical cases	Kot et al.[1]	Chi et al.[4]	Tiwari[14]	Calazans et al.[15]	Bendgude et al.[23]	Flaitz and Felefli[30]
Have the patient's demographic characteristics been clearly described?	yes	yes	yes	yes	yes	yes
Has the patient's medical history been clearly described and presented as a timeline?	no	yes	yes	yes	yes	yes
Was the patient's current clinical condition at the time of presentation clearly described?	yes	yes	yes	yes	yes	yes
Have the diagnostic tests or evaluation methods and results been clearly described?	yes	yes	yes	yes	yes	insecure
Have the intervention or treatment procedures been clearly described?	yes	no	yes	no	yes	no
Has the post-surgery clinical condition been clearly described?	yes	yes	yes	yes	yes	yes
Have any adverse events (damage) or unexpected events been identified and described?	yes	yes	yes	no	yes	yes
Does the clinical case provide takeaway lessons?	yes	yes	yes	yes	yes	yes

have demonstrated efficacy in reducing the duration of anesthesia and minimizing self-inflicted lesions, in line with the results of previous studies.[5,6,16,18]

The pharmacological approach to alleviating self-inflicted soft tissue injuries following local anesthesia includes the administration of reversal agents such as phentolamine mesylate. This adrenergic antagonist has been shown to significantly reduce the duration of anesthesia-induced numbness, decreasing the likelihood of accidental bites and associated trauma.[31,32] Its efficacy in expediting sensory recovery is particularly valuable in pediatric dentistry, where young patients may struggle with the unfamiliar sensation of prolonged numbness. However, while the benefits of phentolamine mesylate in reducing anesthesia-related injuries are well-documented, concerns remain regarding its potential side effects, including transient hypotension, dizziness and local tissue reactions.[33] Additionally, repeated administration in the same anatomical area raises the risk of localized complications, such as tissue irritation or vascular compromise. These factors underscore the importance of exploring non-pharmacological and minimally invasive alternatives to improve patient safety and comfort.

The advantages of low-level laser therapy (LLLT) are especially significant in pediatric dentistry.[34,35] One of its primary benefits is the significant reduction in soft tissue recovery time, which promotes faster healing and minimizes discomfort in young patients.[18] In addition, PBMT provides an effective analgesic effect, relieving pain without the need for pharmaceutical interventions.[36] This is particularly valuable in pediatric populations, where the risk of adverse reactions to anesthesia can pose significant concerns.[37,38] Photobiomodulation therapy provides a noninvasive, drug-free method for managing self-inflicted injuries, such as accidental bites or trauma, which often occur due to residual numbness after local anesthesia.[18] Low-level laser therapy harnesses the healing properties of light to stimulate cellular repair and reduce inflammation, making it a promising and safe option for injury treatment.[35] Its ease of application and minimal risk profile further increase its potential as a valuable tool in pediatric dental care, providing both immediate relief and long-term benefits for young patients.[16] However, there is limited research on the cost-effectiveness and accessibility of implementing PBMT in routine clinical practice, indicating a need for further studies to evaluate these aspects.[39]

The effectiveness of different methods to prevent self-inflicted soft tissue injuries after local anesthesia depends on the specific technique used, patient compliance and clinical feasibility. For instance, the use of phentolamine mesylate can accelerate the reversal of local anesthesia, thereby reducing the risk of accidental soft tissue injuries. However, it may also be associated with side effects such as transient hypotension or dizziness.[4,5,29] Meanwhile, PBMT is a noninvasive option that helps tissues heal faster and reduces the duration of numbness without the need for additional medication.[14,16] Despite the promising benefits of PBMT, concerns remain about its availability, cost and the lack of standardized protocols for routine clinical practice.[37] Non-pharmacological options, like intraoral appliances, have shown success in preventing accidental bites, especially in younger children.[8] However, patient compliance and comfort play a crucial role, as some children may be reluctant to use these devices. Another simple method is giving children unsweetened popsicles as a sensory distraction to reduce biting behavior, but there is limited evidence regarding its long-term effectiveness or potential drawbacks.[26] Even though these techniques are promising, direct comparisons of their safety, effectiveness and feasibility are lacking in the current literature. Most studies evaluate these interventions individually rather

than in comparative trials, making it difficult to determine the most effective approach.

Preventive measures are critical in pediatric dental care to mitigate the risk of self-inflicted injury following procedures involving local anesthesia.[38,40] The use of protective intraoral devices has been shown to significantly reduce accidental bites. A study evaluating 3 types of self-designed intraoral appliances found them effective in preventing biting of the cheeks, lips and tongue in children after local anesthesia.[20] In addition, non-pharmacological interventions, such as offering unsweetened popsicles after treatment, have demonstrated benefits.[41,42] Research indicates that children who received popsicles after dental procedures under local anesthesia experienced less discomfort and a reduced tendency to self-mutilation than those who received a toy.[28] However, the literature does not extensively address the potential adverse effects of these preventive strategies. Nevertheless, given their noninvasive nature, these approaches are likely to pose fewer risks than pharmacological methods, which may be associated with systemic adverse effects.[20]

Caregivers play a vital role in preventing self-inflicted soft tissue injuries in children – especially younger or disabled patients – following local dental anesthesia. Due to temporary numbness, children may unintentionally bite or chew on their lips, cheeks or tongue, leading to painful injuries.[4] To minimize this risk, caregivers should closely monitor the child until the anesthetic wears off, discourage eating solid foods or drinking hot beverages, and provide soft or cold foods instead.[43] Additionally, engaging the child in distraction techniques, such as supervised play, can help reduce the likelihood of injury.[19] Educating caregivers about these precautions is essential for ensuring a safe and comfortable recovery.[44] These strategies not only improve postoperative comfort but also play a critical role in preventing complications associated with residual numbness, thereby improving the overall quality of pediatric dental care.[38,40–42,45,46]

Limitations

This study has several limitations, including variability in anesthesia protocols, differences in dosages and administration methods and the heterogeneity of pediatric populations, which affect the generalizability of findings. The broad age range of examined children introduces additional variability, as younger and older children may respond differently to anesthesia and have distinct risks of self-inflicted injuries. The lack of longitudinal studies further limits insights into long-term effects, such as cognitive or developmental outcomes. Future research should focus on standardized protocols, narrower age groups and larger, more diverse control groups. In addition, the considerable variability among the studies included prevents us from performing a meta-analysis. However, additional research is needed to make a meta-analysis feasible.

Conclusions

This systematic review highlights the high prevalence of self-inflicted soft tissue injuries among pediatric dental patients, caused primarily by residual numbness after local anesthesia. The findings underscore the need for comprehensive preventive and therapeutic strategies to effectively address these complications. Innovative approaches such as computerized anesthesia, PBMT and protective intraoral devices have shown significant potential in reducing the incidence of accidental bites and enhancing recovery outcomes. However, the variability of anesthetic protocols and study methodologies underscores the need for standardized practices and further research. Longitudinal studies are essential for evaluating the long-term effects of these interventions, ensuring safety and validating their efficacy in diverse pediatric populations. To enhance clinical application, dental practitioners should prioritize patient and caregiver education on post-anesthetic care, incorporate intraoral protective devices when appropriate, and consider alternative anesthesia techniques to minimize residual numbness. Additionally, implementing structured post-procedure monitoring can help identify and mitigate potential injuries early. By integrating these advanced, minimally invasive approaches, pediatric dental care can prioritize both patient safety and comfort while addressing the unique challenges of soft tissue injury management.

Consent for publication

Not applicable.

Use of AI and AI-assisted technologies

Not applicable.

ORCID iDs

Aneta Olszewska https://orcid.org/0000-0003-1286-6779
Julia Kensy https://orcid.org/0009-0008-1680-793X
Agata Czajka-Jakubowska https://orcid.org/0000-0002-1692-2910
Daniele Pergolini https://orcid.org/0000-0001-8885-0496
Maurizio Bossù https://orcid.org/0000-0002-6539-9134
Umberto Romeo https://orcid.org/0000-0003-2439-2187
Jacek Matys https://orcid.org/0000-0002-3801-0218

References

1. Kot K, Krawczuk-Molęda E, Marek E, Lipski M. Self-inflicted injury as a complication following dental local anaesthesia in children: Case reports. *J Stomatol*. 2018;72(2):203–211. doi:10.5114/jos.2018.80673
2. Ho JPTF, Van Riet TCT, Afrian Y, et al. Adverse effects following dental local anesthesia: A literature review. *J Dent Anesth Pain Med*. 2021; 21(6):507. doi:10.17245/jdapm.2021.21.6.507
3. Orzechowska-Wylęgała BE, Wylęgała AA, Zalejska-Fiolka J, Czuba Z, Toborek M. Pro-inflammatory cytokines and antioxidative enzymes as salivary biomarkers of dentofacial infections in children [published online as ahead of print on June 19, 2024]. *Dent Med Probl*. 2024. doi:10.17219/dmp/185733
4. Chi D, Kanellis M, Himadi E, Asselin ME. Lip biting in a pediatric dental patient after dental local anesthesia: A case report. *J Pediatr Nurs*. 2008;23(6):490–493. doi:10.1016/j.pedn.2008.02.035

5. Tavares M, Goodson JM, Studen-Pavlovich D, et al. Reversal of soft-tissue local anesthesia with phentolamine mesylate in pediatric patients. *J Am Dent Assoc*. 2008;139(8):1095–1104. doi:10.14219/jada.archive.2008.0312
6. Nourbakhsh N, Shirani F, Babaei M. Effect of phentolamine mesylate on duration of soft tissue local anesthesia in children. *J Res Pharm Pract*. 2012;1(2):55–59. doi:10.4103/2279-042X.108371
7. Thyssen JP, Menné T, Elberling J, Plaschke P, Johansen JD. Hypersensitivity to local anaesthetics: Update and proposal of evaluation algorithm. *Contact Dermatitis*. 2008;59(2):69–78. doi:10.1111/j.1600-0536.2008.01366.x
8. Lipiński P, Ługowska A, Tylki-Szymańska A. Chronic acid sphingomyelinase deficiency diagnosed in infancy/childhood in Polish patients: 2024 update. *Adv Clin Exp Med*. 2024;33(10):1163–1168. doi:10.17219/acem/193696
9. Ghafoor H, Haroon S, Atique S, et al. Neurological complications of local anesthesia in dentistry: A review. *Cureus*. 2023;15(12):e50790. doi:10.7759/cureus.50790
10. Marshall A, Alam U, Themistocleous A, Calcutt N, Marshall A. Novel and emerging electrophysiologicalb biomarkers of diabetic neuropathy and painful diabetic neuropathy. *Clin Ther*. 2021;43(9):1441–1456. doi:10.1016/j.clinthera.2021.03.020
11. Huang X, Lin J, Demner-Fushman D. Evaluation of PICO as a knowledge representation for clinical questions. *AMIA Annu Symp Proc*. 2006;2006:359–363. PMID:17238363. PMCID:PMC1839740.
12. Page MJ, McKenzie JE, Bossuyt PM, et al. The PRISMA 2020 statement: An updated guideline for reporting systematic reviews. *BMJ*. 2021;372:n71. doi:10.1136/bmj.n71
13. Watson PF, Petrie A. Method agreement analysis: A review of correct methodology. *Theriogenology*. 2010;73(9):1167–1179. doi:10.1016/j.theriogenology.2010.01.003
14. Tiwari A. A traumatic ulcer caused by accidental lip biting following topical anesthesia: A case report. *Cureus*. 2023;15(4):e38316. doi:10.7759/cureus.38316
15. Calazans T, De Campos P, Melo A, et al. Protocol for low-level laser therapy in traumatic ulcer after troncular anesthesia: Case report in pediatric dentistry. *J Clin Exp Dent*. 2020;12(2):e201–e203. doi:10.4317/jced.56176
16. Ghajari MF, Kiaepour Z, Fekrazad R, Hartoonian S, Shekarchi F. Expediting the reversal of inferior alveolar nerve block anesthesia in children with photobiomodulation therapy. *Lasers Med Sci*. 2024;39(1):148. doi:10.1007/s10103-024-04096-x
17. Helmy RH, Zeitoun SI, El-Habashy LM. Computer-controlled intraligamentary local anaesthesia in extraction of mandibular primary molars: Randomised controlled clinical trial. *BMC Oral Health*. 2022;22(1):194. doi:10.1186/s12903-022-02194-2
18. Olszewska A, Matys J, Grzech-Leśniak K, Czajka-Jakubowska A. Enhanced recovery of local anesthesia in pediatric patients: The impact of photobiomodulation on reversing anesthesia effects. *Med Sci Monit*. 2024;30:e941928. doi:10.12659/MSM.941928
19. Bagattoni S, D'Alessandro G, Gatto MR, Piana G. Self-induced soft-tissue injuries following dental anesthesia in children with and without intellectual disability: A prospective study. *Eur Arch Paediatr Dent*. 2020;21(5):617–622. doi:10.1007/s40368-019-00506-9
20. Alghamidi W, Alghamdi S, Assiri J, Almathami A, Alkahtani Z, Togoo R. Efficacy of self-designed intraoral appliances in prevention of cheek, lip and tongue bite after local anesthesia administration in pediatric patients. *J Clin Exp Dent*. 2019;11(4):e315–e321. doi:10.4317/jced.55477
21. Alinejhad D, Bahrololoomi Z, Navabazam A, Asayesh MA. Comparison of visual analog scale scores in pain assessment during pulpotomy using different injection materials in children aged 6 to 8 and 8 to 10 years. *J Contemp Dent Pract*. 2018;19(3):313–317. PMID:29603705.
22. Baillargeau C, Lopez-Cazaux S, Charles H, et al. Post-operative discomforts in children after extraction of primary teeth. *Clin Exp Dent Res*. 2020;6(6):650–658. doi:10.1002/cre2.316
23. Bendgude V, Akkareddy B, Jawale BA, Chaudhary S. An unusual pattern of self-inflicted injury after dental local anesthesia: A report of 2 cases. *J Contemp Dent Pract*. 2011;12(5):404–407. doi:10.5005/jp-journals-10024-1067
24. Coulthard P, Rolfe S, Mackie IC, Gazal G, Morton M, Jackson-Leech D. Intraoperative local anaesthesia for paediatric postoperative oral surgery pain: A randomized controlled trial. *Int J Oral Maxillofac Surg*. 2006;35(12):1114–1119. doi:10.1016/j.ijom.2006.07.007
25. College C, Feigal R, Wandera A, Strange M. Bilateral versus unilateral mandibular block anesthesia in a pediatric population. *Pediatr Dent*. 2000;22(6):453–457. PMID:11132502.
26. Adewumi A, Hall M, Guelmann M, Riley J. The incidence of adverse reactions following 4% septocaine (articaine) in children. *Pediatr Dent*. 2008;30(5):424–428. PMID:18942603.
27. Townsend JA, Ganzberg S, Thikkurissy S. The effect of local anesthetic on quality of recovery characteristics following dental rehabilitation under general anesthesia in children. *Anesth Prog*. 2009;56(4):115–122. doi:10.2344/0003-3006-56.4.115
28. Ram D, Berson T, Moskovitz M, Efrat J. Unsweetened ice popsicles impart a positive feeling and reduce self-mutilation after paediatric dental treatment with local anaesthesia. *Int J Paediatr Dent*. 2010;20(5):382–388. doi:10.1111/j.1365-263X.2010.01059.x
29. Sixou JL, Barbosa-Rogier ME. Efficacy of intraosseous injections of anesthetic in children and adolescents. *Oral Surg Oral Med Oral Pathol Oral Radiol Endodontol*. 2008;106(2):173–178. doi:10.1016/j.tripleo.2007.12.004
30. Flaitz CM, Felefli S. Complications of an unrecognized cheek biting habit following a dental visit. *Pediatr Dent*. 2000;22(6):511–512. PMID:11132513.
31. Suri N, Kalra G, Kumar M, Avasthi A, Kalra T, Singh R. A literature review on various complications associated with administration of local anesthesia in dentistry. *IP Int J Maxillofac Imaging*. 2022;8(2):63–66. doi:10.18231/j.ijmi.2022.015
32. Cummings DR, Yamashita DDR, McAndrews JP. Complications of local anesthesia used in oral and maxillofacial surgery. *Oral Maxillofac Surg Clin North Am*. 2011;23(3):369–377. doi:10.1016/j.coms.2011.04.009
33. Meechan JG. Local anaesthesia: Risks and controversies. *Dent Update*. 2009;36(5):278–283. doi:10.12968/denu.2009.36.5.278
34. Dehgan D, Şermet Elbay Ü, Elbay M. Evaluation of the effects of photobiomodulation with different laser application doses on injection pain in children: A randomized clinical trial. *Lasers Med Sci*. 2022;38(1):6. doi:10.1007/s10103-022-03674-1
35. Karu T. Is it time to consider photobiomodulation as a drug equivalent? *Photomed Laser Surg*. 2013;31(5):189–191. doi:10.1089/pho.2013.3510
36. Olszewska A, Forszt D, Szymczak A, et al. Effectiveness of phentolamine mesylate, vibration and photobiomodulation in reducing pain and the reversal of local anesthesia: A systematic review [published online as ahead of print on November 9, 2024]. *Adv Clin Exp Med*. 2024. doi:10.17219/acem/190202
37. Mass E, Palmon Y, Zilberman U. Local anesthesia in pediatric dentistry: How much is enough? *Dentistry*. 2018;8(4):1000480. doi:10.4172/2161-1122.1000480
38. Gupta S, Gupta S, Gupta T, Mehra M, Grover R. Painless anesthesia in pediatric dentistry: An updated review. *IOSR J Dent Med Sci*. 22(9):16–21. doi:10.9790/0853-2209041621
39. Sleep SL, Walsh LJ, Zuaiter O, George R. PBM for dental analgesia and reversal from injected local anesthetic agents: A systematic review. *Laser Dent Sci*. 2024;8(1):52. doi:10.1007/s41547-024-00268-8
40. Coté CJ, Wilson S; American Academy of Pediatrics; American Academy of Pediatric Dentistry. Guidelines for monitoring and management of pediatric patients before, during, and after sedation for diagnostic and therapeutic procedures. *Pediatrics*. 2019;143(6):e20191000. doi:10.1542/peds.2019-1000
41. Jung RM, Rybak M, Milner P, Lewkowicz N. Local anesthetics and advances in their administration: An overview. *J Pre Clin Clin Res*. 2017;11(1):94–101. doi:10.26444/jpccr/75153
42. Elheeny AAH. Articaine efficacy and safety in young children below the age of four years: An equivalent parallel randomized control trial. *Int J Paediatr Dent*. 2020;30(5):547–555. doi:10.1111/ipd.12640
43. Use of local anesthesia for pediatric dental patients. *Pediatr Dent*. 2017;39(6):266–272. PMID:29179367.
44. Kiliś-Pstrusińska K, Anna M, Adamczyk P, et al. Depressive disorders in children with chronic kidney disease treated conservatively. *Adv Clin Exp Med*. 2024;33(11):1189–1199. doi:10.17219/acem/175236
45. Van Eeden SP, Patel MF. Prolonged paraesthesia following inferior alveolar nerve block using articaine. *Br J Oral Maxillofac Surg*. 2002;40(6):519–520. doi:10.1016/S0266435602002231
46. Kingon A, Sambrook P, Goss A. Higher concentration local anaesthetics causing prolonged anaesthesia: Do they? A literature review and case reports. *Aust Dent J*. 2011;56(4):348–351. doi:10.1111/j.18t34-7819.2011.01358.x